Structural Engineering Report No. 49

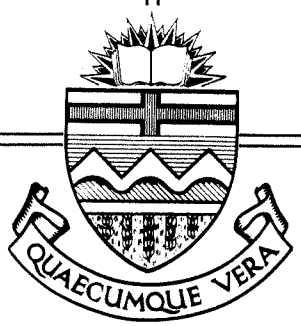

THE SECOND-ORDER ANALYSIS OF REINFORCED CONCRETE FRAMES

by

S. E. HAGE and

J. G. MacGREGOR

October, 1974

RECENT STRUCTURAL ENGINEERING REPORTS

Department of Civil Engineering

University of Alberta

24. *Prestressed Concrete Beams with Web Reinforcement Under Combined Loading* by P. Mukherjee and J. Warwaruk, May 1970.

25. *Studies of Reinforced Concrete Shear Wall-Frame Structures* by R.P. Nikhed, J.G. MacGregor and P.F. Adams, June 1970.

26. *Buckling Strengths of Hot Rolled Hat Shaped Sections* by D.A. Heaton and P.F. Adams, July 1970.

27. *Experimental and Analytical Investigation of the Behavior of Coupled Shear Wall-Frame Structures* by S.N.G. Majumdar and P.F. Adams, August 1970.

28. *Comparative Study of Slab-Beam Systems* by J. Misic and S.H. Simmonds, September 1970.

29. *Elastic-Plastic Analysis of Three Dimensional Structures* by J.H. Wynhoven and P.F. Adams, September 1970.

30. *Flexural and Lateral-Torsional Buckling Strengths and Double Angle Struts* by N.J. Nuttall and P.F. Adams, September 1970.

31. *Stiffness Influence Coefficients for Non-Axisymmetrical Loading on Closed Cylindrical Shells* by S.H. Iyer and S.H. Simmonds, October 1970.

32. *CSA-S16-1969 Steel Structures for Buildings - Seminar Notes* by P.F. Adams, G.L. Kulak and J. Longworth, November 1970.

33. *Experiments on Steel Wide-Flange Beam-Columns Subjected to Lateral Loads* by G.W. English and P.F. Adams, May 1971.

34. *Finite Element Analysis of Thin-Walled Members of Open Section* by S. Rajasekaran, September 1971.

35. *Finite Element Programs for Beam Analysis* by S. Rajasekaran, September 1971.

36. *Seminar on Building Code Requirements, ACI-318-71* by J.G. MacGregor, S.H. Simmonds and J. Warwaruk, July 1971.

37. *Stability of Braced Frames* by J.H. Davison and P.F. Adams, October 1971.

38. *Time Dependent Deflections of Reinforced Concrete Slabs* by A. Scanlon and D.W. Murray, December 1971.

THE UNIVERSITY OF ALBERTA

THE SECOND-ORDER ANALYSIS OF REINFORCED CONCRETE FRAMES

by

SVEN EGIL HAGE

A THESIS

SUBMITTED TO THE FACULTY OF GRADUATE STUDIES AND RESEARCH

IN PARTIAL FULFILLMENT OF THE REQUIREMENTS FOR THE DEGREE

OF MASTER OF SCIENCE

DEPARTMENT: CIVIL ENGINEERING

EDMONTON, ALBERTA

FALL, 1974

ABSTRACT

This thesis presents a study of the second-order effects in reinforced concrete frames.

The load-deformation response of reinforced concrete sway frames was obtained using realistic moment - axial load - curvature diagrams and the concepts of column deflection curves and sway subassemblages. The results of this analysis were used to study the applicability of the moment magnifier and $P\Delta$ - methods of analysis.

The parameters which have been studied include deflections at ultimate load and service load, second-order moments, stability effects and the effective stiffnesses of reinforced concrete columns and beams.

Both the moment magnifier method and $P\Delta$ - method were found to be applicable to material failures, but neither is satisfactory when dealing with stability failures. Approximate methods have been established to predict the failure mode.

Deflections were found to exceed current code prescribed values in most cases. Stability failures exhibited the largest deflections.

TABLE OF CONTENTS

LIST OF SYMBOLS

A_s	Area of reinforcement.
c	Coefficient in the Slope-Deflection Equations.
D	Dead load.
E_c	Modulus of elasticity of concrete.
E_s	Modulus of elasticity of steel.
$(EI/L)_b$	Stiffness parameter for beams.
$(EI/L)_c$	Stiffness parameter for columns.
F	Equivalent axial load on beam-column.
h	Depth of cross-section.
I_g	Moment of inertia of gross concrete section about the centroidal axis of the member cross-section.
I_s	Moment of inertia of reinforcement about the centroidal axis of the member cross-section.
J_u/J_o	0.5s(1-c) for no sway, 0.5s(1+c) for full sway.
k	Effective length factor.
K_b	$(EI/L)_b$
K_c	$(EI/L)_c$
l	Length of column.
l_b	Length of beam.
L	l/2 (live load in Equations (4.4) and (4.5).
L_b	$l_b/2$
l_n	Story height between floors n and n-1.
L_{CDC}	Half wave length of column deflection curve.
m	Coefficient defining the point of intersection

M	End moment on beam-column.
M_E	Externally applied moment.
M_{GM}	Fixed end moment of beam caused by gravity loads.
M_{mj}	Mean moment in the j'th segment.
M_i	Moment at upper end of column in the i'th story (counted from the top of the building).
M_r	Resisting moment produced by the beams.
M_{SM}	Beam end moment caused by lateral load.
M_u	Ultimate moment capacity of cross-section.
P	Axial load on column.
P_{cr}^b	Critical load based on a sway prevented condition.
P_{cr}^s	Critical load based on a sway permitted condition.
P_n	Axial load on the column in the n'th story.
P_s	Axial service load on column.
P_u	Axial design load on column.
q	$(P/EI)^{1/2}$
Q	Lateral load.
Q_n	Lateral load on the n'th floor (counted from the top of the building).
r	Radius of gyration about the axis of bending.
s	Coefficient in the Slope-Deflection Equations.
v, v_x, v_j	Deflection of column deflection curve from the line of action of the force F, at distance x and at the end of the j'th segment.
w	Uniformly distributed load.
W	Wind load.
U	Ultimate load effect

α_o Initial angle of CDC measured relative to the direction of the force F.

α_j Angle between tangent and the direction of the force F at the end of the j'th segment.

β Ratio of minimum end moment to maximum end moment. Positive for double curvature.

δ_j Length of the j'th segment of the CDC curve.

Δ One half of story deflection. Inflection point assumed at mid-height of column.

Δ_n Deflection of the n'th floor relative to the floor below.

γ Angle between the lines of action of the forces F and P.

λ Shear distribution factor.

μ M_{GM}/M_u

η M_{SM}/M_u

ρ Ratio of reinforcement area to the area of the cross-section.

ϕ_j Curvature of the j'th segment of the CDC curve.

ϕ_{mj} Mean curvature of the j'th segment.

CHAPTER I

INTRODUCTION

In recent years the use of slender buildings and building components has become very common, and from a structural point of view this trend has made it necessary to consider certain aspects of structural behaviour that are not important when members and structures have a low height to width ratio.

Of particular interest in the analysis of building frames are the deflections produced by the lateral loads. These deflections can be relatively large when the building has a large height to width ratio. The axial loads acting in the columns will produce additional moments and forces in the structure when acting through the lateral displacement of the columns. When these effects are taken into account in the structural analysis of the building, the analysis is referred to as a "second-order analysis." Fig. 1.1 (a) shows a simple frame acted upon by a lateral load Q and vertical loads P applied at the top of the columns. The deformed shape of the frame is shown in Fig. 1.1 (b). From this figure it is seen that when the structure has deflected laterally the vertical load P will also contribute to the lateral sway of the frame. When the frame has reached its final deflected position the axial load produces a sway moment $P\times\Delta$ which is commonly referred to as the "$P\Delta$-moment".

The purpose of this thesis is to study the effect of the $P\Delta$-moments on the behaviour of reinforced concrete frames. A computer analysis is used to generate the load-deformation behaviour of the

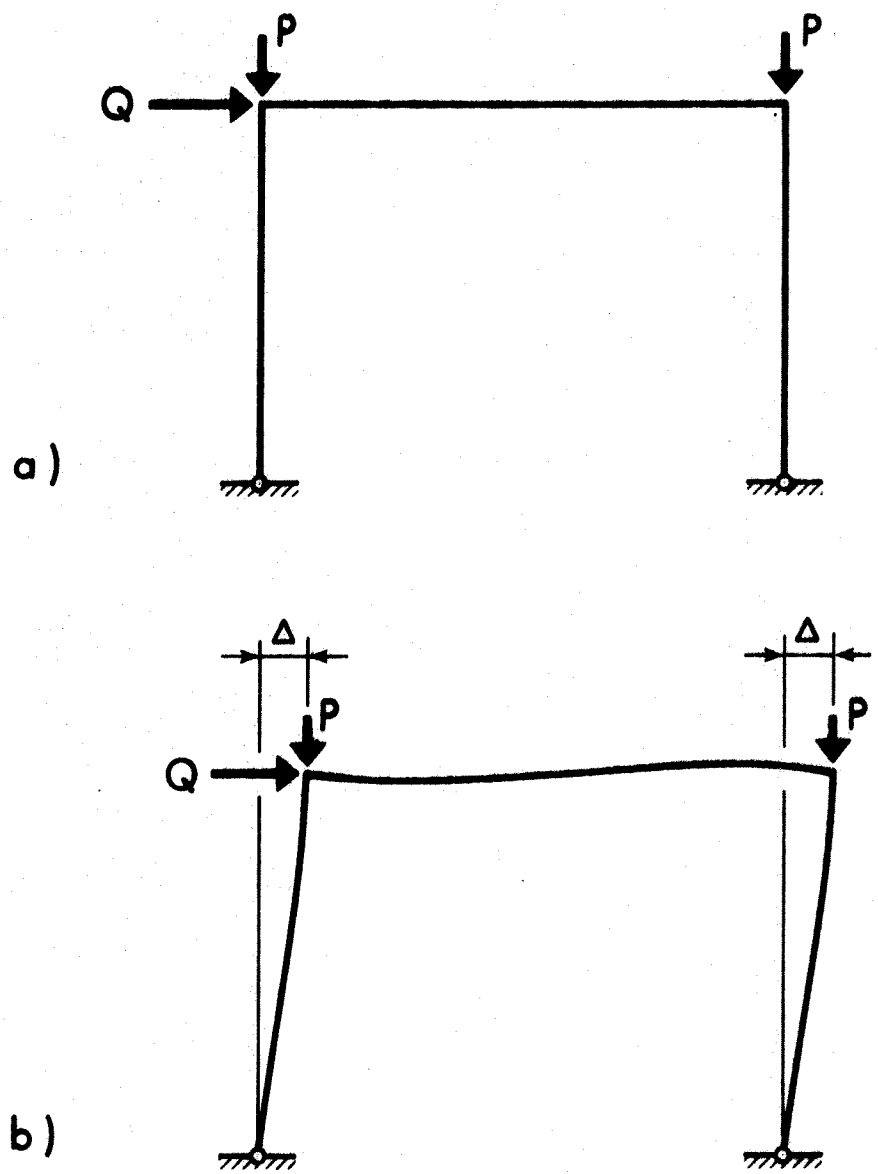

FIG. 1.1 SECOND-ORDER EFFECTS ON SWAY PERMITTED FRAMES

analytical model and the results of this analysis are used to study the applicability of current design methods and a proposed method of second-order analysis.

The general theory which forms the basis of the computer analysis is presented in Chapter III. Moment-axial load-curvature curves are generated to establish the load-deformation behaviour of the member cross-section and the concepts of column deflection curves and sway subassemblages are also presented.

Chapter IV presents the analytical model used in the computer analysis and load-deformation curves of the model. These curves were computed using the concepts presented in Chapter III. The significance of the deflection indices obtained in the analysis is discussed and effective elastic column stiffnesses are presented. Finally, the use of the sway subassemblage concept in frame analysis is discussed. An extensive set of sway subassemblage charts are presented in Appendix A.

Effective elastic EI values for reinforced concrete beams are studied in Chapter V and recommended design values of flexural stiffness are presented.

Chapter VI is devoted to the discussion of stability problems in multi-story frames. Results from current methods of second-order analysis are compared to the results obtained in the computer analysis. An alternate method of analysis is also proposed and its applicability and limitations are discussed.

CHAPTER II

REVIEW OF CURRENT METHODS OF SECOND-ORDER ANALYSIS OF BUILDING FRAMES

2.1 Introduction

The importance of a realistic second-order analysis has become evident in recent years due to the use of smaller load factors and more slender compression members in building frames. Deflection limits based on serviceability requirements have become an important design criterion in current building codes and in many cases are a governing factor in the design of tall buildings.

Although large deflections frequently do not affect the strength of beams or low structures, this is not so in frames which are free to sway under lateral loads. The lateral deflections give rise to additional moments and may produce a significant reduction in the load carrying capacity of the structure. It is, therefore, essential that these second-order effects can be computed in order to establish a rational design procedure, and considerable research has been carried out in recent years to improve existing methods and to develop new methods of accounting for second-order effects.

Due to the complexity in carrying out an exact second-order analysis, approximate methods of various types have been developed for design office use. Most building codes suggest design methods for compression members which are of a semi-empirical nature or are based on approximate theorectical solutions.

2.2 Approaches to Frame Stability Problems in Building Codes

There are two main methods of considering the stability of concrete columns and frames in use to-day. One is the moment

magnifier method presented in ACI 318-71 [1,2,3] and the other is the complementary moment method adopted by the CEB (Comité Européen du Beton)[4,5].

In the moment magnifier method the moments obtained from a first-order analysis are multiplied by a magnification factor which is a function of the ratio of the applied axial load to the critical load of the column. To account for the end restraints on columns in rigid frames an effective length factor k is introduced. The restrained column is then replaced by a pin-ended column of length kl which is designed for the applied axial load and the magnified moment. Nomographs [2] obtained from an elastic solution may be used to determine k for columns which are assumed to be either free to sway or fully braced. The accuracy of the method depends to a large extent on the accuracy of the relative values of column to beam stiffness. The ACI Code provides expressions to compute the column stiffness as a function of the stiffness of the gross concrete section $E_c I_g$, and the stiffness of the reinforcement $E_s I_s$. The variation in stiffness due to the axial load is not included.

The CEB method, which has been adopted in one form or another by many European countries, accounts for second-order effects by adding a complementary moment to the first order moment. The CEB Recommendations present a simplified method for computing the complementary moment which is given as a function of the effective length and approximate expressions for the curvature. The effect of rotational end restraint on the column is accounted for in

a manner similar to that in the moment magnifier method. The actual column is replaced by an equivalent pin-ended column of length kl which is then used to determine the complementary moment. The effective length factor is assumed to be obtained from a linear elastic analysis and is therefore subject to the same assumptions as used in establishing beam and column stiffnesses. No specific method is suggested in the CEB recommendations for evaluating k.

The calculation of effective lengths is discussed more fully in Section 6.3 of this thesis.

2.3 Iterative Procedures

Several authors have suggested the use of iterative procedures, often referred to as P-Δ methods, to carry out second-order frame analysis [6,7,8,9,10]. The basic idea behind these procedures is that the moments produced by the total vertical load P, acting through a lateral deflection Δ at a certain level in a building may be replaced by equivalent lateral shears applied at floor levels.

The equivalent shears are computed from the deflections obtained in a first order analysis and added to the applied lateral loads. This process is repeated until the deflections in one cycle agree, within specified limits, with the deflections obtained in the previous cycle.

A rapid convergence of the process is essential to make it feasible for design office use, thus no more than three iterations should be necessary. When the axial load has a value close to the critical load the convergence tends to become very slow.

K. Aas-Jakobsen[11] has proposed a finite element approach to solve for secon-order effects under linear-elastic conditions. The stiffness matrix [K] is assumed to be the sum of two stiffness matrices $[K_1]$ and $[K_2]$ where $[K_1]$ is the first order stiffness matrix and $[K_2]$ is the non-linear second-order stiffness matrix. The matrix $[K_2]$ is obtained through an iteration procedure. When unit displacements are applied to the member the axial load required to maintain equilibrium is unknown and can only be obtained by trial and error. Aas-Jakobsen suggests that the axial load be set equal to zero in the first cycle. From the first order forces obtained in the first cycle an equivalent axial load can be computed and used in the second cycle. The process is repeated until the axial load found in one cycle is close to the value computed in the previous cycle. Aas-Jakobsen states that the process will usually converge rapidly so that two cycles are generally sufficient.

2.4 Non - Linear Analysis

The majority of today's structures are designed using a straight line force - deformation relationship. The validity of such an assumption depends largely on the degree to which non-linearities affect the distribution of forces. The moment in continous beams are relatively insensitive to the value of EI used unless the relative EI changes during the loading history. Building codes usually specify EI values that will give results on the conservative side. On the other hand, in second-order analysis where the actual lateral deflections are important, a reasonably good approximation to the actual

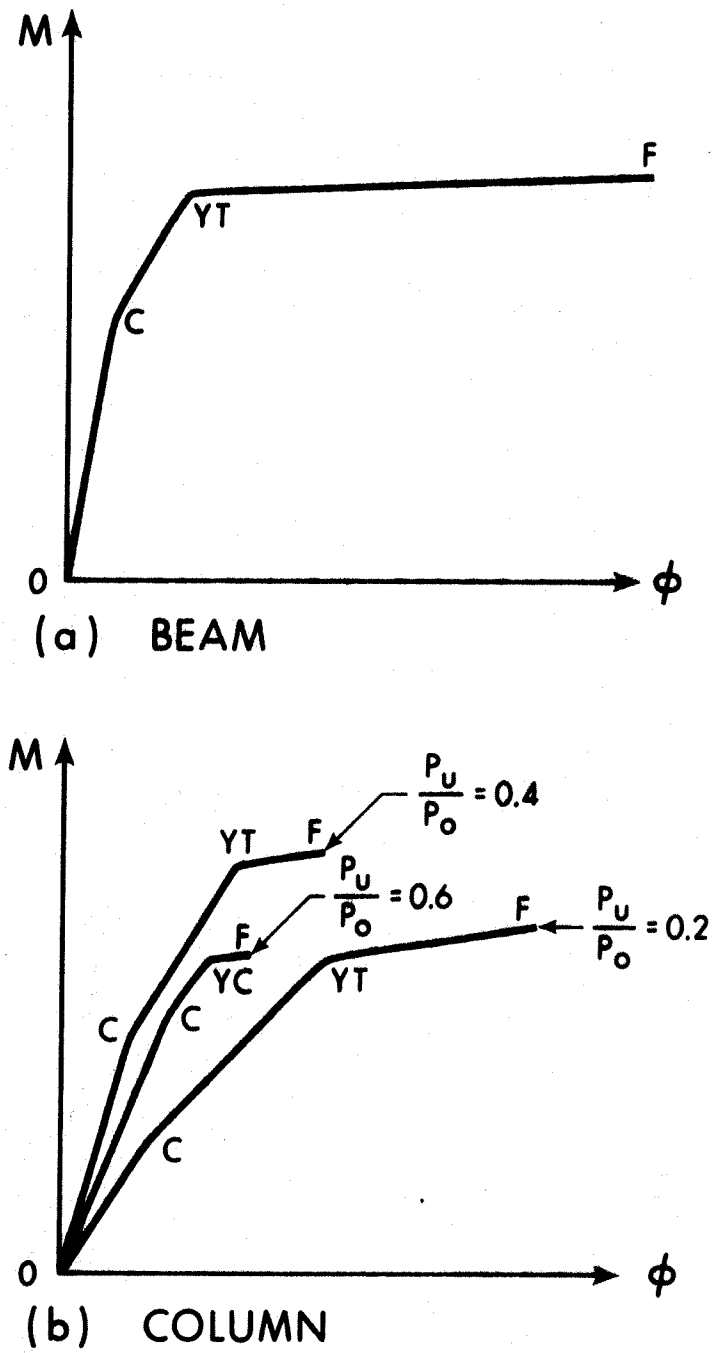

FIG. 2.1 SIMPLIFIED NON-LINEAR M-ϕ DIAGRAMS

load-deformation curve is necessary to properly predict the effect of lateral deflections.

Structural analysis based on a load-deformation curve which is approximated by a non-linear smooth curve or by several straight lines are usually referred to as "non-linear analysis".

Due to the difficulty in representing the load-deformation curve of reinforced concrete cross-sections by an analytical expression, straight line approximations have been suggested [12]. It has been found that three straight lines are sufficient to give results close to test results [13,14,15]. Fig. 2.1 shows some typical straight line moment-curvature diagrams for various members and loading conditions. The points C,YT,YC and F represent cracking of concrete in tension, yielding of the tension reinforcement, yielding of the compression reinforcement and failure due to crushing of the concrete, respectively.

The region o-c represents the uncracked state. When cracking has occurred, region C-YT, there is a loss of stiffness but the member is still behaving elastically. There is a further reduction in stiffness after yielding of the reinforcement in YT-F, and the member no longer behaves elastically.

A non-linear analysis of complex structures requires considerable computation and its use will usually not be justified in practice. Hence, it is desirable, in the case of reinforced concrete structures, to find elastic stiffnesses that lead to acceptable results or to find other ways of carrying out the structural analysis. Both techniques are explored more fully later in this thesis. Section 4.5 in Chapter IV presents an

investigation into effective EI values for reinforced concrete columns and in Chapter V the same problem is considered for reinforced concrete beams. Chapter IV also presents the development of an alternate method of analysis as applied to reinforced concrete structures.

Breen [16] used a numerical integration process to compute the relationship between end moment and end rotation for reinforced concrete members taking into account the non-linearity of the moment-axial load-curvature diagram. By plotting the individual beam and column moment-rotation curves on the same graph he showed that the moment-rotation curve of a frame joint could be established and from these curves the loading capacity of the frame was predicted.

2.5 The Sway Subassemblage Concept

A semi-graphical method for designing girders and beam columns in rigidly jointed unbraced frames has been proposed by Daniels and Lu [17].

The procedure starts by analyzing a frame whose members have been selected in a preliminary analysis. Each story is subdivided into a number of sway subassemblages consisting of a column and one or two adjacent beams, depending on whether the column under consideration is an exterior or interior column.

To trace the load-deformation behavior of each subassemblage a set of restrained columns design charts is used. These are non-dimensional plots of lateral load against lateral deflection of half a column for various values of end restraint, slenderness ratio and axial load and include the effect of

lateral deflections on the load carrying capacity of the column.

When the load-deflection curve has been established for each of the subassemblages in a story for a given axial load level, the curves are combined to give the overall load-deflection curve for that story for that axial load level. The lateral load at which the slope of the curve for the story becomes negative corresponds to instability of the story. In this manner the load-deflection relationships of a story may be determined without prior design of other parts of the frame.

In Chapter III the development of sway subassemblage charts for reinforced concrete columns will be discussed in more detail.

CHAPTER III

DEVELOPMENT OF COLUMN DEFLECTION CURVES AND SWAY SUBASSEMBLAGE CHARTS FOR REINFORCED CONCRETE COLUMNS

3.1 Introduction

In the analysis of a building for lateral loads each story of the frame can be divided into a series of subassemblages each consisting of a half column and adjoining beams. The subassemblages can be analyzed separately and their individual lateral load-deflection curves superimposed to obtain an overall lateral load-deflection curve for the story. Sway subassemblage charts consisting of a series of restrained column curves for various degrees of end restraint have been developed to aid in the analysis of structural steel subassemblages as described in Section 2.6. The development of such charts for reinforced concrete columns will be discussed in this chapter. The properties and use of these charts and curves will be discussed in Chapter IV.

The sway subassemblage charts and restrained column curves are developed using Column Deflection Curves, usually referred to as CDC curves. A CDC curve is a plot of the deflected shape of a column subjected to a given axial load with a given slope at the point where the moment equals zero. Such a curve may be used to represent the deflected shape of a beam-column having the same axial load, but different end conditions, which may vary from hinged to fully fixed. If a family of such curves exists for a certain axial load it is possible to determine the relationship between the applied lateral load and the corres-

ponding lateral deflection that must exist for the system to be in equilibrium under given end restraints.

In order to compute a CDC curve it is necessary to know the response of the column cross section to external loads, which, in this case, is conveniently represented by Moment-Axial Load-Curvature curves (hereafter referred to as M-P-ϕ curves). The shape of these curves is a function of material properties, geometry and external loads.

The steps involved in establishing the sway subassemblage charts may be summarized as follows:

1. Determine material stress-strain relationships,
2. Compute the M-P-ϕ curve for the cross-section for a given axial load,
3. Generate a family of CDC curves for the given axial load,
4. Compute the sway subassemblage charts for the given axial load and various values of end restraint.

Each of these steps will be discussed more fully in the following sections.

3.2 Material Properties

3.2.1 Stress-Strain Curves for Concrete

The stress-strain relationships assumed for concrete in compression and tension are shown in Fig. 3.1(a). The compression curve is similar to the one proposed by Hognestad [18].

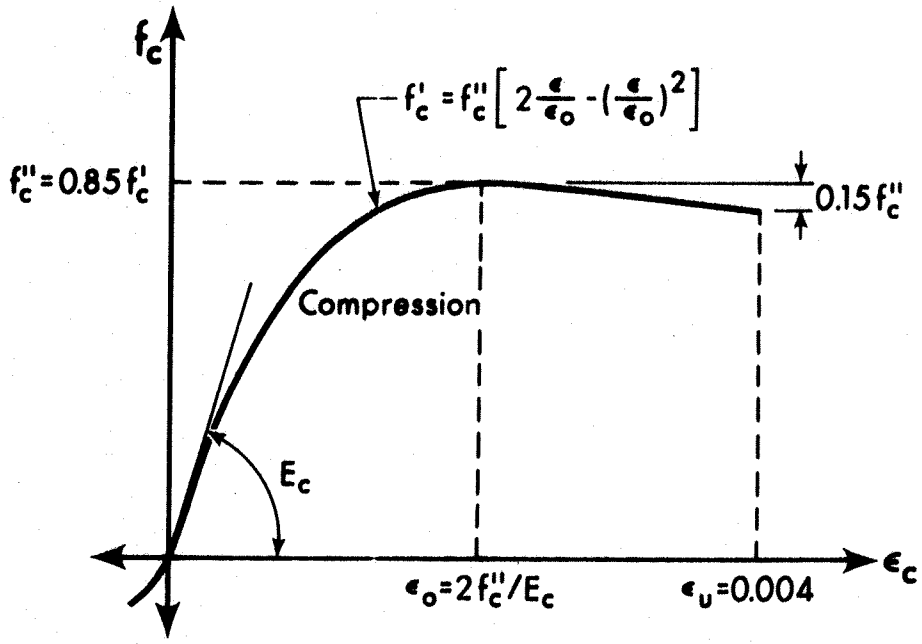

FIG. 3.1(a) STRESS-STRAIN DIAGRAM FOR CONCRETE IN FLEXURE

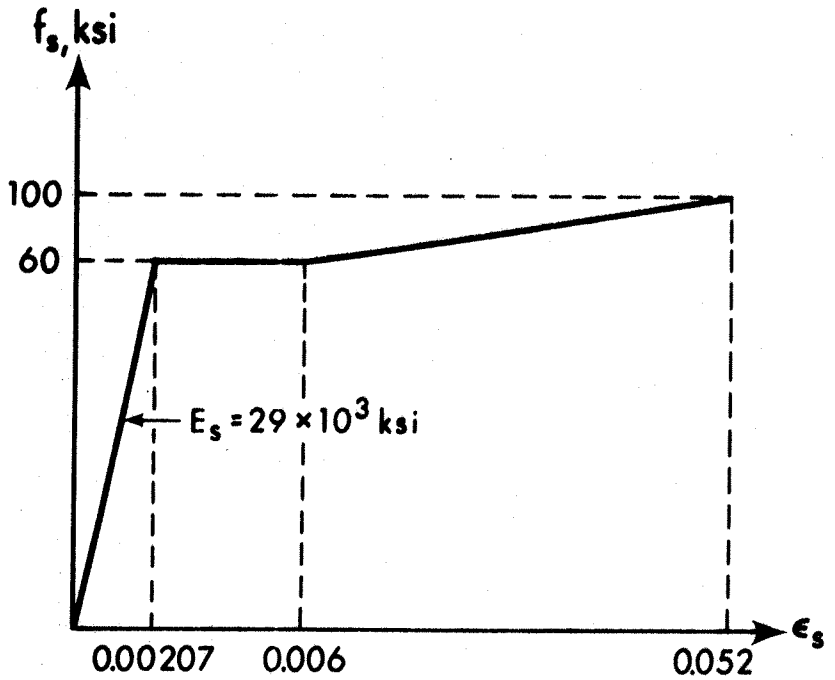

FIG. 3.1(b) REINFORCEMENT STRESS-STRAIN DIAGRAM

The non-linear part of the compression curve is given by Equation (3.1) and the stress-strain relationship for concrete in tension is represented by Equation (3.2) [19]:

$$\frac{f_c}{f_c''} = 2\left[\frac{\varepsilon}{\varepsilon_o}\right] - \left[\frac{\varepsilon}{\varepsilon_o}\right]^2 \qquad (3.1)$$

$$\frac{f_t}{f_t'} = 2\left[\frac{\varepsilon}{\varepsilon_{ult}}\right] - \left[\frac{\varepsilon}{\varepsilon_{ult}}\right]^3 \qquad (3.2)$$

where

$$\varepsilon_o = \frac{2f_c''}{E_c}$$

The value of the modulus of elasticity of concrete has been taken as

$$E_c = 18 \times 10^5 + 500\, f_c'' \text{ psi}$$

The compressive strength of concrete loaded in flexure, f_c'', was assumed to be 85 percent of the strength of control cylinders [18] and under the same loading conditions the ultimate strain was taken as 0.004.

The split cylinder strength f_t' is assumed to be equal to $7.0\sqrt{f_c'}$ and the ultimate tensile strain, ε_{ult}, may be expressed as $2f_t'/E_c$.

3.2.2 Reinforcing Steel Stress-Strain Curve

Only reinforcing steel with f_y = 60000 psi has been considered in this study and the assumed stress-strain curve for this

study and the assumed stress-strain curve for this steel is shown in Fig. 3.1(b). It consists of three parts; the initial elastic region, a flat yield plateau and a strain hardening region. The length of the flat plateau has been assumed slightly longer than what is usually indicated by tests. The effect of this is to overestimate somewhat the deflections at ultimate. This in turn results in an overestimate of the second order moments and therefore tends to be conservative. The slope of the strain hardening portion was based on the average value from a number of available stress-strain curves.

3.3 Moment-Axial Load-Curvature Relationships

3.3.1 Calculation of M-P-ϕ Curves

The computation of the M-P-ϕ curves is based on the following assumptions:

a) Plane sections remain plane.

b) The stress-strain diagram of concrete is as described in section 3.2.1.

c) The concrete is assumed to crush when the strain in the extreme compression fibre reaches 0.004.

d) The concrete cracks when the tensile strain exceeds the ultimate tensile strain.

e) The stress-strain diagram for steel is as described in Section 3.2.2 and shown in Fig. 3.1 (b).

For a given axial load the moment-curvature relationship can be computed using a trial and error procedure to find the neutral axis.

This process is rather tedious for hand calculations and a computer program [20] was therefore used.

The program can handle any shape of section provided there is bending about one axis only, and includes the effect of tensile stresses in the concrete and strain hardening in the reinforcement. The basic steps in the computations are as follows:

1. Divide the cross section into a number of elements of sufficiently small size such that the variations in strain across the element is relatively small.
2. Assume a small value of the curvature and a position of the neutral axis.
3. Compute strains, stresses and forces for each element.
4. Check if the forces acting on the cross section are in equilibrium. If they are not, choose a new position of the neutral axis and repeat.
5. When equilibrium has been established, compute the internal moment.
6. Repeat 1 through 5 for increasing values of curvature until the ultimate concrete strain in compression has been reached.

3.3.2. The Effect of Various Parameters on the M-P-ϕ Curve

The major variables affecting the shape of the M-P-ϕ curves include:

a. The axial load ratio Pu/Po (or Pu/P_b)

b. The steel percentage, ρ

c. Material strengths, f'_c, f_y.

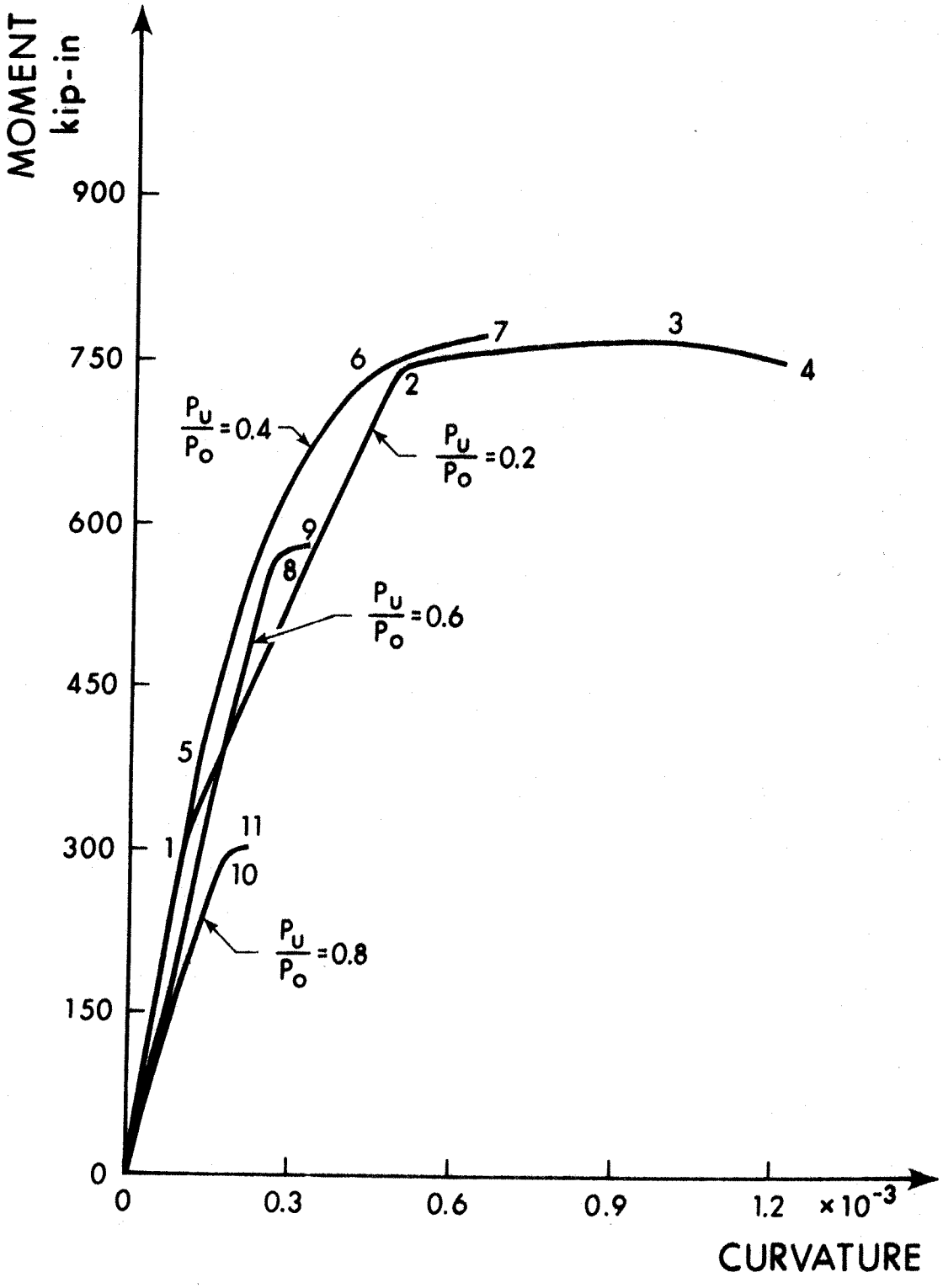

FIG. 3.2 MOMENT-AXIAL LOAD-CURVATURE DIAGRAMS FOR A TIED COLUMN WITH BARS IN TWO FACES (PROPERTIES GIVEN IN Fig. 4.1)

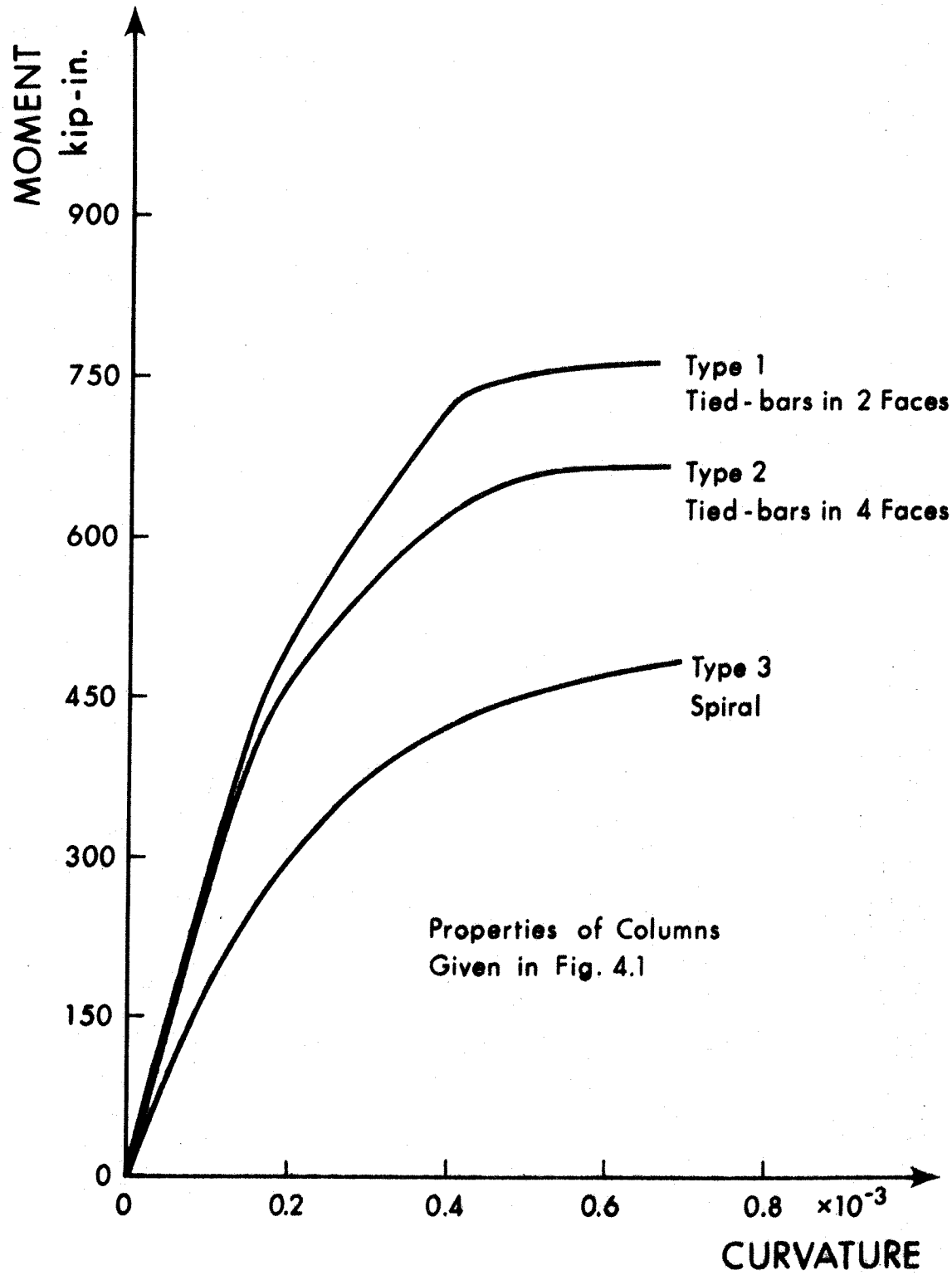

FIG. 3.3 MOMENT-AXIAL LOAD-CURVATURE DIAGRAMS
COLUMN TYPES 1, 2 and 3 (See Fig. 4.1)
$P_u/P_o = 0.4$

d. Cover ratio, γ

e. Shape and size of cross-section

f. Distribution of reinforcement over the cross-section.

Only axial load, shape of cross-section and distribution of reinforcement will be considered here.

Fig. 3.2 shows four curves computed for the same columns with four different values of axial load.

As the axial load is increased the failure mode changes from ductile failure, shown by point 4 in this figure, to brittle failure,point 11. The increase in axial load also delays the opening of cracks on the tension side of the column. Initiation of cracking occurred at points 1,5 and just above 8. The heavily loaded columns experience little reduction in stiffness until the compression steel yields at 8 and 10. Yielding of the tension steel occurs at 2 while 6 represents yielding of the compression steel followed by cracking of the concrete. Points 3,7,9 and 11 represent points of maximum moment capacity for P/P_o equal to 0.2, 0.4, 0.6 and 0.8 respectively.

In Fig. 3.3 the M-P-ϕ relationship has been plotted for the three different types of column for the same axial load ratio. The cross-sectional properties are given in Figure 4.1. All three columns had the same total steel percentage and the same cover. All sections show practically the same amount of rotation capacity at ultimate but the moment capacities are reduced considerably for

type 2 and type 3 due to the less efficient placing of the reinforcement. Some of the reduction for type 3 is also due to less efficient distribution of the concrete.

Distributing the reinforcement over the cross-section is seen (Fig. 3.3.) to produce a much smoother transition from the elastic to the inelastic range.

3.4 Column Deflection Curves

3.4.1 Introduction

In 1910 von Karman used CDC's to determine the strength of beam-columns with small eccentricities [21]. Chwalla generalized von Karman's work in 1934 to include other loading conditions [22]. Since then several investigators have expanded Chwalla's basic ideas in various directions [23 to 29].

The basis of the use of CDC's as applied in this thesis was established by Ojalvo[27].

3.4.2 Basic Relationships of Column Deflection Curves

A typical beam-column under applied loads is shown in Fig. 3.4(a). The equilibrium equations of this member may be established in the usual manner from statics, and the external moment at any cross section a distance x from the left hand end is:

$$M_E = M\left[1+\frac{x}{l}(\beta-1)\right]+ Pv_x \qquad (3.3)$$

where v_x is the deflection at distance x and β is the end moment ratio, positive for double curvature.

The external moment must equal the internal moment. Thus:

$$M_E = M_I = f(\phi) = f(-v_x'') \qquad (3.4)$$

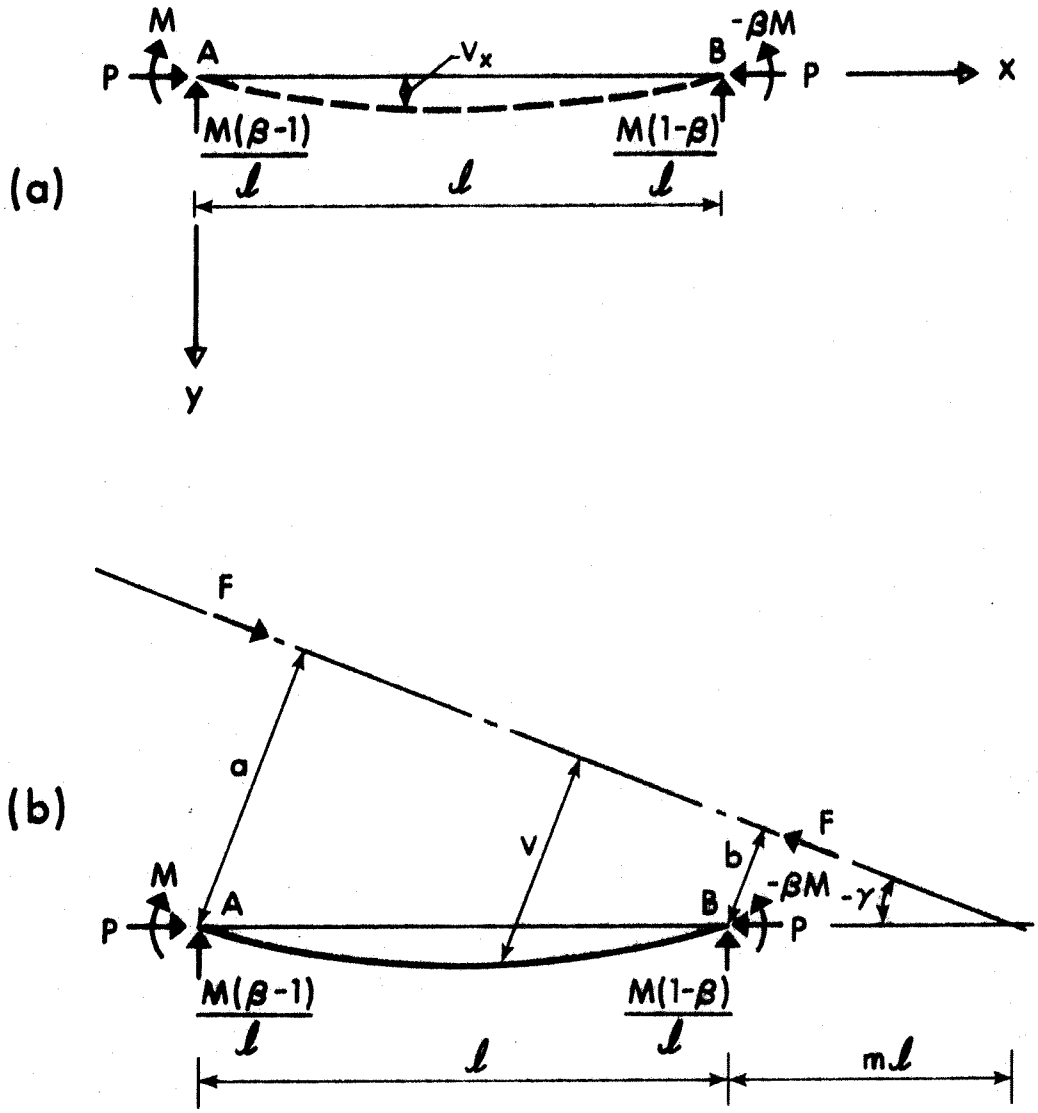

FIG. 3.4 FORCES ON A BEAM-COLUMN

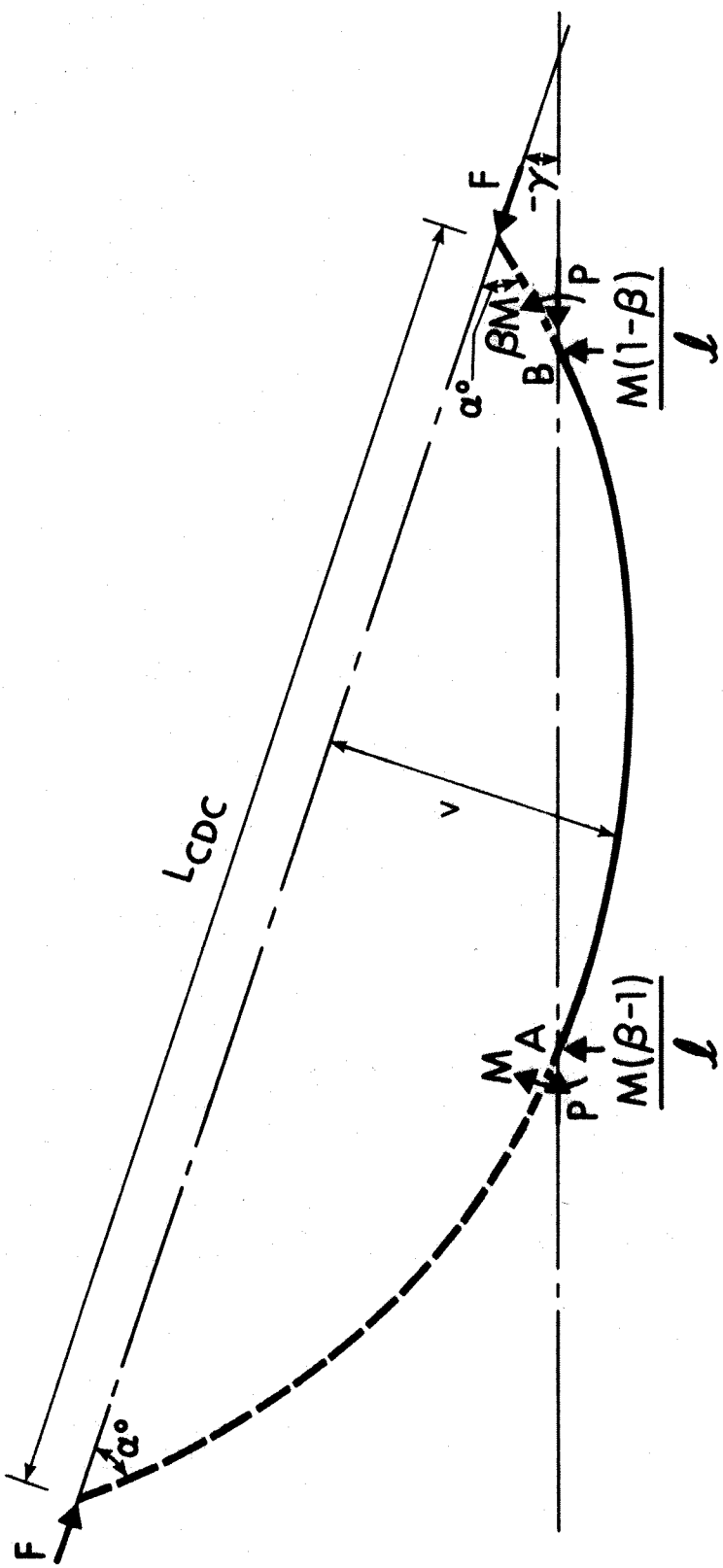

FIG. 3.5 BEAM-COLUMN AS PART OF A CDC

or:

$$M\left[1 + \frac{x}{l}(\beta-1)\right] + Pv_x = f(-v_x'') \tag{3.5}$$

where $f(\phi)$, etc. means a function of ϕ, etc.

However, a different approach may be used to express equilibrium. The system of forces in Fig. 3.4(a) may be replaced by a single force F as shown in Fig. 3.4(b).

The direction of the force is defined by the angle γ such that

$$Fa = M \text{ and } Fb = \beta M,$$

and in general

$$M_E = Fv = f(-v'') \tag{3.6}$$

Summation of moments about A and B taking counterclockwise moments as positive yields, respectively,

$$Fl(m+1)\sin(-\gamma) = -M \tag{3.7}$$

and

$$Fml[\sin(-\gamma)] = \beta M \tag{3.8}$$

Combining Eqns. (3.7) and (3.8) gives the point of intersection between the line of action of F and the line AB,

$$m = \frac{-\beta}{1+\beta} \tag{3.9}$$

To satisfy the axial load requirement it is necessary that

$$F = \frac{P}{\cos\gamma} \tag{3.10}$$

and by combining Eqns. (3.8),(3.9) and (3.10) the angle γ may be determined from

$$\tan\gamma = \frac{(1+\beta)M}{Pl} \tag{3.11}$$

Thus Eqns. (3.9),(3.10) and (3.11) define completely the magnitude, location and direction of F, and the equilibrium equation is now Equation (3.6).

To obtain the deflected shape of the beam-column it is necessary to integrate Equation (3.6), and the M-P-ϕ curves form the basis for this integration. The process does not have to be confined to the section AB, but may be carried beyond these points. This is illustrated in Fig. 3.5 where the curve has been extended to intersect the line of action of F. The beam-column AB is a part of this half wavelength whose length and initial angle are L_{CDC} and α_o, respectively. Just as the portion AB of the CDC represents the equilibrium of the beam-column under discussion, so another portion of the CDC is the shape of another beam-column. Thus any one CDC can give information about an infinite number of beam-columns with various end conditions. Fig. 3.6 shows some examples of how the CDC may be used to represent various types of beam-columns. Column AB is hinged at A and has applied moment at B. CD is bent in double curvature with end moments of equal magnitude and EF is a column bent in single curvature with unequal end moments.

3.4.3 Assumptions in the CDC Calculations

Since the M-P-ϕ curves form the basis for CDC calculations it follows that the CDC's are subject to the same assumptions which were used in developing the load-deformation response of the cross section.

Furthermore, it is common to assume that the equivalent axial force F is equal to the actual axial load P_u. From Eqn. (3.10) it is clear that this assumption holds for small values of γ. However,

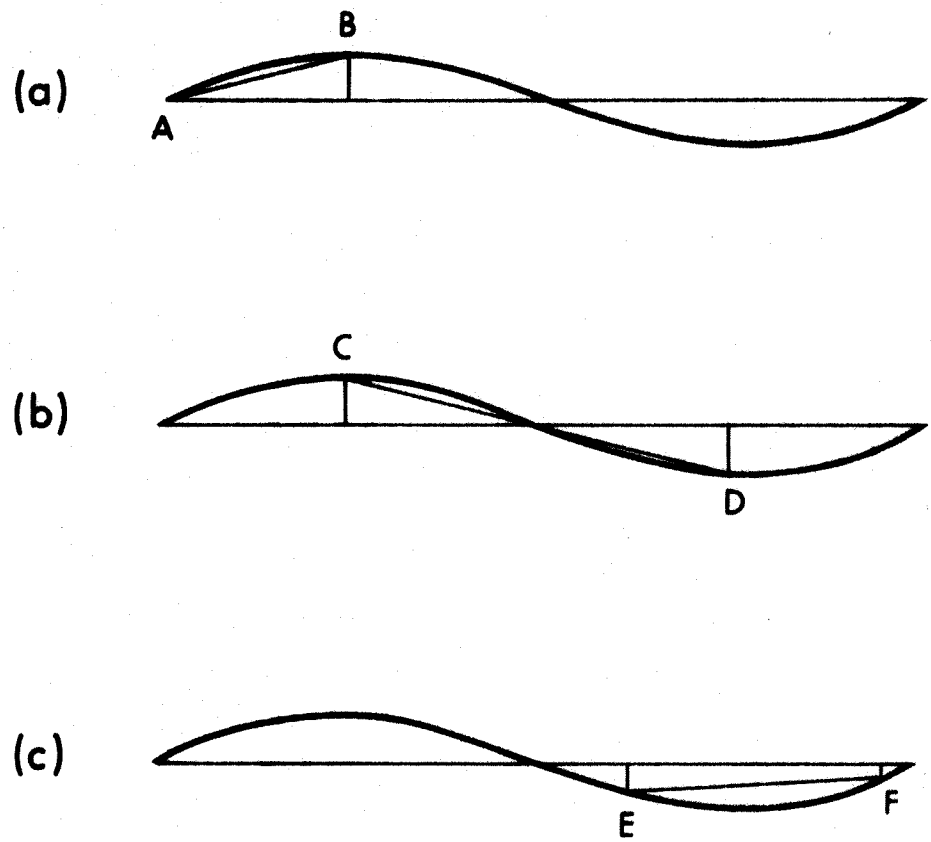

FIG. 3.6 CDC'S REPRESENTING VARIOUS TYPES OF BEAM-COLUMNS

Eqn. (3.11) indicates that for a beam-column of length l and end moments M and βM, tan γ may become large for small values of axial load and non-zero values of $(1 + \beta)$. If the end moments are equal and opposite ($\beta = -1$, single curvature) $\gamma = 0$, $F = P$ and the solution is always exact. But as the ratio of end moments increases to a maximum of + 1, i.e. perfect double curvature, tan γ increases to a maximum of $2M/Pl$ The worst situation arises for a short column with a low axial load and a maximum moment equal to the ultimate moment. Consider the values from Table 4.1 for a load ratio of 0.2 and a slenderness ratio $l/h = 70$. From Eqns. (3.11) and (3.10) it is found that

$$F = 1.04P$$

Thus by using $F = 0.2P$ in the analysis the column has in fact been analyzed for an axial load which is less than the actual value. In this case the discrepancy is only about 4% but for shorter columns and for smaller axial load the error would be more severe. For practical purposes, however, this is not likely to be a serious problem since most columns will not have a combination of P/P_o and l/h within the critical range.

3.4.4 Calculation of CDC Curves

The basic principles underlying the concept of column deflection curves were outlined in Section 3.4.2. In this section the equations required to compute the shape of the CDC curve will be presented.

To account for the distribution of cracking along the member it is necessary to divide the curve into a number of segments. The length of the segment should be such that the degree of cracking

is nearly constant within the segment. Galambos[30] has suggested that a segment length equal to 4r will give good results for steel members. A somewhat shorter length would probably be appropriate for reinforced concrete members since 4r generally exceeds the thickness of the column. In the calculations reported in this thesis the segment length was arbitrarily chosen as 5 inches.

A typical segment of a CDC curve is shown in Fig. 3.7. If the segment is short it may be assumed that the curve is a circular arc. The radius of the j'th segment is then $1/\phi_j$.

From the geometry of Fig. 3.7 the following relationships may be established (ignoring second-order terms such as $\alpha_o\phi_1$, α_o^2 and ϕ_1^2):

$$v_1 = bd - cd$$

$$bd = \alpha_o\delta_1$$

$$\text{angle } dac = \frac{\delta_1\phi_1}{2}$$

$$ac \simeq \delta_1$$

$$\therefore \quad cd \simeq \delta_1^2\phi_1/2$$

The deflection and the angle of the tangent at the end of the first segment may now be written as

$$v_1 = \alpha_o\delta_1 - (\delta_1^2\phi_1/2) \tag{3.12}$$

and

$$\alpha_1 = \alpha_o - \delta_1\phi_1 \tag{3.13}$$

And in general at the end of the j'th segment

$$v_j = v_{j-1} + \alpha_{j-1}\delta_j - \frac{\delta_j^2\phi_j}{2} \tag{3.14}$$

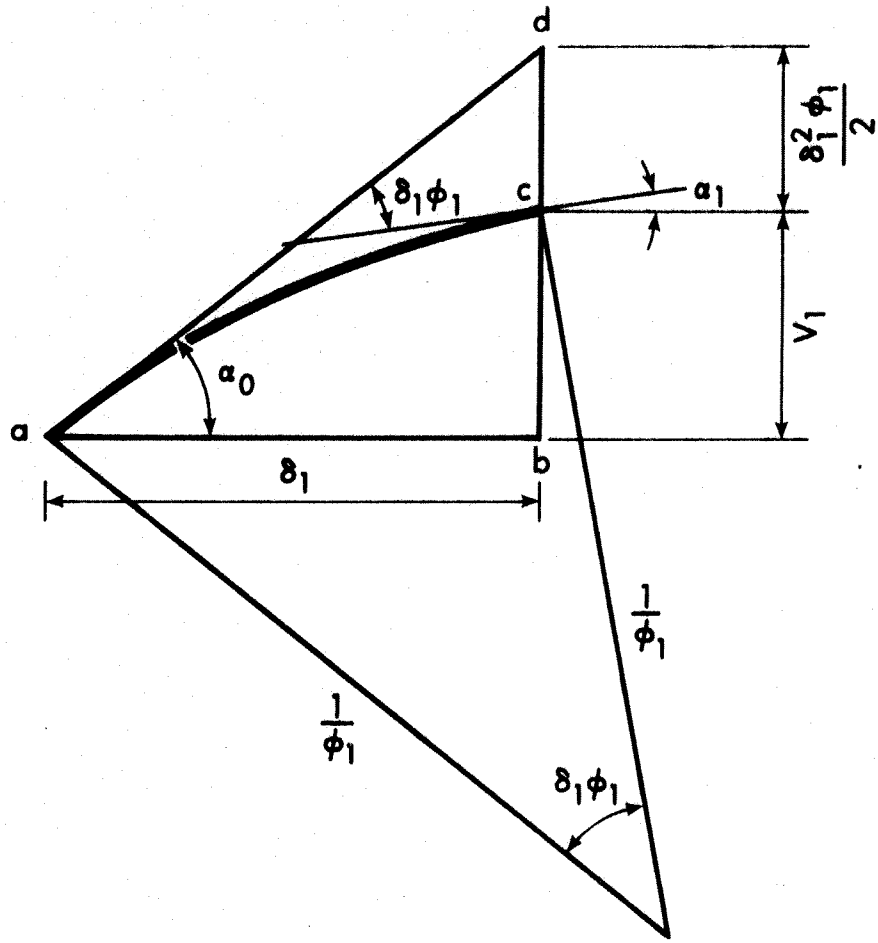

FIG. 3.7 SEGMENT OF COLUMN DEFLECTION CURVE

$$\alpha_j = \alpha_{j-1} - \delta_j \phi_j \tag{3.15}$$

The values of v_j and α_j are now used to determine v_{j+1} and α_{j+1}.

The first step in the calculations is to determine a value of α_o and δ. The length need not be the same for all segments but usually is for convenience. The value of ϕ may be determined from the M-P-ϕ diagram when the moment has been determined. This moment is taken as the mean moment in the segment and the general expression for the mean moment in the j'th segment is

$$M_{mj} = Pv_{j-1} + \frac{P}{2} \delta_j \alpha_{j-1} \tag{3.16}$$

By entering the M-P-ϕ curve with the value of M_{mj} the curvature of the j'th segment may be determined.

Due to the difficulty in obtaining a relatively simple analytical expression for the M-P-ϕ diagram, this curve was approximated by a number of straight lines. A high degree of accuracy may be obtained by using a sufficient number of lines. A typical example of such an approximation is shown in Fig. 3.8.

If it is assumed that $M_i < M_{mj} < M_{i+1}$, where the subscript i refers to the i'th point on the M-P-ϕ curve, then the curvature corresponding to M_{mj} is given

by

$$\phi_{mj} = \phi_i + \left[\frac{M_{mj}-M_i}{M_{i+1}-M_i}\right] \left[\phi_{i+1}-\phi_i\right] \tag{3.17}$$

The value of ϕ_{mj} is now substituted for ϕ_j into Eqns. (3.14) and (3.15) to compute the deflection and the slope of the tangent, respectively, at the end of the j'th segment.

The computations may be terminated when one quarter of the curve has been computed since the curve is symmetrical. When M_{mj}

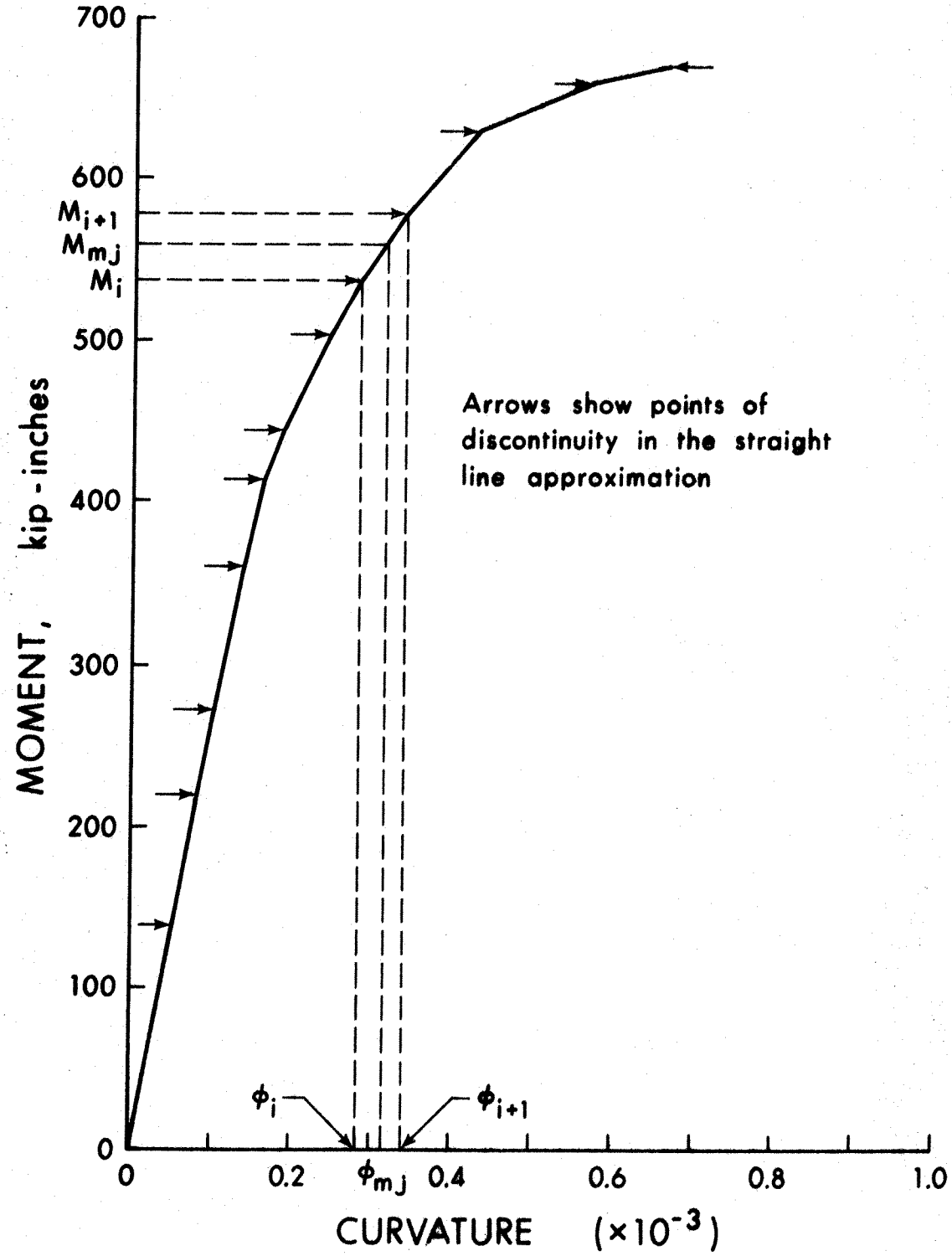

FIG. 3.8 LINEARIZED MOMENT-CURVATURE DIAGRAM - TIED COLUMN WITH BARS IN FOUR FACES, $P_u/P_o = 0.4$

reaches the moment capacity of the cross section the above equations are no longer valid because they do not account for angular discontinuity at the hinge.

3.4.5 Comparison of CDC Calculations with Test Results

The theoretical calculations have been compared to tests carried out by Breen[16] and Chang[31]. The CDC's corresponding to failure of the columns are plotted with the test results in Fig. 3.9 and Fig. 3.10.

The test specimens had heavy end brackets and hence the section properties were not uniform along the length of the member. To get a meaningful comparison it was necessary to ignore the end brackets and measure deflections from the line joining the ends of the actual column. This part of the member is represented on the CDC by the distance AB. The test results were plotted using AB as the horizontal axis allowing for the deflection at the end of the bracket.

The maximum deflections from the CDC calculations are about four percent below Breen's test result and about ten percent above Chang's result. Thus the deflected shape of these columns was predicted with reasonable accuracy from the column deflection curve.

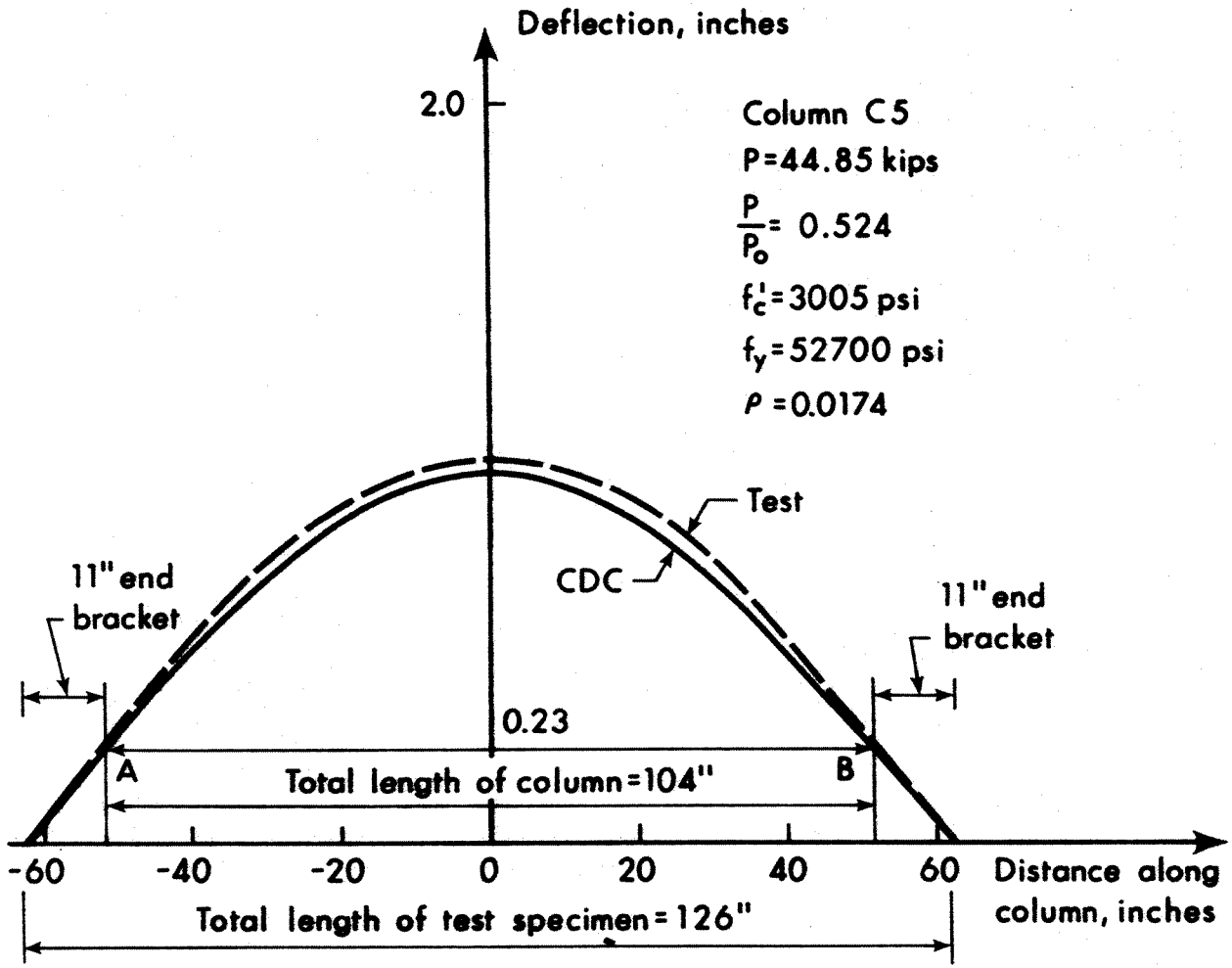

FIG. 3.9 COMPARISON OF CDC CALCULATIONS TO TEST CARRIED OUT BY BREEN.

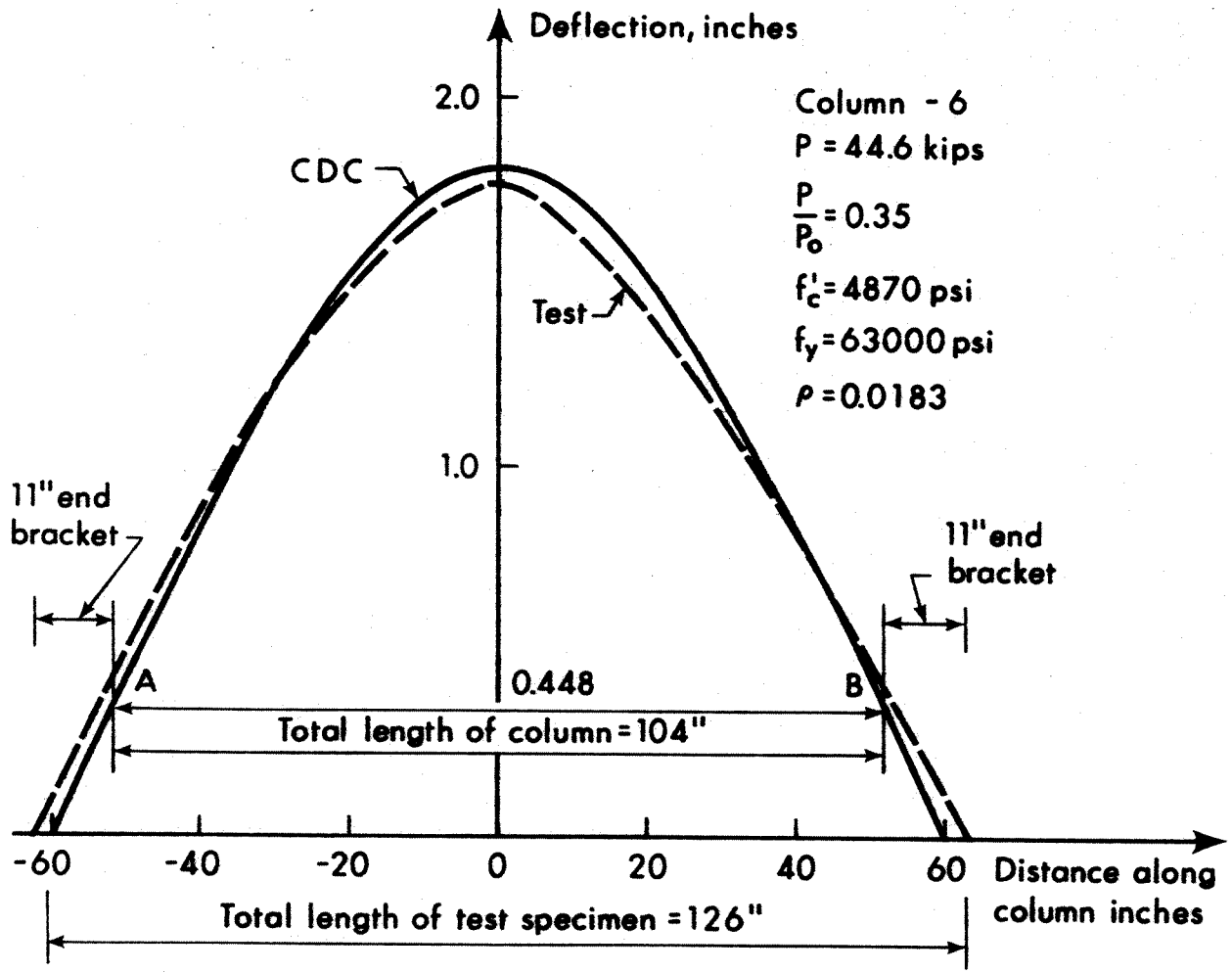

FIG. 3.10 COMPARISON OF CPC CALCULATIONS TO TEST CARRIED OUT BY CHANG

3.5 Sway Subassemblage Charts

3.5.1 Basic Equations

The basic ideas behind the subassemblage concept were introduced in Section 2.6, and the tools required to apply the concept, i.e. M-P-ϕ diagrams and CDC curves, were presented in Sections 3.3 and 3.4, respectively. It is clear from those discussions that considerable computational work is required if this method is used from first principles and that it would be quite unsuitable for hand calculations. A more practical approach is to develop standard design curves which are applicable to a large number of cases. Such curves have been developed to aid in the design of steel structures[17].

A multi-story frame is shown in Fig. 3.11(a). The subassemblage consisting of the n'th floor girders between column lines B and D and half of the column in line C between floors n and n+1 is shown in Fig. 3.11(b). A point of contraflexure has been assumed at mid-height of the column.

The model is acted upon by a lateral load

$$Q_n = \lambda \sum_{i}^{n} H_i \qquad (3.18)$$

Where λ is a column shear distribution factor, the axial load P_n which is the sum of all vertical loads acting on column line C above level n and the moment M_{n-1} which is produced by the column shears above the n'th floor. A further simplification has been made in Fig. 3.11(c) where M_r represents the total restraining action supplied by the girders. The angle θ is the rotation of the joint and γ is the angle between the chord and a tangent to the

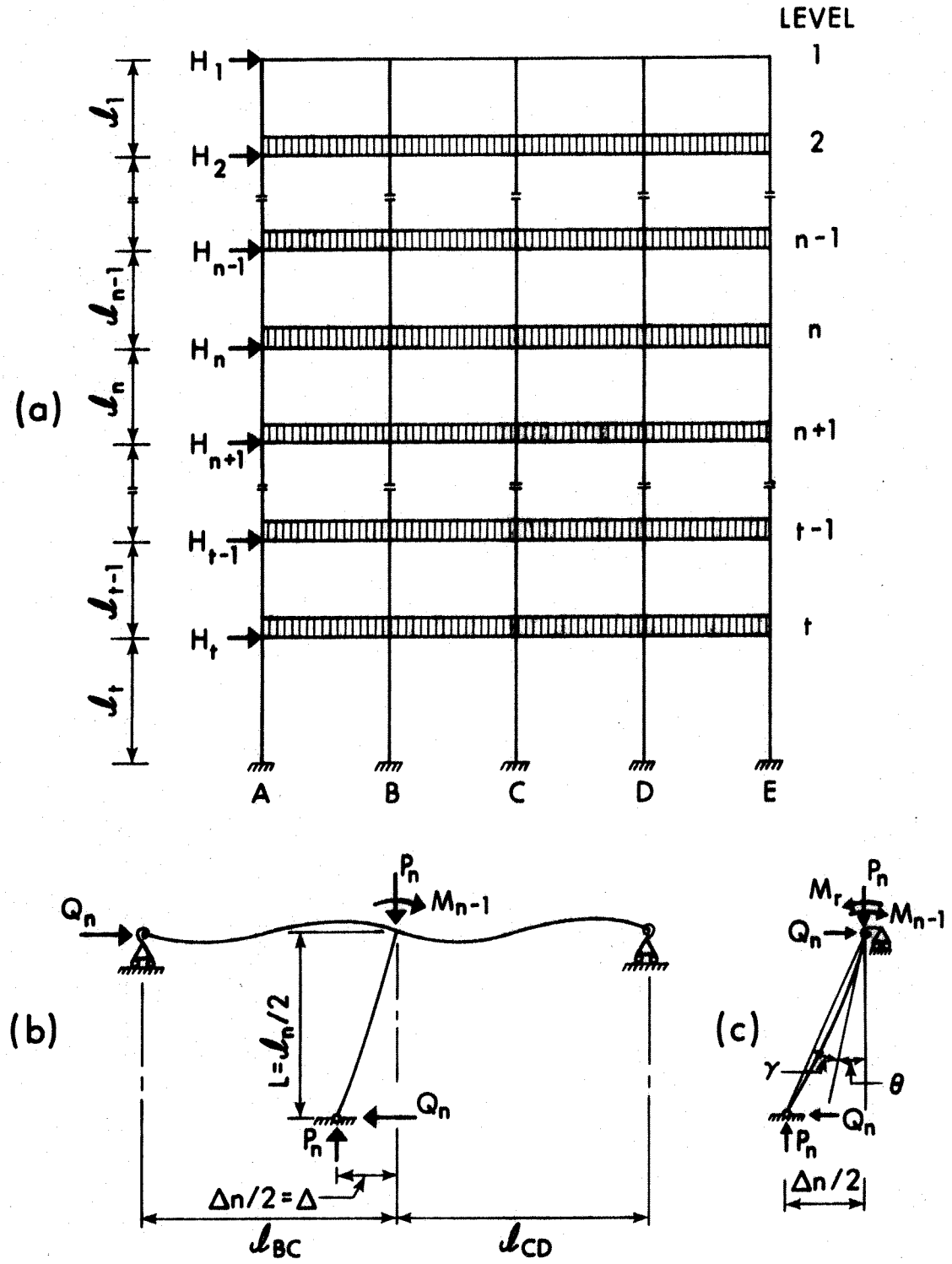

FIG. 3.11 TYPICAL SWAY SUBASSEMBLAGE

upper end of the column curve. γ is determined from the CDC curves and at the end of the j'th element it is given by equation (3.19).

$$\gamma = \frac{v_j}{j\delta} - \delta_j \tag{3.19}$$

The moment at the upper end of the column is given by the equilibrium Equation (3.20).

$$M_n = \frac{Q_n l_n}{2} + P_n \frac{\Delta_n}{2} \tag{3.20}$$

Equilibrium of moments at the upper end requires that

$$M_r = M_n + M_{n-1} \tag{3.21}$$

The moment M_{n-1} may be expressed as

$$M_{n-1} = Q_{n-1} \frac{l_{n-1}}{2} + P_{n-1} \frac{\Delta_{n-1}}{2} \tag{3.22}$$

Since $Q_{n-1} < Q_n$ and $P_{n-1} < P_n$ the value of M_{n-1} will always be smaller than M_n unless Δ_{n-1} is appreciably greater than Δ_n. Normally, $\Delta_n > \Delta_{n-1}$ and M_{n-1} may be assumed to be equal to M_n. This assumption will then be conservative.

Equation (3.20) may be rewritten as

$$M_r = 2M_n \tag{3.23}$$

The relationship between the rotations γ, θ and Δ_n/l_n is found from the geometry of Fig. 3.11(c) and is given by

$$\frac{\Delta_n}{l_n} = \theta + \gamma \tag{3.24}$$

If the restraining action provided by the beams is assumed to be linear the restraining moment may be expressed as

$$M_r = K\theta M_u \tag{3.25}$$

where K is the beam stiffness and M_u is the ultimate moment capacity of the column.

3.5.2 Procedure for Computing Subassemblage Curves

The computations for a given subassemblage curve start by specifying a value of the axial load and the restraining function. For various values of θ the restraining moment is calculated from Equation (3.25) and the moment at the top of the column is determined from Equation (3.23). When the rotation γ has been found, usually from a CDC analysis, the story deflection is determined from Equation (3.24). The lateral load which is compatible with the joint rotation and the forces acting on the column is found from Equation (3.20).

The results can conveniently be plotted in a non-dimensional form of lateral load against story deflection. To accomplish this Equation (3.20) is written in the form given by Eqn.(3.26) and $Q_n l_n/2M_u$ is plotted against Δ_n/l_n.

$$\frac{Q_n l_n}{2 M_u} \equiv \frac{M_n - P_n\left[\frac{\Delta_n}{l_n}\right] l_n}{M_u} \tag{3.26}$$

A computer program was written to generate the restrained column curves and a description of this program is presented in Appendix B. The properties and use of these curves are discussed in Chapter IV.

CHAPTER IV

RESTRAINED COLUMN CURVES FOR REINFORCED CONCRETE COLUMNS

4.1 Introduction

The load deformation response of a sway subassemblage can be described by means of restrained column curves which represent the load-deformation characteristics of a column having a given rotational end restraint. The load-deflection relationship of a subassemblage at any given stage of loading is obtained from the restrained column curve corresponding to the same end restraint as that provided by the beams of the subassemblage. Section 4.7 describes in more detail how restrained column curves are used to obtain the complete load-deformation response of a sway subassemblage.

The general theory relating to restrained column curves and sway subassemblages was presented in Section 3.5. In this chapter the theory will be used to generate restrained column curves for reinforced concrete columns. The series of curves, contained in Appendix A were generated by the computer program in Appendix B.

4.2 The Analytical Model and Variables Studied

To study the general properties of subassemblage charts for reinforced concrete members and to provide comparison with other design methods, charts were generated for three columns:

Type 1. square column with reinforcement in two faces,

Type 2. square column with reinforcement distributed in all four faces,

Type 3. circular column with reinforcement distributed along the circumference.

The column cross-sections are shown in Fig. 4.1 along with the material properties.

The subassemblage considered in this analysis is shown in Fig. 4.2(a). The springs at the ends of the beam and the column represent the net restraint provided by the frame which the subassemblage is assumed to be a part of. It will be assumed that the stiffness of the springs is such that the members are bent in double curvature with a point of contraflexure in the middle. Thus the model may be represented by Fig. 4.2(b).

It will be assumed that no upper column frames into the beam-column joint. Hence, Equation (3.23) may be modified to read

$$M_r = M \tag{4.1}$$

The equilibrium equation for the column may be written down from Fig. 4.2(c)

$$M = QL + P\Delta, \tag{4.2}$$

and in non-dimensional form

$$\frac{QL}{M_u} = \frac{M - P\left[\frac{\Delta}{L}\right]L}{M_u} \tag{4.3}$$

The lateral load vs. lateral deformation relationship may be traced by plotting QL/M_u against Δ/L.

The model was analysed for five values of beam stiffness K (see Equation (3.25)): 100, 200, 400, 600, and infinity. The values of K derived in Section 5.3 for a representative T-beam and flat plates are about 500 - 2000 and 50 - 140, respectively, when combined with the columns shown in Fig. 4.1.

Eight values of the slenderness ratio l/h were used, varying from 5 to 40 in steps of 5.

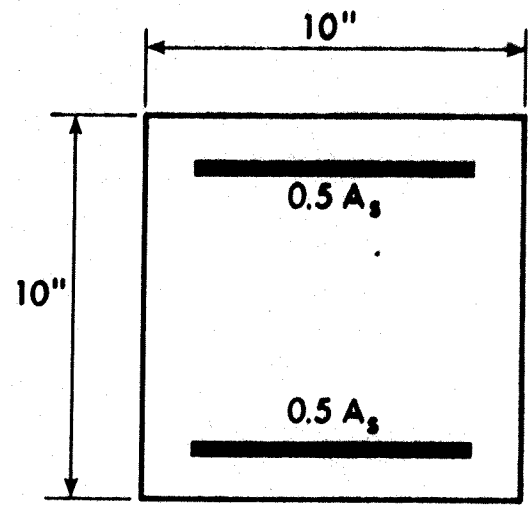

(a) TYPE 1

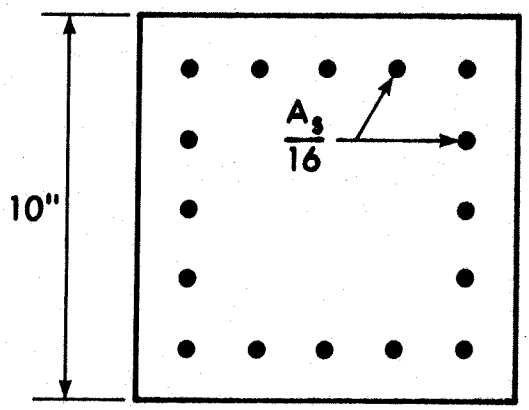

(b) TYPE 2

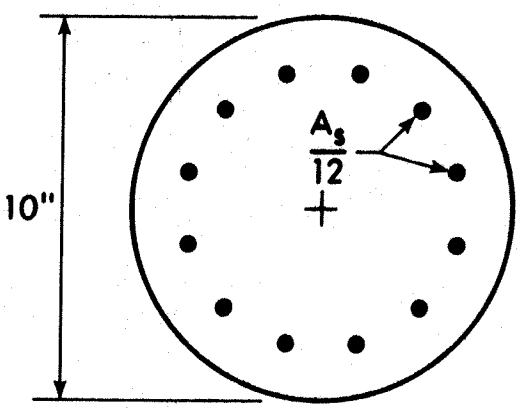

(c) TYPE 3

f'_c = 4000 psi

f_y = 60000 psi

ρ = 0.02

γ = 0.75

COVER 1.25 in

FIG. 4.1 COLUMN CROSS-SECTIONS

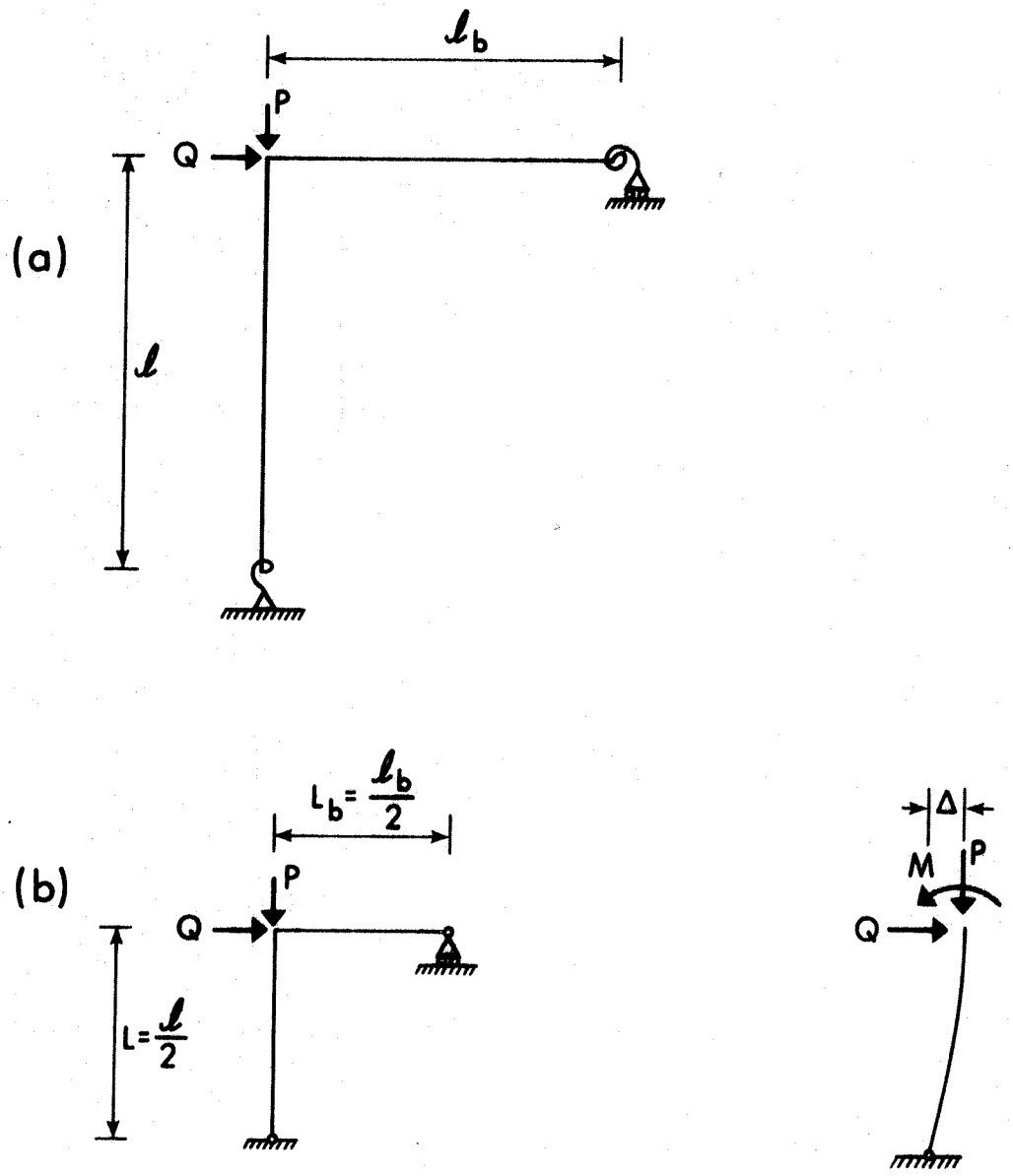

FIG. 4.2 ANALYTICAL MODEL FOR DEVELOPMENT OF RESTRAINED COLUMN CURVES

The complete set of charts obtained from this analysis is presented in Appendix A. A total of 146 charts are presented for 690 individual combinations of length, shape and end restraint.

The coordinates of the linearized M-P-ϕ diagrams used in the analysis are given in Tables 4.1, 4.2 and 4.3.

4.3 Basic Properties of Subassemblage Curves

Some typical results from the analysis are shown in Figs. 4.3 and 4.4, and the moment curvature diagram used in the calculations of these curves is shown in Fig. 4.5.

The line ab in Fig. 4.3 represents the locus of columns failing as a result of material failure, due to reaching the cross-sectional capacity at the top of the column. This line slopes because the PΔ moments reduce the lateral load capacity. Lines parallel to ab give the capacity of the subassemblage when a plastic hinge forms in the beams prior to the column reaching its capacity. Thus the capacity of the subassemblage is limited by the line cd when the restraining capacity of the beams is 0.75 M_u.

The point A in Figs. 4.3 and 4.4 corresponds approximately to point 1 on the M-P-ϕ curve shown in Fig. 3.2. This is the point where the column starts to crack and there is a loss of stiffness, but it continues to behave elastically.

While the short column in Fig. 4.3 reaches its ultimate capacity with a corresponding maximum value of $Q\ell / M_u$ the longer column in Fig. 4.4 exhibits material failure under a lateral load which is less than its load carrying capacity. The practical limit of this column is reached on the line mn. For any increase in load

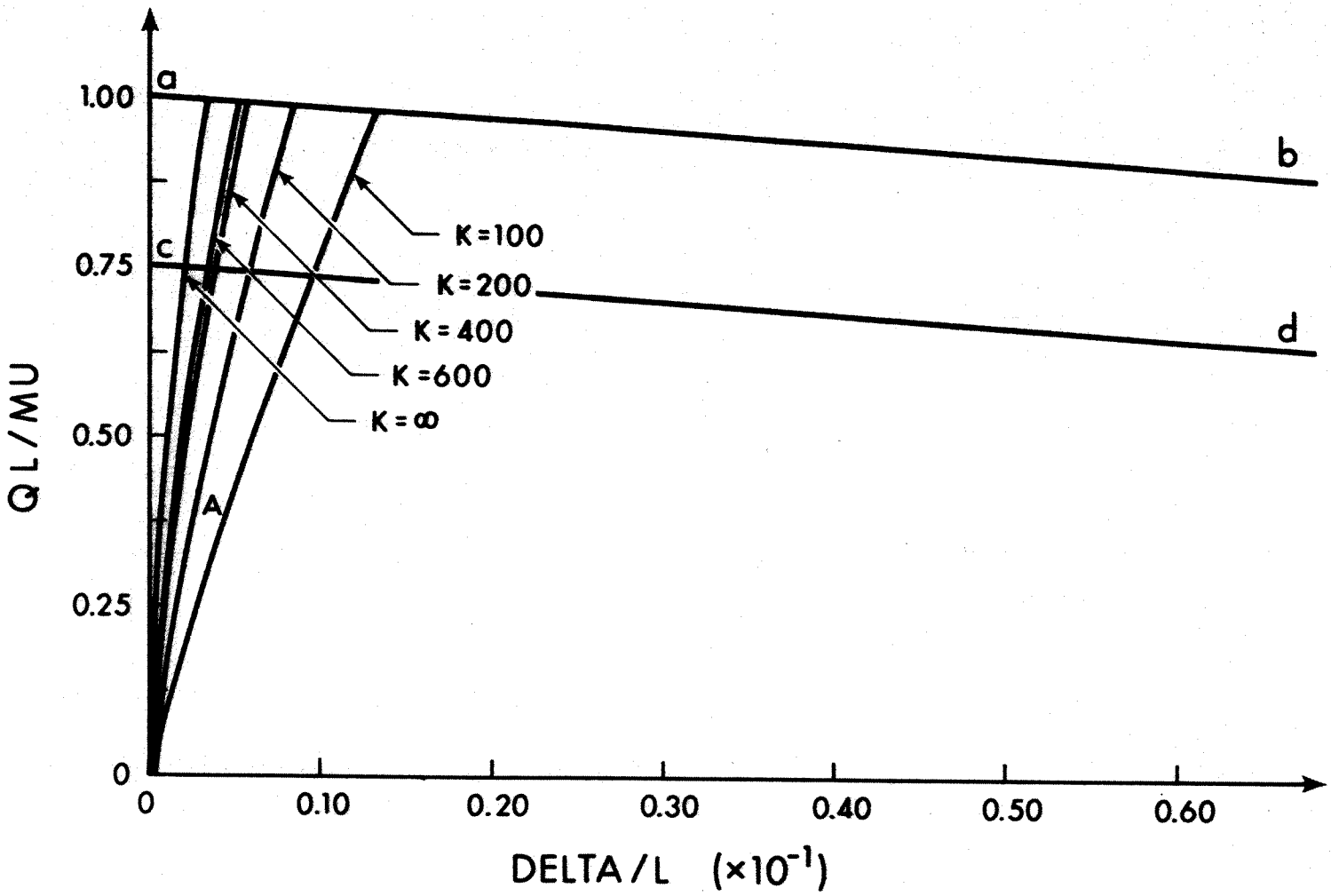

FIG. 4.3 LOAD-DEFLECTION DIAGRAM FOR TIED COLUMN WITH BARS IN 2 FACES, $\frac{P_u}{P_o}$ =0.1 and ℓ/h=5

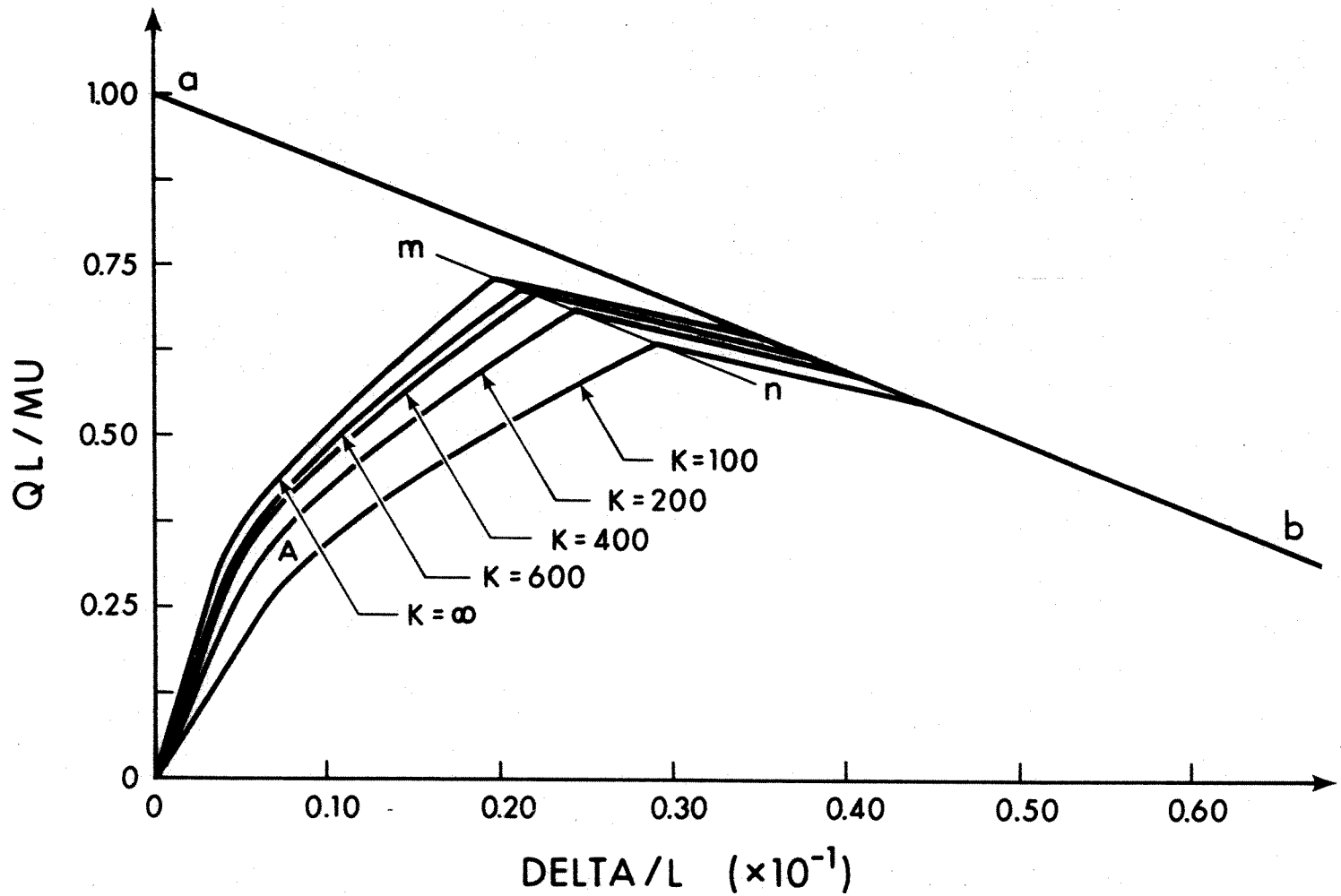

FIG. 4.4 LOAD-DEFLECTION DIAGRAM FOR TIED COLUMN WITH BARS IN 2 FACES, $\frac{P_u}{P_o}$ =0.1 and ℓ/h=30

Point No.		Axial load ratio, P_u/P_o							
		0.1	0.2	0.3	0.4	0.5	0.6	0.7	0.8
1	Moment	226.5	315.0	360.0	410.0	410.0	290.0	210.0	155.0
	$\phi x10^3$	0.071	0.100	0.120	0.147	0.158	0.123	0.093	0.085
2	Moment	616.0	555.0	392.5	453.0	490.0	450.0	330.0	203.0
	$\phi x10^3$	0.424	0.310	0.136	0.163	0.193	0.197	0.162	0.114
3	Moment	630.0	667.0	496.0	490.0	589.0	530.0	387.0	259.0
	$\phi x10^3$	0.790	0.416	0.218	0.186	0.270	0.246	0.197	0.153
4	Moment	643.0	740.0	587.0	563.0	652.0	562.0	434.0	296.0
	$\phi x10^3$	1.190	0.491	0.295	0.245	0.329	0.269	0.288	0.182
5	Moment	671.0	749.0	663.0	663.0	665.0	574.0	447.0	299.0
	$\phi x10^3$	1.880	0.557	0.365	0.341	0.377	0.326	0.296	0.200
6	Moment		759.0	784.0	735.0	672.0			300.0
	$\phi x10^3$		0.710	0.500	0.424	0.464			0.212
7	Moment		768.0	801.0	754.0				
	$\phi x10^3$		0.876	0.525	0.533				
8	Moment			828.0	766.0				
	$\phi x10^3$			0.592	0.647				

Units: moment is inch-kips, curvature is 1/inch.

TABLE 4.1

Coordinates for linearized M-P-ϕ diagrams for Type 1 column.

Point No.		Axial load ratio, P_u/P_o							
		0.1	0.2	0.3	0.4	0.5	0.6	0.7	0.8
1	Moment	210.0	210.0	290.0	250.0	210.0	170.0	120.0	80.0
	$\phi x10^3$	0.069	0.069	0.102	0.094	0.086	0.077	0.063	0.050
2	Moment	234.0	290.0	380.0	330.0	330.0	290.0	200.0	140.0
	$\phi x10^3$	0.108	0.098	0.148	0.126	0.139	0.137	0.107	0.090
3	Moment	271.0	423.0	445.0	415.0	410.0	370.0	280.0	180.0
	$\phi x10^3$	0.155	0.243	0.214	0.166	0.177	0.180	0.155	0.119
4	Moment	416.0	479.0	516.0	440.0	468.0	410.0	338.0	200.0
	$\phi x10^3$	0.318	0.308	0.293	0.188	0.208	0.203	0.196	0.162
5	Moment	508.0	557.0	572.0	504.0	500.0	450.0	382.0	254.0
	$\phi x10^3$	0.422	0.404	0.365	0.245	0.237	0.230	0.232	0.185
6	Moment	522.0	618.0	668.0	538.0	532.0	495.0	403.0	262.0
	$\phi x10^3$	0.546	0.489	0.513	0.285	0.277	0.268	0.288	0.204
7	Moment	556.0	639.0	693.0	578.0	571.0	509.0	410.0	267.0
	$\phi x10^3$	0.610	0.581	0.580	0.342	0.333	0.317	0.332	0.235
8	Moment	562.0	666.0		628.0	588.0	517.0		270.0
	$\phi x10^3$	0.677	0.733		0.420	0.414	0.447		0.269
9	Moment	592.0			556.0	600.0			
	$\phi x10^3$	1.077			0.553	0.543			
10	Moment	594.0			664.0				
	$\phi x10^3$	1.136			0.668				
11	Moment	597.0							
	$\phi x10^3$	1.410							

Units: moment is inch-kips, curvature is 1/inch.

TABLE 4.2

Coordinates for linearized M-P-ϕ diagrams for Type 2 column.

Point No.		Axial load ratio, P_u/P_o							
		0.1	0.2	0.3	0.4	0.5	0.6	0.7	0.8
1	Moment	135.0	130.0	223.0	140.0	150.0	150.0	90.0	87.0
	$\phi x10^3$	0.072	0.069	0.129	0.079	0.108	0.099	0.053	0.057
2	Moment	168.0	184.0	303.0	220.0	230.0	210.0	130.0	111.0
	$\phi x10^3$	0.118	0.103	0.220	0.134	0.151	0.151	0.091	0.086
3	Moment	236.0	237.0	337.0	273.0	270.0	250.0	170.0	136.0
	$\phi x10^3$	0.227	0.166	0.268	0.172	0.183	0.187	0.132	0.118
4	Moment	280.0	260.0	369.0	364.0	301.0	290.0	210.0	155.0
	$\phi x10^3$	0.300	0.196	0.323	0.292	0.212	0.228	0.174	0.144
5	Moment	383.0	316.0	414.0	400.0	320.0	319.0	240.0	175.0
	$\phi x10^3$	0.468	0.285	0.411	0.356	0.236	0.262	0.219	0.174
6	Moment	416.0	362.0	460.0	428.0	341.0	334.0	257.0	181.0
	$\phi x10^3$	0.579	0.363	0.516	0.420	0.268	0.285	0.232	0.190
7	Moment	439.0	416.0	497.0	442.0	388.0	340.0	267.0	190.0
	$\phi x10^3$	0.731	0.467	0.637	0.470	0.348	0.300	0.250	0.213
8	Moment	452.0	453.0	507.0	463.0	405.0	356.0	283.0	195.0
	$\phi x10^3$	0.862	0.540	0.707	0.557	0.396	0.356	0.285	0.260
9	Moment	458.0	477.0	508.0	478.0	420.0	367.0	290.0	198.0
	$\phi x10^3$	0.947	0.630	0.772	0.670	0.463	0.467	0.325	0.304
10	Moment	460.0	487.0			428.0	368.0	294.0	
	$\phi x10^3$	1.089	0.691			0.572	0.532	0.362	
11	Moment		500.0					296.0	
	$\phi x10^3$		0.908					0.436	

Units: moment is inch-kips, curvature is 1/inch.

TABLE 4.3

Coordinates for linearized M-P-ϕ diagrams for Type 3 column.

beyond this line the column and beam structures represented become unstable in a sidesway mode.The line mn will therefore be considered an instability failure condition. The line of instability corresponds to a point slightly above point 2 on the M-P-ϕ curve. This type of instability occurs because equilibrium between external and internal forces is no longer possible due to the P-Δ moments and the reduction in member stiffness with increasing moments.

In the balance of this report the type of failure described by Fig. 4.3 will be referred to as a "material failure" while that corresponding to Fig. 4.4 will be called a "stability failure". Because the distinction between the two is difficult in some cases, the name stability failure has been reserved in this report for structures in which the moment at which the structure becomes unstable is more than five percent below the moment capacity of the cross-section.

The effect of slenderness and second-order effects is evident from the comparison of Figs. 4.3 and 4.4. For K=100 the P-Δ moments account for about two percent of the failure moment for the short column and about 31 percent for the long column. For infinite beam restraint the values are 0.6 and 21 percent respectively.

4.4 Normalized Subassemblage Charts

One of the major difficulties in any attempt to develop a standard set of sway subassemblage charts for reinforced concrete columns is the wide variation in the M-P-ϕ curves due to variations in geometrical properties, steel percentage, axial load and material properties. As a result, each particular cross-section has a unique

set of charts which cannot be applied to any other cross-section. This puts severe limitations on the use of the subassemblage concept for reinforced concrete structures since extensive calculations would have to be carried out for each case.

An attempt was made to develop a normalized version of the M-P-ϕ curves which would apply to a wide range of columns, but insufficient accuracy was attained for the methods tried.

4.5 Deflections

Few building codes specify limits on the deflection index Δ/l. In North America the National Building Code of Canada[32] is the only one to do so and the limit is set at 1/500 at service loads both for the story rotation and for the buildings as a whole. The same limit has been suggested by ACI Committee 435 "Allowable Deflections"[33]. When code prescribed values do not exist, values ranging from 1/300 to 1/1000 have been used in practice, depending on the type of building and the judgement of the engineer.

A rigorous deflection analysis for concrete structures requires a considerable amount of computation and as a result approximate methods are usually preferred.

However, the subassemblage analysis provides a better estimate if a realistic M-P-ϕ curve is used. The deflections obtained from the subassemblage charts have been used for comparison with the deflection limits accepted in practice and to study the relationship between loading, deflections, geometry and mode of failure.

Service load conditions were considered for two cases based on Equations (4.4) and (4.5)

$$U = 1.4D + 1.7L \tag{4.4}$$

$$U = 0.75\ (1.4D + 1.7L + 1.7W) \tag{4.5}$$

where D,L and W are dead loads, live loads and wind loads, respectively. These equations are identical to Equations (9.1) and (9.2) in ACI 318-71.

The two cases considered were:

1. Maximum service load based on Equation (4.4) with L/D=5.0

and 2. Minimum service load based on Equation (4.5) with L/D=0.2

The service load was assumed to be given by Equation (4.6)

$$P_s = D + L \tag{4.6}$$

From these relationships the axial service loads are equal to $0.61P_u$ and $0.92P_u$ for case 1 and 2, respectively. The corresponding load factors for lateral loads are 1.7 and 1.275. Thus the service lateral loads were taken as 1/1.7 and 1/1.275 times the maximum QL/M_u value for the ultimate load case.

In figs. 4.5 through 4.14 the lateral load-deflection curves for ultimate loading conditions have been plotted for 10 cases in addition to similar curves for the two axial loads corresponding to the maximum and minimum service load conditions. The service lateral loads have been obtained by dividing the lateral load by the appropriate load factors and the service load deflections were obtained from the appropriate load-deflection curve. The results are presented numerically in Table 4.4. The curves plotted in Figs. 4.5 through 4.14 were chosen to study the effect that the shape of the cross-section, the slenderness and the beam restraint have on deflect-

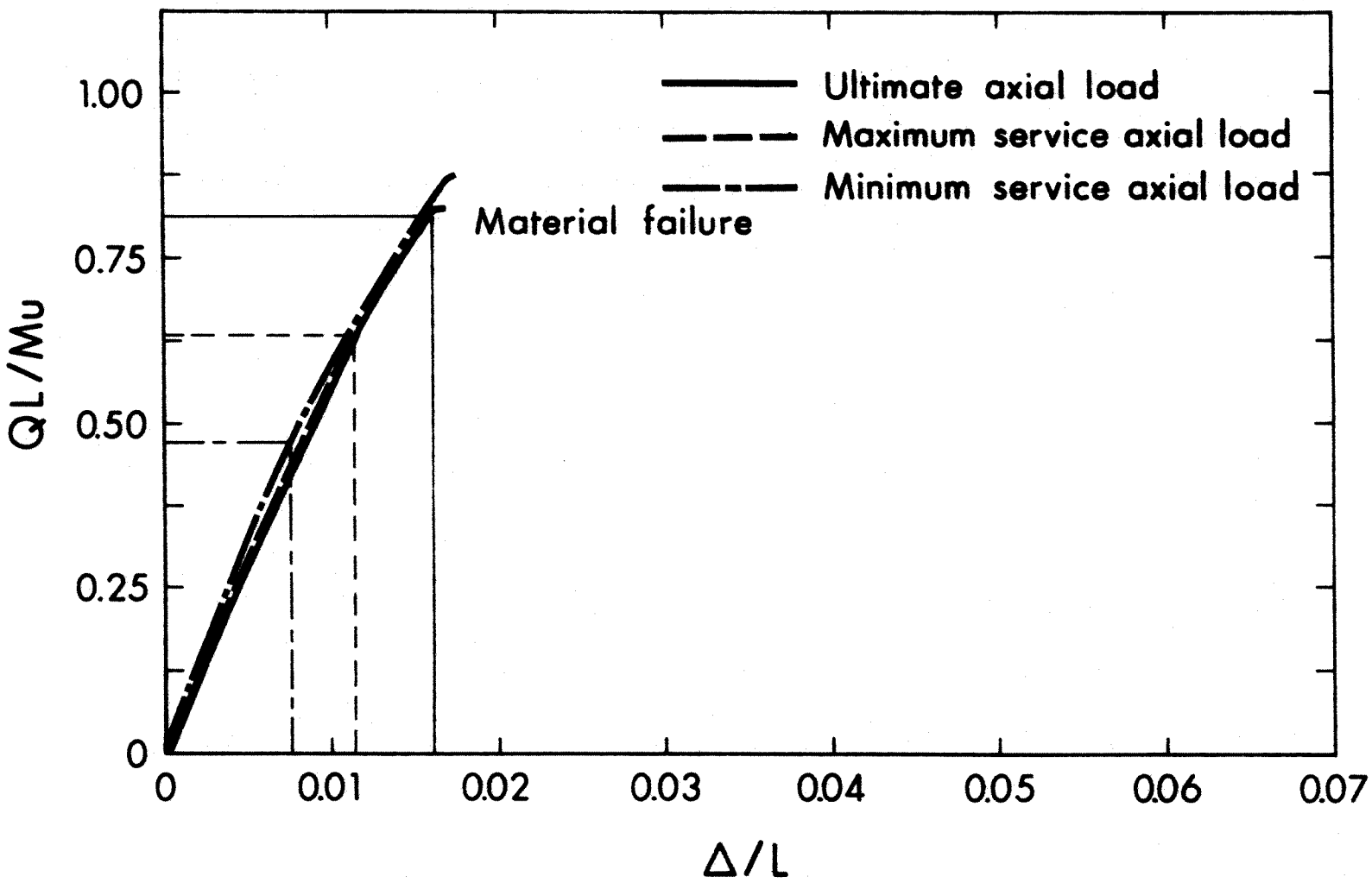

TIED COLUMN-BARS IN 2 FACES

P_u/P_o = 0.4 ℓ/h = 10 K = 100

FIG. 4.5 COMPARISON OF DEFLECTIONS AT SERVICE AND ULTIMATE LOAD

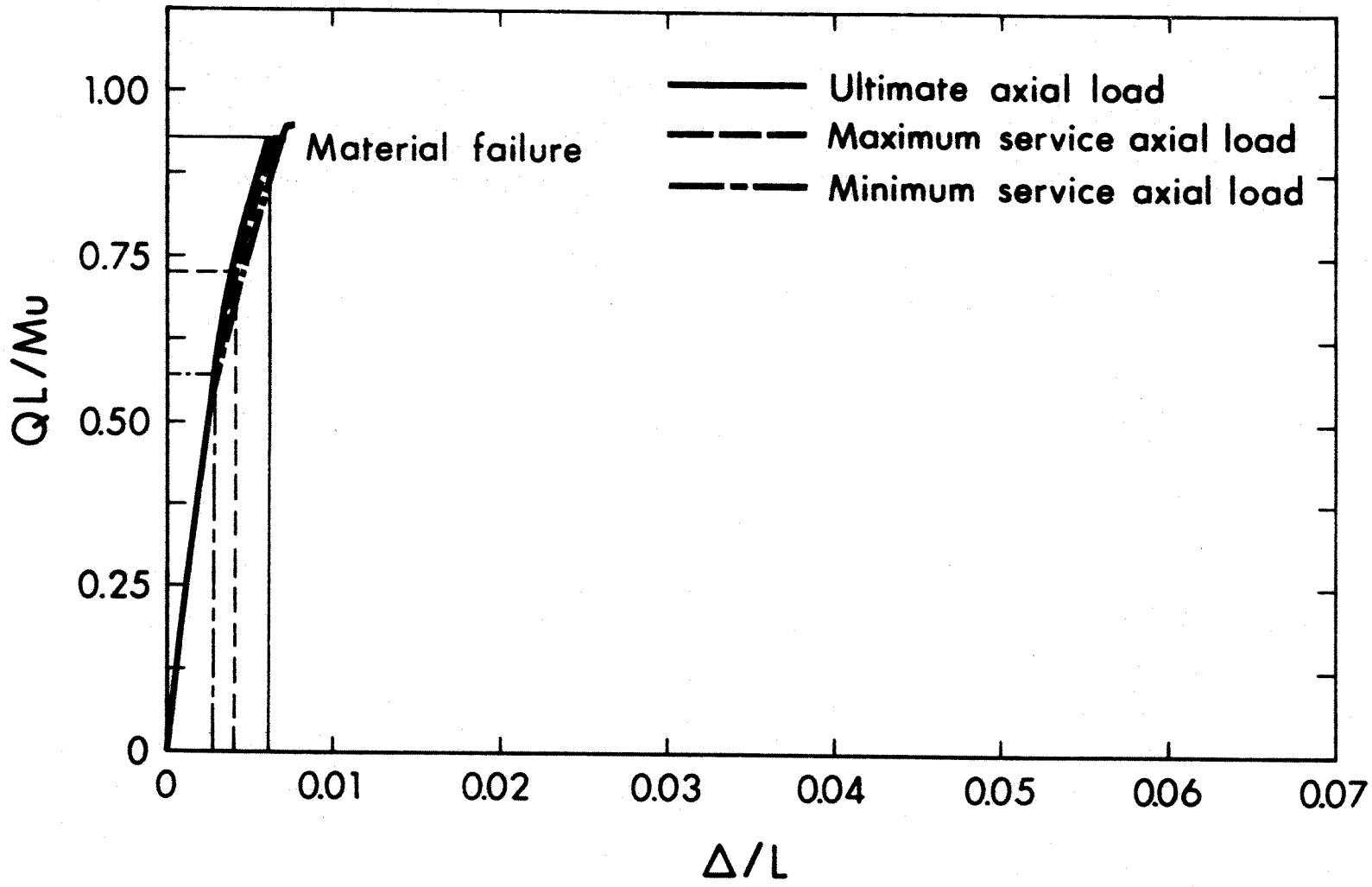

TIED COLUMN-BARS IN 2 FACES

$P_u/P_o = 0.4$ $\ell/h = 10$ $K = \infty$

FIG. 4.6 COMPARISON OF DEFLECTIONS AT SERVICE AND ULTIMATE LOAD

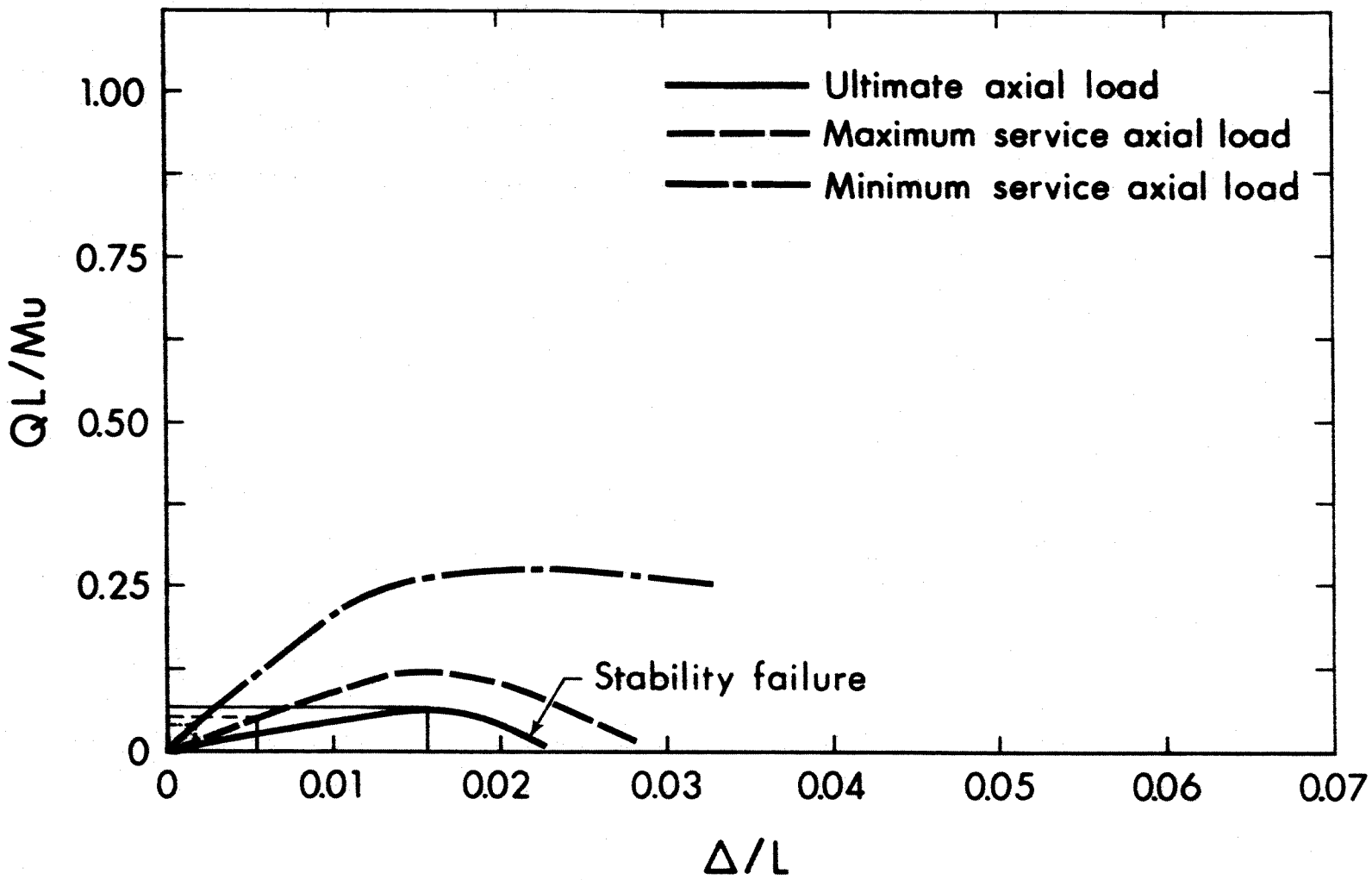

TIED COLUMN-BARS IN 2 FACES

P_u/P_o = 0.4 ℓ/h = 30 K = 100

FIG. 4.7 COMPARISON OF DEFLECTIONS AT SERVICE AND ULTIMATE LOAD

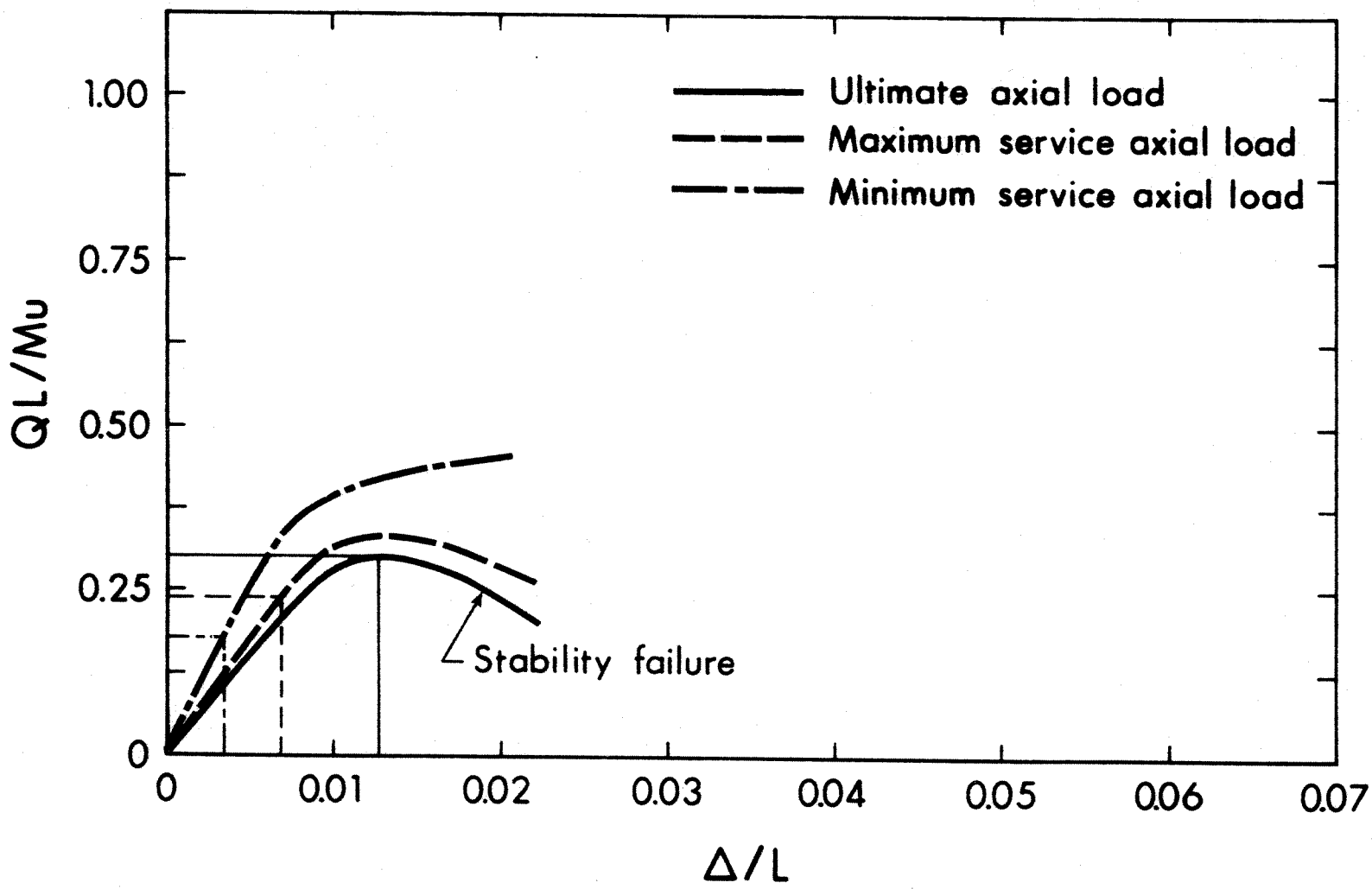

TIED COLUMN-BARS IN 2 FACES

$P_u/P_o = 0.4$ $\ell/h = 30$ $K = \infty$

FIG. 4.8 COMPARISON OF DEFLECTIONS AT SERVICE AND ULTIMATE LOAD

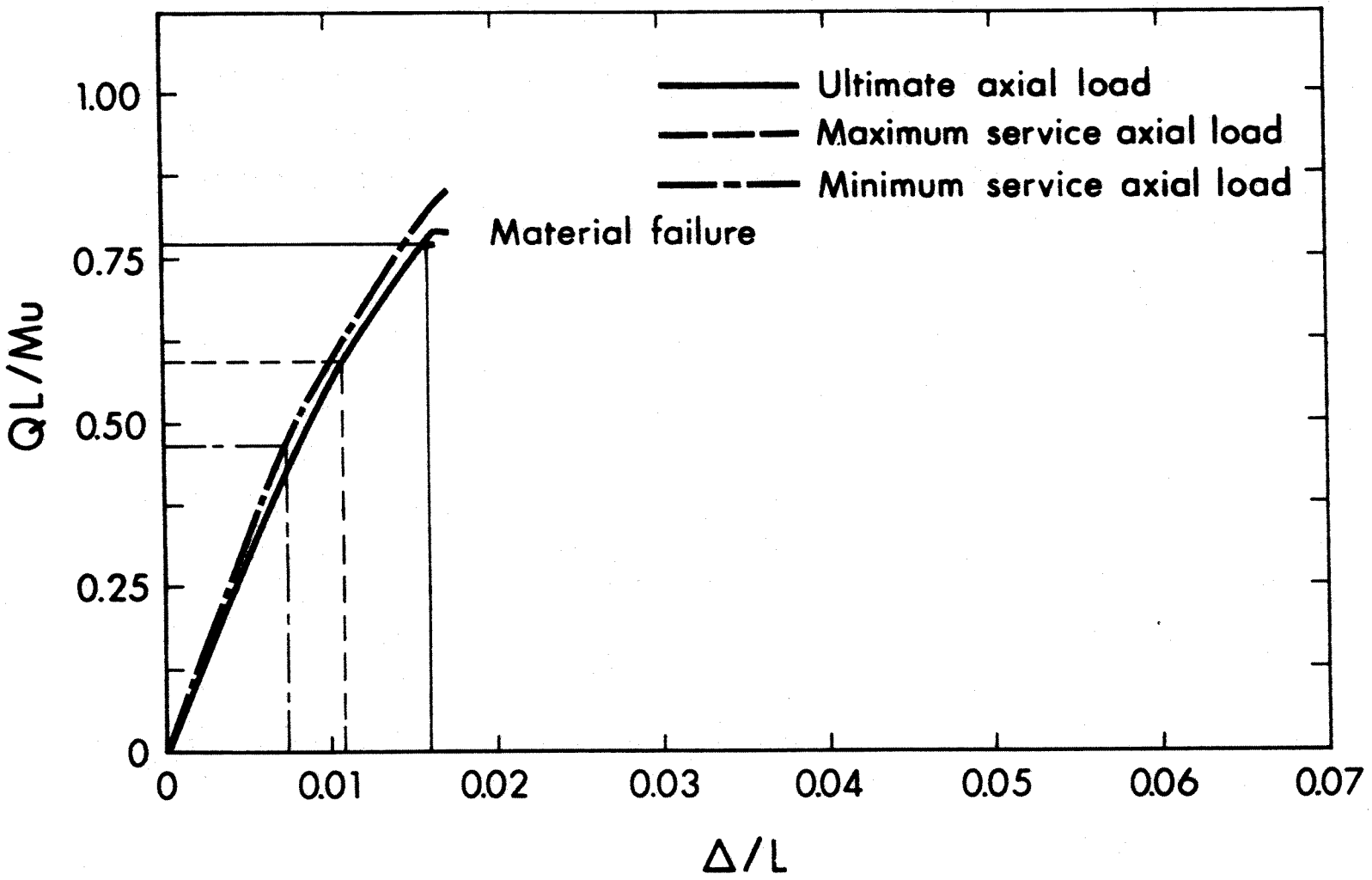

TIED COLUMN-BARS IN 4 FACES

$P_u/P_o = 0.4$ $\quad \ell/h = 10$ $\quad K = 100$

FIG. 4.9 COMPARISON OF DEFLECTIONS AT SERVICE AND ULTIMATE LOAD

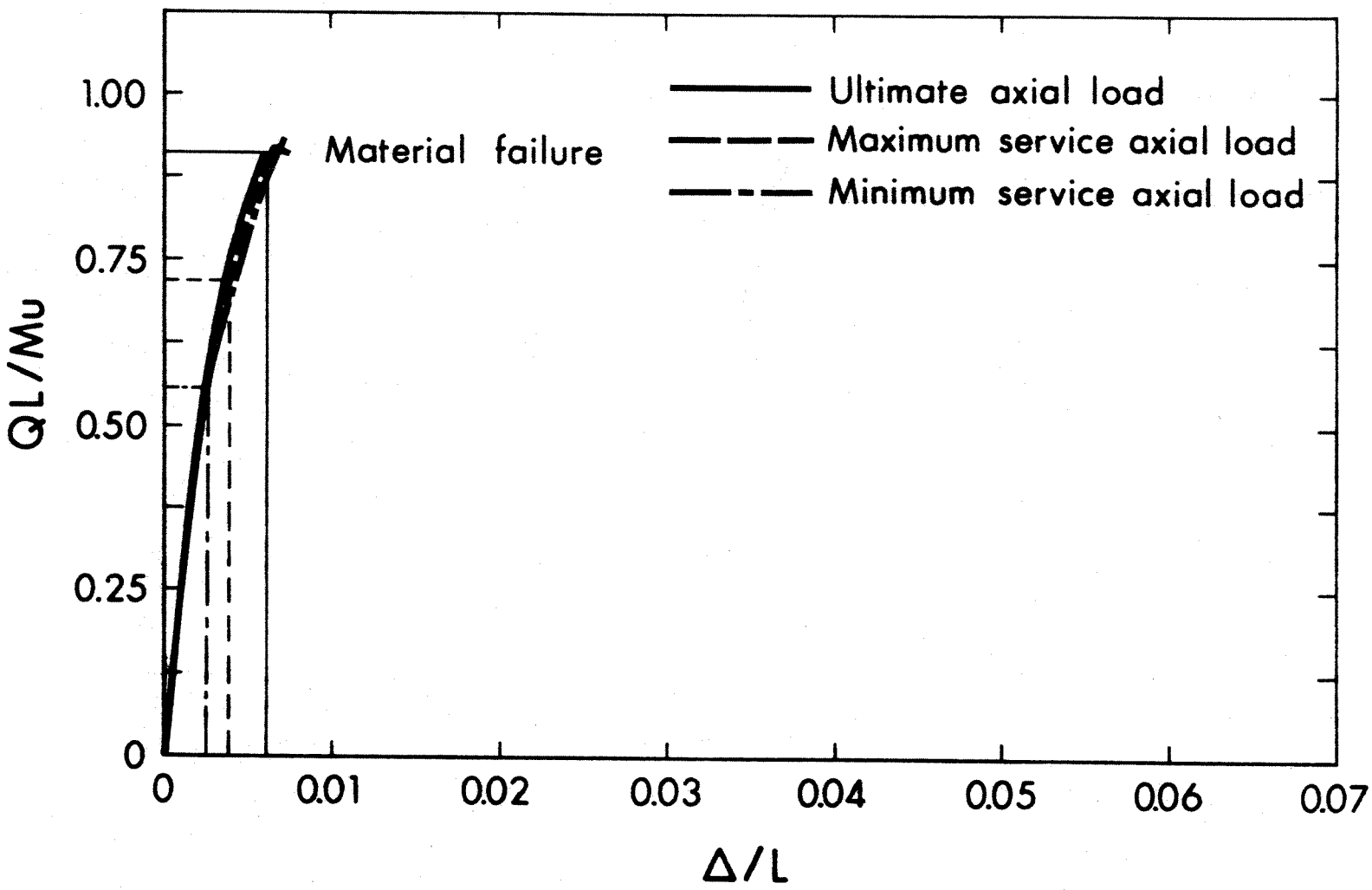

TIED COLUMN-BARS IN 4 FACES

$P_u/P_o = 0.4$ $\ell/h = 10$ $K = \infty$

FIG. 4.10 COMPARISON OF DEFLECTIONS AT SERVICE AND ULTIMATE LOAD

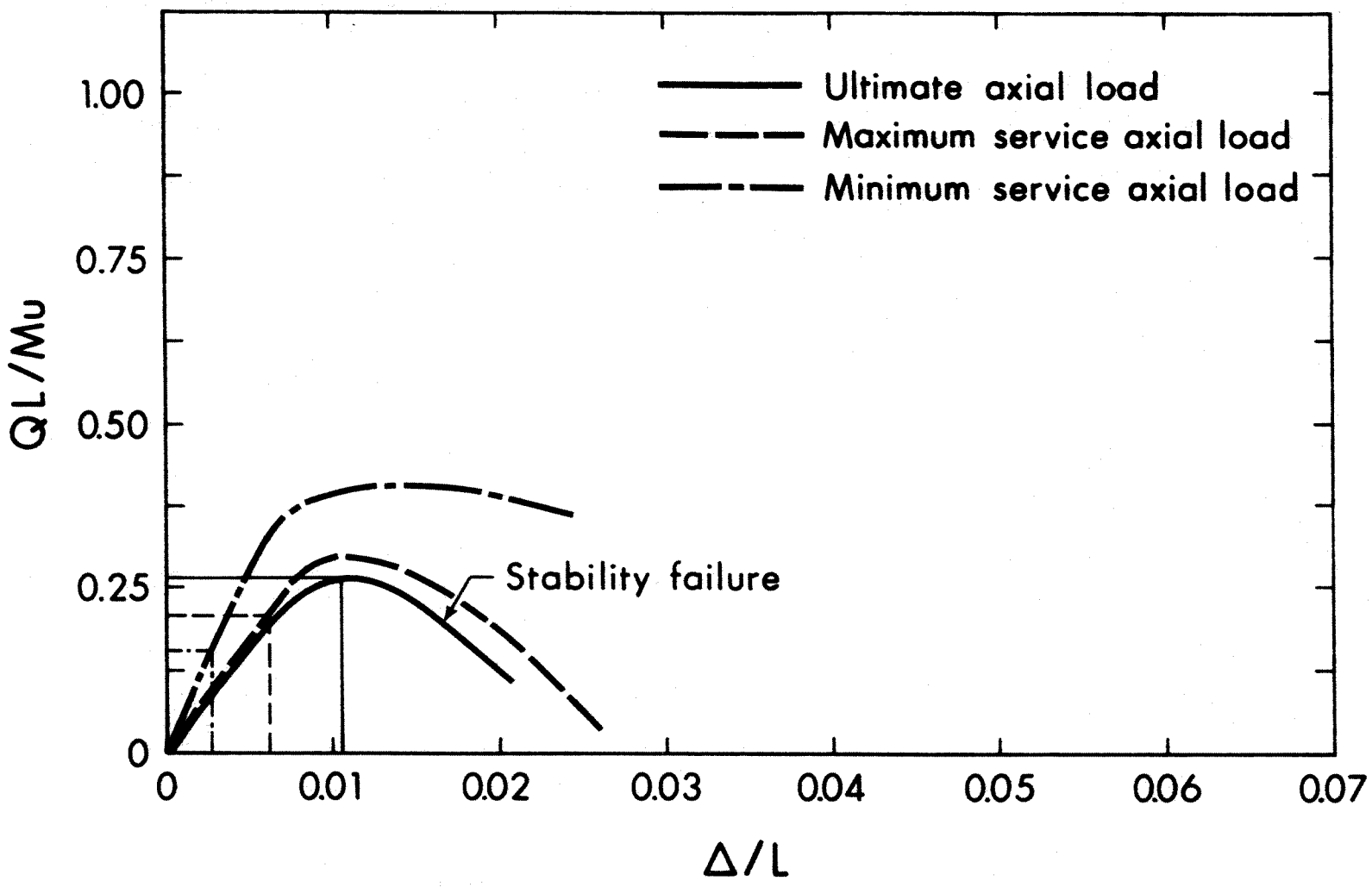

TIED COLUMN-BARS IN 4 FACES

$P_u/P_o = 0.4$ $\ell/h = 30$ $K = \infty$

FIG. 4.11 COMPARISON OF DEFLECTIONS AT SERVICE AND ULTIMATE LOAD

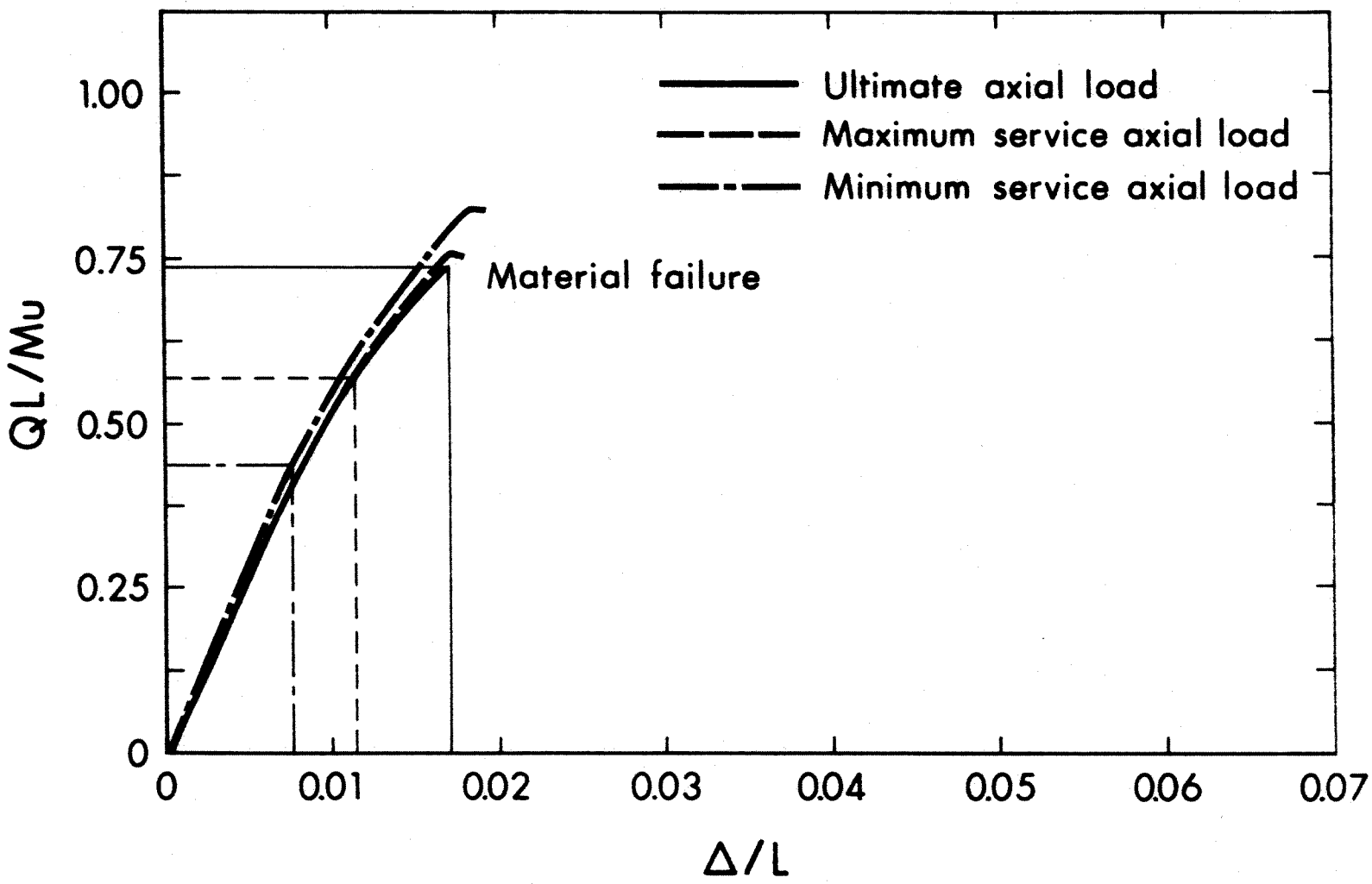

SPIRAL COLUMN

$P_u/P_o = 0.4$ $\ell/h = 10$ $K = 100$

FIG. 4.12 COMPARISON OF DEFLECTIONS AT SERVICE AND ULTIMATE LOAD

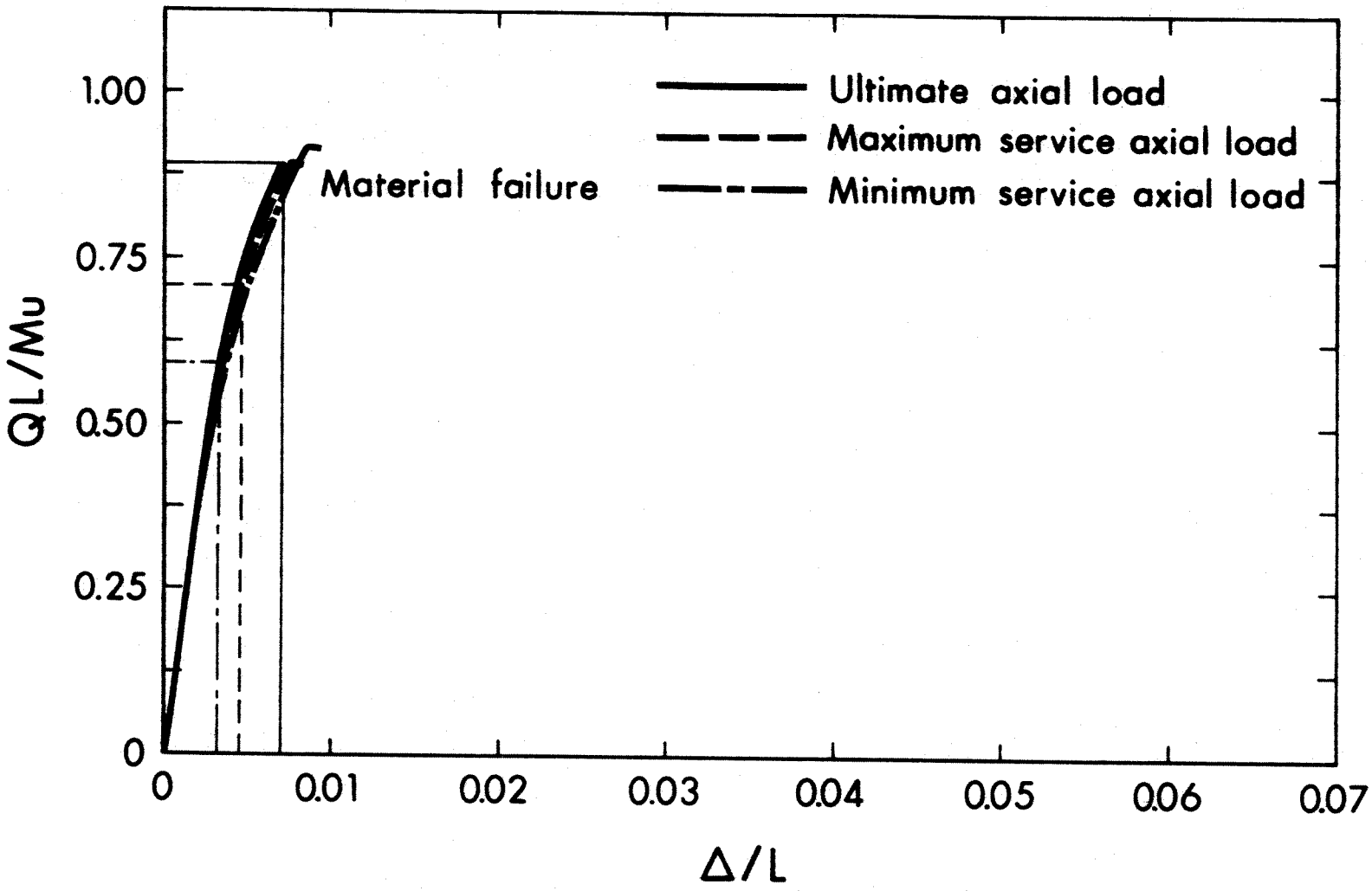

SPIRAL COLUMN

$P_u/P_o = 0.4$ $\quad \ell/h = 10$ $\quad K = \infty$

FIG. 4.13 COMPARISON OF DEFLECTIONS AT SERVICE AND ULTIMATE LOAD

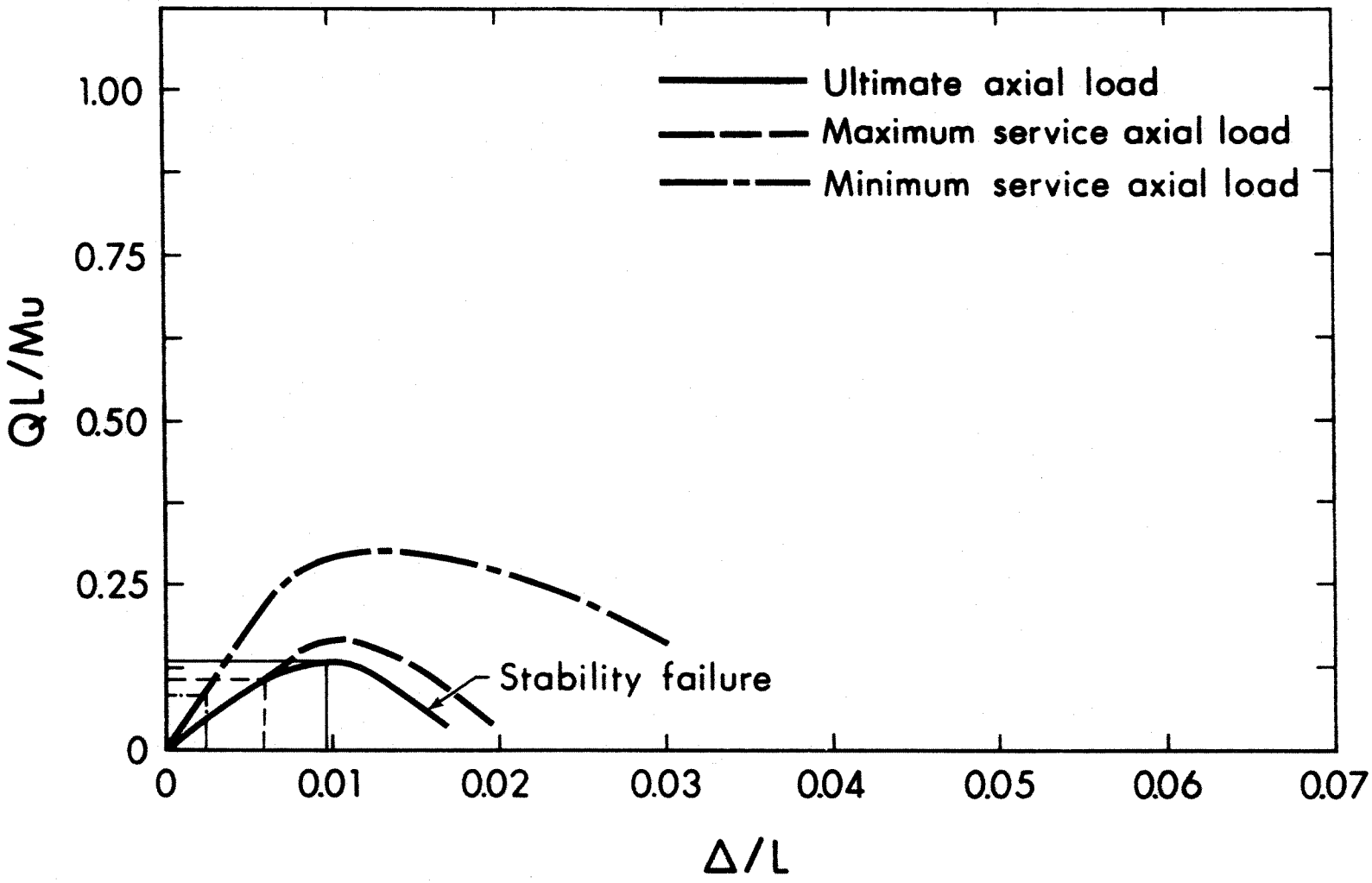

SPIRAL COLUMN

$P_u/P_o = 0.4$ $\quad \ell/h = 30$ $\quad K = \infty$

FIG. 4.14 COMPARISON OF DEFLECTIONS AT SERVICE AND ULTIMATE LOAD

Type of loading	Type of column	Δ/L			
		l/h=10		l/h=30	
		K=100	K= ∞	K=100	K= ∞
Ultimate	1	0.0161	0.0061	0.0157	0.0126
	2	0.0157	0.0058	unstable	0.0106
	3	0.0171	0.0071	unstable	0.0097
Service load, case 2	1	0.0115	0.0041	0.0056	0.0066
	2	0.0110	0.0037	unstable	0.0061
	3	0.0116	0.0044	unstable	0.0058
Service load, case 1	1	0.0078	0.0027	0.0017	0.0034
	2	0.0072	0.0023	unstable	0.0028
	3	0.0076	0.0029	unstable	0.0022

TABLE 4.4

Deflection index for ultimate and service load conditions for loads corresponding to $P_u/P_o=0.4$

ions.

It can be seen from these figures that the shape of the cross-section has little effect on the deflections. The slenderness ratio is important for service load deflections and is also significant for ultimate deflections for strong beam-weak column combinations. As expected the deflections increase with reductions of the beam stiffness. This effect is more pronounced for material failures than for stability failures.

All the deflection indices obtained in the analysis are shown graphically in Figs. 4.15 through 4.22. A total of 690 cases were studied, 217 of which were stability failures. A stability failure was assumed to occur when the moment at which the structure became unstable was more than five percent below the moment capacity of the column.

Deflection indices at ultimate (Fig. 4.15, 4.18) showed wide variation with results ranging from about 1/700 to 1/30.

The results for the two service load conditions (Fig. 4.16, 4.17) gave a somewhat more narrow distribution with values between 1/760 and 1/50 for case 2 and 1/820 to 1/70 for case 1. The service load deflections may vary from about 10 to 80 percent of the ultimate deflections depending on the shape of the load deflection diagram and the service load condition. If the curve is very steep the service load deflections will reach the upper limit; in the case of large ultimate deflections the value will be closer to the lower limit. Material failures will normally have relatively small deflections while stability failures exhibit much larger deformations at ultimate. Typical examples are shown

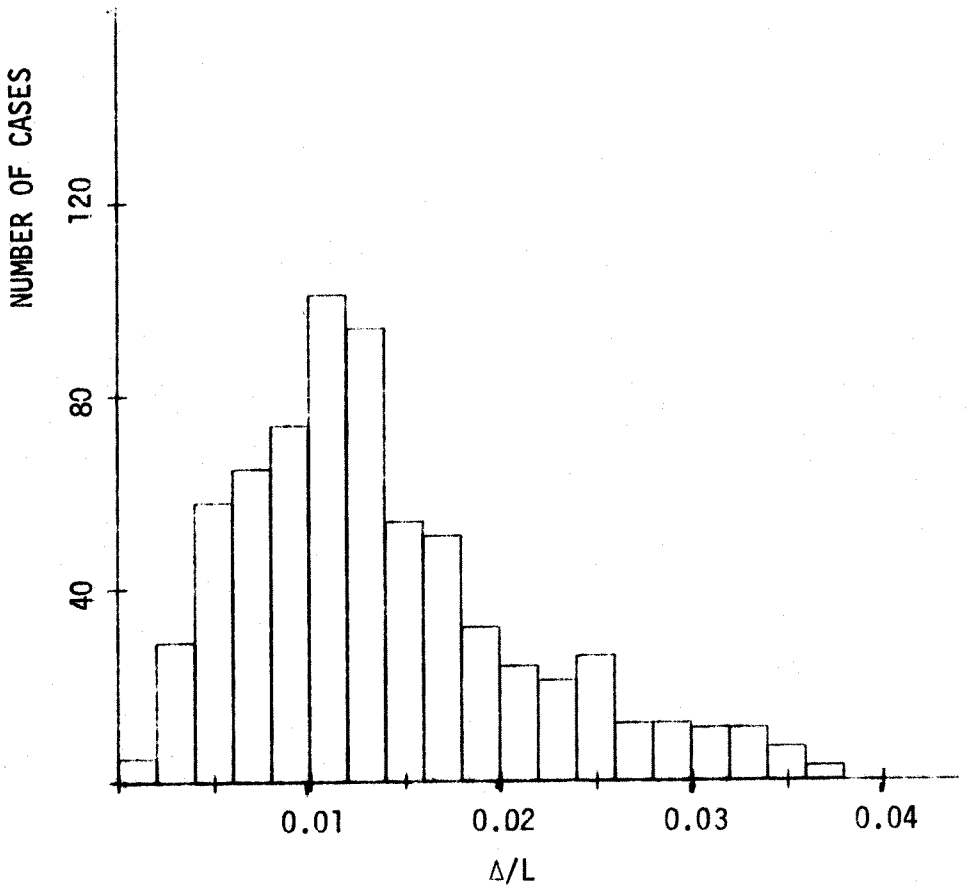

FIG. 4.15 DISTRIBUTION OF DEFLECTION INDICES AT ULTIMATE LOAD

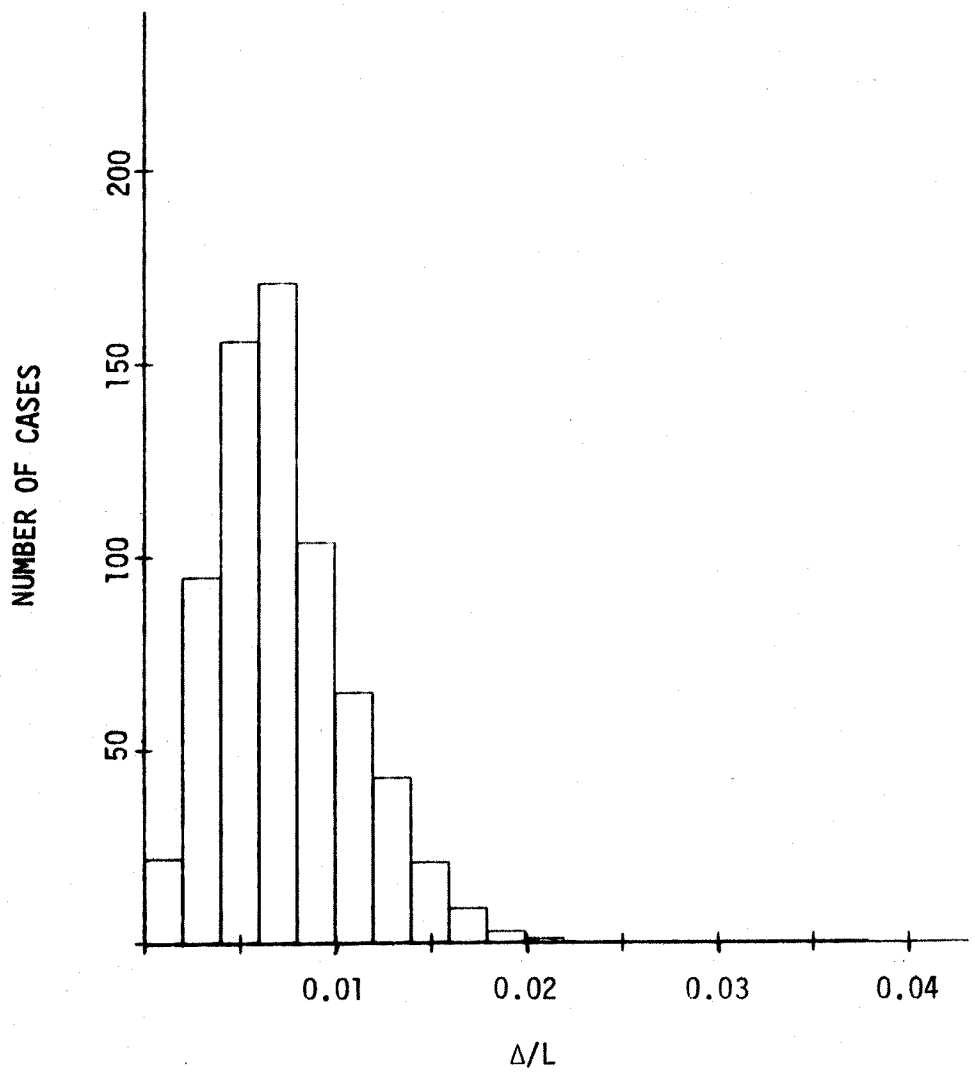

FIG. 4.16 DISTRIBUTION OF DEFLECTION INDICES FOR MAXIMUM SERVICE LOADS

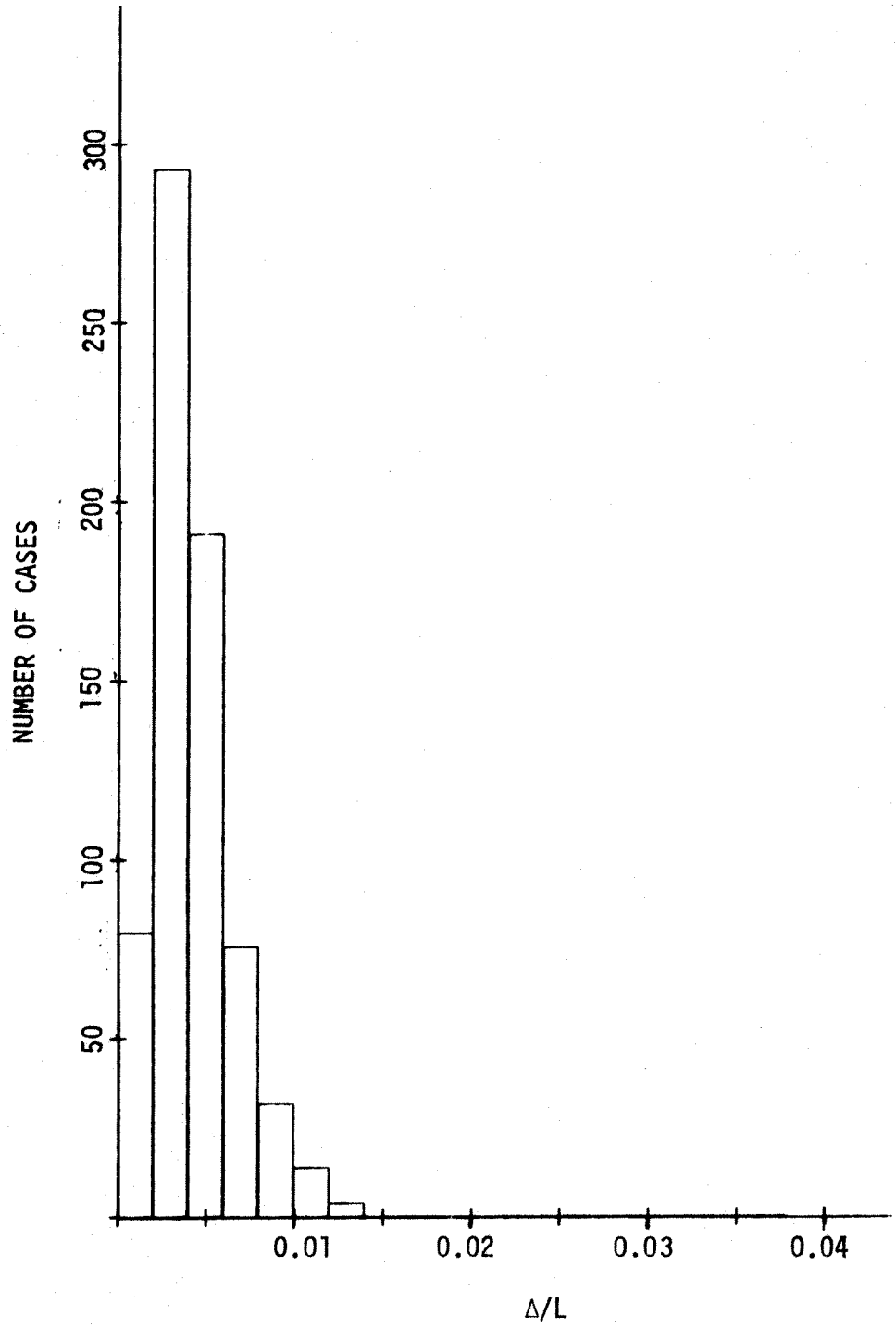

FIG. 4.17 DISTRIBUTION OF DEFLECTION INDICES FOR MINIMUM SERVICE LOAD

in Figs. 4.5 through 4.14.

Structures failing as a result of material failure were found to have service load deflections of about 1/3 to 2/3 of the ultimate deflection. If the loading condition corresponds to minimum service load the values will be in the lower range, say 1/3 to 1/2, with weak beam-strong column combinations giving the higher values. For maximum service loads the values range from 1/2 to 2/3 of the ultimate deflection.

In Figs. 4.20 through 4.22 the computed values have been compared to allowable values of Δ/L of 1/500 and 1/250 for service load and ultimate load, respectively. For all three cases only a small percentage of the results falls below the specified limits. Thus, for the columns considered, deflections would likely be the governing design criterion rather than strength.

Stability failures usually occur at relatively large deflections. Fig. 4.19 shows that no stability failures occurred for Δ/L less than 1/200. For allowable values below this figure the design would be governed by deflections or strength. This limit is used to set limits on the applicability of the $P\Delta$ type of analysis in Section 6.43.

To investigate a possible relationship between deflection, loading and slenderness ratio the deflection index at ultimate was plotted against slenderness ratio for various values of axial load, Fig. 4.23 through 4.25. These plots show that the relationship between slenderness ratio and deflection index is close to being a straight line for relatively small values of kl/r. For higher values of kl/r the results become more scattered and the deflection

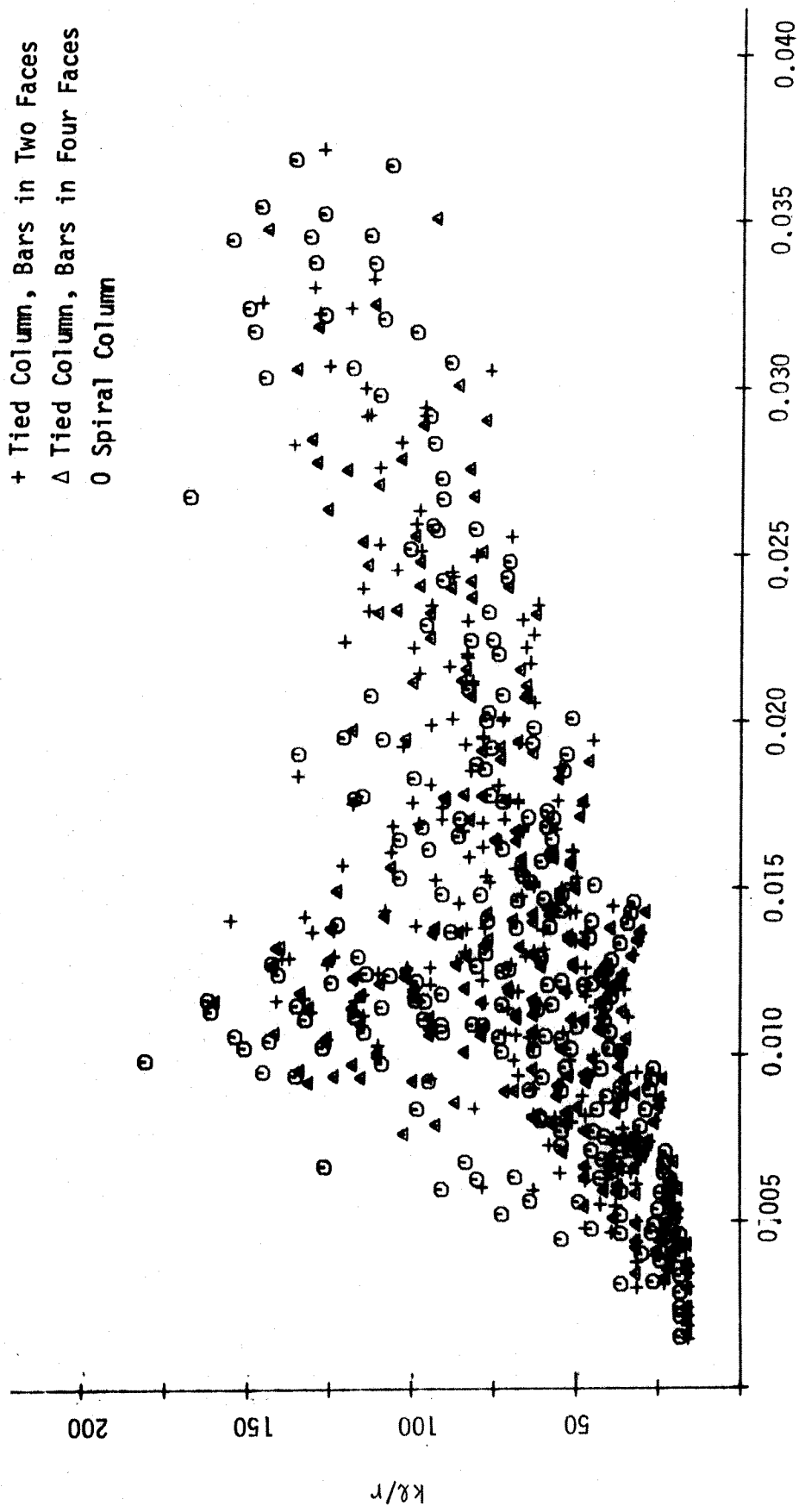

FIG. 4.18 DEFLECTION INDICES PLOTTED AGAINST SLENDERNESS RATIO FOR 690 CASES STUDIED.

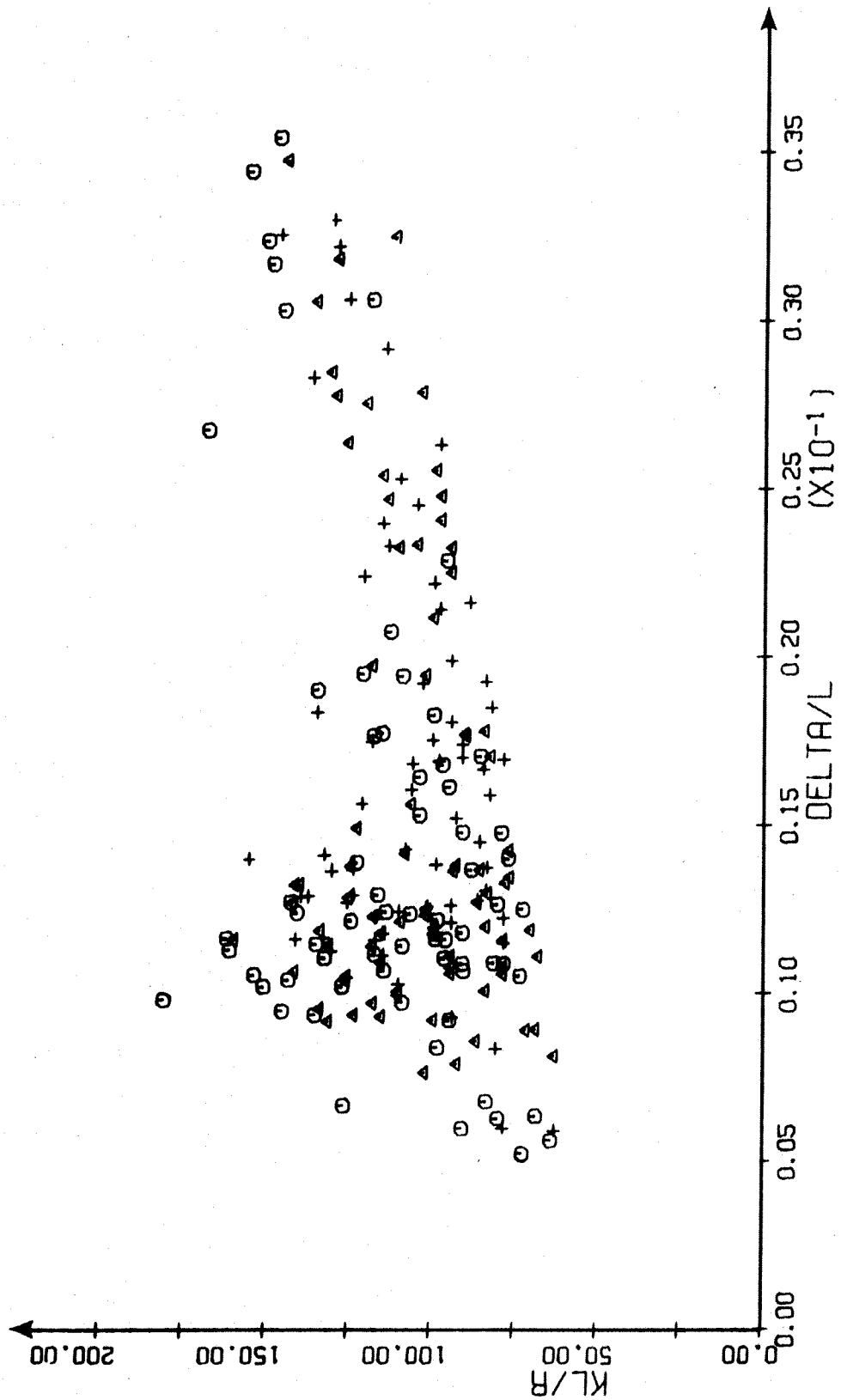

FIG. 4.19 DEFLECTION INDICES PLOTTED AGAINST SLENDERNESS RATIO FOR 217 STABILITY FAILURES

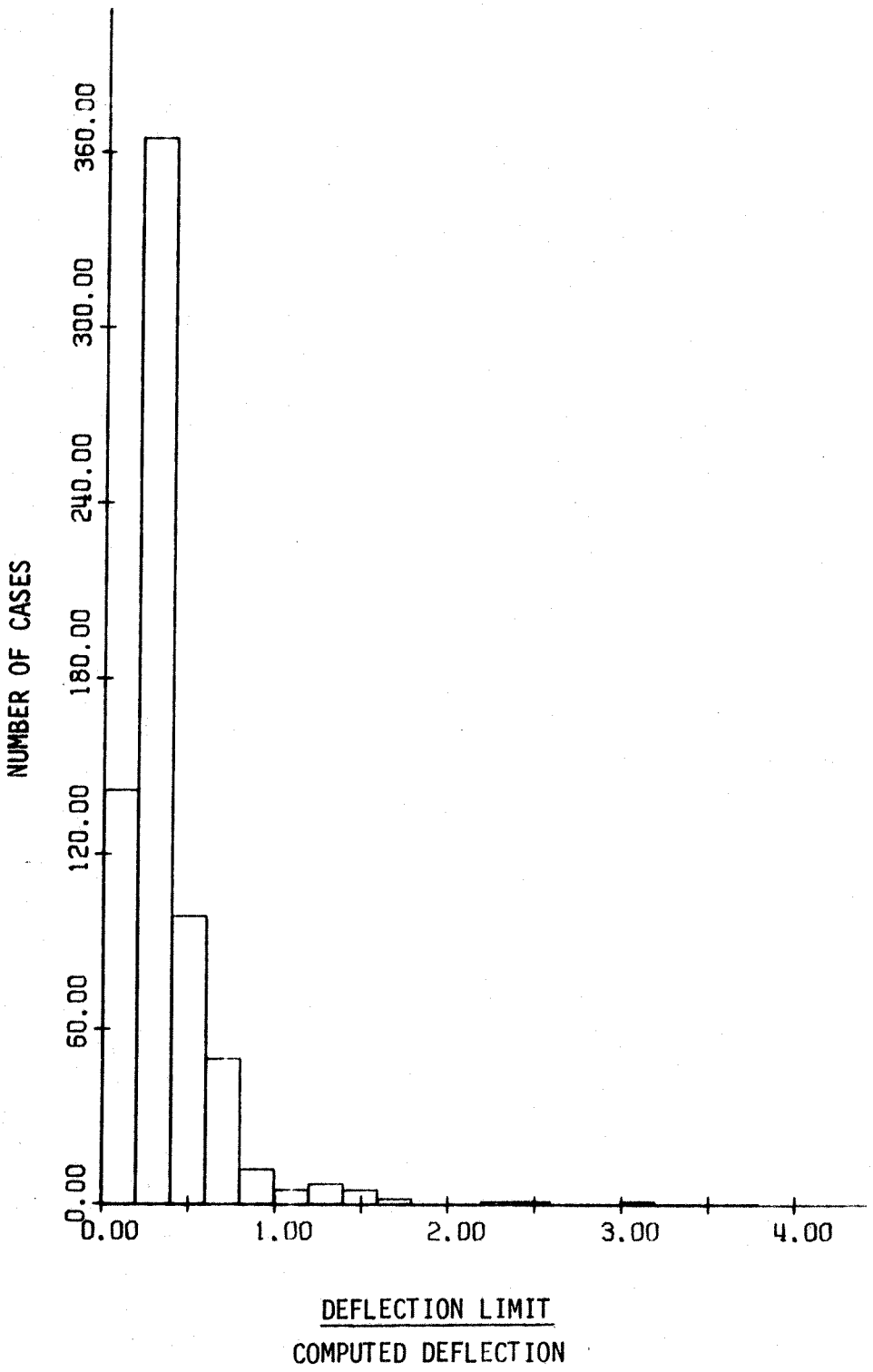

FIG. 4.20 COMPARISON OF COMPUTED DEFLECTIONS WITH DEFLECTION LIMIT OF 1/500 MAXIMUM SERVICE LOAD

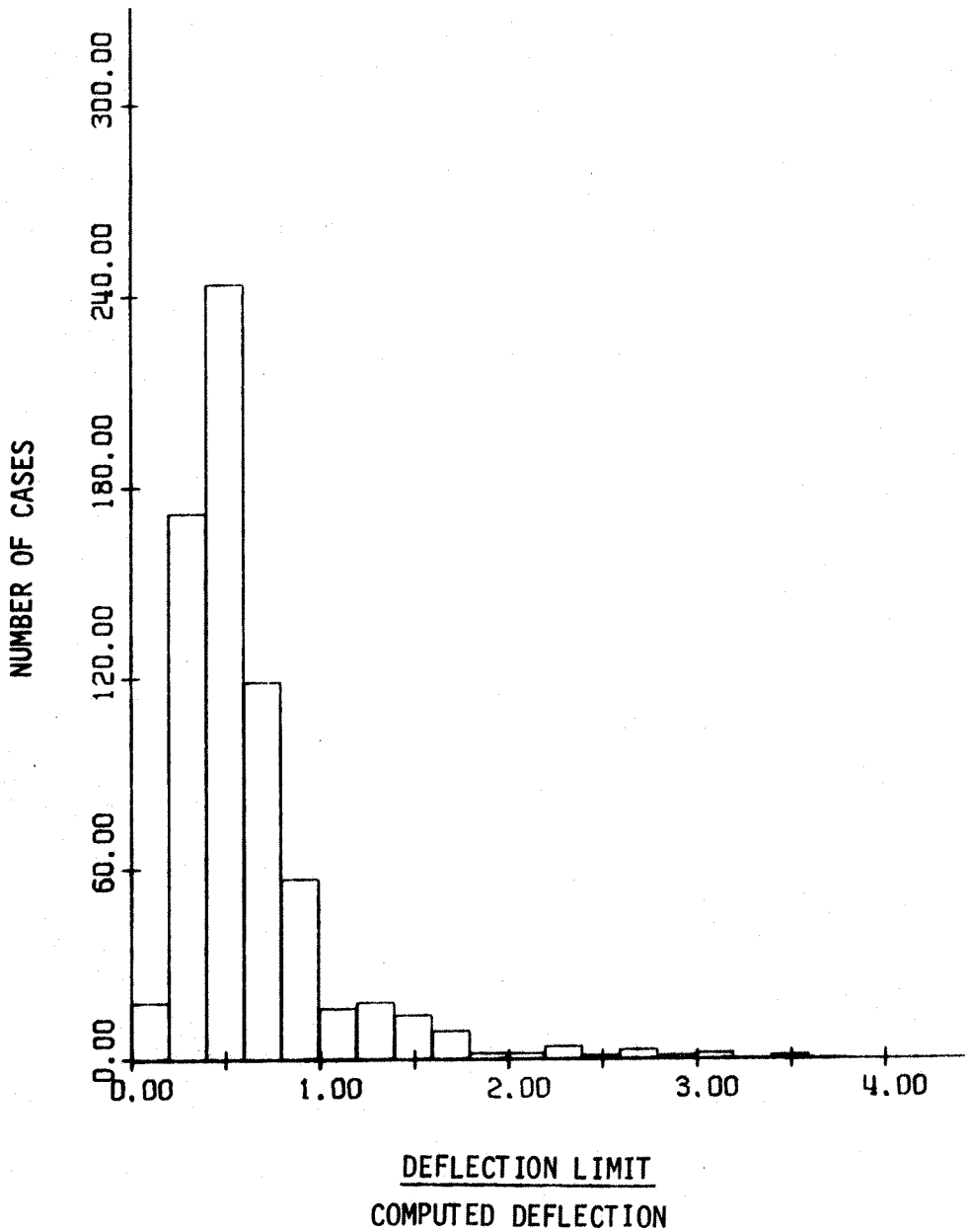

FIG. 4.21 COMPARISON OF COMPUTED DEFLECTIONS WITH DEFLECTION LIMIT OF 1/500 MINIMUM SERVICE LOAD.

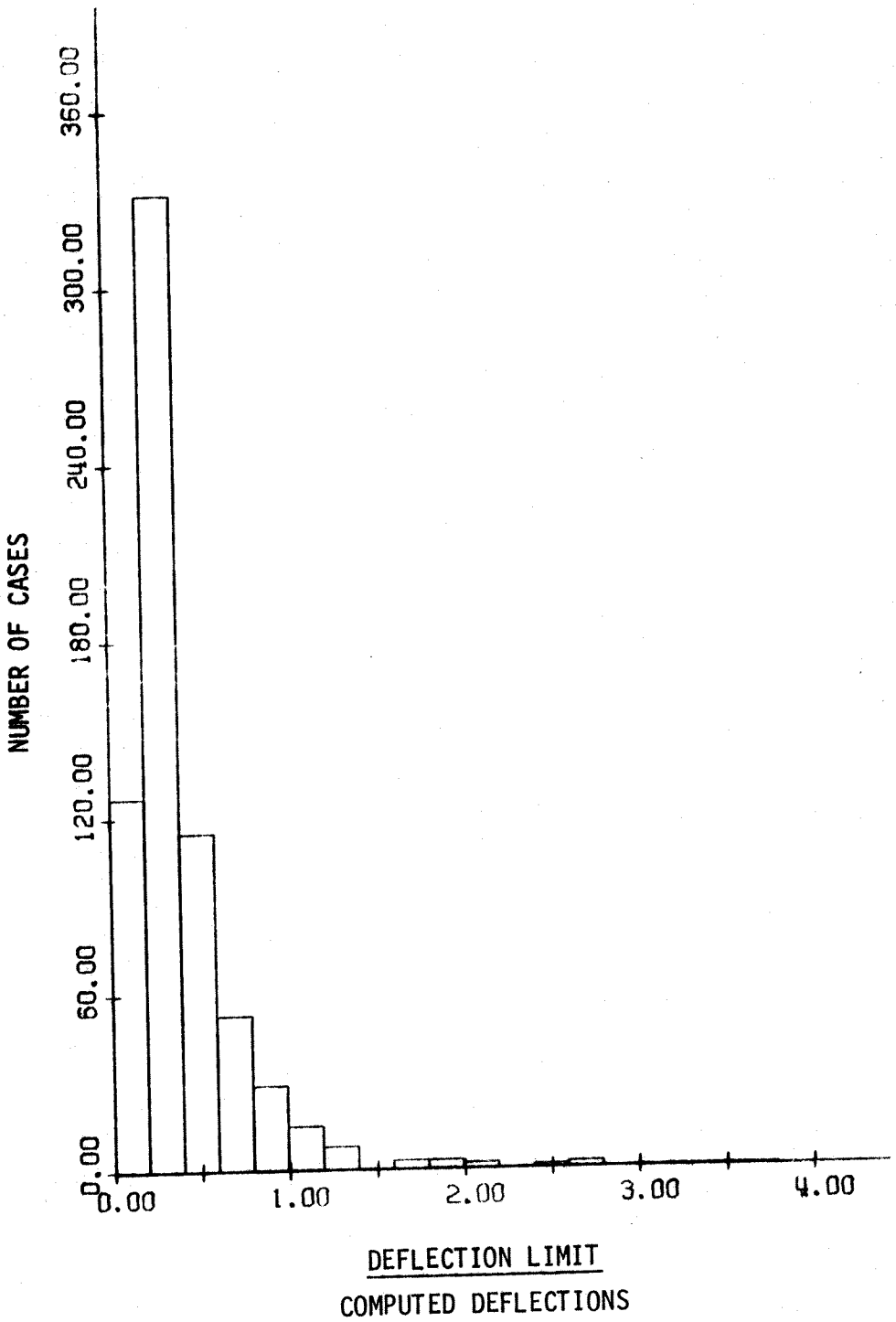

FIG. 4.22 COMPARISON OF COMPUTED DEFLECTIONS WITH DEFLECTION LIMIT OF 1/250 ULTIMATE LOAD

index reaches values which would normally be unacceptable in design. A straight line relationship between kl/r and $(\Delta/l)_u$ was therefore chosen such that it would give a reasonably good estimate of small deflection indices.

The following empirical equation was taken to represent the deflection index at ultimate as a function of the slenderness ratio of the column and the axial load:

$$\left(\frac{\Delta}{L}\right)_u = \left[\frac{3.4 - 2.75\ \frac{P_u}{P_o}}{10^4}\right] \frac{kl}{r} \qquad (4.7)$$

This equation has been plotted in Fig. 4.23 through 4.25 for P_u/P_o equal to 0.1, 0.4 and 0.7.

4.6 Column Stiffness Analysis

It was previously pointed out that the member stiffness is probably the most important parameter in any second-order analysis. A linear-elastic analysis will yield good results if the assumed stiffness is close to the effective elastic stiffness for the particular point in the load-deflection diagram being considered.

Before determining an equivalent linear-elastic value of EI a desicision must be made as to what point on the load-deflection diagram should be used since the stiffness depends on the magnitude of the load and the loading history of the structure.

If the coordinates of a point on the load-deflection curve are known, the equivalent stiffness may be computed from the following equations, derived from Fig. 4.2 using standard elastic formulae.

The equivalent column stiffness is given by

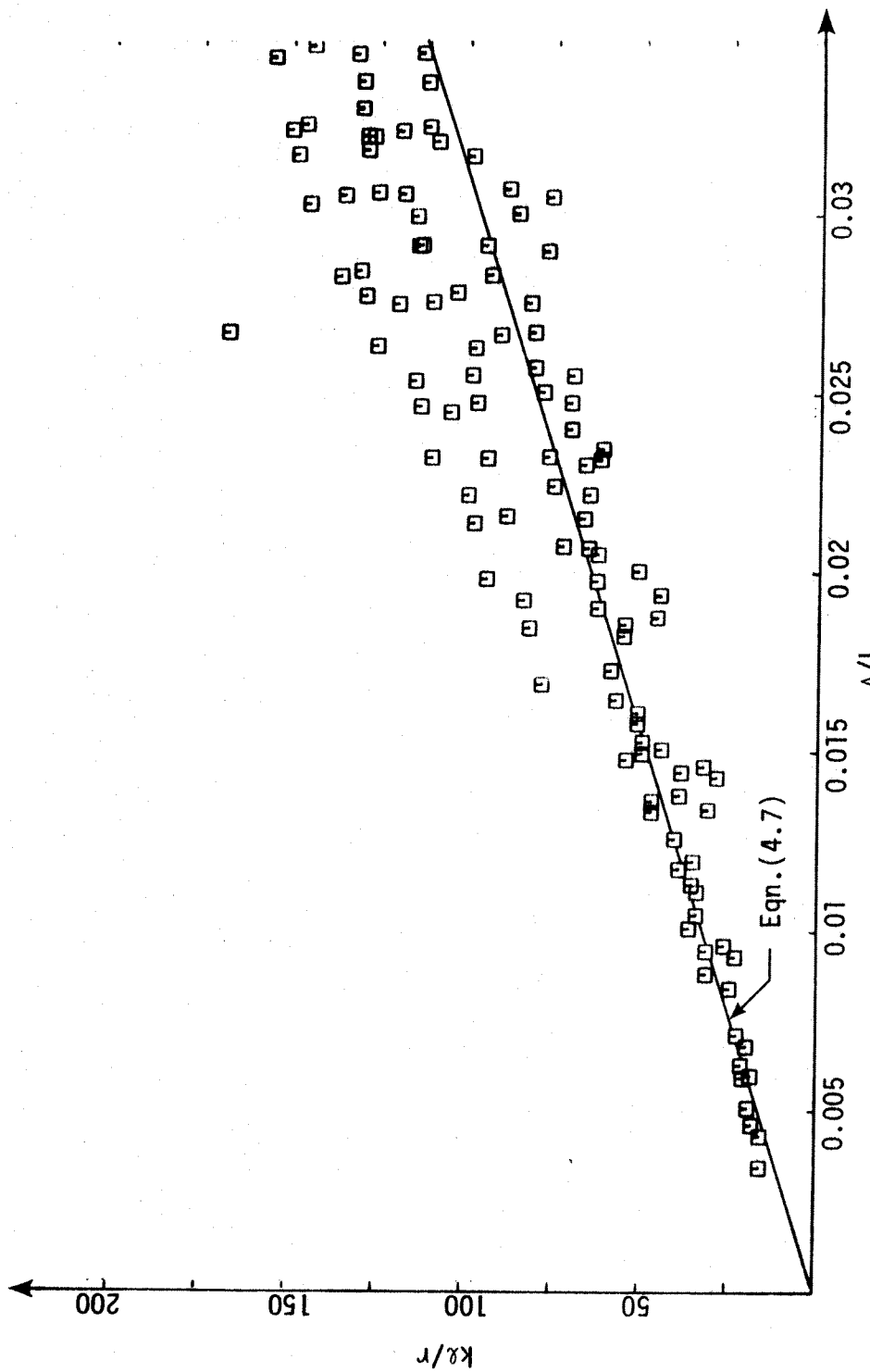

FIG. 4.23 DEFLECTIONS AT ULTIMATE FOR $P_u/P_o = 0.1$

ALL COLUMNS

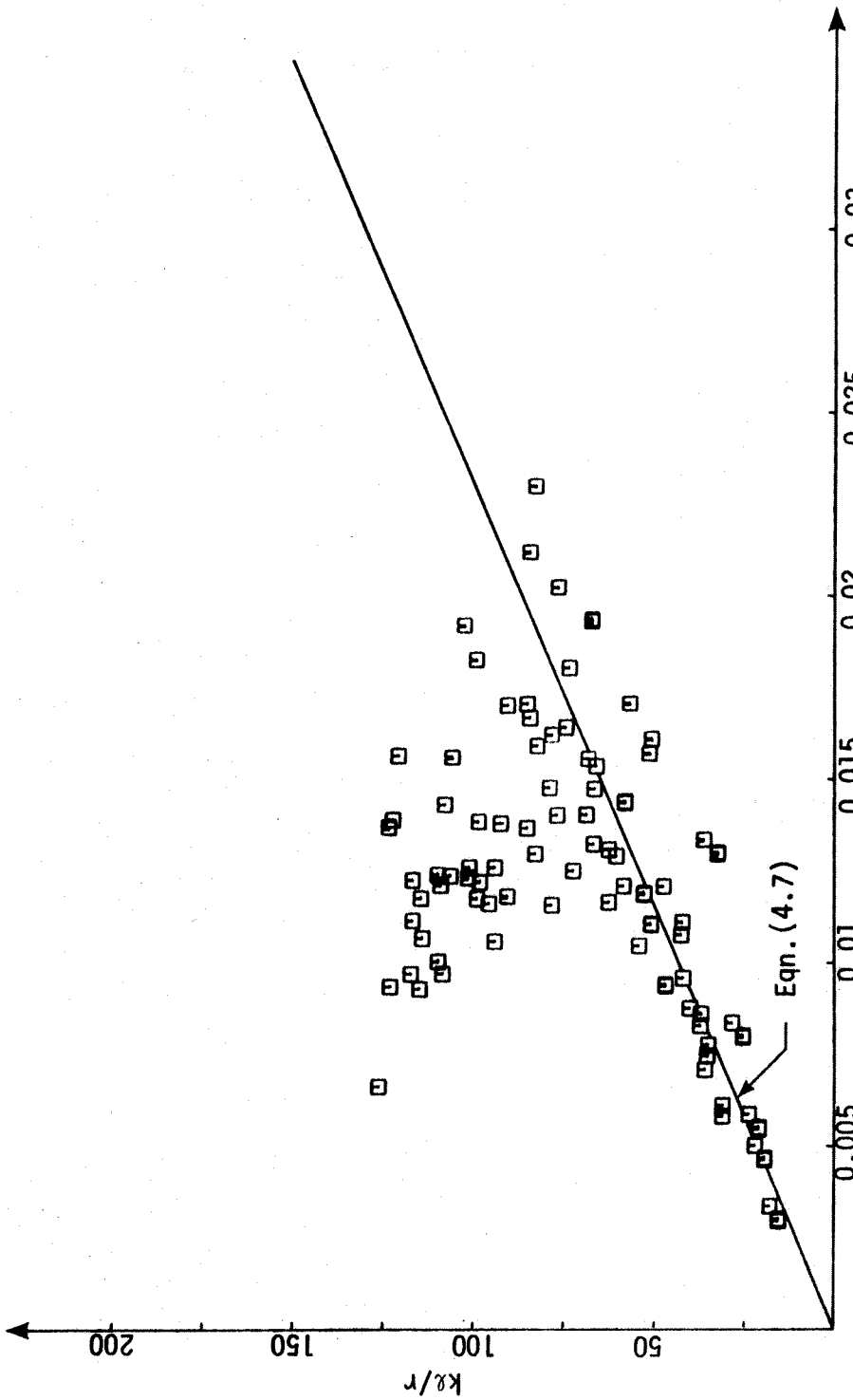

FIG. 4.24 DEFLECTIONS AT ULTIMATE FOR P_u/P_o = 0.4
ALL COLUMNS

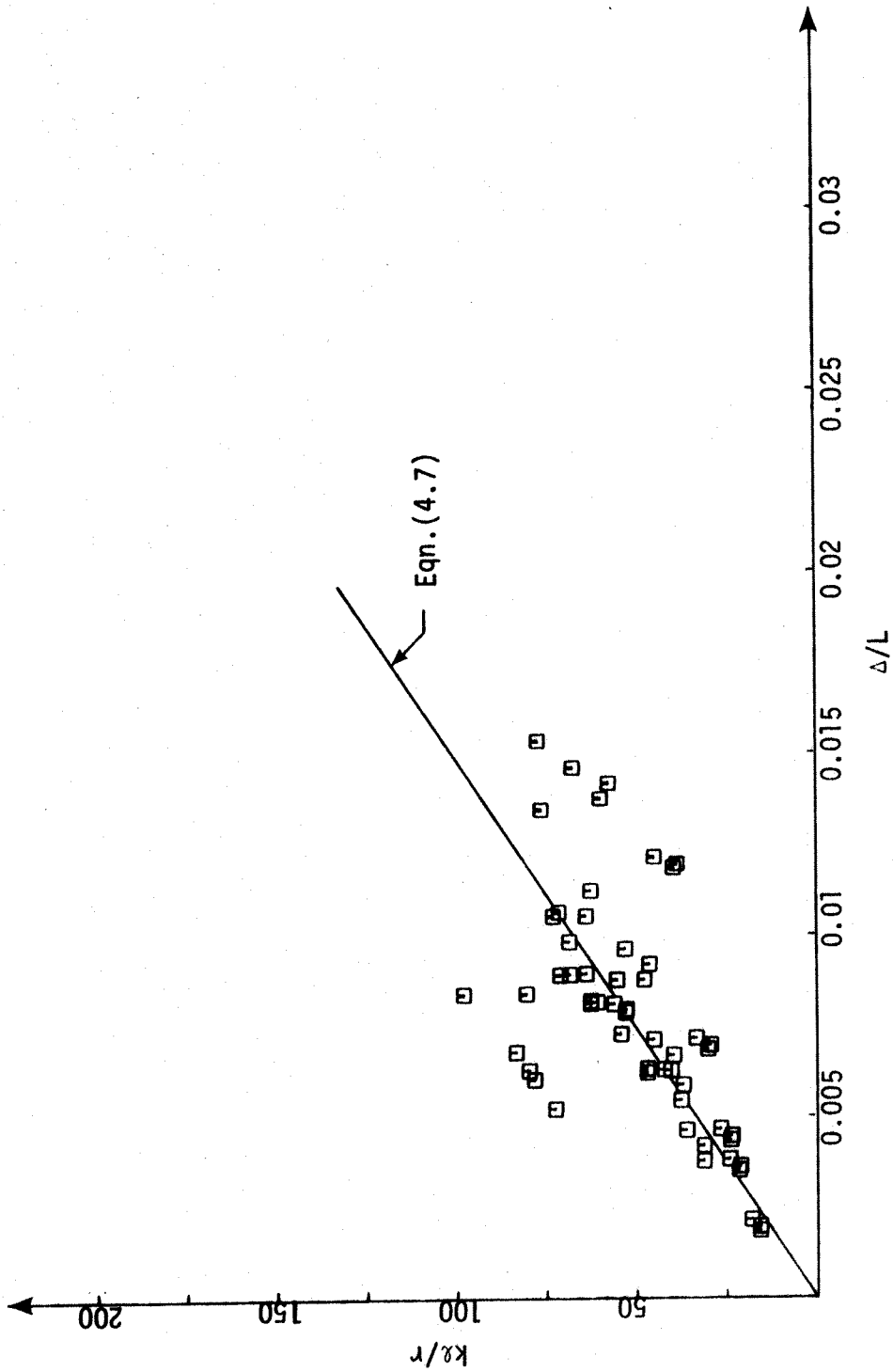

FIG. 4.25 DEFLECTIONS AT ULTIMATE FOR P_u/P_o = 0.7

ALL COLUMNS

$$(EI)_c = \frac{ML_c^2}{3(\Delta - \frac{ML_c}{3K_b})} \tag{4.8}$$

where $$K_b = \frac{(EI)_b}{L_b} \tag{4.9}$$

From Equation (3.25)

$$M_r = K\theta M_u = \frac{3(EI)_b}{L_b}\theta \tag{4.10}$$

$$\therefore K_b = \frac{KM_u}{3} \tag{4.11}$$

The moment M is given by Equation (4.2).

Fig. 4.26 shows a typical load-deflection diagram. If this structure had been loaded up to point B the elastic load-deformation relationship corresponding to failure would be given by the line OB. If, on the other hand, the allowable or ultimate deflections limit the ultimate load on the structure to that corresponding to point A the ultimate deflection would be Δ_1 rather than Δ_2 given by the EI based on line OB. This overestimate will result in a corresponding overestimate of the P-Δ moments, in this idealized case of about 60 percent. Similarly, if a point below A is chosen for computing the equivalent stiffness, an unsafe estimate of deflections and second-order moments will result.

The discrepancies pointed out above will normally be severe only for structures exhibiting a very ductile behaviour. For a load-deformation characteristic such as that shown in Fig. 4.6 only minor errors would occur.

It will be appreciated from the above discussion that choosing the correct point on the load-deflection diagram to define EI will

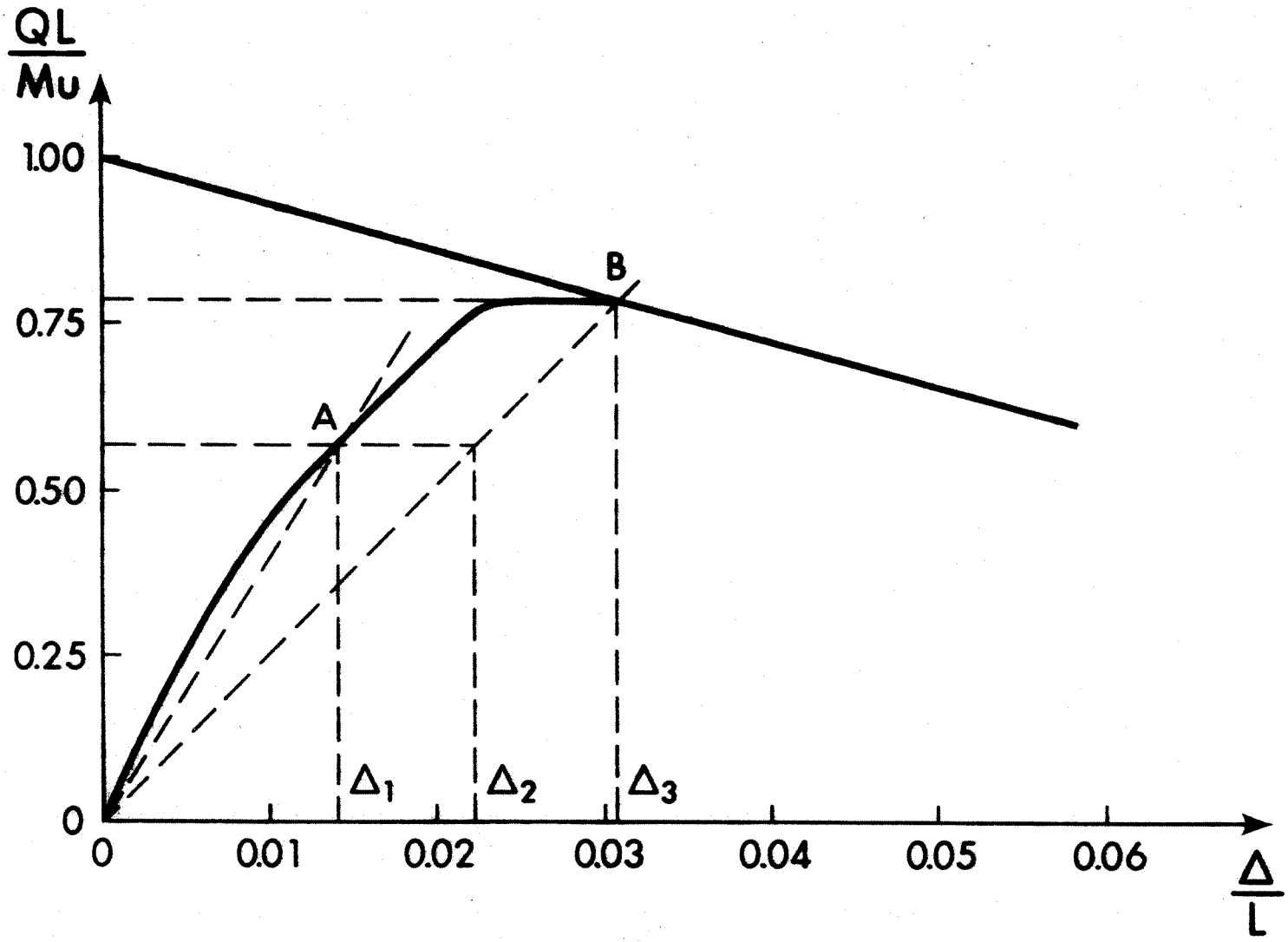

FIG. 4.26 EFFECTIVE STIFFNESS RELATED TO THE LOAD-DEFLECTION RESPONSE

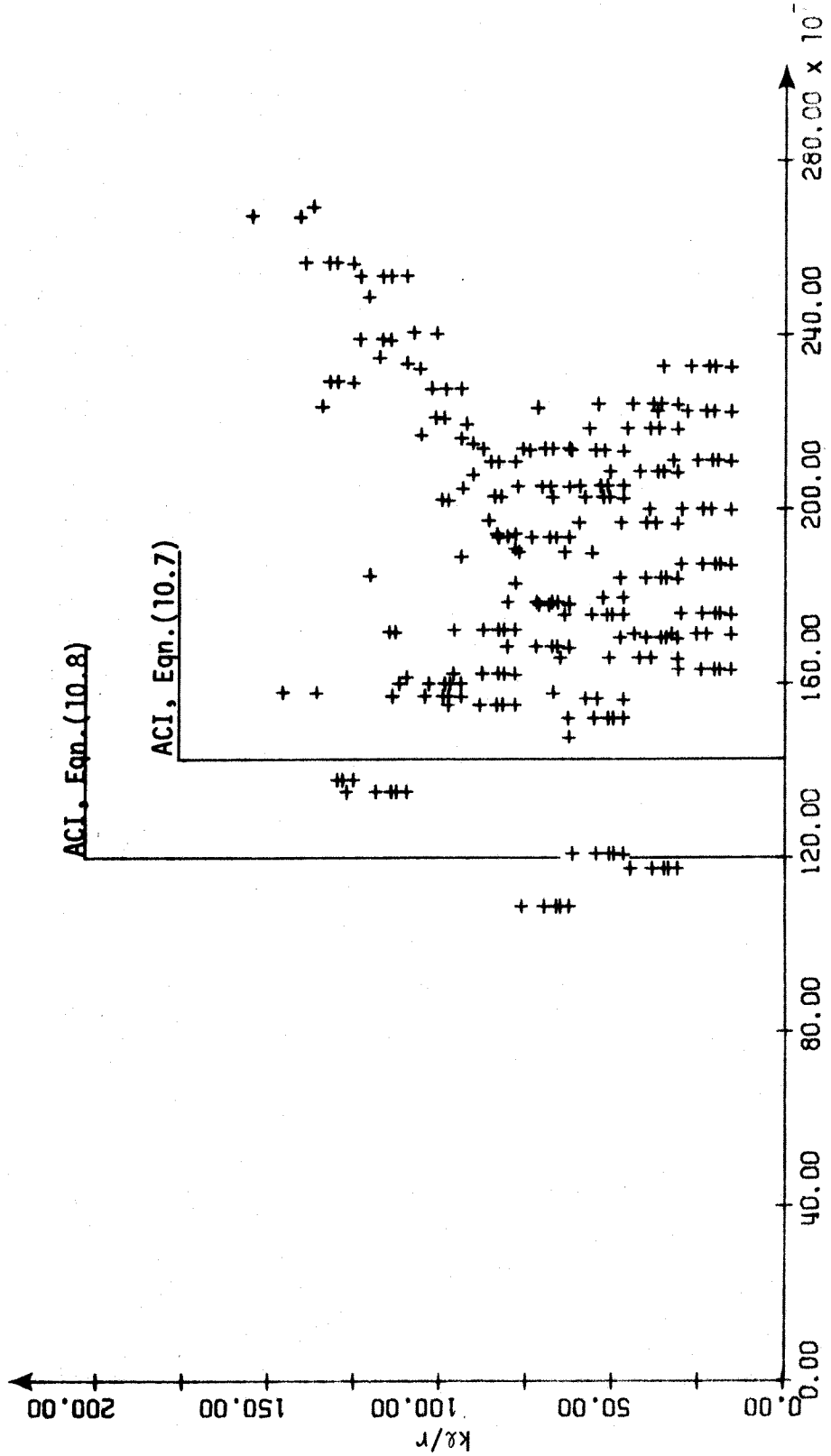

FIG. 4.27 EFFECTIVE STIFFNESS VALUES FOR TIED COLUMN, BARS IN TWO FACES MATERIAL AND STABILITY FAILURES

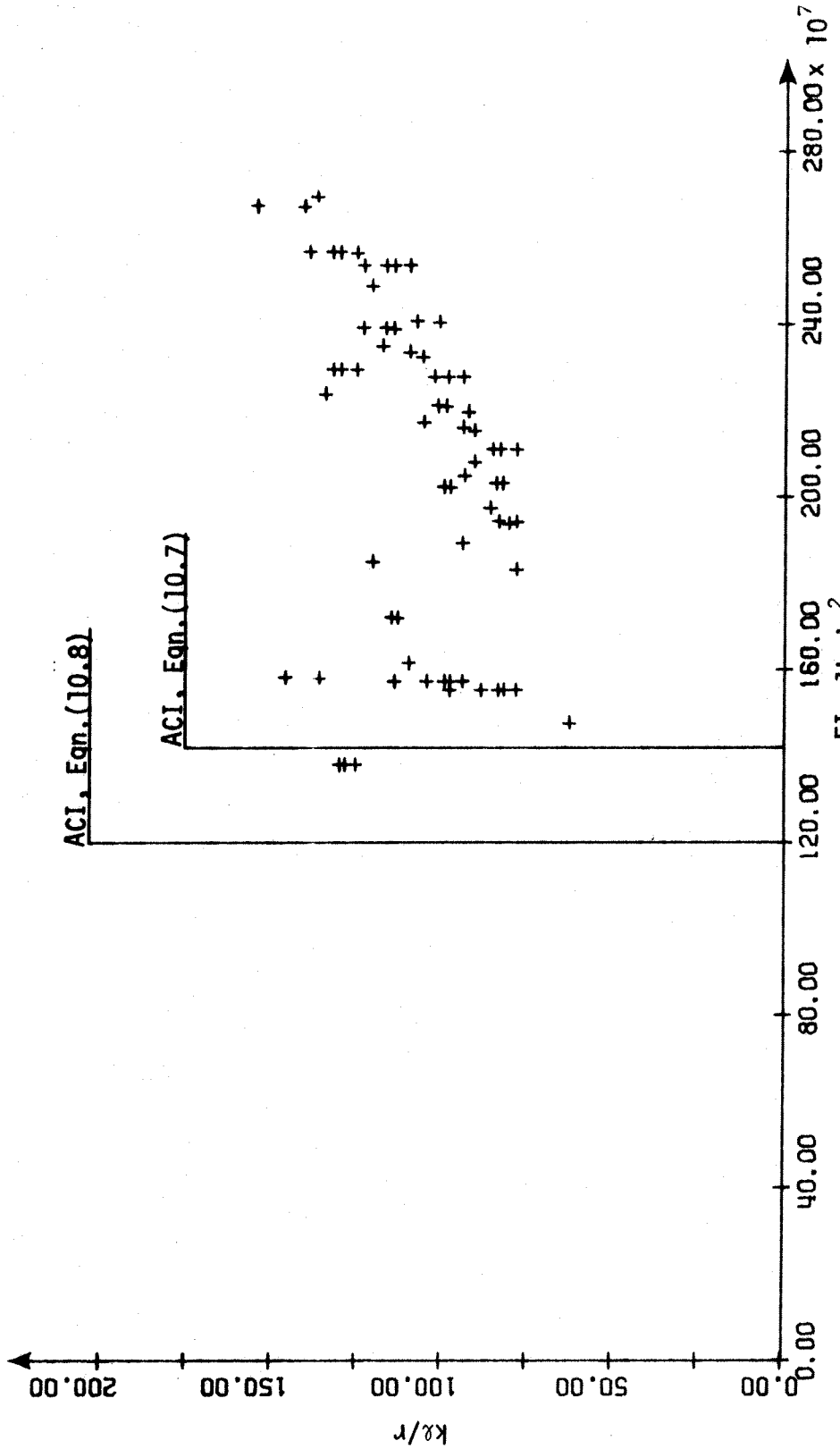

FIG. 4.28 EFFECTIVE STIFFNESS VALUES FOR TIED COLUMN, BARS IN TWO FACES

STABILITY FAILURES

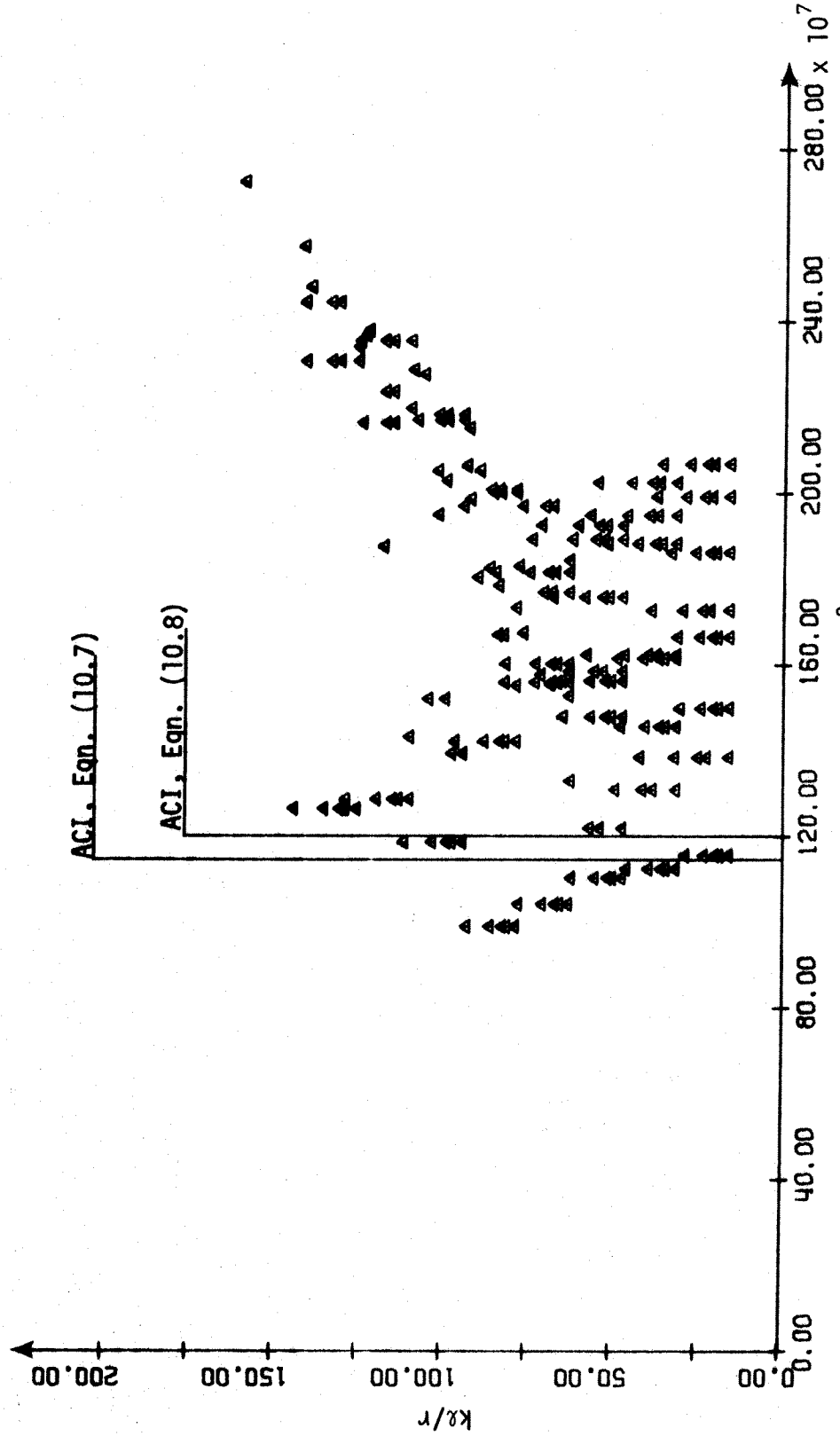

FIG. 4.29 EFFECTIVE STIFFNESS VALUES FOR TIED COLUMN, BARS IN FOUR FACES

MATERIAL AND STABILITY FAILURES

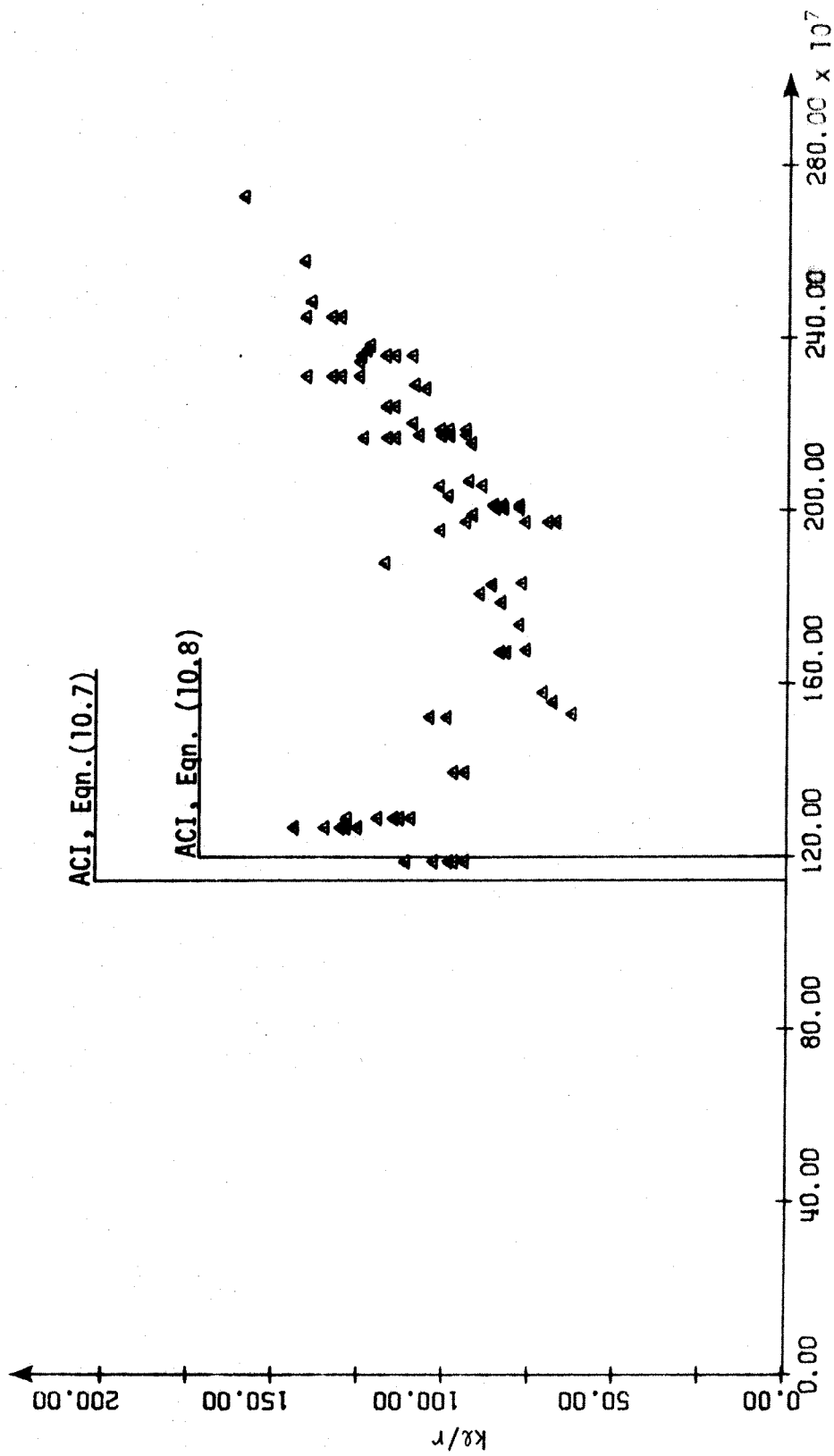

FIG. 4.30 EFFECTIVE STIFFNESS VALUES FOR TIED COLUMN, BARS IN FOUR FACES

STABILITY FAILURES

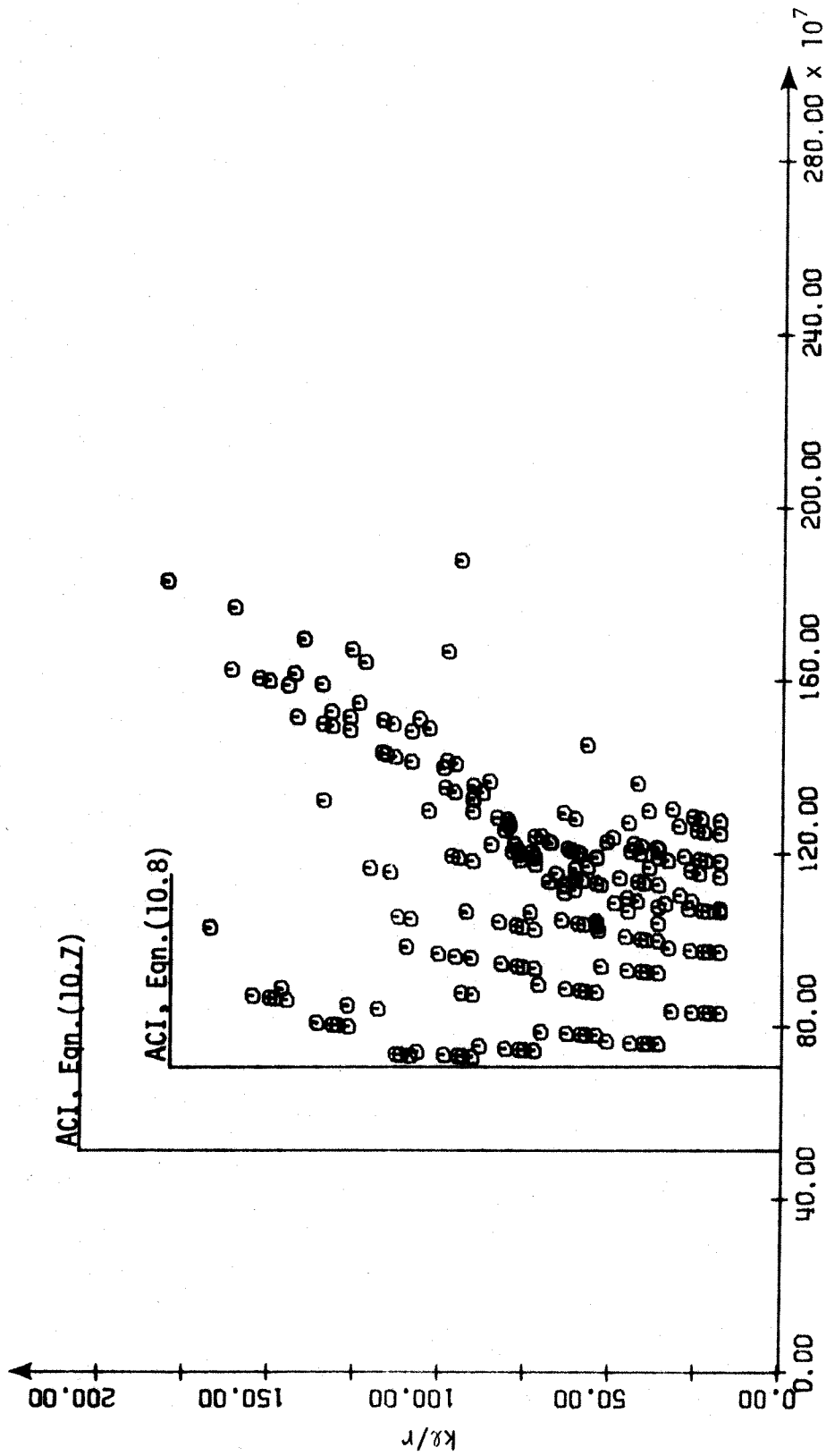

FIG. 4.31 EFFECTIVE STIFFNESS VALUES FOR SPIRAL COLUMN MATERIAL AND STABILITY FAILURES

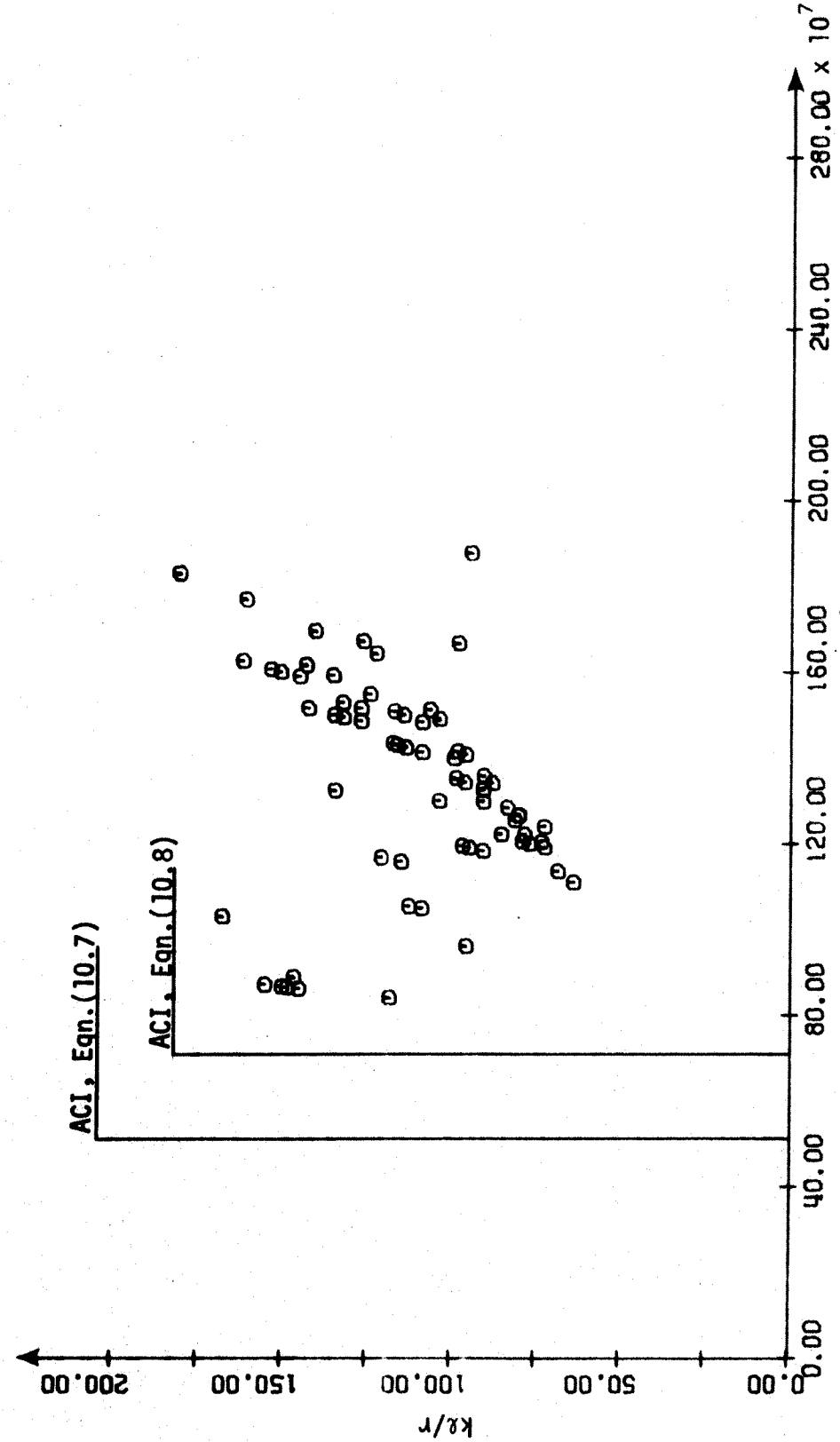

FIG. 4.32 EFFECTIVE STIFFNESS VALUES FOR SPIRAL COLUMN STABILITY FAILURES

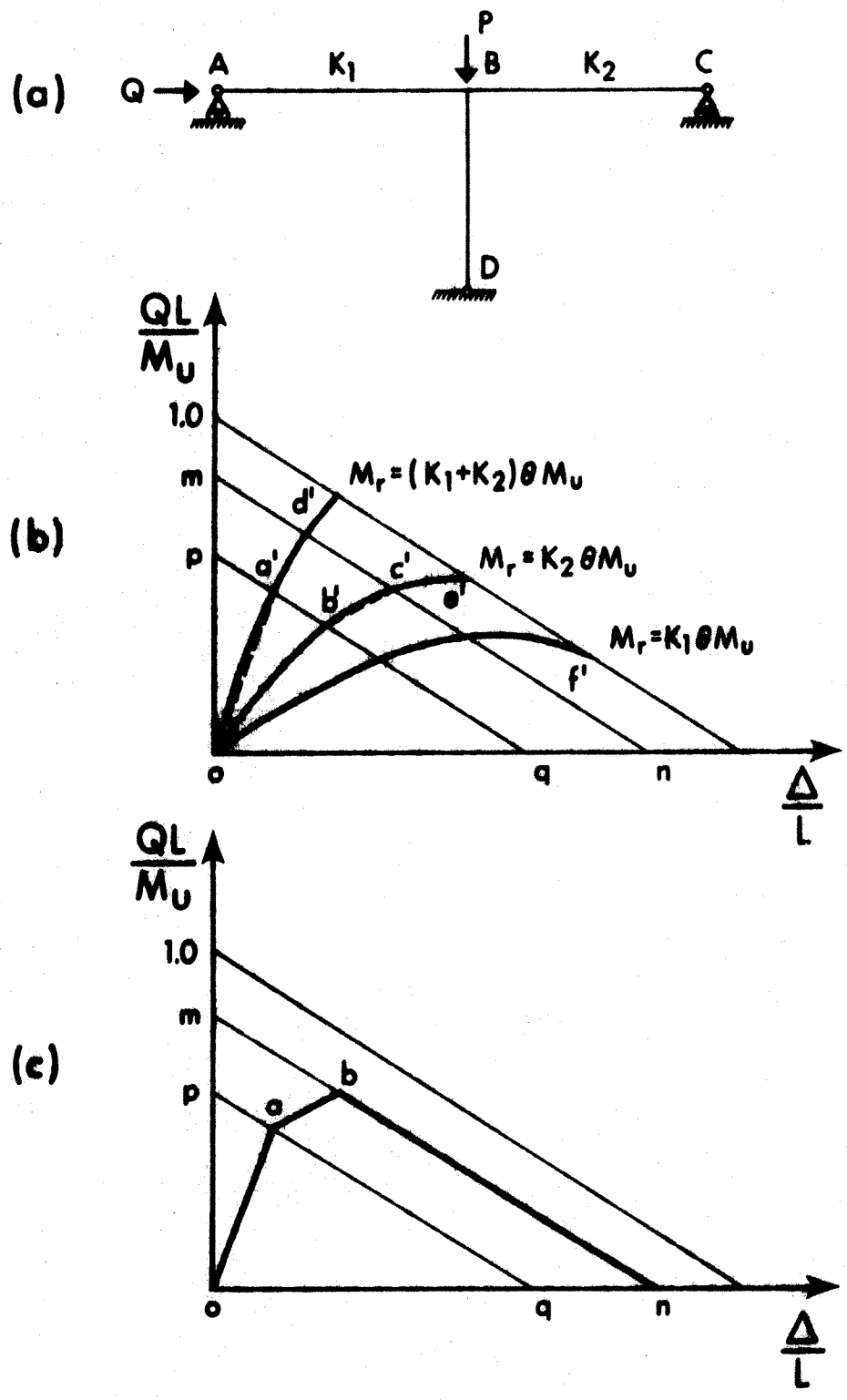

FIG. 4.33 CONSTRUCTION OF LOAD-DEFLECTION CURVE FOR SINGLE STORY INTERIOR SUBASSEMBLAGE

depend on several factors and becomes a complex matter. The point corresponding to the maximum value of QL/M_u was therefore chosen to be used in the calculations. This will always give conservative estimates of both first and second-order deflections.

The computed effective linear-elastic stiffness values have been plotted against slenderness ratio in the form of scatter diagrams in Figs. 4.27 through 4.32. A comparison with values computed from ACI 318-71 equations (10-7) and (10-8) shows that only a small number of the computed results are below the ACI values, and that for a large number of cases the code equations give extremely conservative results. The few cases where the effective EI is smaller than that computed from the ACI equations corresponded to low values of P_u/P_o. For $P_u/P_o < 0.2$ the most conservative of the ACI equations gives the best estimate of EI.

In the case of stability failures the columns tend to have rather high stiffness because the curvature at failure is relatively small and thus the effect of cracking is less severe. High EI values were also found to occur for material failures when the axial load was fairly close to the balanced load.

It should be noted that the ACI Moment Magnifier procedure treats stability failures as material failures. To do this it is necessary for the EI value for use in the ACI procedure to be based on the point of intersection of the load deflection curves with the sloping curve representing the cross-sectional strength. Thus, in the case shown in Fig. 4.4, the effective EI corresponding to the maximum value of QL/M_u (points along line mn) will be considerably larger than the EI corresponding to the eventual failure of the section (points along line ab).

4.7 Use of Sway Subassemblage Diagrams in Frame Analysis

The response of a story subjected to lateral loads and gravity loads can be determined by superposition of the response of each individual column in the story. In order to establish the column response the story is subdivided into a number of subassemblages as outlined in Section 2.6 and the load-deformation characteristics of each subassemblage is determined using the restrained column curves.

A typical subassemblage of an interior column in a single story frame is shown in Fig. 4.33(a). The restraining action provided by the beams is $K_1\theta M_u$ for beam AB and $K_2\theta M_u$ for beam BC. The restrained column curves relevant to this subassemblage are shown in Fig. 4.33(b). Line o-d$'$ is the restrained column curve for a column restrained by both beams, line o-f$'$ and o-e$'$ are for the same column restrained only by beam AB or only be beam BC, respectively. The lines m-n and p-q correspond to the formation of plastic hinges in beam BC and beam AB respectively.

The load-deflection curve for the subassemblage has been constructed in Fig. 4.33(c). Initially, the load-deformation response is given by the line Oa which is parallel to Oa$'$ in Fig. 4.33(b). At 'a' a plastic hinge forms in beam AB and a further increase in load is resisted only by the beam BC. The line ab is parallel to the line b$'$c$'$ in Fig. 4.33(b). At 'b' a plastic hinge is formed in the beam BC as well and the structure becomes unstable. Thus the ultimate load capacity of this subassemblage is given by point b.

If either one or both of the beams had a moment capacity equal to or greater than that of the column the load-deflection curve would reach the upper inclined line. If neither beam developed hinges the load deflection curve would be given by oa$'$d$'$, and if only the weaker beam

developed a hinge the line ab would be replaced by b' c' e'.

When the load-deflection curve has been constructed for all subassemblages in a story the total shear resistance may be determined by a graphical super-position of the individual load-deflection curves.

In a multi-story frame the overturning moment produced by the column above must be considered (see Section 3.5.1 and Fig. 3.11). If restrained column curves based on the model in Fig. 4.2 are to be used for a multi-story frame a modification must be made to the beam stiffness K. From Equations (3.23), (3.25) and (4.1) the following two expressions for the joint rotation θ are obtained for a single-story and a multi-story frame respectively:

$$\theta = \frac{M_n}{KM_u} \tag{4.12}$$

$$\theta = \frac{2M_n}{KM_u} = \frac{M_n}{(\frac{K}{2})M_u} \tag{4.13}$$

Thus, for a multi-story structure the sway subassemblage load-deflection curves should be based on restrained column curves corresponding to a beam stiffness of one half of the actual beam stiffness.

References 17,34 and 35 present design examples and design aids for the design of multi-story steel structures by the subassemblage method. These design curves differ from those presented here in that they are based on the assumption that an upper column frames into the joint and thus, if the curves are used for a single story frame the curve corresponding to a beam twice as stiff as the actual beam should be used to determine the load-deflection response.

CHAPTER V

EFFECTIVE STIFFNESS OF REINFORCED CONCRETE BEAMS

5.1 Introduction

No firmly established method exists for computing the effective stiffness of reinforced concrete beams. Various approximate methods are used in practice, some of which sacrifice accuracy for simplicity.

However, a reasonable accuracy in the estimate of the restraining action of the beams is essential in any second-order analysis and some guidelines are therefore required for its computation.

In this chapter the effective stiffness of reinforced concrete beams will be studied for various loading conditions and loading intensities. An attempt will be made to establish some simple rules which may be used in second-order analysis.

5.2 Method of Analysis

A cracked reinforced concrete beam behaves as a beam having a varying moment of inertia along its length. The effective moment of inertia at any section of the beam is a function of the bending moment at the section and may also depend on the loading history of the structure.

To account for the effect of the change in bending moment along the beam the beam was divided into a number of small segments such that the bending moment in each segment is approximately constant. Thus it is assumed that the distribution of cracks is uniform throughout each segment.

If the moment-curvature relationship of the cross-section is

known the stiffness of a segment having a certain bending moment is easily obtained as the slope of the moment-curvature diagram at the point being considered. To simplify the computation of the slope, the M-ϕ curve was approximated by a number of straight lines as previously outlined in Section 3.4.4.

The moment capacity of the cross-section was assumed to be reached when the tension steel yielded, thus ignoring the effect of strain hardening. This assumption gave failure moments in close agreement with values obtained from standard design formulae for computing ultimate moments.

The moment in each segment was assumed to be the mean of the moments at the ends of the segment and from the M-ϕ curve the stiffness, EI, corresponding to the mean moment was determined. The flexibility coefficents were obtained by loading the beam with the M/EI diagram corresponding to unit end moments and applying the conjugate beam theorems to compute the resulting end rotations. The rotational stiffness coefficients were then established by inverting the flexibility matrix.

It should be noted that the distribution of moments was a function of the distribution of stiffnesses which in turn were a function of the distribution of moments. An iteration procedure was required to reach a distribution of moments and stiffnesses which were compatible with the applied loads. The rotational stiffnesses were calculated based on the final distribution of stiffnesses.

It was found that the redistribution of moments did not cause significant changes in the stiffness values. This could also be anticipated by considering the idealized shape of the M-ϕ curve

since only elements which initially had a moment value close to points of discontinuity would have its stiffness affected by a change in moment. The idealized M-ϕ curves have only one or two points of discontinuity and as a result only the stiffnesses of a few elements are affected by the redistribution of moments.

Effective stiffness values were computed for three loading conditions:

1. gravity load only.
2. lateral load only.
3. gravity load and lateral load combined.

Each case was investigated for various values of load intensity.

The load intensity may conveniently be expressed as a function of the end segment moment capacity. In the case of gravity load the beam was assumed to have fixed ends and the nominal fixed-end moment M_{GM} may be expressed as

$$M_{GM} = \frac{wl_b^2}{12} = \eta M_u \tag{5.1}$$

where w is the uniformly distributed load on the beam, l_b is the length of the beam, M_u is the moment capacity of the end segment and η is a coefficient which may have values between zero and one.

The end moments, M_{SM}, caused by lateral loads can be written as

$$M_{SM} = \mu M_u \tag{5.2}$$

where μ is a coefficient varying between zero and one.

For combined loads the applied end moment at the most heavily loaded end is given by

$$(M_{GM} + M_{SM}) = - (\eta + \mu) M_u \tag{5.3}$$

and at the other end

$$(M_{GM} - M_{SM}) = (\eta - \mu)M_u \qquad (5.4)$$

assuming counterclockwise moments to be positive and the lateral load to be applied from left to right.

5.3 Effective Stiffness of T-Beams and Rectangular Slabs

Two different shapes of cross-section were considered in the analysis, a T-section and a rectangular flat slab section (Figs. 5.1 and 5.2).

The T-section had a total depth of 22.5 inches and a web width of 13 inches. The flange was 4.5 inches deep and 78 inches wide. The effective span was 25 feet. The slab was 12 inches wide, 7.5 inches deep and had an effective span of 18 feet.

Both members were symmetrically reinforced about the centre line and were divided into two end sections and a middle section. All three sections had equal amounts of top and bottom reinforcement, the ends being more heavily reinforced than the middle. The details of the cross-sections are shown in Fig. 5.1 and Fig. 5.2.

Typical M-ϕ diagrams obtained for the T-section and the slab are shown in Figs. 5.3 through 5.5. Fig. 5.3 shows the response of the T-section when loaded such that the flange is in compression while in Fig. 5.4 the flange is loaded in tension. The latter case shows a large and sudden drop in moment capacity as cracks develop in the flange. However, this is an artificial equilibrium condition which shows up in the computations because the moment capacity is computed from predetermined increments in the curvature. The transition line from the point of cracking to the point TY was used in the

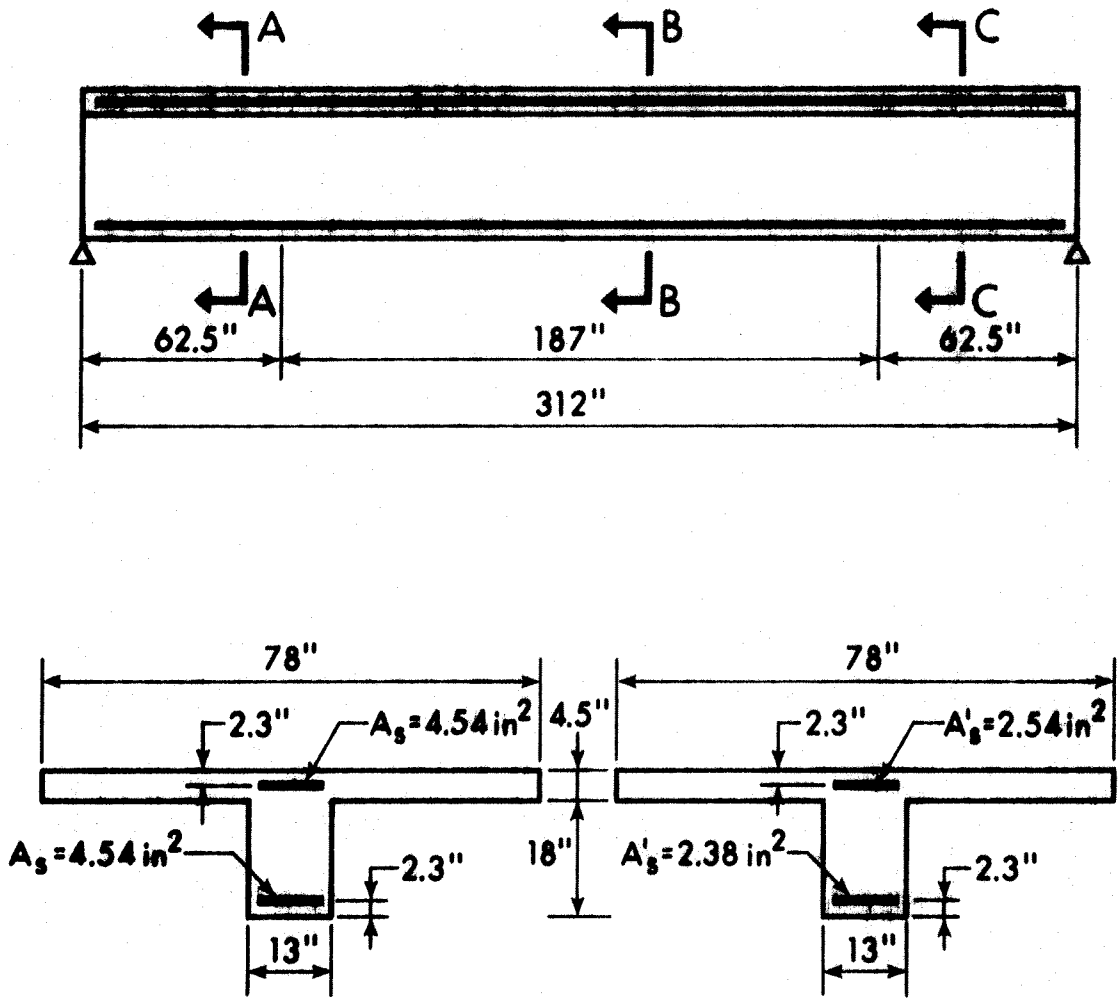

FIG. 5.1 T-BEAM FOR STIFFNESS ANALYSIS

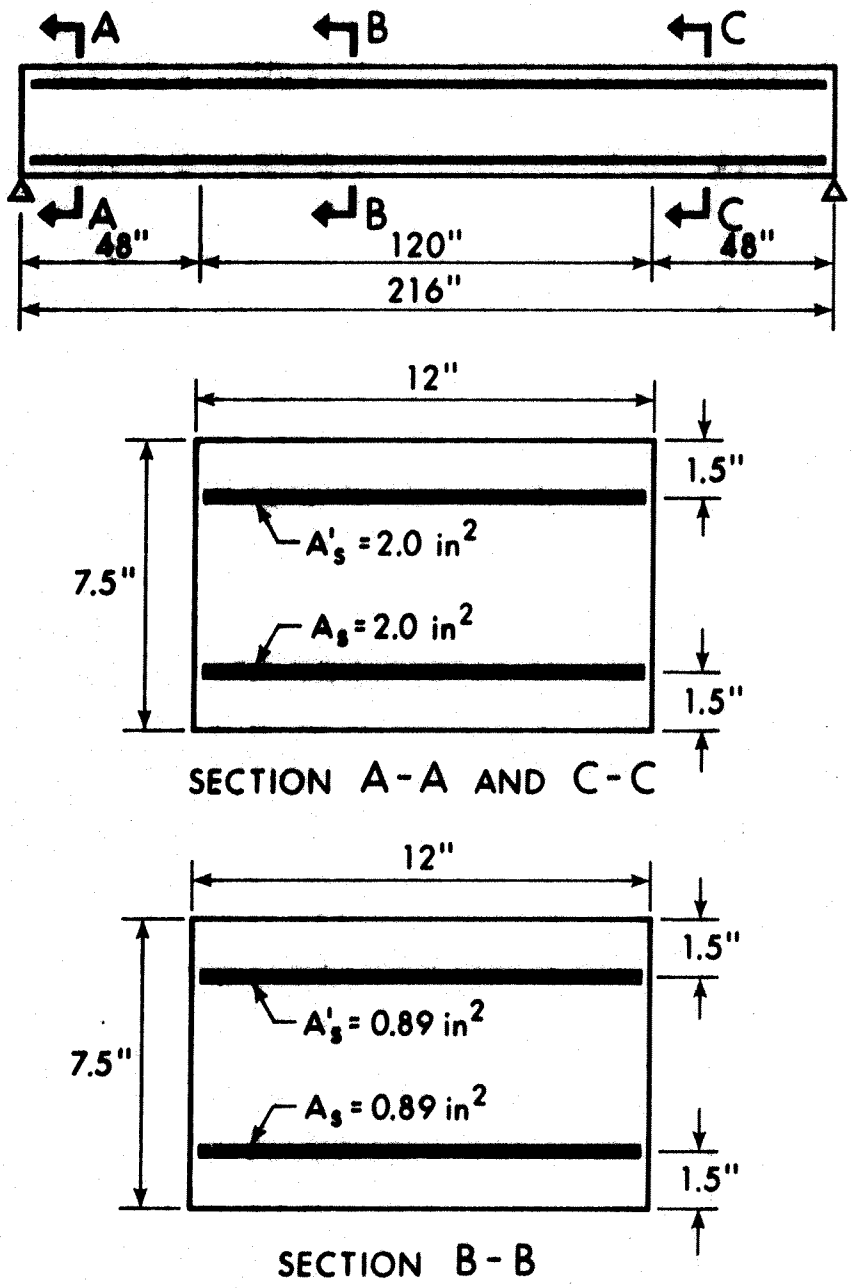

FIG. 5.2 SLAB FOR STIFFNESS ANALYSIS

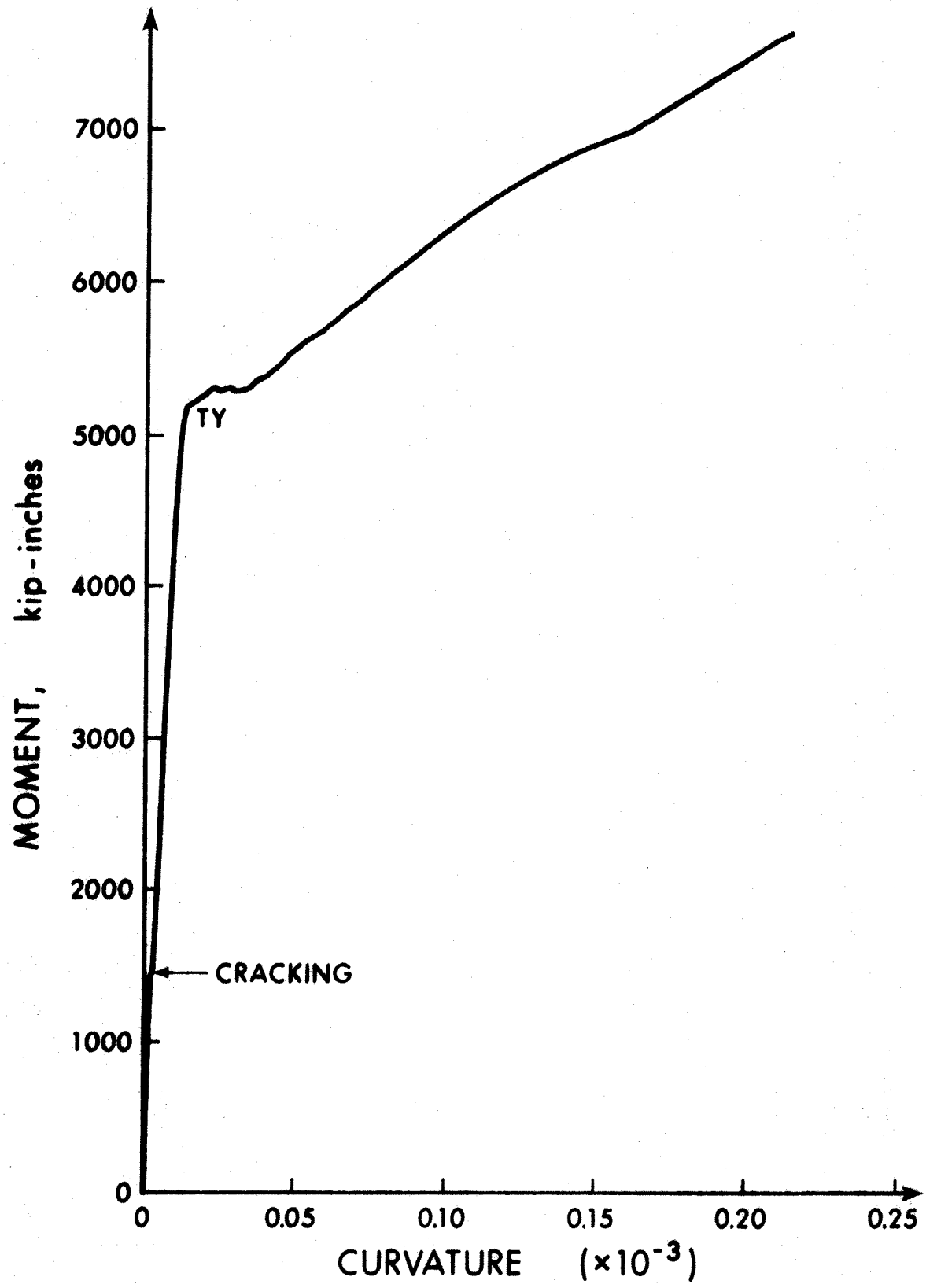

FIG. 5.3 M-ϕ DIAGRAM FOR T-SECTION WITH FLANGE IN COMPRESSION

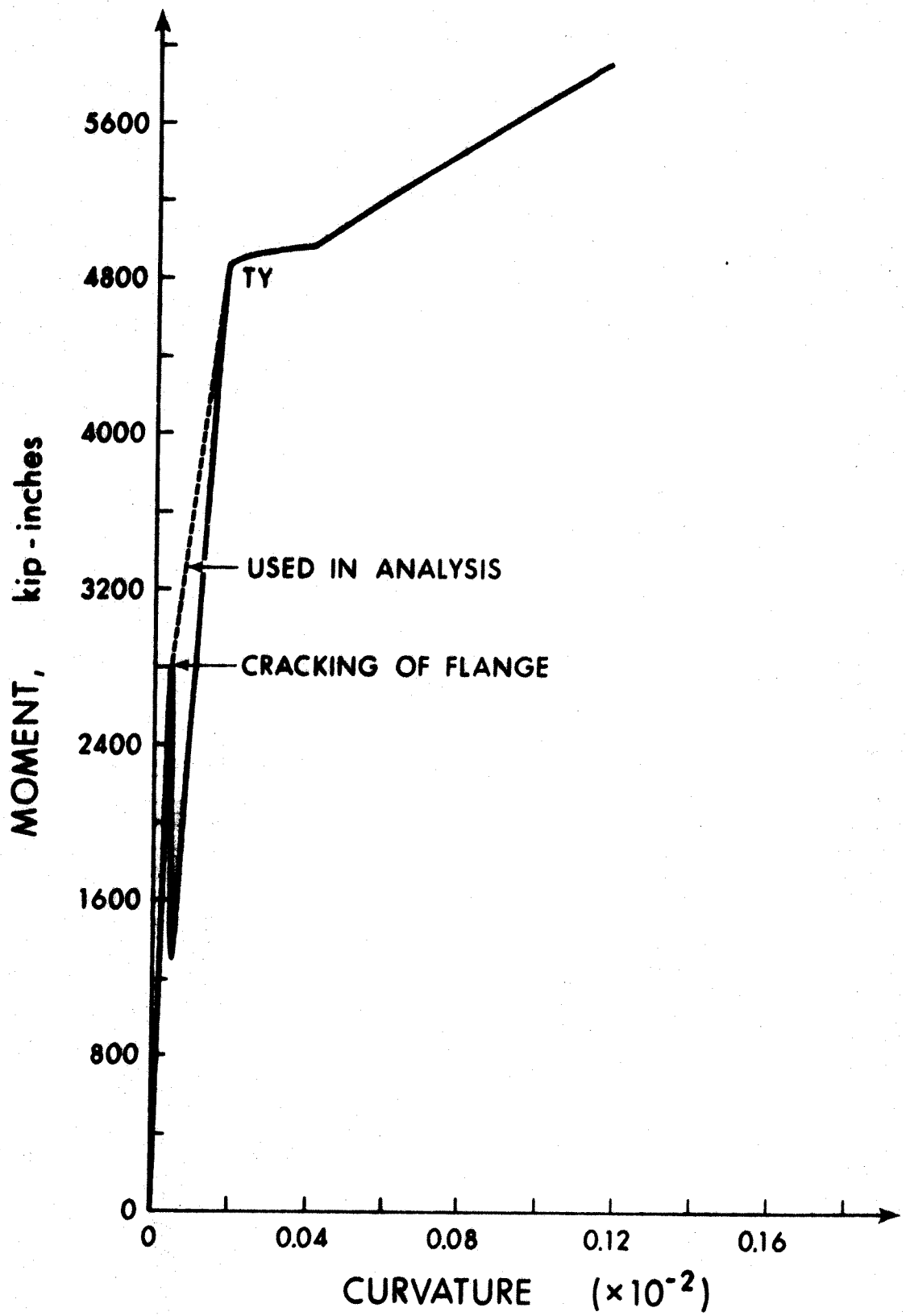

FIG. 5.4 M-ϕ CURVE FOR T-SECTION WITH FLANGE IN TENSION

computations. Fig. 5.3 shows a similar decrease in stiffness after the initiation of cracking, but the transfer is much smoother. The M-ϕ response of the slab shown in Fig. 5.5 is similar to that of the T-section with the flange in compression.

A few trial calculations were carried out to investigate what length of segments should be used to attain sufficient accuracy. It was found that for a given length of segment the accuracy was dependent upon the type of loading, and the largest inaccuracies seemed to occur for combined gravity and lateral loads. If high accuracy is sought a fairly short segment length should be used.

In these calculations 40 segments were used for the T-beam and 72 segments for the slab.

The results of the calculations have been plotted in Fig. 5.6 for the T beam section and Fig. 5.7 for the slab section. Considering the members under pure gravity load (Figs. 5.6a and 5.7a) shows clearly the reduction in stiffness as the load intensity is increased and the cracked zones extend.

The T-beam is seen to keep 95 percent of its uncracked, untransformed stiffness $E_c I_g$, for values of η below 0.5. For higher loads the stiffness is reduced rapidly and for $\eta = 0.9$ it has dropped to 46 percent of the uncracked stiffness.

The effects of cracking become evident at fairly low load levels for the slab and once the first cracks have opened up there is a rapid decrease in stiffness. However, as the load intensity is increased the rate of stiffness reduction is reduced. When the moment at the ends has reached 90 percent of the capacity of the end segment the stiffness has dropped to 53 percent of the uncracked stiffness.

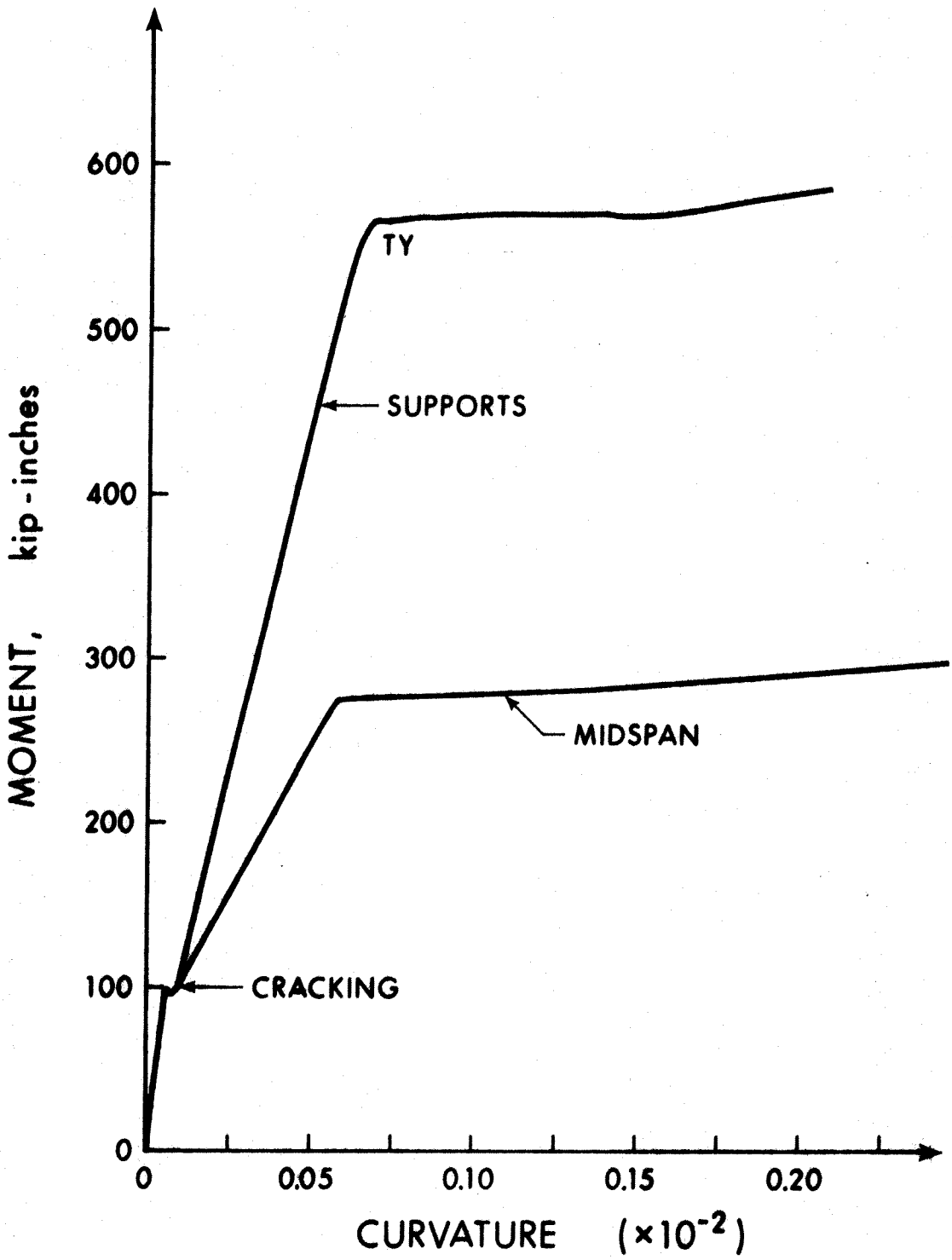

FIG. 5.5 M-ϕ CURVE OF SLAB CROSS-SECTION

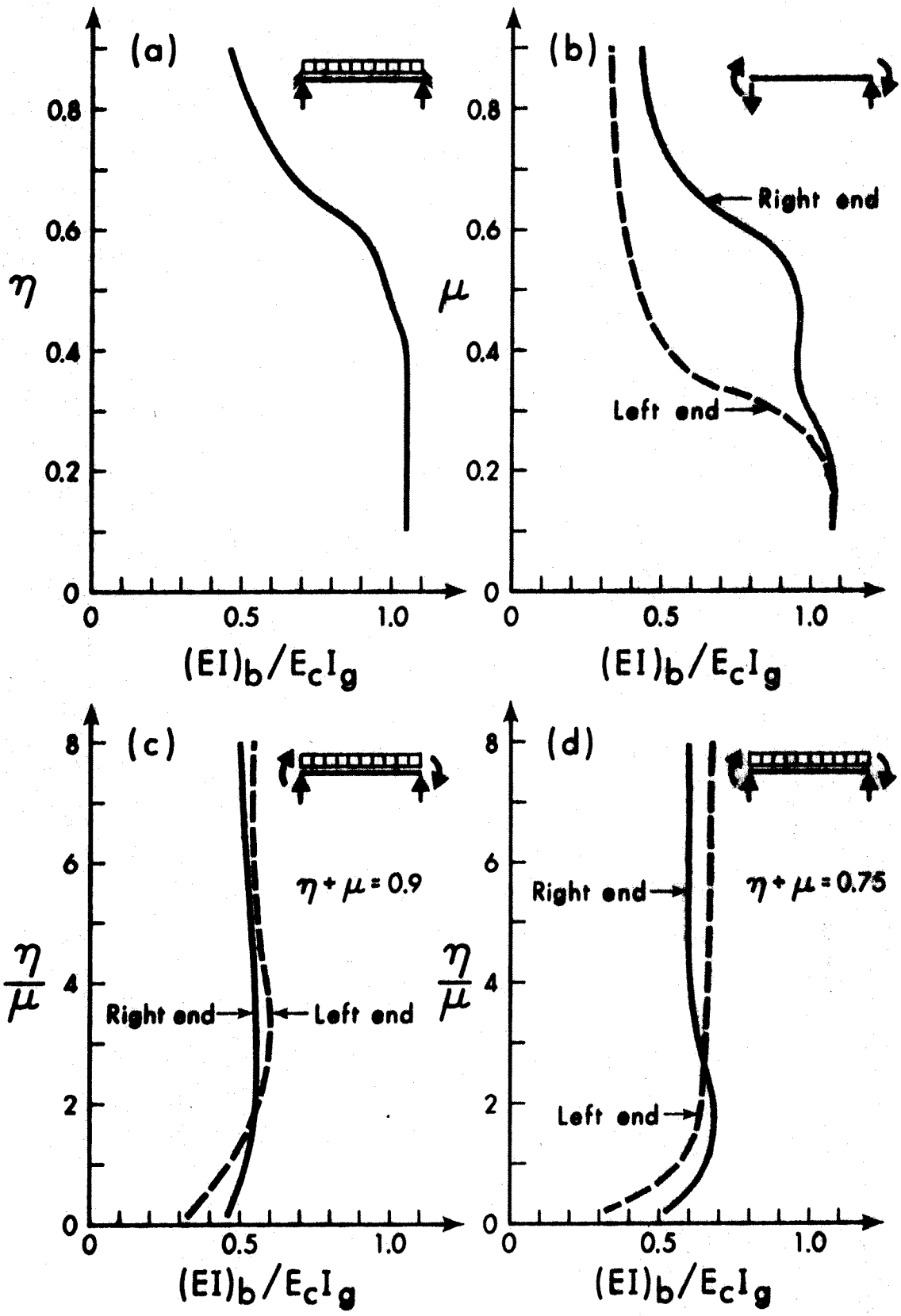

FIG. 5.6 EFFECTIVE STIFFNESS VALUES OF T-BEAM

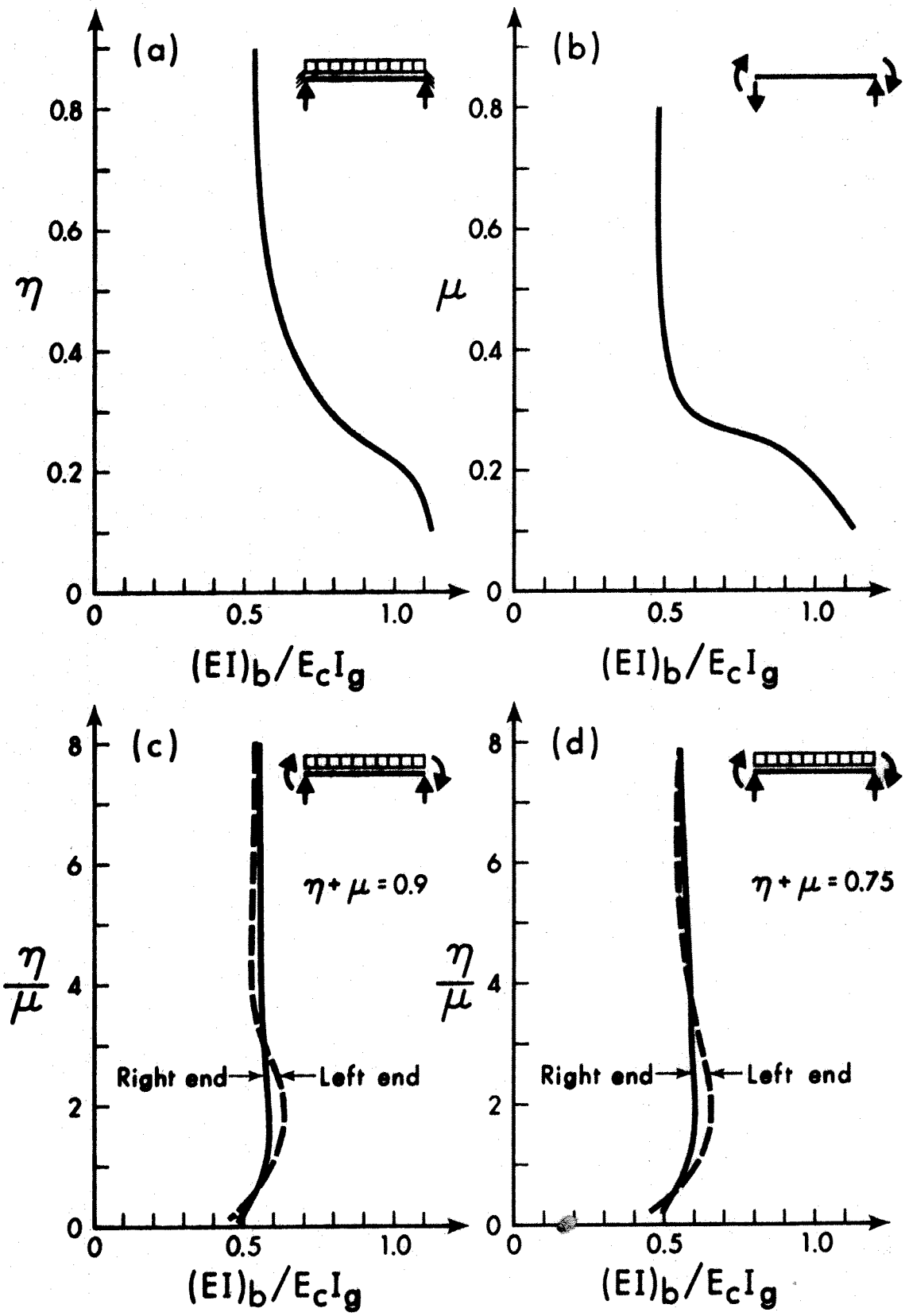

FIG. 5.7 EFFECTIVE STIFFNESS VALUES OF SLAB

In a second-order analysis the beam will be loaded according to load case 3. The variation in stiffness for various combinations of fixed end moment and sway moment is shown in Fig. 5.6(c),(d) and Fig. 5.7(c),(d) for two values of load intensity. The plots show only small variations in stiffness with variations in the ratio η/μ. For very small values of η/μ, say below 1.0, corresponding to high lateral load moments and small gravity load moments it would be more appropriate to use value from load case 2, i.e. sway moments only, as shown in Fig. 5.6(b) and Fig. 5.7(b). As one would expect, reducing the load intensity $(\eta+\mu)$ results in higher stiffness values, although for the slab this increase is negligible. In practice one would expect to find values of $(\eta+\mu)$ in the range 0.75 to 0.90 and the results presented herein suggest that values of $(EI)_b$ between 0.5 and 0.6 times E_cI_g may be used for this type of loading condition if η/μ is greater than 1.0.

The steel percentage will of course affect the stiffness of the member to some extent. This maybe taken into account by expressing $(EI)_b$ as

$$(EI)_b = E_c\ (aI_g + nI_s) \qquad (5.5)$$

where a is a coefficient, n is the modular ratio of steel and concrete and I_s is the moment of inertia of the reinforcement about the neutral axis of the gross concrete section.

For load case 3 and η/μ greater than 1.0 the value of the coefficient 'a' may be taken as 0.2 for the T-beam and 0.15 for the slab. For a modular ratio of 8 this gives the stiffness values $0.496E_cI_g$ for the T-beam and $0.53E_cI_g$ for the slab.

The effective moment of inertia of T-sections is often

expressed in terms of the moment of inertia of the web alone, I_w. In this case the ratio I_g/I_w is equal to 2.0 and the effective $(EI)_b$ is therefore between 1.0 and 1.2 times E_cI_w. This is somewhat lower than a commonly accepted [36] assumption that $(EI)_b=2(E_cI_w)$ and higher than a method assuming the effective flange width equal to twice the web width[37]. $2(E_cI_w)$ is equivalent to an effective flange width of about three times the web width.

The stiffness parameter K, used in the sway subassemblage analysis, may be computed for these beams by using Equation (4.11). The moment capacity of the column, M_u will be assumed to vary between 828 k-in and 300 k-in (Type 1 column, see Fig. 4.1 and Table 4.1). The T-section will then have K values varying from about 500 to about 2000 before cracking and only about one half of these values after cracking. For the slab the values vary between 50 and 140 before cracking and again about one half of these values after cracking.

CHAPTER VI

ANALYSIS OF MULTI-STORY FRAMES FOR STABILITY EFFECTS

6.1 Introduction

There are two types of stability failures that may be encountered in a frame analysis. One is known as "bifurcation of equilibrium," or buckling, and occurs when the applied axial load reaches the critical buckling load. The other type is referred to as "instability through disturbance of equilibrium" and occurs because equilibrium between external and internal forces cannot be achieved due to such things as imperfections and reduction in stiffness. This type of instability occurs for an axial load smaller than the bifurcation load of the member. In sway frames where the members exhibit a load-deformation response as shown in Fig. 6.13(a), sidesway instability will occur before the ultimate moment has been reached. When instability occurs, a small increment in the lateral load produces additional $P\Delta$ moments, which in turn cause additional deflections. Because the applied moment is a function of the lateral deflection and because the stiffness decreases with increasing moments, the required internal moment resistance is not achieved. The $P\Delta$ effect is, therefore, a key parameter which must be considered in the analysis of sway permitted frames.

Modern building codes attempt to predict stability failures by means of simple approximate methods. The accuracy of these methods may be quite good in some cases, while in others they are highly inaccurate but generally conservative.

A rigorous stability analysis of reinforced concrete frames

is a rather complicated matter due to such things as the non-linear load-deformation relationships of concrete columns and beams and the effect of the steel percentage and axial loads on the member stiffness. A general method which would give good accuracy in all cases would have to consider the effect of these variables, resulting in a very complicated procedure.

The subassemblage procedure provides a good method for predicting instability and the results from such an analysis will be used as a basis for comparison when investigating the applicability of current procedures for second-order analysis.

6.2 Sway Preventing Action in Frames

Prior to embarking on the design of columns in a frame by traditional means it is necessary to determine whether the frame is braced or unbraced since the behaviour of these two types of frames differs greatly. The problem is how much lateral restraint is required to allow a frame to be designed as a braced frame.

The ACI Code Commentary[2] states that the bracing elements (shear walls, trusses, etc.) should have a lateral stiffness of at least six times the lateral stiffnesses of all the columns in the story being considered. This requirement may not apply equally well to all structures, however.

A more rational evaluation of the sway preventing action in frames has been presented by Lay [38,39]. The analytical model used by Lay is shown in Fig. 6.1. The end conditions of the column are represented by the rotational stiffness coefficients k_A and k_B, and the translational stiffness coefficient k_s. The restraining actions at the end

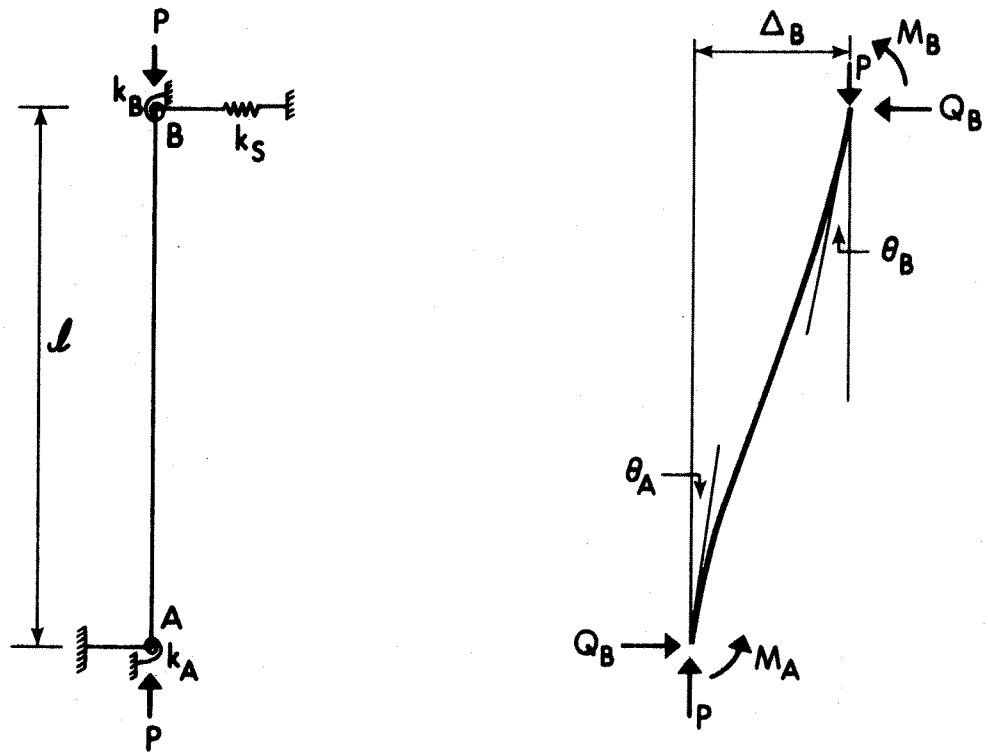

FIG. 6.1 LAY'S MODEL FOR INVESTIGATING SWAY PREVENTING ACTION IN FRAMES

of the member can be written as

$$M_A = k_A \frac{EI}{L} \theta_A \tag{6.1}$$

$$M_B = k_B \frac{EI}{L} \theta_B \tag{6.2}$$

$$Q_B = k_s \frac{EI}{L^2} \left(\frac{\Delta}{L}\right) \tag{6.3}$$

The equilibrium equation is

$$P\Delta = M_A + M_B + Q_B L \tag{6.4}$$

M_A and M_B may be determined from the slope-deflection equations and substituted into Equation 6.4.

The solution is then:

$$k_s = \pi^2 \left(\frac{P}{P_{cr}}\right) - s(1+c) \frac{2+s(1-c)\left(\frac{1}{k_A} + \frac{1}{k_B}\right)}{1+s\frac{1}{k_A} + \frac{1}{k_B} + \frac{s^2}{k_A k_B}(1-c^2)} \tag{6.5}$$

where P_{cr} is the buckling load, s and c are the standard slope-deflection coefficients modified for axial load and are given by Equations (6.6) and (6.7)

$$s = \frac{1-u \cot u}{\tan \frac{u}{2} - \frac{u}{2}} \left(\frac{u}{2}\right) \tag{6.6}$$

$$c = \frac{u \csc u - 1}{1 - \cot u} \tag{6.7}$$

$$u = \pi\sqrt{P}/P_E \tag{6.8}$$

$$P_E = \frac{\pi^2 EI}{l^2} \tag{6.9}$$

Lay[39] suggested three ways to use Equation (6.5) to investigate the sway stiffness necessary to ensure sway prevented action in

frames:

1. An exact evaluation of k_s using Equation (6.5)
2. If the numerator of Equation (6.5) is positive and k_A and k_B are both positive, which is always the case if $P/P_E < 1.0$, the lateral stiffness necessary to allow the column to reach its no-sway buckling load may be approximated by:

$$k_s \geq \pi^2 \frac{P}{P_{cr}} \tag{6.10}$$

This will give a conservative value of the critical k_s provided the rotational end restraints are positive. Negative end restraints will rarely occur in ordinary building frames due to the low axial load usually carried by the beams. Thus, this will be conservative provided that the numerator is positive, i.e.

$$2 + s(1-c)\left(\frac{1}{k_A} + \frac{1}{k_B}\right) \geq 0 \tag{6.11}$$

If the required lateral restraint exists according to Equation (6.5) or Equations (6.10) and (6.11) the effective length factor may be determined from the nomograph for braced frames. When doing so, Trahair's method[40] (Equation (6.21), Section 6.3.2) should be used to determine the parameter ψ. Because the frame is braced the effective lengths will be less than the actual lengths.

3. The buckling load may be approximated by Equation (6.10) without any further checks if the effective length is not taken less than the actual length.

The derivation of these stiffness criteria was based on a linear-elastic load-deformation relationship.

Telwar and Cohn[41] have suggested four bracing criteria for tall buildings containing shear walls:

1. To limit the deflections at service load to a value of 1/500th of the story height they proposed that:

$$\frac{P_{cr}}{P} \geq \frac{700\ Q}{P} + 1 \tag{6.12}$$

where P_{cr} is the critical load for the entire structure and Q and P are lateral and vertical service loads.

2. A stability criterion to ensure that the frame could be designed for gravity loads only was the basis of Equation (6.13):

$$\frac{P_{cr}}{P} \geq 20 \tag{6.13}$$

3. They also proposed that

$$\frac{P_{cr}^{w}}{P_{cr}} \geq 0.5 \tag{6.14}$$

where P_{cr}^{w} is the critical load for the wall standing on its own.

4. The fourth criterion was intended to prevent excessive moments due to unsymmetrical loading and for a pseudoelastic frame was expressed by Equation (6.15)

$$P_{cr}^{w} = \text{Max}\left[\left(\frac{1}{i}\right)\left(\frac{12k_c}{h}\right)\left(\frac{\bar{Q}^{f}}{\bar{Q}_c}\right)\right] \tag{6.15}$$

where i is the story under consideration (counting from the top), h is the story height, k_c is the EI/h for the column in the story carrying the greatest shear and $\bar{Q}^{f}$ and $\bar{Q}^{c}$ are the shears on the frame and the column, respectively. The third and fourth criteria are based on assumptions about desirable behaviour and may fail to

recognize the entire spectrum from fully braced structures through structures free to sway.

One or more of the criteria presented in this section may be used to evaluate the sway preventing action of the bracing elements in a frame before a method of analysis is decided upon.

A further study of the sway preventing action in frames is presented in Section 6.4.2.

6.3 Effective Length Factor Method

6.3.1 Introduction

Traditionally the effect of frame action has been accounted for in column design by means of effective length factors. This method has been described in Section 2.2. In this section the results obtained from this method will be compared to those obtained in the subassemblage analysis. Three factors are of prime interest; the effective length factor itself, the magnitude of the amplified moment and the mode of failure.

6.3.2 Some Remarks on the Effective Length Concept

In both the ACI column design method[1] and the CEB column design method [4] there are two very important parameters involved in determining the second-order effects, namely the stiffness, EI (or curvature in CEB), and the effective length factor k. The latter is a function of EI since it depends on the ratio of the sum of the stiffnesses of the columns framing into a joint to the sum of stiffnesses of all the beams framing into the same joint. This may be expressed as

$$\psi = \frac{\Sigma(EI/l)_c}{\Sigma(EI/l)_b} \qquad (6.16)$$

This expression is an approximation to enable the effective length nomographs to be used for irregular frame lay-outs.

Lay[39] has investigated the validity of this approximation and from an elastic slope-deflection analysis he developed the following expression for the relative stiffness parameter

$$\psi' = \frac{(EI/l)_{dc}}{\Sigma(\frac{EI}{l})_b + \Sigma\left[\frac{Ju}{Jo}(\frac{EI}{l})_b\right]} \tag{6.17}$$

where $(EI/l)_{dc}$ is the stiffness of the column being designed,

$$\frac{Ju}{Jo} = \frac{s(1-c)}{2} \text{ for braced frames} \tag{6.18a}$$

$$\frac{Ju}{Jo} = \frac{s(1+c)}{2} \text{ for sway frames} \tag{6.18b}$$

s and c are the slope-deflection stiffness coefficients including axial load effects as defined in Section 6.2.

Once the end stiffness ratios are computed the effective length factor, k, can be obtained from nomographs presented in Reference 2 or from approximate equations such as those given by Furlong[42] or in the British Standard Code of Practice CP110[43].

An examination of the nomographs shows that the value of k is reduced as the value of ψ is reduced, which in turn implies that the critical load of the column is increased. Thus it follows that the discrepancy between Equation (6.16) and Equation (6.17) will result in an unsafe estimate only when

$$\psi < \psi' \tag{6.19}$$

which will occur when

$$\Sigma\left[\frac{Ju}{Jo}(\frac{EI}{l})_{mc}\right] < (\frac{EI}{l})_{mc} \tag{6.20}$$

where the subscript mc refers to the upper column framing into the joint.

From Equation (6.18) it can be seen that this can only occur for braced frames and substitution of Equation (6.6.) into Equation (6.18a) shows that a second condition is that u (Equation 6.8) must be greater than π. Thus, Equation (6.16) will lead to a safe estimate of k in braced frames if $P < P_E$.

To simplify the use of Equation (6.17) Lay suggests that an approximate method developed by Trahair[41] may be used. This method approximates Equation (6.17) by the following expression

$$\psi' = \frac{(\frac{EI}{l}) \text{ column being designed}}{\Sigma(1-\frac{P}{P_E})(\frac{EI}{l}) \text{ all other members}} \qquad (6.21)$$

The term $(1-P/P_E)$ approximates the effect of axial load on the member stiffness and will normally be significant only for the columns since the beams usually have negligible axial load.

Although Equation (6.16) will give conservative results for sway frames Lay[39] suggests that the modified Equation (6.21) be used since there are considerable economic advantages to be gained from it.

Rosenblueth[44], MacGregor, Breen and Pfrang[3]and, Springfield and Adams[45] have pointed out shortcomings in the effective length concept in dealing with sway frames where the columns in a particular story have widely varying effective length factors. The extreme case of a pin-ended column supported by a sway frame occurs frequently. The nomographs suggest that the pin-ended column will not be able to carry any vertical load since $k = \infty$ because sway can occur, and therefore $P_{cr} = 0$ for the hinged member. Some modification of the method

must therefore be considered where ψ is very large for both ends of the member or where ψ varies widely between columns in a frame.

The 1971 ACI Code attempts to treat this case by replacing the P/P_{cr} term in the moment magnifier equation by the term $\Sigma P/\Sigma P_{cr}$ whose variations in effective length is recognized by treating the entire story as a unit[1,3].

6.3.3 Comparison of Results from the Moment Magnifier Method and the Subassemblage Analysis

The accepted practical procedure for determining the effective length factor, k, is to use the nomographs [2,46,16,34] mentioned in Section 6.3.2. The magnified moment, according to ACI 318-71, is then given by

$$M_c = \frac{M_2 C_m}{1 - \frac{P}{\pi^2 (EI)_c} (kl)^2} \tag{6.22}$$

where M_c is the magnified moment, M_2 is the first-order moment and C_m is an equivalent moment factor.

Equation (6.22) may be rearranged to give an expression for the effective length factor k, and using the subassemblage model in Fig. 4.2 it can be written as:

$$k^2 = \frac{\pi^2 (EI)_c}{Pl^2} \left[1 - \frac{Ql}{Ql + P\Delta} C_m \right] \tag{6.23}$$

Thus, the results from the subassemblage analysis may be used to compute the effective length factor which would have to be used in Equation (6.22) to give the correct second-order moment.

The quantity ψ needed to find the value of k from the nomographs is defined by Equation (6.16) with the denominator of the equation determined from Equation (4.10). The parameter $(EI)_c$ was

calculated according to Section 4.5.

In this case there is no upper column framing into the joint and thus Equation (6.16) is in agreement with Trahair's method, Equation (6.21).

The quantity C_m will be taken as 1.0 in this derivation according to ACI 318-71 rather than the value of 0.85 as given by an elastic analysis for the sway case. This gives values of k somewhat below the correct value. C_m is a function of the first-order deflection and since this is not known due to the non-linearity of the load-deflection curve, a precise value of C_m is difficult to obtain for reinforced concrete columns.

In Fig. 6.2 the effective length factors obtained from the nomographs and from the subassemblage analysis have been plotted against relative stiffness. The two curves show fairly good agreement, with the nomographs giving the higher values. The maximum percentage discrepancy between the two curves is about seven percent and occurs for low values of k. This percentage decreases with increasing k and for values of k about 3.5 the error is only one percent. If the correct value of C_m had been used, the effect would have been to bring the two curves closer together, which indicates that the nomographs predict quite well the length of the equivalent pin-ended column.

Figures 6.3 through 6.10 show the relationship between the short column interaction diagram (l/h=0), an interaction diagram for material or stability failure, taken as Point 1 in Fig. 6.13 (a) or (b) and a design interaction diagram based on the moment-magnifier procedure using Eqn.(6.22)and either the effective EI from Eqn(4.8) or the EI from ACI Eqn.(10-7). Results are plotted for values of end

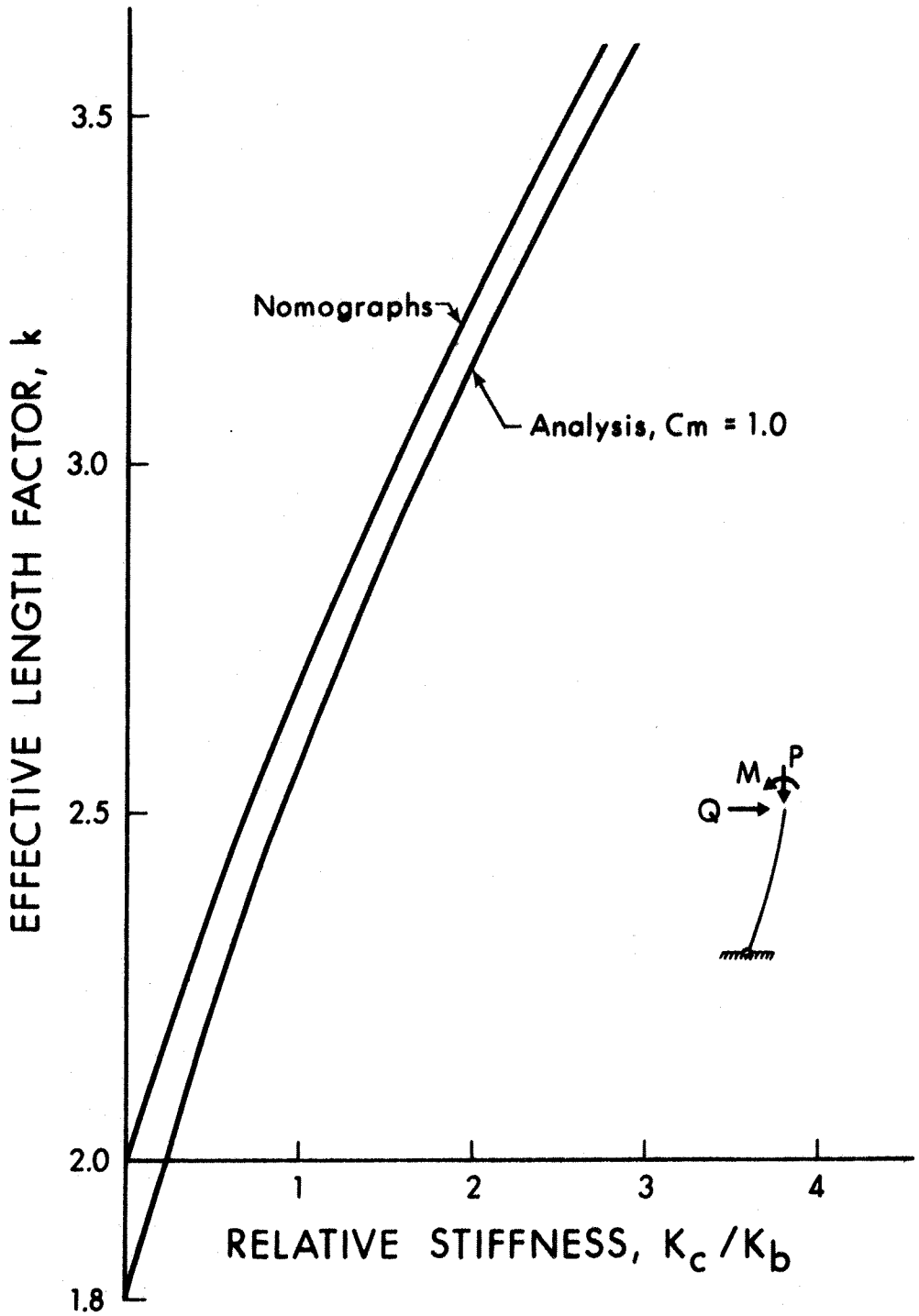

FIG. 6.2 COMPARISON OF EFFECTIVE LENGTH FACTORS OBTAINED FROM NOMOGRAPHS AND SUBASSEMBLAGE ANALYSIS

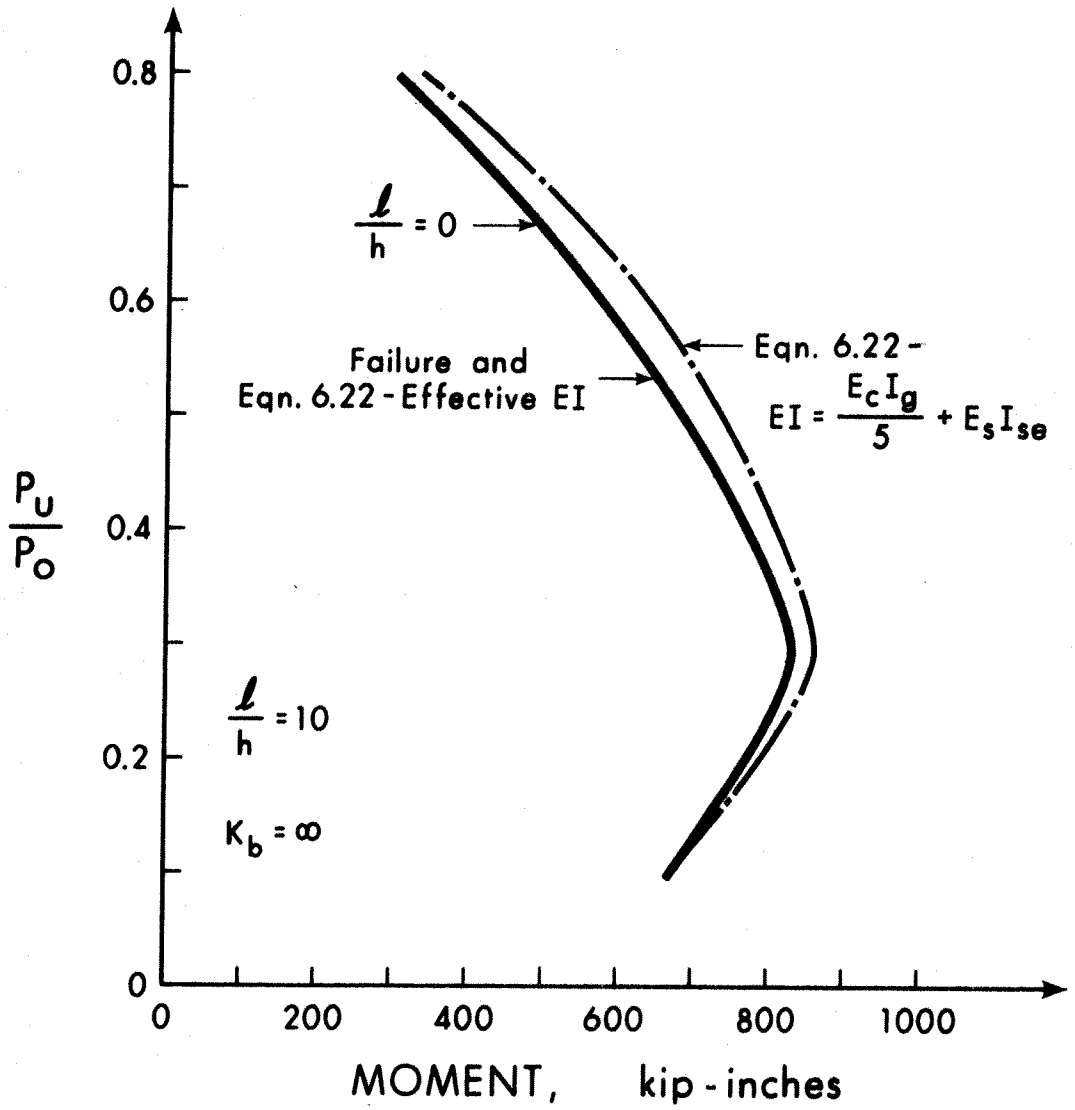

FIG. 6.3 LOAD-MOMENT RELATIONSHIP AT ULTIMATE OBTAINED FROM THE SUBASSEMBLAGE AND MOMENT MAGNIFIER METHODS OF ANALYSIS

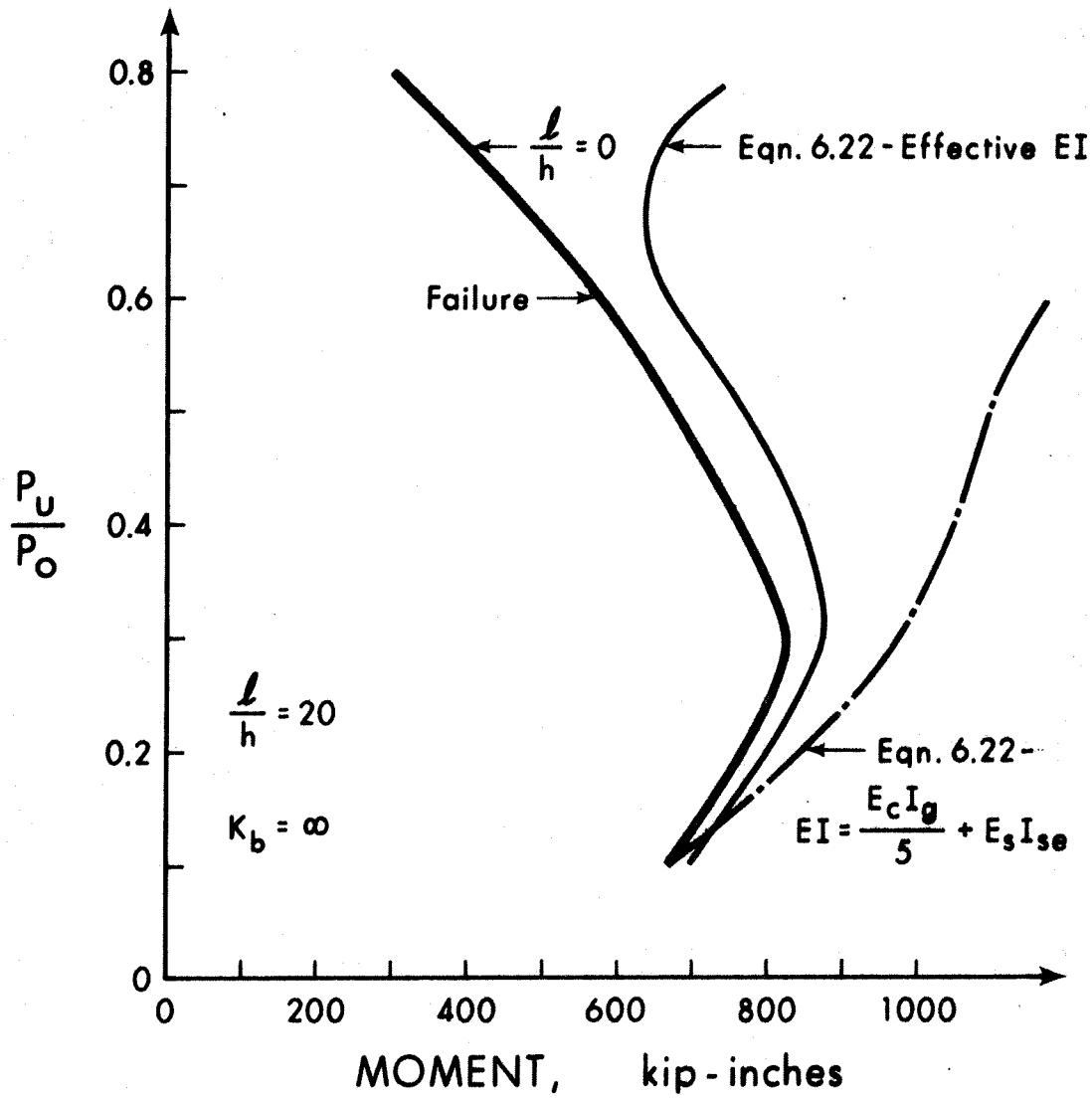

FIG. 6.4 LOAD-MOMENT RELATIONSHIP AT ULTIMATE OBTAINED FROM THE SUBASSEMBLAGE AND MOMENT MAGNIFIER METHODS OF ANALYSIS

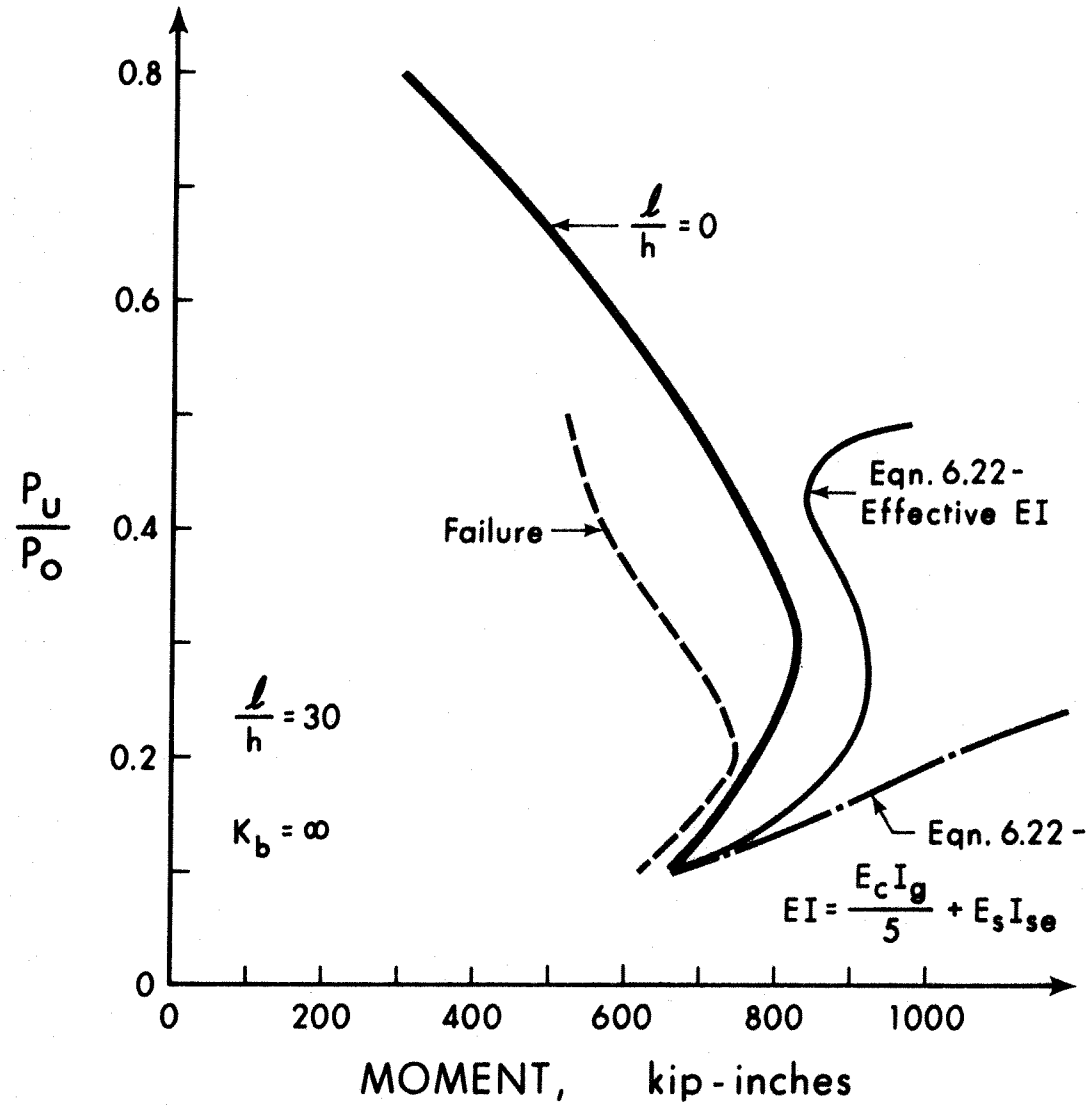

FIG. 6.5 LOAD-MOMENT RELATIONSHIP AT ULTIMATE OBTAINED FROM THE SUBASSEMBLAGE AND MOMENT MAGNIFIER METHODS OF ANALYSIS

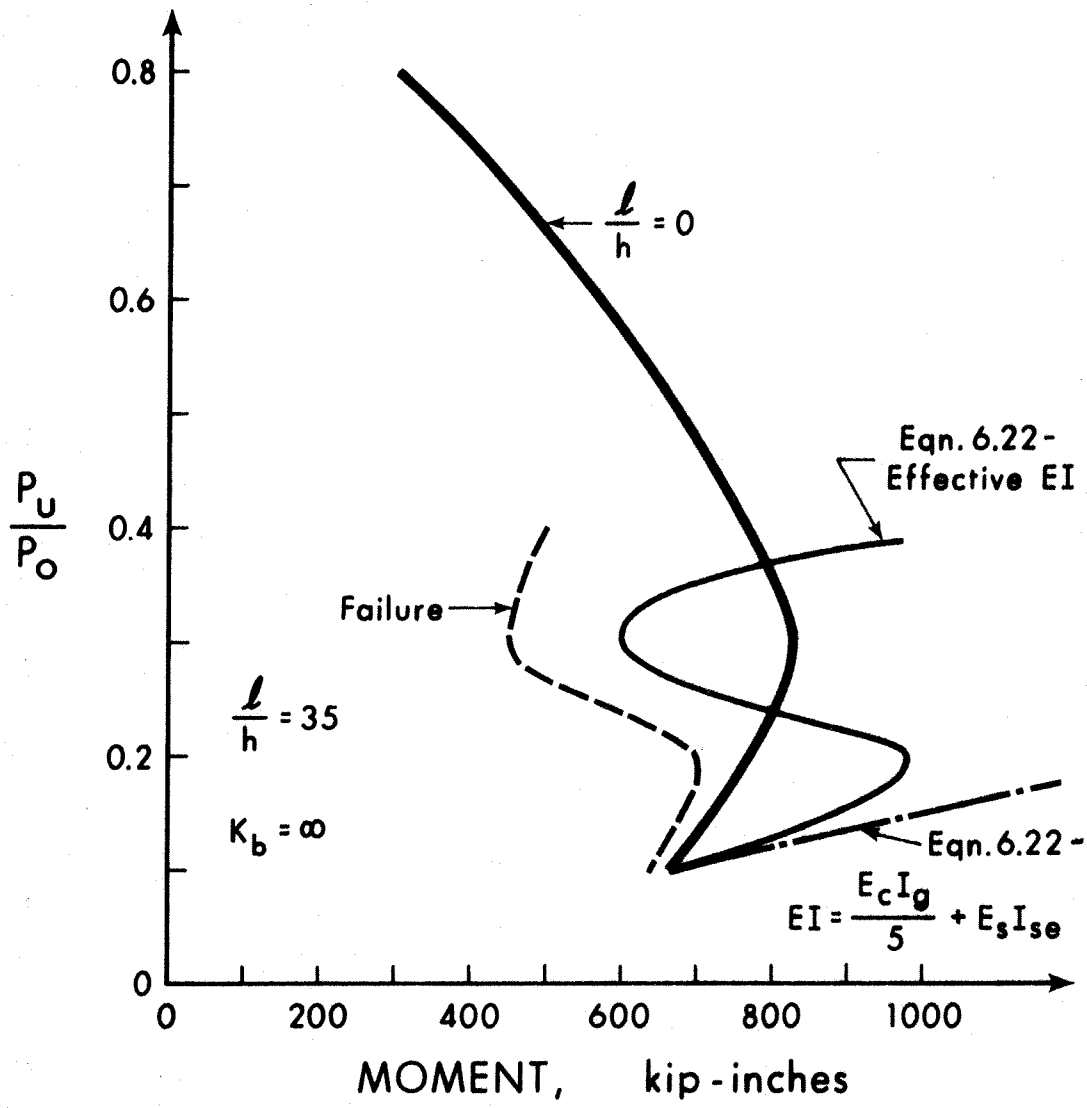

FIG. 6.6 LOAD-MOMENT RELATIONSHIP AT ULTIMATE OBTAINED FROM THE SUBASSEMBLAGE AND MOMENT MAGNIFIER METHODS OF ANALYSIS

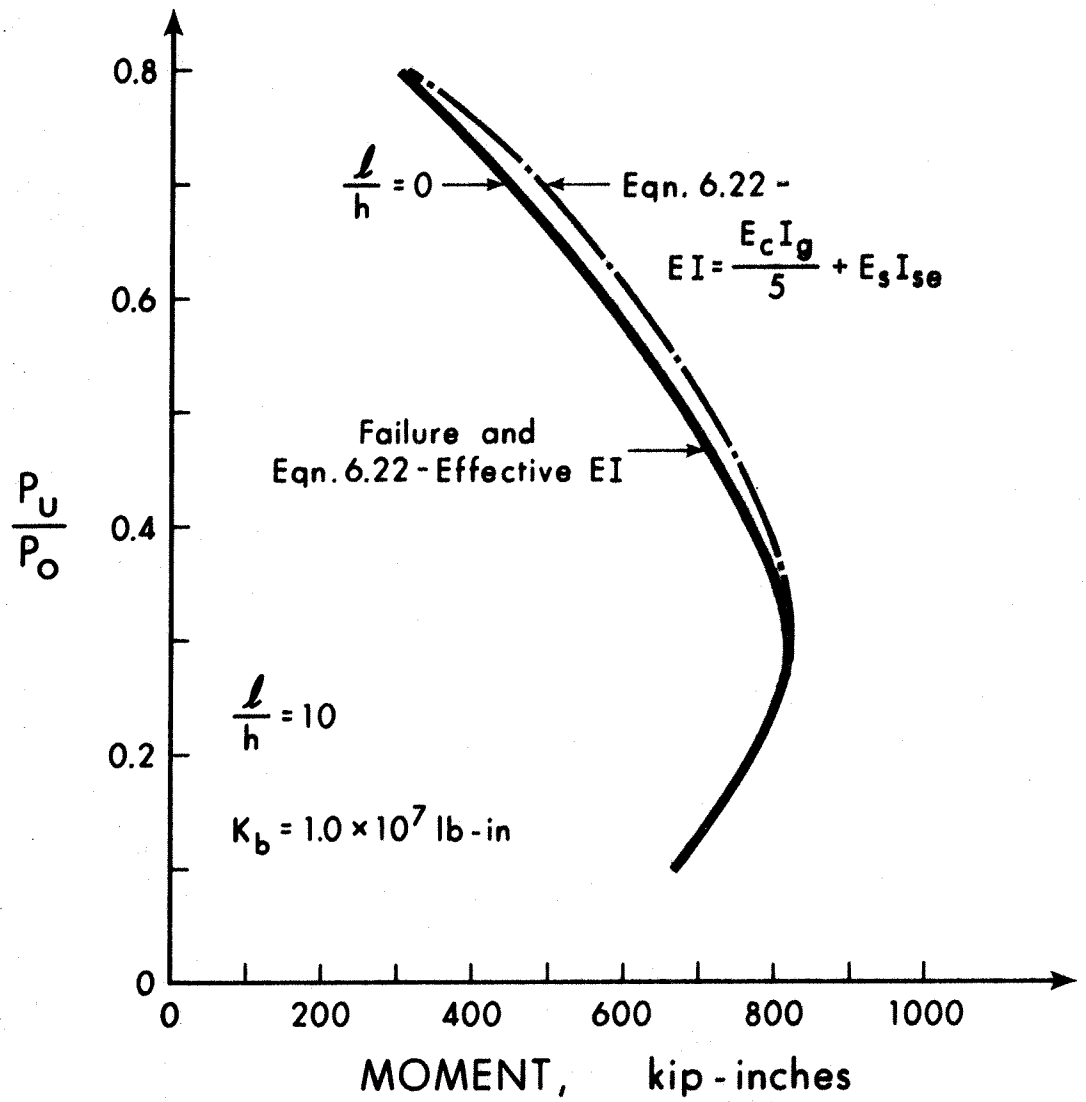

FIG. 6.7 LOAD-MOMENT RELATIONSHIP AT ULTIMATE OBTAINED FROM THE SUBASSEMBLAGE AND MOMENT MAGNIFIER METHODS OF ANALYSIS

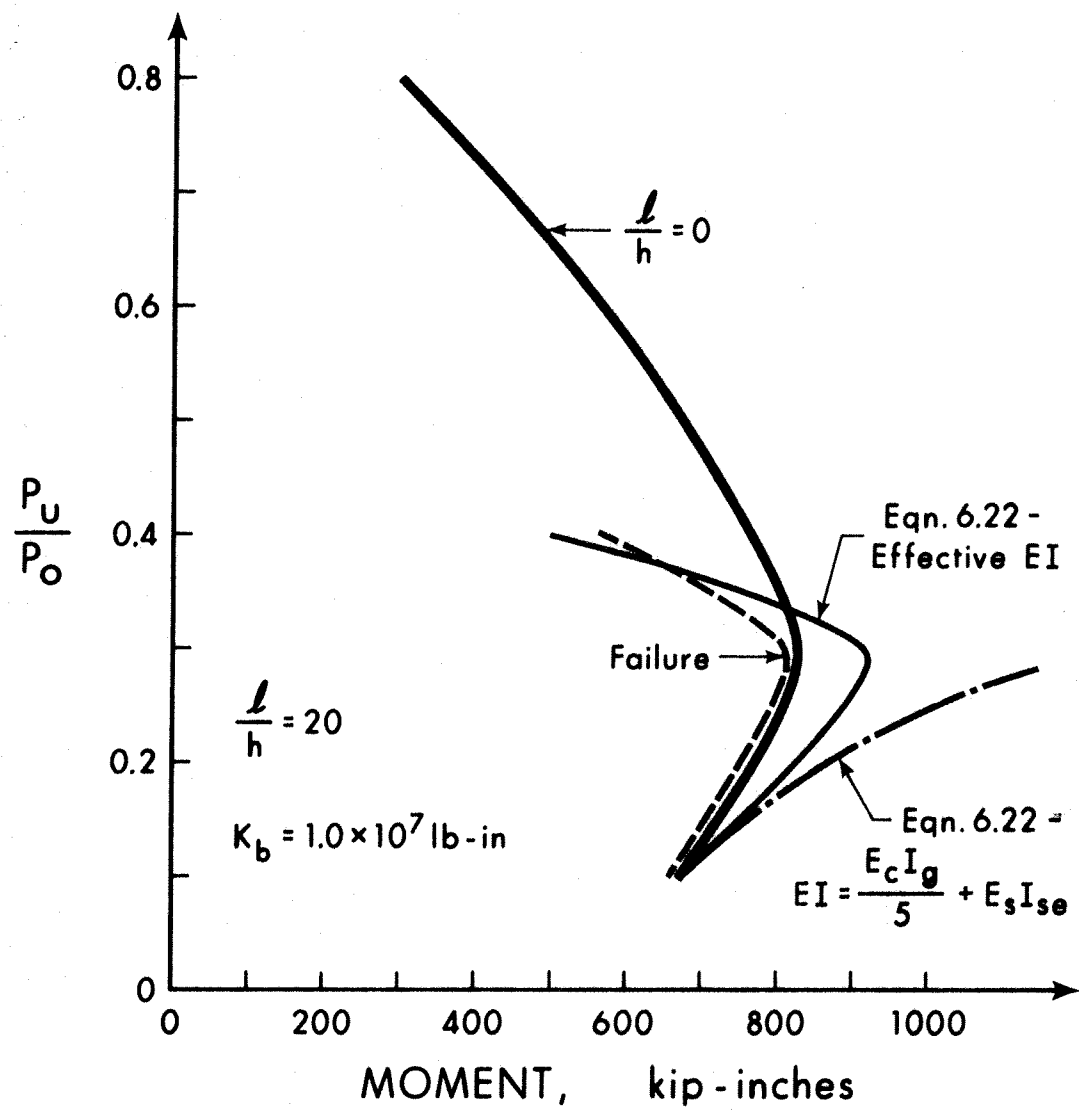

FIG. 6.8 LOAD-MOMENT RELATIONSHIP AT ULTIMATE OBTAINED FROM THE SUBASSEMBLAGE AND MOMENT MAGNIFIER METHODS OF ANALYSIS

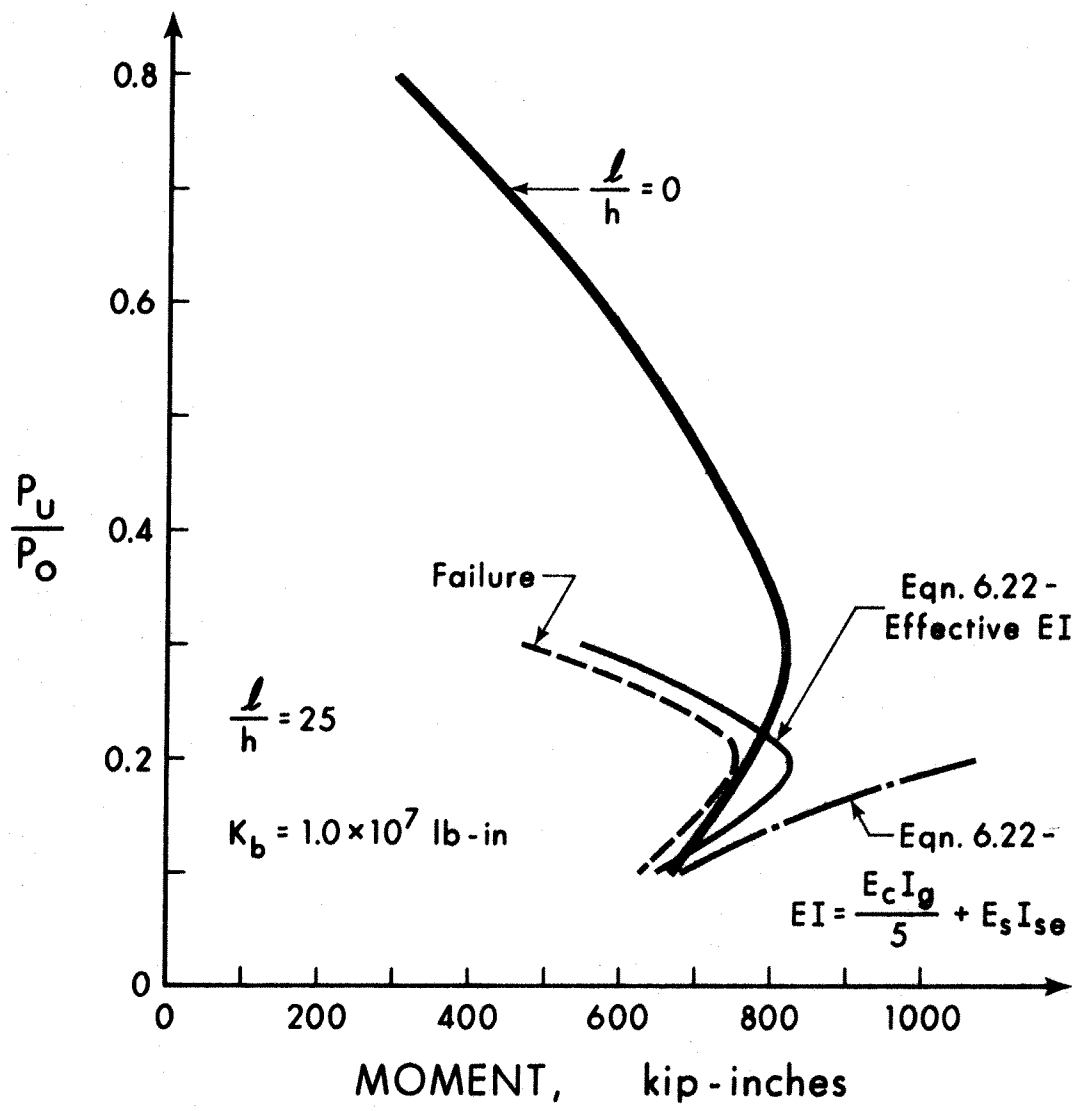

FIG. 6.9 LOAD-MOMENT RELATIONSHIP AT ULTIMATE OBTAINED FROM THE SUBASSEMBLAGE AND MOMENT MAGNIFIER METHODS OF ANALYSIS

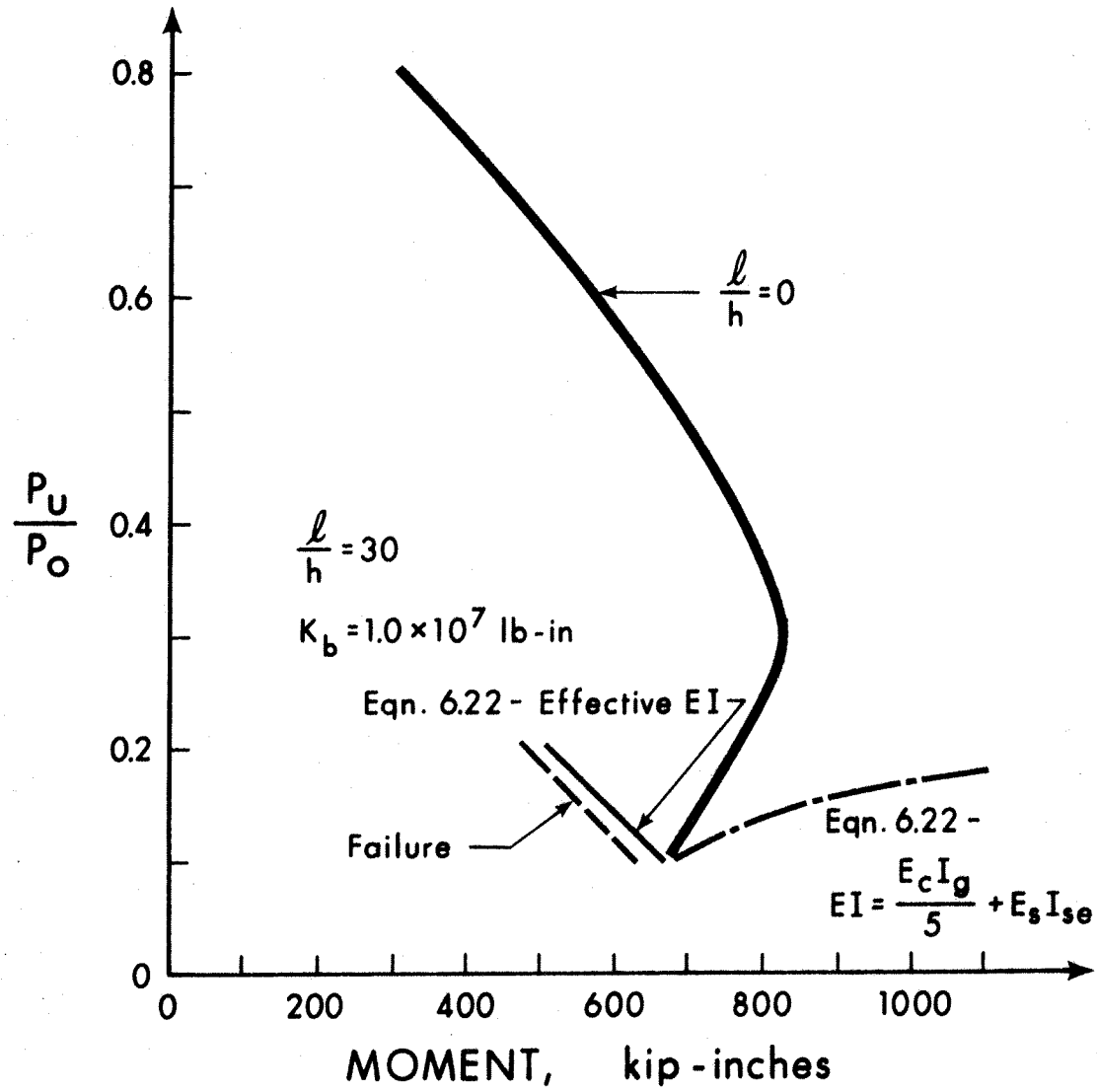

FIG. 6.10 LOAD-MOMENT RELATIONSHIP AT ULTIMATE OBTAINED FROM THE SUBASSEMBLAGE AND MOMENT MAGNIFIER METHODS OF ANALYSIS

restraint $K_b = \infty$ and $K_b = 1 \times 10^7$ k-in, a value close to the lowest practical limit for beam stiffness, and various slenderness ratios. All plots are for a tied column with bars in two faces (Type 1 column).

For l/h greater than about 20 the failure line lies inside the interaction diagram indicating stability failures. Interaction diagrams based on the moment magnifier equation using the effective EI correspond reasonably well to the failure interaction diagram as they should, since the effective EI values were derived from Point 1 in Fig. 6.13(a) or (b). If design were based on the use of this interaction diagram, the design would require less steel than actually necessary. If, on the other hand, design were based on the moment magnifier and the ACI EI value, the design interaction diagram lies outside the cross-sectional interaction diagram indicating that more reinforcement is required than actually needed. Thus the ACI Code procedure predicts the second order moments well for short columns (Figs. 6.3 and 6.7) but tends to overestimate the moments for slender columns.

6.4 Iterative P-Δ Procedure

6.4.1 General Principles

The basic principles of the P-Δ method were outlined in Section 2.4. This section will be devoted to a more detailed investigation of the method and its application in the design of building frames [47].

Fig. 6.11 shows a diagram of a column in the i^{th} story of a frame carrying both lateral and vertical loads. The deflection Δ is computed ignoring the effect of P_n. From equilibrium requirements the additional shears produced by the axial load acting

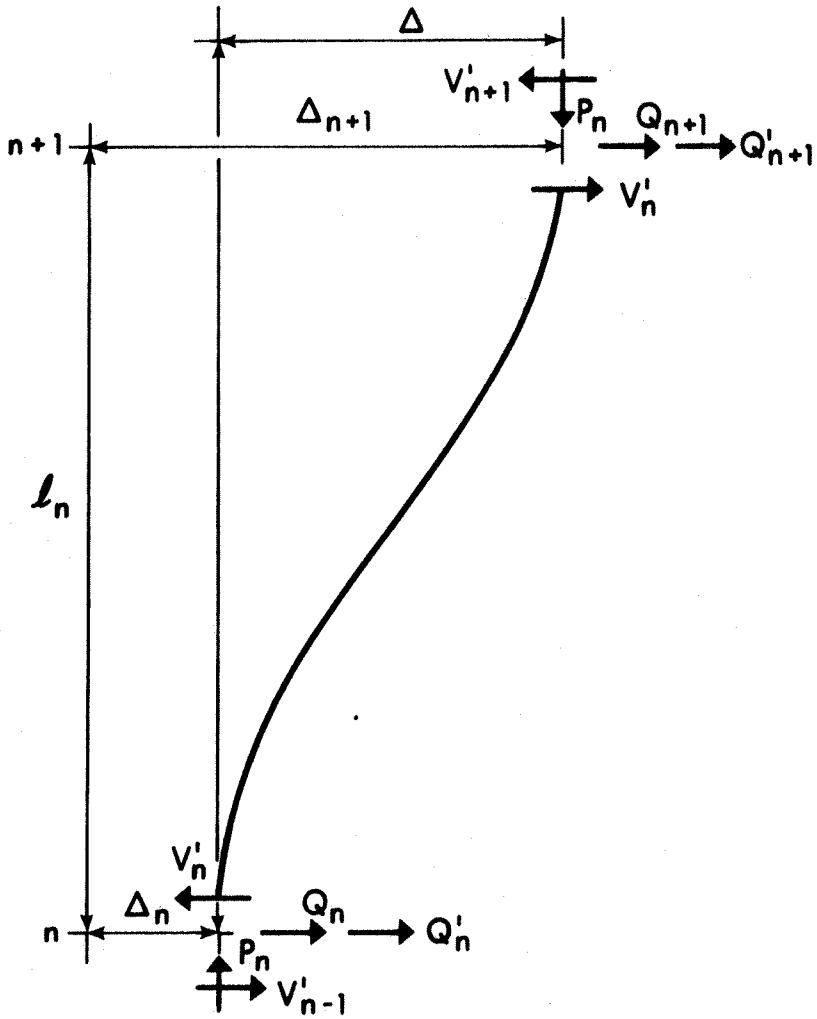

FIG. 6.11 SWAY FORCES DUE TO VERTICAL LOADS

through a deflection Δ may be written as

$$V_n' = \frac{\Sigma P_n}{l_n} (\Delta_{n+1} - \Delta_n) \qquad (6.24)$$

where V_n' = additional shear in story n due to axial loads, ΣP_n = sum of column axial load in story n, l_n = height of story n, Δ_{n+1}, Δ_n = deflection of floor level n + 1 and n respectively. The net additional sway force at level n due to axial loads is given by

$$Q_n' = V_{n+1}' - V_n' \qquad (6.25)$$

This force is now added to the applied lateral load at level n and a first order analysis is again carried out. The deflections obtained in that analysis are substituted into Eqn. (6.24) to give a new set of story shears which in turn are used to compute a new set of additional sway forces. The process is repeated until the moments or deflections in one cylce are only slightly larger than those of the previous cycle.

The rate of convergence of the iteration process could be used as an indication as to the possibility of a stability failure occurring. Some results from the P-Δ analysis are shown in Tables 6.1 and 6.2, where Δ_i is the deflection in the i'th cycle and Δ_f is the final second-order deflection as obtained in the sub-assemblage analysis. The short column interaction diagrams and the failure curves for these columns are shown in Figs. 6.3 through 6.10. The iteration process is seen to converge slowly for stability failures and it appears that if the process converges within five iterations there is no danger of a stability failure occurring.

$\frac{l}{h}$	$\frac{P_u}{P_{cr}}$	$\frac{P_u}{P_o}$	Effective $(EI)_c$			ACI Eqn. (10-7)		
			$\frac{\Delta_i}{\Delta_{i-1}}$	$\frac{\Delta_f}{\Delta_i}$	No.of cycles	$\frac{\Delta_i}{\Delta_{i-1}}$	$\frac{\Delta_f}{\Delta_i}$	No.of cycles
10	0.106	0.1	1.010	1.003	3	1.009	1.063	3
	0.189	0.2	1.031	1.008	3	1.035	0.954	3
	0.270	0.3	1.018	1.007	4	1.020	0.872	4
	0.360	0.4	1.035	1.019	4	1.043	0.891	4
	0.451	0.5	1.025	1.022	5	1.035	0.853	5
	0.542	0.6	1.047	1.057	5	1.037	0.839	6
	0.652	0.7	1.049	1.095	6	1.045	0.868	7
	0.777	0.8	1.047	1.175	8	1.045	0.986	9
20	0.268	0.1	1.049	1.014	3	1.014	0.949	4
	0.506	0.2	1.029	1.028	5	1.037	0.908	5
	0.764	0.3	1.042	1.097	7	1.045	0.813	8
	0.848	0.4	1.044	1.235	10	1.050	0.105	32

$(EI/l)_b = 10^7$ lb-in^2

TABLE 6.1

Results from the PΔ iteration procedure.

$\frac{l}{h}$	$\frac{P_u}{P_{cr}}$	$\frac{P_u}{P_o}$	Effective $(EI)_c$			ACI Eqn. (10-7)		
			$\frac{\Delta_i}{\Delta_{i-1}}$	$\frac{\Delta_f}{\Delta_i}$	No. of cycles,i	$\frac{\Delta_i}{\Delta_{i-1}}$	$\frac{\Delta_f}{\Delta_i}$	No. of cycles,i
10	0.054	0.1	1.047	1.000	2	1.042	1.137	3
	0.081	0.2	1.006	1.000	3	1.006	0.885	3
	0.117	0.3	1.005	1.040	3	1.007	0.876	3
	0.143	0.4	1.016	1.000	3	1.024	0.767	3
	0.173	0.5	1.023	1.006	3	1.036	0.731	3
	0.205	0.6	1.033	1.007	3	1.050	0.733	3
	0.255	0.7	1.045	1.021	3	1.019	0.776	4
	0.324	0.8	1.019	1.008	4	1.027	0.880	4
20	0.200	0.1	1.025	1.004	3	1.016	1.288	3
	0.266	0.2	1.046	1.012	3	1.015	0.841	4
	0.379	0.3	1.028	1.015	4	1.043	0.778	4
	0.480	0.4	1.050	1.039	4	1.044	0.667	5
	0.567	0.5	1.034	1.037	5	1.036	0.508	7
	0.709	0.6	1.039	1.064	6	1.046	0.436	9
	0.713	0.7	1.042	1.165	9	1.050	0.386	15

$(EI/l)_b = 5.0 \times 10^7$ lb-in^2

TABLE 6.2

Results from the PΔ iteration procedure.

Tables 6.1 and 6.2 also show how the deflections and the rate of convergence is affected by using EI values computed from ACI Equation (10-7). Because the Code equation underestimates the stiffness in most cases the deflections are overestimated and the ratio Δ_f/Δ_i is therefore less than one. The rate of convergence is seen to decrease with increasing P_u/P_{cr}, and as a result, using a smaller value of EI will reduce the rate of convergence.

6.4.2 Direct Solution

The process described in Section 6.4.1 may be expressed in a more convenient form. Let Q_1 and Δ_1 represent the applied lateral load and the corresponding first order deflection, respectively. Also, let the appropriate axial load be P, the deflection caused by a unit lateral load be k_s and let Q_i (i=2,3,--∞) be the sum of the applied and additional lateral loads in the i'th cycle.

Then the iteration process may be expressed in the following manner:

$$\text{1st iteration:} \quad \Delta_1 = k_s Q_1 \tag{6.26}$$

$$\text{2nd iteration:} \quad \Delta_2 = k_s Q_2 = k_s Q_1 \left(1+\frac{P}{1}k_s\right) \tag{6.27}$$

$$\text{3rd iteration:} \quad \Delta_3 = k_s Q_3 = k_s Q_1 \left(1+\frac{P}{1}k_s+\left(\frac{P}{1}\right)^2 k_s^2\right) \tag{6.28}$$

and the general term for the i'th iteration is

$$\Delta_i = k_s Q_1 \left[1+\frac{P}{1}k_s+\left(\frac{P}{1}\right)^2 k_s^2+---+\left(\frac{P}{1}\right)^{i-2} k_s^{i-2}+\left(\frac{P}{1}\right)^{i-1} k_s^{i-1}\right] \tag{6.29}$$

This is a geometric series which converges if $\frac{P}{1}\, k_s<1.0$, and in that case the sum of the infinite series is

$$\frac{1}{1-\frac{P}{1}k_s} = \frac{1}{1-\frac{P\Delta_1}{Q_1 1}} \tag{6.30}$$

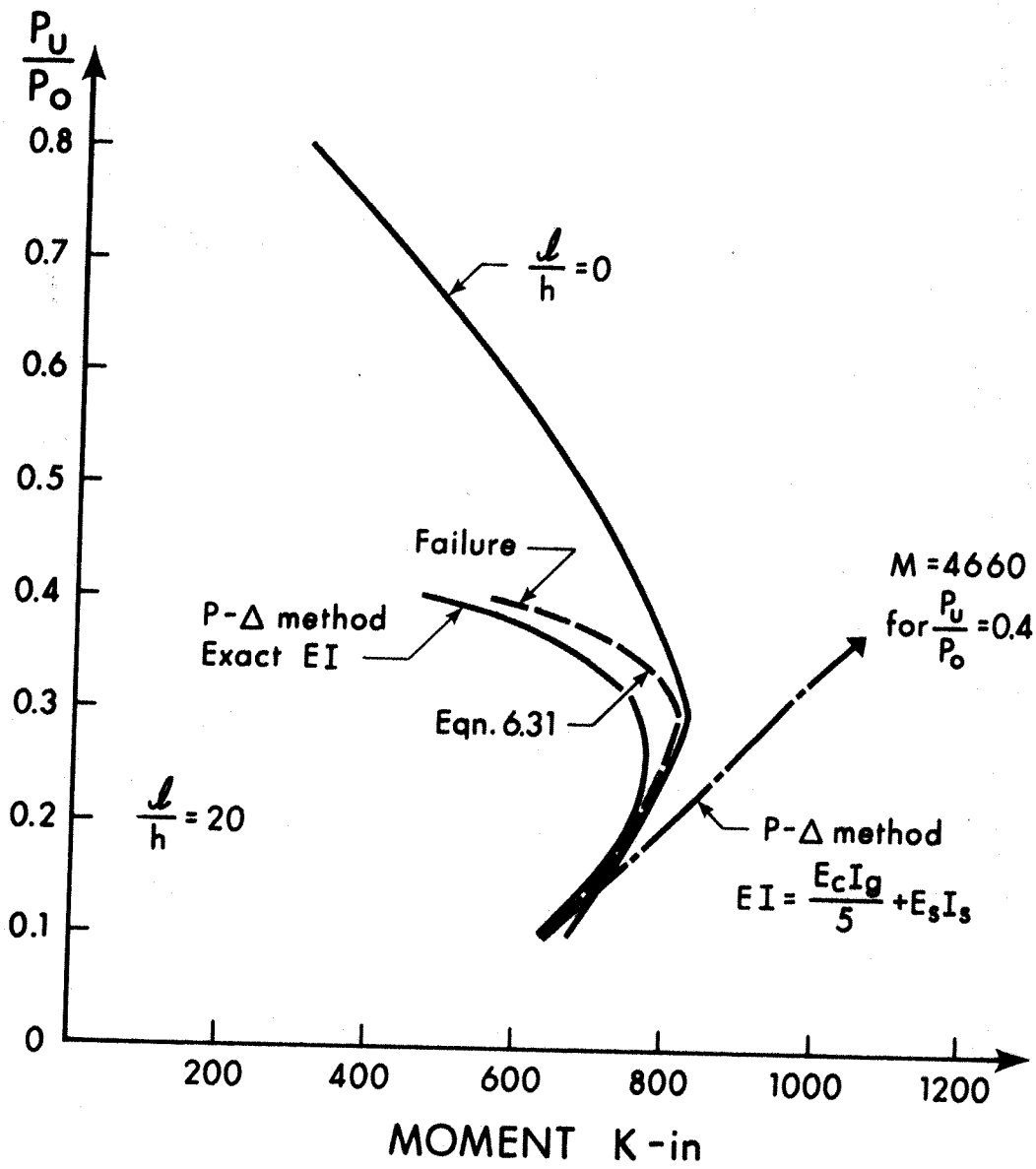

FIG. 6.12 P-Δ ANALYSIS COMPARED TO SUBASSEMBLAGE ANALYSIS

$K_b = 10^7$ k-in.

And since $k_s Q_1 = \Delta_1$ the process converges to the final second-order deflection Δ_2.

$$\Delta_2 = \frac{\Delta_1}{1 - \frac{P\Delta_1}{Q_1 I_1}} \tag{6.31}$$

Equation (6.31) is identical to the equations proposed by Fey[9], Parme[10] and Goldberg[7] and shows that the second-order deflections may be computed directly from the results of a first-order analysis in the case of a straight line moment-curvature relationship. If a non-linear M-P-ϕ curve is approximated by a number of straight lines, Equation (6.31) may still be used if the lateral load is applied in increments to allow for appropriate adjustments of the EI value with increasing moment.

The obvious advantage of using Equation (6.31) rather than the actual iteration process is that only two first order analyses are required to obtain the second-order moments and forces in an elastic structure.

The accuracy of Equation (6.31) may be studied by considering Fig. 6.12. This figure shows interaction diagrams obtained from: a) the actual iteration process, b) using Equation (6.31) and c) the subassemblage analysis. The iteration process was carried out using both the effective EI and ACI equation (10-7). The results from Equation (6.31) were obtained using the effective EI.

It can be seen that the use of Equation (6.31), with the correct EI, gives results identical to those obtained in the sub-assemblage analysis while the iteration procedure gives smaller moments. The moments from the P-Δ analysis were lower because the

P-Δ calculation converges on the correct answer from below and the convergence criterion normally used in the iteration process was that the deflections obtained from two successive iterations should agree to within a certain limit, in this case five percent. When the iteration process is slow, the deflections obtained from two successive cycles do not differ very much, but they may still be inaccurate compared to the correct final deflection. This is shown in Table 6.1 where, for P_u/P_o=0.4 and l/h=20, the error is about 23 percent. However, this type of inaccuracy will not occur when the process converges rapidly.

In Section 6.4.1 it was suggested that the rate of convergence could be used as a check on whether a stability failure is imminent. To enable this criterion to be used with Equation (6.31) it is necessary to express the convergence check in a different form. If the iteration process is considered to have converged when the deflection in the i^{th} cycle is within five percent of the final deflection, this condition can be expressed by Equation (6.32).

$$\frac{\dfrac{\Delta_1}{1 - \dfrac{P\Delta_1}{Q_1 l}}}{\Delta_1\left(1 + \dfrac{P}{l} k_s + \text{---} + \left(\dfrac{P}{l}\right)^{i-1} k_s^{\,i-1}\right)} \leq 1.05 \qquad (6.32)$$

Equation (6.32) may be rearranged to read

$$\left(\frac{P}{l}\right)^i k_s^i \leq 0.05 \qquad (6.33)$$

Thus, the number of iterations required to achieve five percent accuracy is given by

$$i = - \frac{1.30}{\log\left(\frac{P\Delta_1}{Q_1 l}\right)} \tag{6.34}$$

For the particular case where i is not to exceed five, Equation (6.35) must be satisfied.

$$\frac{P\Delta_1}{Q_1 l} \leqq 0.55 \tag{6.35}$$

Equation (6.35) shows that the deflections obtained in the first-order analysis may be used to check on stability failures, and if Equation (6.35) is not satisfied, the member stiffnesses may be modified until the first-order analysis gives acceptable results before proceeding with the calculation of the final second-order deflections and stress resultants.

Alternately, the check on the iteration process may also be based on the convergence of the moments rather than the deflections, and the convergence criterion may be expressed as

$$\frac{Q_1 l + P\Delta_2}{Q_1 l + P\Delta_i} \leqq 1.05 \tag{6.36}$$

By substituting for Δ_2 and Δ_i from Equations (6.31) and (6.29) in Equation (6.36) it reduces to

$$\left(\frac{P\Delta_1}{Q_1 l}\right)^{i+1} \leqq 0.05 \tag{6.37}$$

When i = 0, Equation (6.37) is identical to Equation (6.13), and thus defines the values of $P\Delta_1/Q_1 l$ for which a second-order analysis may be ommitted. With i = 1 it becomes

$$\frac{P\Delta_1}{Q_1 l} \leq 0.22 \tag{6.38}$$

In this case sufficiently accurate moments will be obtained by adding $P\Delta_1$ to the first-order moments and the second-order deflection Δ_2 need not be computed. For values of $P\Delta_1/Q_1 l$ greater than 0.22 the second-order deflections must be computed and are easily obtained from Equation (6.31).

6.4.3 The Effect of Sidesway Instability on the Accuracy of The PΔ Analysis

Methods currently used to predict stability failures only consider the bifurcation load which is independent of the lateral load. However, when stability failure may occur as a result of a reduction in member stiffness, the magnitude of the lateral load becomes an important parameter.

A typical load-deflection diagram for a slender column whose load carrying capacity has been sharply reduced due to a reduction in member stiffness is shown in Fig. 6.13(a). This column is stable if the lateral load is less than Q_1. If the applied lateral load is between Q_1 and Q_2 the design may be unsafe. This will always be the case in a PΔ analysis since the second-order moment will be less than M_u but greater than the actual failure moment. For the typical case of a stability failure shown in Fig. 6.5 this would mean that the second-order moment lies between the failure curve and the short column interaction diagram, and since it is less than M_u the column would normally be considered adequate.

Fig. 6.13(b) shows a typical load-deflection diagram for a material failure. In this case the lateral load carrying capacity

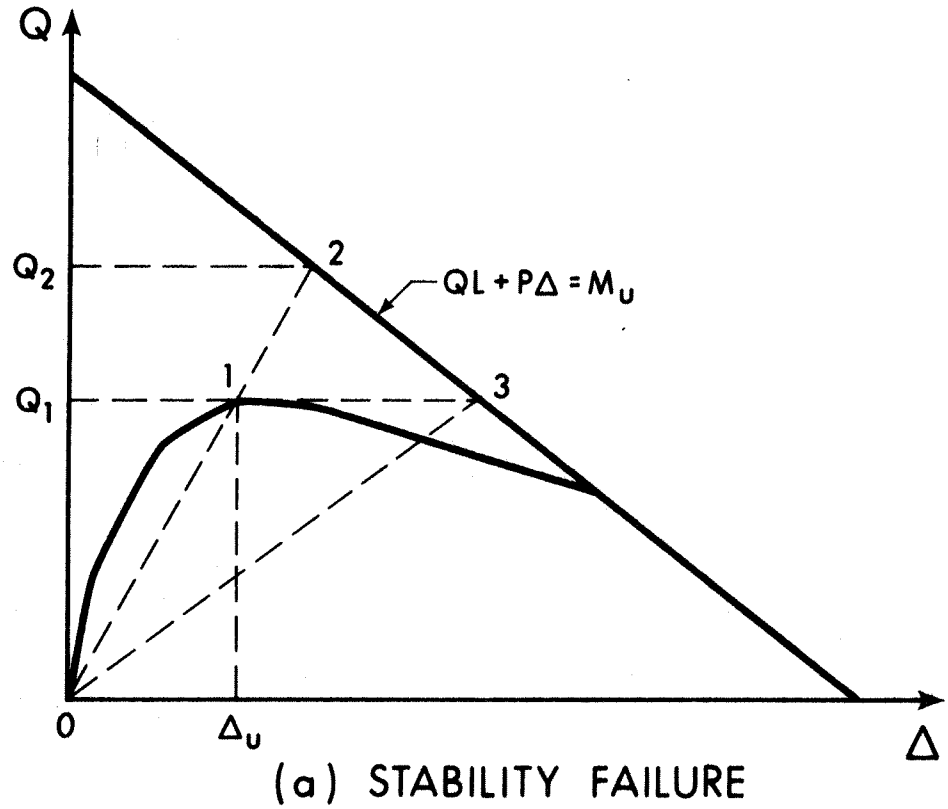

(a) STABILITY FAILURE

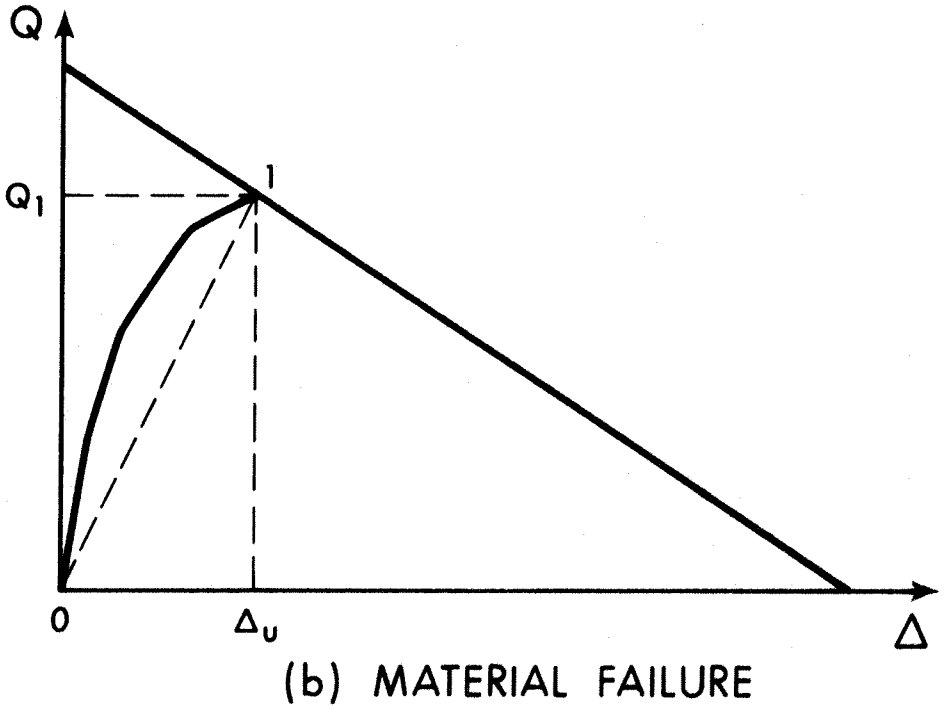

(b) MATERIAL FAILURE

FIG. 6.13 TYPICAL LOAD-DEFLECTION DIAGRAMS

is governed by the moment capacity of the cross-section and cannot be overestimated unless the lateral stiffness is assumed greater than the slope of the line 0-1. The same conclusion can be drawn from Fig. 6.3 where the failure curve and the short column interaction diagram coincide.

An unsafe design does not necessarily arise for stability failures in the moment magnifier method, even if the lateral load is between Q_1 and Q_2 in Fig. 6.13(a), since the moment magnifier is a function of P_u/P_{cr}. If P_u/P_{cr} is large enough the magnified moment will be greater than M_u and a column with a larger moment capacity is required. This may help in two ways to produce a safe design; firstly, the new column may change the failure mode from a stability failure to a material failure; secondly, the new lateral load carrying capacity Q_1 may be greater than the applied load. However, there is at present no simple method to investigate this type of stability failure and the correct failure mode is normally not known to the designer.

If the lateral load carrying capacity could be predicted by the use of subassemblage charts, for example, the mode of failure would also be known. This will normally involve rather extensive computations which makes this method unsuitable for design. This is doubly true because the lateral load carrying capacity depends on many variables which makes it difficult to establish simple empirical expressions or general charts.

6.4.4 Deflection Limits to Prevent Sway Stability Failures

Rather than attempting to predict accurately the lateral load at which instability occurs, it is simpler to define certain

limits which will indicate when a sidesway instability failure is likely to occur. Such criteria may be established as a relationship between slenderness ratio, axial load and deflection index.

Fig. 6.14 is a plot of slenderness ratio against the deflection index for stability failure for all the columns studied in this thesis. It includes data for 217 separate cases involving three column cross sections, five slenderness ratios and five different end restraints. The Δ/L values plotted correspond to the value Δ_u in Fig. 6.13(a). This was divided by the real length L of the column rather than the effective length kL since sway indices for buildings are generally expressed as Δ/L. Data for columns developing material failure, as shown in Fig. 6.13(b), have not been included in this figure. It is seen that the following relationships may be used to define values of slenderness ratio and deflection index for which stability failures did not occur:

$$\left(\frac{\Delta}{L}\right)_u \leq \frac{kL}{18000r} \text{ for } \frac{kL}{r} \geq 90 \tag{6.39}$$

and

$$\left(\frac{\Delta}{L}\right)_u \leq 0.005 \text{ for } \frac{kL}{r} < 90 \tag{6.40}$$

Equations (6.39) and (6.40) have been plotted in Fig. 6.14. The scatter diagram also indicates that for a given slenderness ratio there is an upper limit of Δ/L above which no stability failures occurred. However, in these cases the deflections would by far exceed acceptable limits and they have therefore not been included.

Equations (6.39) and (6.40) are based on the effective stiffness values computed from the subassemblage analysis. In practice the correct effective stiffness is seldom known and thus the effective

length factor k is subject to errors. Also, difficulties may arise in defining k if it is not obvious whether the frame is free to sway or is braced.

An alternate approach is to express slenderness by the ratio l/h rather than kl/r. Values of $(\Delta/L)_u$ for which stability failures were not observed may in this case be established from Fig. 6.15, which is a plot of ultimate deflections against l/h for 217 stability failures and is expressed analytically by Equation (6.41).

$$\left(\frac{\Delta}{L}\right)_u \leqq \frac{l}{4400h} \quad \text{for } \frac{l}{h} \geqq 22 \tag{6.41}$$

For l/h < 22 Equation (6.40) still applies.

Similar criteria may also be based on service load deflections. Figs. 6.16 and 6.17 show plots of minimum and maximum service load deflections, respectively, plotted against l/h for the 217 cases of stability failures. These plots show that no stability failures were observed with deflection indices below 1/300 for minimum service loads and 1/250 for maximum service loads.

To consider the effect of the axial load, P_u/P_o was plotted against the smallest value of slenderness ratio and deflection index at which a stability failure occurred. These plots are shown in Fig. 6.18 and Fig. 6.19, respectively.

Based on these plots the following empirical expressions were chosen to define regions where no stability failures were observed:

$$\frac{kL}{r} \leqq 90 - 50\,\frac{P_u}{P_o} \tag{6.42}$$

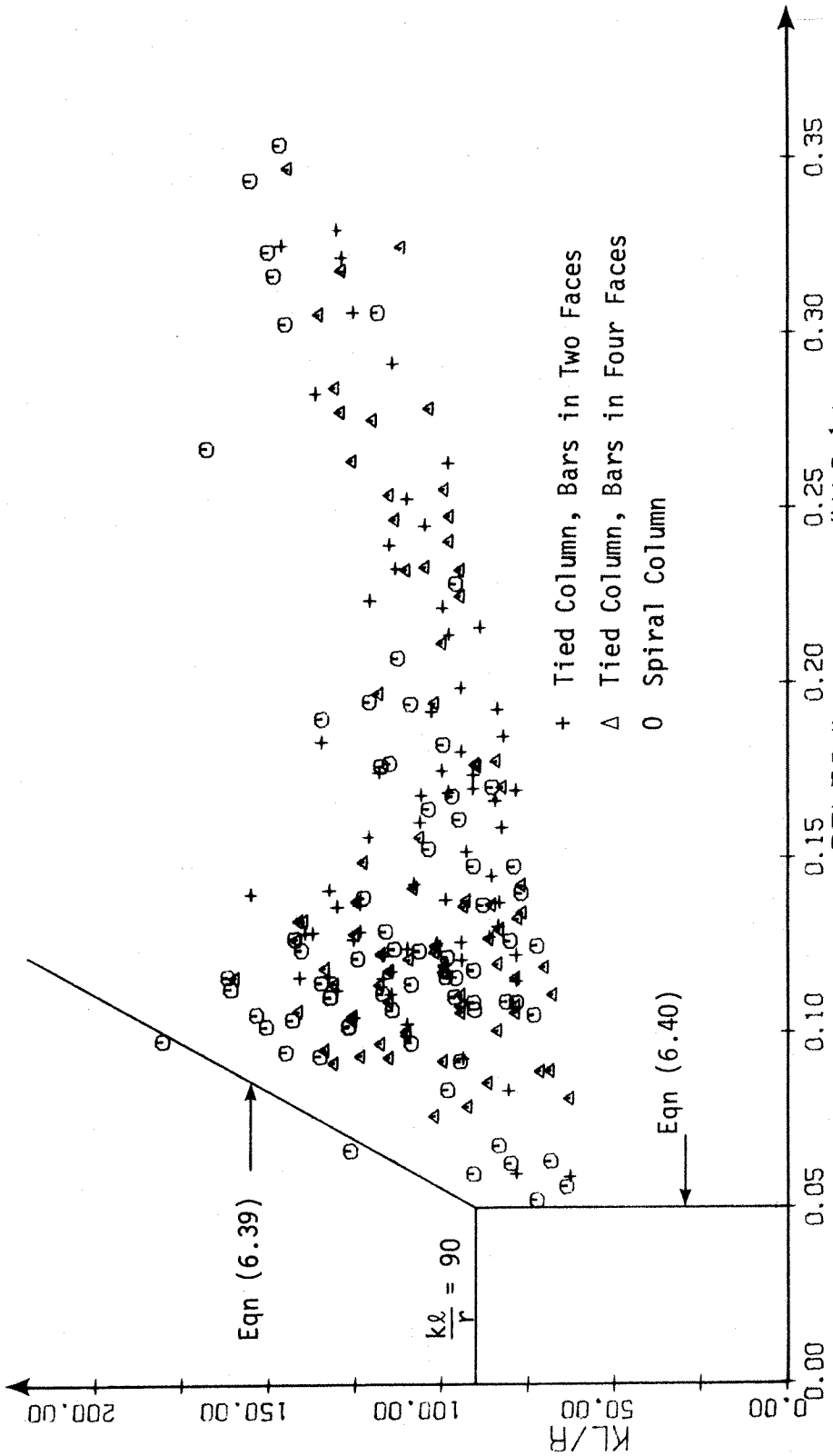

FIG. 6.14 DEFLECTION INDICES AT ULTIMATE VS. kℓ/r FOR STABILITY FAILURES

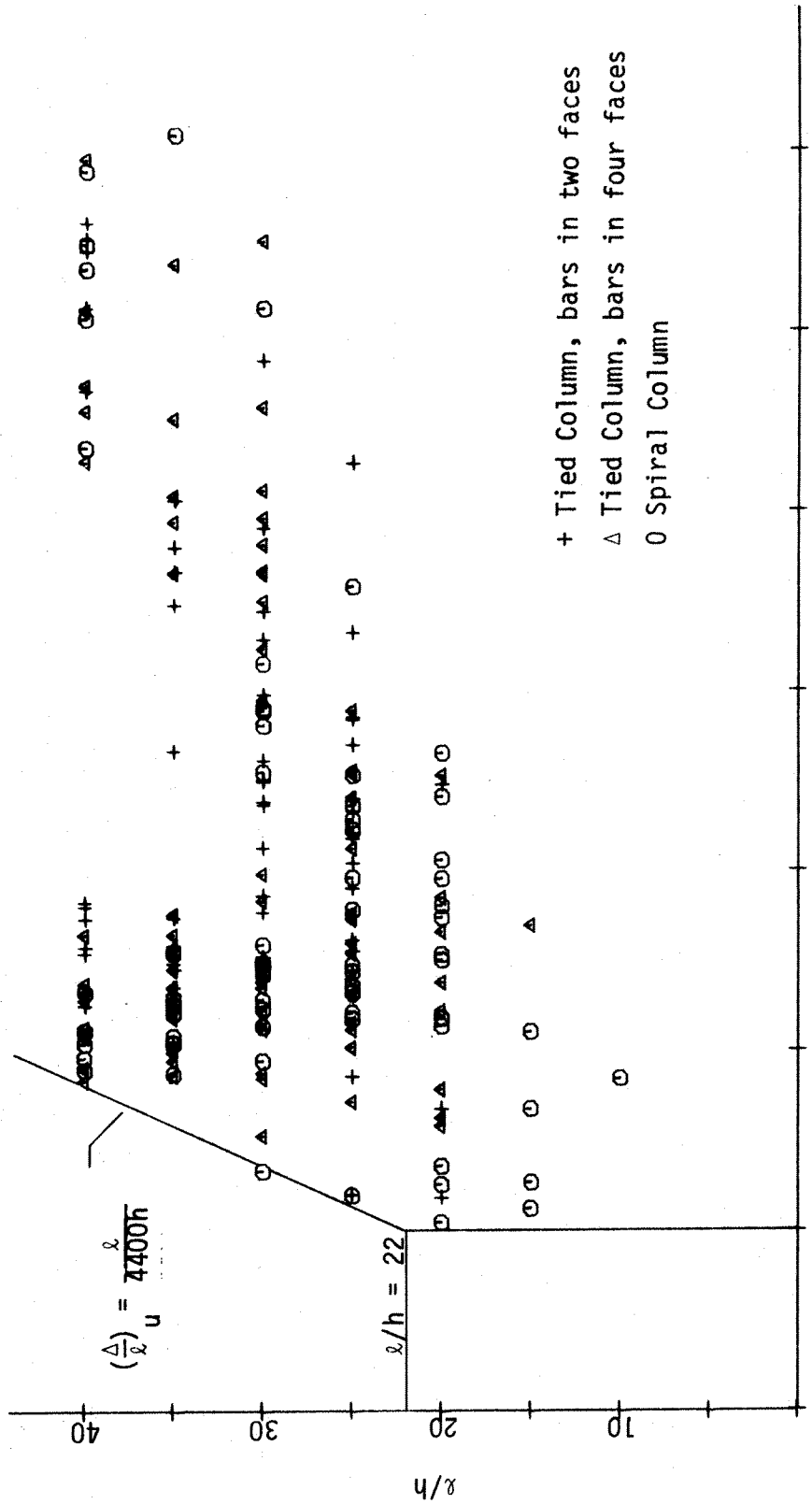

FIG. 6.15 DEFLECTION INDECES AT ULTIMATE vs. ℓ/h FOR STABILITY FAILURES

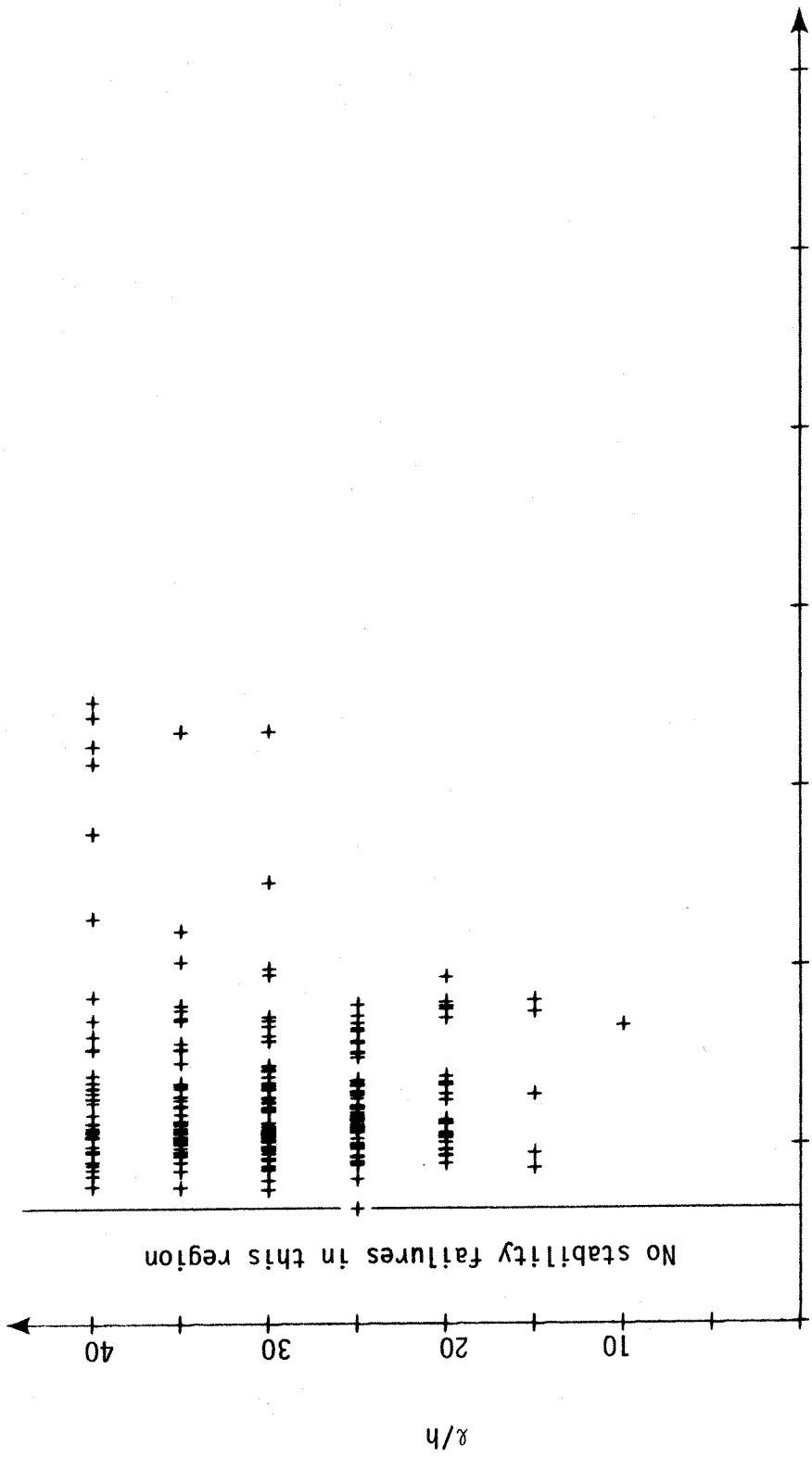

FIG. 6.16 DEFLECTION INDECES AT MINIMUM SERVICE LOAD vs. ℓ/h FOR STABILITY FAILURES

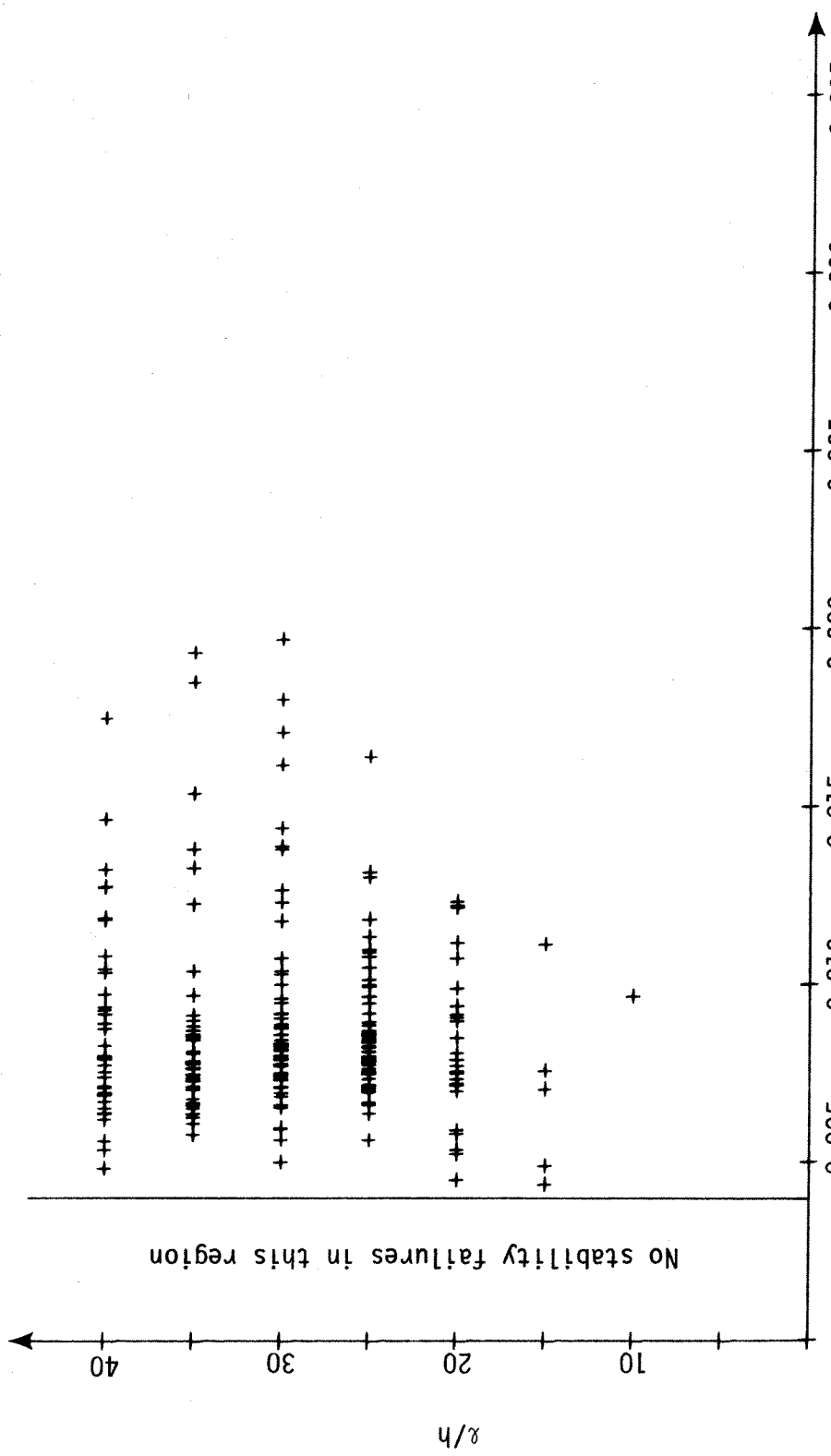

FIG. 6.17 DEFLECTION INDECES AT MAXIMUM SERVICE LOAD vs. ℓ/h FOR STABILITY FAILURES

$$\left(\frac{\Delta}{L}\right) \leqq \frac{0.00095}{\frac{P_u}{P_o} - 0.035} + 0.0035 \qquad (6.43)$$

These equations have also been plotted in Figs. 6.18 and 6.19. For the columns studied, columns having kL/r or $(\Delta/L)_u$ falling below these curves developed material failure rather than stability failure.

Equations (6.42) and (6.43) may be combined to give a plot of slenderness ratio against deflection index as shown in Fig. 6.20. The condition that will have to be satisfied to ensure a material failure may then be expressed as

$$\left(\frac{\Delta}{L}\right) \leqq \frac{0.00095}{1.765 - 0.02\left(\frac{kL}{r}\right)} + 0.0035 \qquad (6.44)$$

A column with a given kL/r and P_u/P_o value will be stable if its $(\Delta/L)_u$ is restricted to less than the value given by Equation (6.44). Within the range covered by Eqn. (6.44), Equation (6.44) is less conservative than Equations (6.39) and (6.40). If Equation (6.44) is not satisfied Equations (6.42) and (6.43) may be checked to see if one of them is satisfied.

The results on which Equation (6.44) is based do not include values of P_u/P_o less than 0.1 or greater than 0.8. It is particularly important that the equation is not used for $P_u/P_o<0.1$ due to the asymptotic nature of the curve.

The practical significance of Equations (6.39) to (6.44) is that the P-Δ approximation to the second-order frame analysis can be used for frames having Δ/L values at ultimate which are less than the values given by these equations. Based on Fig. 6.14 and Equations (6.39) and (6.40), the P-Δ analysis can be used safely for frames having sway deflection indices Δ/L less than 0.005, or 1/200, at ultimate or sway indices less than

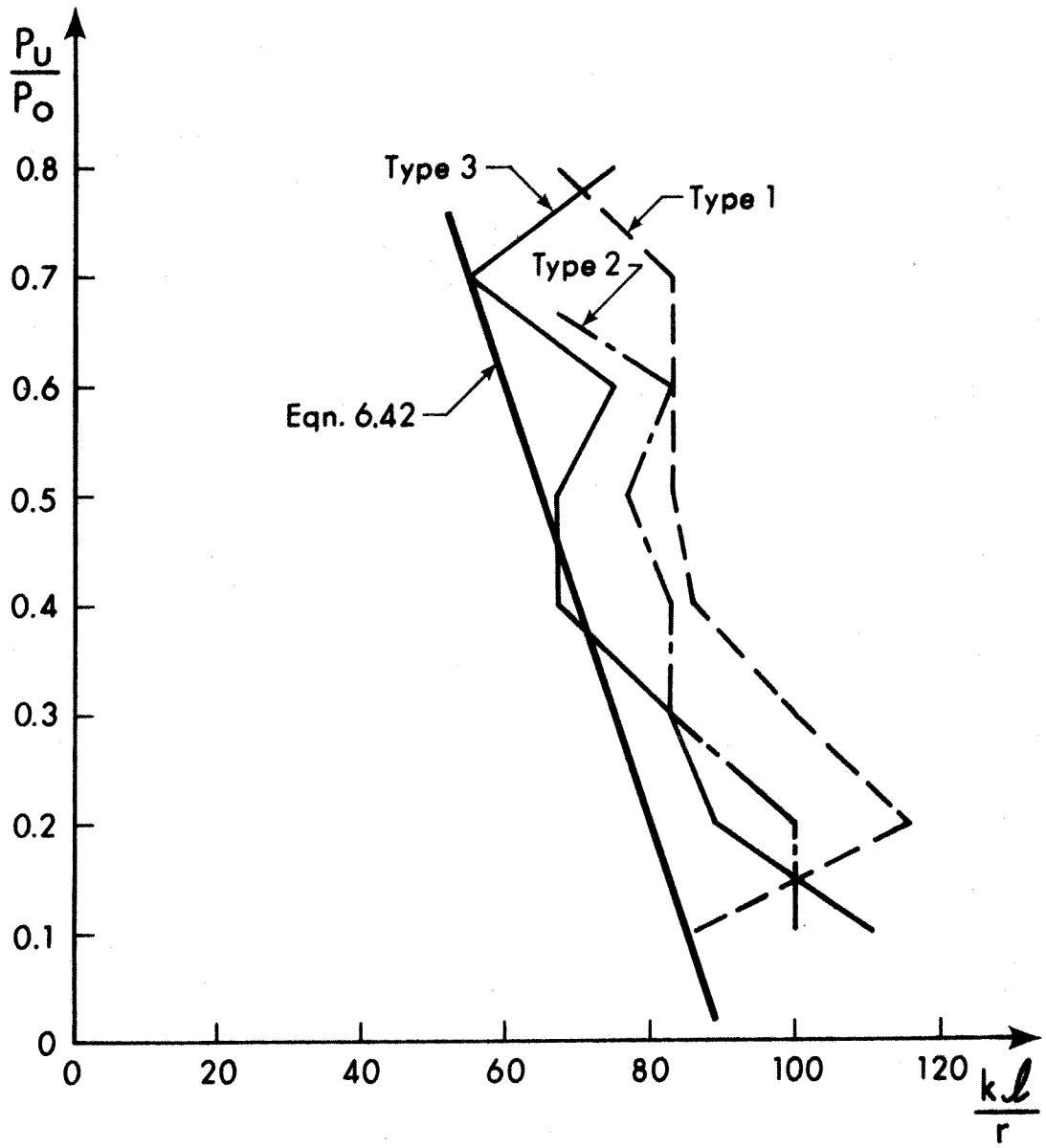

FIG. 6.18 LOWER VALUES OF SLENDERNESS RATIO FOR STABILITY FAILURES

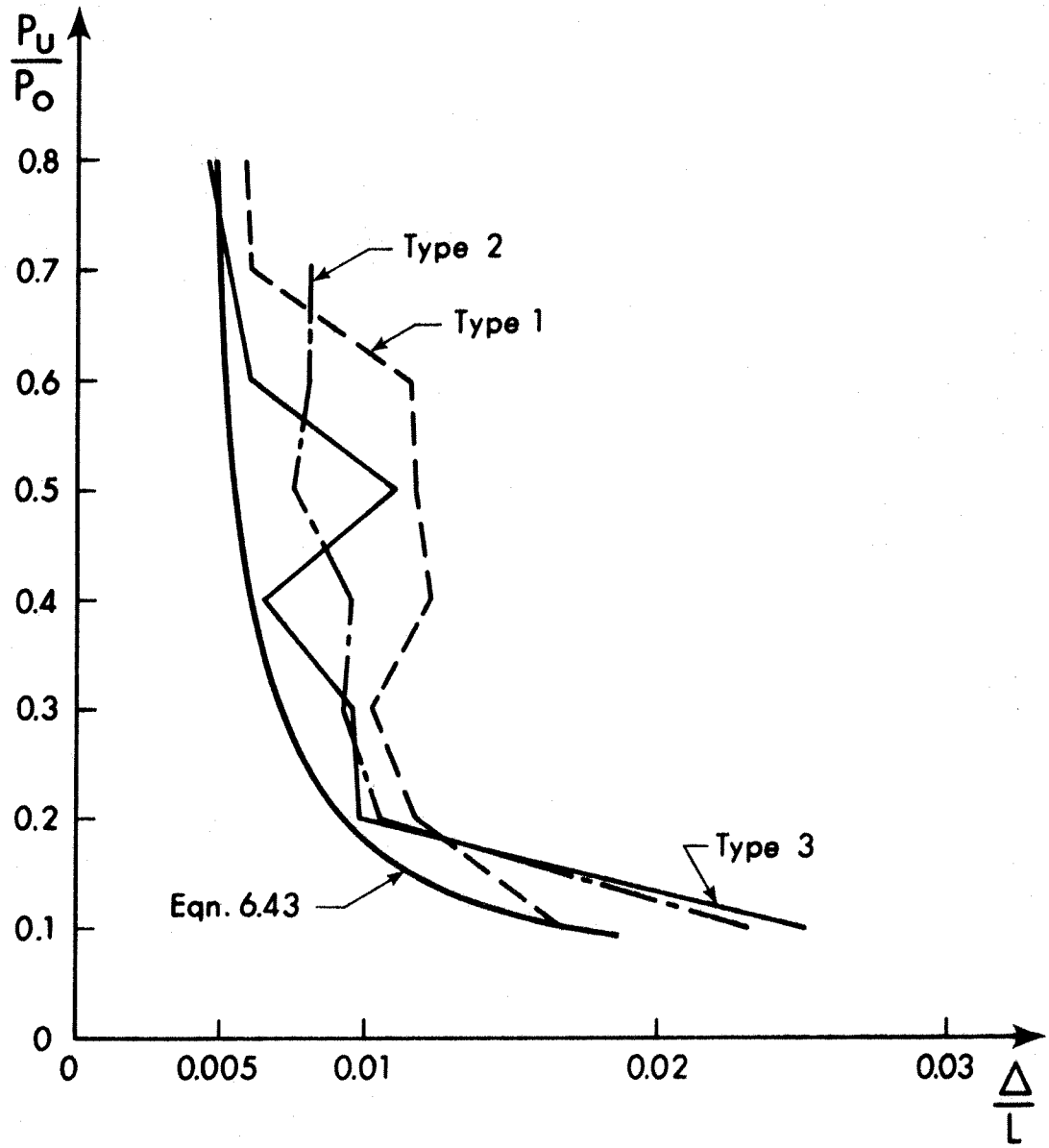

FIG. 6.19 LOWER DEFLECTION INDICES FOR STABILITY FAILURES

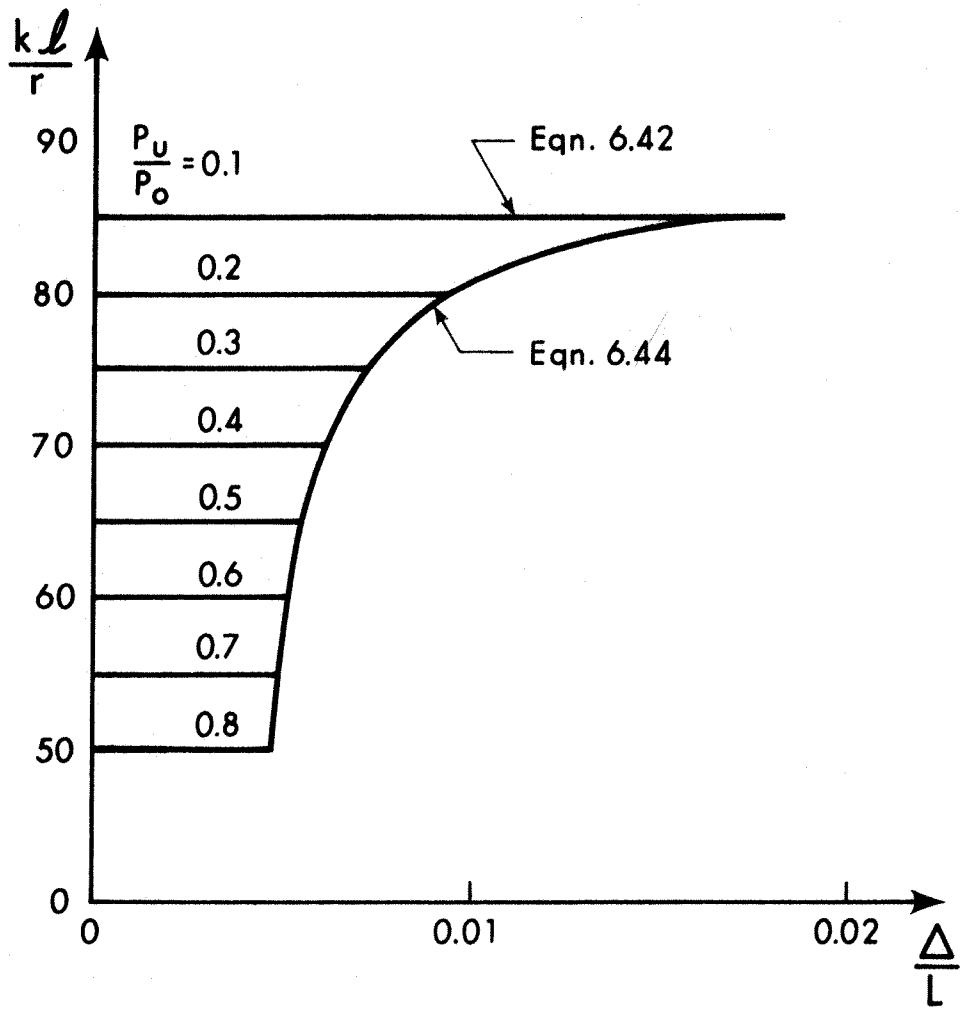

FIG. 6.20 LOWER VALUES OF $k\ell/r$, P_u/P_o and Δ/L BELOW WHICH STABILITY FAILURES WERE NOT OBSERVED

1/300 at service loads. While this conclusion has only been checked for three particular column cross-sections in sway frames, the properties of sway subassemblage curves suggest that similar limits could be used for the design of all practical column cross-sections.

6.5 Determining the Maximum Moment in Beam-Columns in Sway Frames

The methods of second-order analysis of sway frames discussed in previous sections will give the values of the end moments acting on the columns. These moments are not always the maximum moments in the columns and it is necessary to investigate when the end moment is the maximum moment. To do so the moment produced by the axial load as a result of the column not being straight must be included. This can be done by considering the standard differential equation for a beam-column.

Referring to Fig. 6.21(a) the equation for the moment in the column can be written as

$$M_x = M_i + P_y = - EI \frac{d^2y}{dx^2} \tag{6.45}$$

where M_i is the moment at the section ignoring the axial load.
By putting $q^2 = P/EI$ the equation can be written

$$\frac{d^2y}{dx^2} + q^2y = - \frac{M_i}{EI} \tag{6.46}$$

Differentiating Equation (6.46) twice and substituting d^2M_x/dx^2 for $(d^4y/dx^4)EI$ and M_x for $(d^2y/dx^2)EI$ it takes the form

$$\frac{d^2M_x}{dx^2} + q^2M_x = \frac{d^2M_i}{dx^2} \tag{6.47}$$

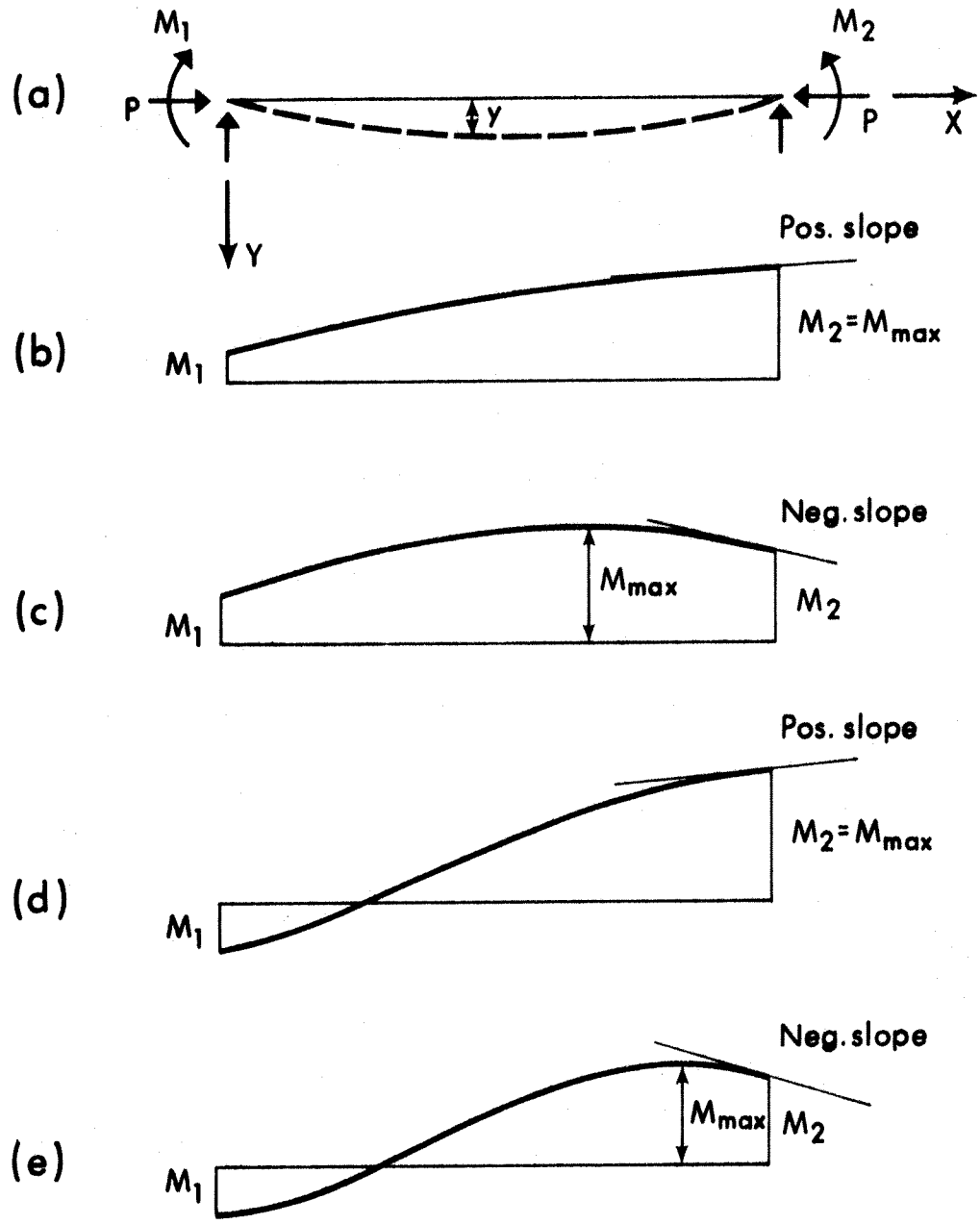

FIG. 6.21 MOMENTS IN A BEAM-COLUMN

and the final solution for the moment at any cross-section is

$$M_x = M_2 \left[\frac{\sin qx + (M_1/M_2) \sin (ql - qx)}{\sin ql}\right] \tag{6.48}$$

M_1 and M_2 are the numerically smaller and larger end moments, resptively. The ratio M_1/M_2 is negative for double curvature and positive for single curvature.

Fig. 6.21(b) through 6.21(e) shows various shapes of the moment diagram that may occur in a beam-column. From these diagrams it is clear that if the maximum moment occurs at the end of the member the slope of the moment diagram must be positive at the end. Thus

$$\left(\frac{dM_x}{dx}\right)_{\substack{x=l \\ x=0}} \geq 0 \tag{6.49}$$

Differentiating Equation (6.48) and putting x=l gives

$$\cos ql \geq \frac{M_1}{M_2} \tag{6.50}$$

for x=0 Equation (6.49) becomes

$$\cos ql \leq \frac{M_2}{M_1} \tag{6.51}$$

Equation (6.51) is clearly satisfied for positive M_2/M_1. In the case of double curvature the equation may be satisfied for $M_2/M_1 = -1$ but cannot be satisfied for $M_2/M_1 < -1$. This is true mathematically, because the cosine is always greater than minus one and physically because the axial load would exceed the critical buckling load. Thus, if Equation (6.50) is satisfied the maximum moment will occur at one end of the member.

If the maximum moment occurs between the ends of the beam-

column its location is obtained by setting Equation (6.49) equal to zero, which yields

$$\tan qx = \frac{\frac{M_2}{M_1} - \cos ql}{\sin ql} \tag{6.52}$$

The solution of Equation (6.52) should always be an angle between zero and π, and may be substituted into Equation (6.48) to obtain the maximum moment.

It has been suggested [35] that when the column end moments include the PΔ moments the moment magnifier concept based on a sway prevented condition may be used to determine the maximum moment. If the moment magnifier turns out to be less than one the maximum moment is assumed to occur at the end.

According to ACI 318-71 the maximum moment is given by Equation (6.53), omitting the capacity reduction factor:

$$M = M_2 \left[\frac{C_m}{1 - \frac{P_u}{P_{cr}}} \right] \tag{6.53}$$

$$\text{where } C_m = 0.6 + 0.4 \frac{M_1}{M_2} \geqq 0.4 \tag{6.54}$$

In a sway frame, with similar columns which are equally loaded, the value of the applied axial load must be less than the critical load based on a sway permitted condition and if P_{cr} is evaluated on the basis of a sway prevented situation the maximum value of the magnifier (for a given C_m) occurs when

$$\frac{P}{P_{cr}} = \frac{P_{cr}^{s}}{P_{cr}^{b}} \tag{6.55}$$

where P_{cr}^{s} and P_{cr}^{b} are critical loads computed on the basis of sway

permitted and sway prevented conditions, respectively. For a given column with given end restraints the right hand side of Equation (6.55) depends only on the effective length factors, and by using the nomographs to determine the effective length factors for various values of end restraint it was found that the maximum value P_{cr}^{s}/P_{cr}^{b} can have is about 0.35. If this value is substituted into Equation (6.53) it is found that the magnifier is less than one for all M_1/M_2 less than 0.125, thus indicating that the maximum moment occurs at the end for smaller values of M_1/M_2. If the applied axial load is only one half of the critical load P_{cr}^{s}, no magnification would be required for M_1/M_2 less than about 0.55.

A comparison between Equations (6.48) and (6.53) may be obtained by assuming values of end restraint and the ratio of applied axial load to the actual critical load. Then the parameter ql may be computed as follows:

$$q^2 = \frac{P_u}{EI} \tag{6.56}$$

$$P_{cr}^{s} = \frac{\pi^2 EI}{(kl)^2} \tag{6.57}$$

$$\therefore \quad ql = \frac{\pi}{k}\sqrt{\frac{P_u}{P_{cr}^{s}}} \tag{6.58}$$

The range of M_1/M_2 values for which the maximum moment occurs at the end is determined from Equation (6.50), and the magnification factor is calculated from Equations (6.52) and (6.48) for cases where the maximum moment occurs between the ends of the column.

Figs. 6.22 and 6.23 show how the moment magnifier varies with the moment ratio M_1/M_2 for various values of end restraint and

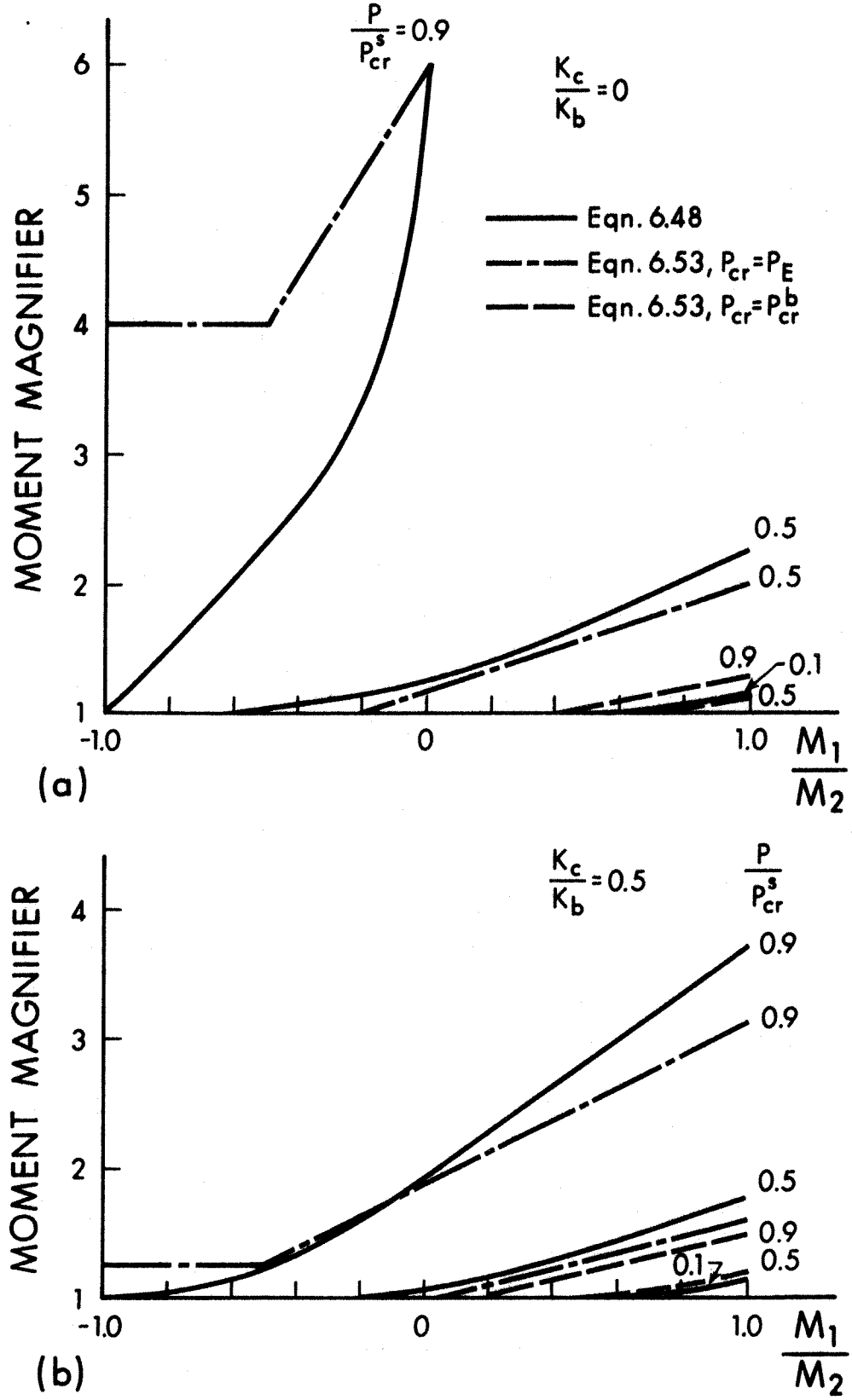

FIG. 6.22 MOMENT MAGNIFICATION IN BEAM-COLUMNS

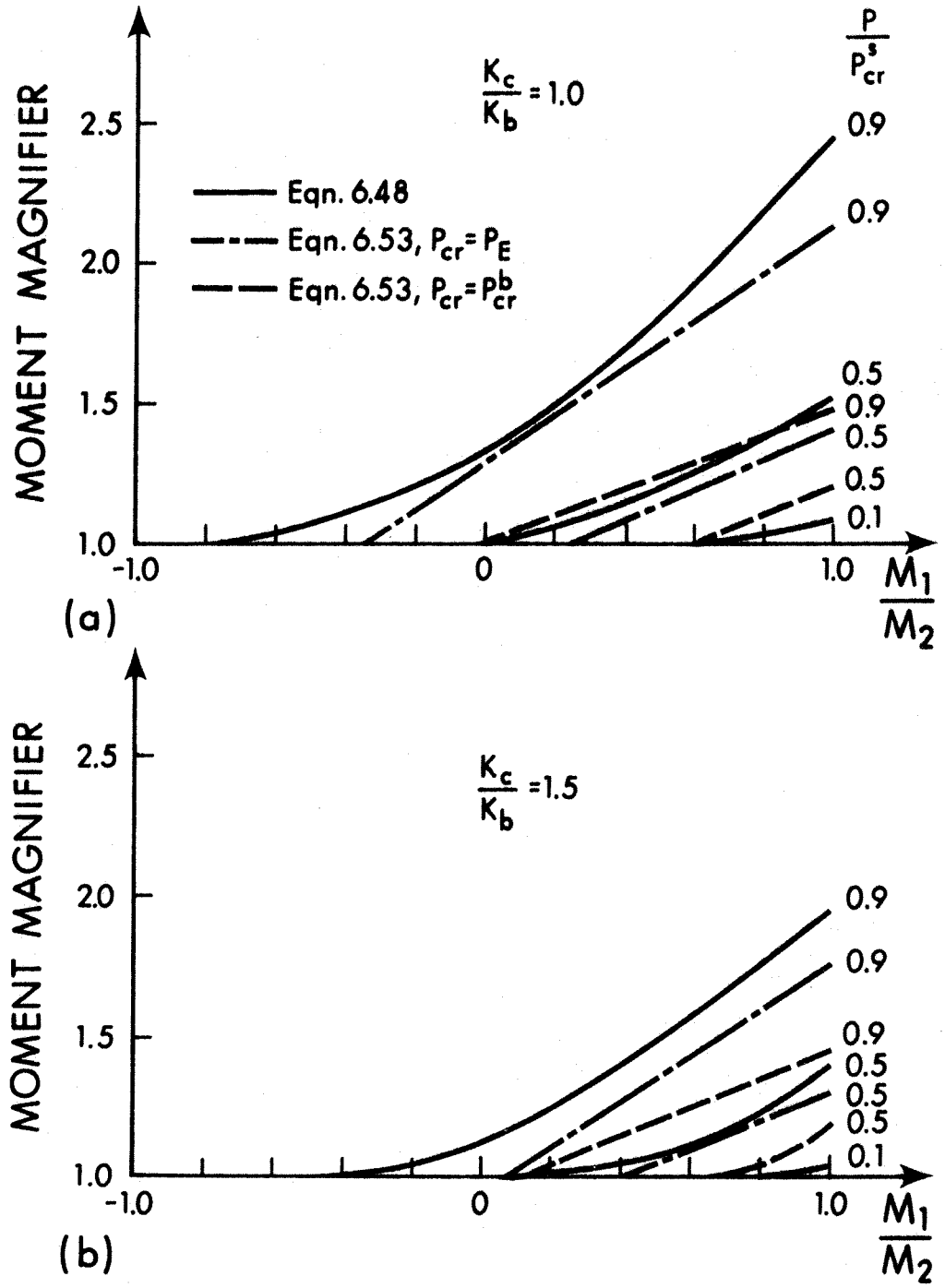

FIG. 6.23 MOMENT MAGNIFICATION IN BEAM-COLUMNS

the ratio P_u/P_{cr}^s. In all cases the restraint has been assumed to be the same at both ends of the column. The ratio P_u/P_{cr} in Equation (6.53) was computed in two different ways: a) $P_{cr} = P_{cr}^b$ and b) $P_{cr} = P_E$, where P_E is the Euler load. The plots show clearly that the use of $P_{cr} = P_{cr}^b$ in Equation (6.52) underestimates the moment magnifier considerably compared to the more accurate solution obtained from Equation (6.48). This is due to the fact pointed out before, that the ratio P_u/P_{cr}^b will always be low in sway frames. A much better approximation is obtained when $P_{cr} = P_E$, except when the column to beam stiffness ratio is very low and P/P_{cr}^s is very high, in which case it tends to give results on the high side. A typical example of this is shown for $P_u/P_{cr}^s = 0.9$ in Fig. 6.22(a) where Equation (6.53) is seen to overestimate the moment magnification by a large amount.

An alternate approximate method may be used to give a better estimate of the moment magnifier. First, Equation (6.50) is used to determine whether the maximum moment occurs at the end of the column. If a magnification is required. the straight line approximation shown in Fig. 6.24 may be used. This approach will always give reasonably conservative values of the magnification factor.

The coordinates of points A and B are easily computed for a given value of ql. The abscissa of point A is simply, from Equation (6.50), equal to cos ql, and the ordinate of point B can be shown from Equations (6.52) and (6.48) to be $\sec(\frac{ql}{2})$. Thus the maximum moment may be expressed by Equation (6.59).

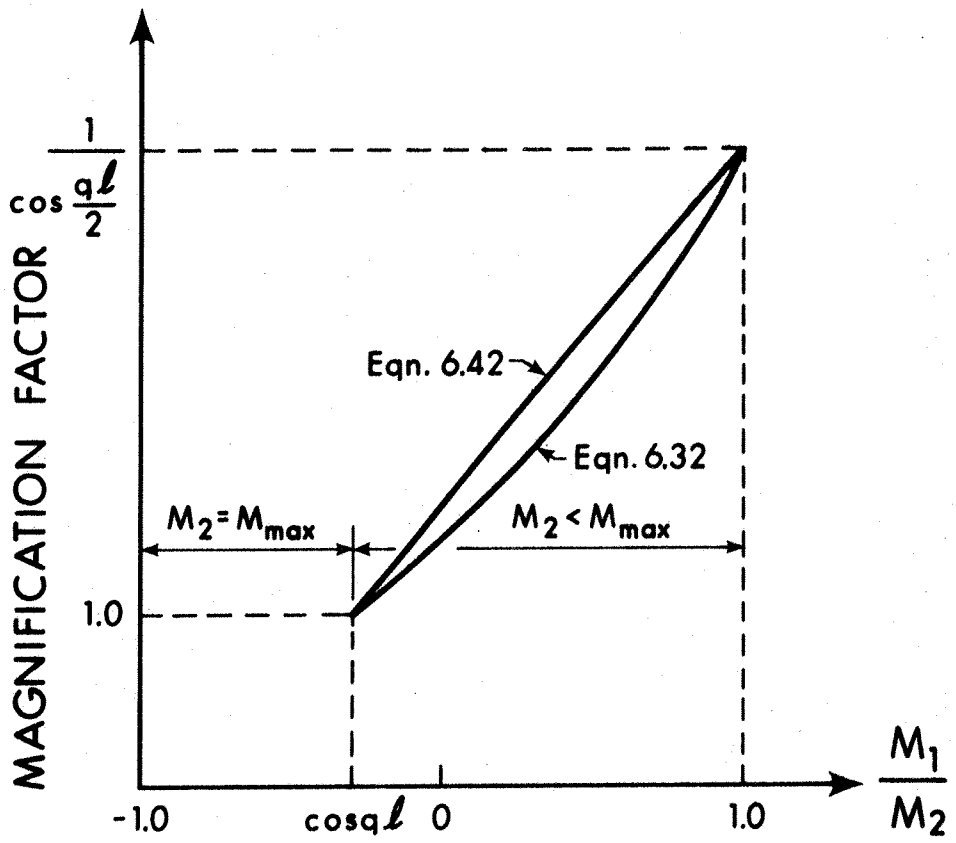

FIG. 6.24 APPROXIMATE MOMENT MAGNIFICATION

$$M_{max} = M_2 \left[\frac{\frac{1}{\cos\frac{ql}{2}} - 1}{1 - \cos ql} \left(\frac{M_1}{M_2} - \cos ql \right) + 1 \right] \qquad (6.59)$$

In practice the moment magnifier equation with $P_{cr} = P_E$ will yield good results in most cases. Only when the effective length factor in the sway permitted condition is close to one, say less than about 1.15, will it be preferable to use Equation (6.59).

The discussion of this section has been based on the assumption that the frame is free to sway such that the columns bend in double curvature. If there is significant lateral restraint provided by bracing elements the deflected shape of the columns will approach single curvature. Thus it is appropriate to evaluate P_{cr} in Equation (6.53) on the basis of the sway prevented nomographs. Since, in practice, there is no such thing as a completely braced or unbraced frame some judgment must be exercised in each case as to which nomograph should be used to evaluate the effective length factor. The bracing criteria of Sections 6.2 and 6.4.2 may be of some assistance in determining the degree of bracing present.

CHAPTER VII

SUMMARY AND CONCLUSIONS

7.1 Summary

In this thesis the second-order analysis of reinforced concrete frames has been investigated.

An analytical model based on the sway subassemblage concept was used to study the load deformation response for 690 combinations of column length, column cross-sections, eight column lengths and five beam stiffnesses were included in the investigation.

The main parameters studied were deflection indices, member stiffnesses, stability parameters and second-order moments.

A computer analysis base on the concepts of column deflection curves and sway subassemblages was carried out using realistic stress-strain diagrams for steel and concrete and taking into account the variation in stiffness along the member caused by cracking.

The current method of second-order analysis prescribed in ACI Code (318-71) and an iterative PΔ-analysis have been compared to the computer analysis to determine their applicability and limitations.

The deflections obtained from the computer analysis were used to establish criteria for predicting stability failures. These criteria are also the practical limits for the use of the simplified design procedures currently in use.

7.2 Conclusions

This study has only considered three column cross-sections and only one value of concrete and steel strength. However, since a fairly wide range of shapes of M-P-ϕ diagrams was used, the results should apply to a wide range of column cross-sections and material strengths.

The analysis showed that the column deflection curve and sway subassemblage concepts may be used to obtain the load-deformation response of reinforced concrete frames. However, the amount of work involved in this kind of anlysis would in most cases make it unsuitable from a practical point of view.

The deflection analysis of Section 4.5 showed that the ultimate deflections corresponding to sway failures are relatively large and that in all but a very few cases exceeded current code deflection limits. Stability failures experienced the largest deflections and none of the 217 cases occurred at a deflection index smaller than 1/200. This indicates that if currently accepted deflection limits are satisfied the structure will exhibit a material failure. Section 6.4.3 presents some approximate methods which can be used to predict the failure mode.

Service load deflections were also found to exceed values specified in most building codes. For high load factors (minimum service load) service load deflections varied between one third and one half of the ultimate deflection and for small load factors (maximum service load) they varied between one half and two thirds. Equation (4.7) may be used to estimate the ultimate deflection.

The moment magnifier and PΔ methods of analysis were both

found to be applicable for material failures, but in the case of stability failures they may produce unsafe designs if the value of EI is greater than that corresponding to line 0-3 in Fig. 6.13(a). In Section 6.4.2 some criteria were established for the use of the PΔ-method, and if they are satisfied the structure will exhibit a material failure. By expressing the PΔ iteration procedure in the form of a geometric series it was found that if $P\Delta_1/Q_1 l$ is less than 0.05 the effect of the axial load may be ignored altogether and if $P\Delta_1/Q_1 l$ is between 0.05 and 0.22 only the effect of the first order deflections need be included. For values greater than 0.22 a second-order analysis is required.

The stiffness analysis of reinforced concrete beams showed that the effective stiffness may be assumed to be between 0.5 and 0.6 times $E_c I_g$. When, in the case of T-sections, the stiffness was expressed in terms of the moment of inertia of the web, values of the effective stiffness were found to be between 1.0 and 1.2 times $E_c I_w$.

REFERENCES

1. A.C.I. COMMITTEE 318. Building Code Requirements for Reinforced Concrete (A.C.I. 318-71), American Concrete Institute, Detroit, 1971.

2. A.C.I. COMMITTEE 318. Commentary on Building Code Requirements for Reinforced Concrete (A.C.I. 318-71), Detroit, 1971.

3. MacGREGOR, J.G., BREEN, J.E., PFRANG, E.O. Design of Slender Columns. Journal American Concrete Institute, Vol. 67, January, 1970.

4. INTERNATIONAL RECOMMENDATIONS FOR THE DESIGN AND CONSTRUCTION OF CONCRETE STRUCTURES. Comite Europeen du Breton, Prague, June, 1970.

5. BULLETIN d'INFORMATION No. 93. Comite Europeen du Beton, Paris, France, July, 1973.

6. ADAMS, P.F. Design of Steel Beam-Columns. Paper presented at the Canadian Structural Engineering Conference 1972, Canadian Steel Industries Construction Council, Toronto, Canada.

7. GOLDBERG, J.E. Approximate Elastic Analysis. State of the Art Report No. 2, Technical Committee No. 14, Proc. of A.S.C.E.-I.A.B.S.E. International Conference on Planning and Design of Tall Buildings, Vol. II, New York, April, 1973.

8. MacGREGOR, J.G. Stability of Reinforced Concrete Building Frames. State of the Art Report No. 1, Technical Committee 23, Proc. of A.S.C.E.-I.A.B.S.E. International Conference on Planning and Design of Tall Buildings, Vol. III, New York, April, 1973.

9. FEY, T. Approximate Second-Order Analysis of Reinforced Concrete Frames. (In German), Bauingenieur, June, 1966.

10. PARME, A.L. Capacity of Restrained Eccentrically Loaded Long Columns. Symposium on Reinforced Concrete Columns, A.C.I. Special Publication SP13, 1966.

11. AAS-JAKOBSEN, K., GRENACHER, M. Berechnung Unelastisher Rahmen Nach Der Theorie 2. Ordnung, Bericht Nr. 45, Institut Für Baustatik, E.T.H. Zürich, January, 1973.

12. MACCHI, G. Theme Report, Technical Committee 22. Proc. of A.S.C.E.-I.A.B.S.E. International Conference on Planning and Design of Tall Buildings, Vol. III, New York, April, 1973.

13. MACCHI, G. Elastic Distribution of Moments on Continuous Beams. International Symposium in the Flexural Mechanics of Reinforced Concrete, A.S.C.E.-A.C.I., Miami, Nov. 1964.

14. MALDAGUE, J.C. Etude de la Deformation de Poutres en Beton Arme. Annales I.T.B.T.P, No.209, May 1965.

15. MACCHI, G. Propositien pour le Calcul des Deformations du Beton Arme en Vue des Calculs Hyperstatiques. C.E.B., Bull. No. 52, 1964.

16. BREEN, J.E. The Restrained Long Column as a Part of a Rectangular Frame. Ph. D. Thesis, The University of Texas, Austin, Texas, June, 1962.

17. DANIELS, J.H., LU, L.W. The Subassemblage Method of Designing Unbraced Multistory Frames. Fritz Engineering Laboratory Report, No. 273.37, Lehigh University.

18. HOGNESTAD, E. A Study of Combined Bending and Axial Load in Reinforced Concrete Members. Bulletin No. 399, University of Illinois, Engineering Experiment Station, November, 1951.

19. WELCH, G.B. Tensile Strains in Unreinforced Concrete Beams. Magazine of Concrete Research, Vol. 78, No. 54 March, 1966.

20. SLIGHT, B. Private Communication, 1973.

21. von KARMAN, T. Untersuchungen über Knickfestigkeit. Mitteilungen uber Forschungsarbeiten auf dem Gebiete des Ingenieurwesens, No. 81, Berlin, 1910.

22. CHWALLA, E. Uber die experimentelle Untersuchung des Tragverhaltens gedruchter Stabe aus Baustahl. Der Stahlbau, Vol. 7, p. 17, 1934.

23. ELLIS, J.S. Plastic Behavior of Compression Members. Journal of the Mechanics and Physics of Solids, Vol.6, p. 282, 1958.

24. NEAL, B.G. and MANSELL, D.S. The Effect of Restraint Upon Collapse Loads of Mild Steel Trusses. International Journal of Mechanical Science, Vol. 5, p. 87, February 1963.

25. HORNE, M.R. The Elastic-Plastic Theory of Compression Members. Journal of the Mechanics and Physics of Solids, Vol. 4, p. 104, 1956.

26. BIJLAARD, P. Buckling of Column with Equal and Unequal End Eccentricities. Proceedings of the 2nd. U.S. National Congress of Applied Mechanics, p. 555, 1954.

27. OJALVO, M. Restrained Columns. Proceedings ASCE, Vol. 86, No. EM5, p. 1, October 1960.

28. LAY, M.G. The Mechanics of Column Deflection Curves. Fritz Engineering Laboratory Report No. 278.12, Lehigh University, June 1964.

29. HAUK, G. and LEE, S.L. Stability of Elasto-Plastic Wide-Flange Columns. Journal of the Structural Division, ASCE, Vol. 89, No. ST6, p. 297, December 1963.

30. GALAMBOS, T.V. Structural Members and Frames. Prentice-Hall, Inc., Englewood Cliffs, N.J., 1968.

31. CHANG, W.F. Long Restrained Reinforced Concrete Columns. Ph.D. Thesis, The University of Texas, Austin, Texas, June 1961.

32. NATIONAL BUILDING CODE OF CANADA 1970, National Research Council, Ottawa, Canada.

33. ACI COMMITTEE 435. Allowable Deflections. Journal American Concrete Institute, Vol. 65, June 1968.

34. Plastic Design of Multi-Story Frames, Lecture Notes, Department of Civil Engineering, Lehigh University.

35. Plastic Design of Multi-Story Frames, Design Aids, Department of Civil Engineering, Lehigh University.

36. Continuity in Concrete Building Frames. 4th. edition, Portland Cement Association, Chicago, 1959.

37. WANG, C.K. and SALMON, C.G. Reinforced Concrete Design. Intext Educational Publishers, New York, 1973.

38. LAY, M.G.The Stability of Members in Plane Frameworks. The Broken Hill Proprietary Company Ltd., Clayton, Victoria, Australia, December 1969.

39. LAY, M.G. Assessment of Sway-Preventing Action in Frames. The Broken Hill Proprietary Company Ltd., Clayton, Victoria, Australia, June 1970.

40. TRAHIR, N.S. Buckling of Plane Frames. Steel Construction (Aust. ISC), 3(1), 1st. Quarter, 1969.

41. TELWAR, S.D. and COHN, M.Z. Shear Wall Bracing Criteria for Tall Buildings. Preliminary Report, 9th. Congress, IABSE, Amsterdam, 1972.

42. FURLONG, R. Column Slenderness and Charts for Design. Journal American Concrete Institute, Vol. 68, January 1971, pp. 9-17.

43. Code of Practice for the Structural Use of Concrete, (CP 110: 1972), British Standards Institution, London.

44. ROSENBLEUTH, E. Slenderness Effects in Buildings. Journal of the Structural Division, ASCE, 91, ST1, January 1965.

45. SPRINGFIELD, J. and ADAMS, P.F. Aspects of Column Design in Tall Buildings. Journal of the Structural Division, ASCE, ST5, May 1972.

46. McGUIRE, W. Steel Structures. Prentice-Hall Inc., Englewood Cliffs, N.J., 1968.

47. MacGREGOR, J.G., MAJUMDAR, S.N.G., NIKHED, R.P. and ADAMS, P.F. Approximate Inelastic Analysis of Shear Wall-Frame Structures. Journal of the Structural Division, ASCE, ST11, November 1972.

APPENDIX A

RESTRAINED COLUMN CURVES

A.1 Introduction

The restrained column curves presented in this section have been prepared for five different values of the beam stiffness parameter K. From left to right the curves are for $K = \infty$, $K = 600$, $K = 400$, $K = 200$ and $K = 100$, respectively. Where there are fewer than five curves on the chart, those corresponding to low values of beam stiffness are missing, indicating an unstable structure for those cases. Thus, if a chart contains three curves they correspond to values of K of ∞, 600 and 400. For K equal to 200 and 100 the structure bacame unstable at a very small value of lateral load.

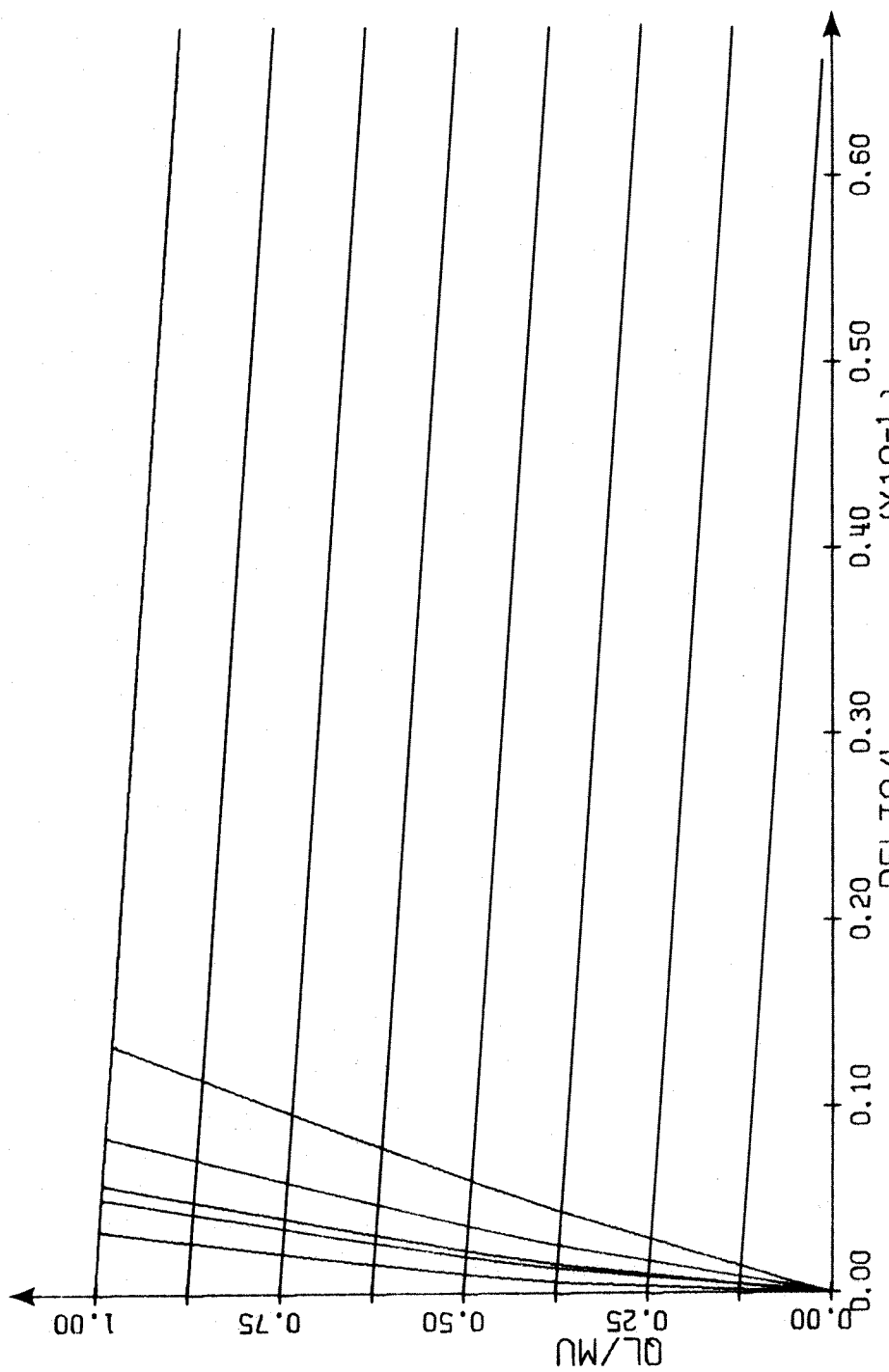

FIG. A-1 LOAD DEFLECTION DIAGRAM. TIED COLUMN. BARS IN 2 FACES
L/H=5 P/P0=0.1

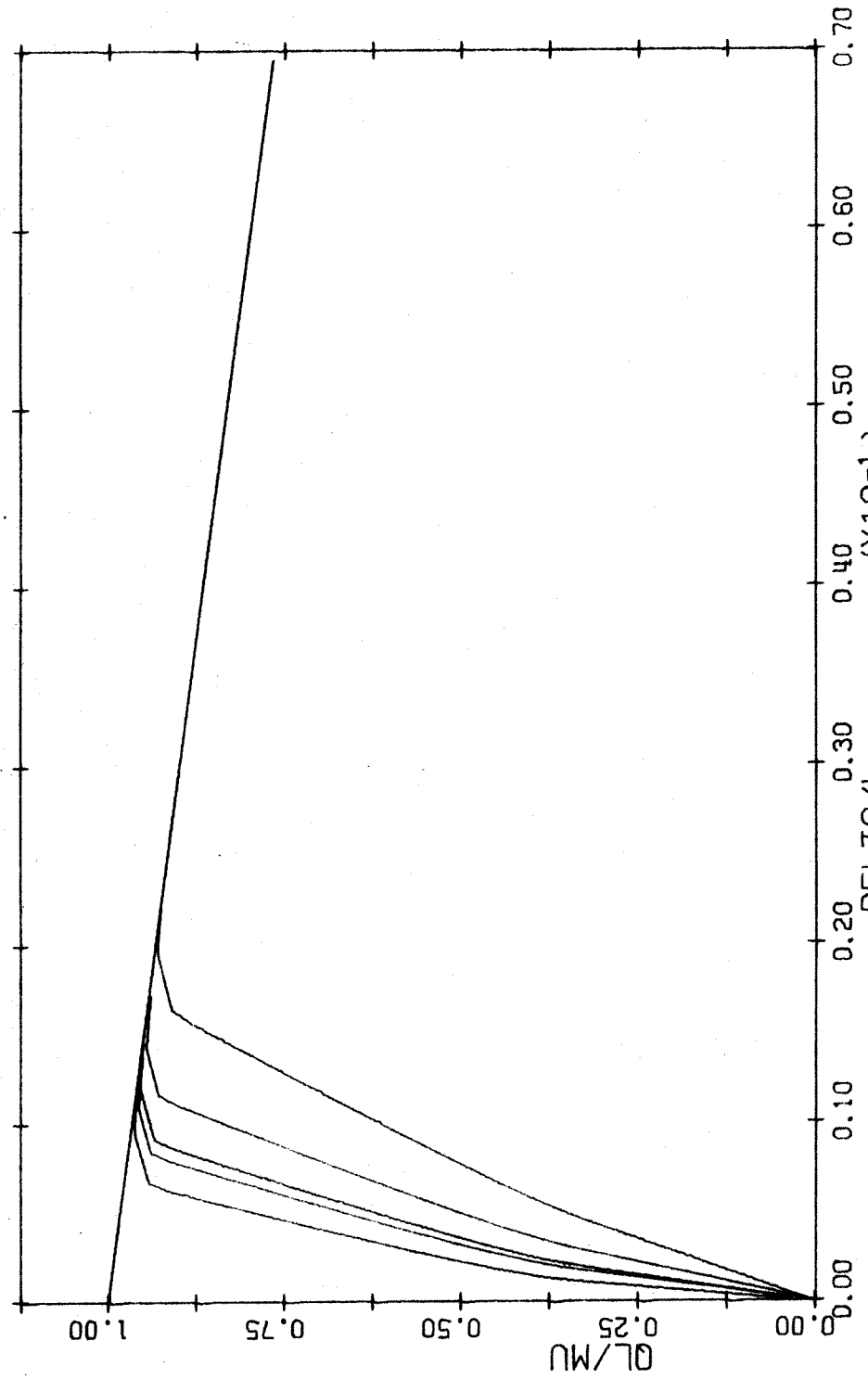

FIG. A-2 LOAD DEFLECTION DIAGRAM. TIED COLUMN. BARS IN 2 FACES
L/H=10 P/P0=0.1

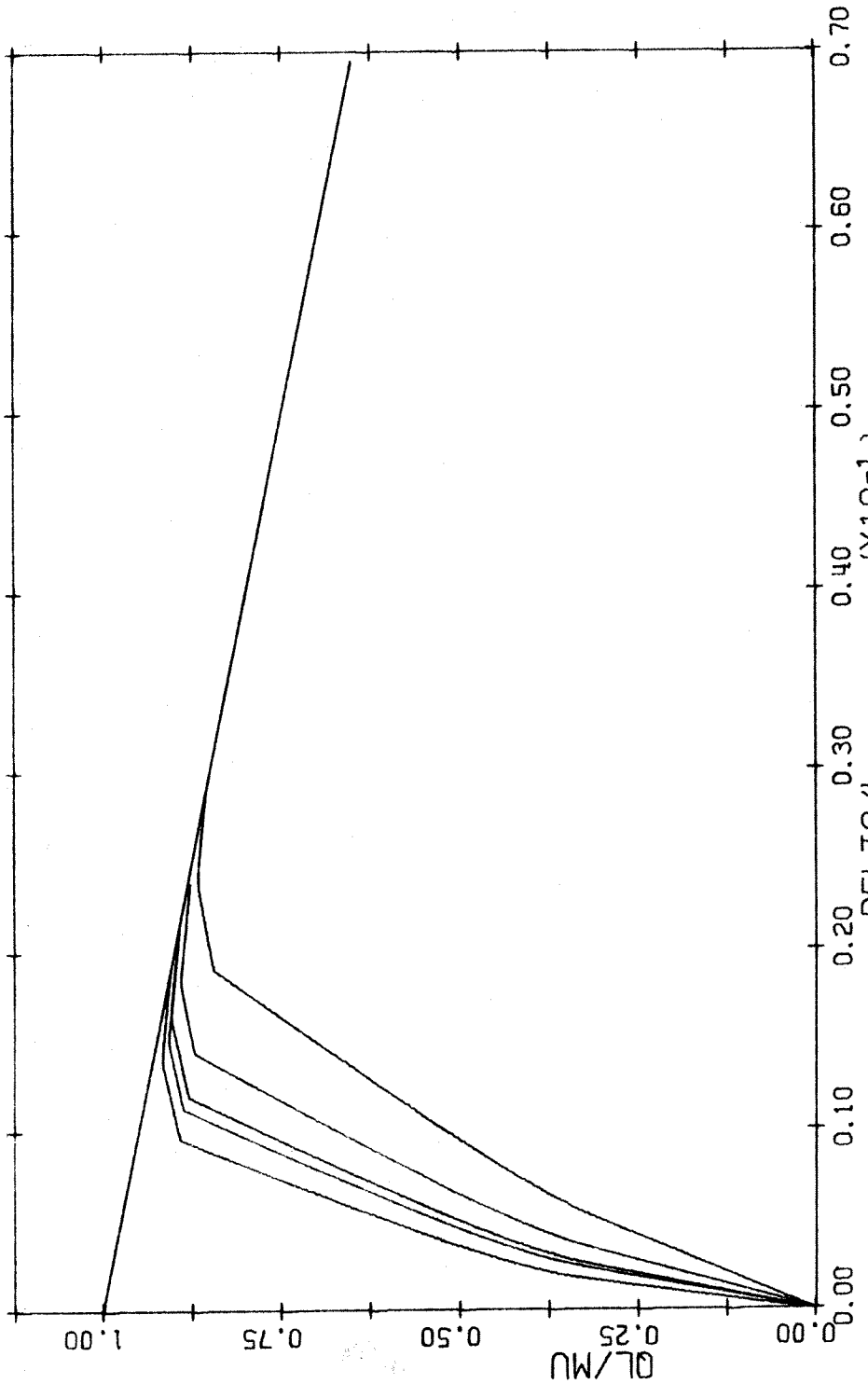

FIG. A-3 LOAD DEFLECTION DIAGRAM. TIED COLUMN. BARS IN 2 FACES
L/H=15 P/P0=0.1

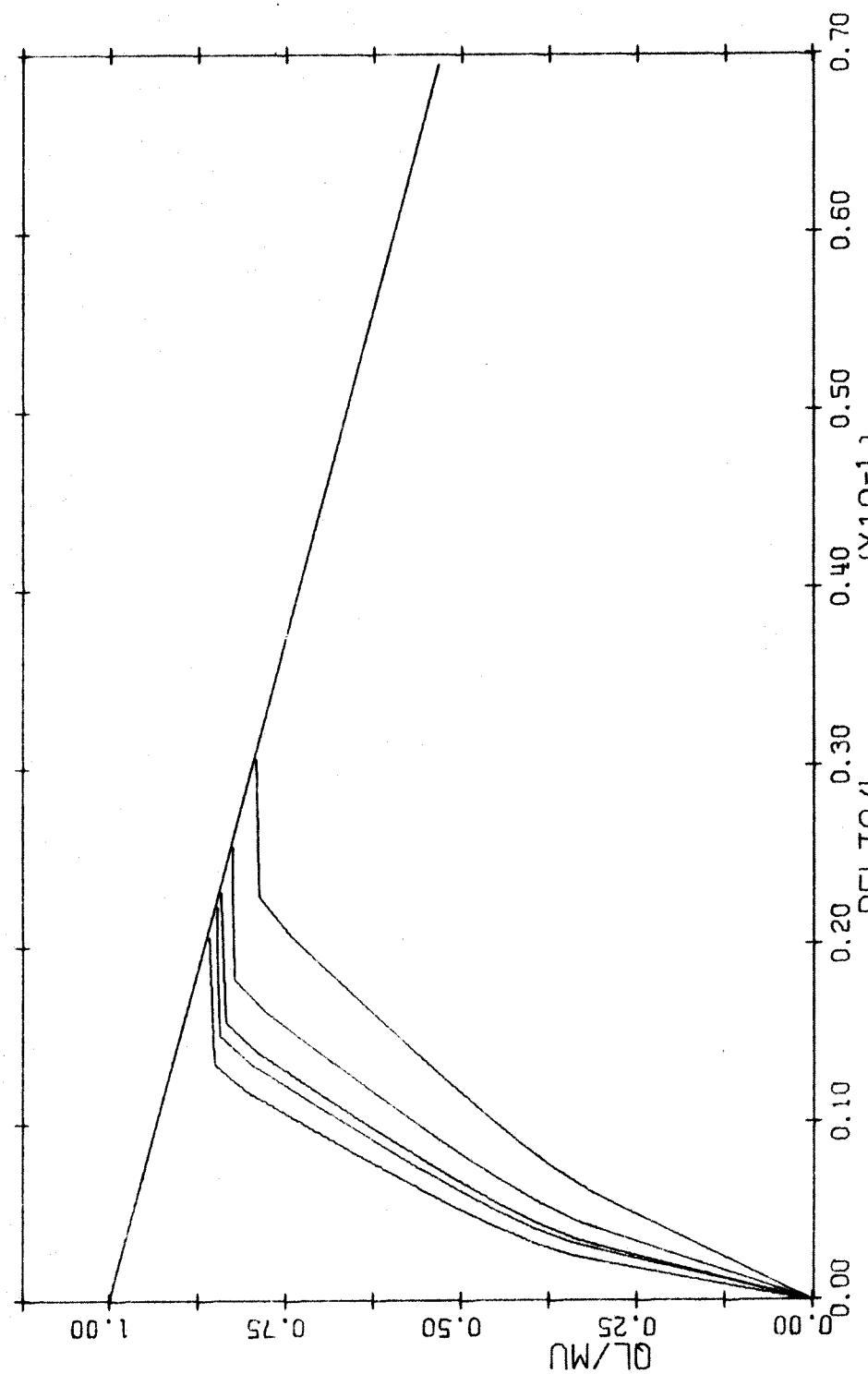

FIG. A-4 LOAD DEFLECTION DIAGRAM. TIED COLUMN. BARS IN 2 FACES
L/H=20 P/P0=0.1

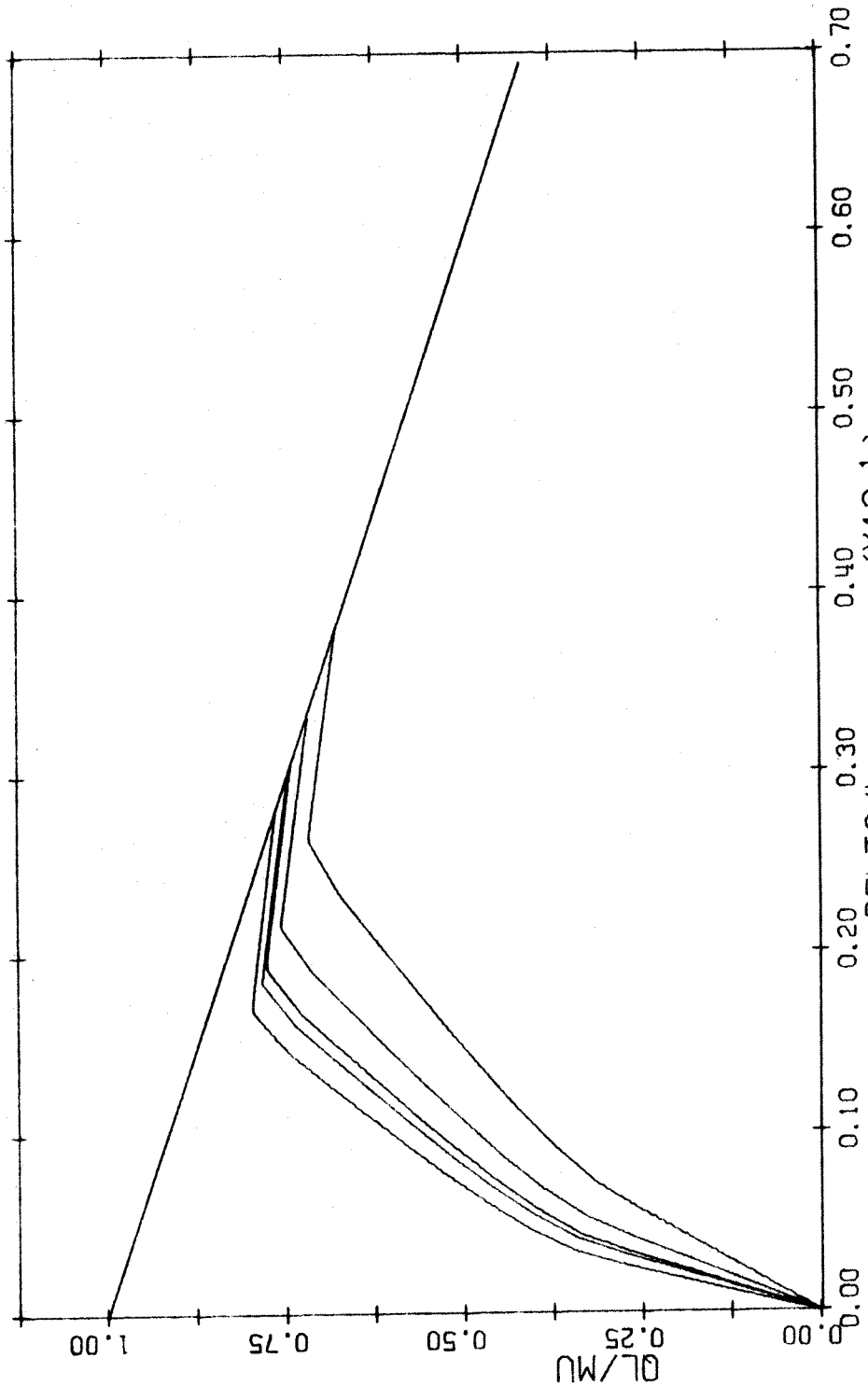

FIG. A-5 LOAD DEFLECTION DIAGRAM. TIED COLUMN. BARS IN 2 FACES
L/H=25 P/P0=0.1

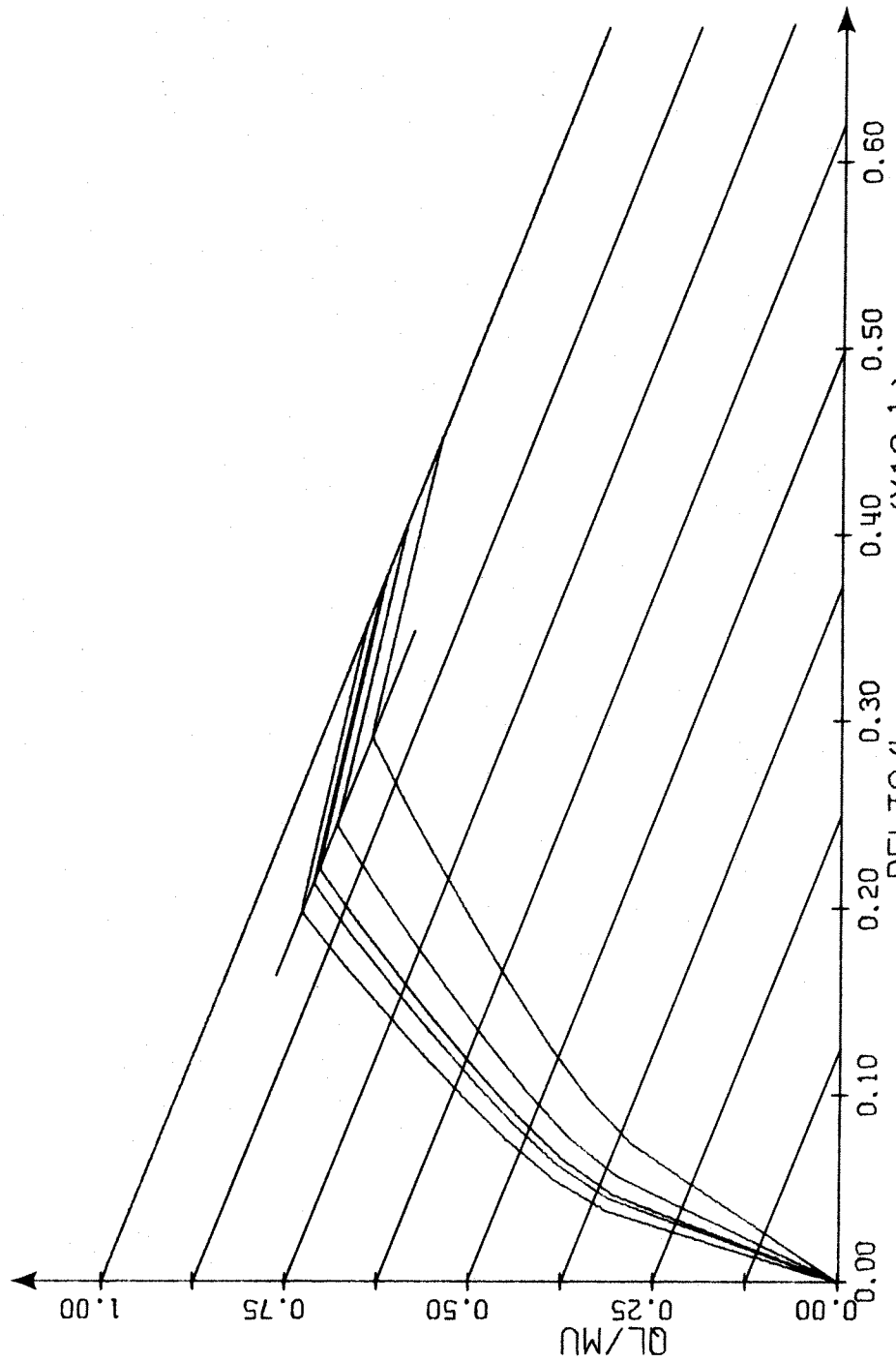

FIG. A-6 LOAD DEFLECTION DIAGRAM. TIED COLUMN. BARS IN 2 FACES
L/H=30 P/P0=0.1

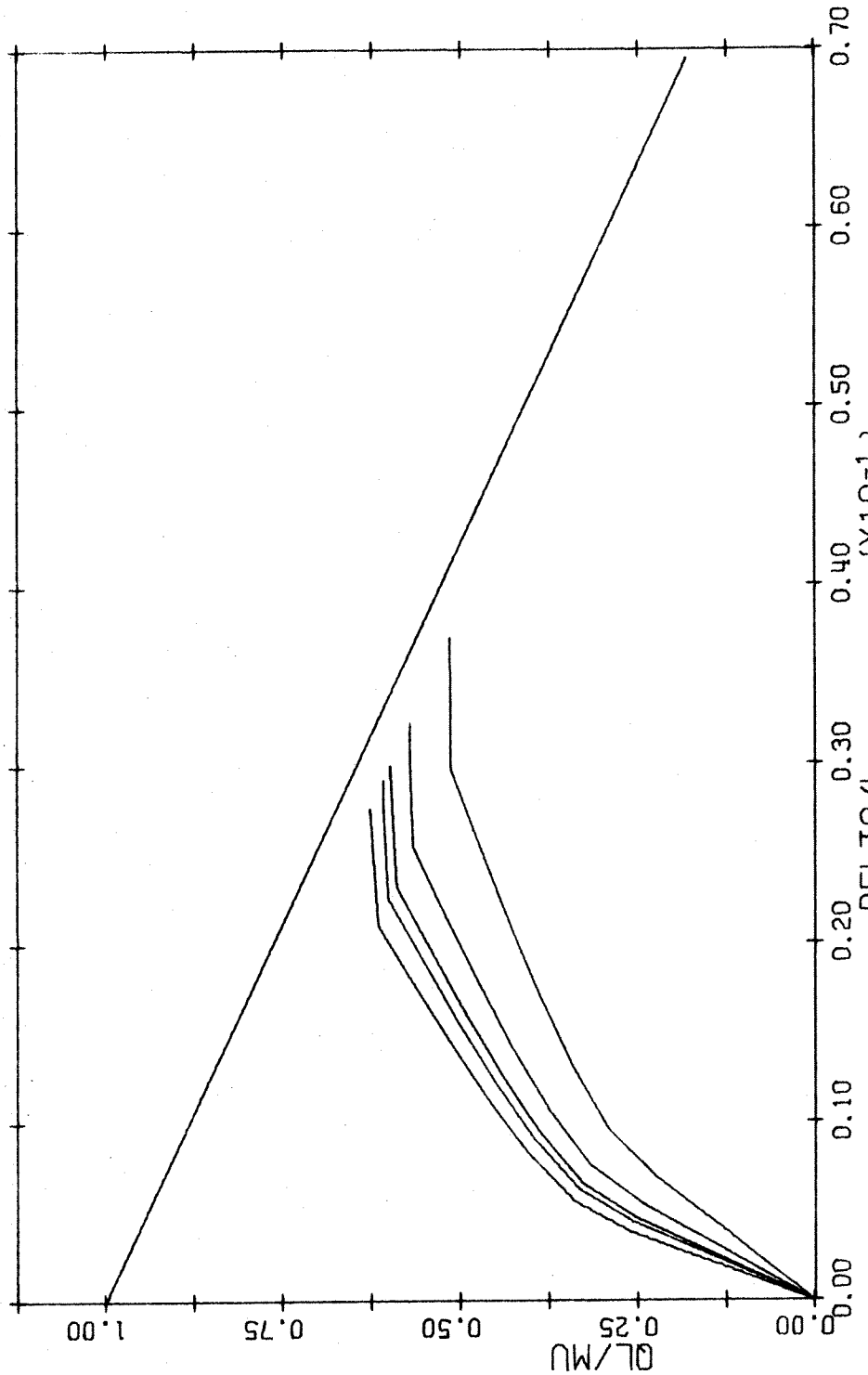

FIG. A-7 LOAD DEFLECTION DIAGRAM. TIED COLUMN. BARS IN 2 FACES
L/H=35 P/P0=0.1

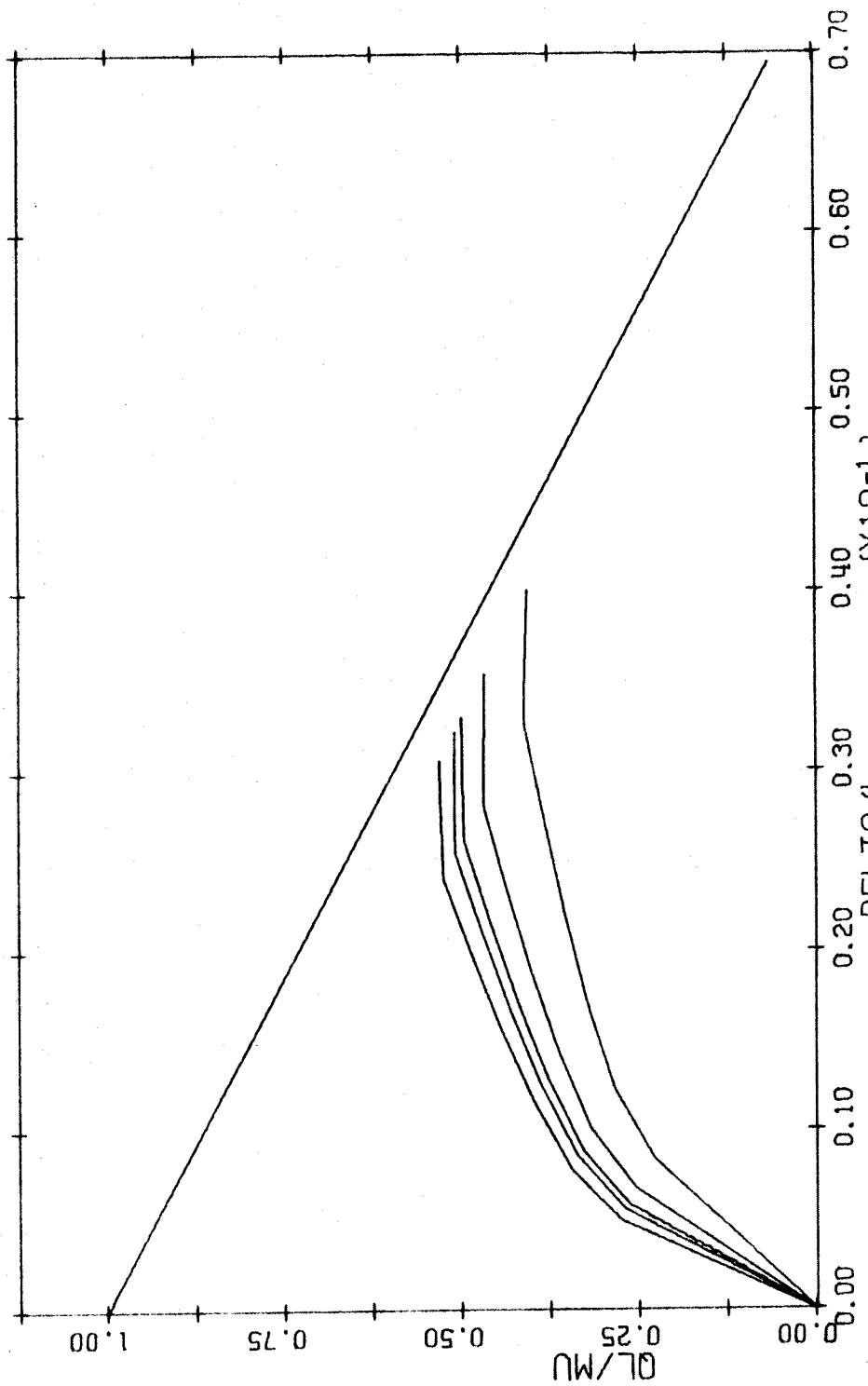

FIG. A-8 LOAD DEFLECTION DIAGRAM. TIED COLUMN. BARS IN 2 FACES
L/H=40 P/P0=0.1

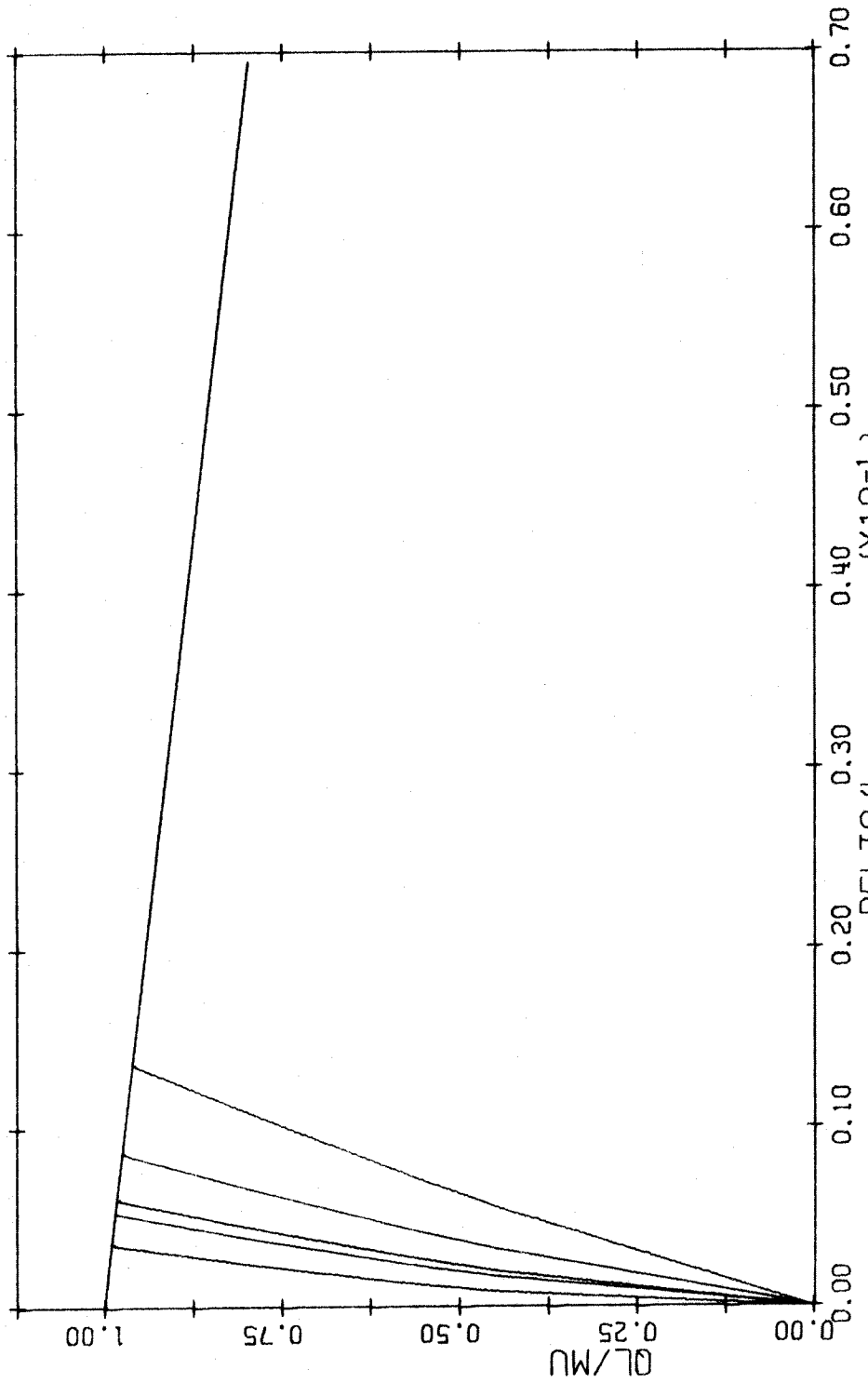

FIG. A-9 LOAD DEFLECTION DIAGRAM. TIED COLUMN. BARS IN 2 FACES
L/H=5 P/P0=0.2

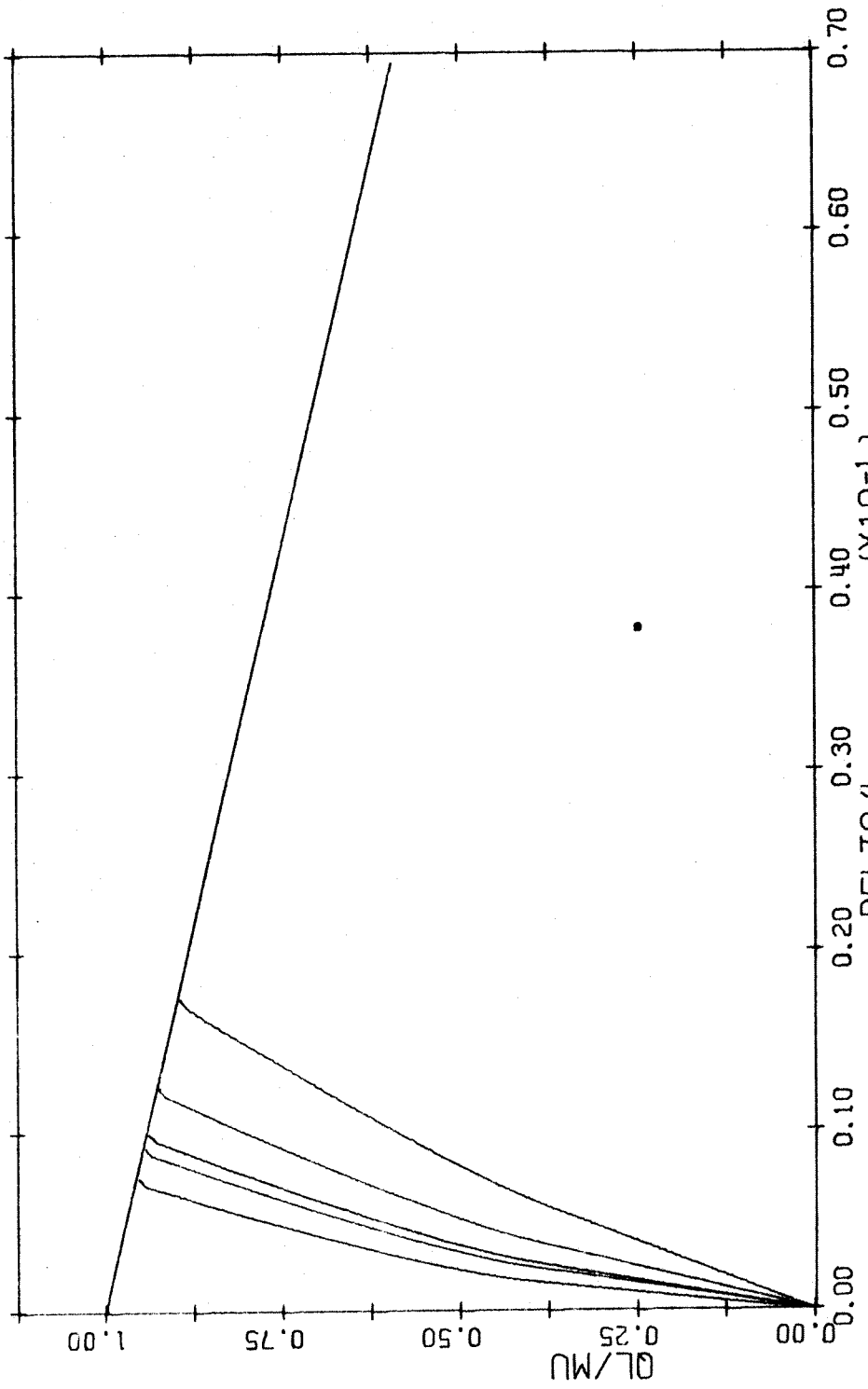

FIG. A-11 LOAD DEFLECTION DIAGRAM. TIED COLUMN. BARS IN 2 FACES
L/H=15 P/PC=0.2

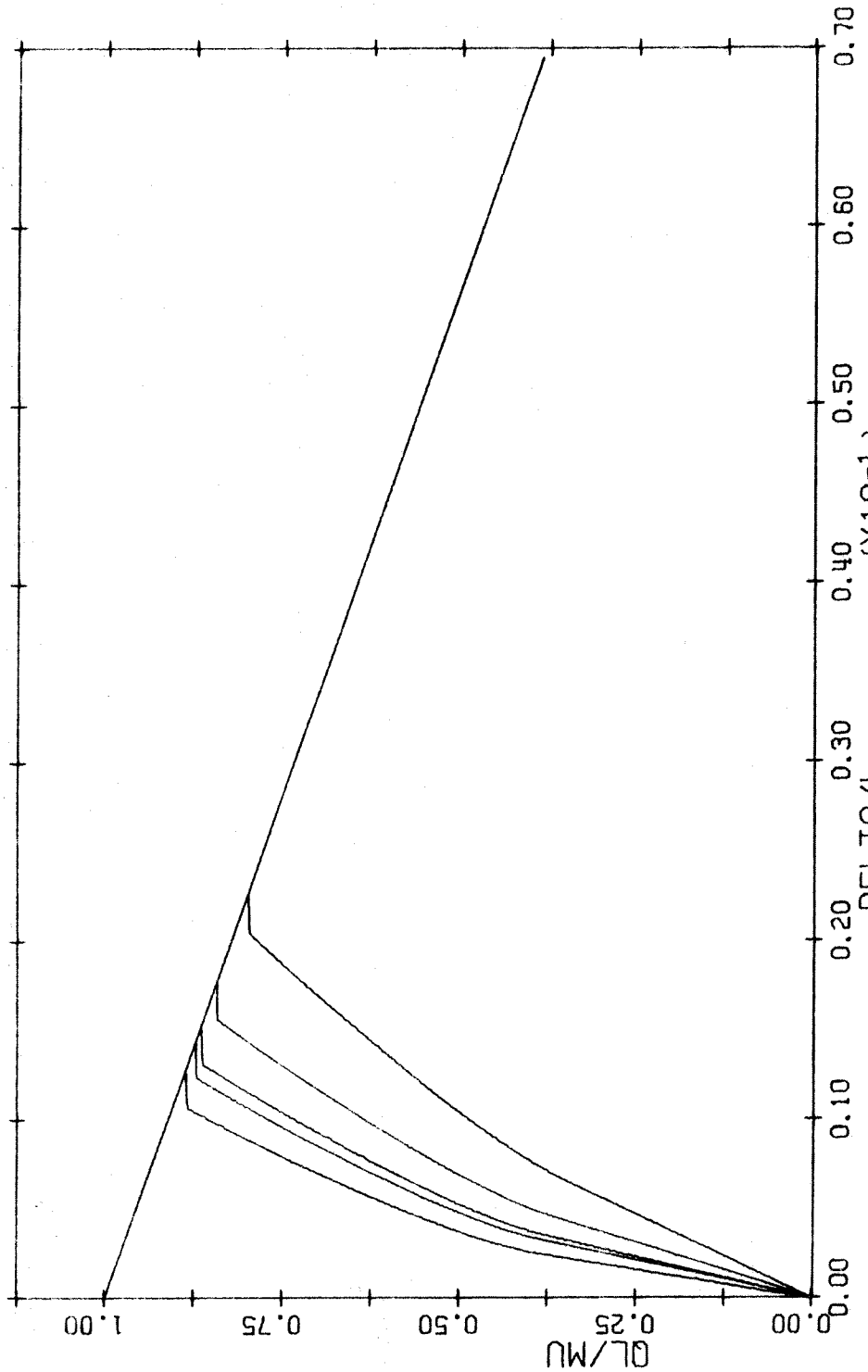

FIG. A-10 LOAD DEFLECTION DIAGRAM. TIED COLUMN. BARS IN 2 FACES
L/H=10 P/P0=0.2

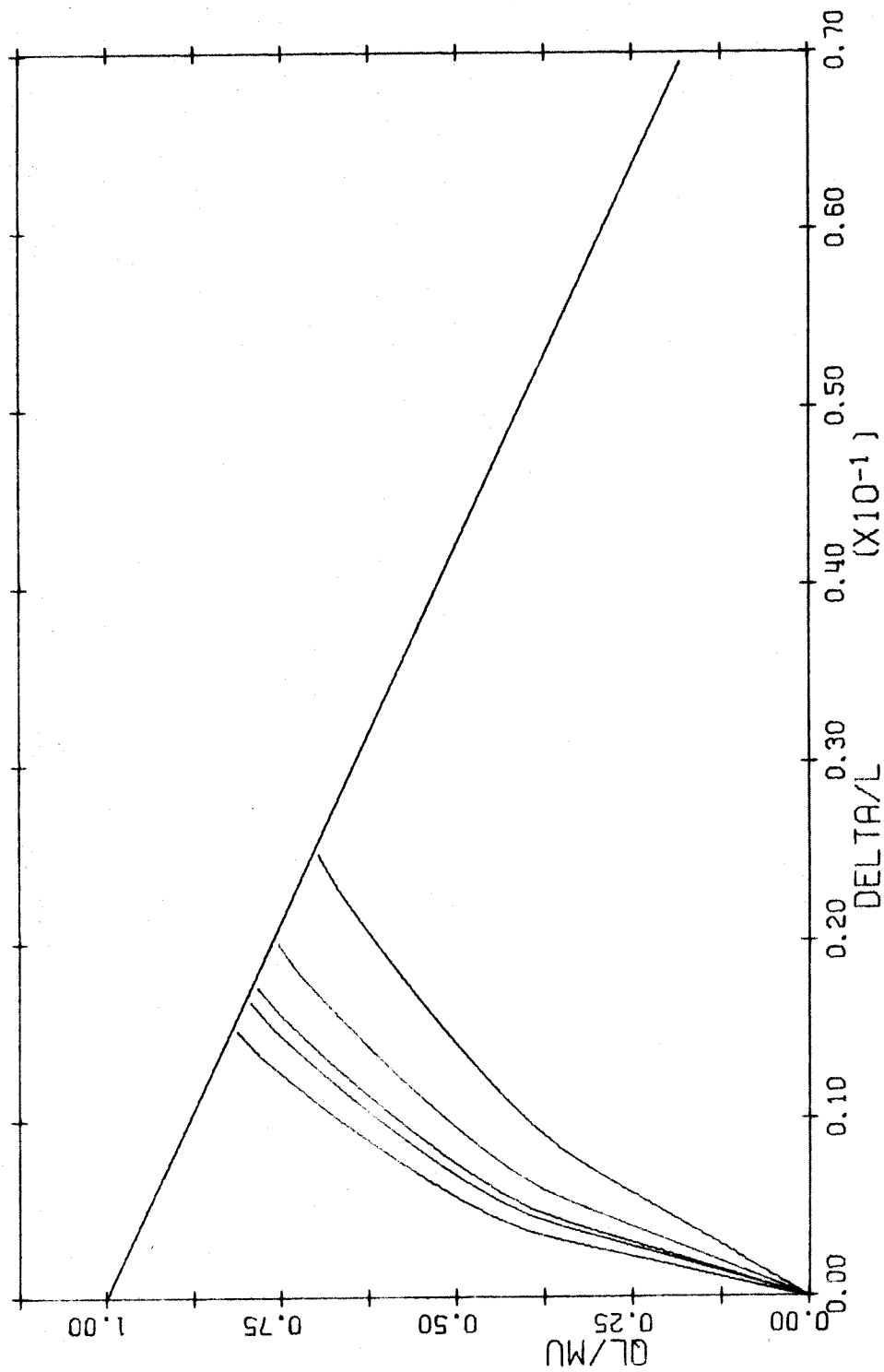

FIG. A-12 LOAD DEFLECTION DIAGRAM. TIED COLUMN. BARS IN 2 FACES
L/H=20 P/PO=0.2

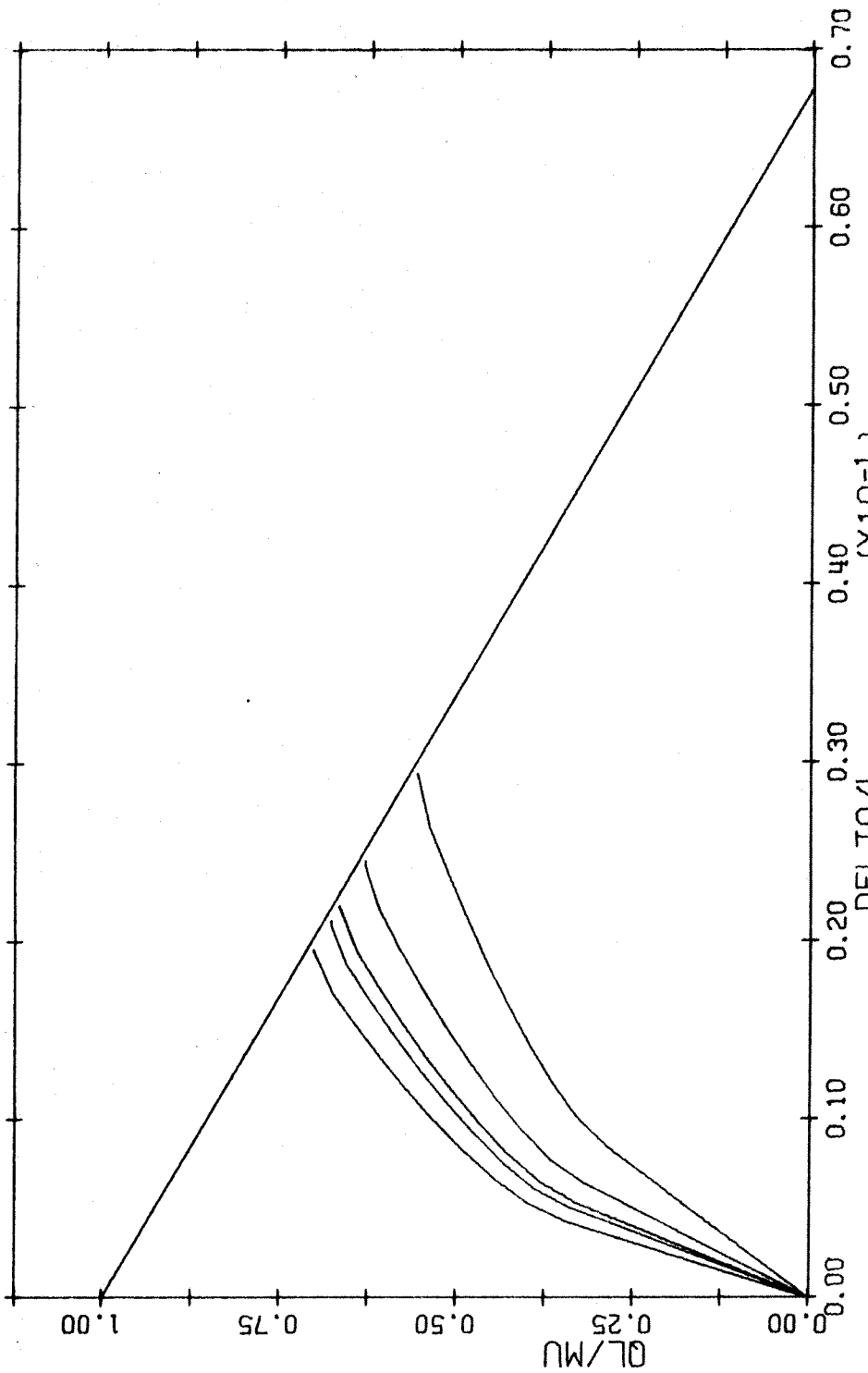

FIG. A-13 LOAD DEFLECTION DIAGRAM. TIED COLUMN. BARS IN 2 FACES
L/H=25 P/P0=0.2

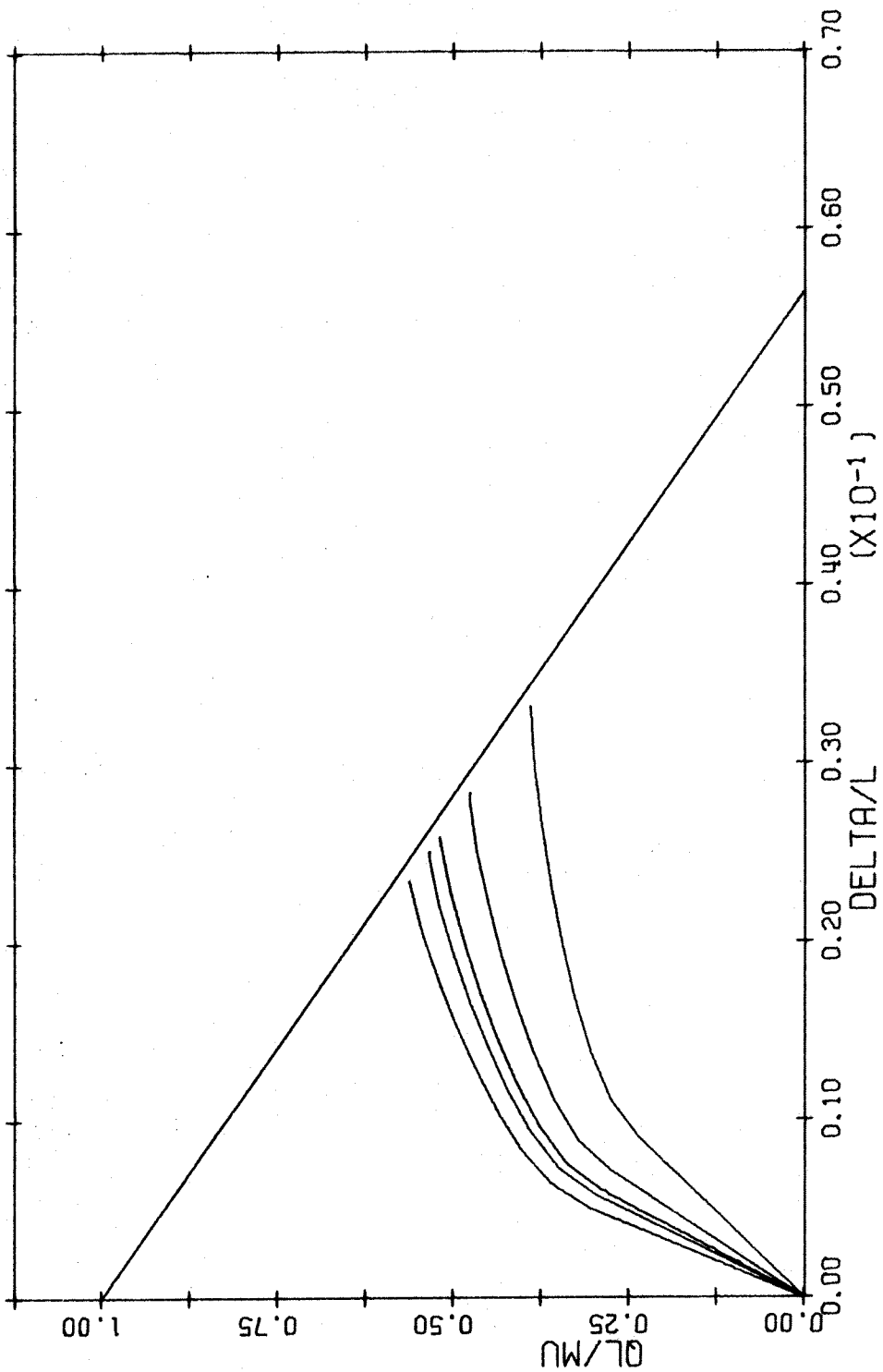

FIG. A-14 LOAD DEFLECTION DIAGRAM. TIED COLUMN. BARS IN 2 FACES
L/H=30 P/P0=0.2

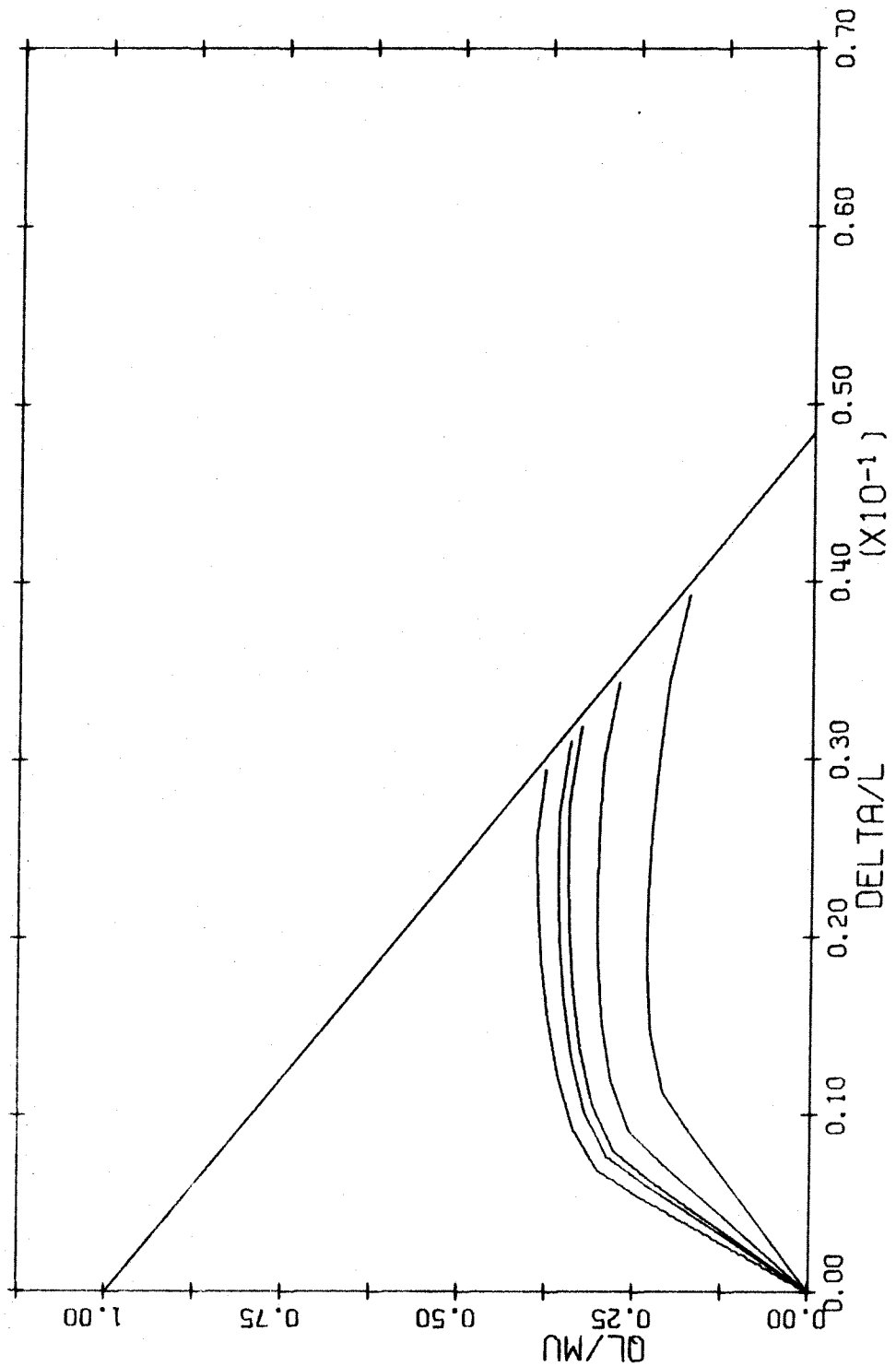

FIG. A-15 LOAD DEFLECTION DIAGRAM. TIED COLUMN. BARS IN 2 FACES
L/H=35 P/PO=C.2

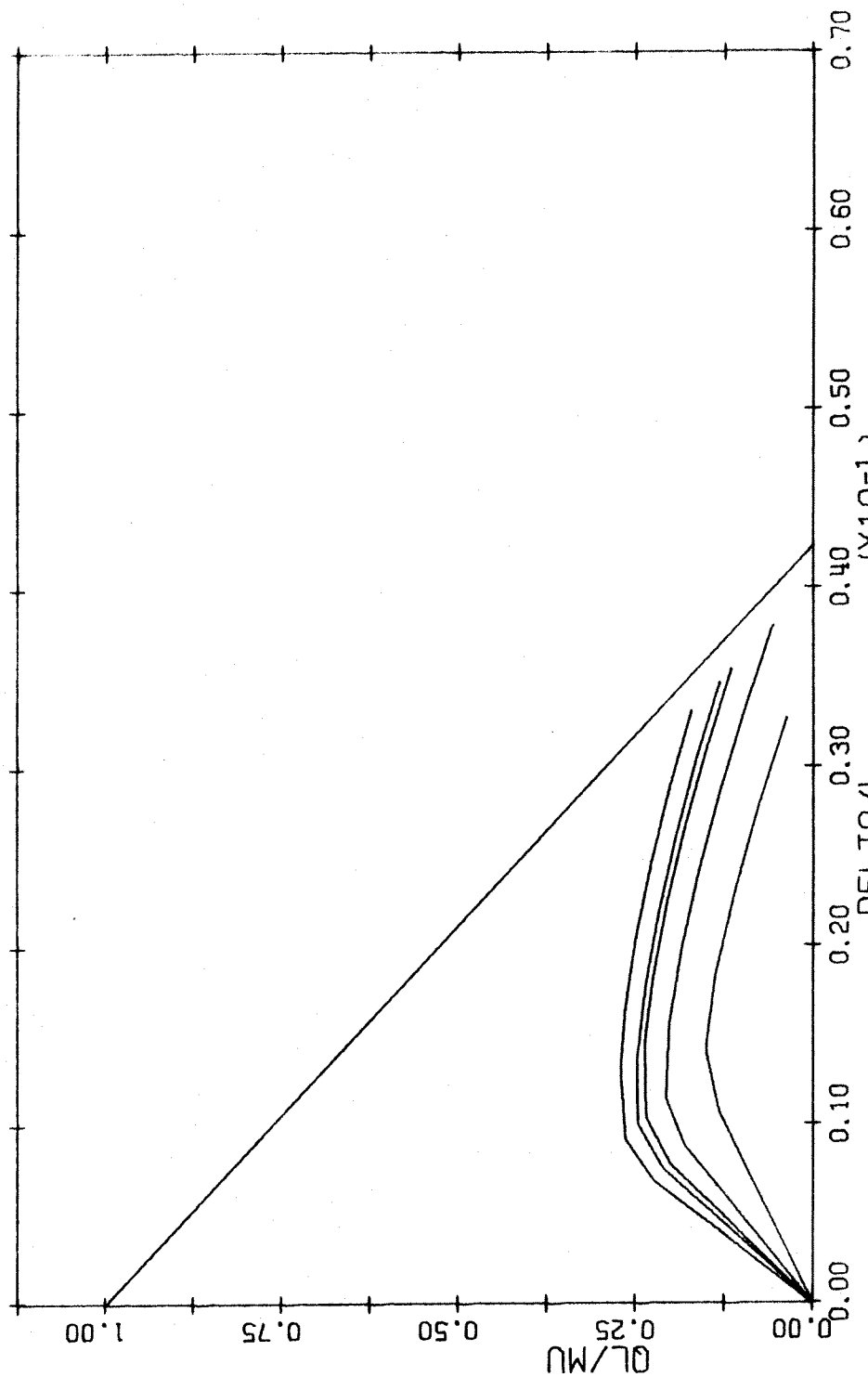

FIG. A-16 LOAD DEFLECTION DIAGRAM. TIED COLUMN. BARS IN 2 FACES
L/H=40 P/P0=0.2

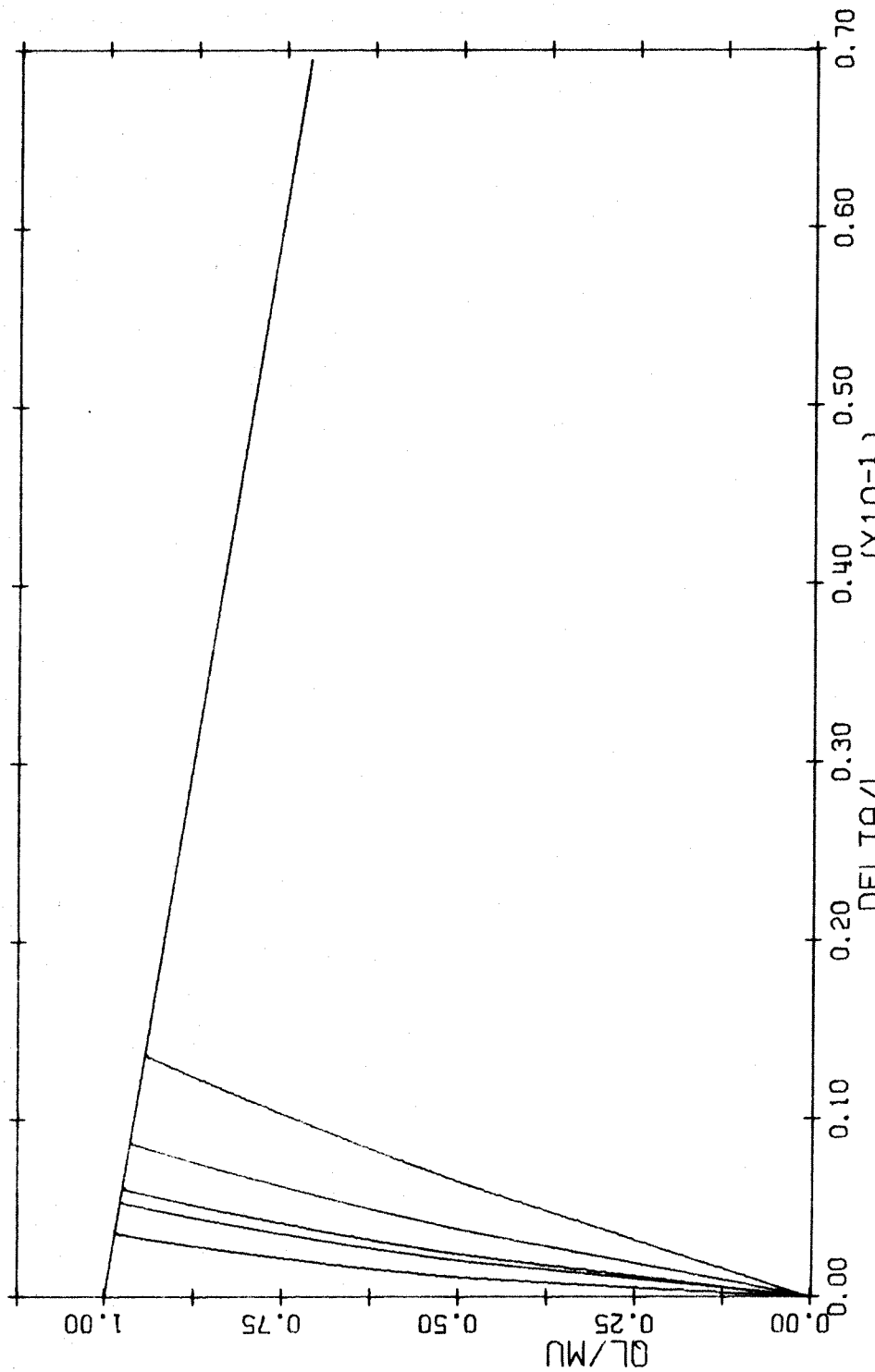

FIG. A-17 LOAD DEFLECTION DIAGRAM. TIED COLUMN. BARS IN 2 FACES
L/H=5 P/PC=0.3

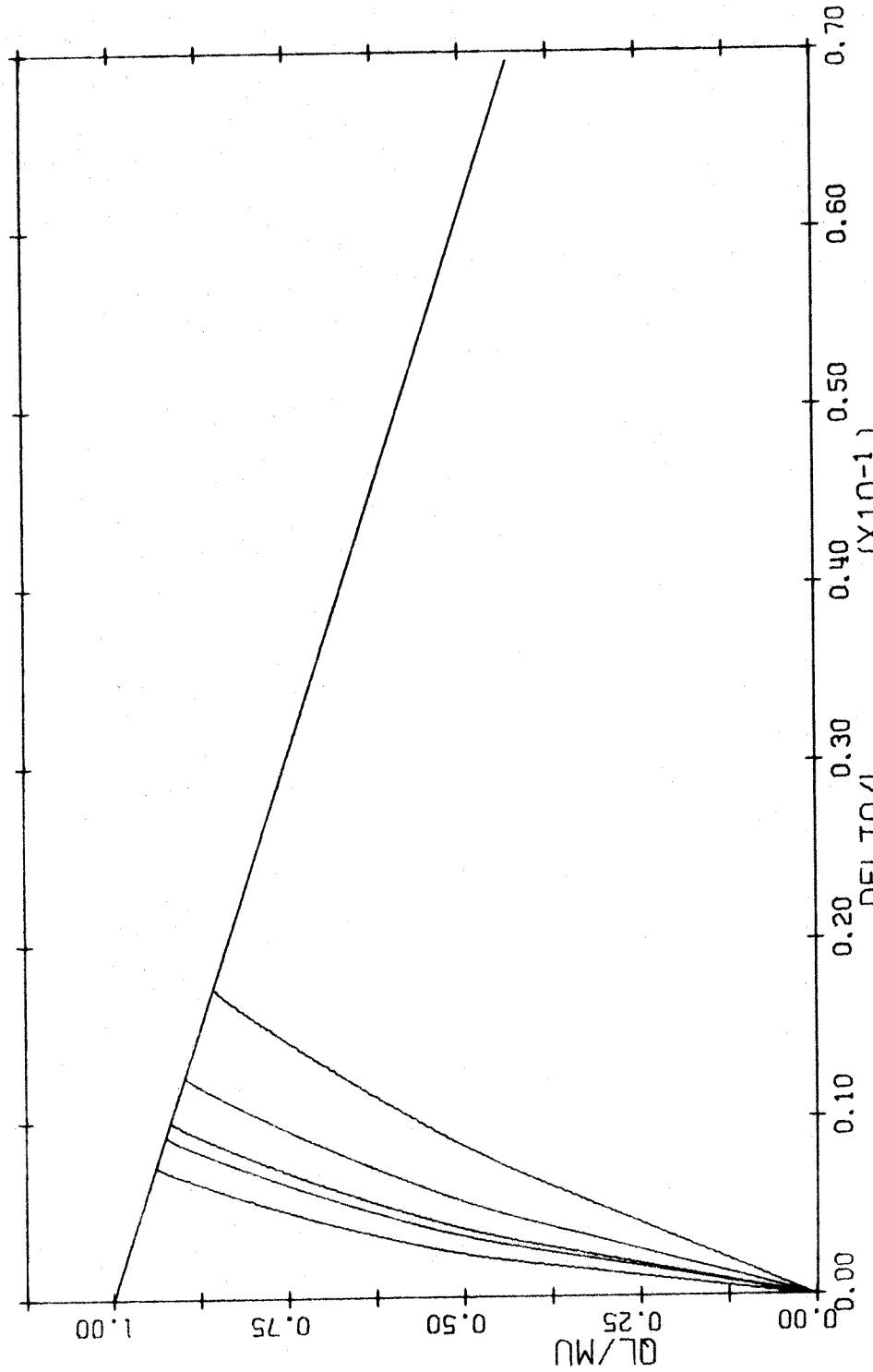

FIG. A-18 LOAD DEFLECTION DIAGRAM. TIED COLUMN. BARS IN 2 FACES
L/H=10 P/P0=0.3

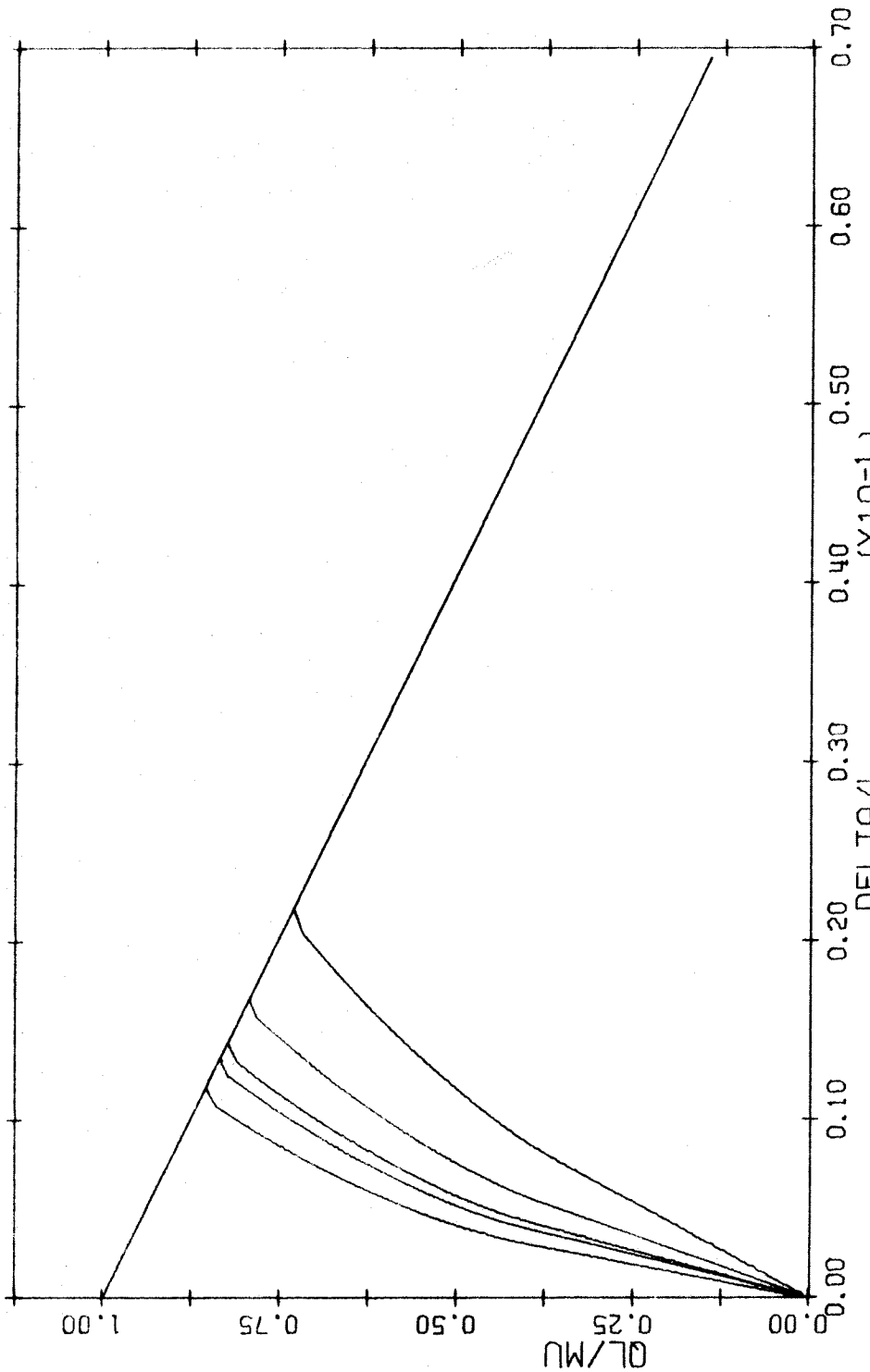

FIG. A-19 LOAD DEFLECTION DIAGRAM. TIED COLUMN. BARS IN 2 FACES
L/R=15 P/P0=0.3

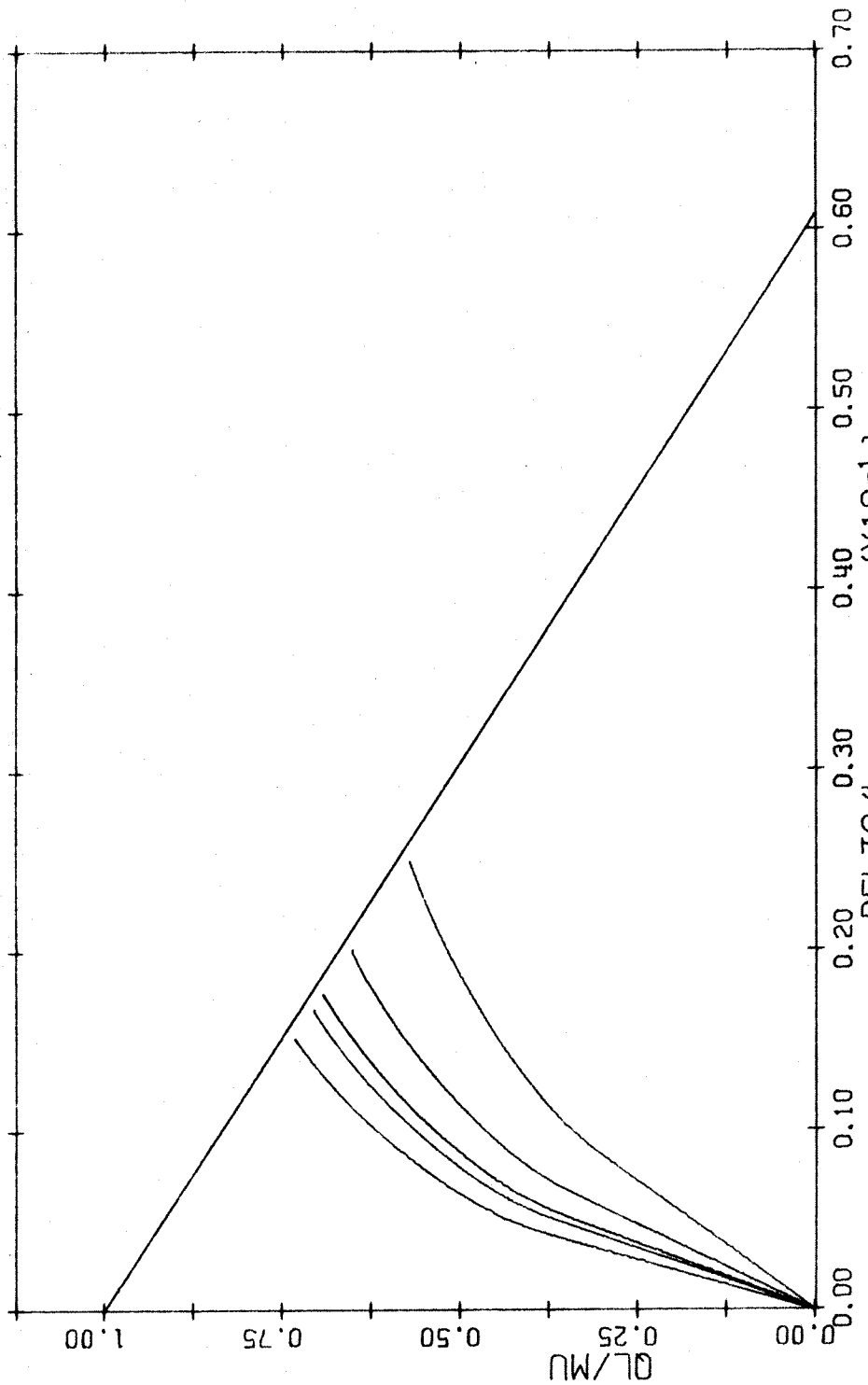

FIG. A-20 LOAD DEFLECTION DIAGRAM. TIED COLUMN. BARS IN 2 FACES
L/H=20 P/P0=0.3

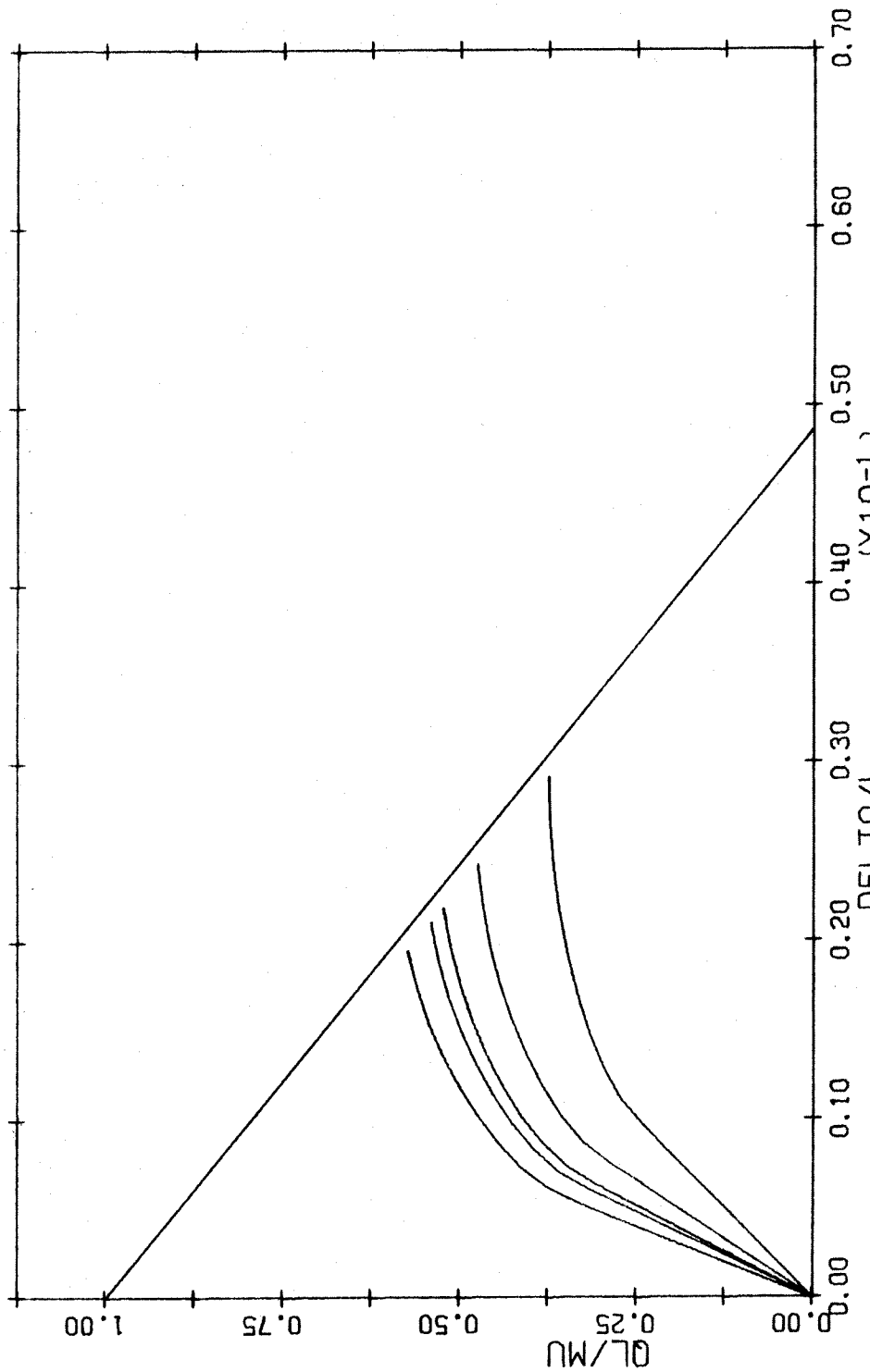

FIG. A-21 LOAD DEFLECTION DIAGRAM. TIED COLUMN. BARS IN 2 FACES
L/H=25 P/PC=0.3

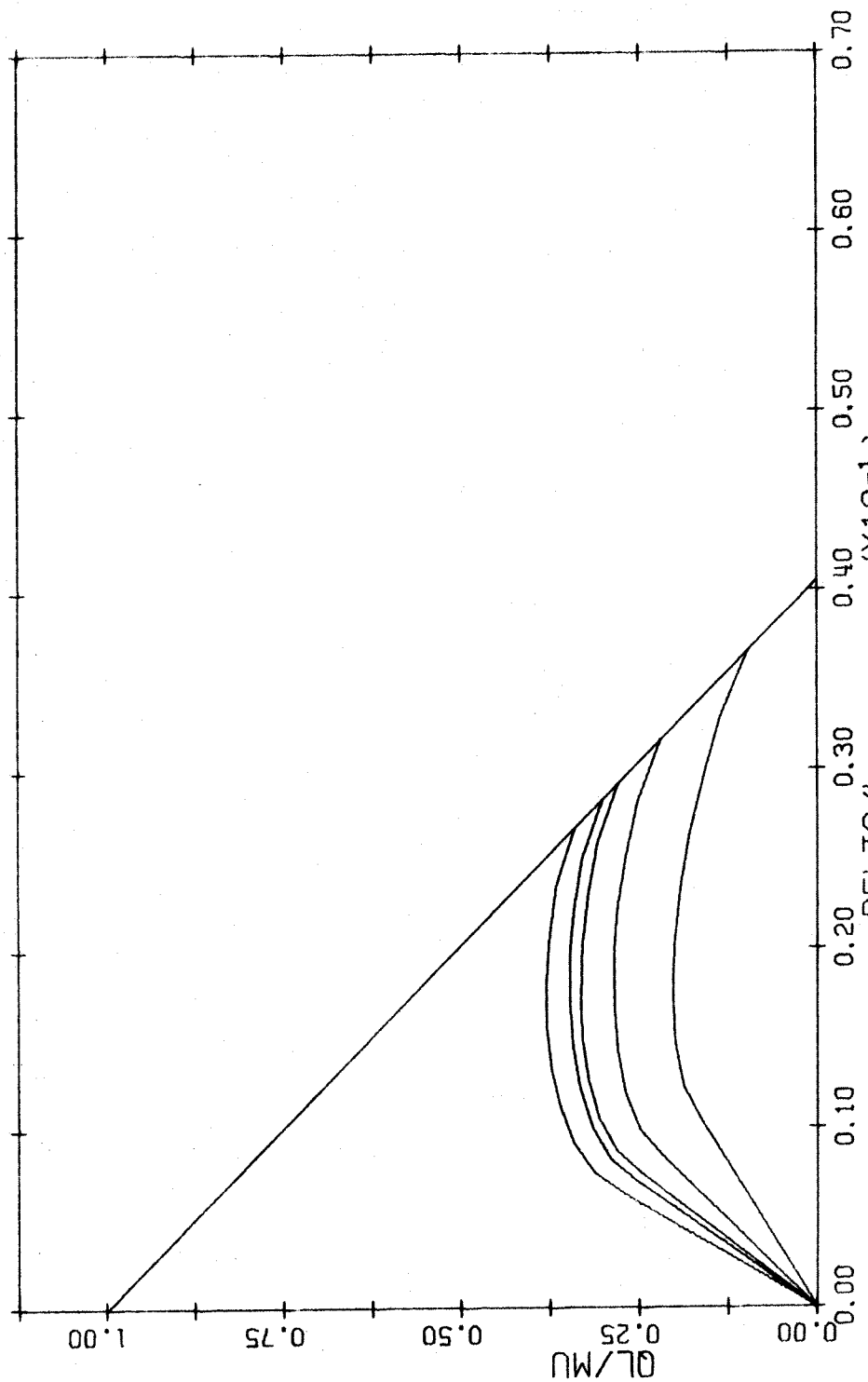

FIG. A-22 LOAD DEFLECTION DIAGRAM. TIED COLUMN. BARS IN 2 FACES
L/H=30 P/P0=0.3

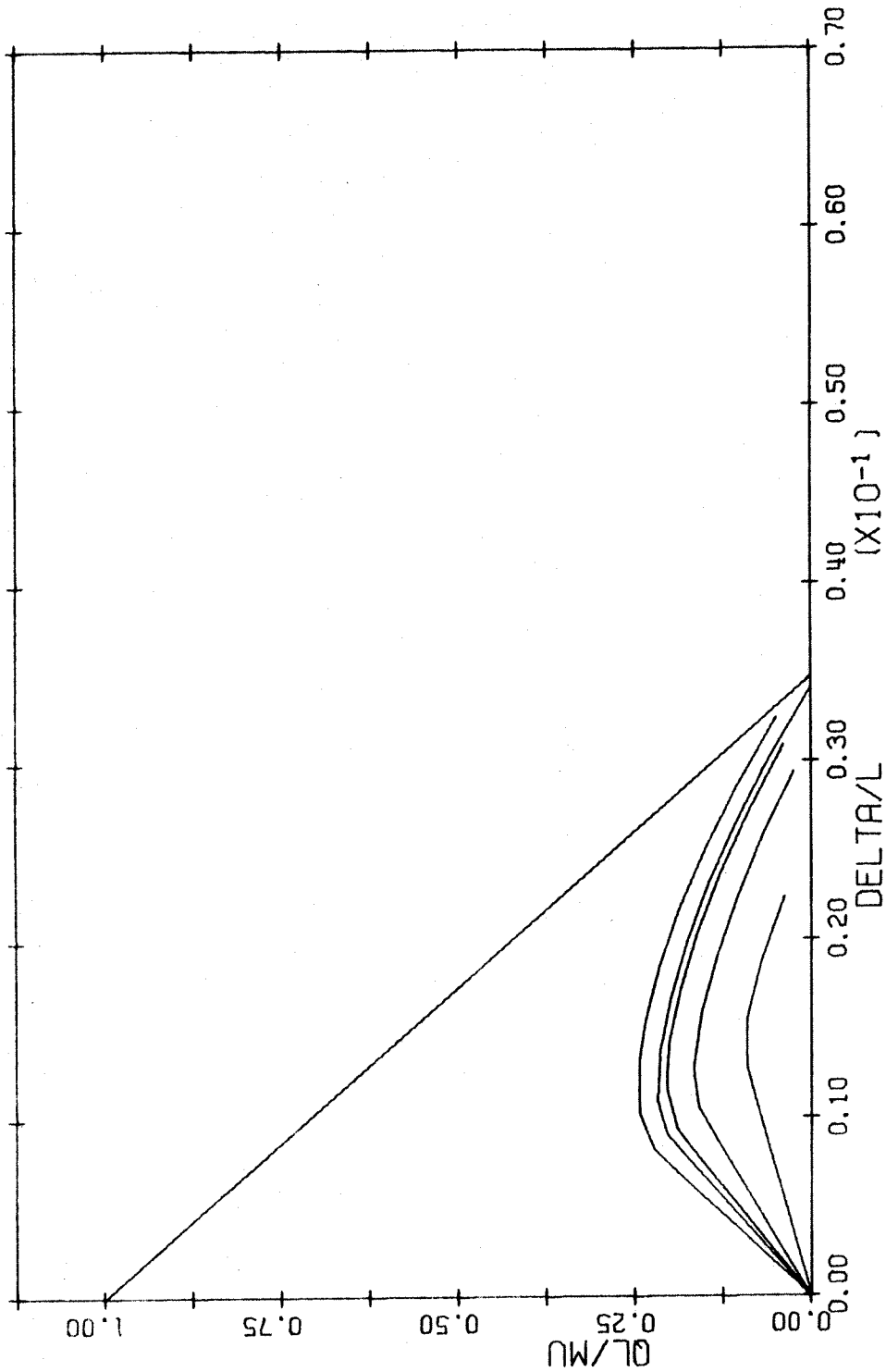

FIG. A-23 LOAD DEFLECTION DIAGRAM. TIED COLUMN. BARS IN 2 FACES
L/H=35 P/P0=0.3

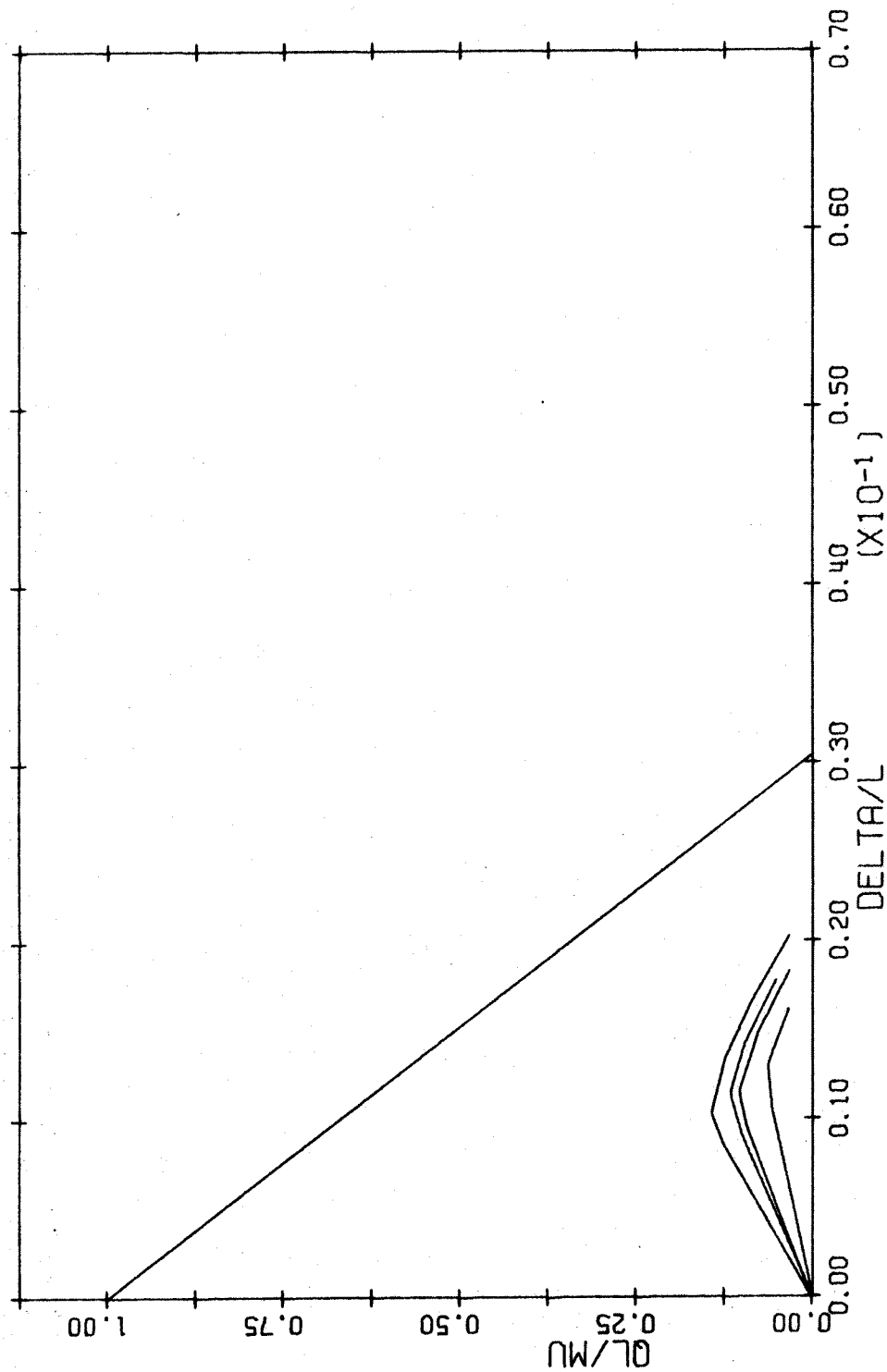

FIG. A-24 LOAD DEFLECTION DIAGRAM. TIED COLUMN. BARS IN 2 FACES
L/H=40 P/P0=0.3

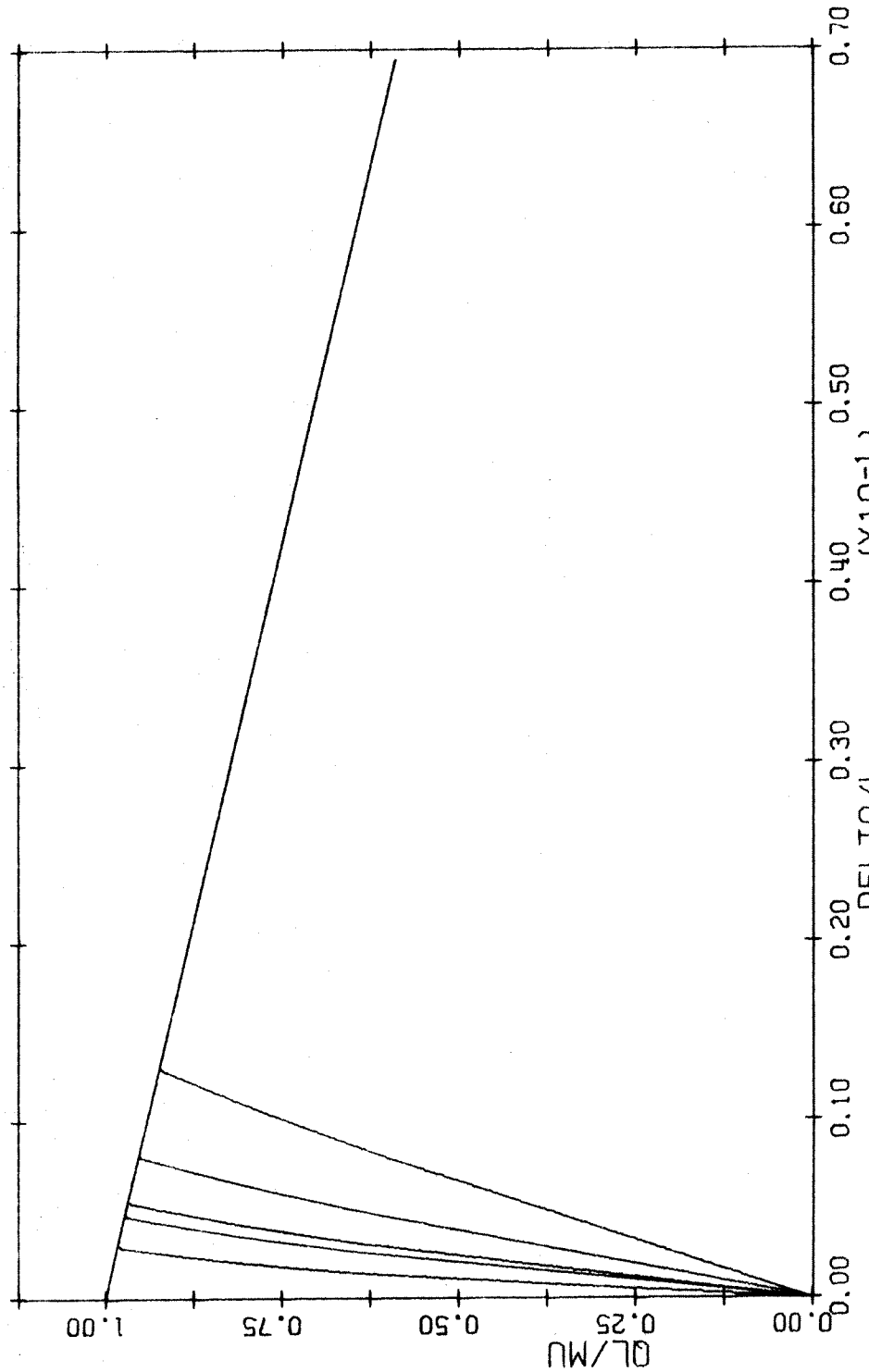

FIG. A-25 LOAD DEFLECTION DIAGRAM. TIED COLUMN. BARS IN 2 FACES
L/H=5 P/P0=0.4

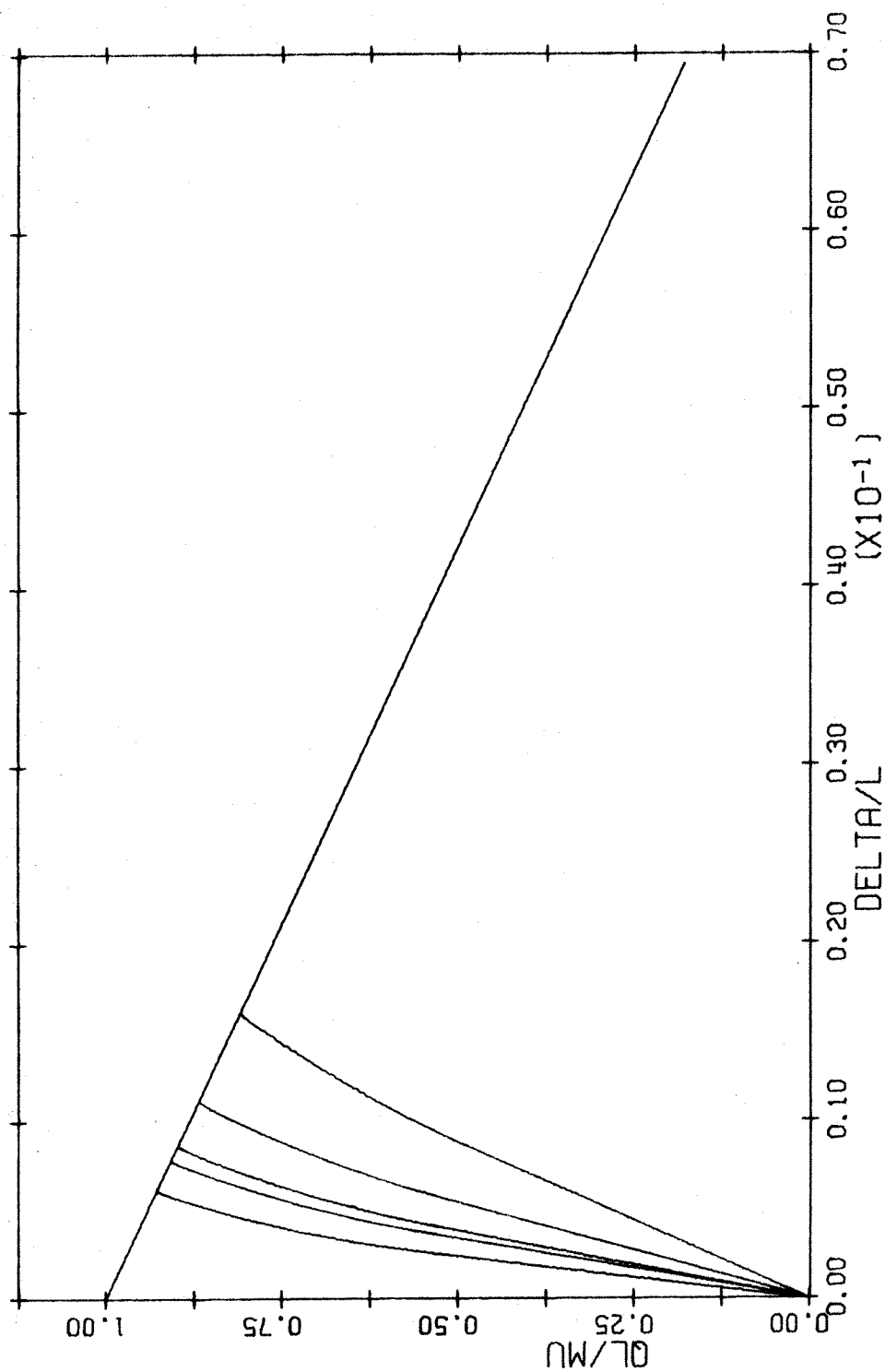

FIG. A-26 LOAD DEFLECTION DIAGRAM. TIED COLUMN. BARS IN 2 FACES
L/H=10 P/P0=0.4

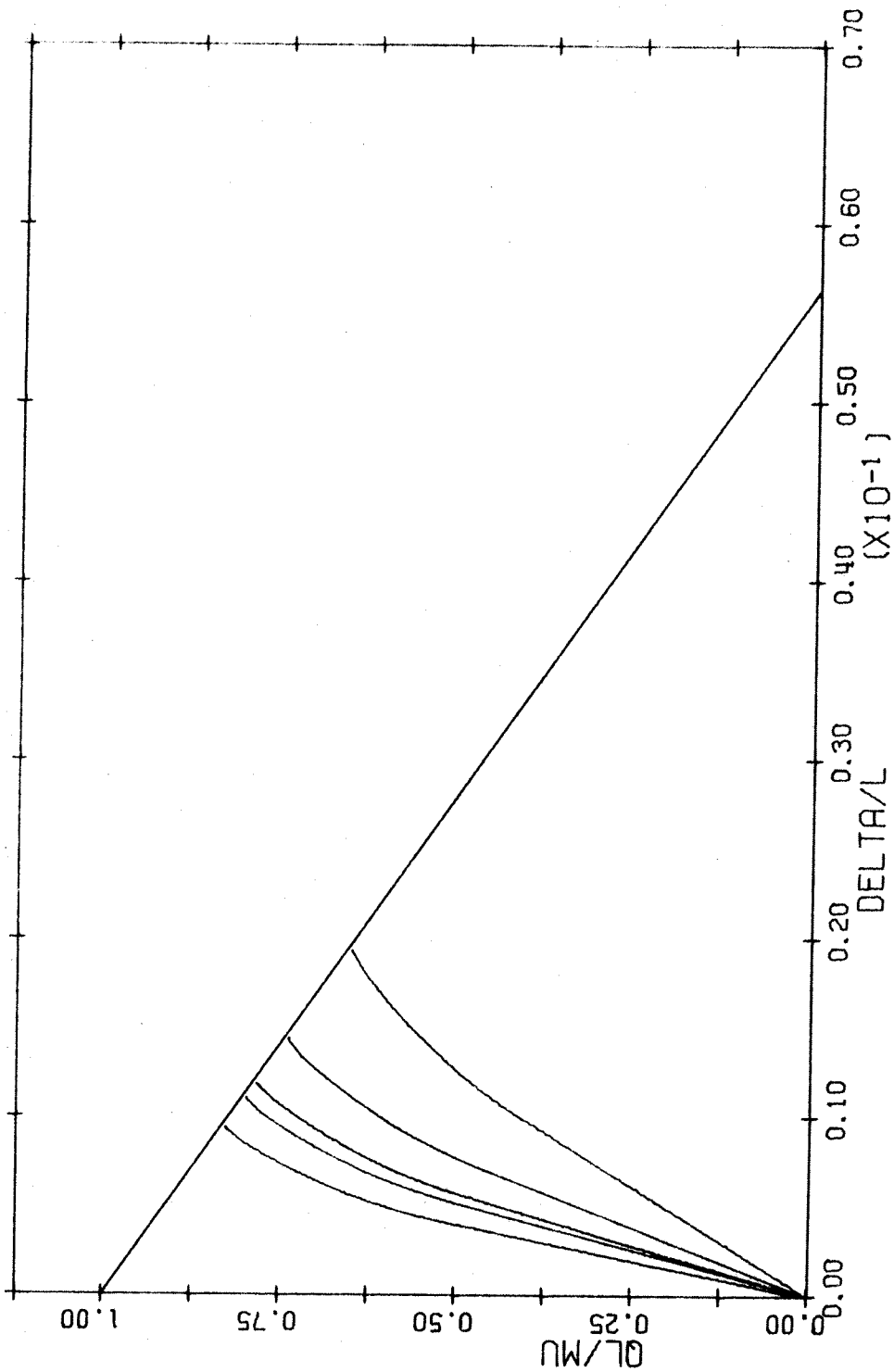

FIG. A-27 LOAD DEFLECTION DIAGRAM. TIED COLUMN. BARS IN 2 FACES
L/H=15 P/P0=0.4

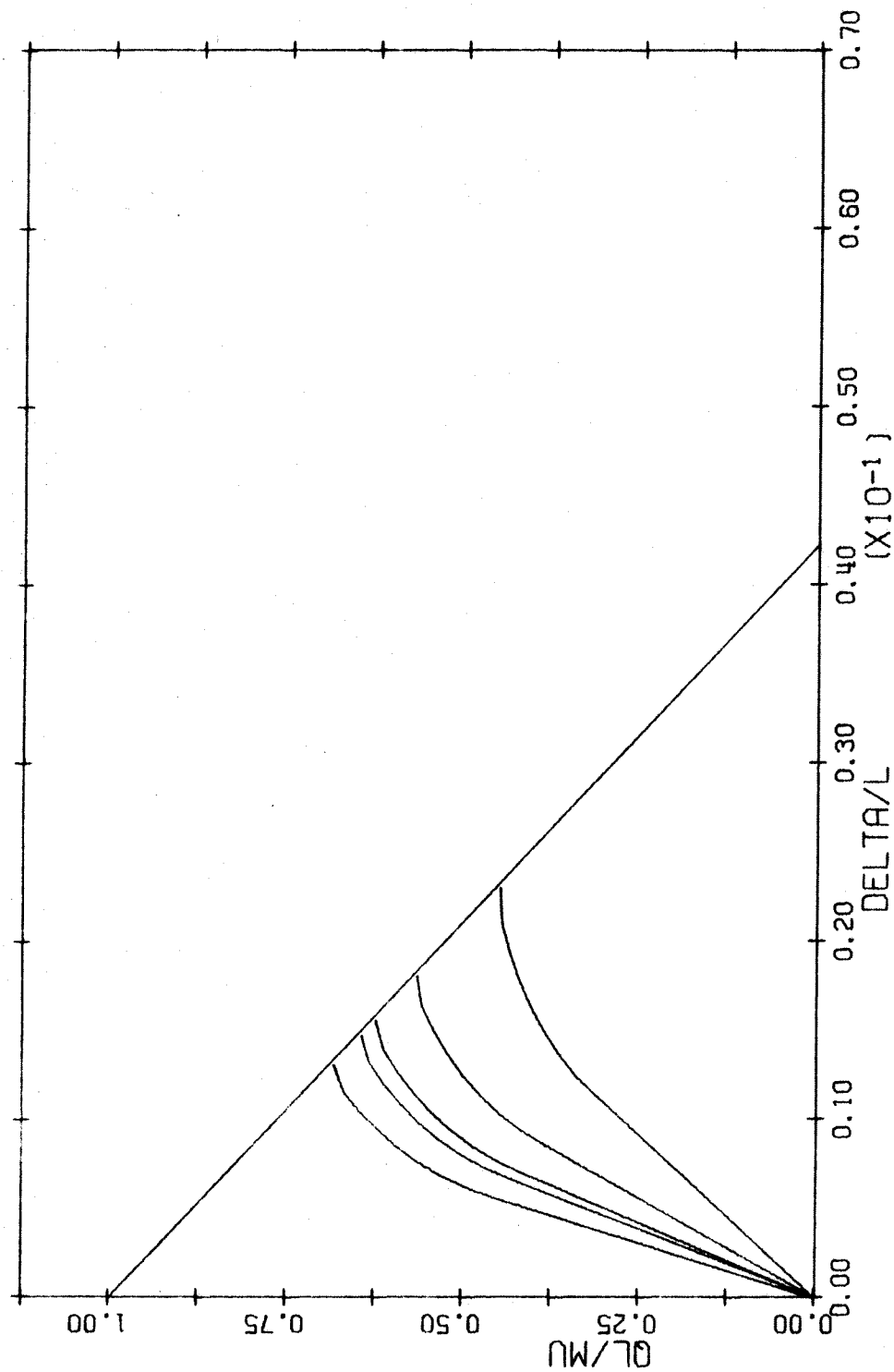

FIG. A-28 LOAD DEFLECTION DIAGRAM. TIED COLUMN. BARS IN 2 FACES
L/H=20 P/P0=0.4

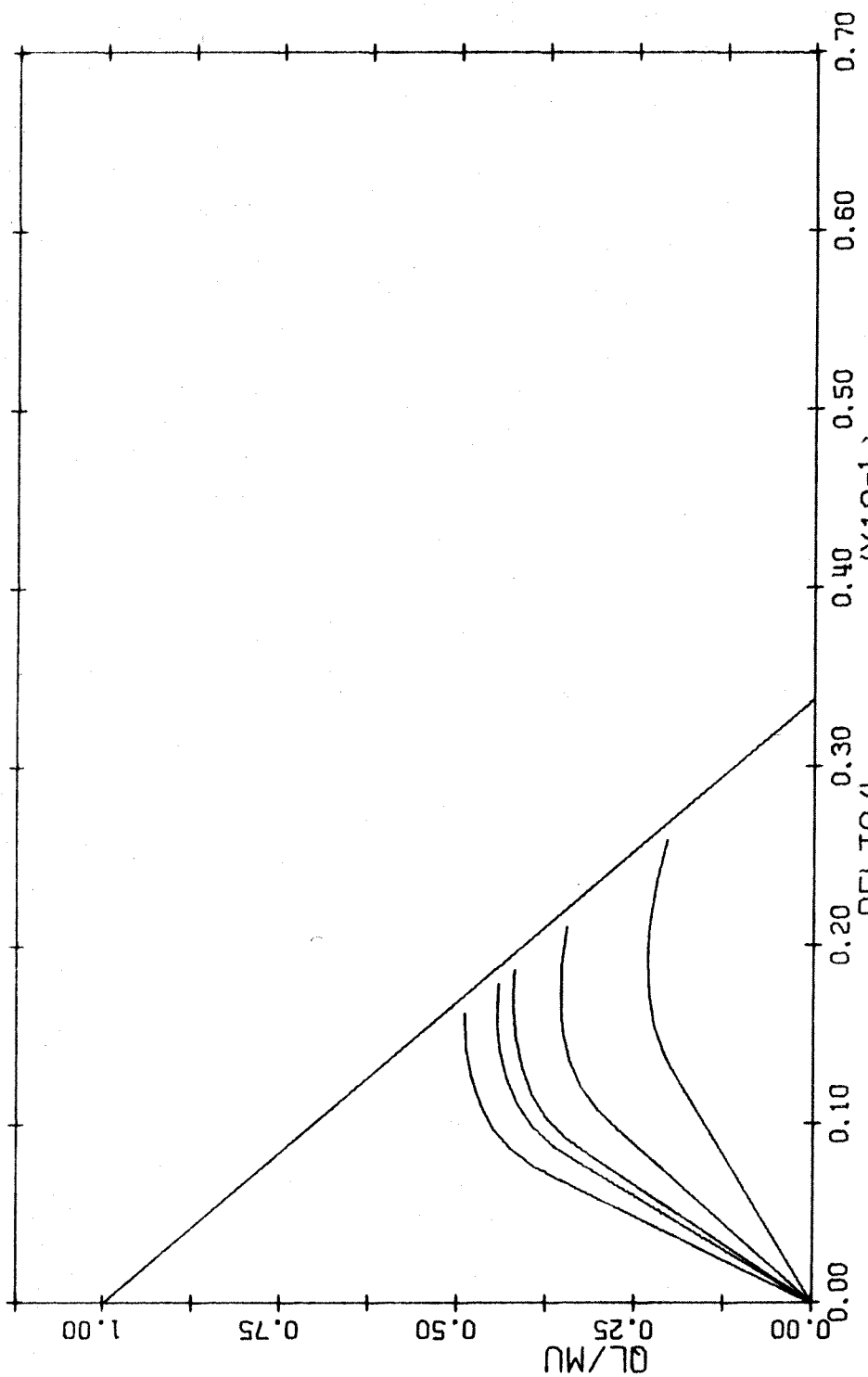

FIG. A-29 LOAD DEFLECTION DIAGRAM. TIED COLUMN. BARS IN 2 FACES
L/H=25 P/P0=0.4

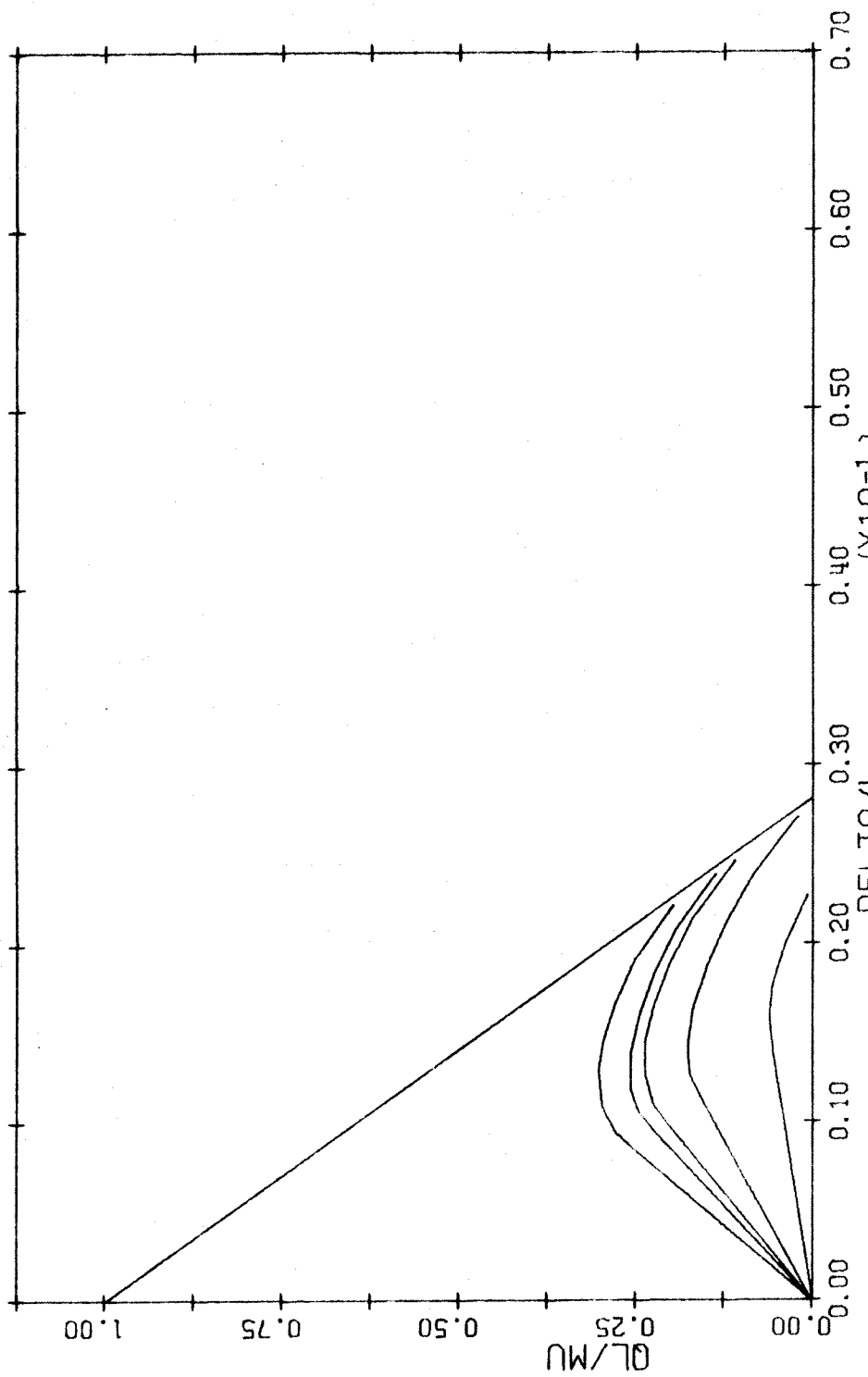

FIG. A-30 LOAD DEFLECTION DIAGRAM. TIED COLUMN. BARS IN 2 FACES
L/H=30 P/P0=0.4

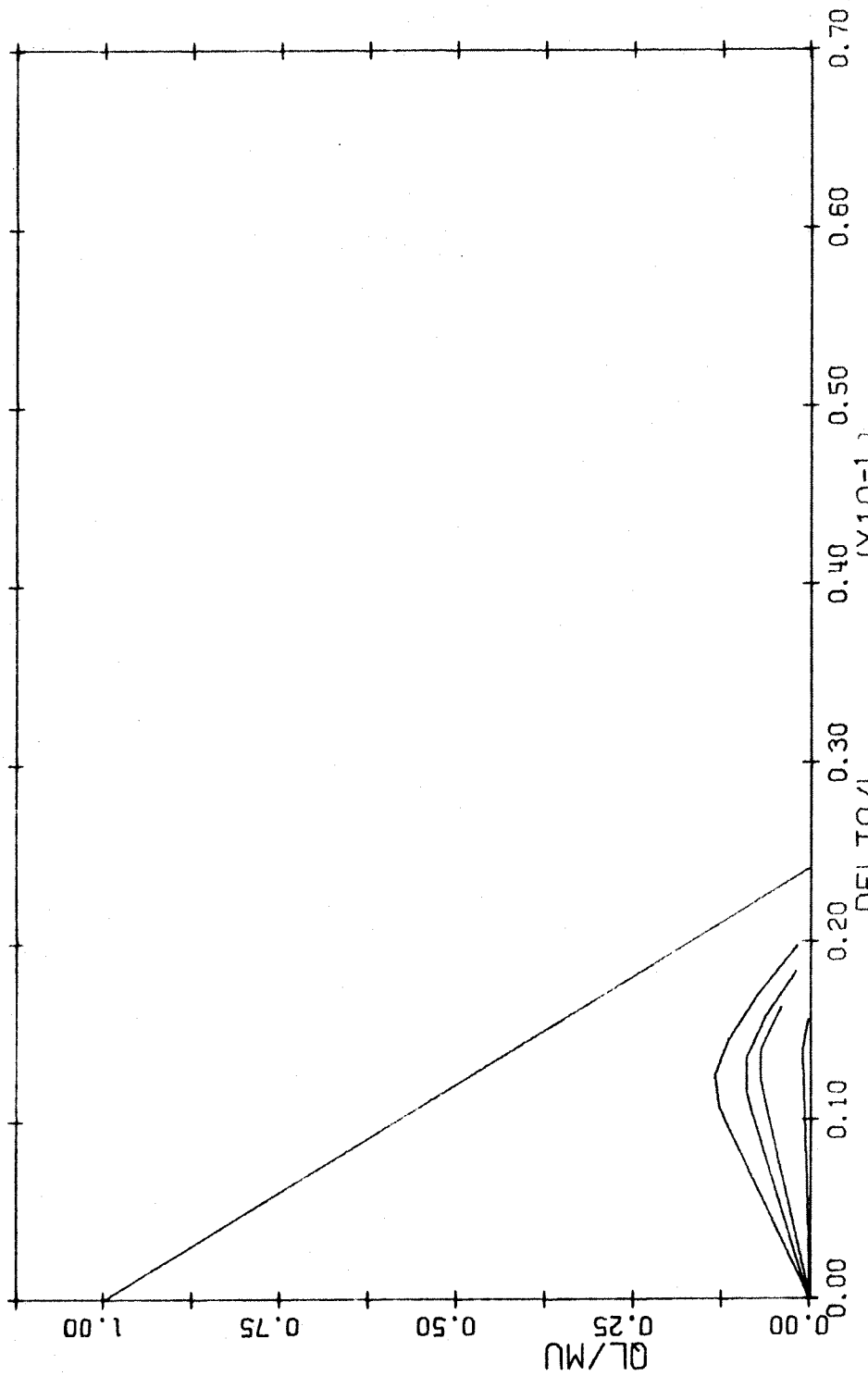

FIG. A-31 LOAD DEFLECTION DIAGRAM. TIED COLUMN. BARS IN 2 FACES
L/H=35 P/PO=0.4

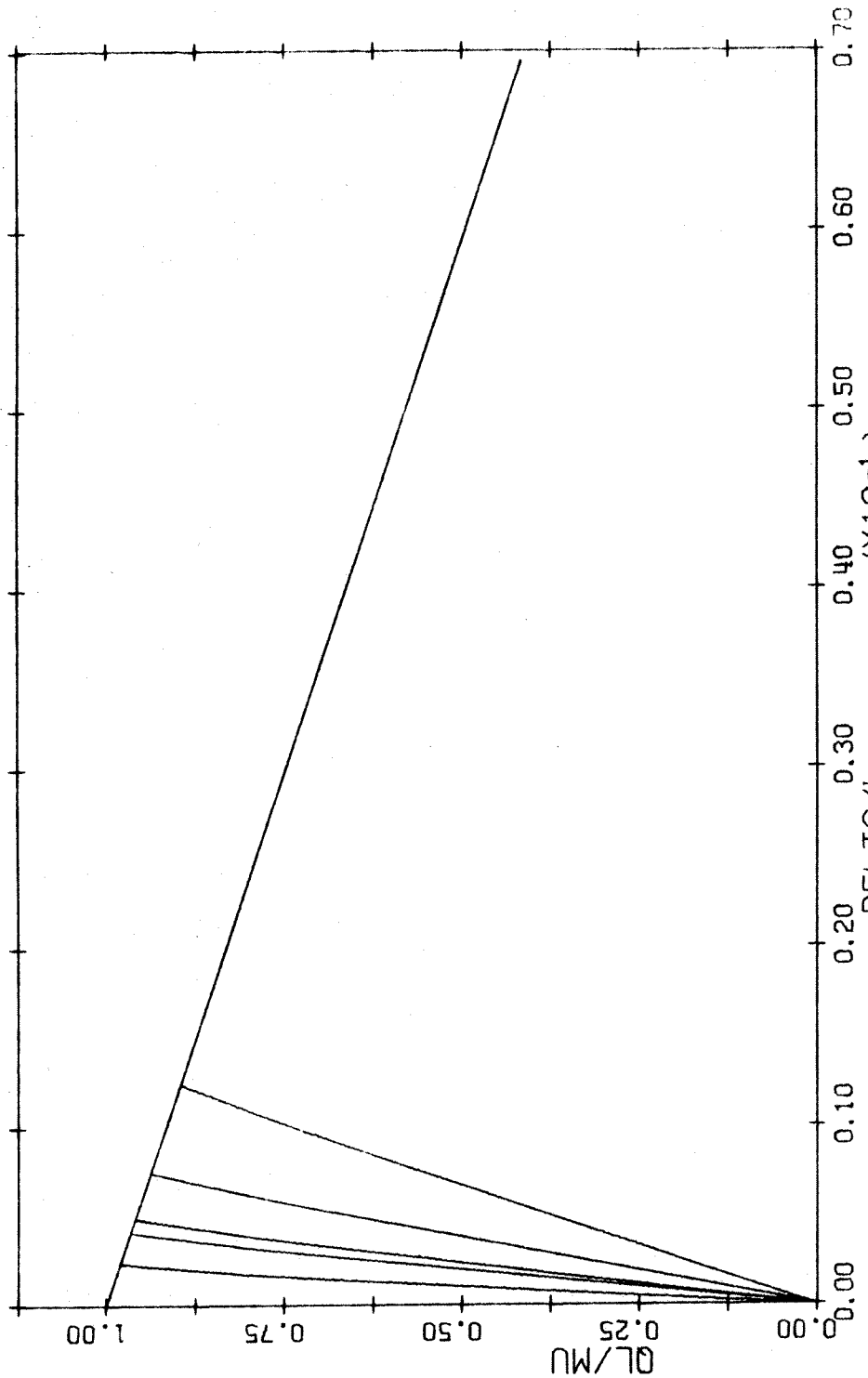

FIG. A-32 LOAD DEFLECTION DIAGRAM. TIED COLUMN. BARS IN 2 FACES
L/H=5 P/P0=0.5

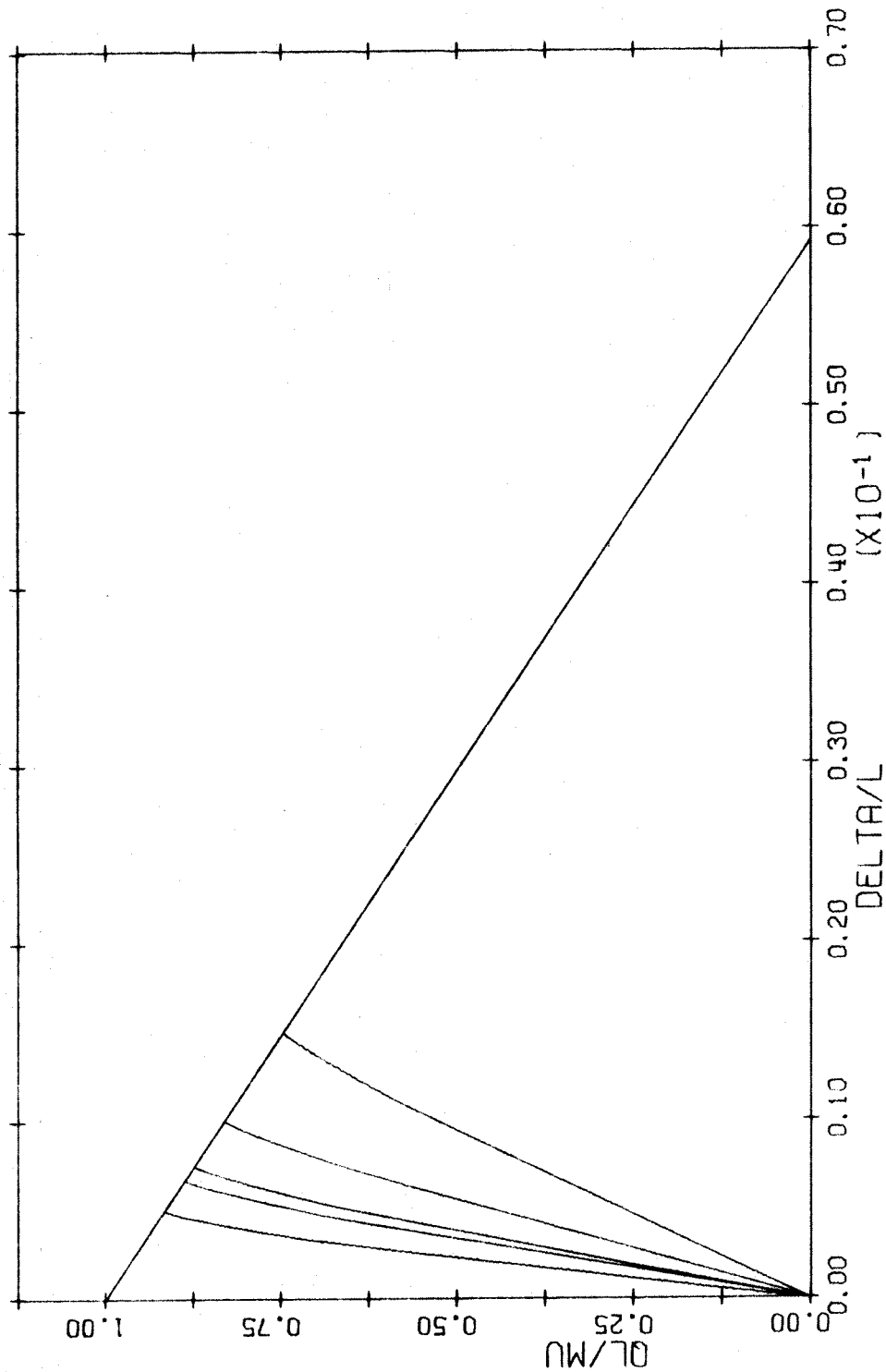

FIG. A-33 LOAD DEFLECTION DIAGRAM. TIED COLUMN. BARS IN 2 FACES
L/H=10 P/P0=0.5

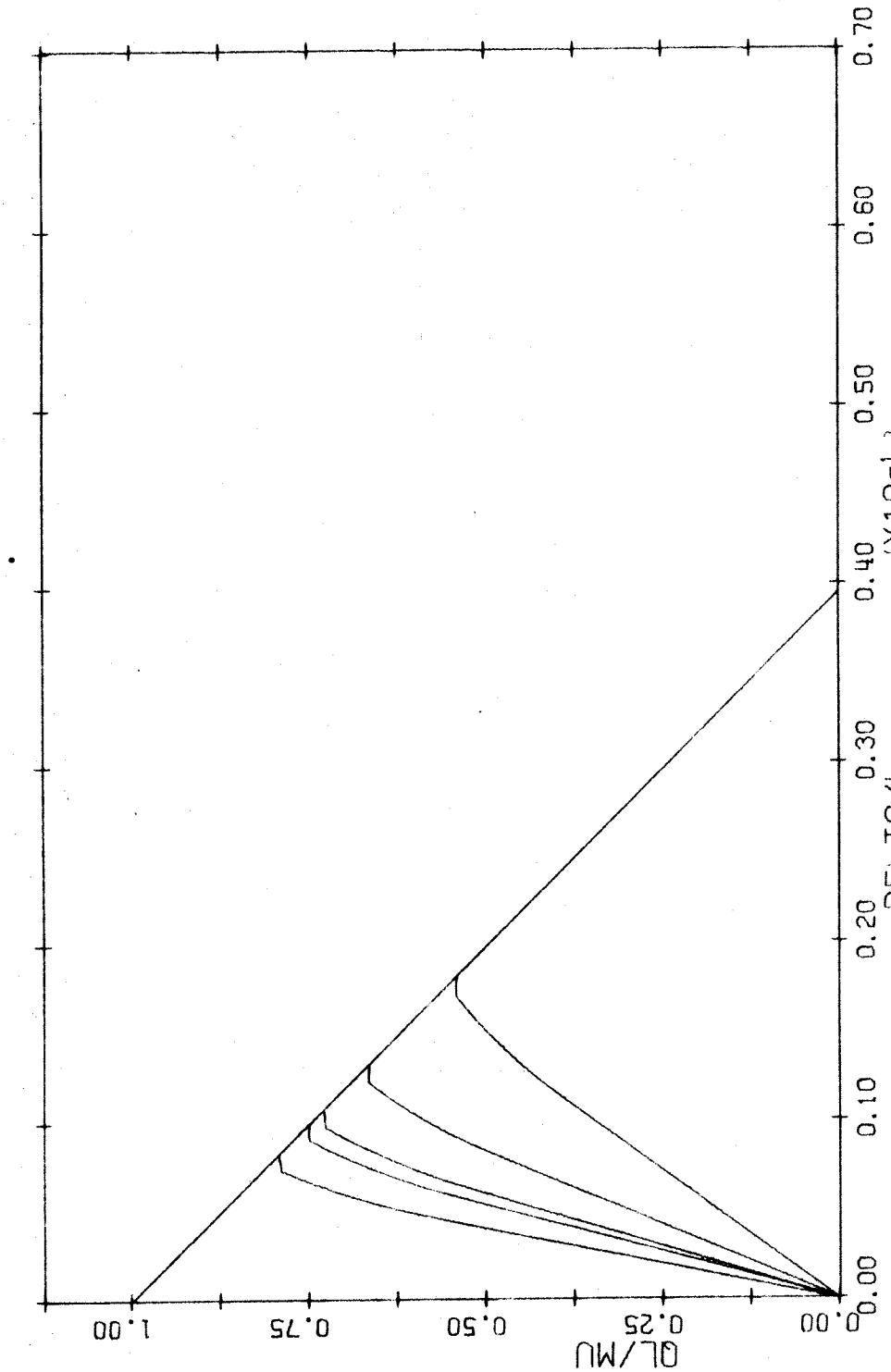

FIG. A-24 LOAD DEFLECTION DIAGRAM. TIED COLUMN. BARS IN 2 FACES
L/H=15 P/P0=0.5

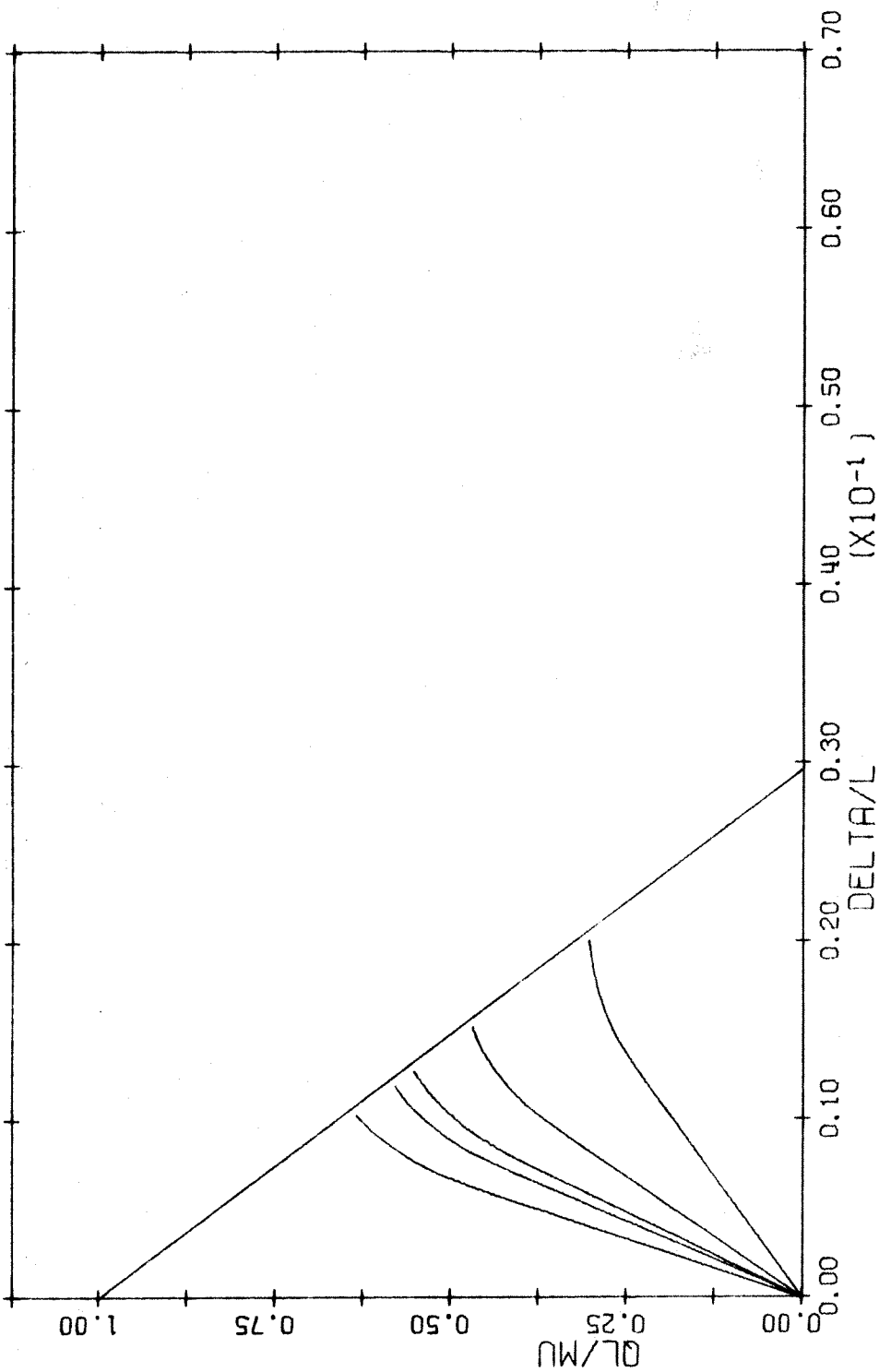

FIG. A-35 LOAD DEFLECTION DIAGRAM. TIED COLUMN. BARS IN 2 FACES
L/H=20 P/P0=0.5

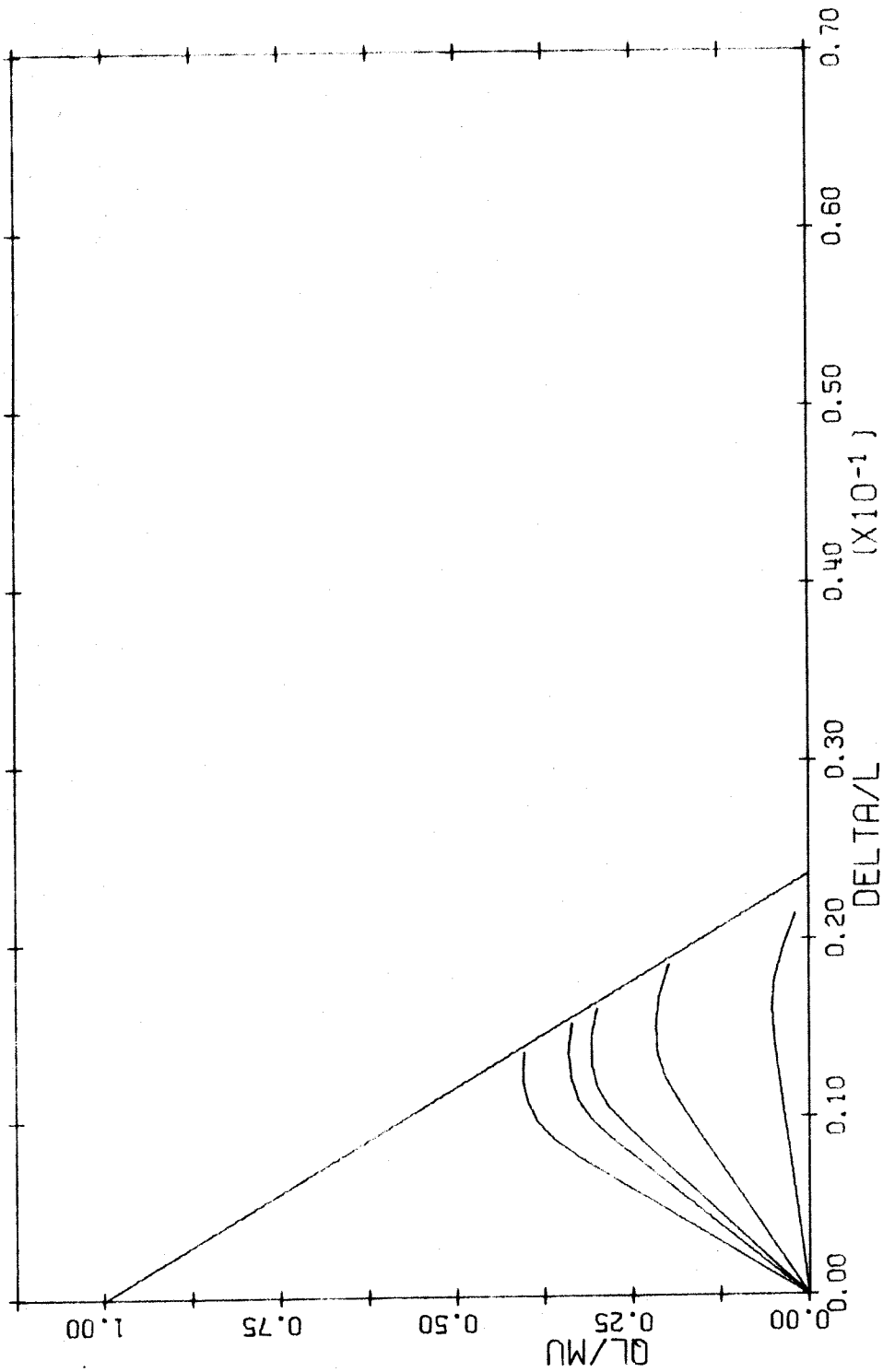

FIG. A-36 LOAD DEFLECTION DIAGRAM. TIED COLUMN. BARS IN 2 FACES
L/H=25 P/P0=0.5

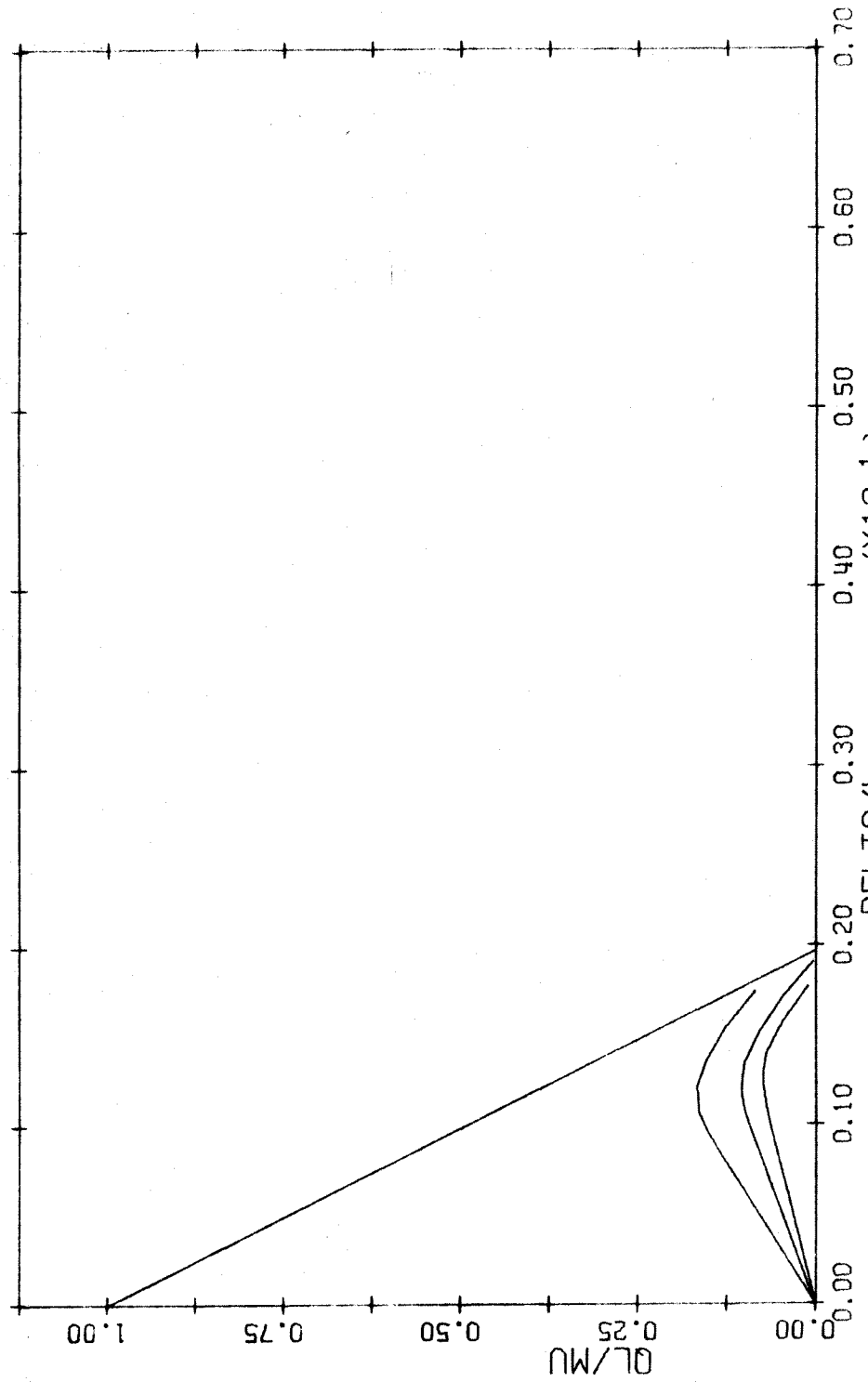

FIG. A-37 LOAD DEFLECTION DIAGRAM. TIED COLUMN. BARS IN 2 FACES
L/H=30 P/P0=0.5

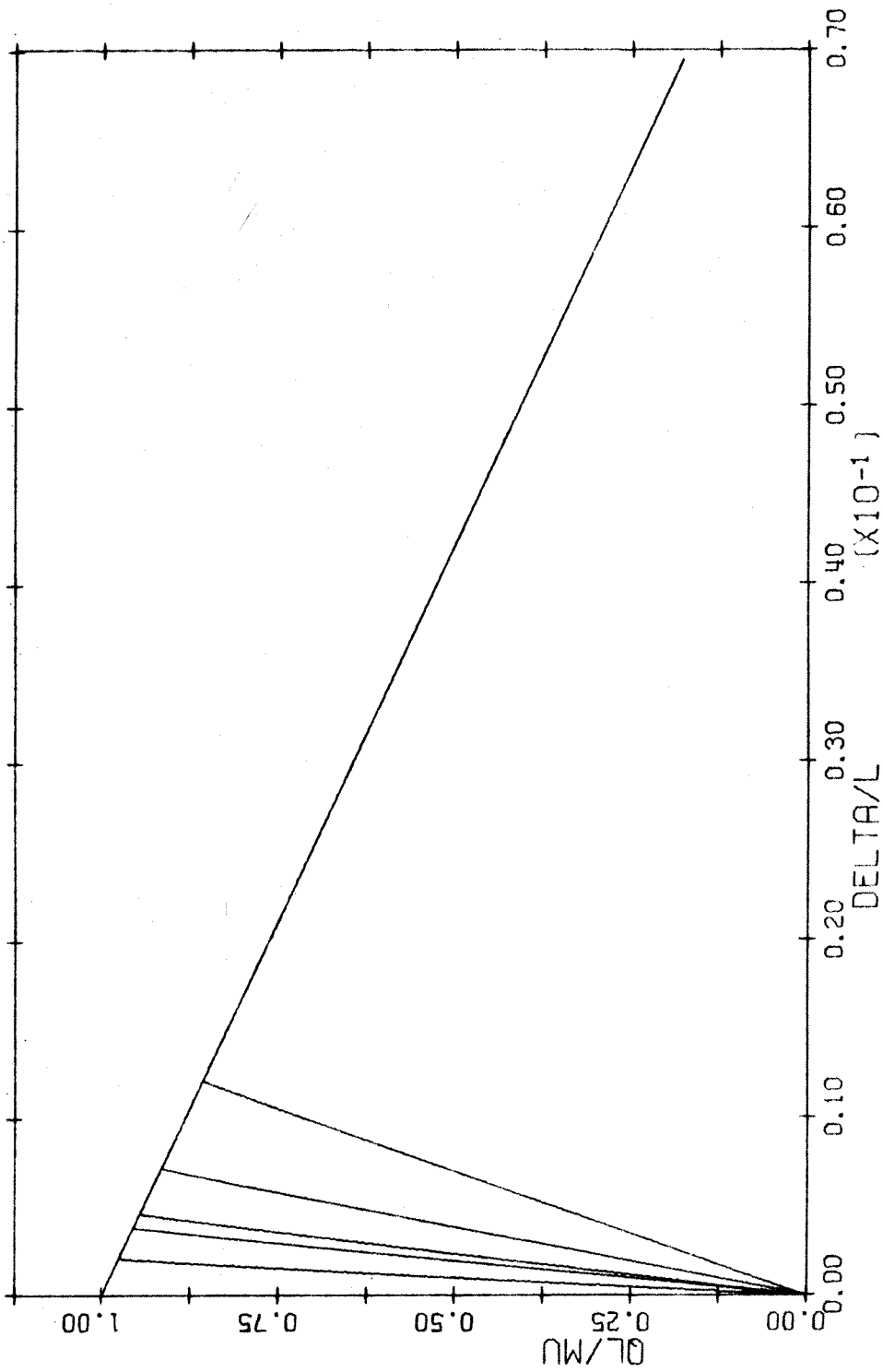

FIG. A-38 LOAD DEFLECTION DIAGRAM. TIED COLUMN. BARS IN 2 FACES
L/H=5 P/P0=0.6

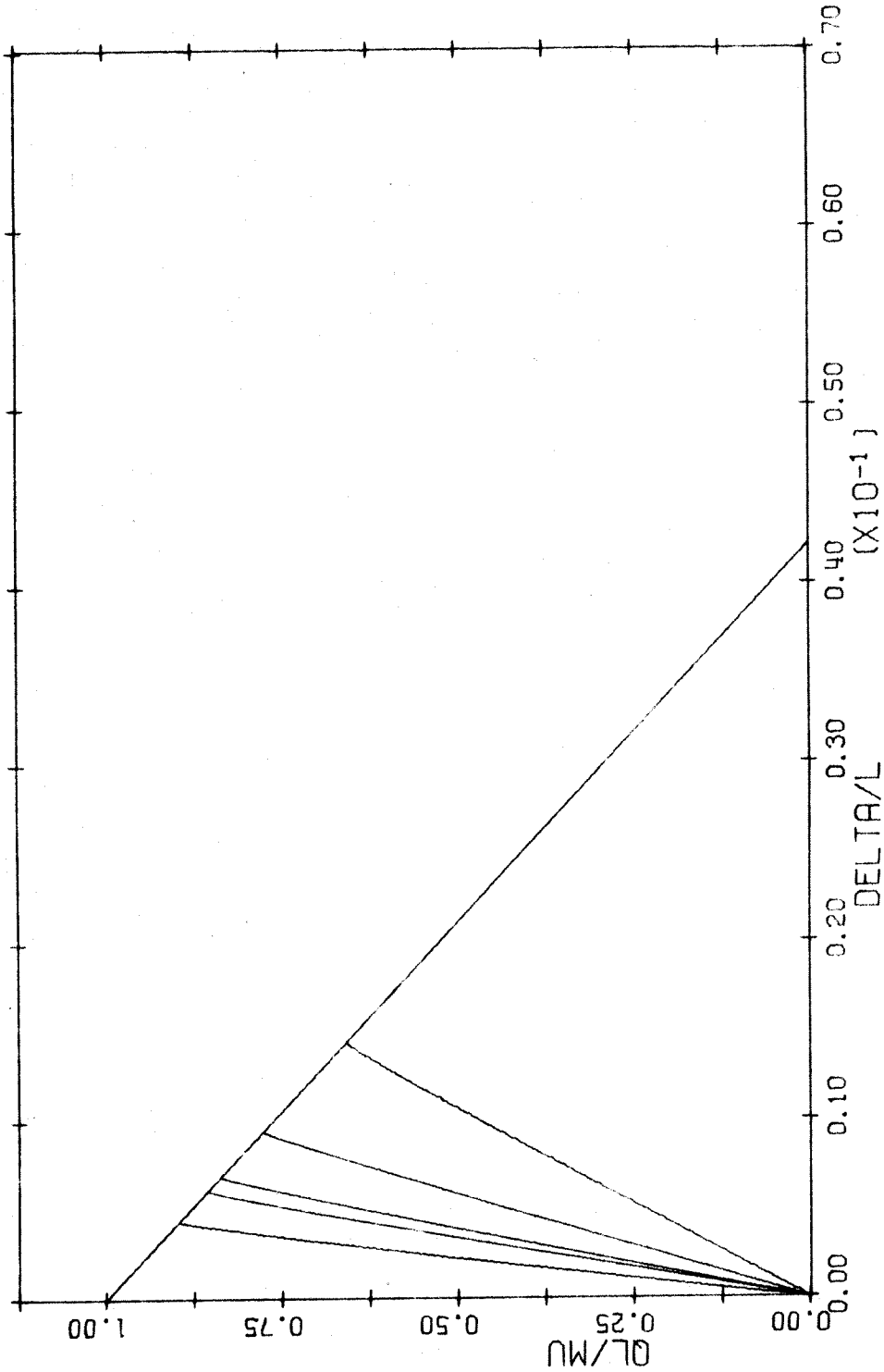

FIG. A-39 LOAD DEFLECTION DIAGRAM. TIED COLUMN. BARS IN 2 FACES
L/H=10 P/P0=0.6

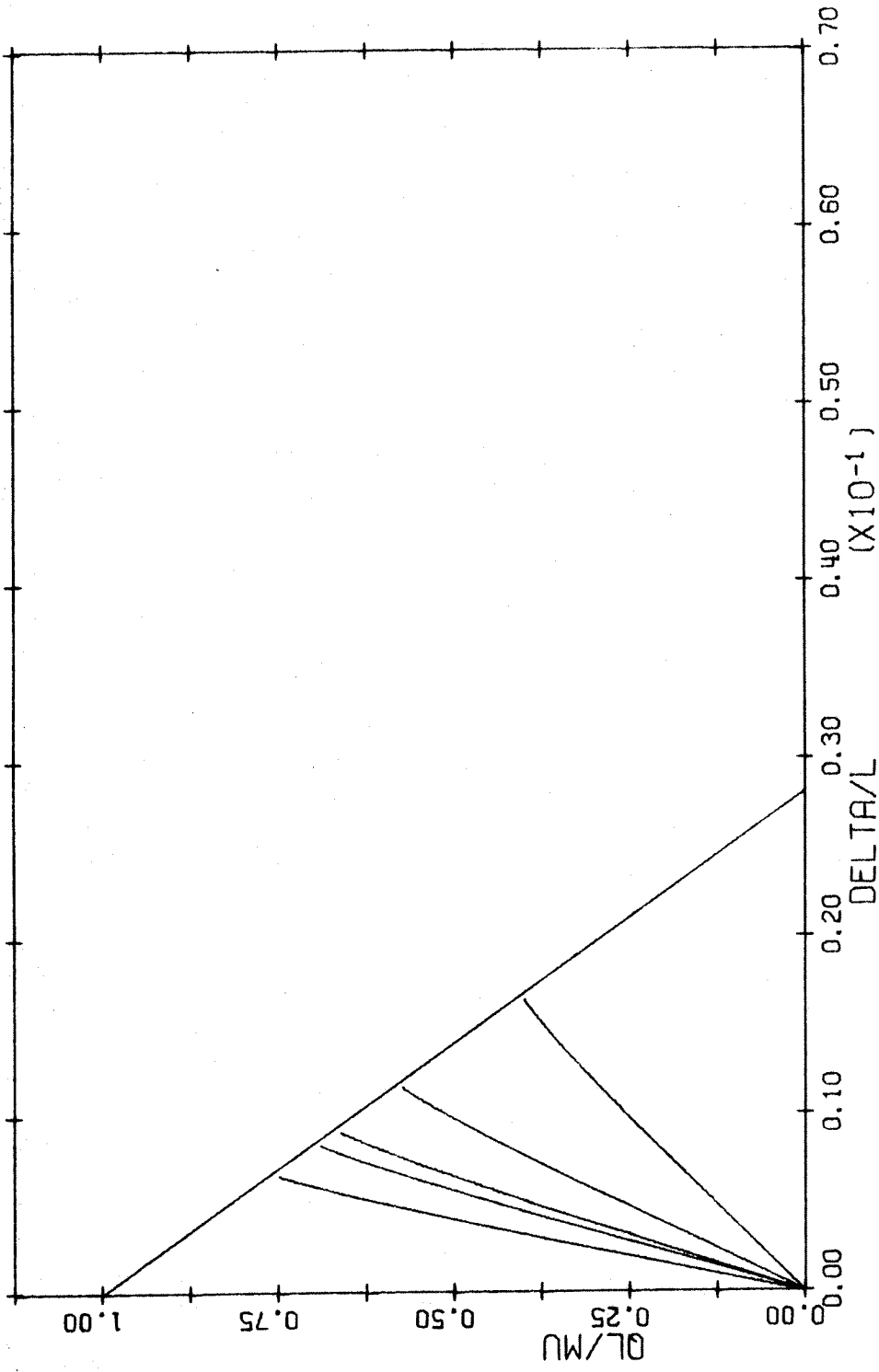

FIG. A-40 LOAD DEFLECTION DIAGRAM. TIED COLUMN. BARS IN 2 FACES
L/H=15 P/P0=0.6

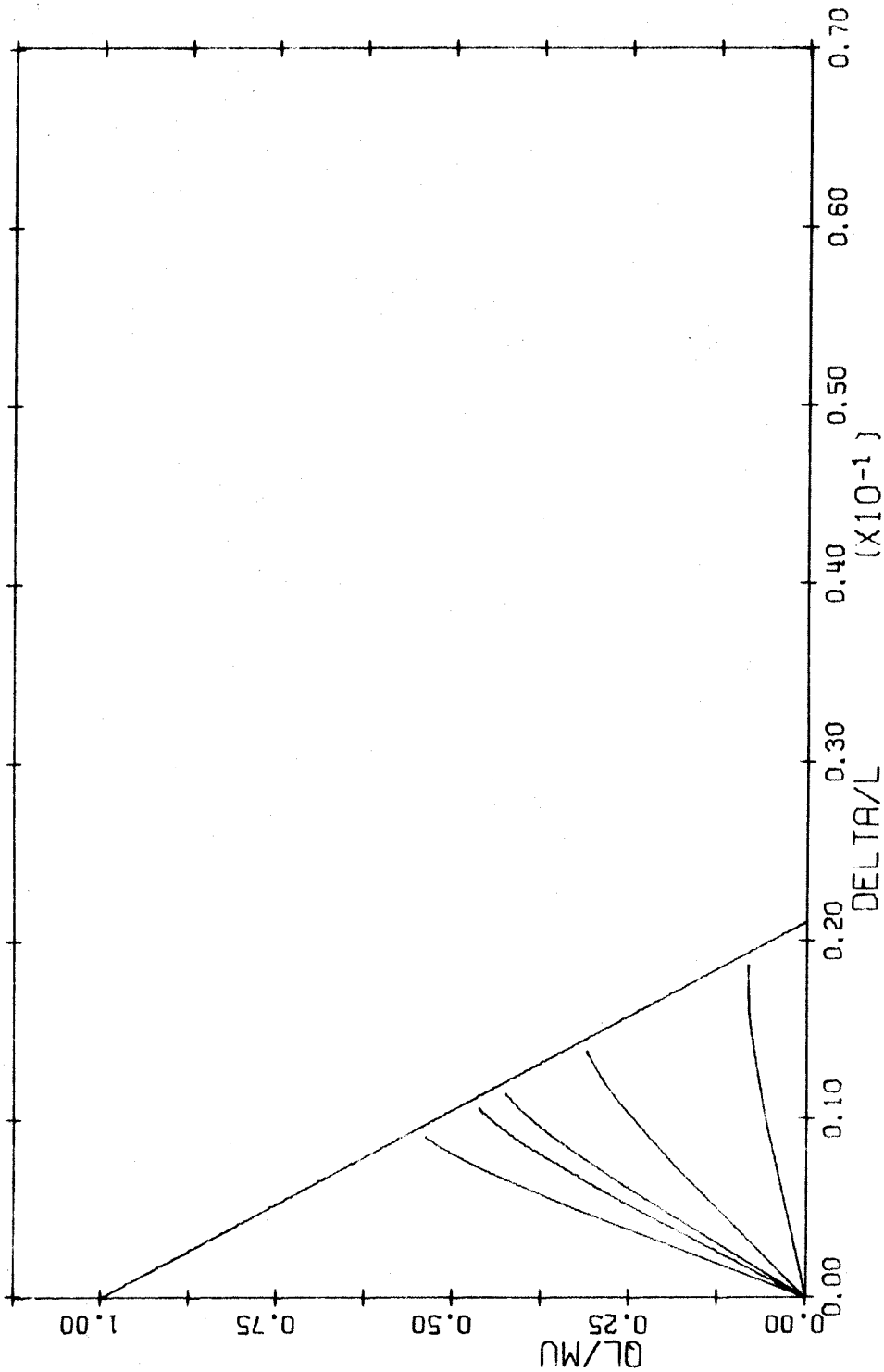

FIG. A-41 LOAD DEFLECTION DIAGRAM. TIED COLUMN. BARS IN 2 FACES
L/H=20 P/P0=0.6

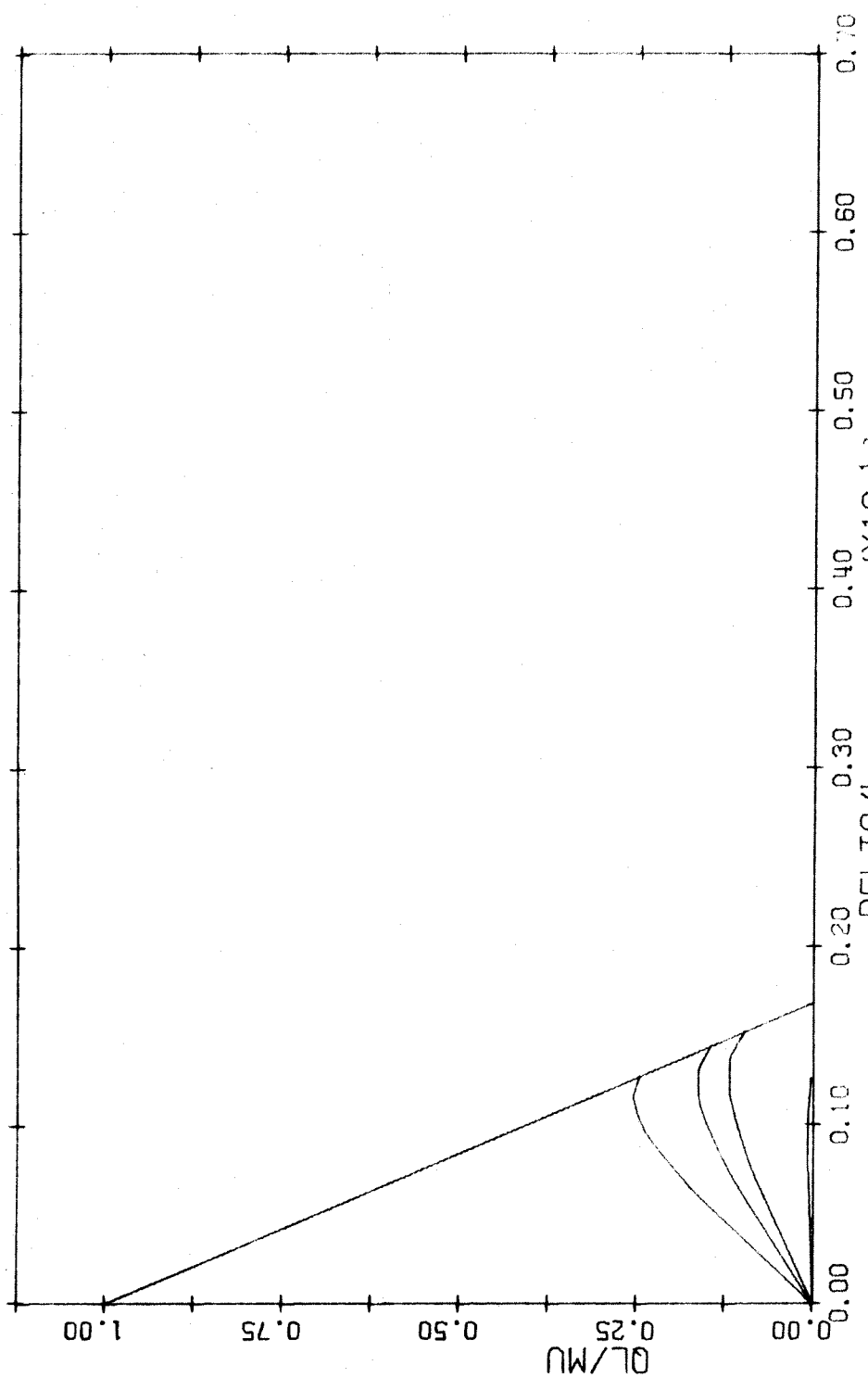

FIG. A-42 LOAD DEFLECTION DIAGRAM. TIED COLUMN. BARS IN 2 FACES
L/H=25 P/PO=0.6

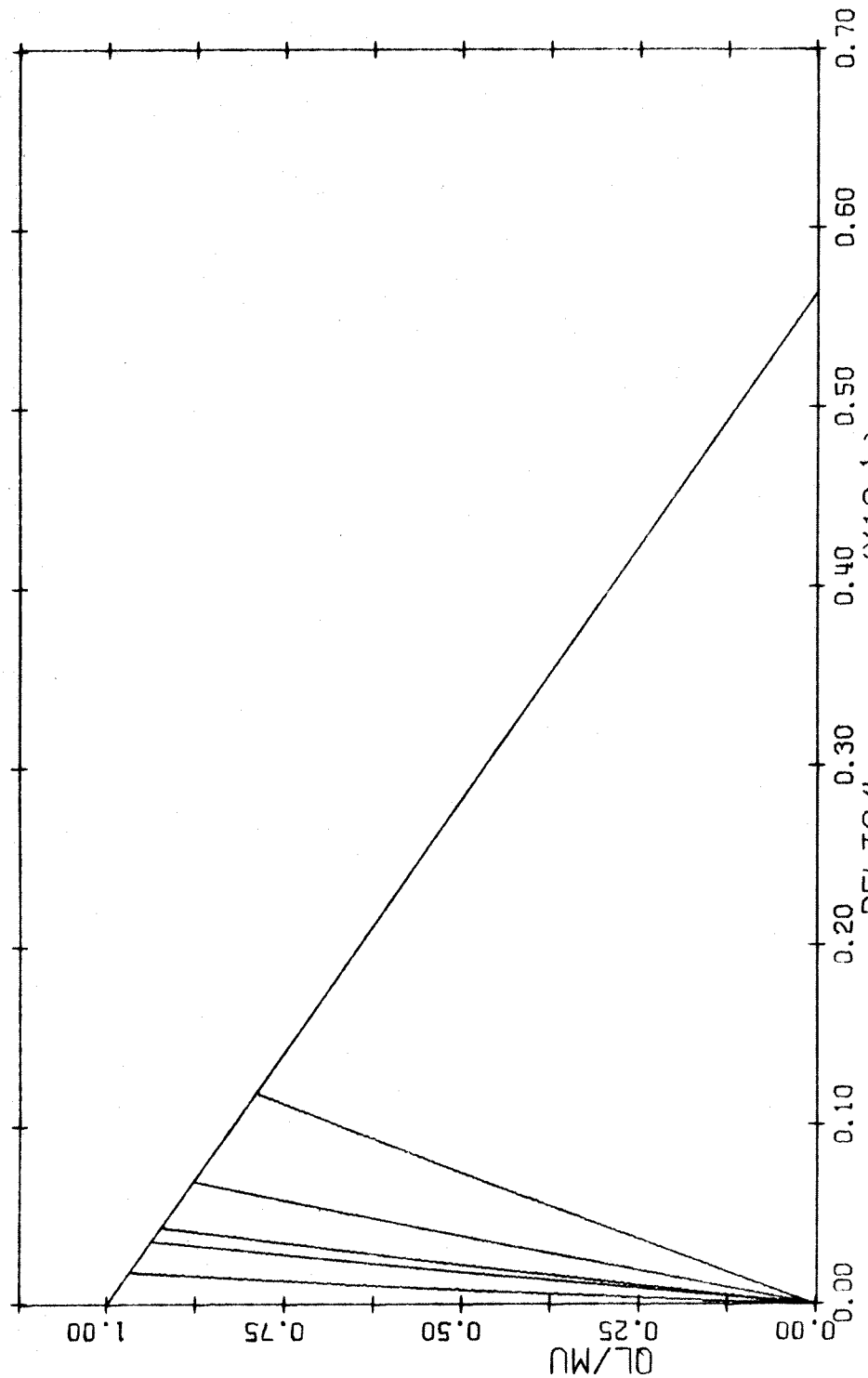

FIG. A-43 LOAD DEFLECTION DIAGRAM. TIED COLUMN. BARS IN 2 FACES
L/H=5 P/P0=0.7

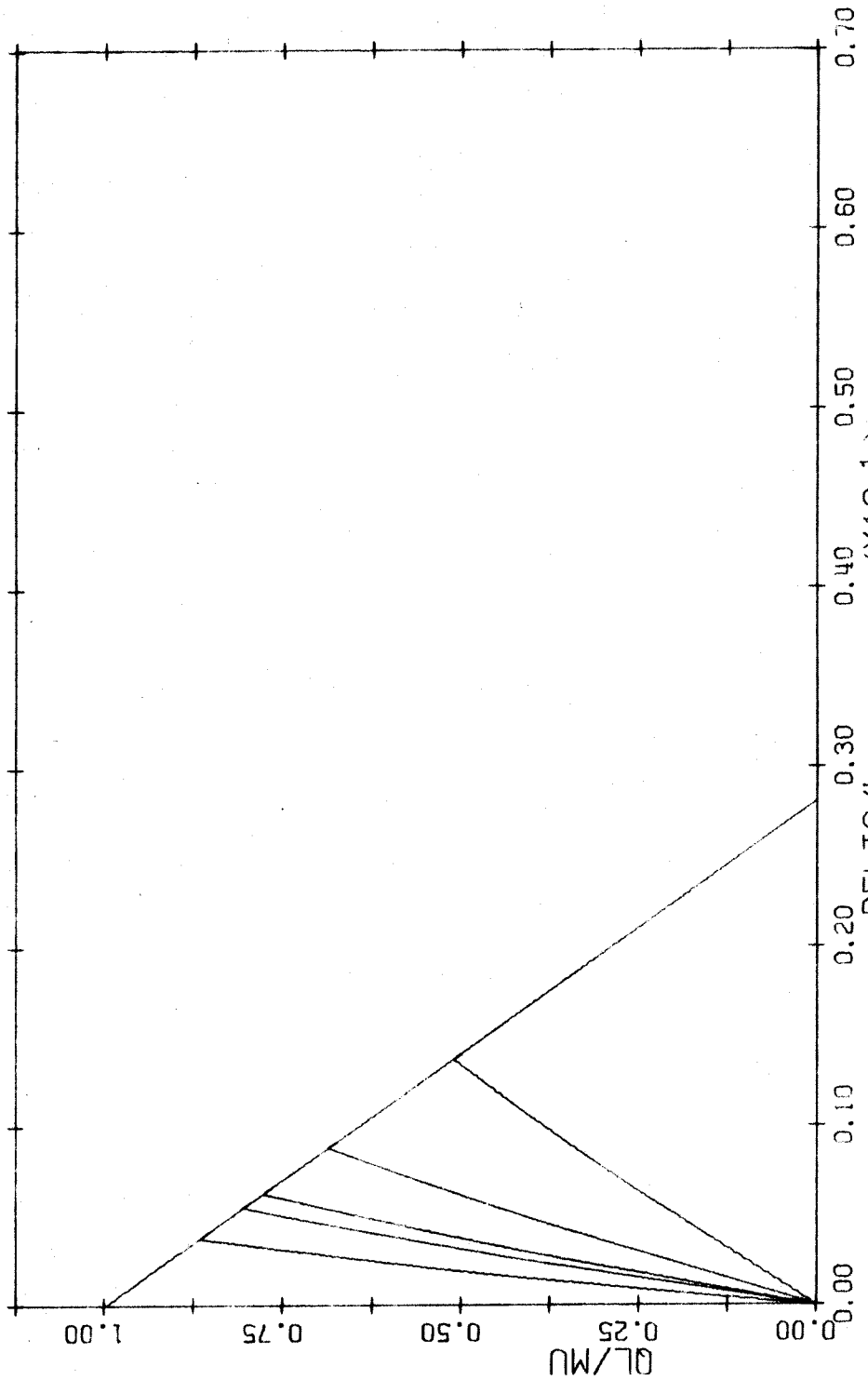

FIG. A-44 LOAD DEFLECTION DIAGRAM. TIED COLUMN. BARS IN 2 FACES
L/H=10 P/PO=0.7

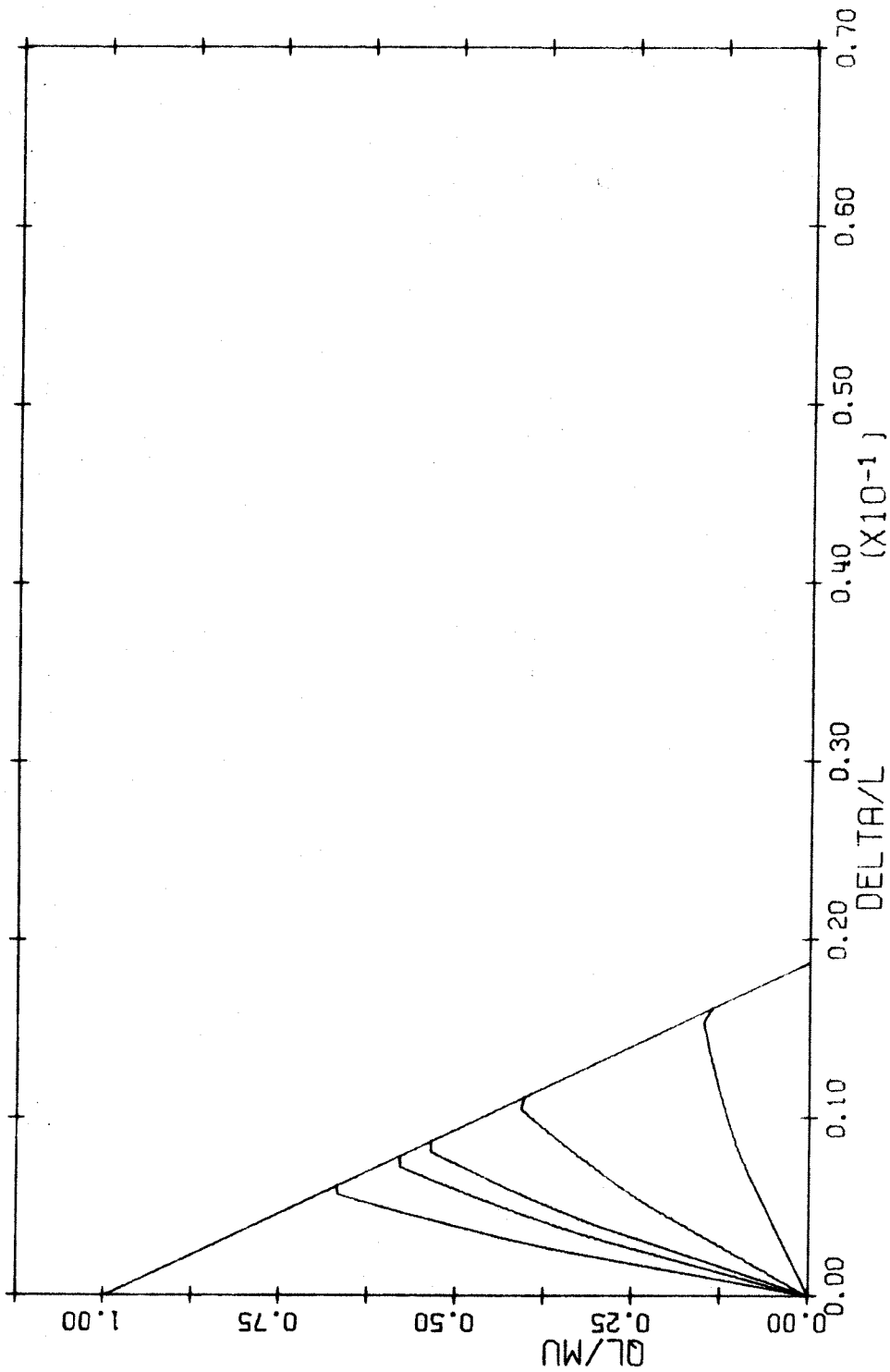

FIG. A-45 LOAD DEFLECTION DIAGRAM. TIED COLUMN. BARS IN 2 FACES
L/H=15 P/P0=0.7

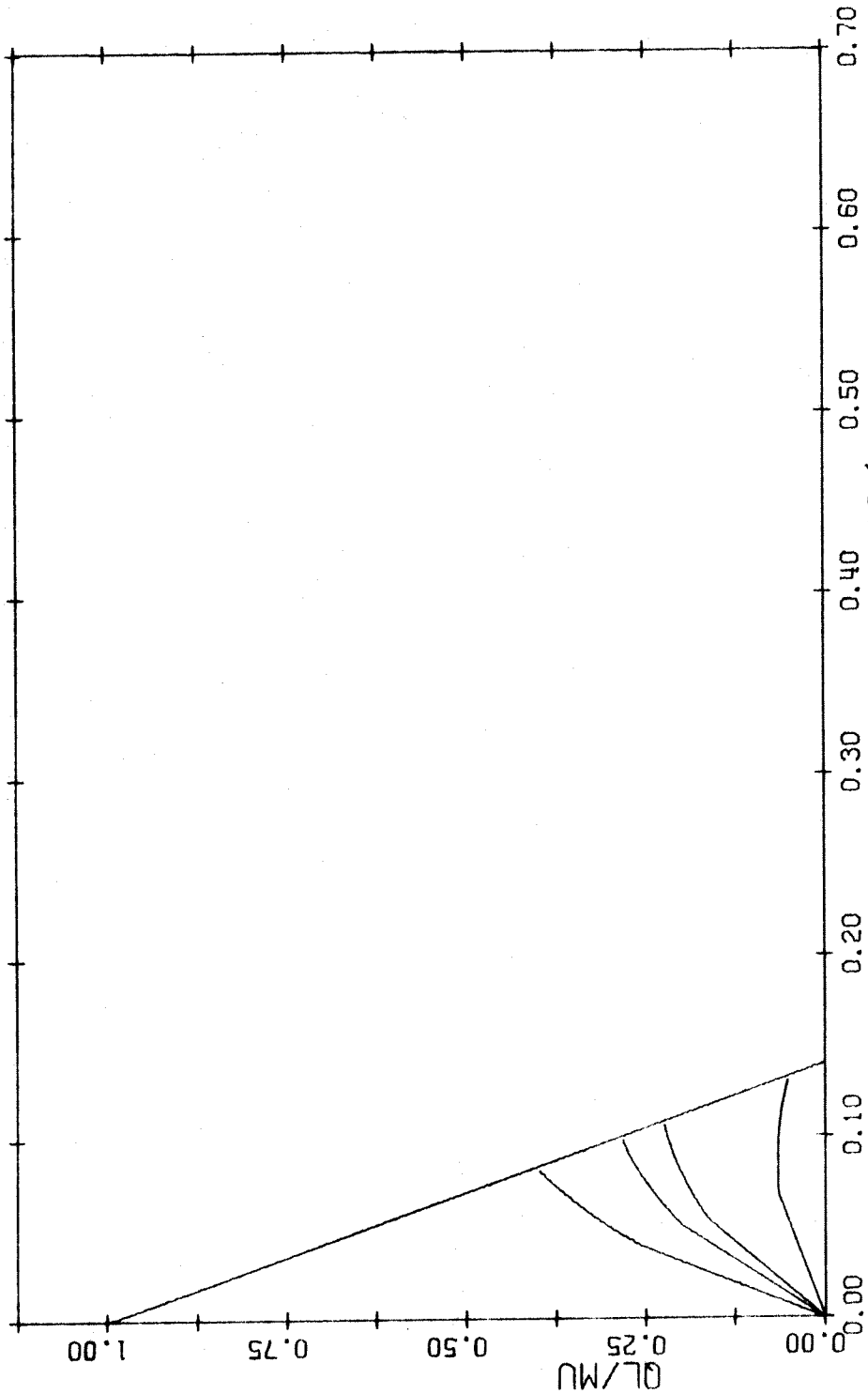

FIG. A-46 LOAD DEFLECTION DIAGRAM. TIED COLUMN. BARS IN 2 FACES
L/H=20 P/PC=0.7

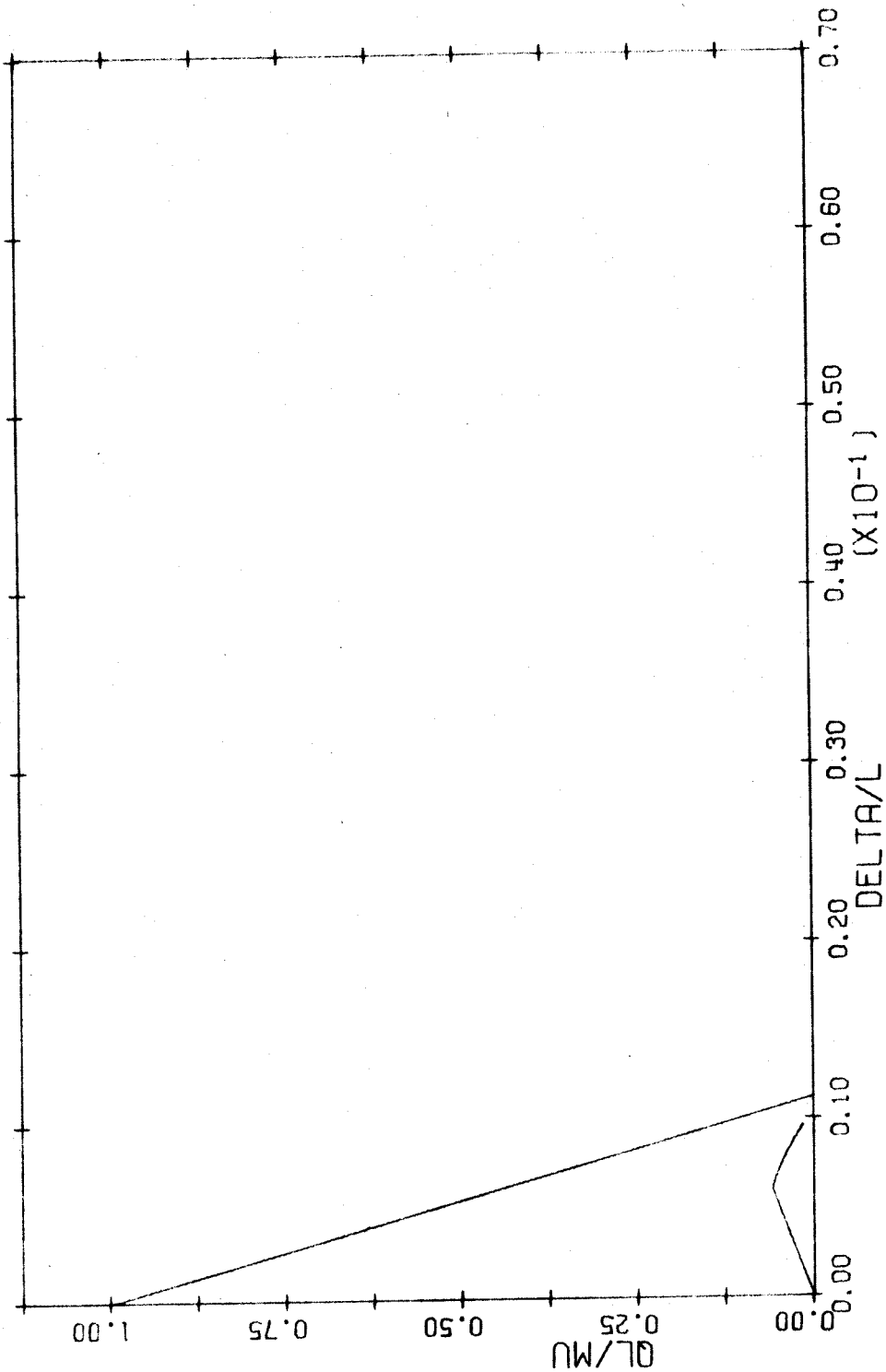

FIG. A-47 LOAD DEFLECTION DIAGRAM. TIED COLUMN. BARS IN 2 FACES
L/H=25 P/P0=0.7

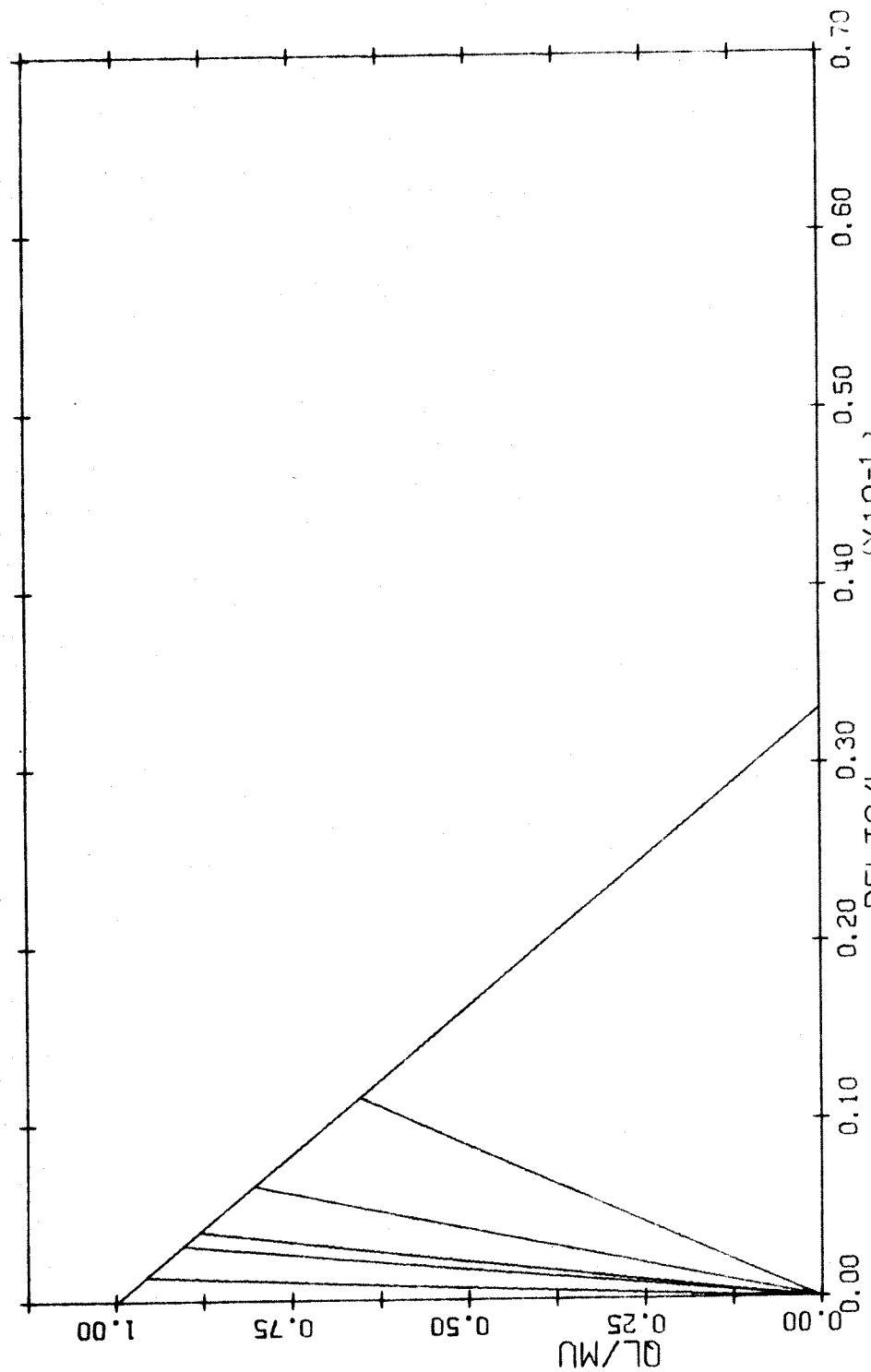

FIG. A-49 LOAD DEFLECTION DIAGRAM. TIED COLUMN. BARS IN 2 FACES
L/H=5 P/PC=0.8

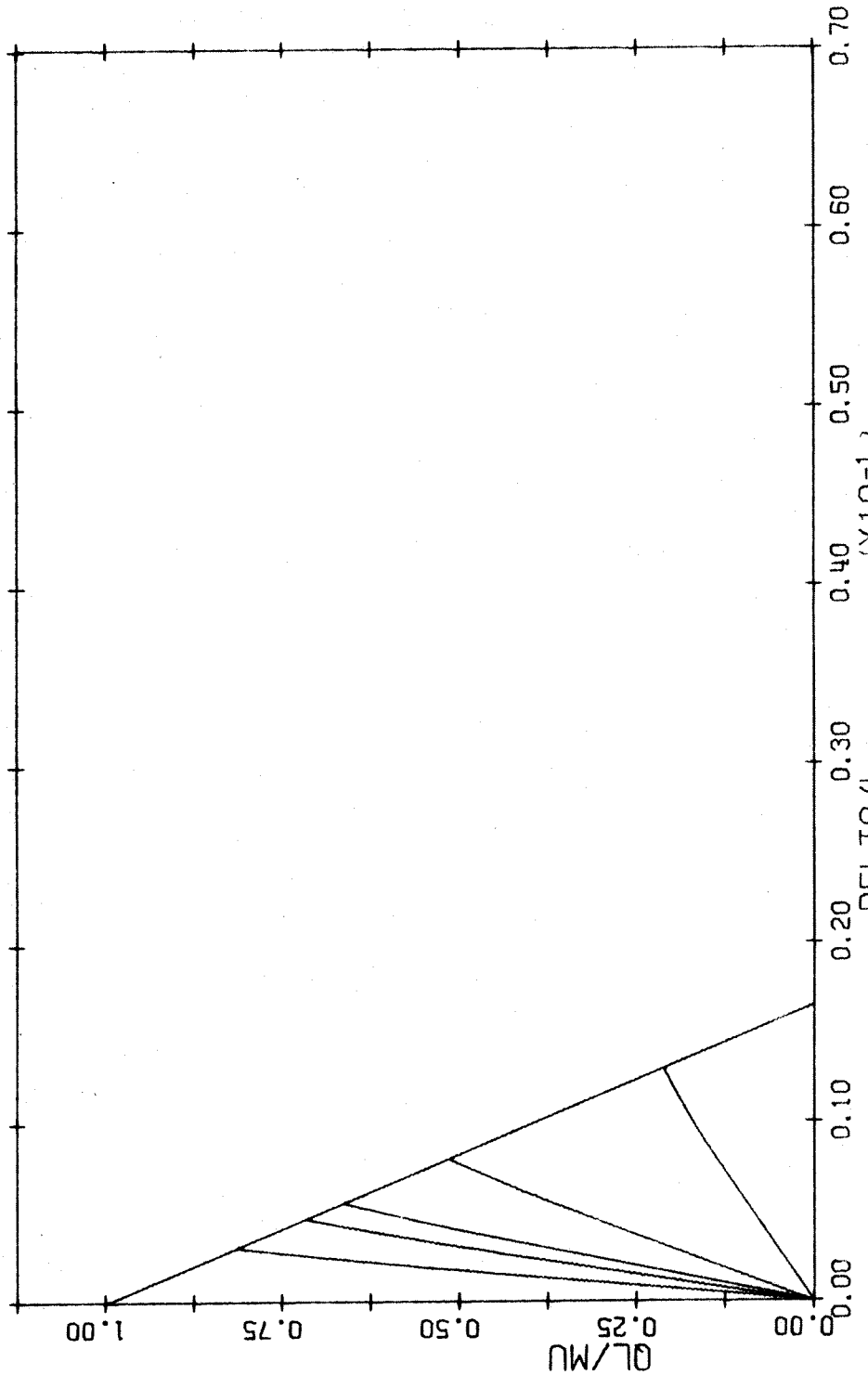

FIG. A-49 LOAD DEFLECTION DIAGRAM. TIED COLUMN. BARS IN 2 FACES
L/H=10 P/PO=0.8

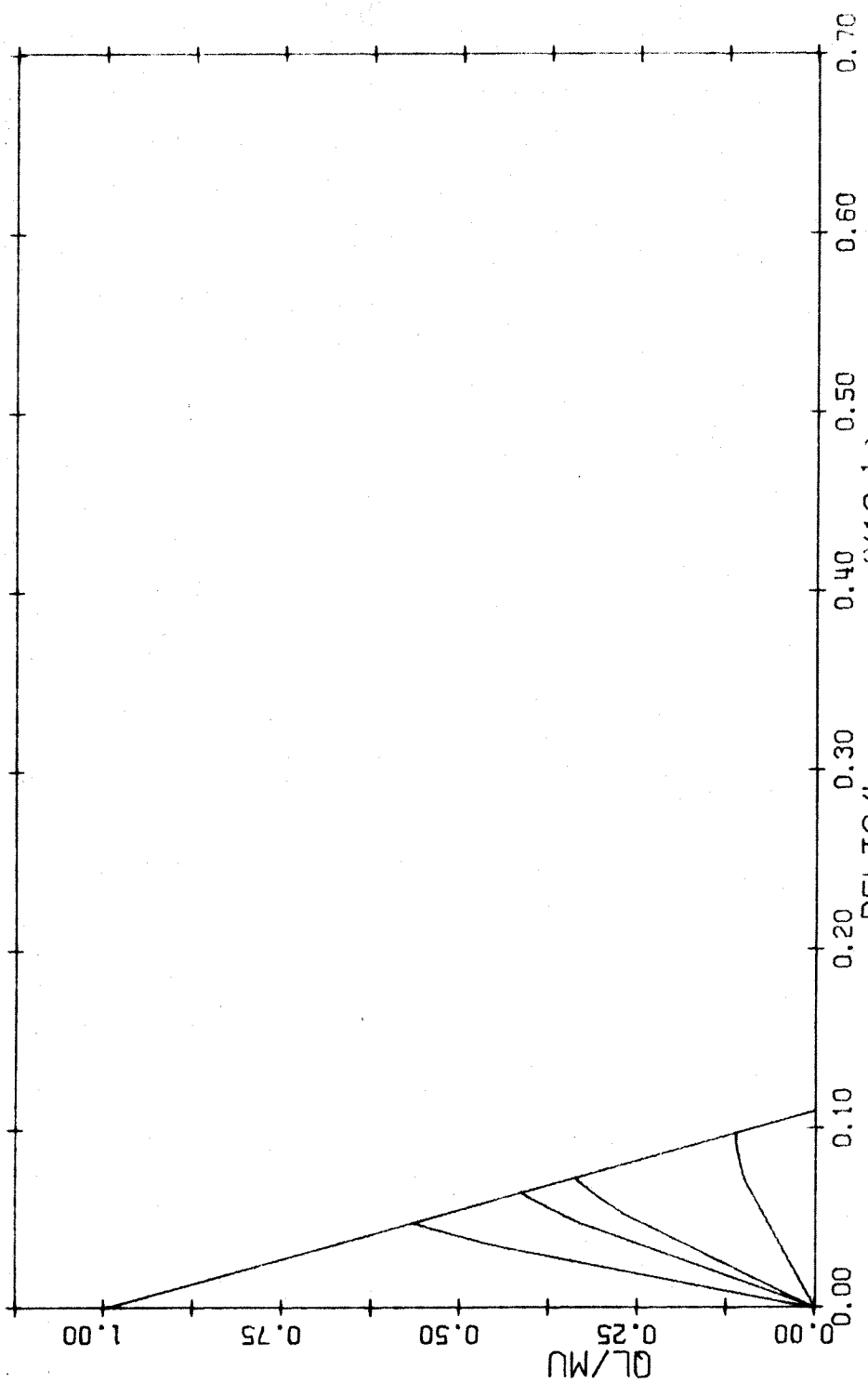

FIG. A-50 LOAD DEFLECTION DIAGRAM. TIED COLUMN. BARS IN 2 FACES
L/H=15 . P/P0=0.8

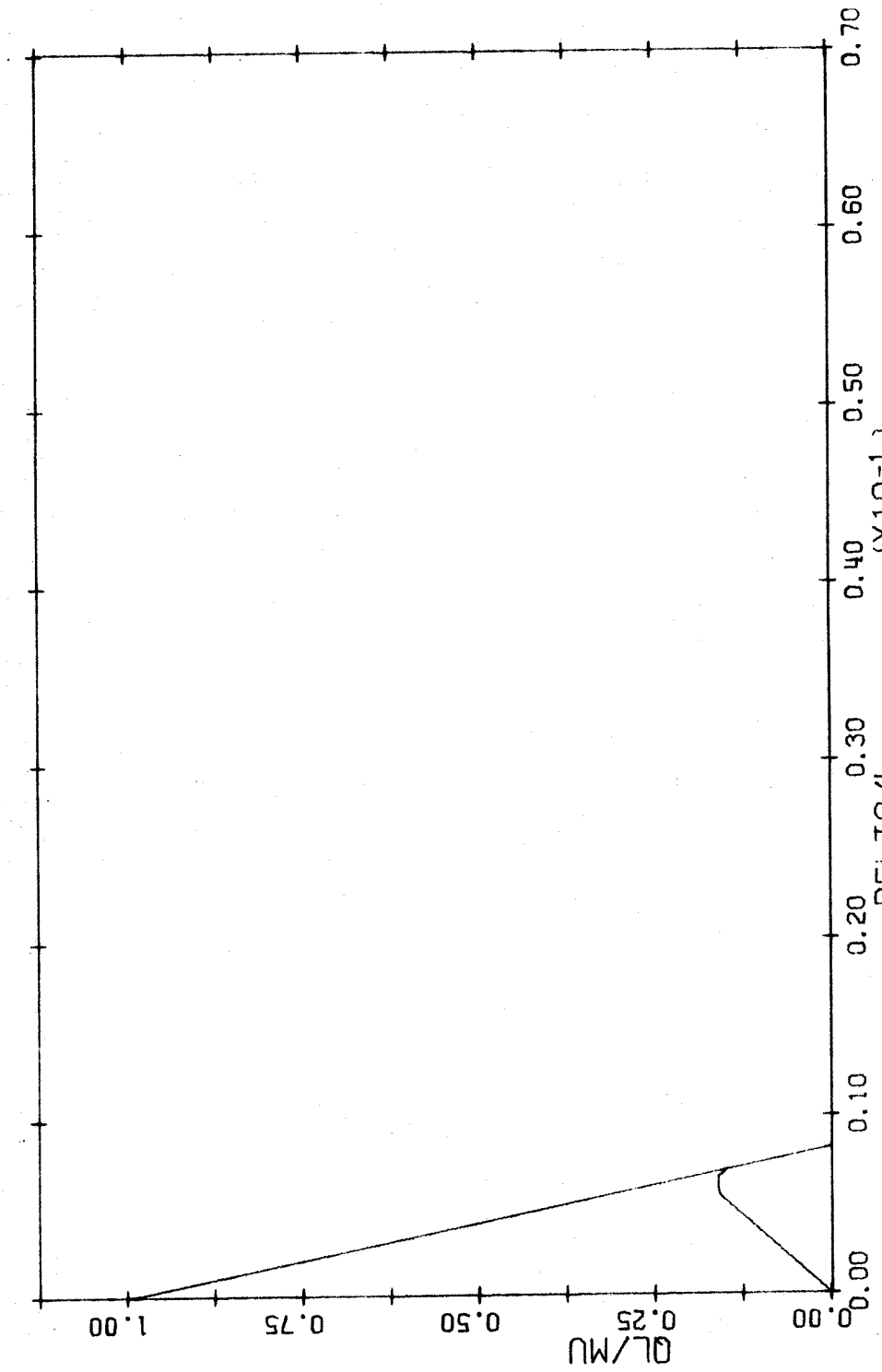

FIG. A-51 LOAD DEFLECTION DIAGRAM. TIED COLUMN. BARS IN 2 FACES
L/H=20 P/P0=0.8

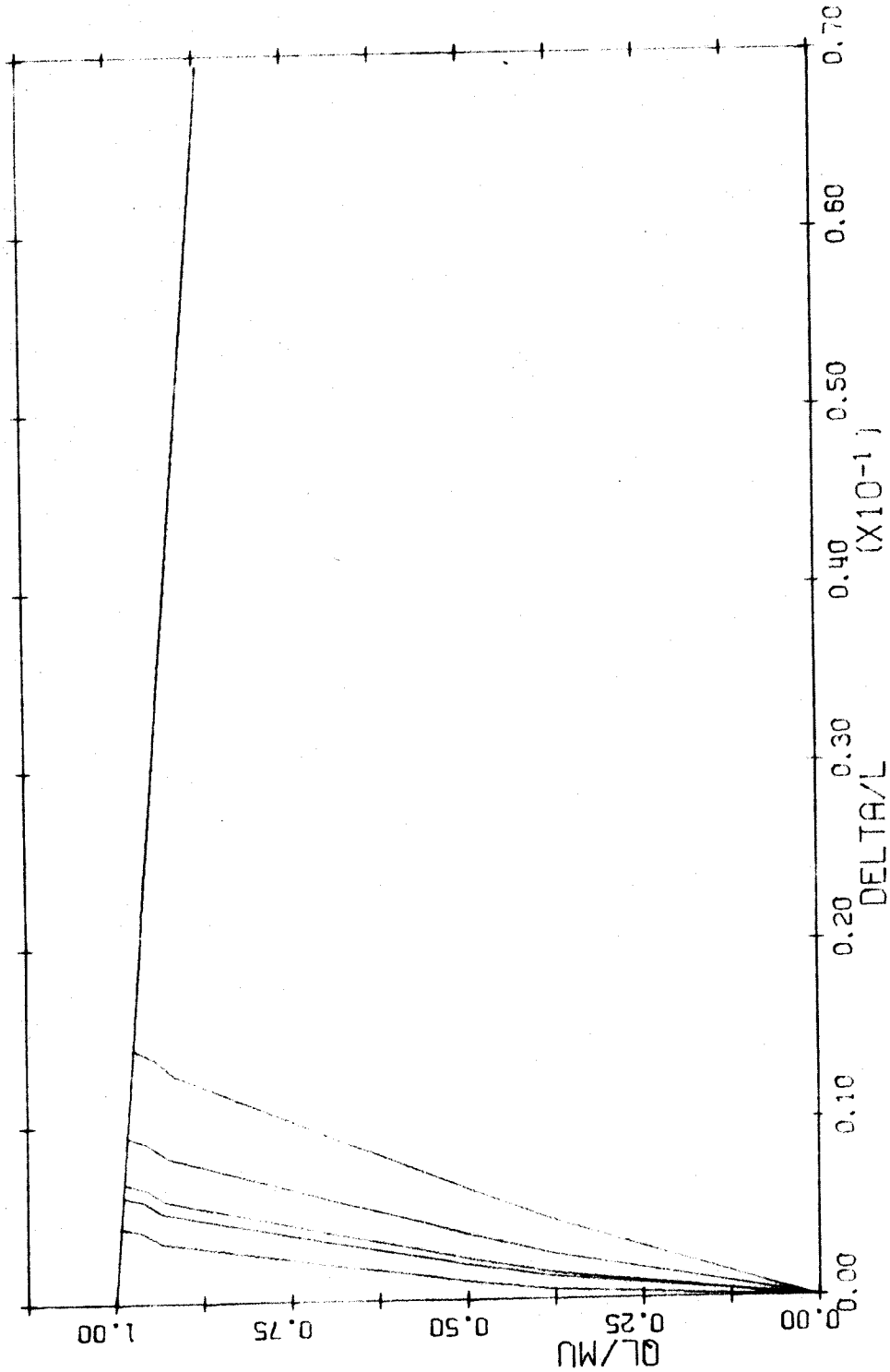

FIG. 3-12 LOAD DEFLECTION DIAGRAM, TIED COLUMN, BARS IN 4 FACES
L/H=5 P/P0=0.1

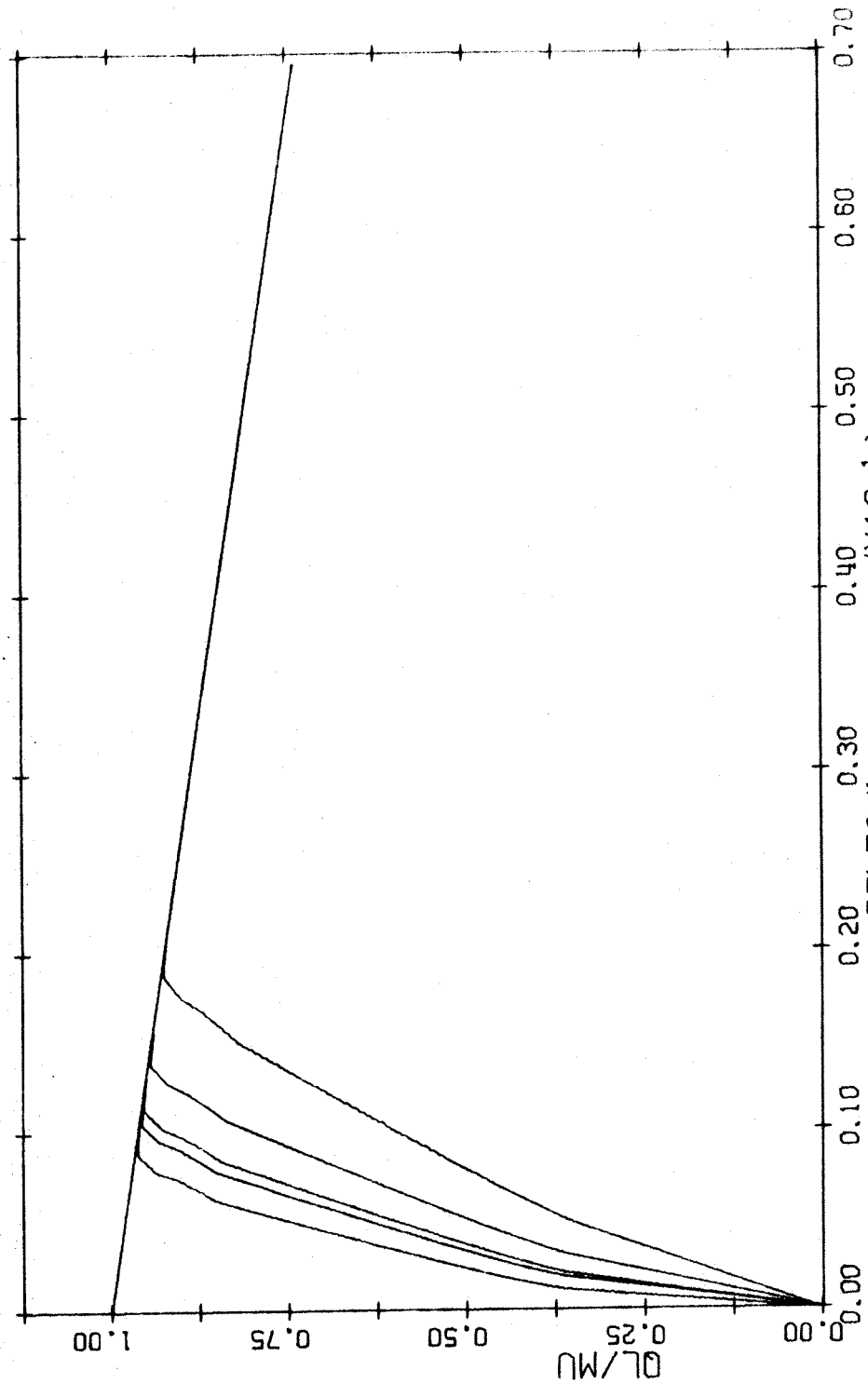

FIG. A-53 LOAD DEFLECTION DIAGRAM. TIED COLUMN. BARS IN 4 FACES
L/H=10 P/P0=0.1

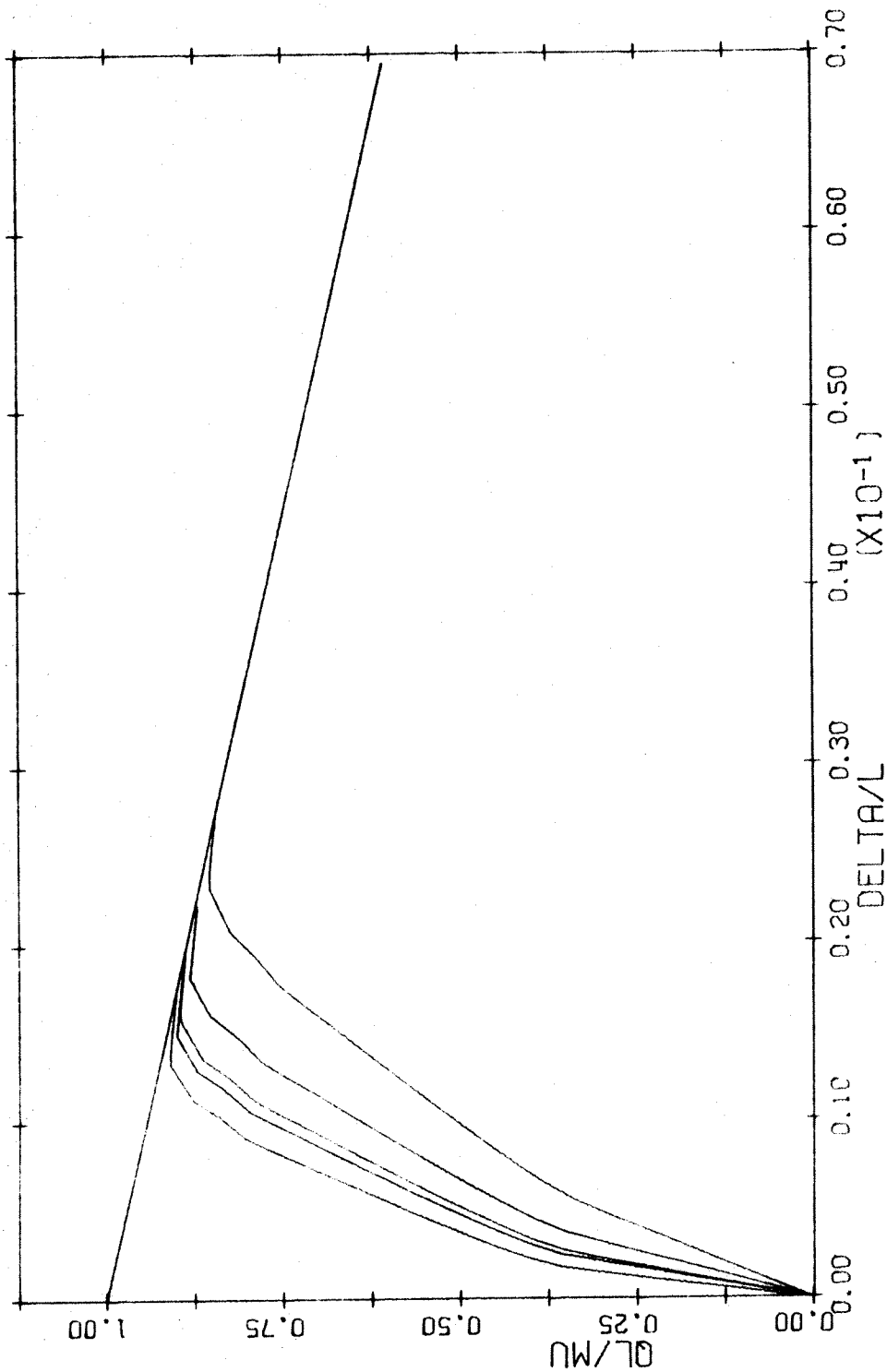

FIG. A-54 LOAD DEFLECTION DIAGRAM. TIED COLUMN. BARS IN 4 FACES
L/H=15 P/P0=C.1

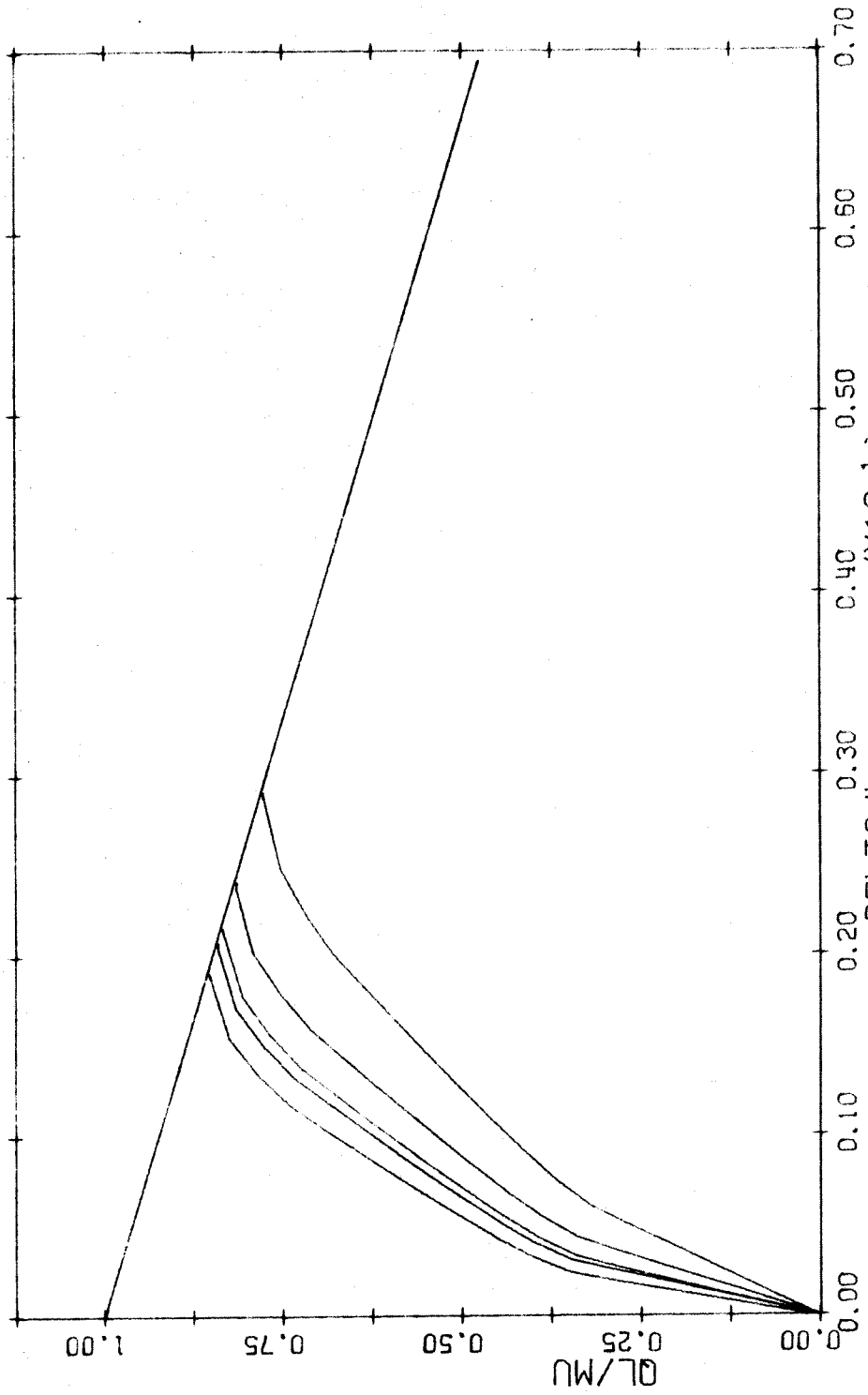

FIG. A-55 LOAD DEFLECTION DIAGRAM. TIED COLUMN. BARS IN 4 FACES
L/H=20 P/P0=0.1

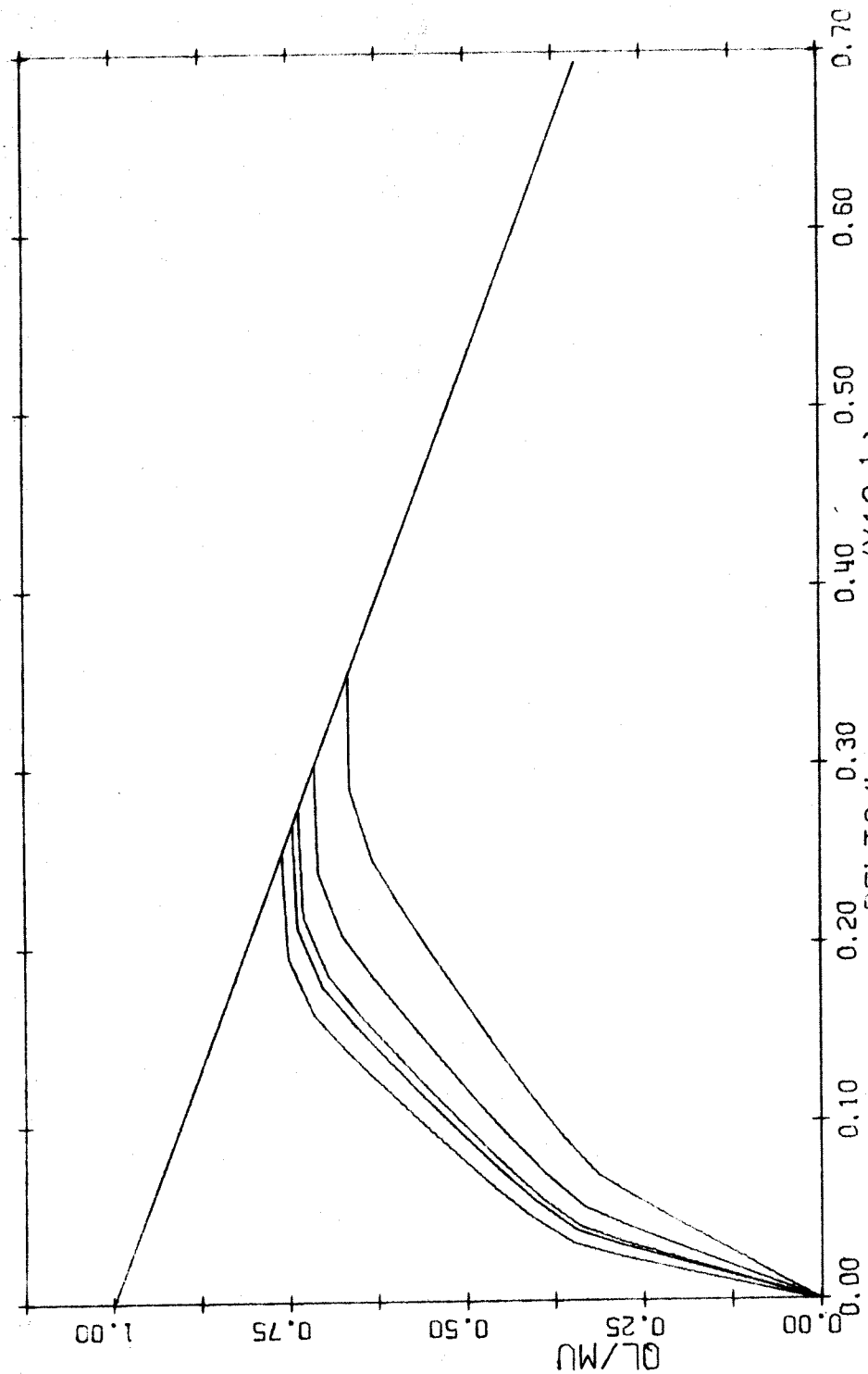

FIG. A-56 LOAD DEFLECTION DIAGRAM. TIED COLUMN. BARS IN 4 FACES
L/H=25 P/PO=0.1

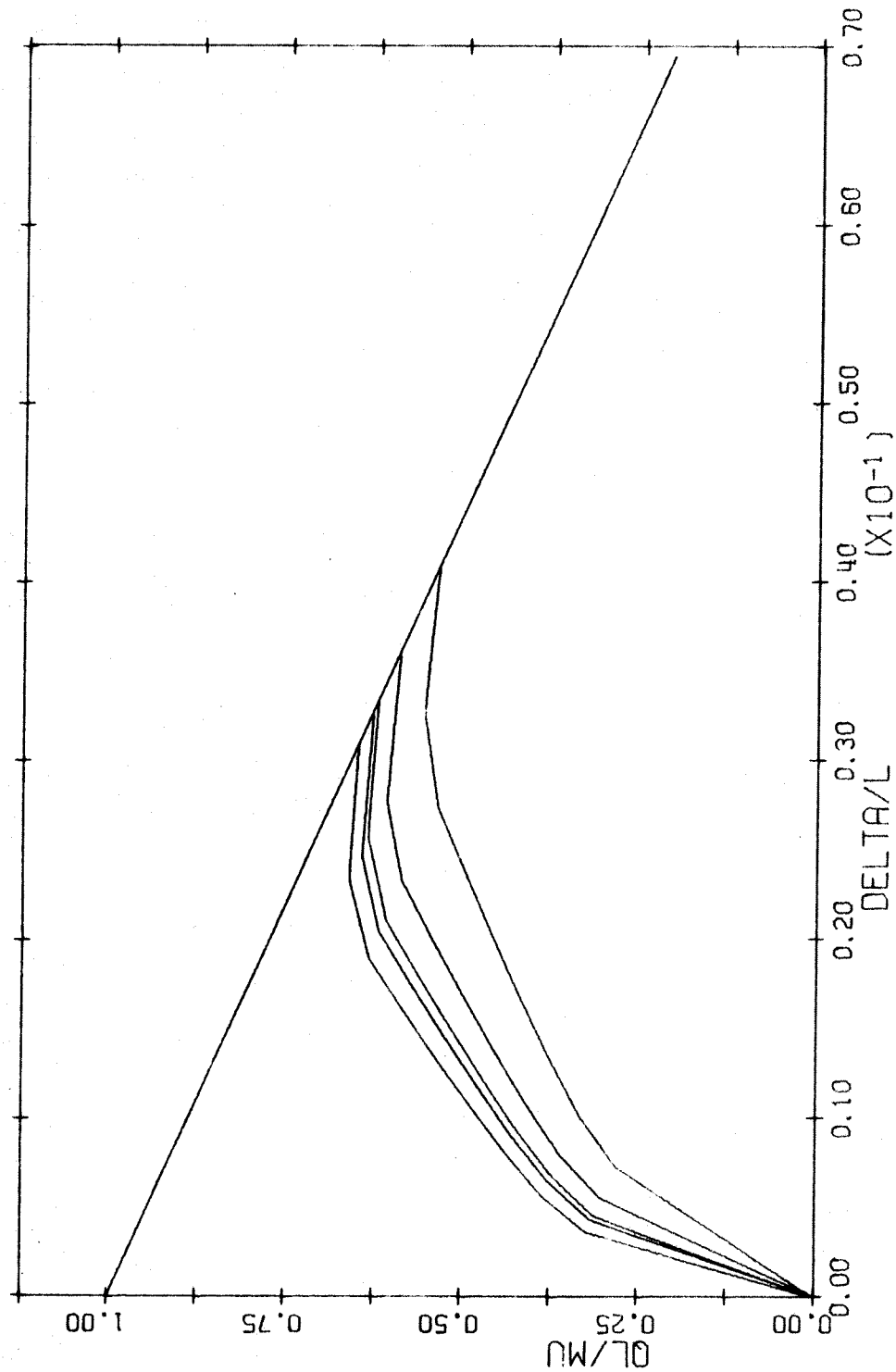

FIG. A-57 LOAD DEFLECTION DIAGRAM. TIED COLUMN. BARS IN 4 FACES
L/H=30 P/P0=0.1

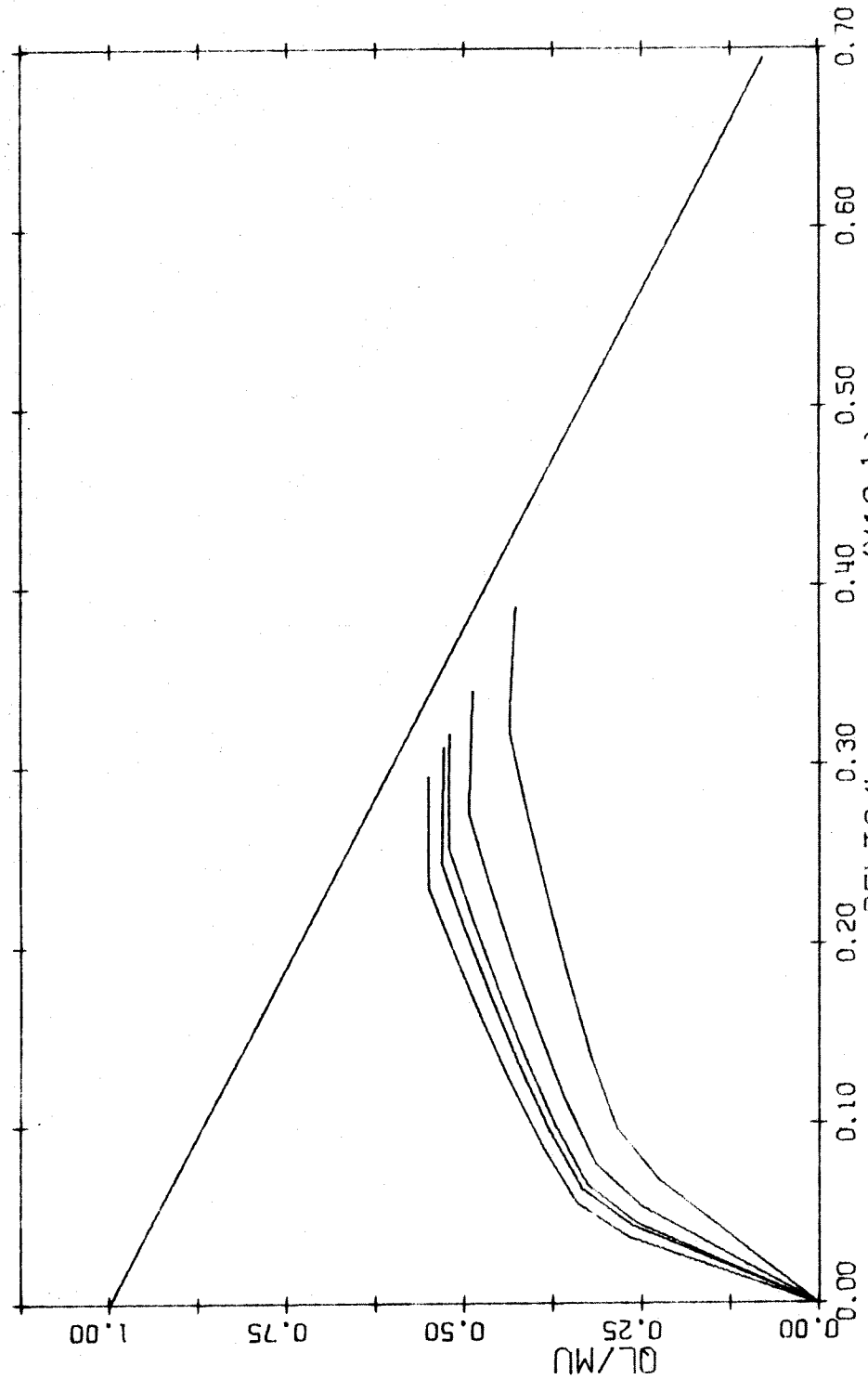

FIG. A-58 LOAD DEFLECTION DIAGRAM. TIED COLUMN. BARS IN 4 FACES
L/H=35 P/P0=0.1

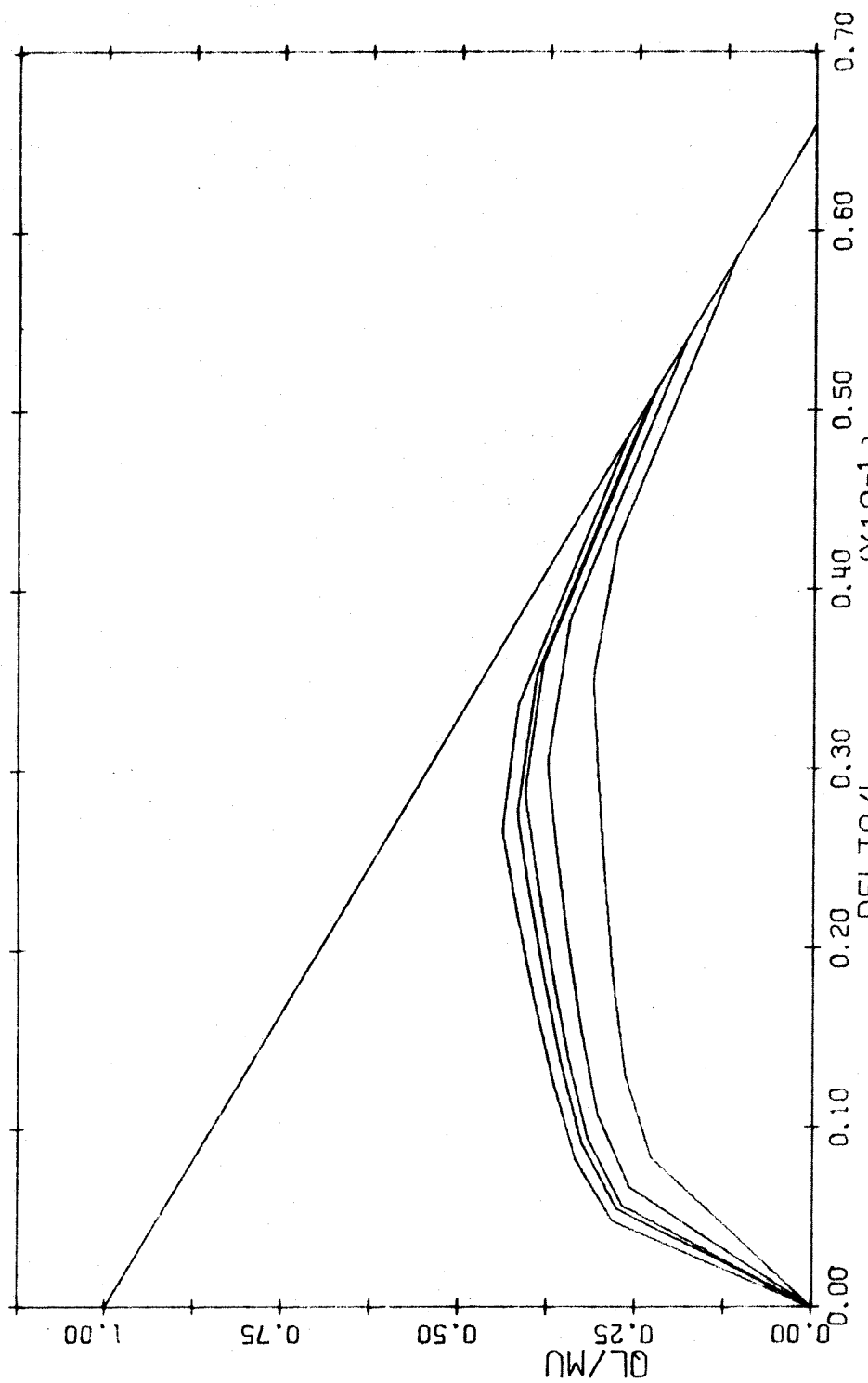

FIG. A-59 LOAD DEFLECTION DIAGRAM. TIED COLUMN. BARS IN 4 FACES
L/H=40 P/PO=0.1

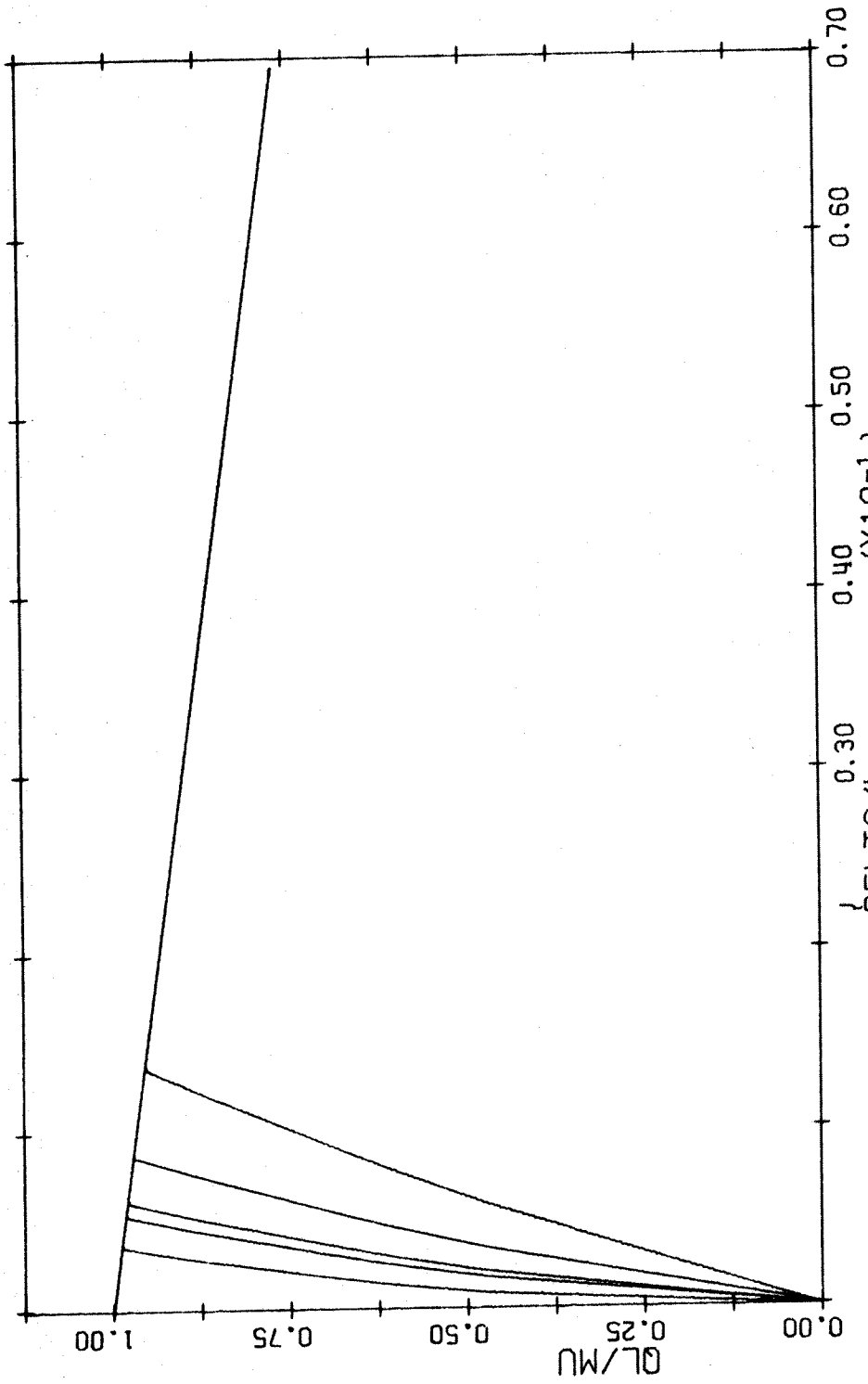

FIG. A-60 LOAD DEFLECTION DIAGRAM. TIED COLUMN. BARS IN 4 FACES
L/H=5 P/P0=0.2

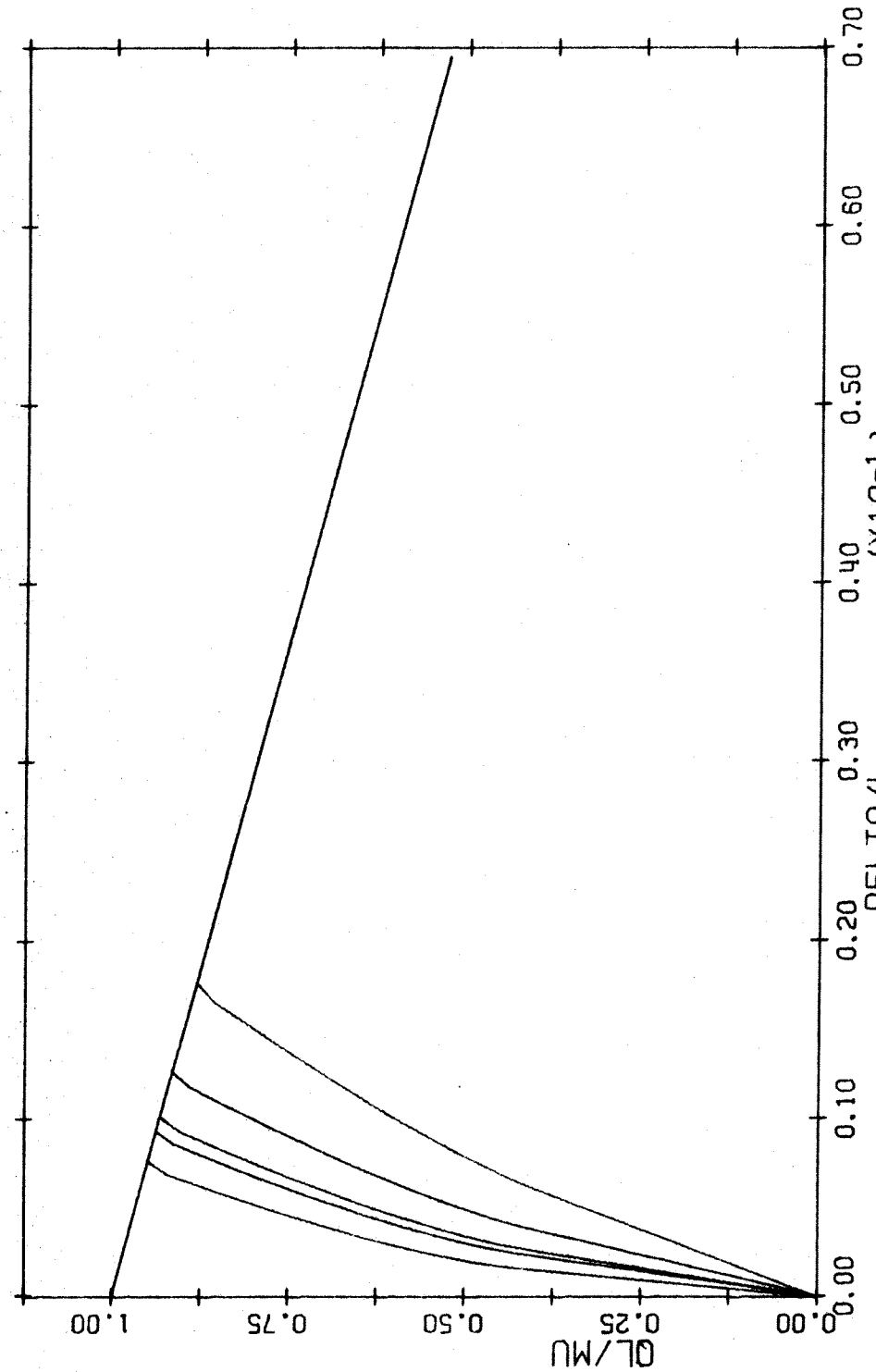

FIG. A-61 LOAD DEFLECTION DIAGRAM. TIED COLUMN. BARS IN 4 FACES
L/H=10 P/P0=0.2

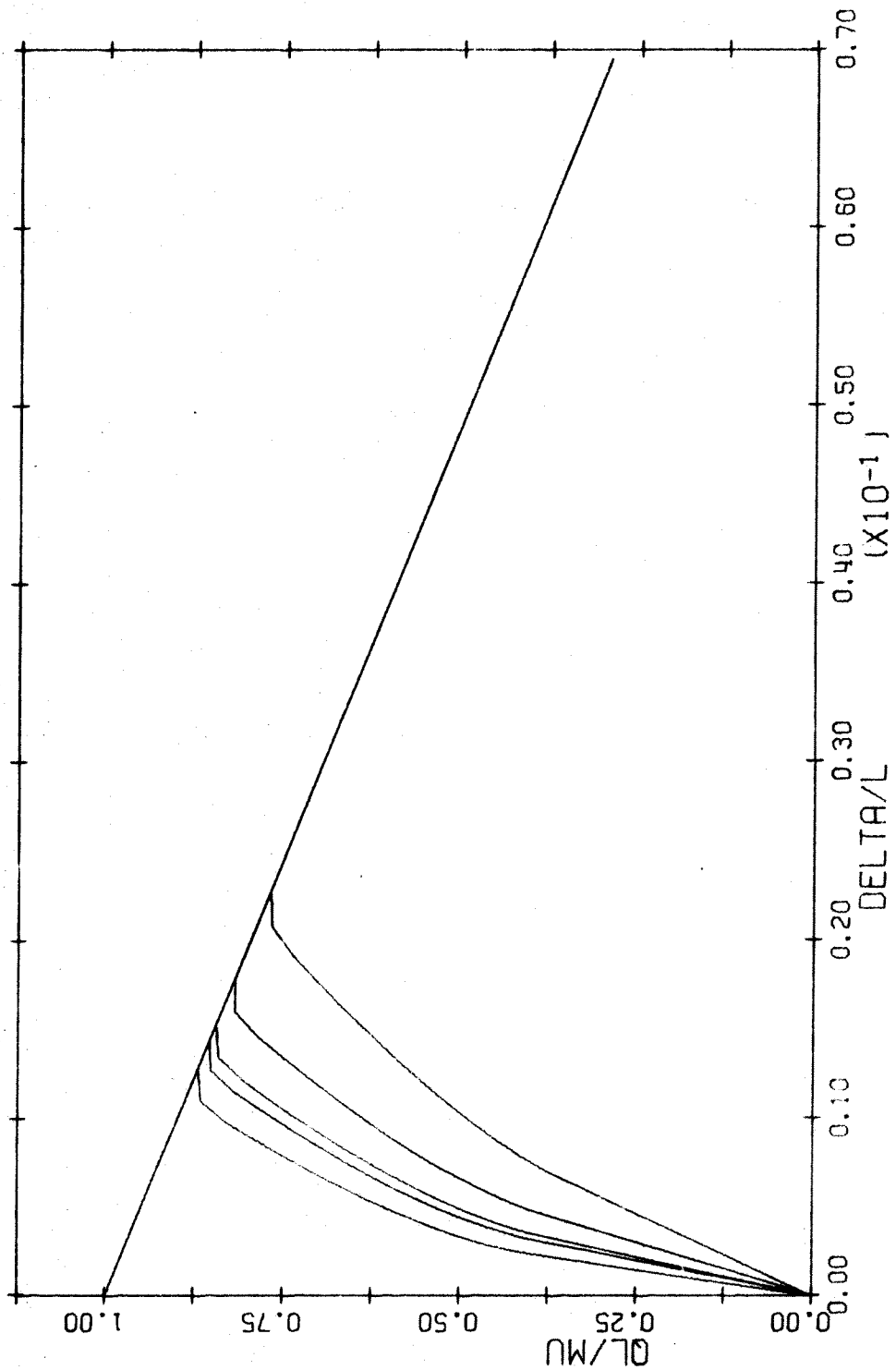

FIG. A-62 LOAD DEFLECTION DIAGRAM. TIED COLUMN. BARS IN 4 FACES
L/H=15 P/P0=0.2

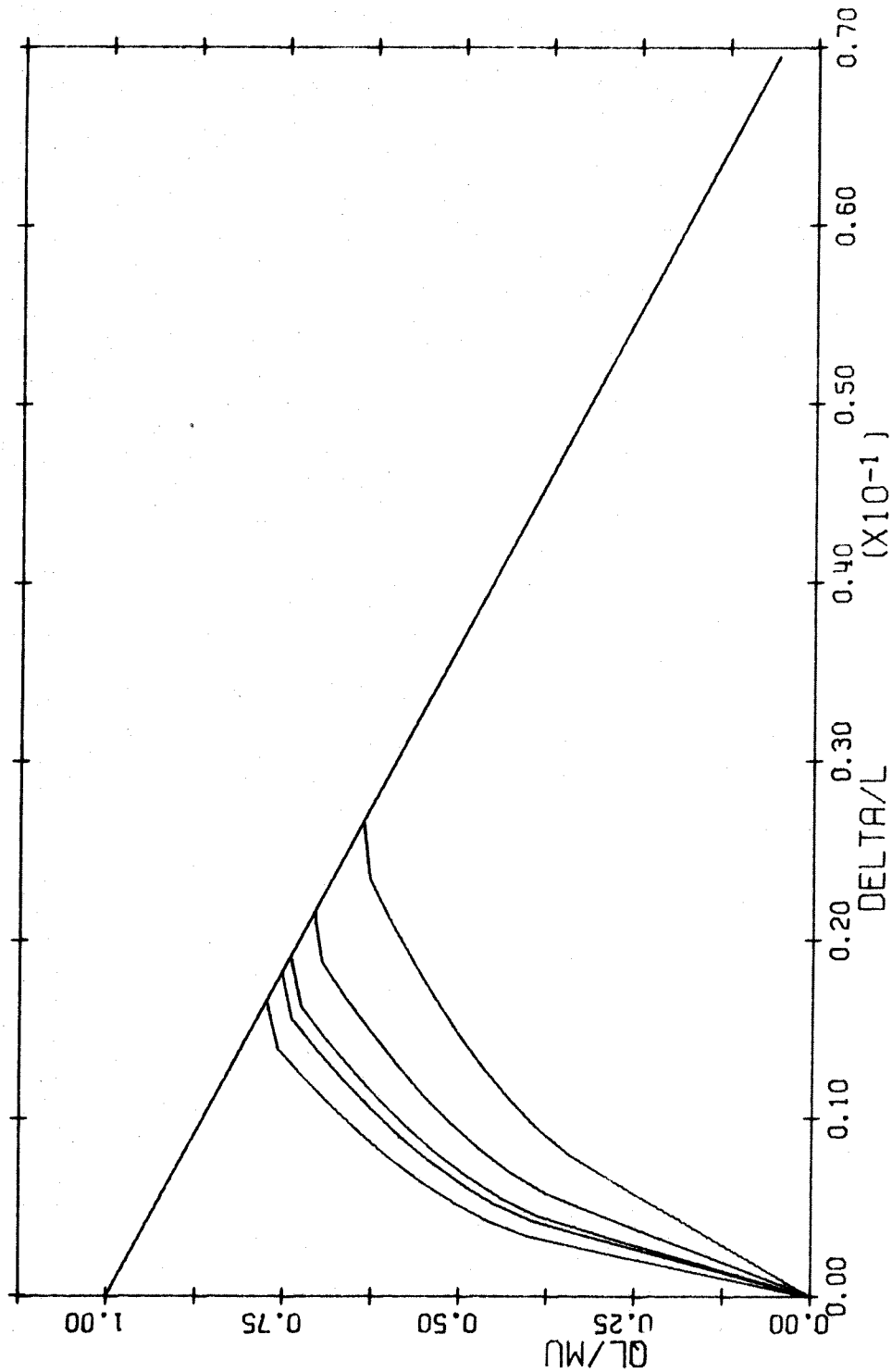

FIG. A-63 LOAD DEFLECTION DIAGRAM. TIED COLUMN. BARS IN 4 FACES
L/H=20 P/P0=0.2

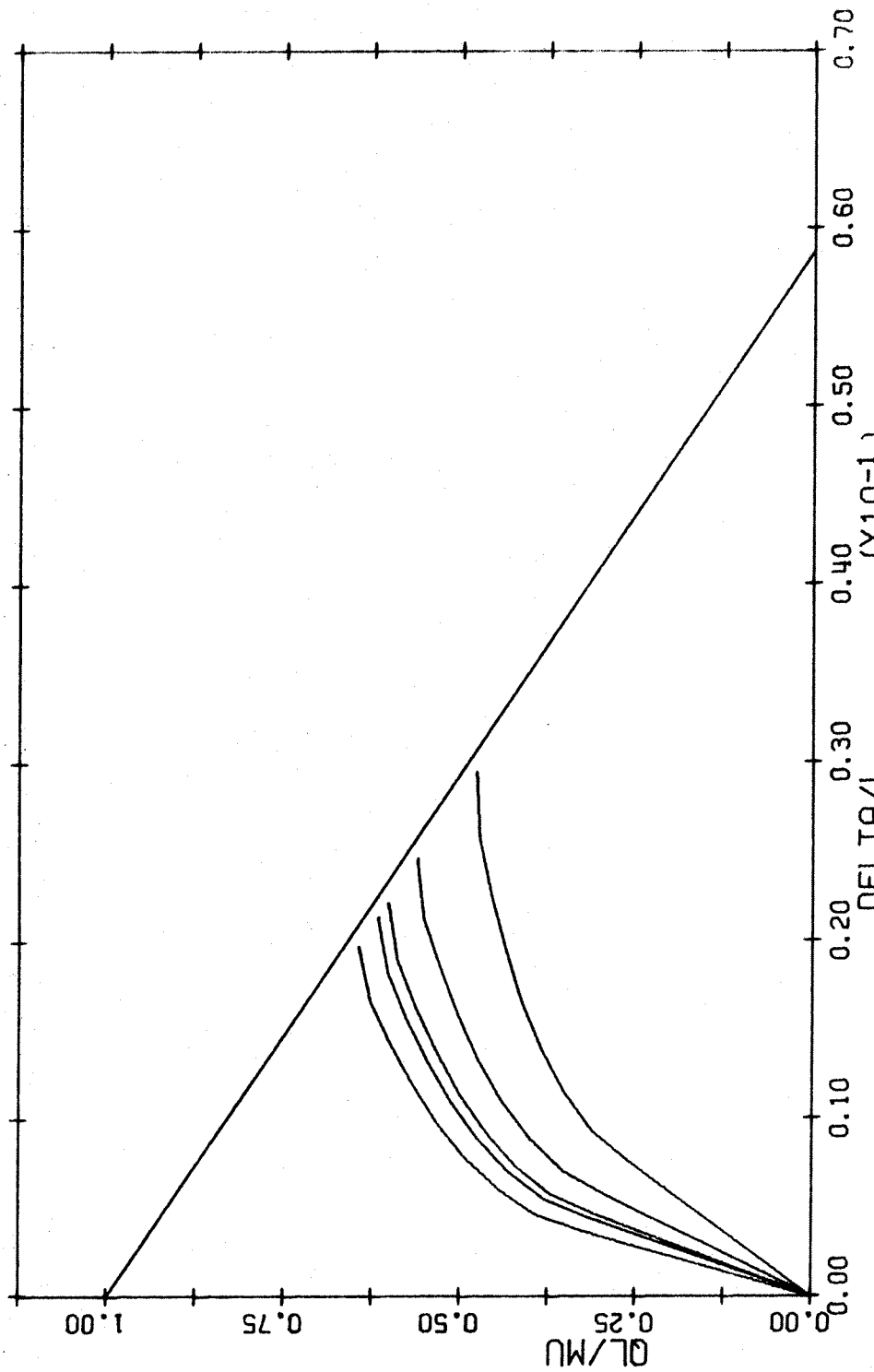

FIG. A-64 LOAD DEFLECTION DIAGRAM. TIED COLUMN. BARS IN 4 FACES
L/H=25 P/P0=0.2

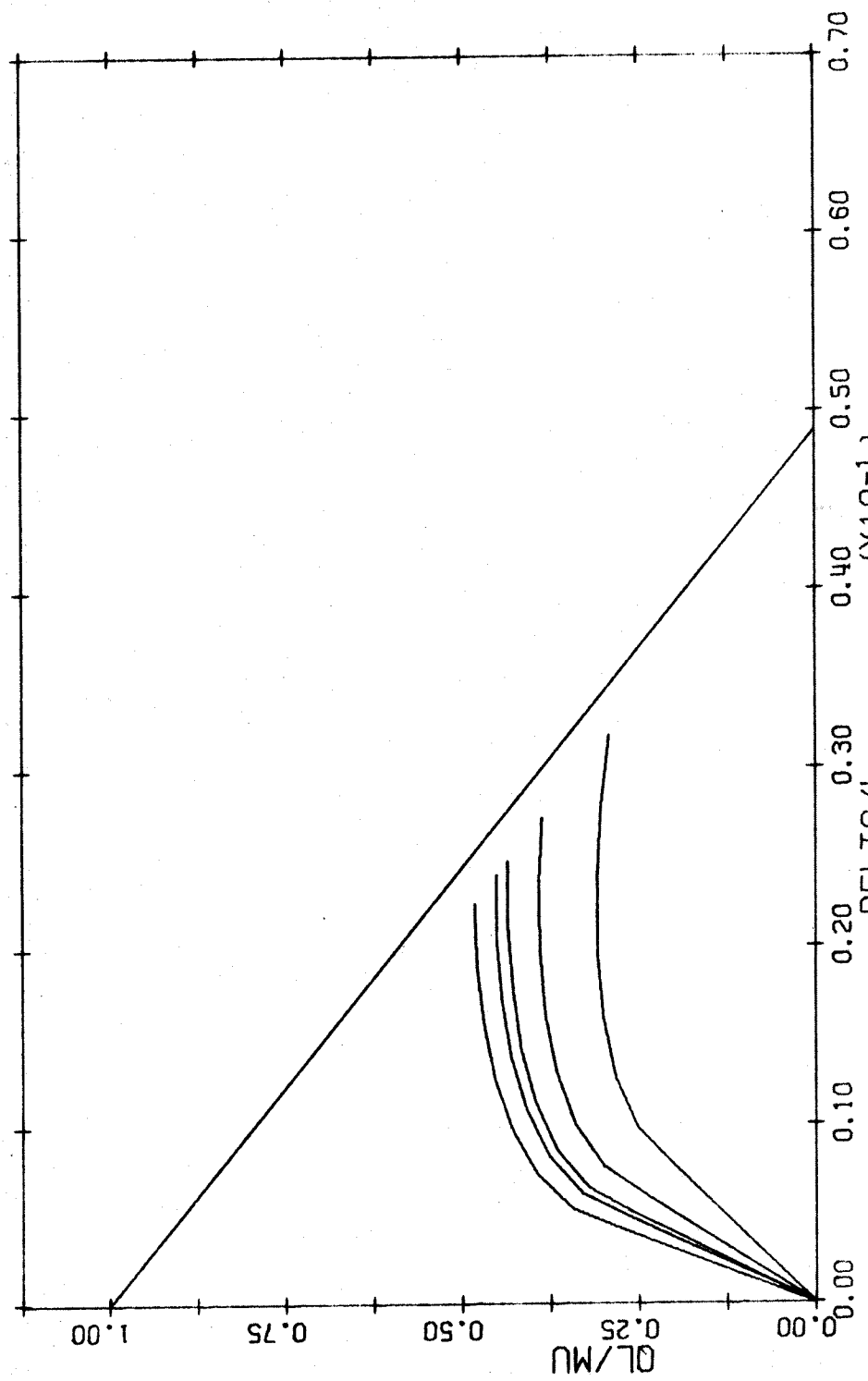

FIG. A-65 LOAD DEFLECTION DIAGRAM. TIED COLUMN. BARS IN 4 FACES
L/H=30 P/P0=0.2

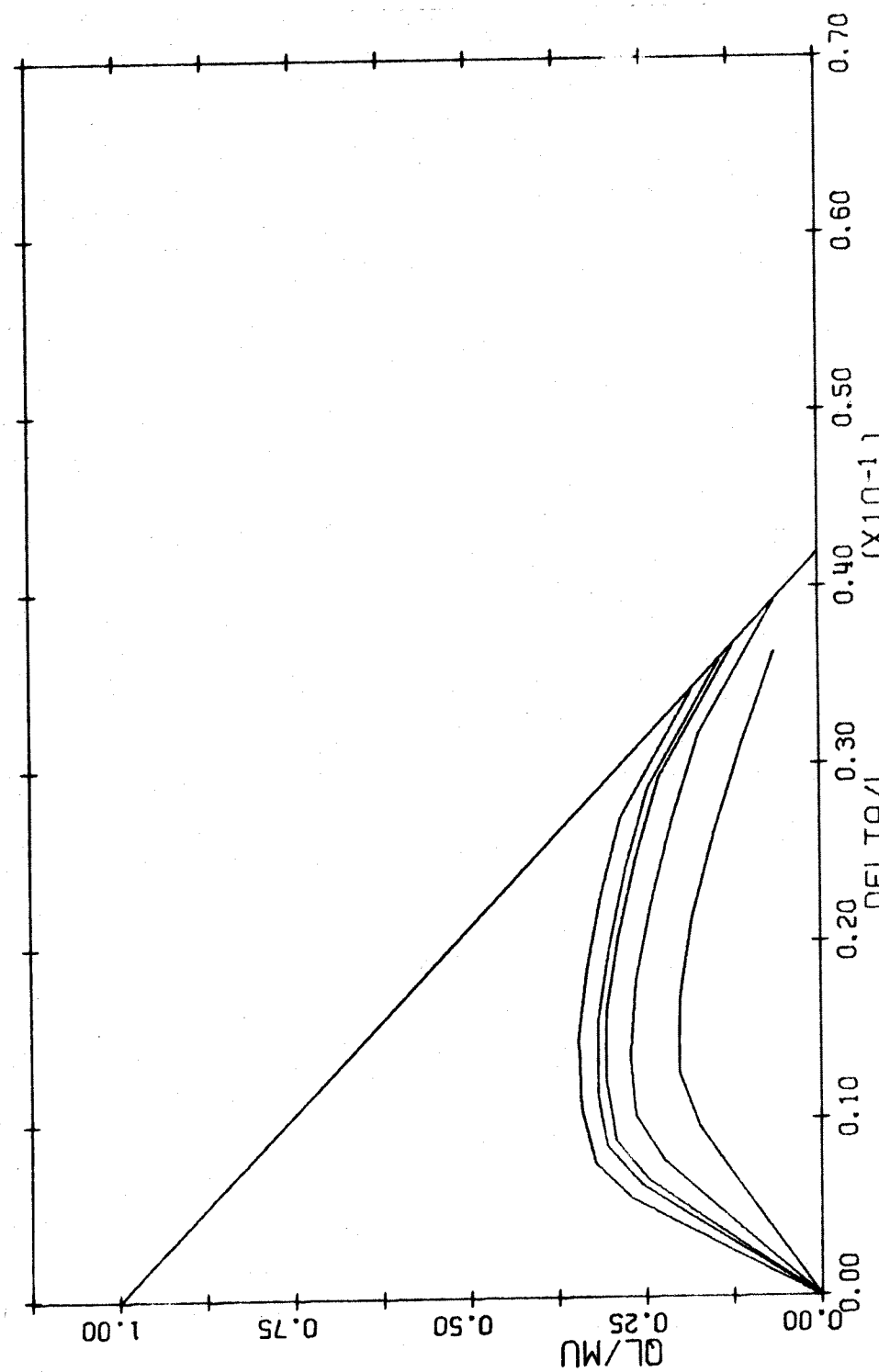

FIG. A-66 LOAD DEFLECTION DIAGRAM. TIED COLUMN. BARS IN 4 FACES
L/H=35 P/P0=0.2

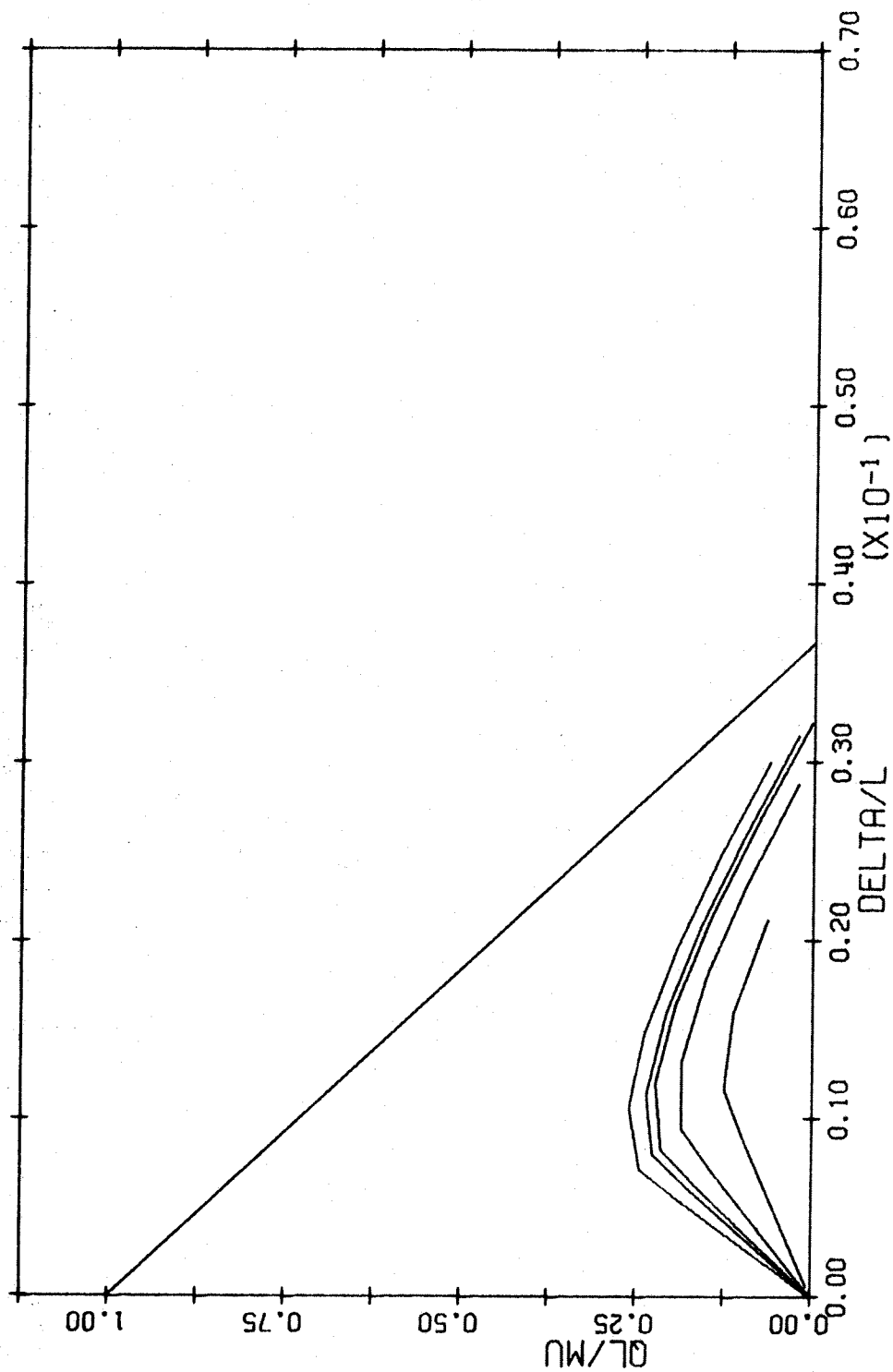

FIG. A-67 LOAD DEFLECTION DIAGRAM. TIED COLUMN. BARS IN 4 FACES
L/H=40 P/P0=0.2

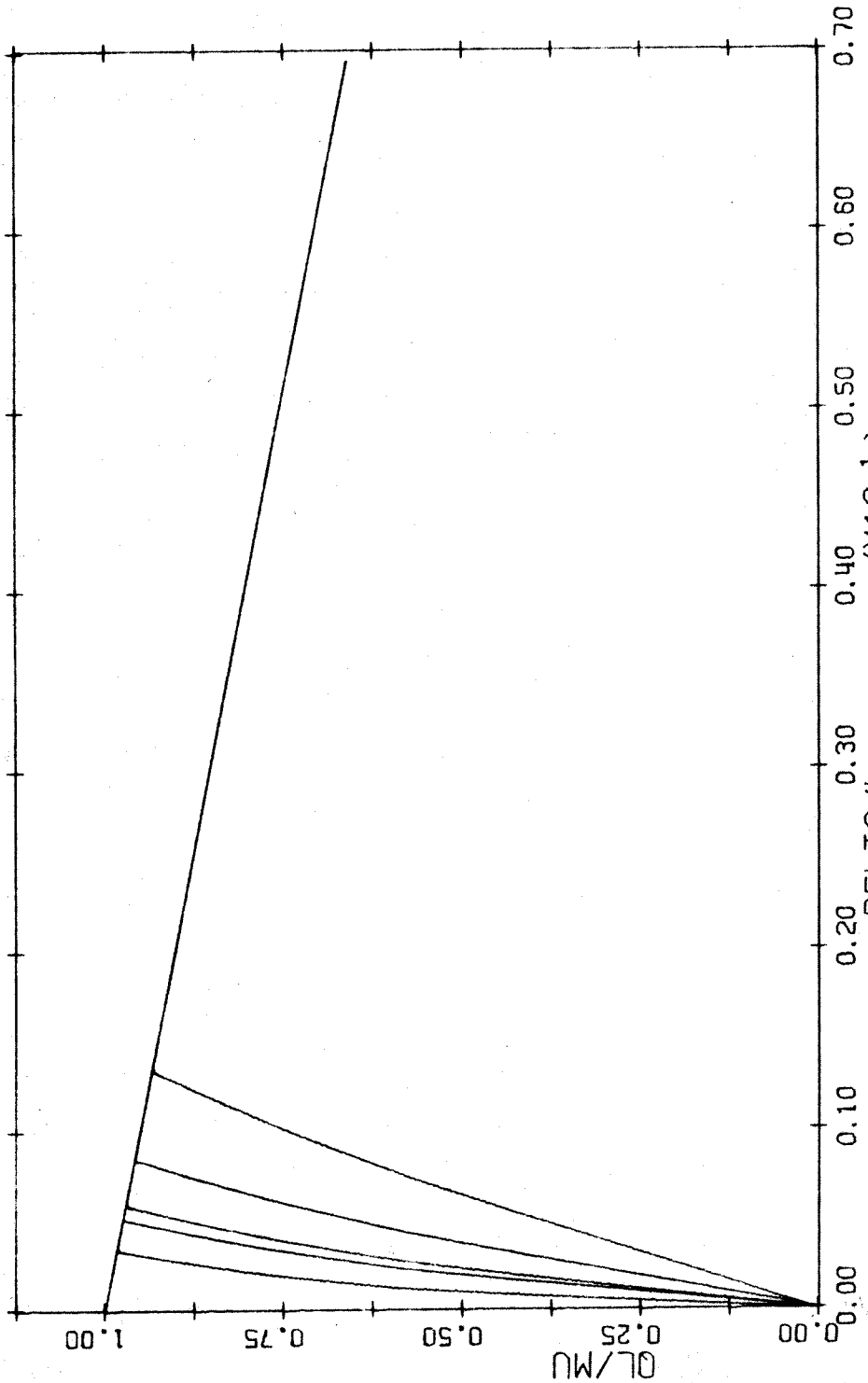

FIG. A-68 LOAD DEFLECTION DIAGRAM. TIED COLUMN. BARS IN 4 FACES
L/H=5 P/P0=0.3

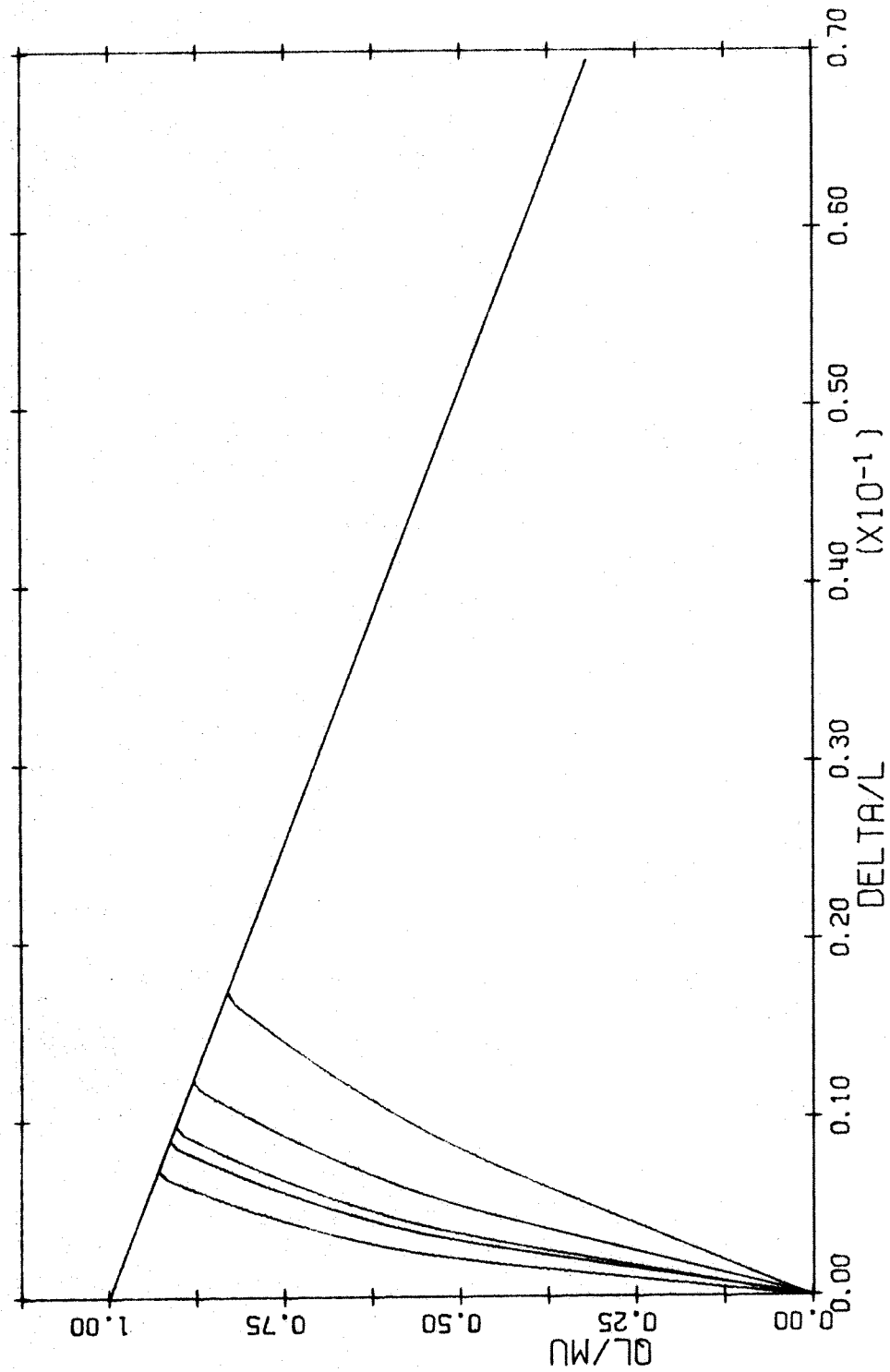

FIG. A-69 LOAD DEFLECTION DIAGRAM. TIED COLUMN. BARS IN 4 FACES
L/H=10 P/P0=0.3

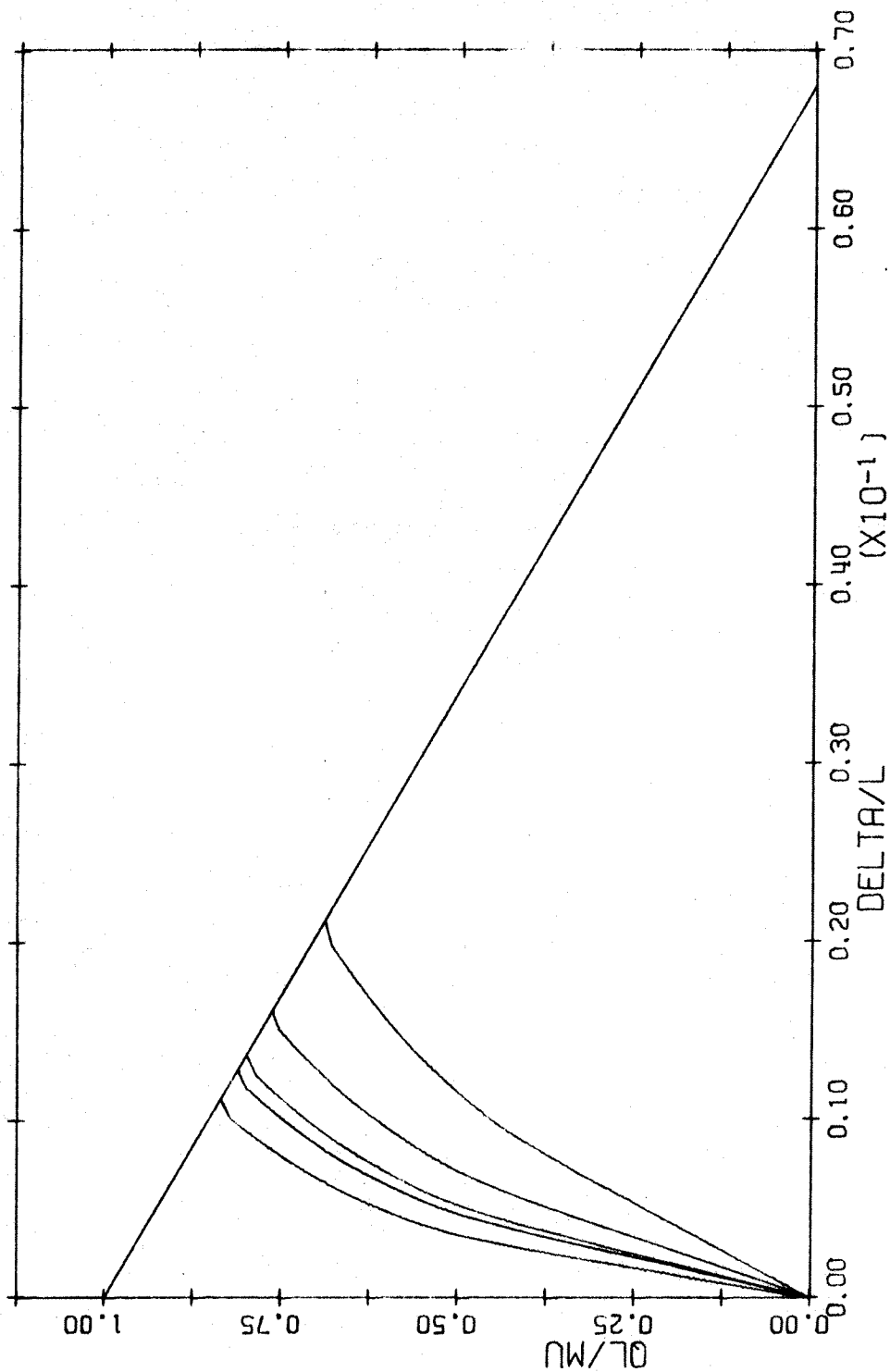

FIG. A-70 LOAD DEFLECTION DIAGRAM. TIED COLUMN. BARS IN 4 FACES
L/H=15 P/PO=0.3

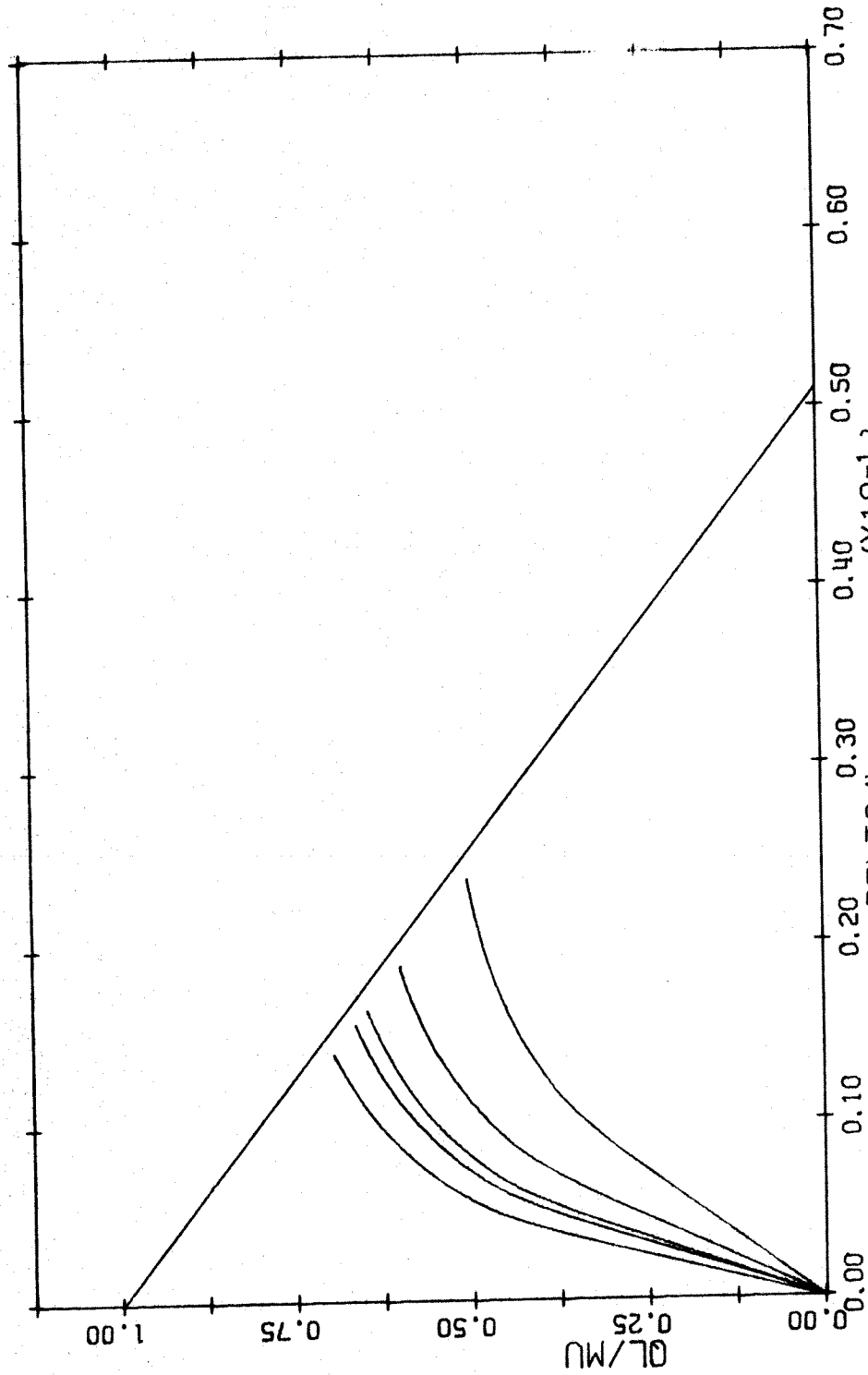

FIG. A-71 LOAD DEFLECTION DIAGRAM. TIED COLUMN. BARS IN 4 FACES
L/H=20 P/P0=0.3

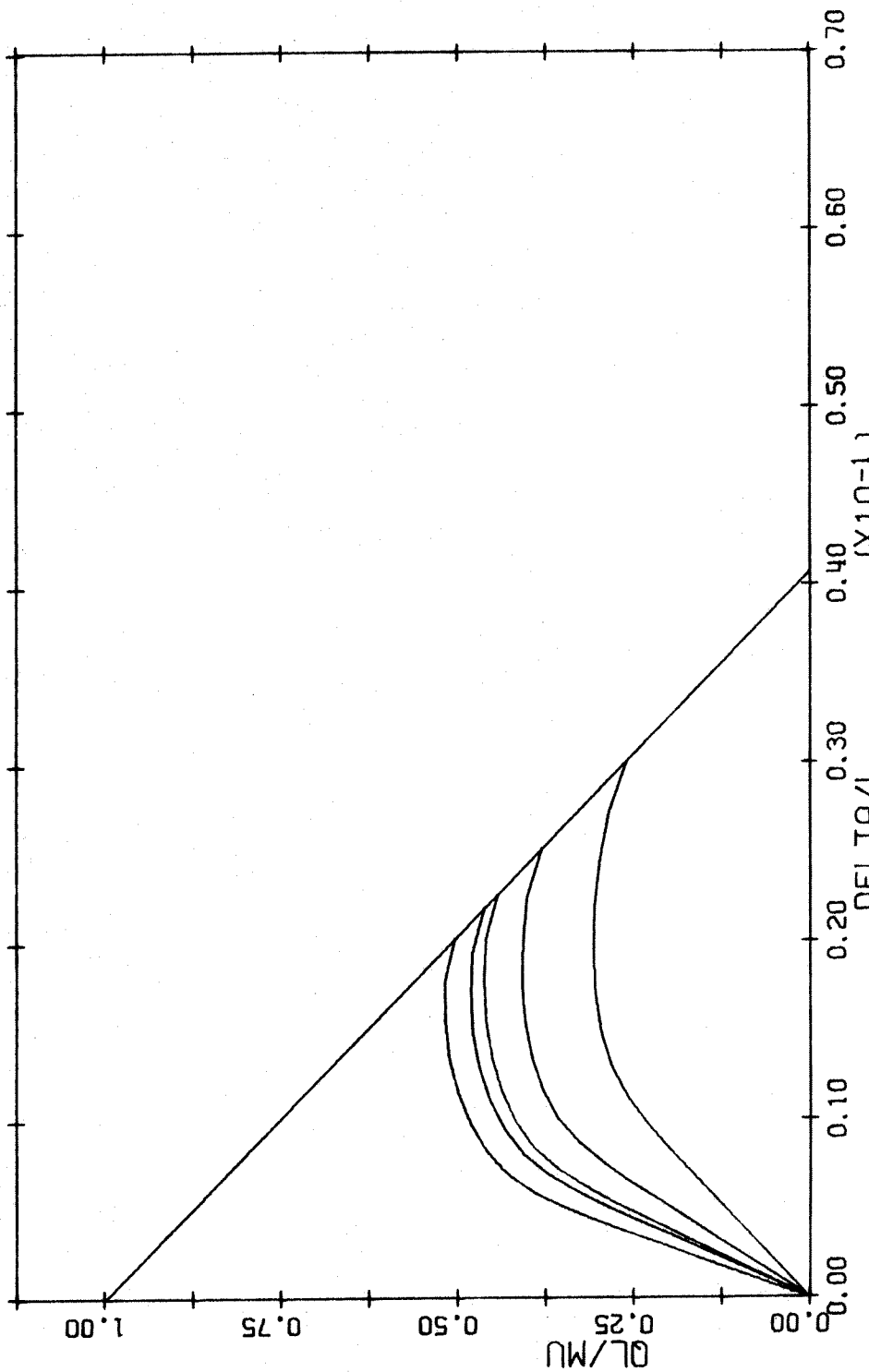

FIG. A-72 LOAD DEFLECTION DIAGRAM. TIED COLUMN. BARS IN 4 FACES
L/H=25 P/P0=0.3

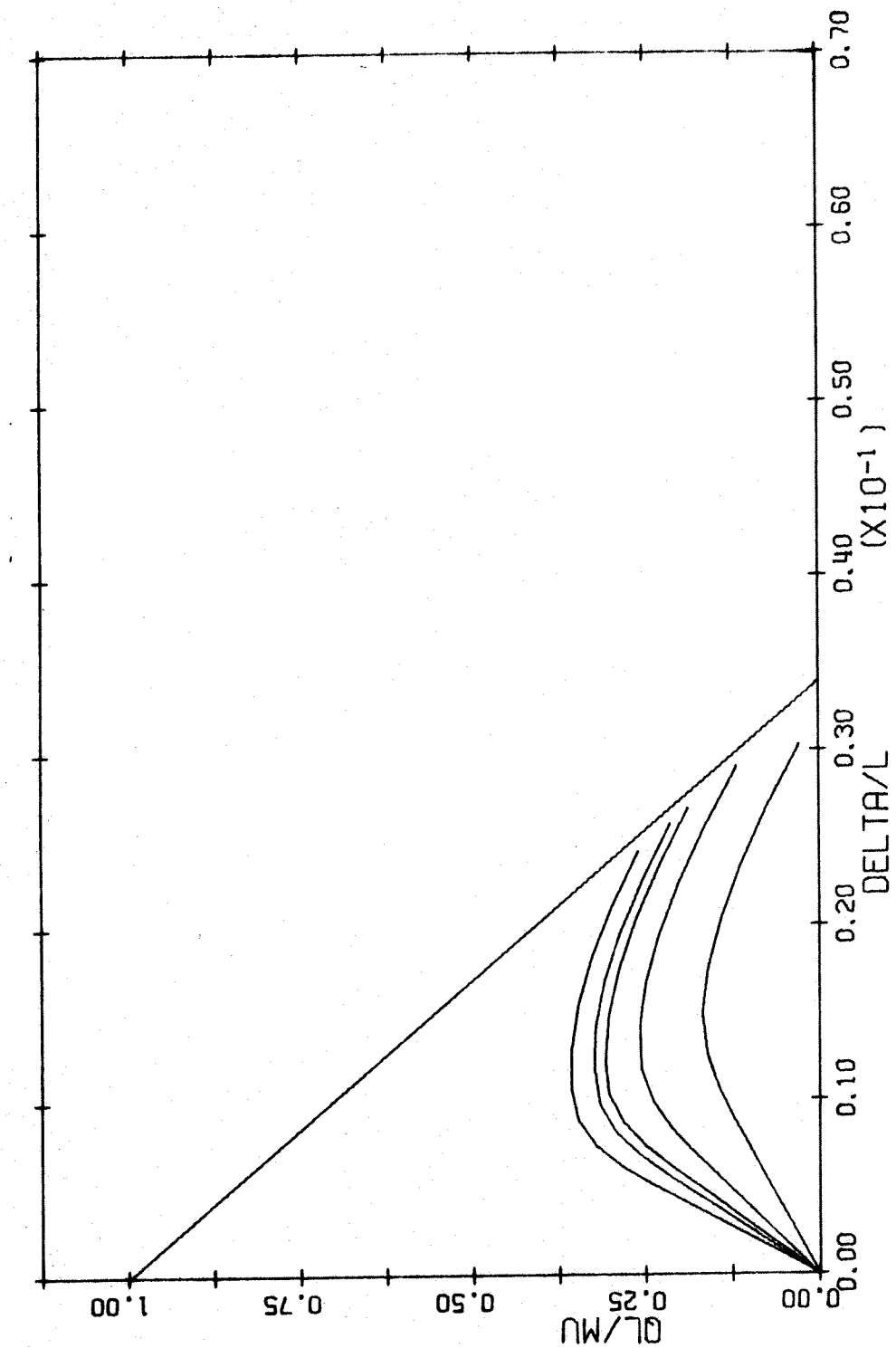

FIG. A-73 LOAD DEFLECTION DIAGRAM. TIED COLUMN. BARS IN 4 FACES
L/H=30 P/P0=0.3

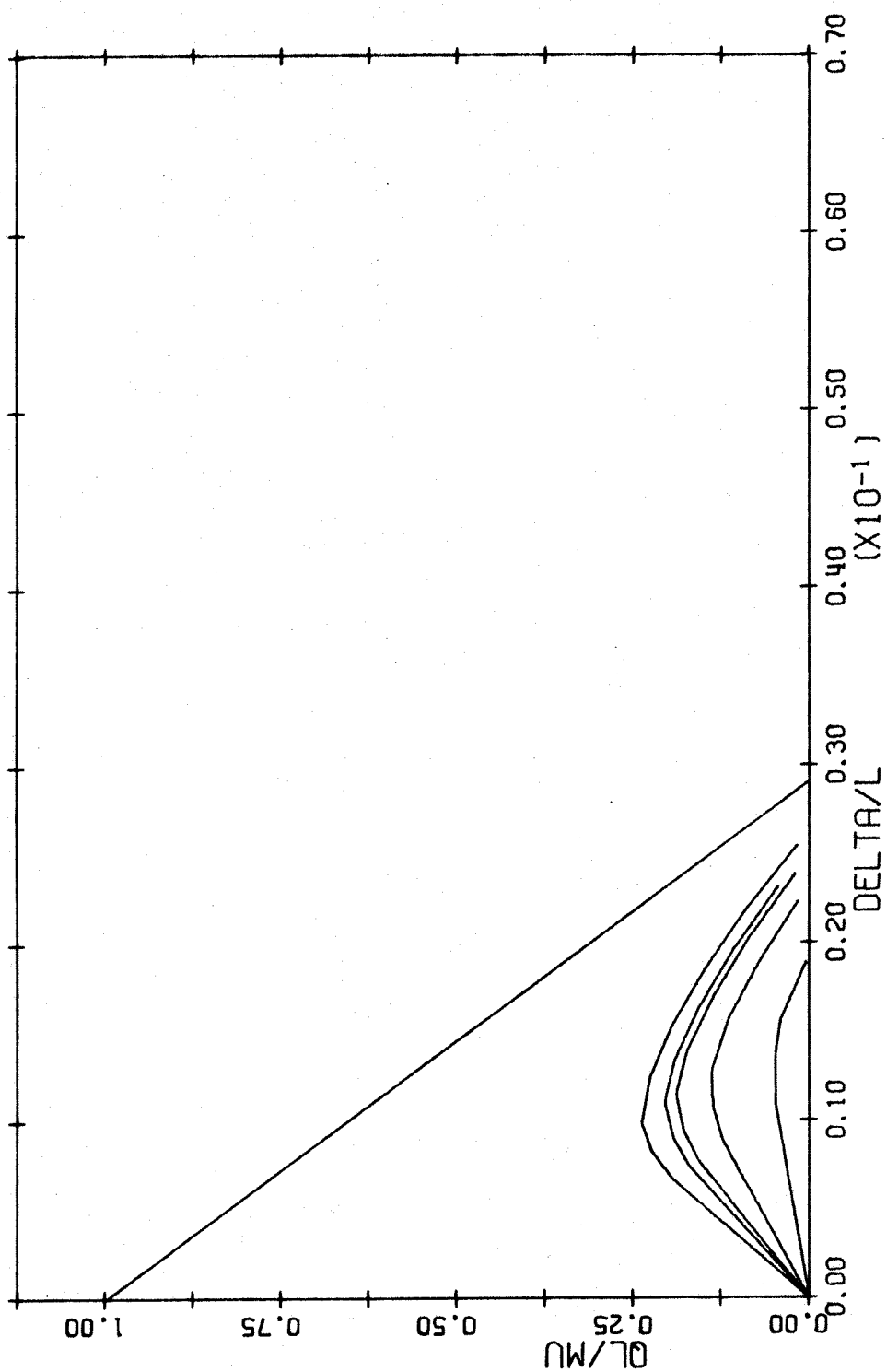

FIG. A-74 LOAD DEFLECTION DIAGRAM. TIED COLUMN. BARS IN 4 FACES
L/H=35 P/PO=0.3

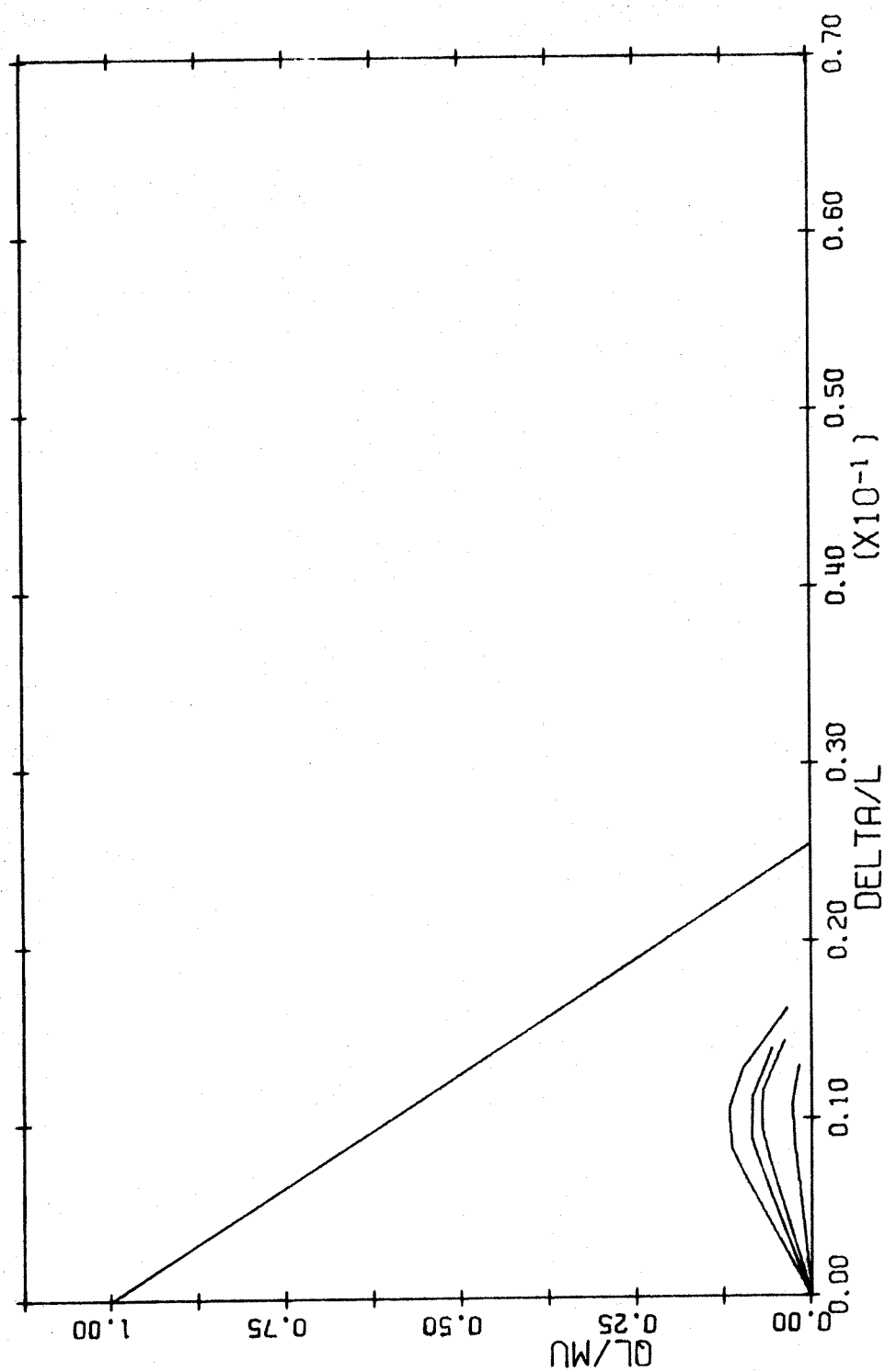

FIG. A-75 LOAD DEFLECTION DIAGRAM. TIED COLUMN. BARS IN 4 FACES
L/H=40 P/P0=0.3

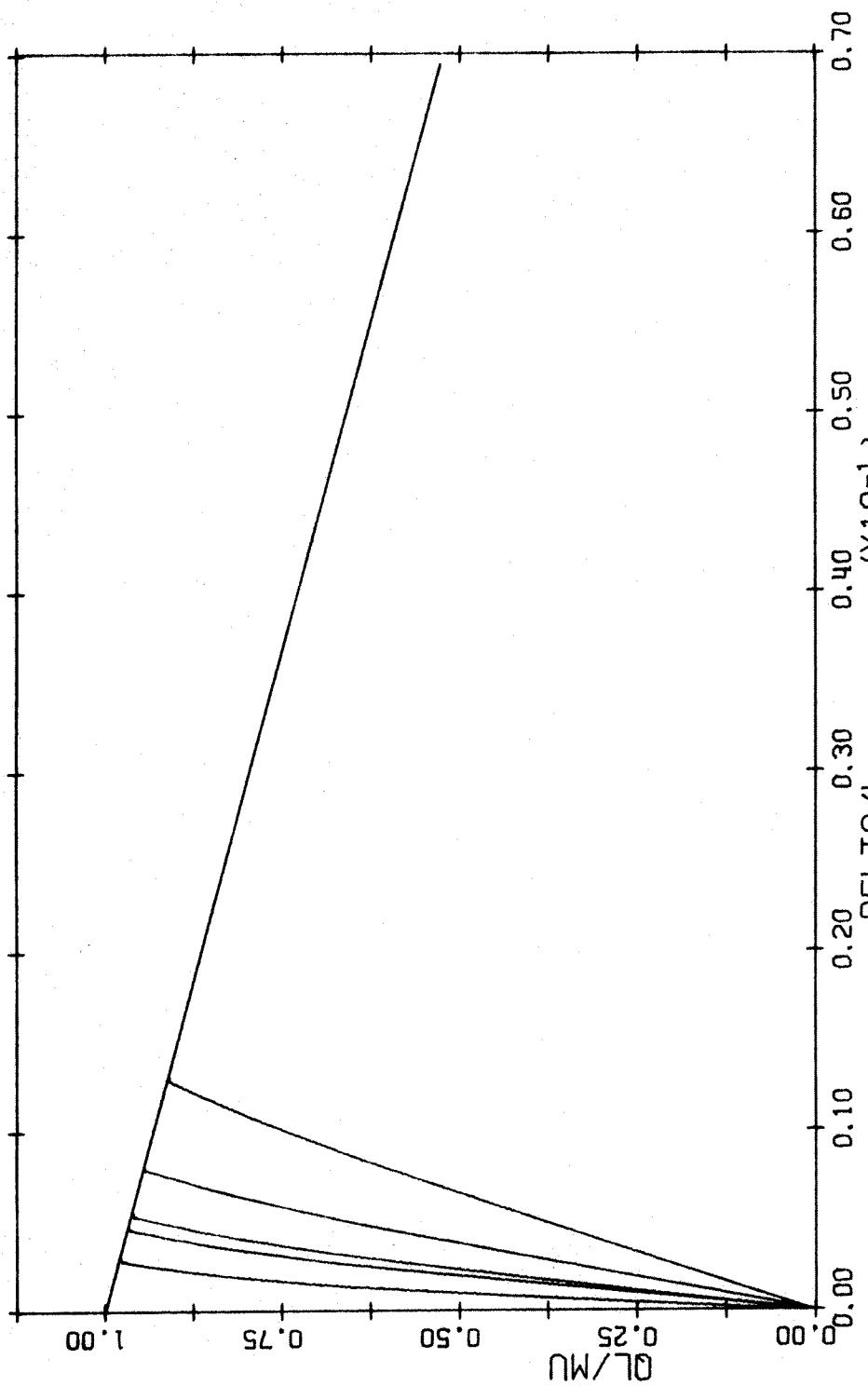

FIG. A-76 LOAD DEFLECTION DIAGRAM. TIED COLUMN. BARS IN 4 FACES
L/H=5 P/PO=0.4

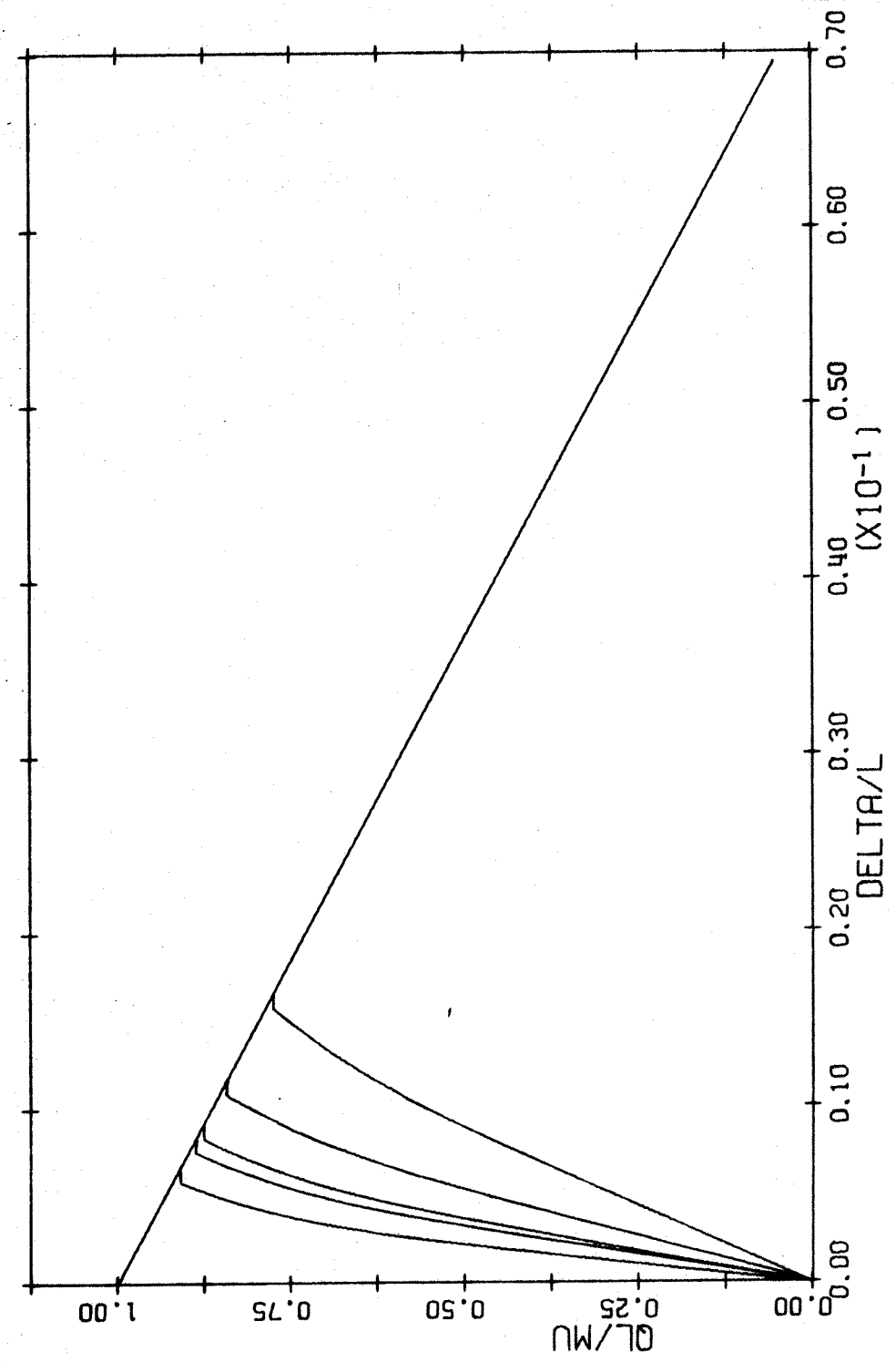

FIG. A-77 LOAD DEFLECTION DIAGRAM. TIED COLUMN. BARS IN 4 FACES
L/H=10 P/P0=0.4

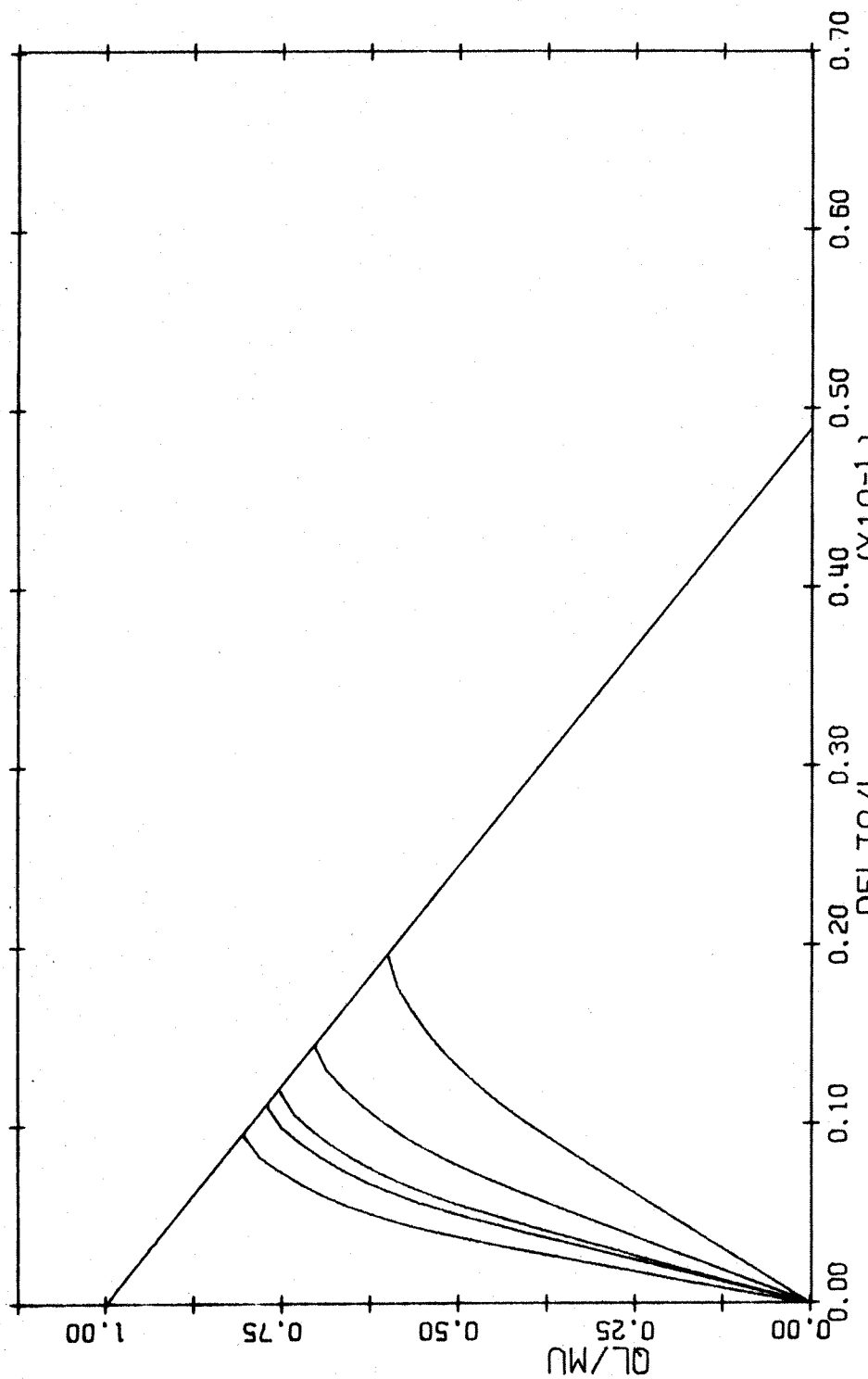

FIG. A-78 LOAD DEFLECTION DIAGRAM. TIED COLUMN. BARS IN 4 FACES
L/H=15 P/P0=0.4

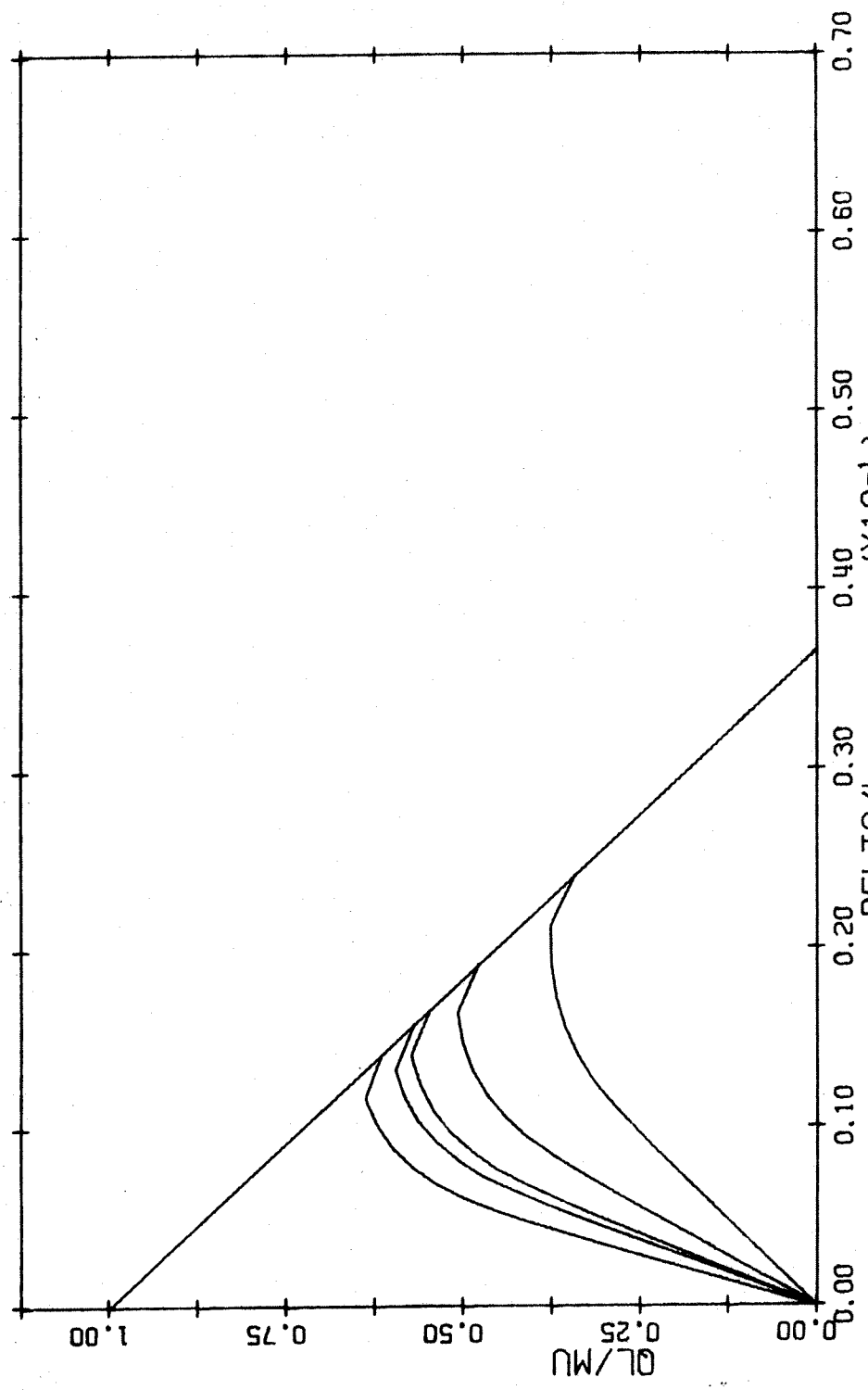

FIG. A-79 LOAD DEFLECTION DIAGRAM. TIED COLUMN. BARS IN 4 FACES
L/H=20 P/P0=0.4

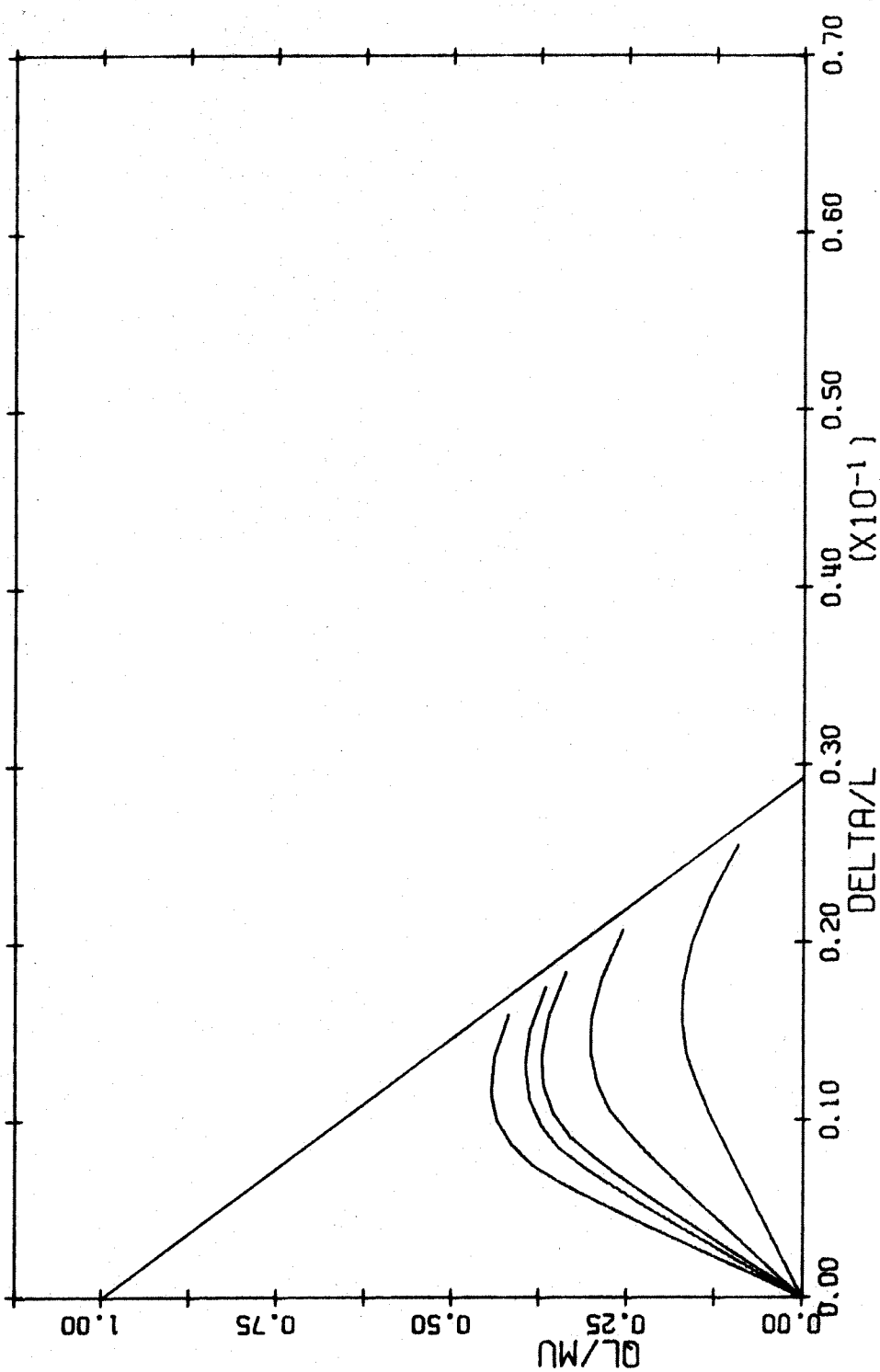

FIG. A-80 LOAD DEFLECTION DIAGRAM. TIED COLUMN. BARS IN 4 FACES
L/H=25 P/PO=0.4

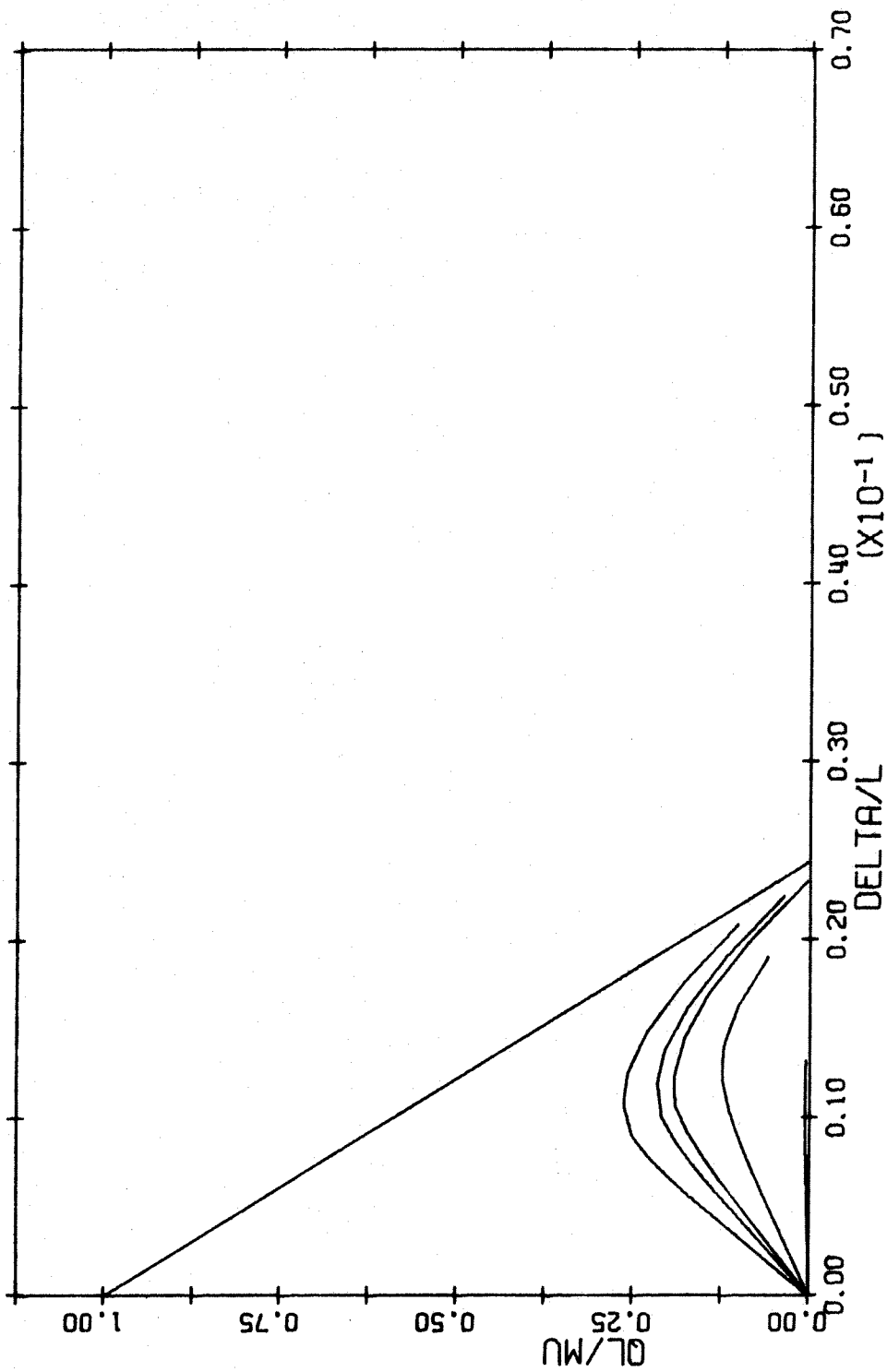

FIG. A-81 LOAD DEFLECTION DIAGRAM. TIED COLUMN. BARS IN 4 FACES
L/H=30 P/PO=0.4

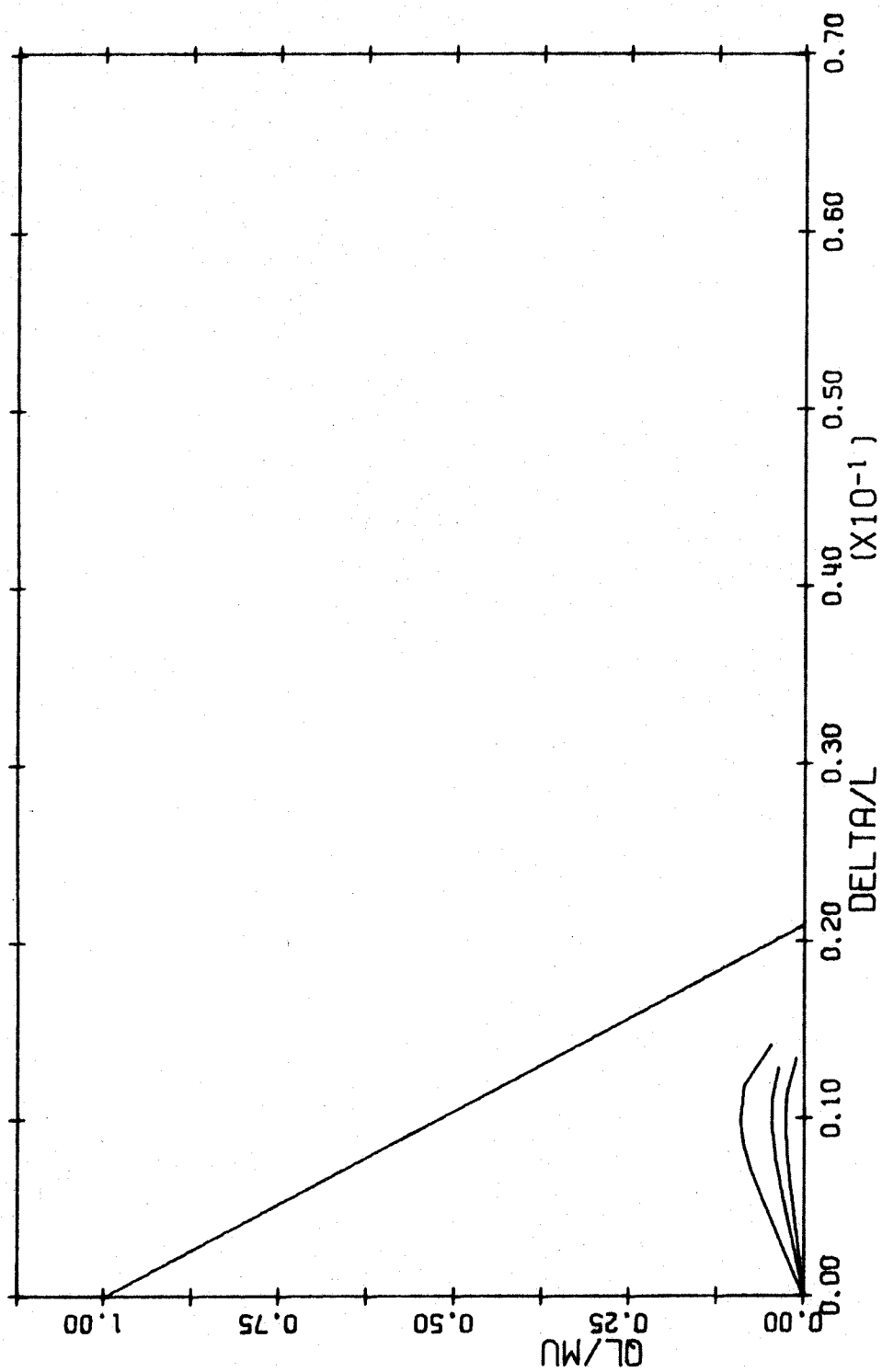

FIG. A-82 LOAD DEFLECTION DIAGRAM. TIED COLUMN. BARS IN 4 FACES
L/H=35 P/P0=0.4

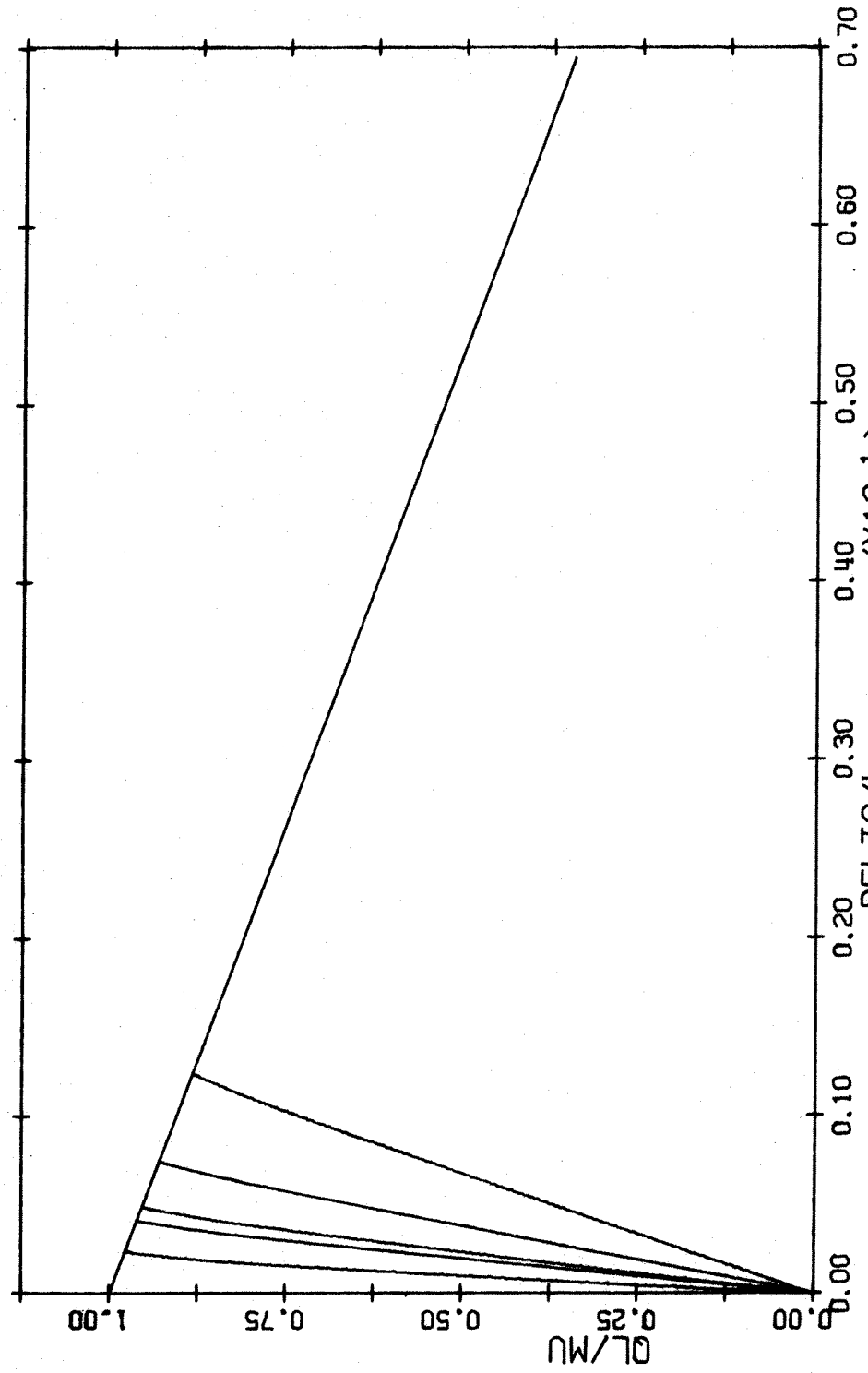

FIG. A-83 LOAD DEFLECTION DIAGRAM. TIED COLUMN. BARS IN 4 FACES
L/H=5 P/P0=0.5

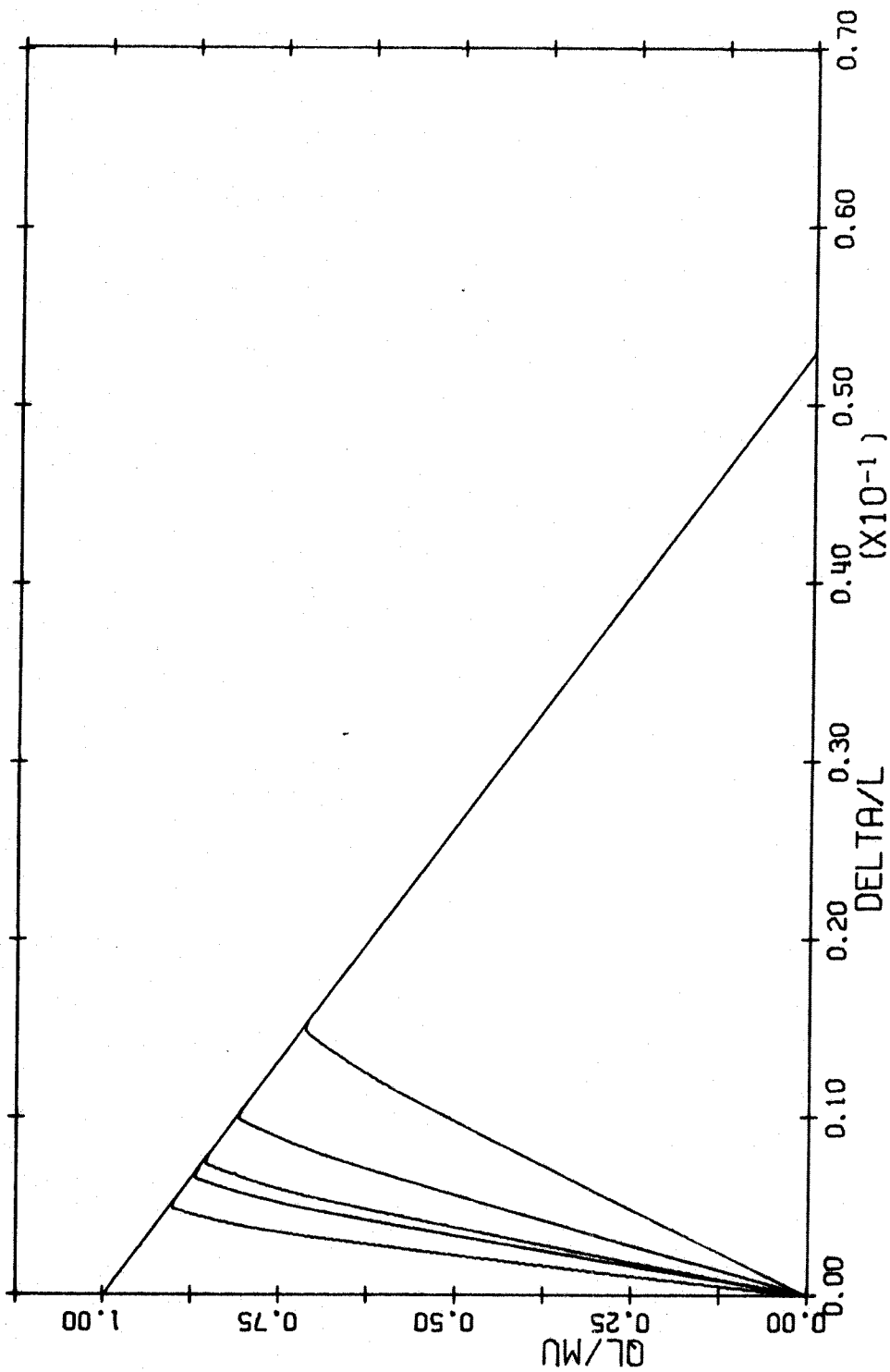

FIG. A-84 LOAD DEFLECTION DIAGRAM. TIED COLUMN. BARS IN 4 FACES
L/H=10 P/PO=0.5

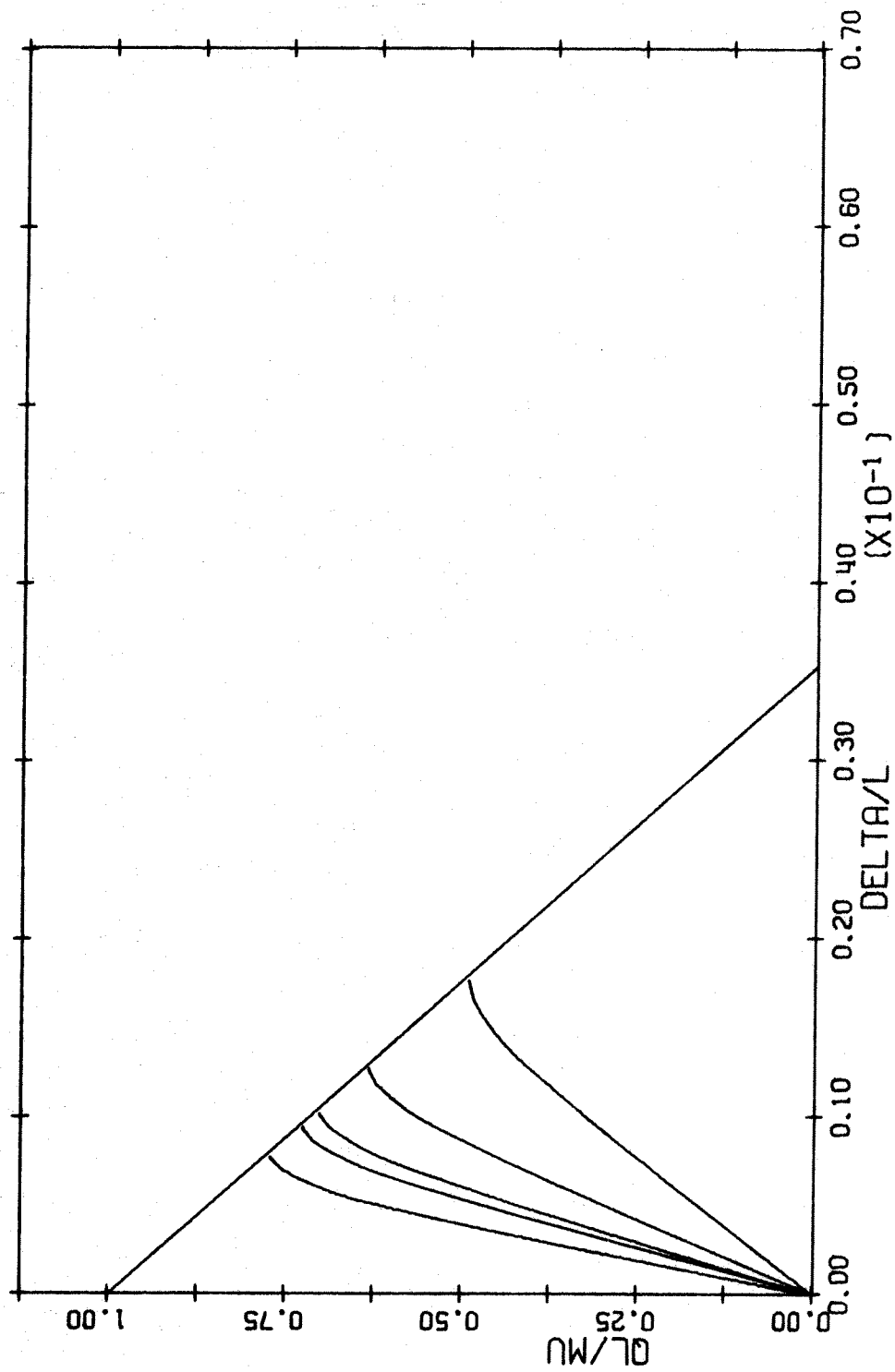

FIG. A-86 LOAD DEFLECTION DIAGRAM. TIED COLUMN. BARS IN 4 FACES
L/H=20 P/P0=0.5

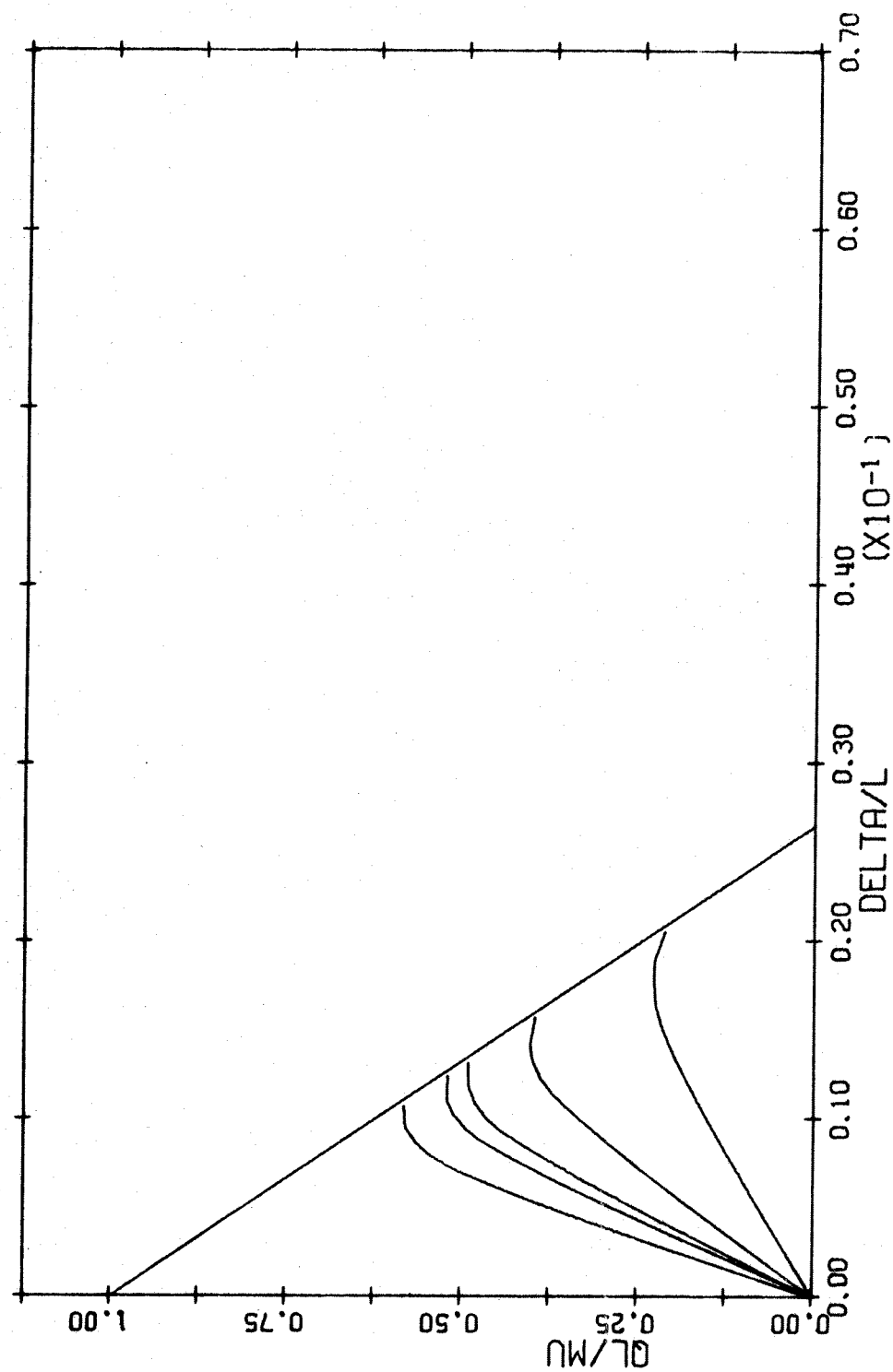

FIG. A-85 LOAD DEFLECTION DIAGRAM. TIED COLUMN. BARS IN 4 FACES
L/H=15 P/P0=0.5

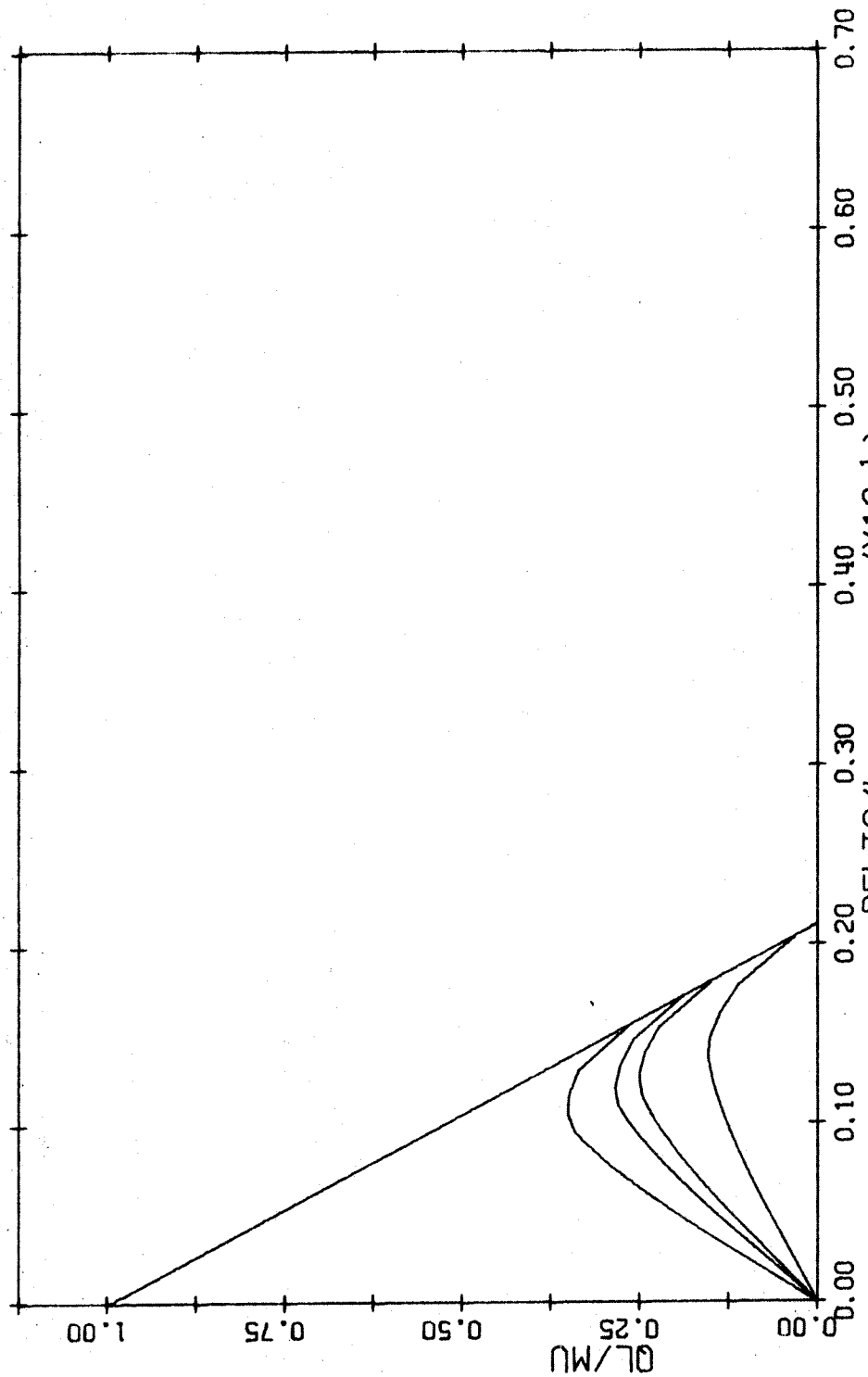

FIG. A-87 LOAD DEFLECTION DIAGRAM. TIED COLUMN. BARS IN 4 FACES
L/H=25 P/P0=0.5

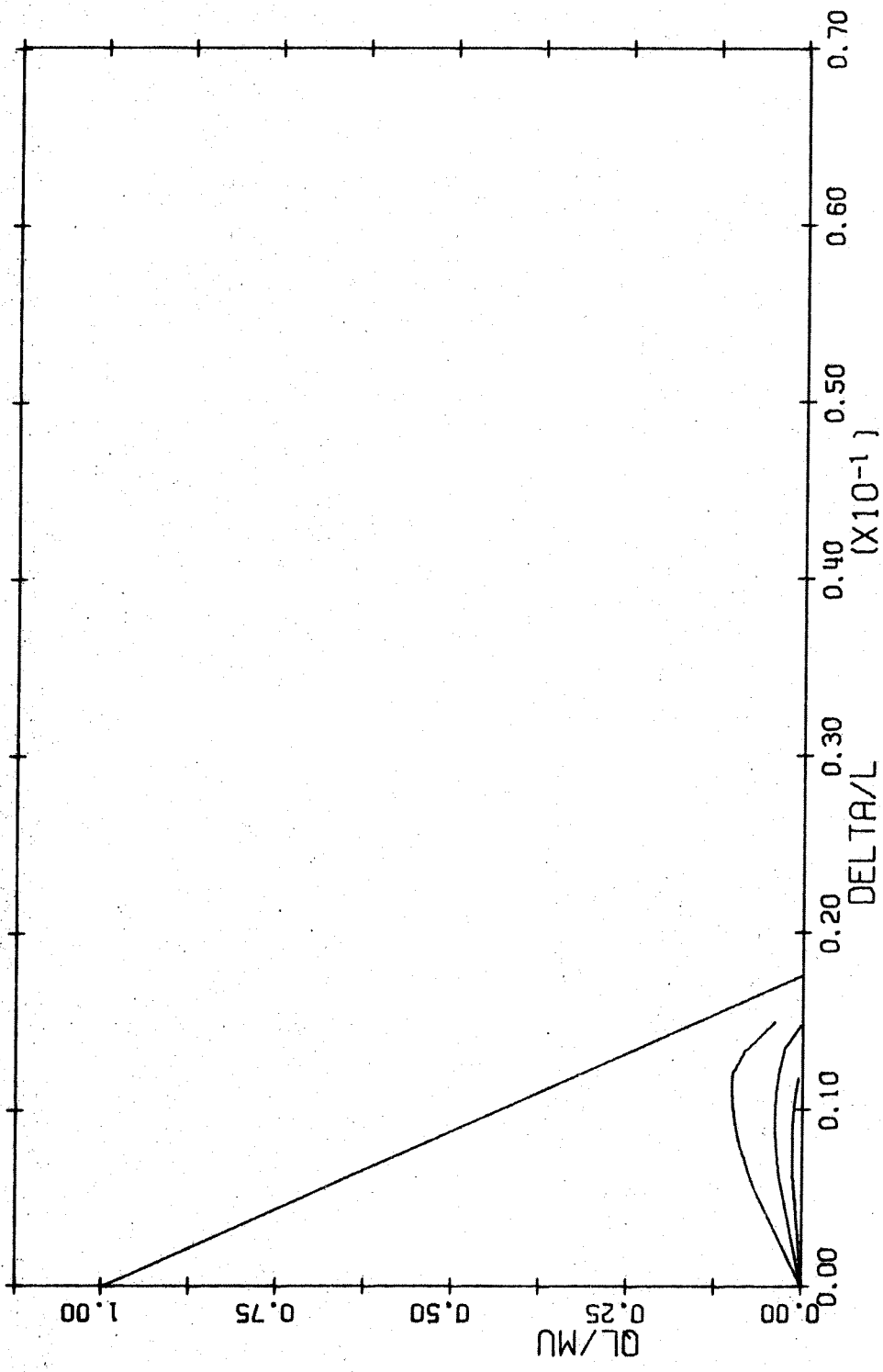

FIG. A-88 LOAD DEFLECTION DIAGRAM. TIED COLUMN. BARS IN 4 FACES
L/H=30 P/P0=0.5

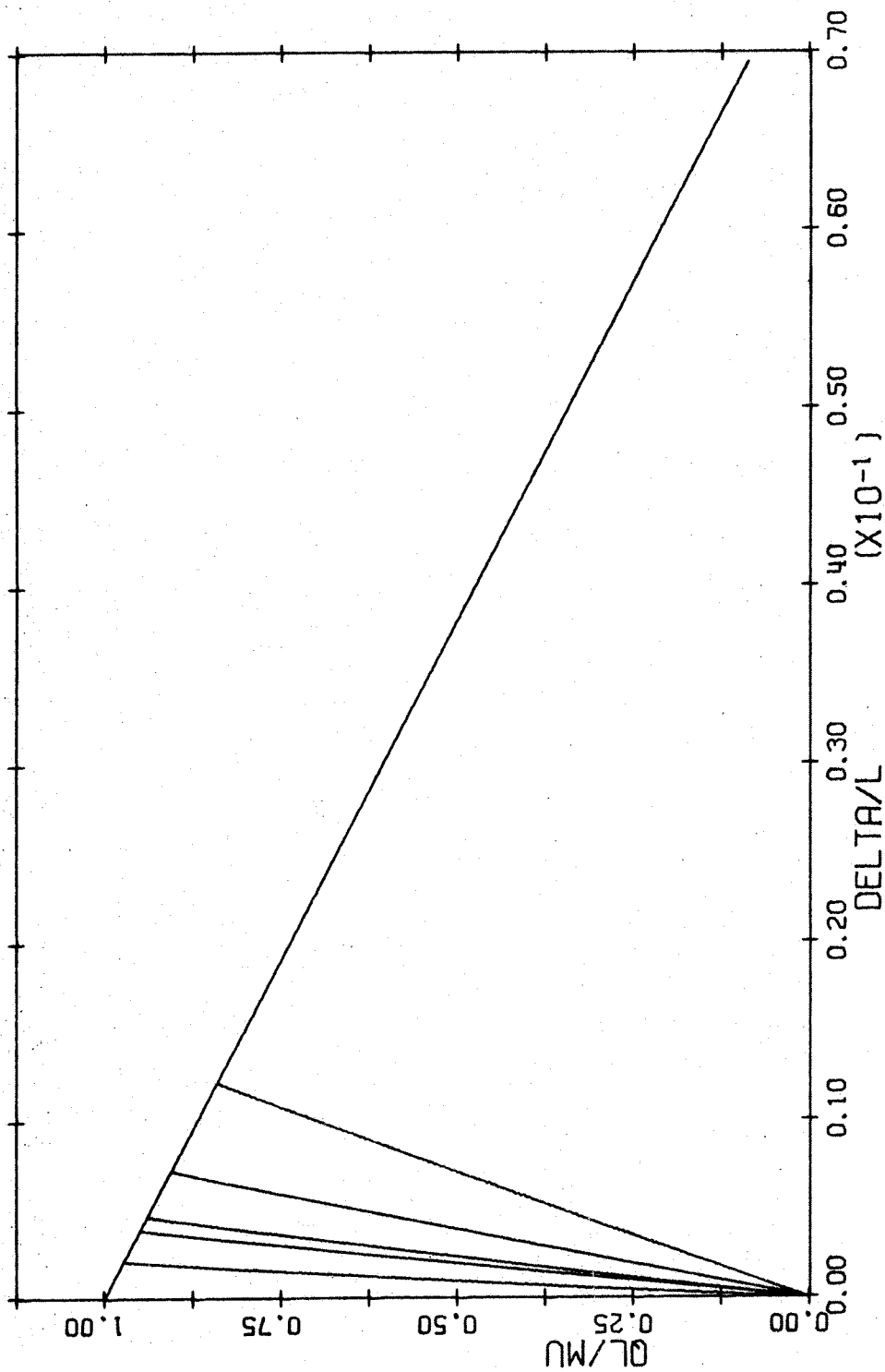

FIG. A-89 LOAD DEFLECTION DIAGRAM. TIED COLUMN. BARS IN 4 FACES
L/H=5 P/P0=0.6

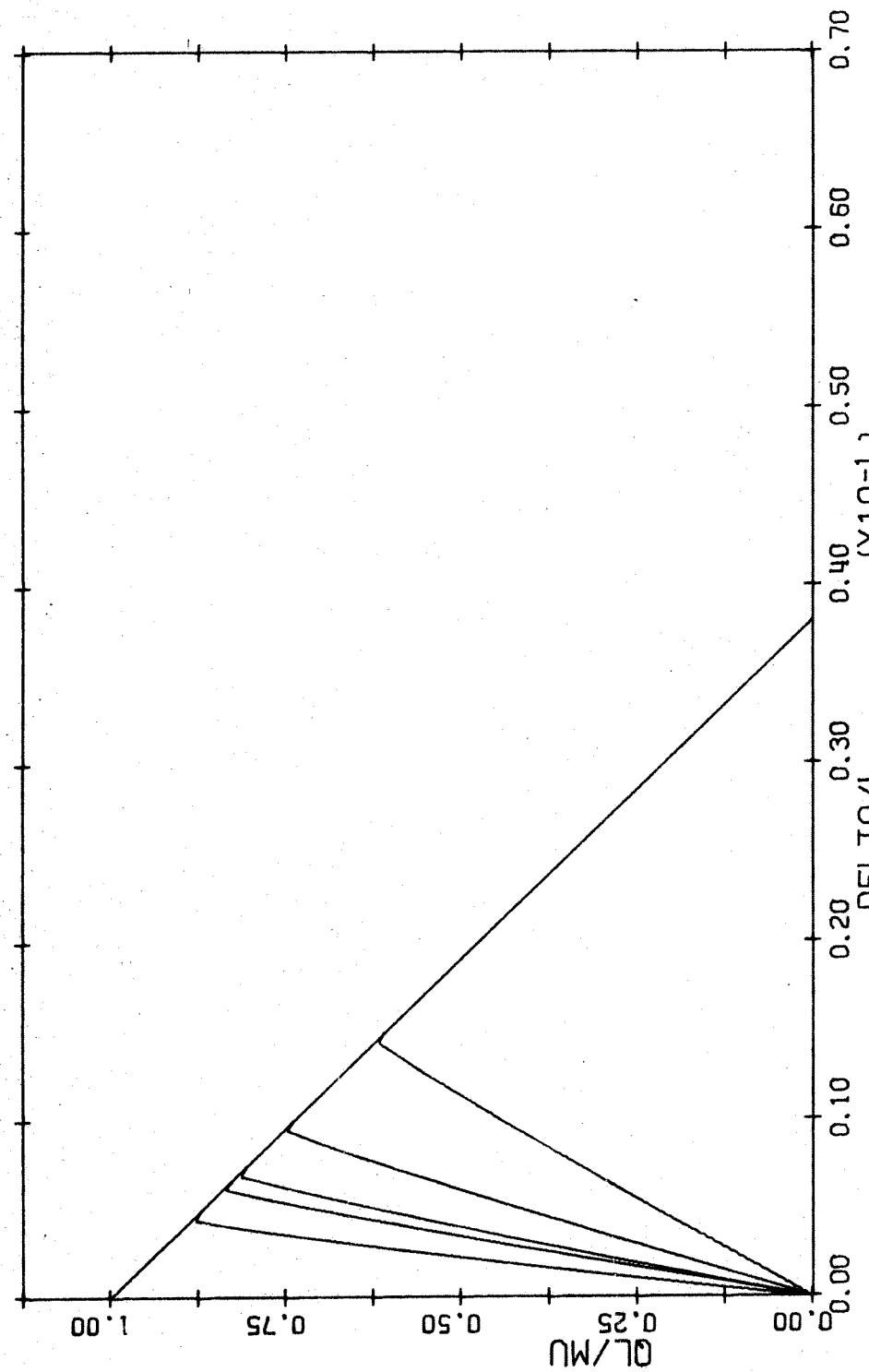

FIG. A-90 LOAD DEFLECTION DIAGRAM. TIED COLUMN. BARS IN 4 FACES
L/H=10 P/P0=0.6

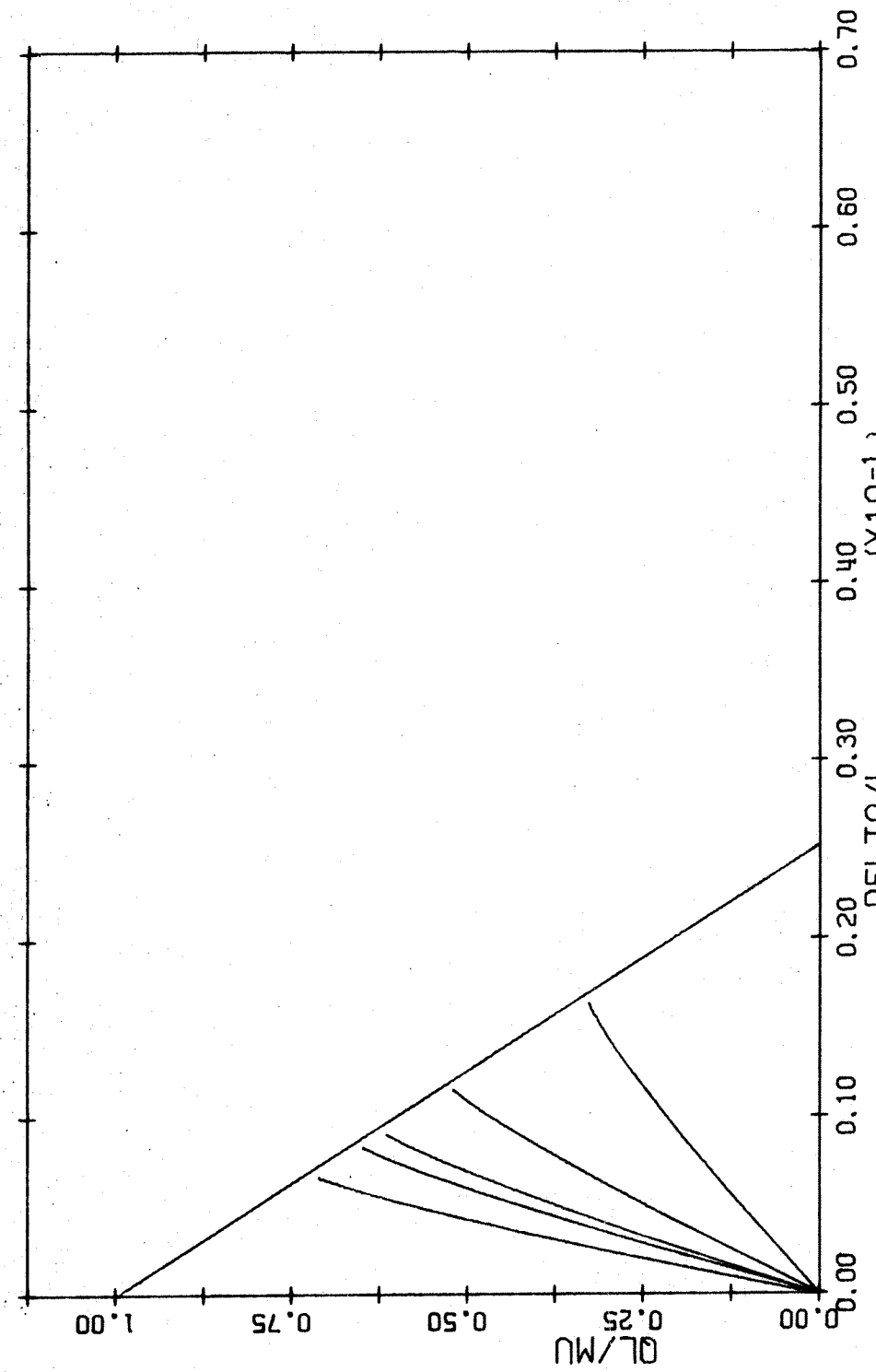

FIG. A-91 LOAD DEFLECTION DIAGRAM. TIED COLUMN. BARS IN 4 FACES
L/H=15 P/P0=0.5

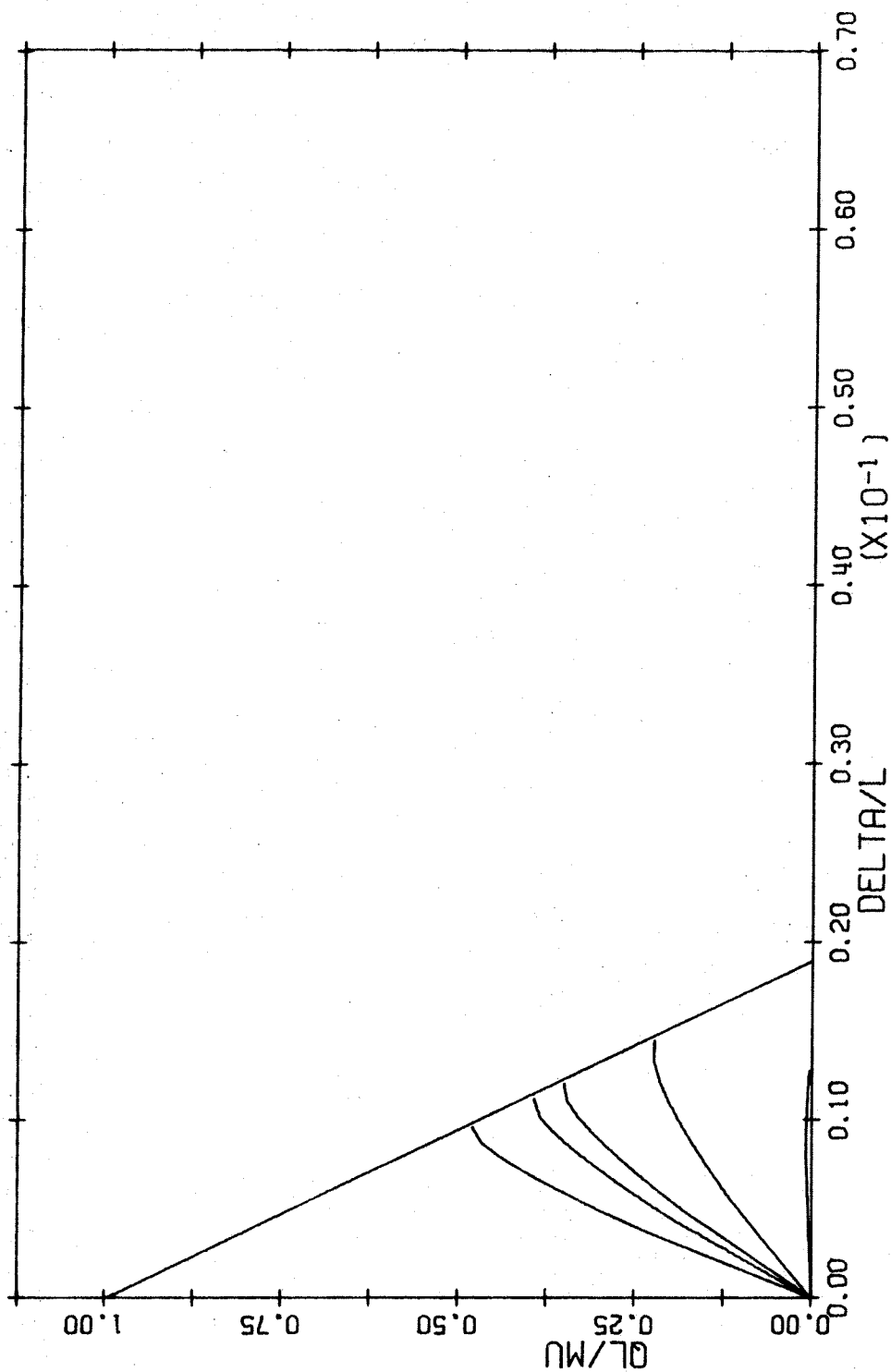

FIG. A-92 LOAD DEFLECTION DIAGRAM. TIED COLUMN. BARS IN 4 FACES
L/H=20 P/P0=0.6

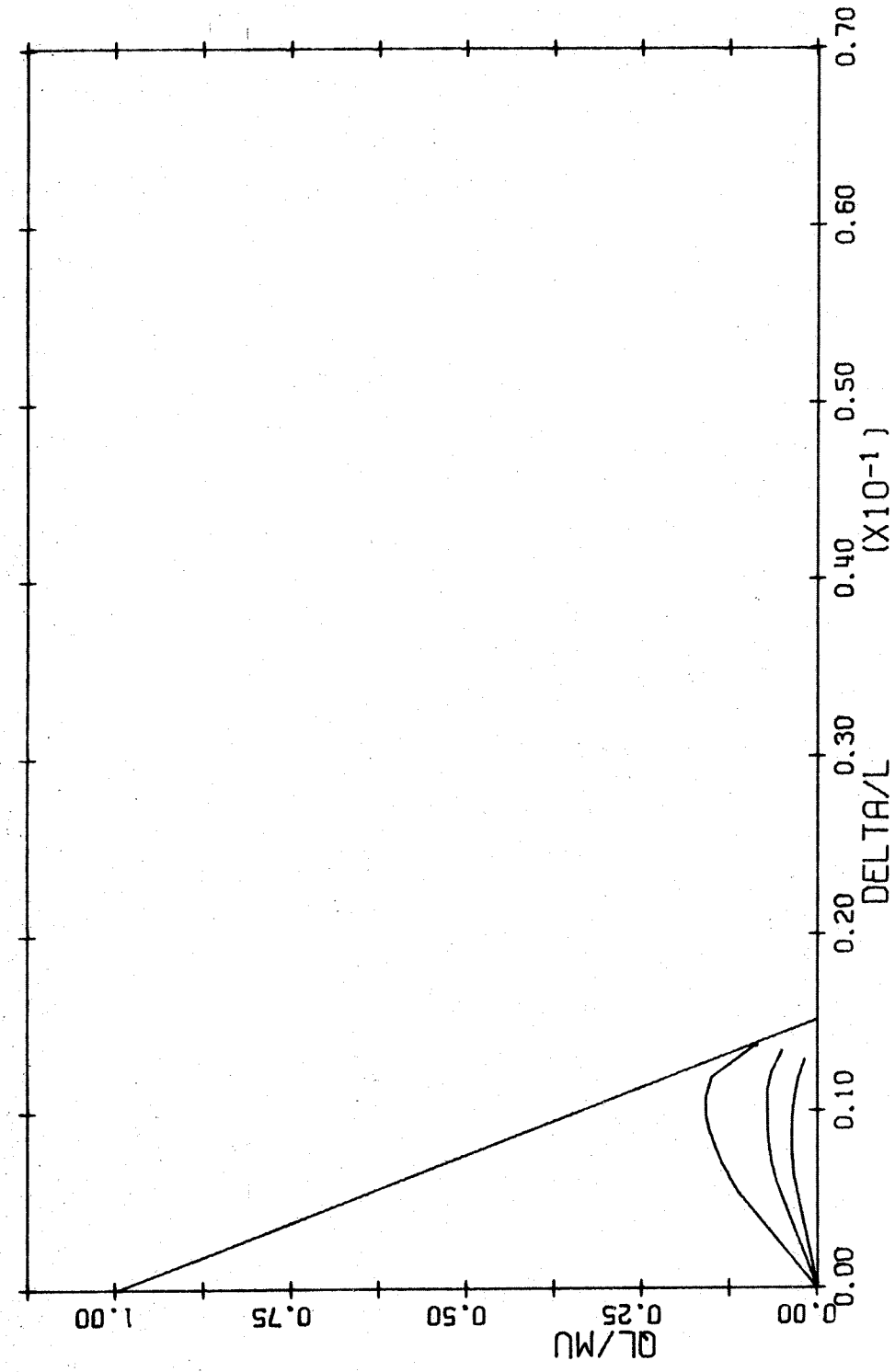

FIG. A-93 LOAD DEFLECTION DIAGRAM. TIED COLUMN. BARS IN 4 FACES
L/H=25 P/P0=0.6

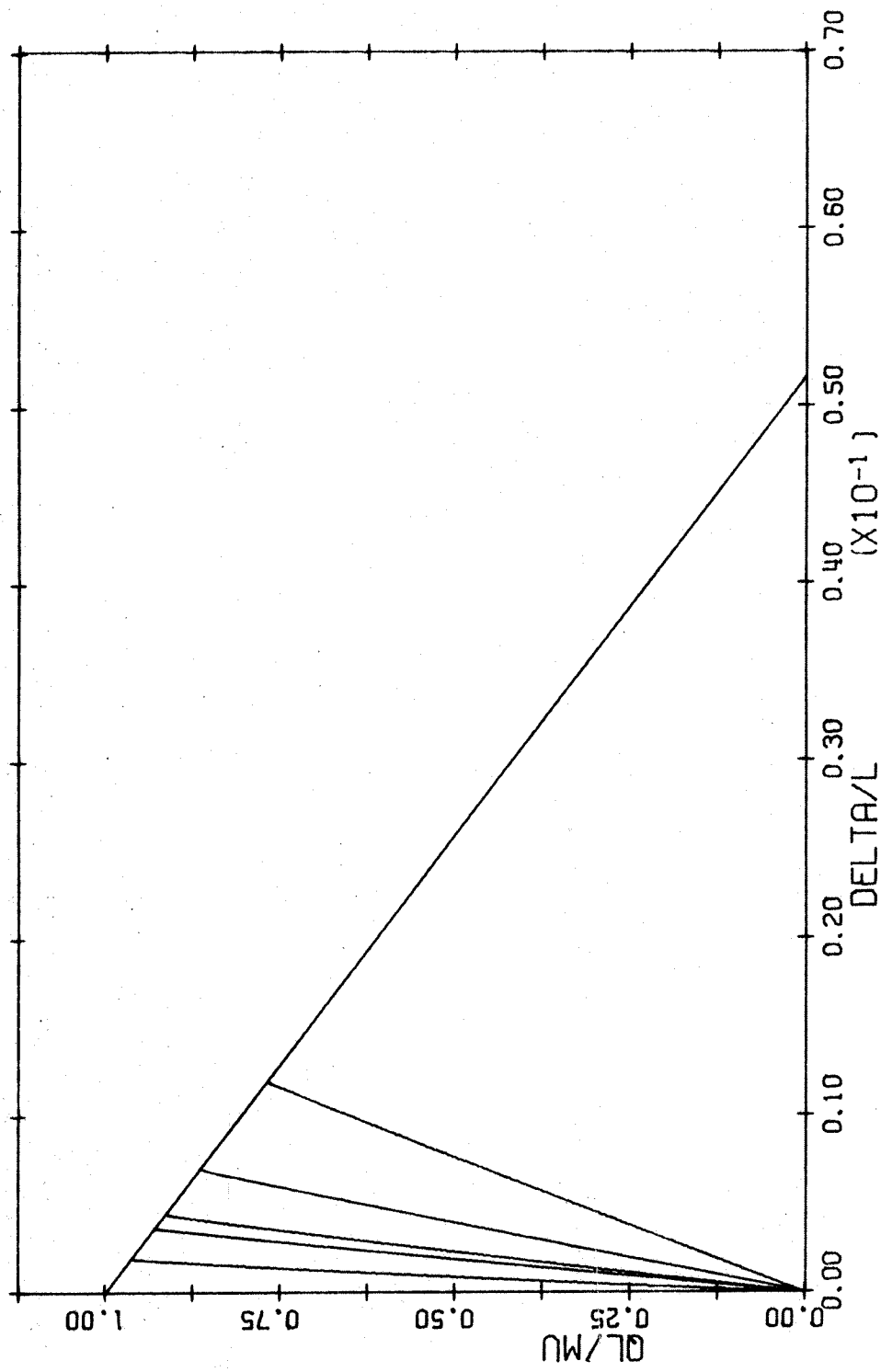

FIG. A-94 LOAD DEFLECTION DIAGRAM. TIED COLUMN. BARS IN 4 FACES
L/H=5 P/P0=0.7

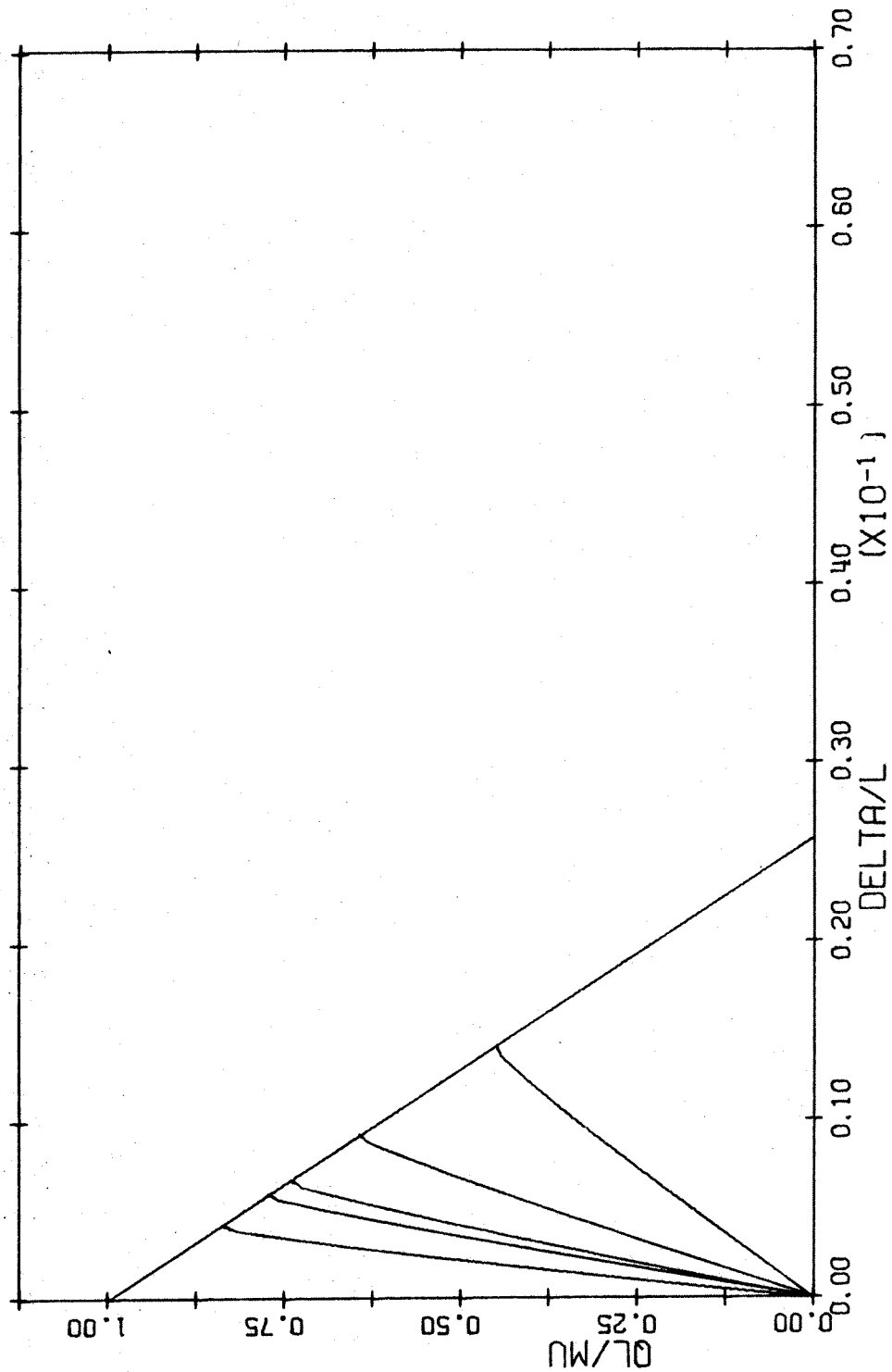

FIG. A-95 LOAD DEFLECTION DIAGRAM. TIED COLUMN. BARS IN 4 FACES
L/H=10 P/P0=0.7

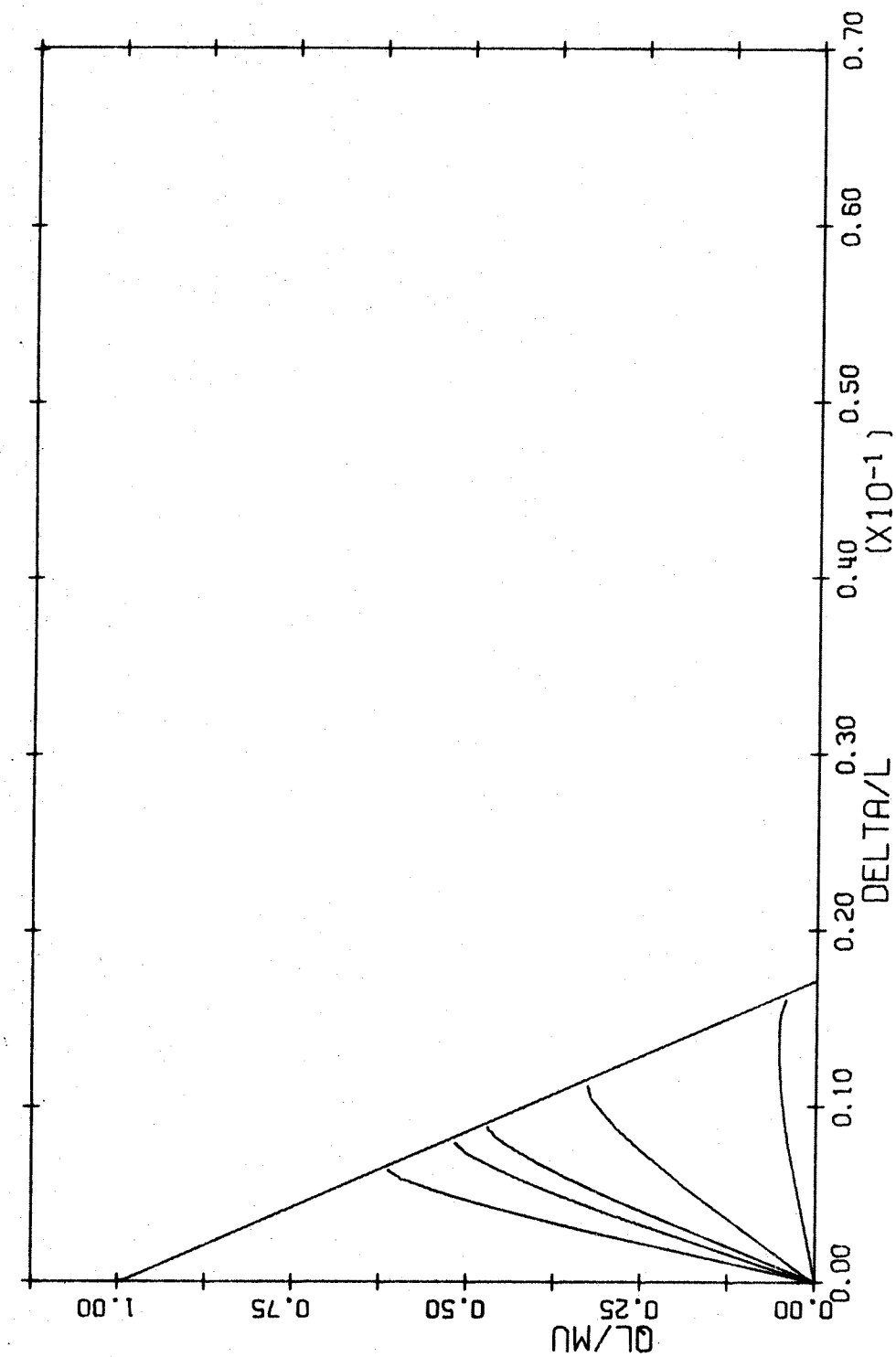

FIG. A-96 LOAD DEFLECTION DIAGRAM. TIED COLUMN. BARS IN 4 FACES
L/H=15 P/P0=0.7

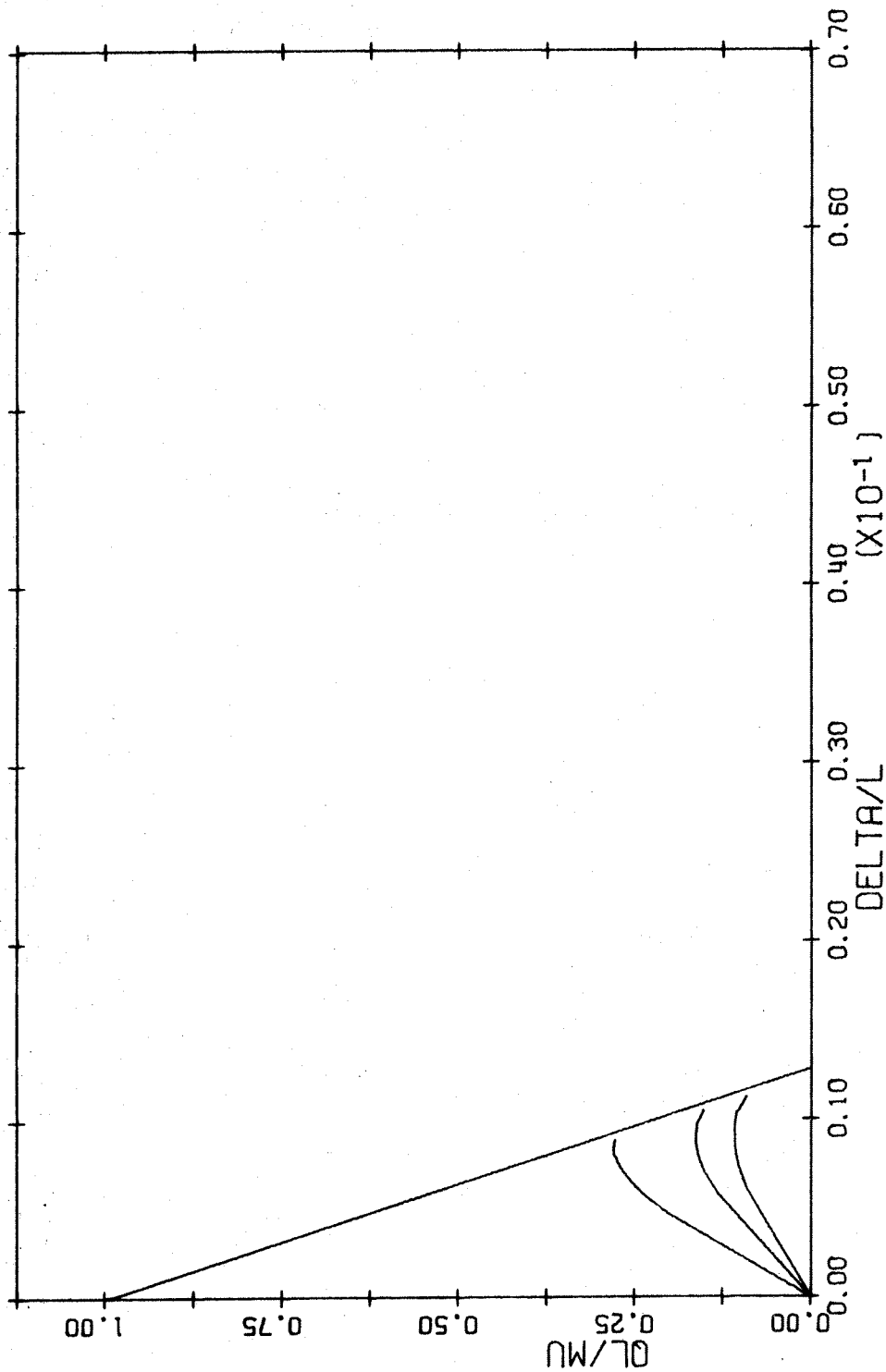

FIG. A-97 LOAD DEFLECTION DIAGRAM. TIED COLUMN. BARS IN 4 FACES
L/H=20 P/P0=0.7

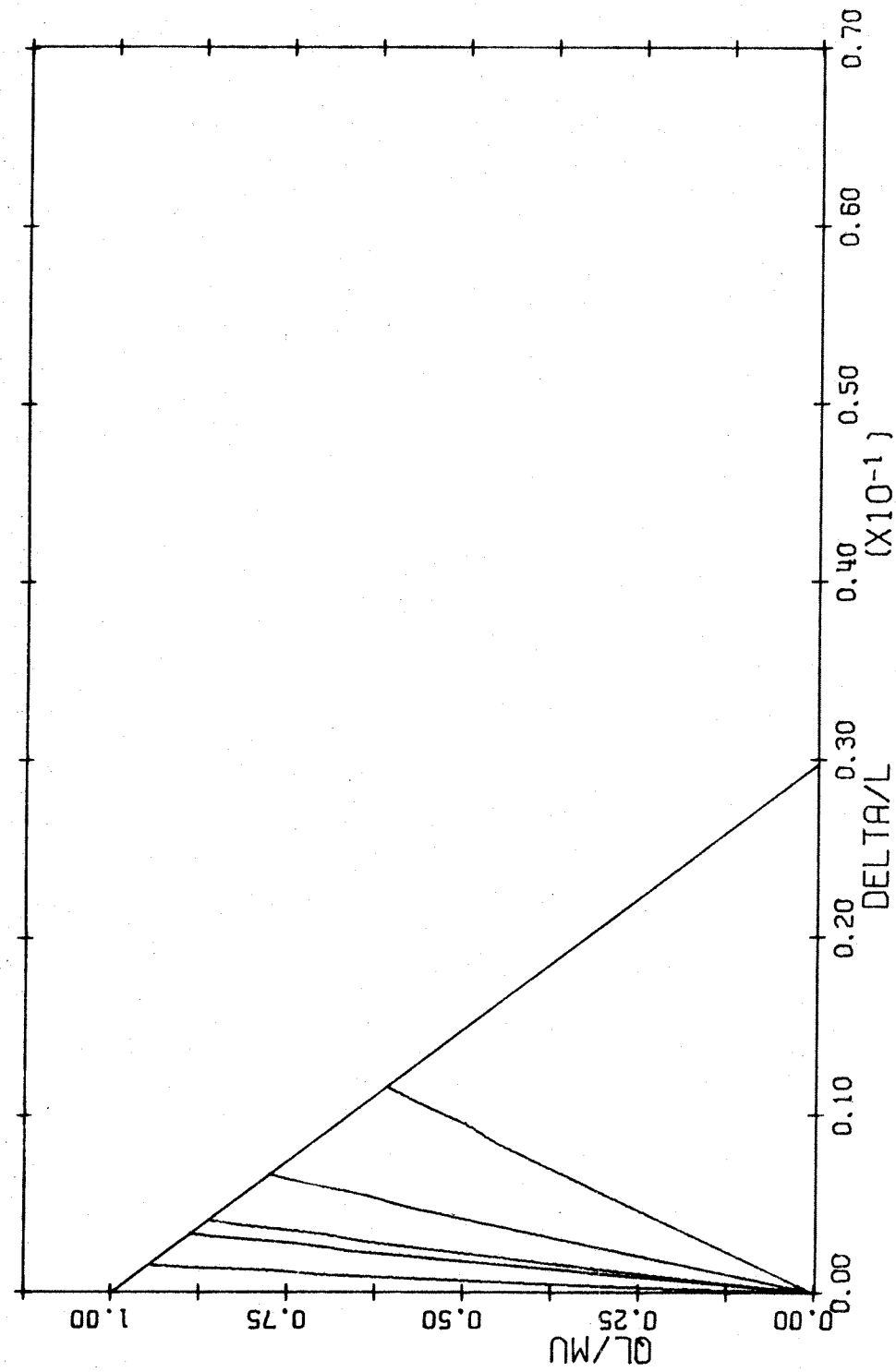

FIG. A-98 LOAD DEFLECTION DIAGRAM. TIED COLUMN. BARS IN 4 FACES
L/H=5 P/P0=0.8

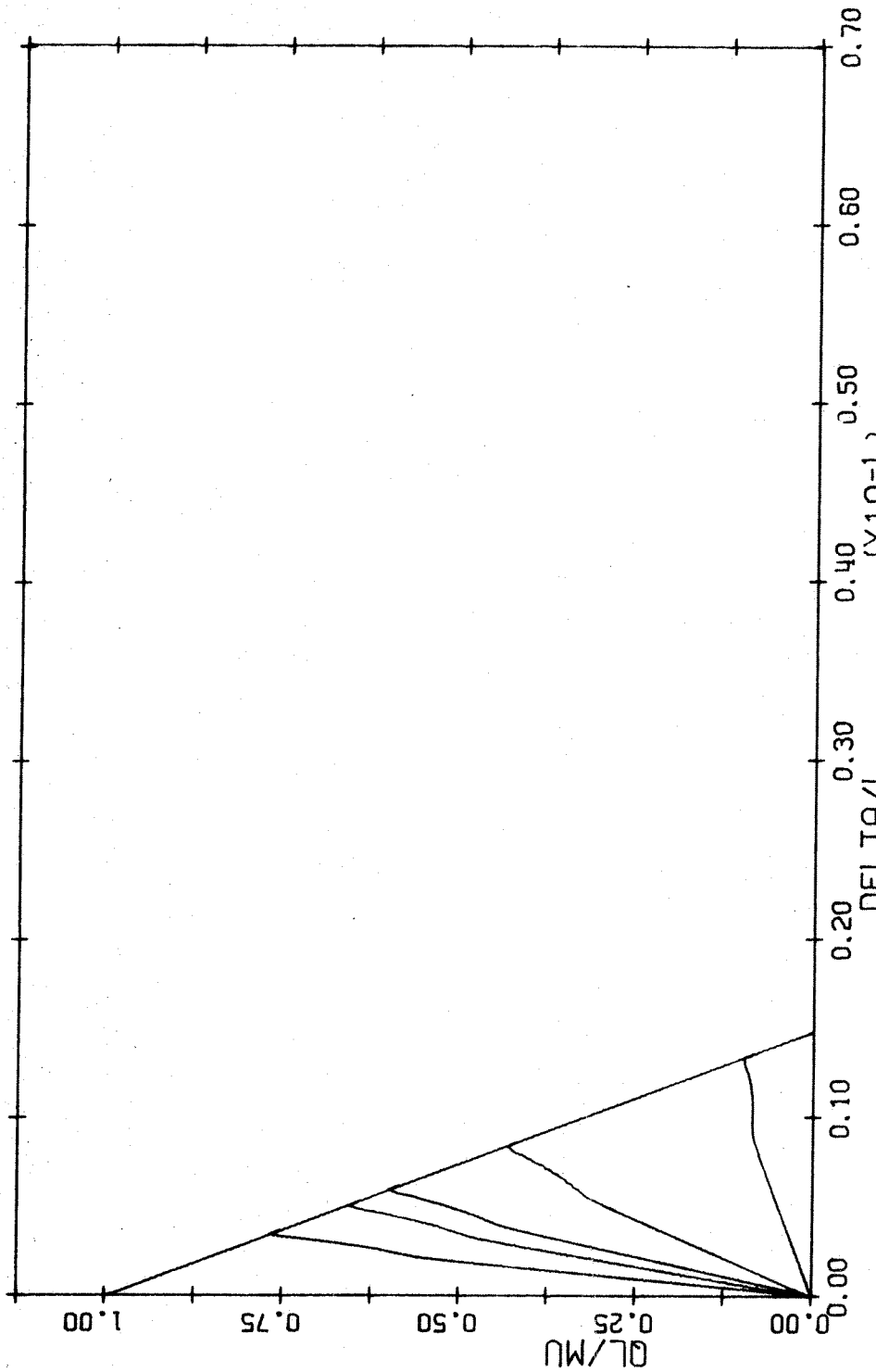

FIG. A-99 LOAD DEFLECTION DIAGRAM. TIED COLUMN. BARS IN 4 FACES
L/H=10 P/P0=0.8

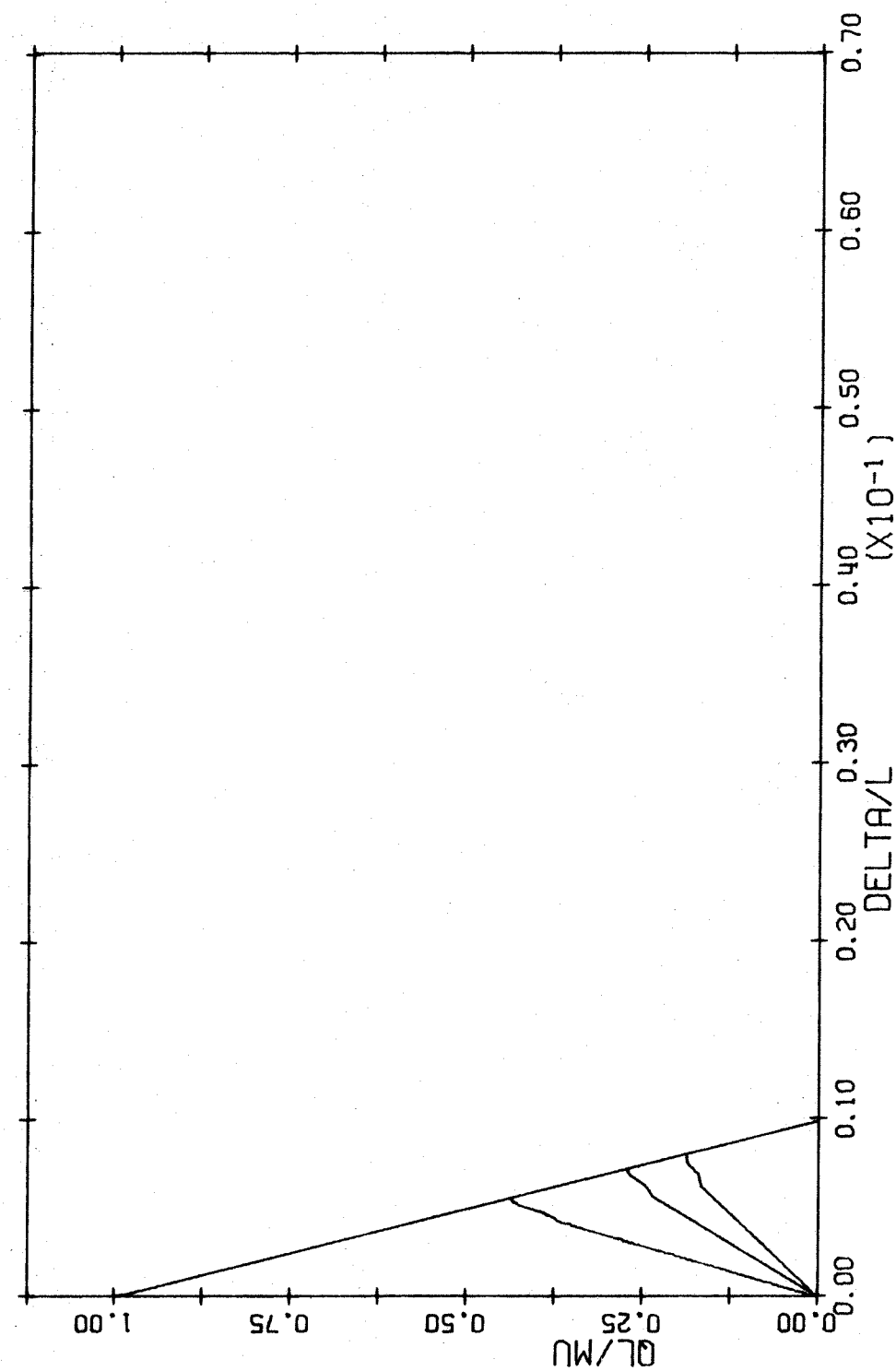

FIG. A-100 LOAD DEFLECTION DIAGRAM. TIED COLUMN. BARS IN 4 FACES
L/H=15 P/P0=0.8

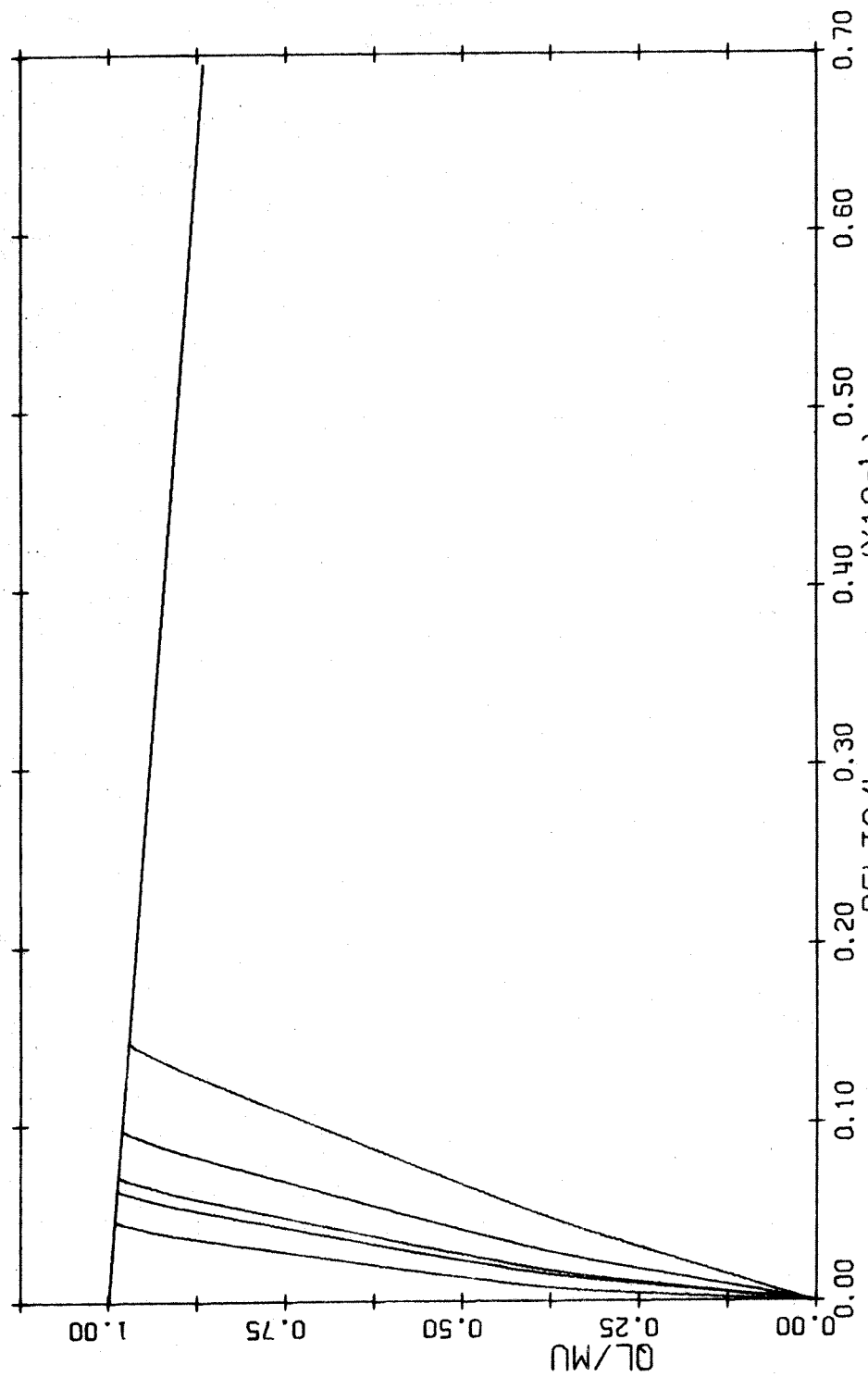

FIG. A-101 LOAD DEFLECTION DIAGRAM. SPIRAL COLUMN.
L/H=5 P/P0=0.1

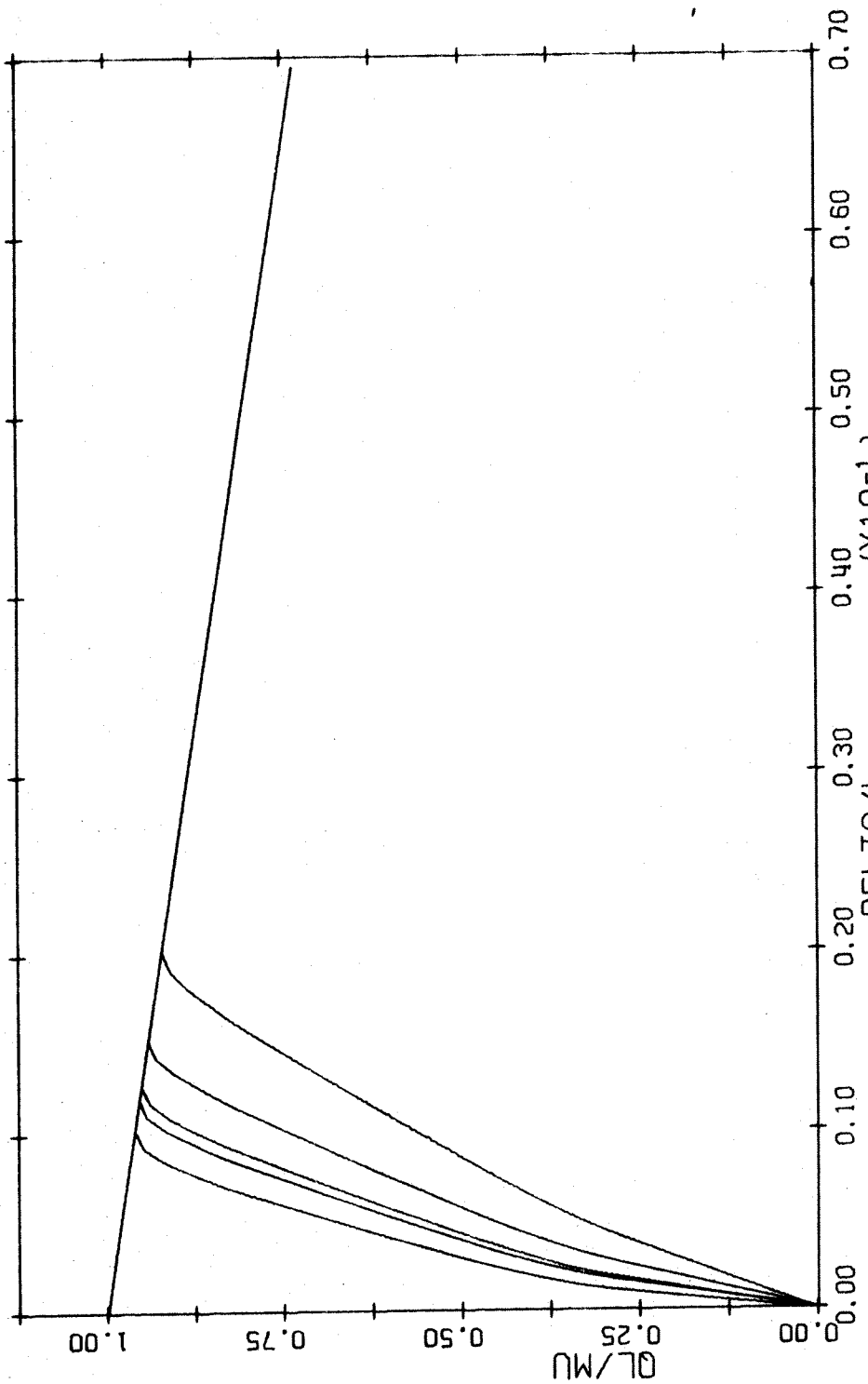

FIG. A-102 LOAD DEFLECTION DIAGRAM. SPIRAL COLUMN.
L/H=10 P/P0=0.1

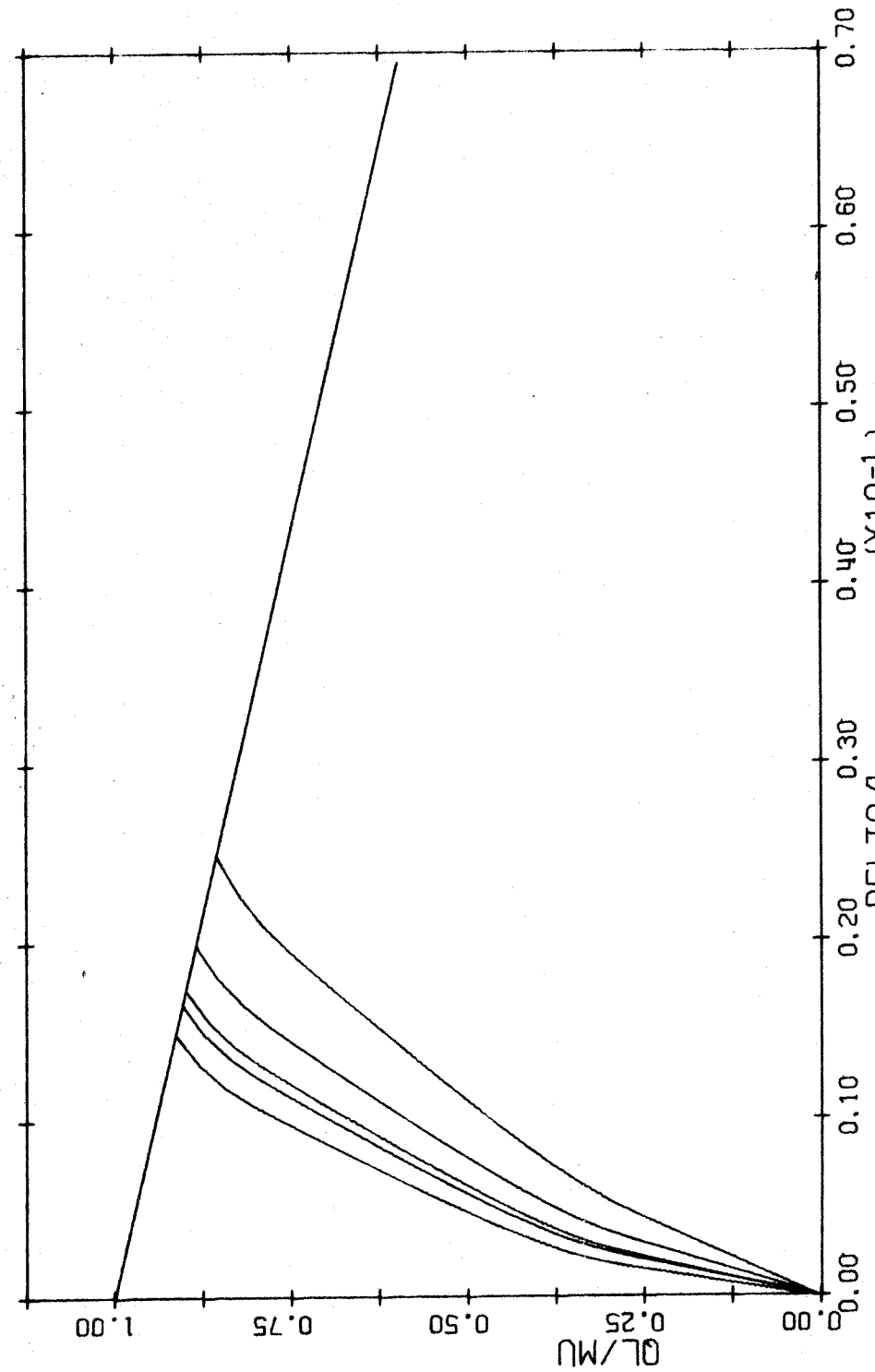

FIG. A-103 LOAD DEFLECTION DIAGRAM. SPIRAL COLUMN.
L/H=15 P/P0=0.1

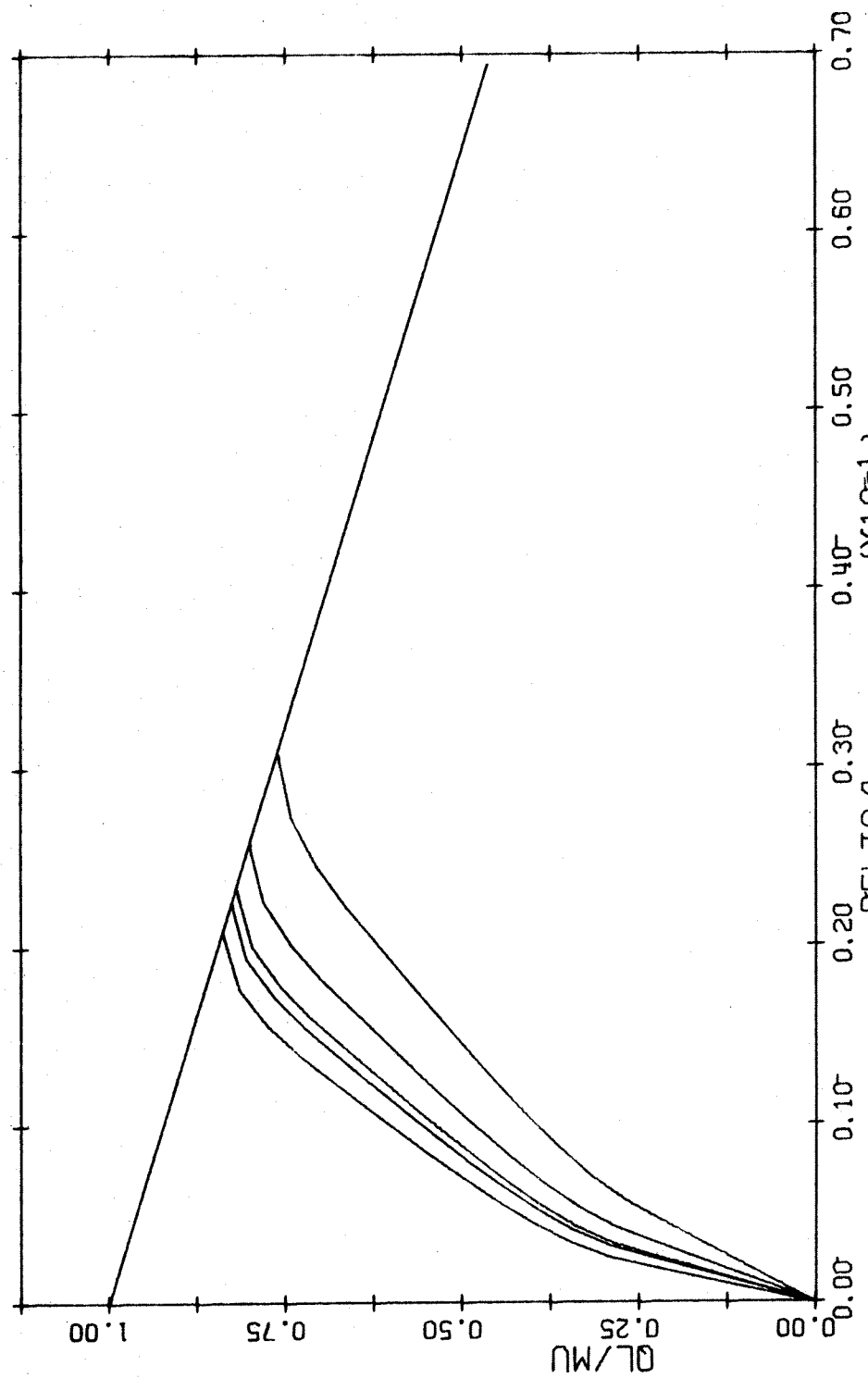

FIG. A-104 LOAD DEFLECTION DIAGRAM. SPIRAL COLUMN.
L/H=20 P/P0=0.1

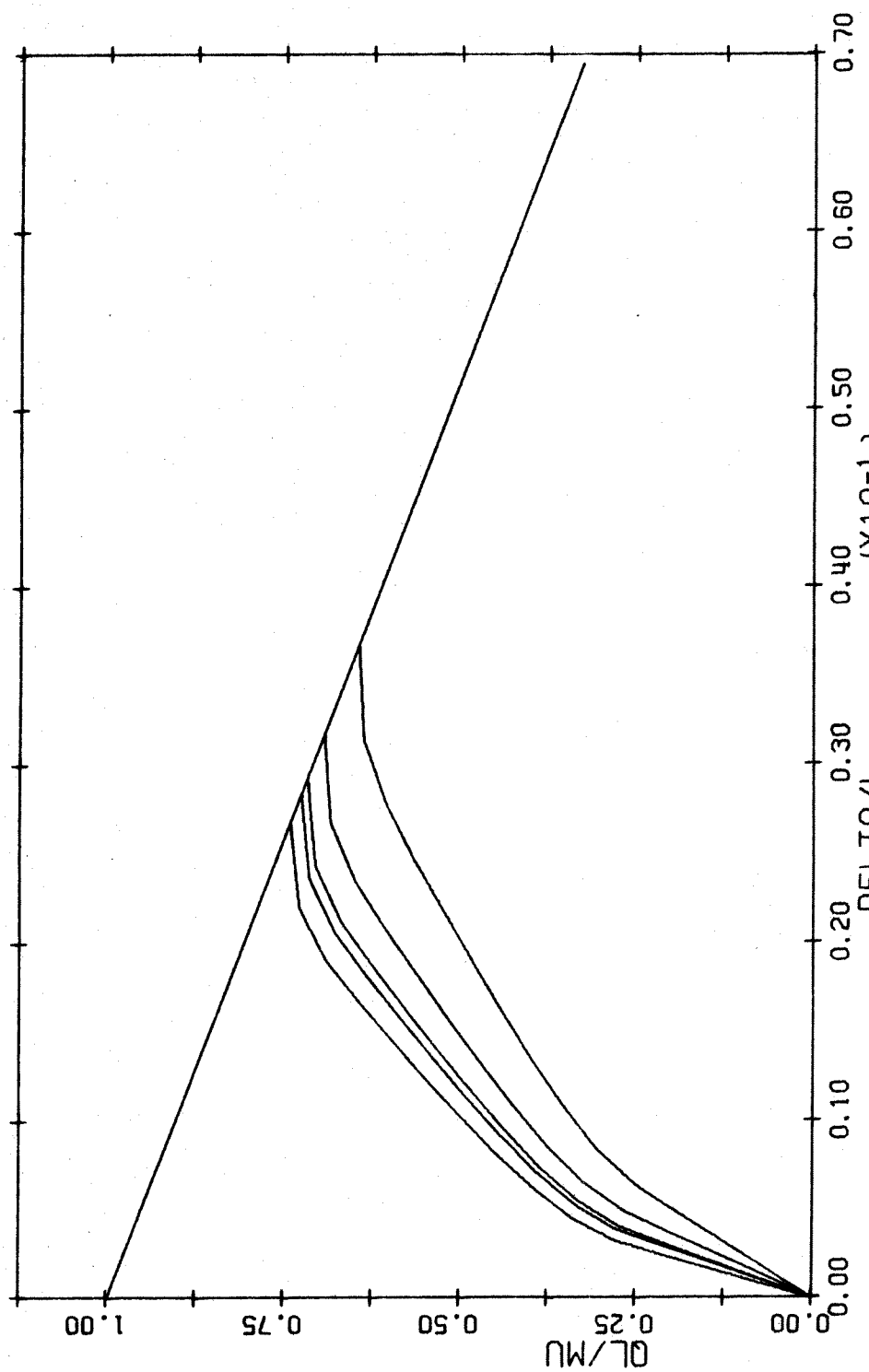

FIG. A-105 LOAD DEFLECTION DIAGRAM. SPIRAL COLUMN.
L/H=25 P/P0=0.1

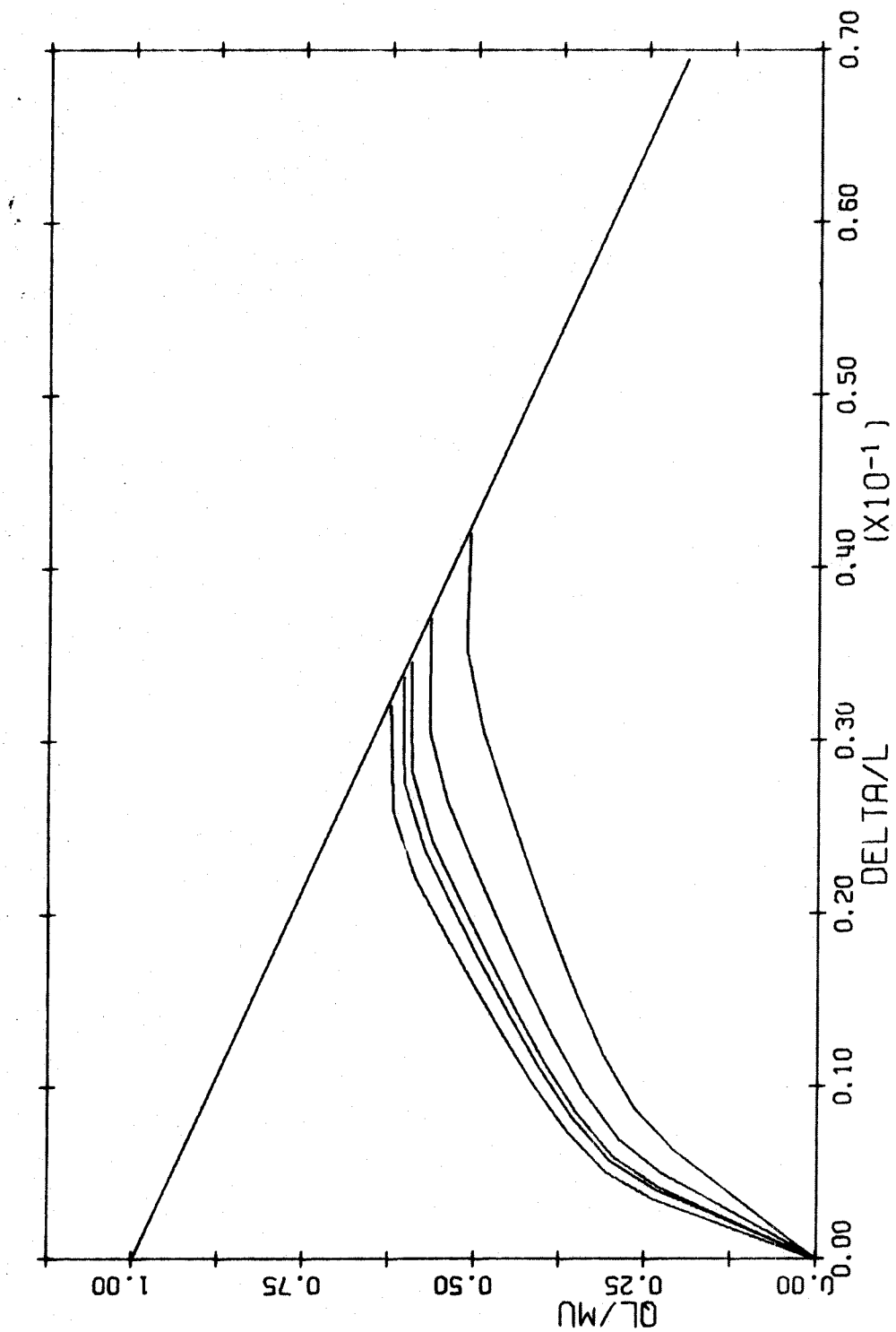

FIG. A-106 LOAD DEFLECTION DIAGRAM. SPIRAL COLUMN.
L/H=30 P/P0=0.1

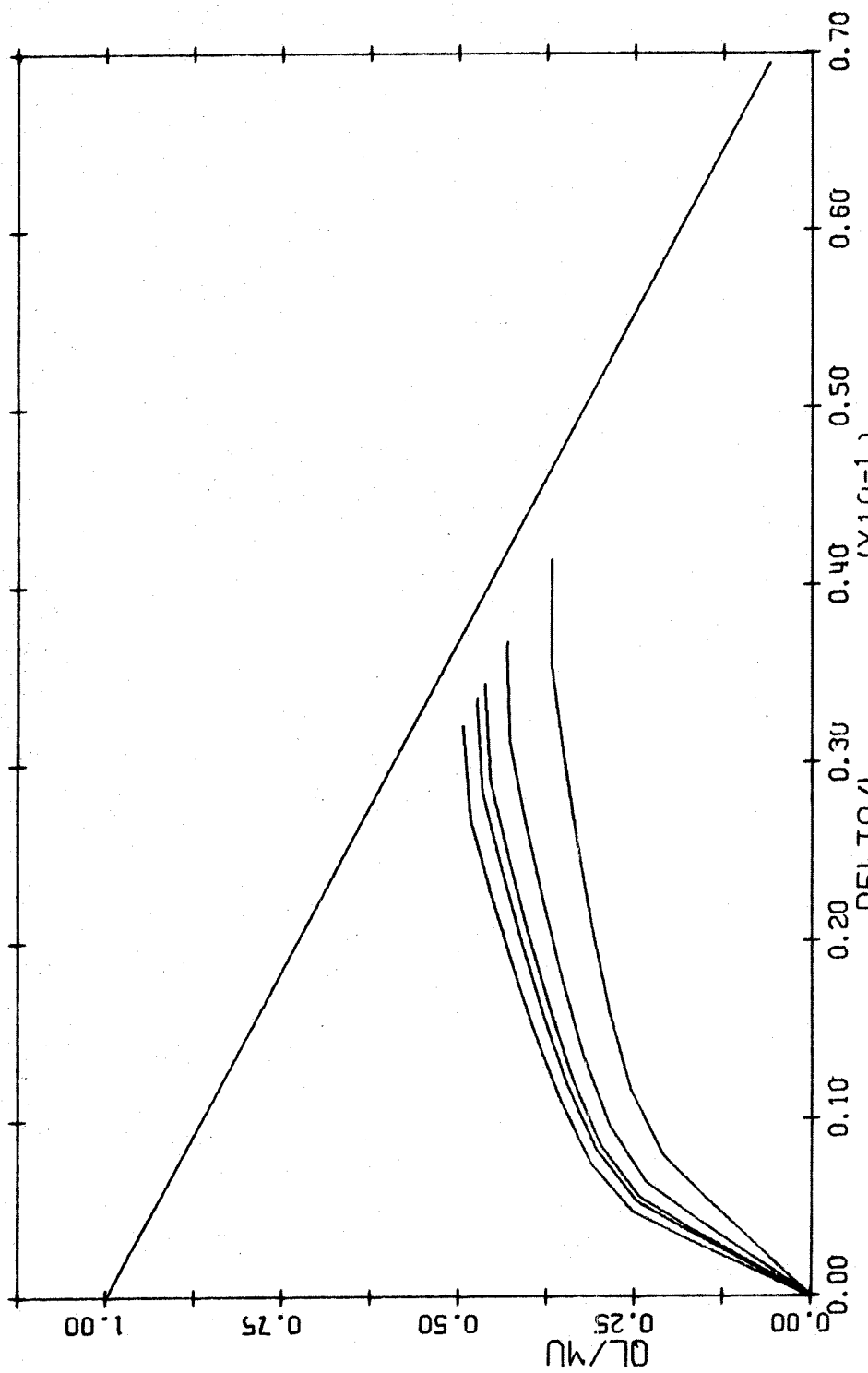

FIG. A-107 LOAD DEFLECTION DIAGRAM. SPIRAL COLUMN.
L/H=35 P/P0=0.1

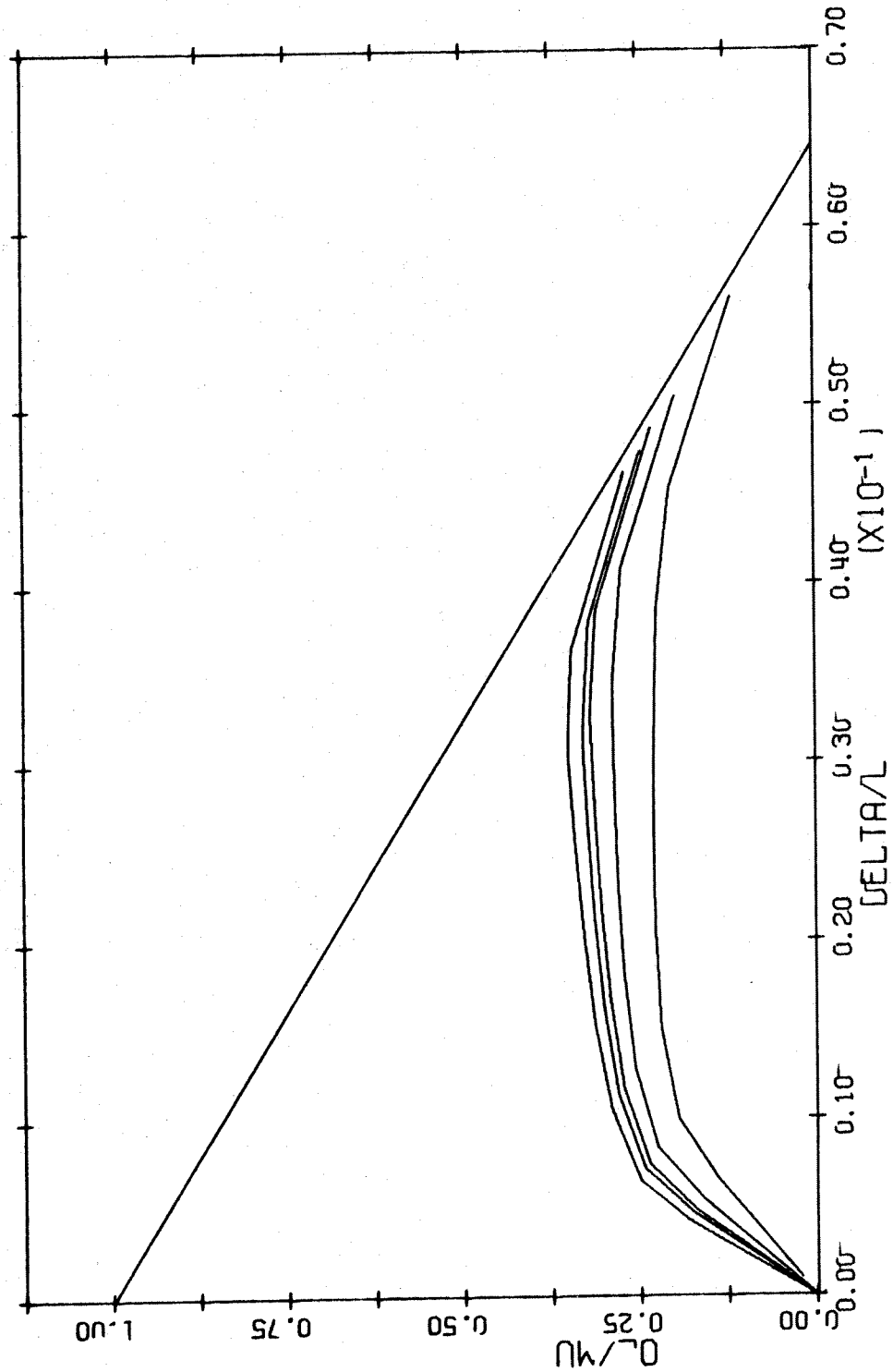

FIG. A-108 LOAD DEFLECTION DIAGRAM. SPIRAL COLUMN.
L/H=40 P/P0=0.1

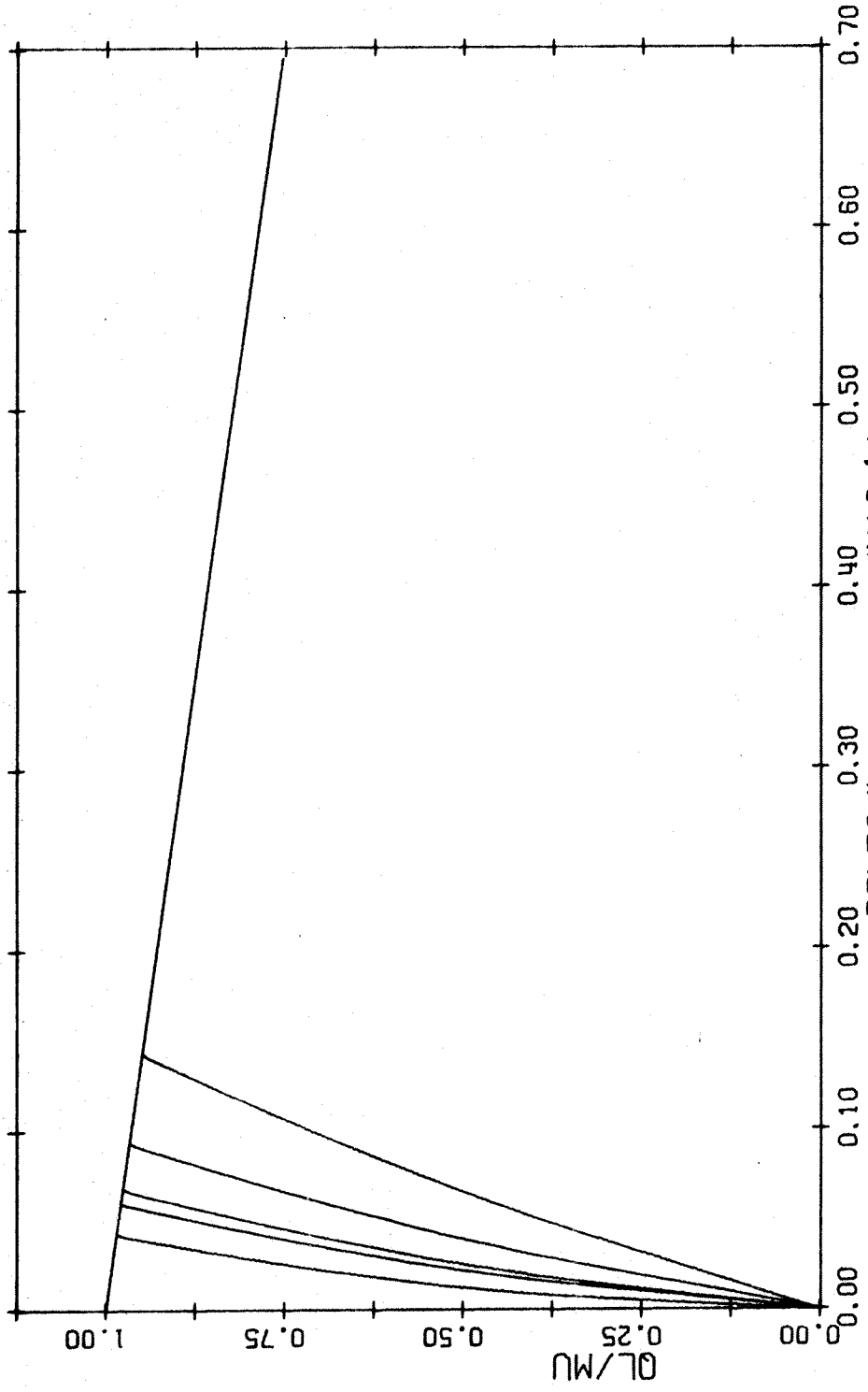

FIG. A-109 LOAD DEFLECTION DIAGRAM. SPIRAL COLUMN.
L/H=5 P/P0=0.2

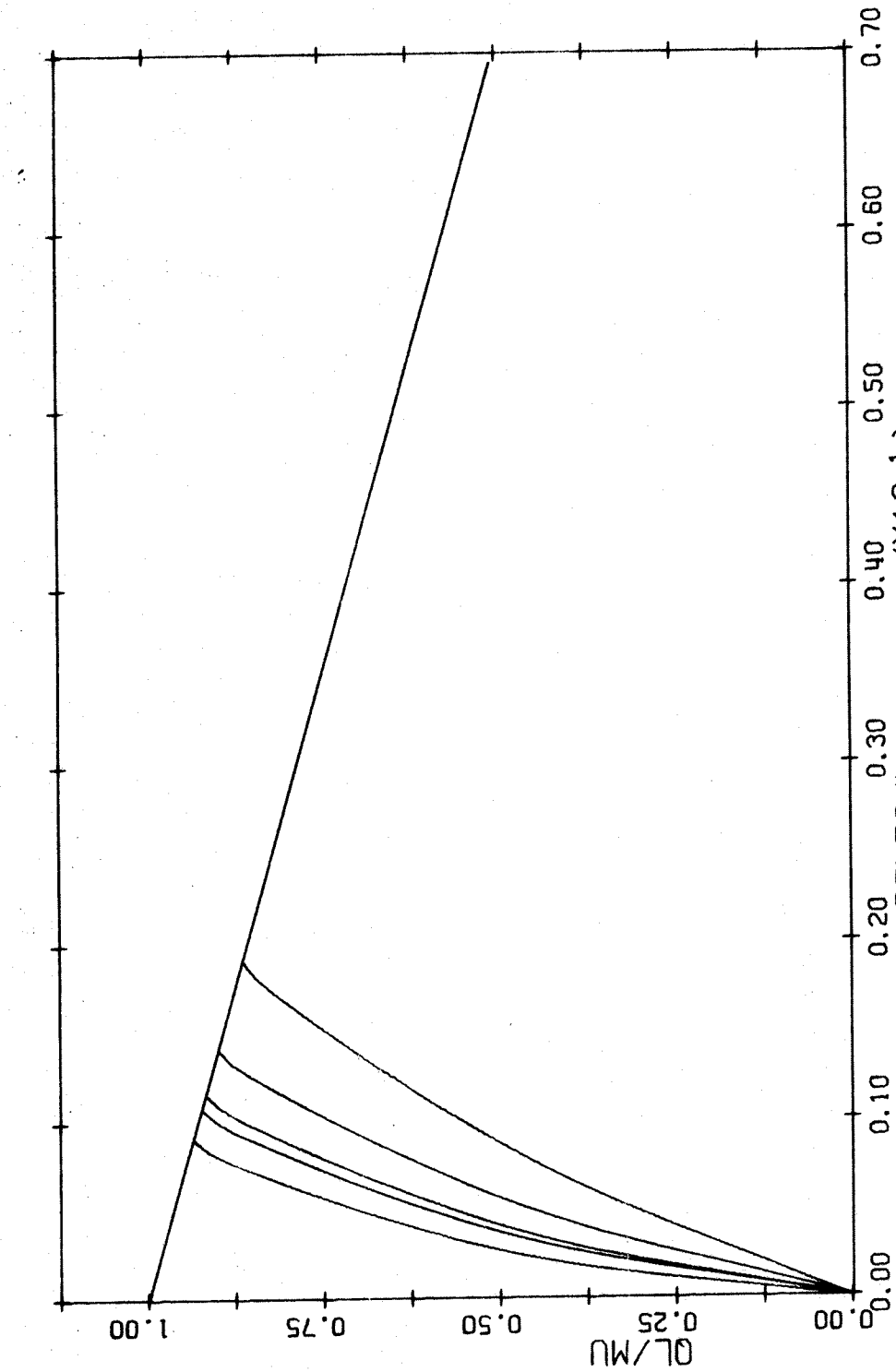

FIG. A-110 LOAD DEFLECTION DIAGRAM. SPIRAL COLUMN.
L/H=10 P/P0=0.2

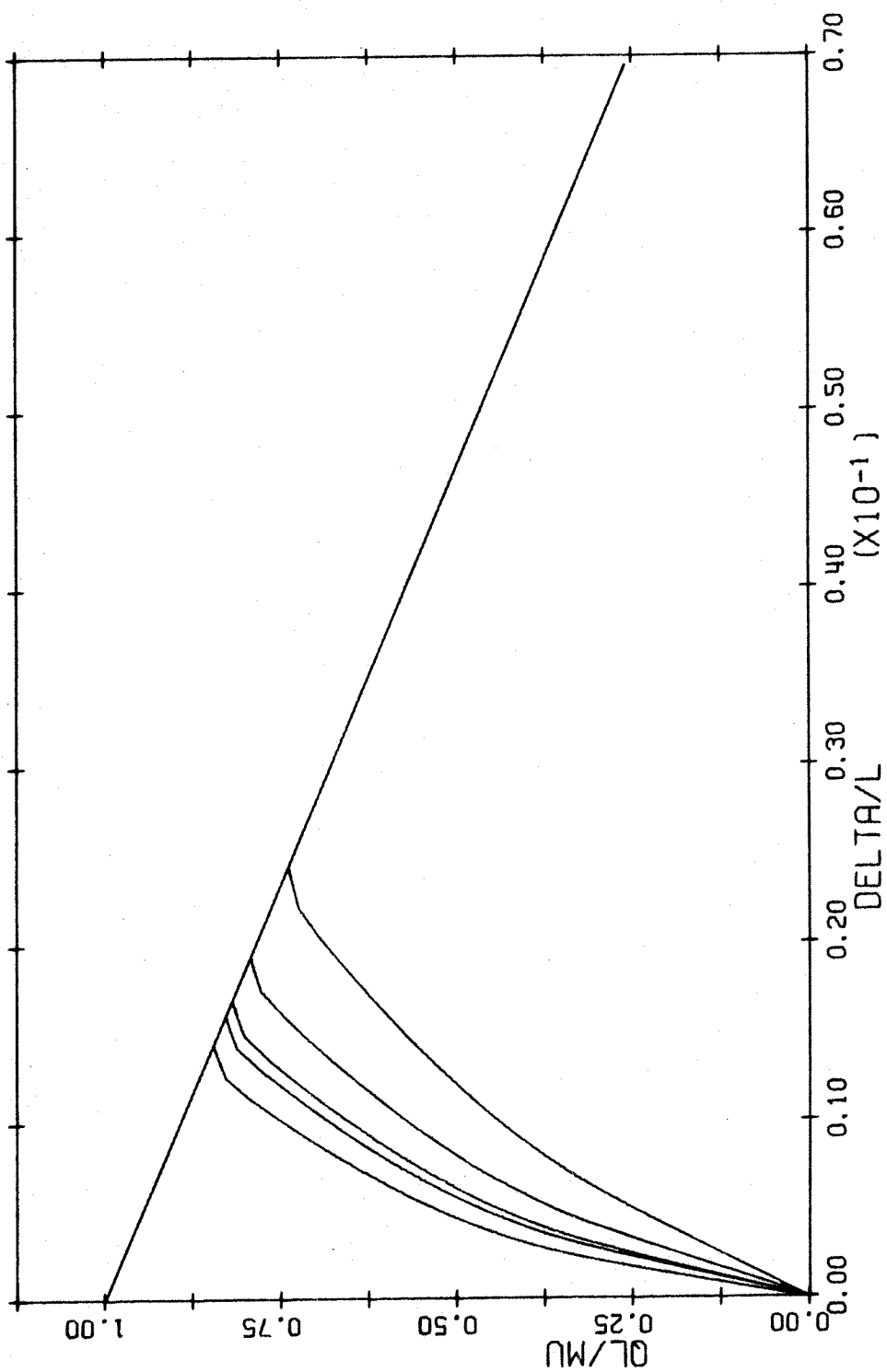

FIG. A-111 LOAD DEFLECTION DIAGRAM. SPIRAL COLUMN.
L/H=15 P/P0=0.2

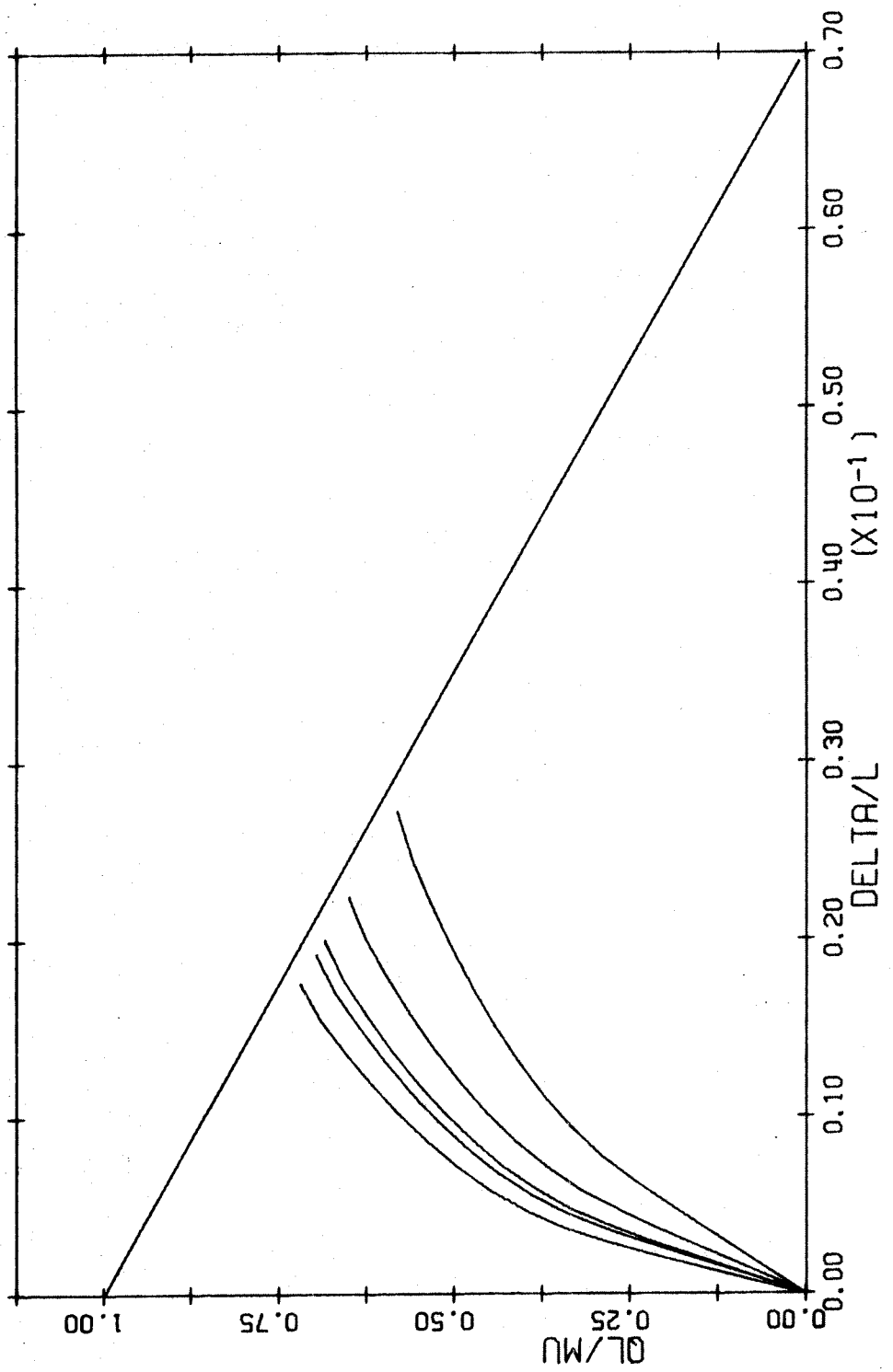

FIG. A-112 LOAD DEFLECTION DIAGRAM. SPIRAL COLUMN.
L/H=20 P/P0=0.2

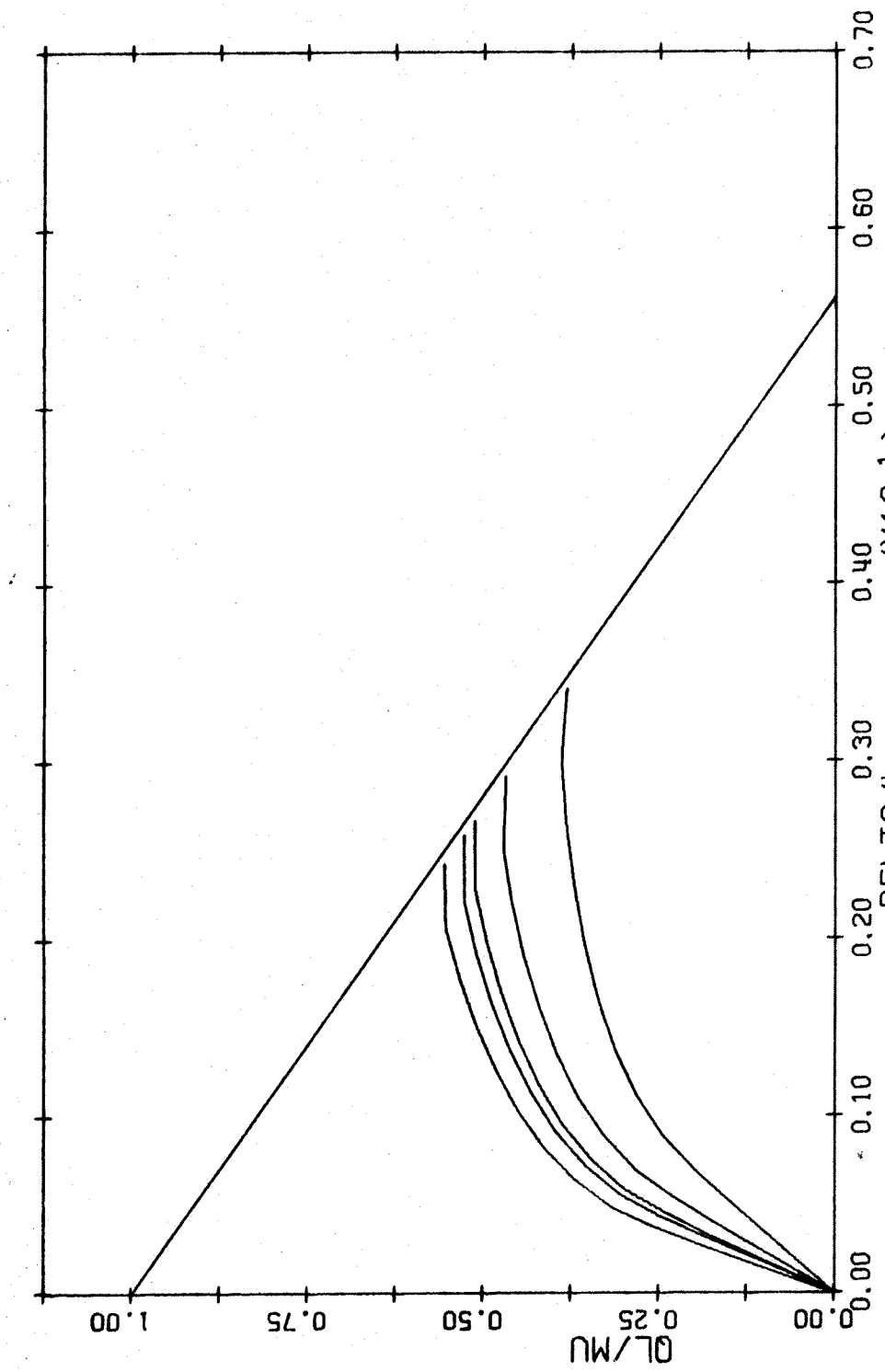

FIG. A-113 LOAD DEFLECTION DIAGRAM. SPIRAL COLUMN.
L/H=25 P/P0=0.2

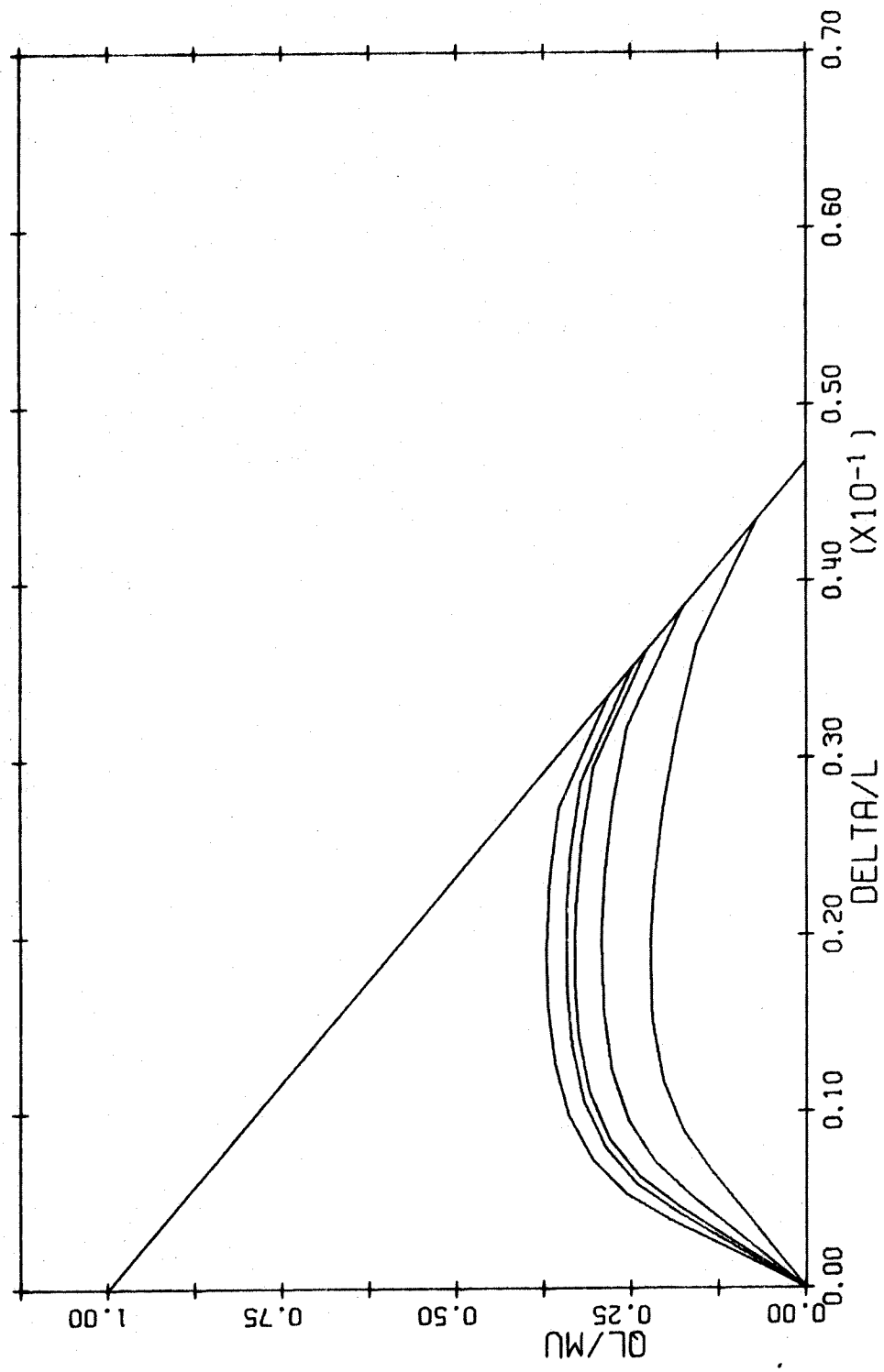

FIG. A-114 LOAD DEFLECTION DIAGRAM. SPIRAL COLUMN.
L/H=30 P/P0=0.2

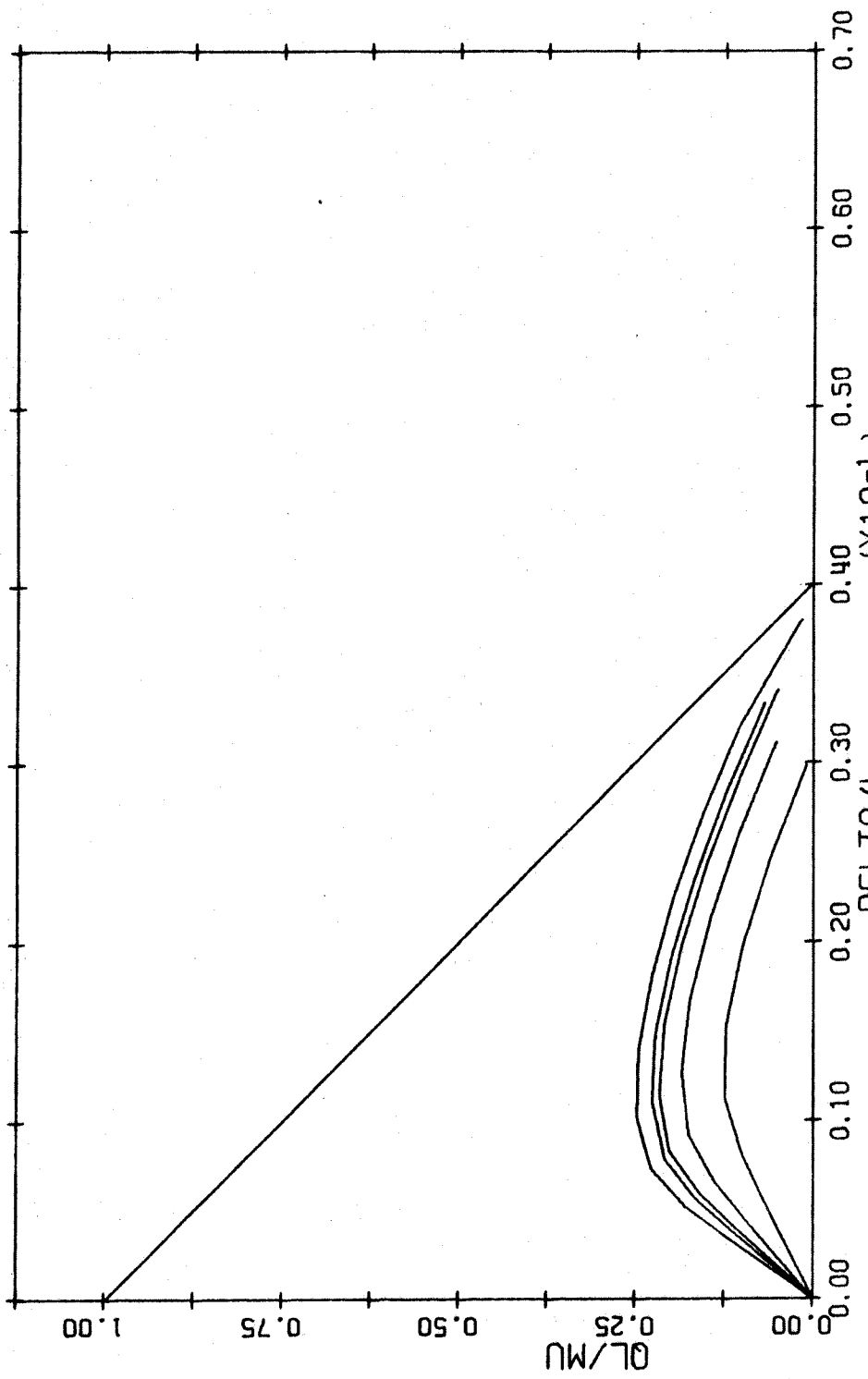

FIG. A-115 LOAD DEFLECTION DIAGRAM. SPIRAL COLUMN.
L/H=35 P/P0=0.2

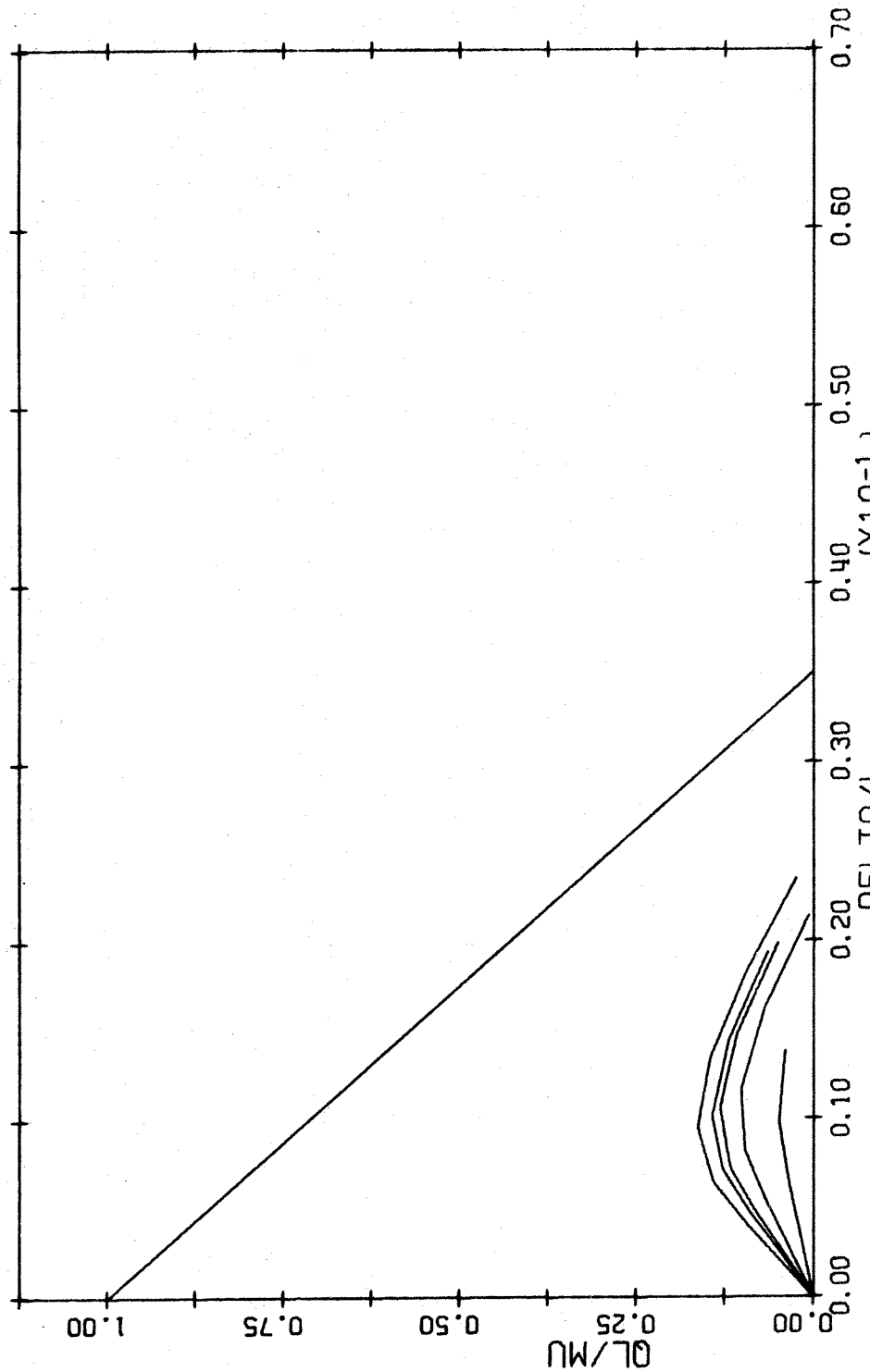

FIG. A-116 LOAD DEFLECTION DIAGRAM. SPIRAL COLUMN.
L/H=40 P/P0=0.2

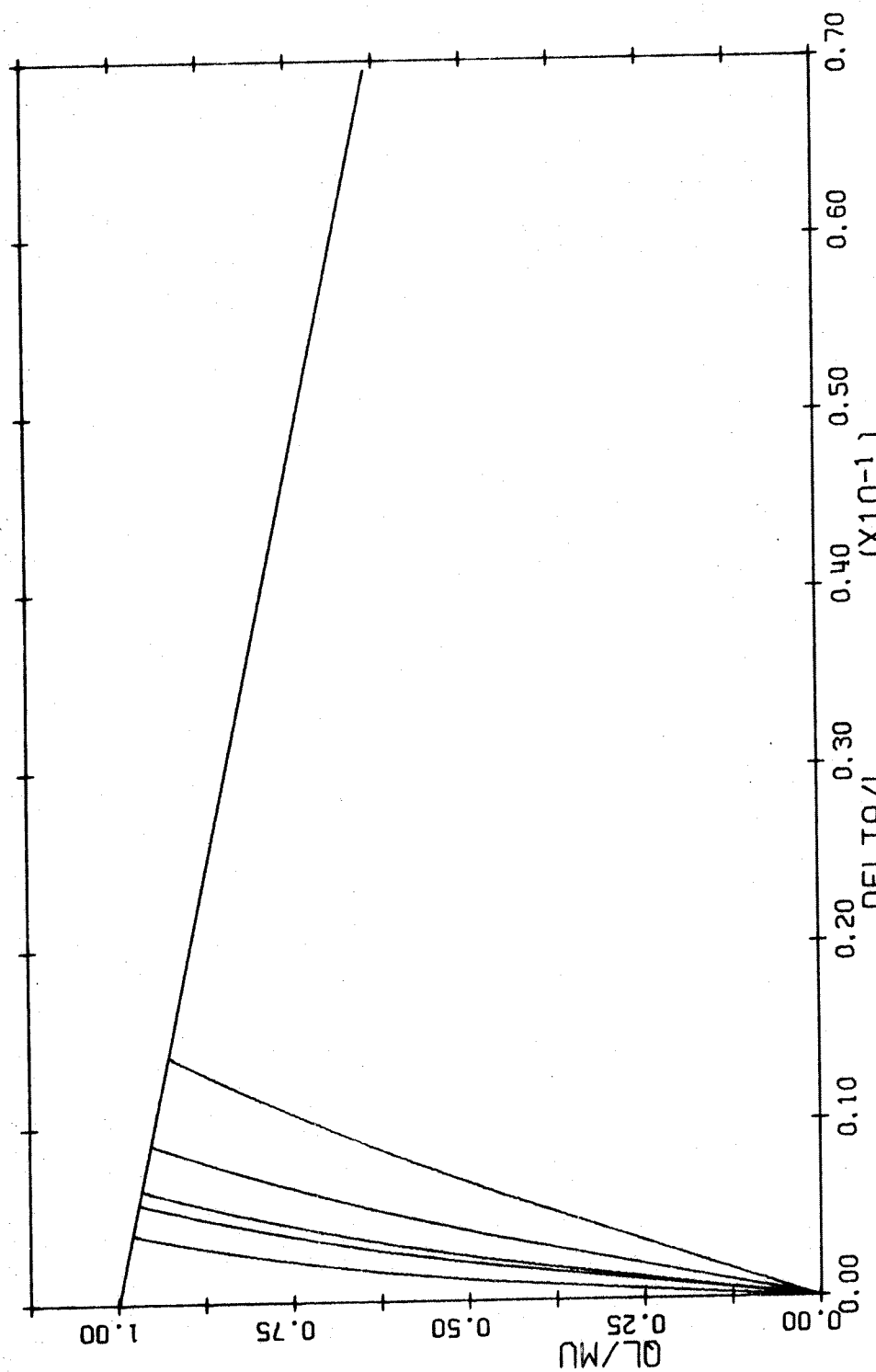

FIG. A-117 LOAD DEFLECTION DIAGRAM. SPIRAL COLUMN.
L/H=5 P/P0=0.3

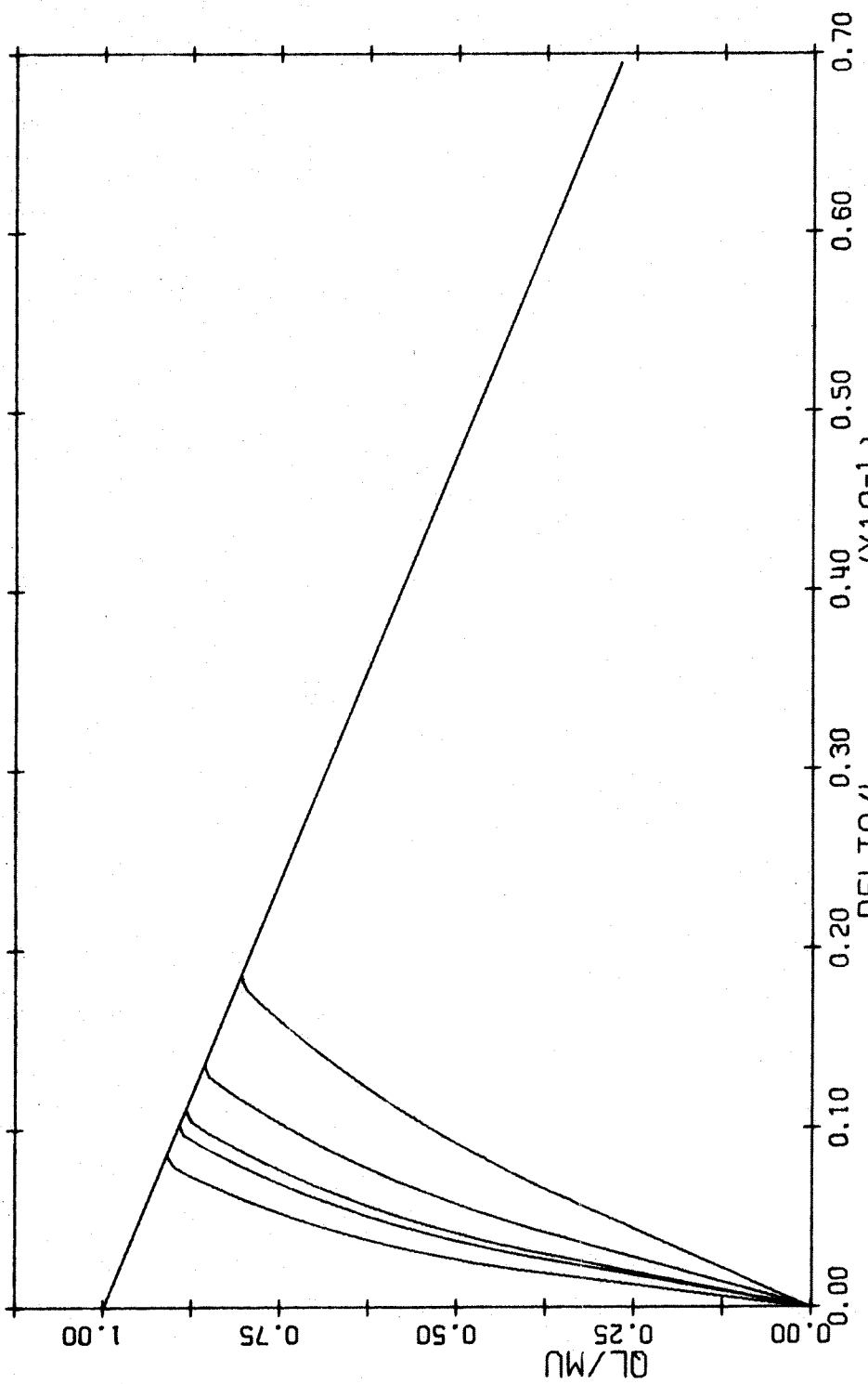

FIG. A-118 LOAD DEFLECTION DIAGRAM. SPIRAL COLUMN.
L/H=10 P/P0=0.3

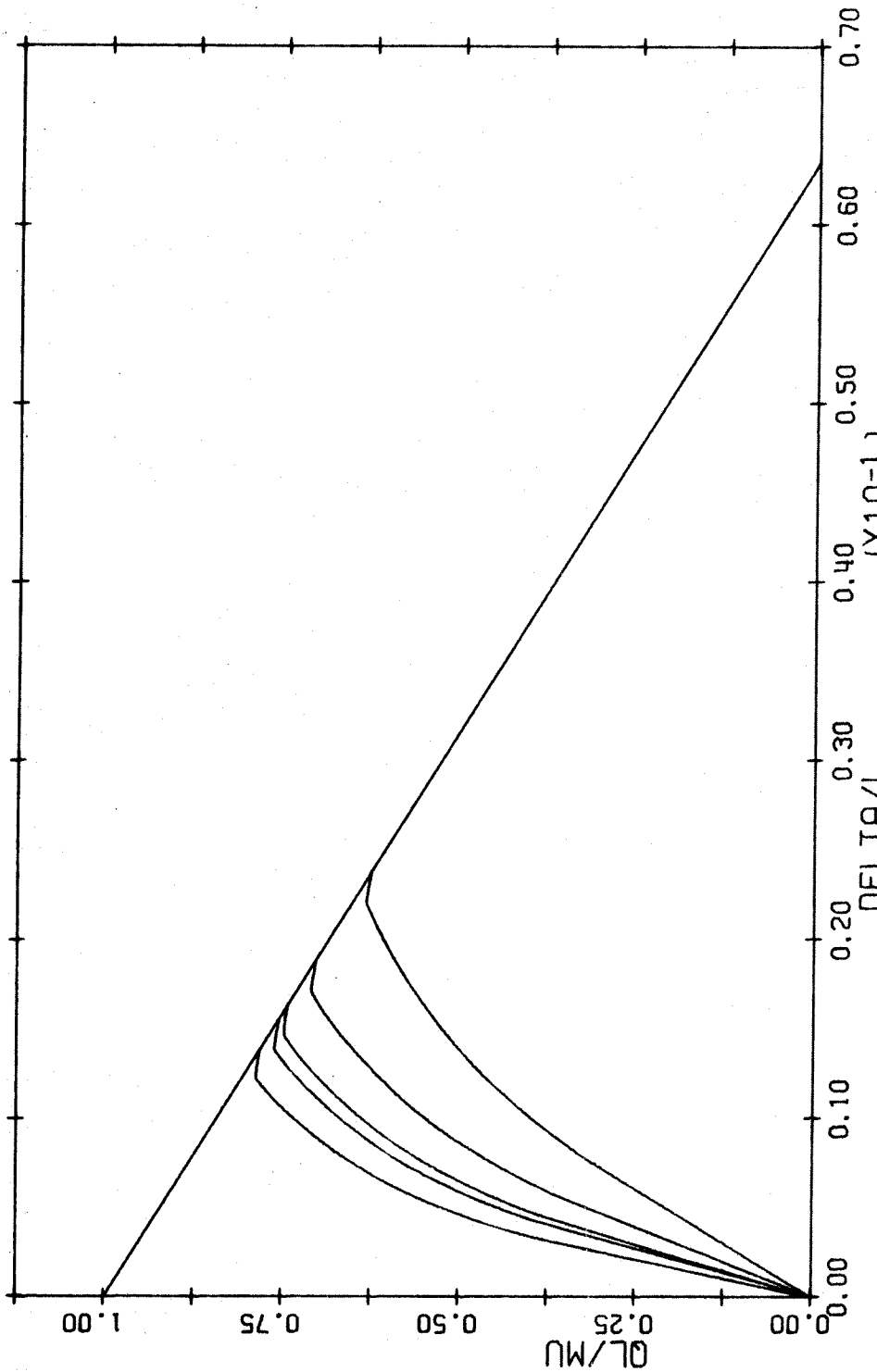

FIG. A-119 LOAD DEFLECTION DIAGRAM. SPIRAL COLUMN.
L/H=15 P/P0=0.3

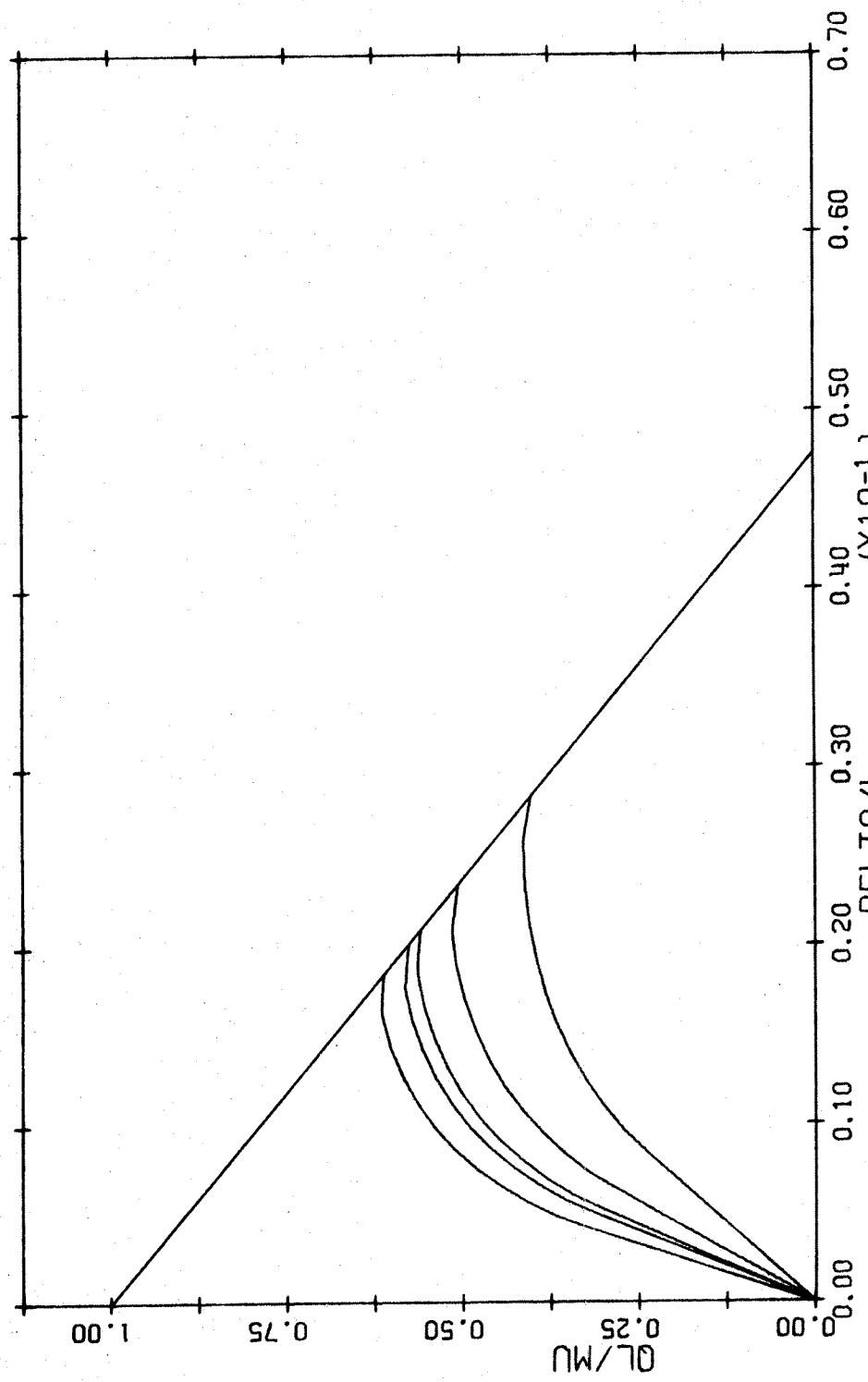

FIG. A-120 LOAD DEFLECTION DIAGRAM. SPIRAL COLUMN.
L/H=20 P/P0=0.3

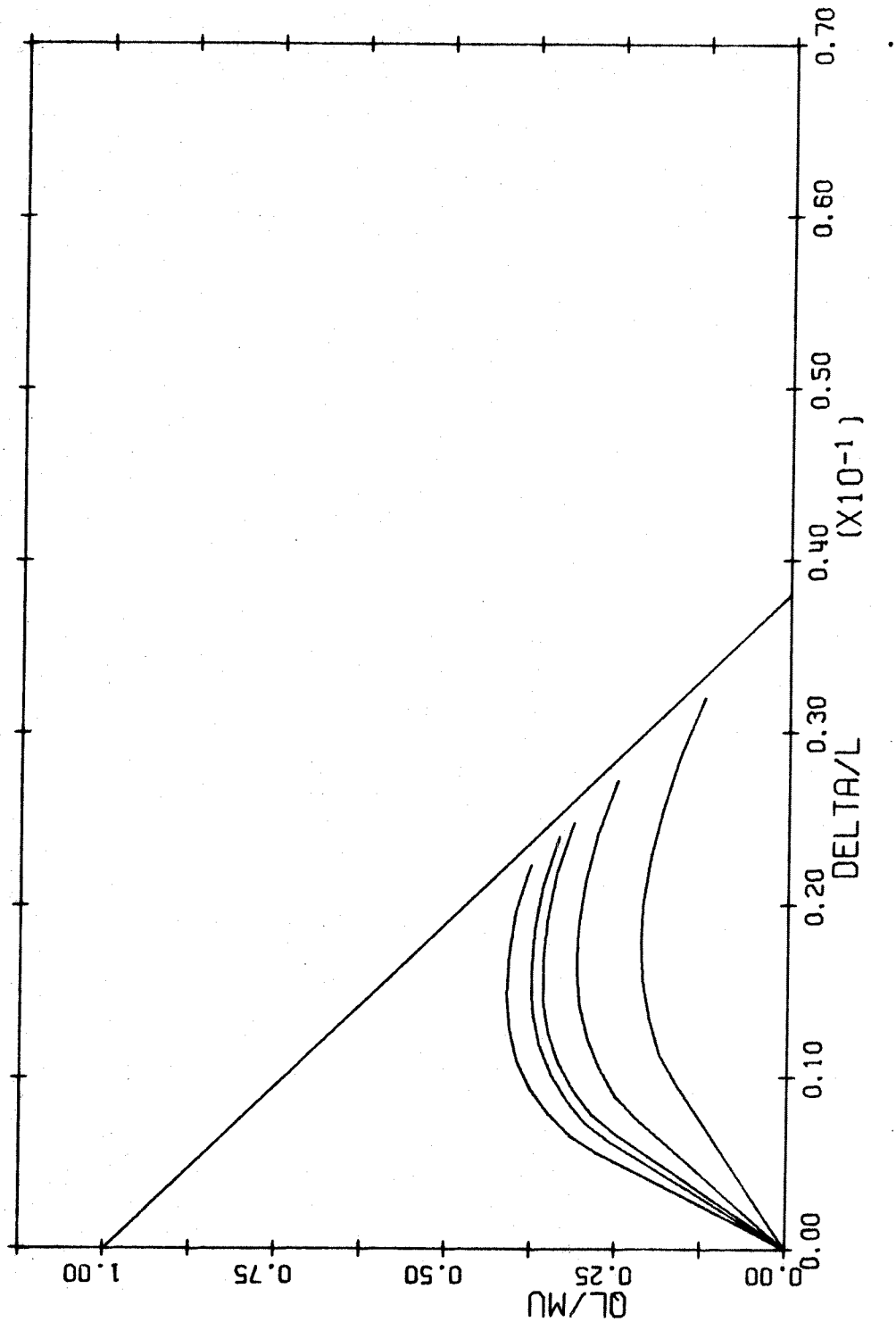

FIG. A-121 LOAD DEFLECTION DIAGRAM. SPIRAL COLUMN.
L/H=25 P/P0=0.3

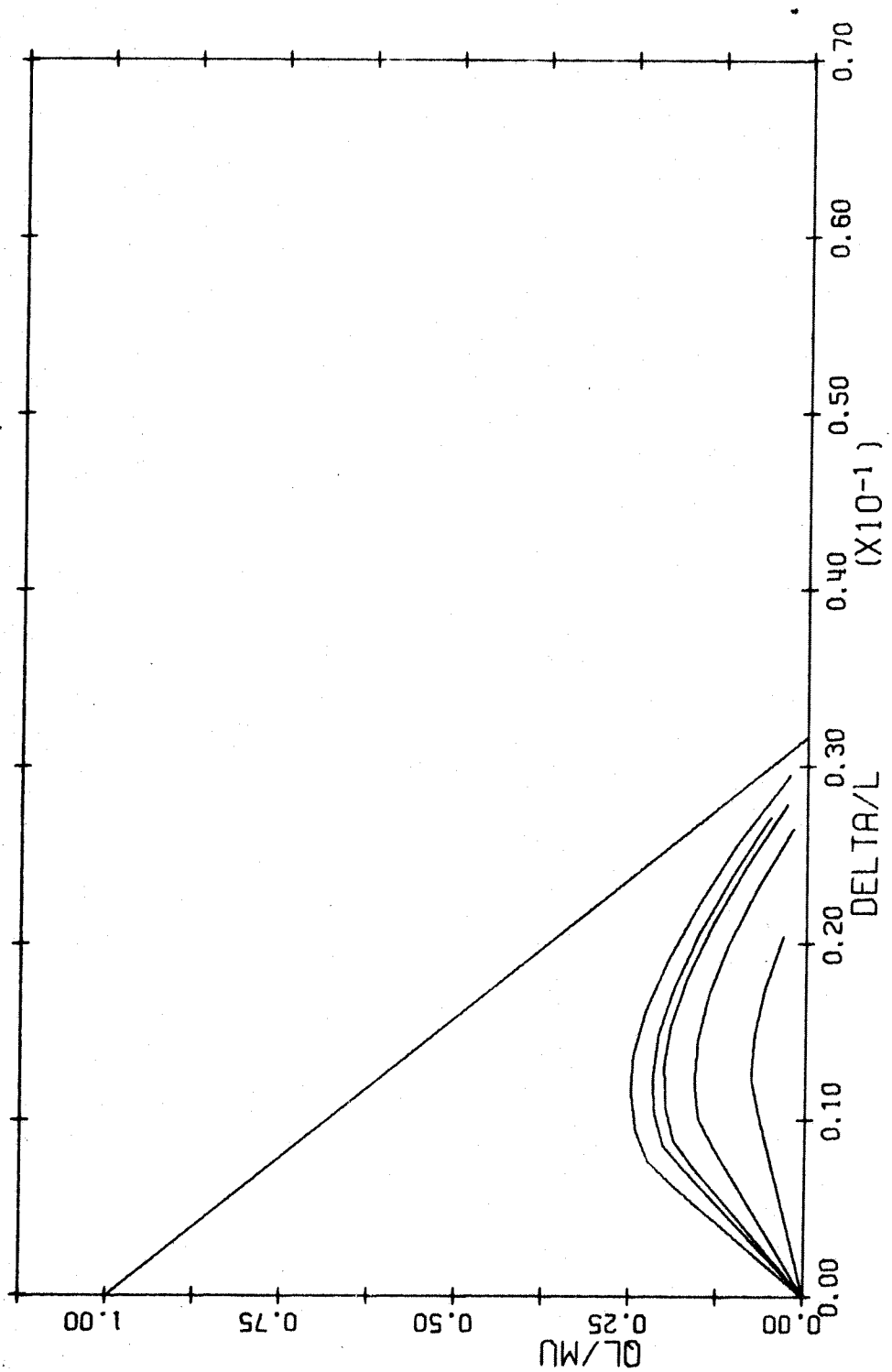

FIG. A-122 LOAD DEFLECTION DIAGRAM. SPIRAL COLUMN.
L/H=30 P/P0=0.3

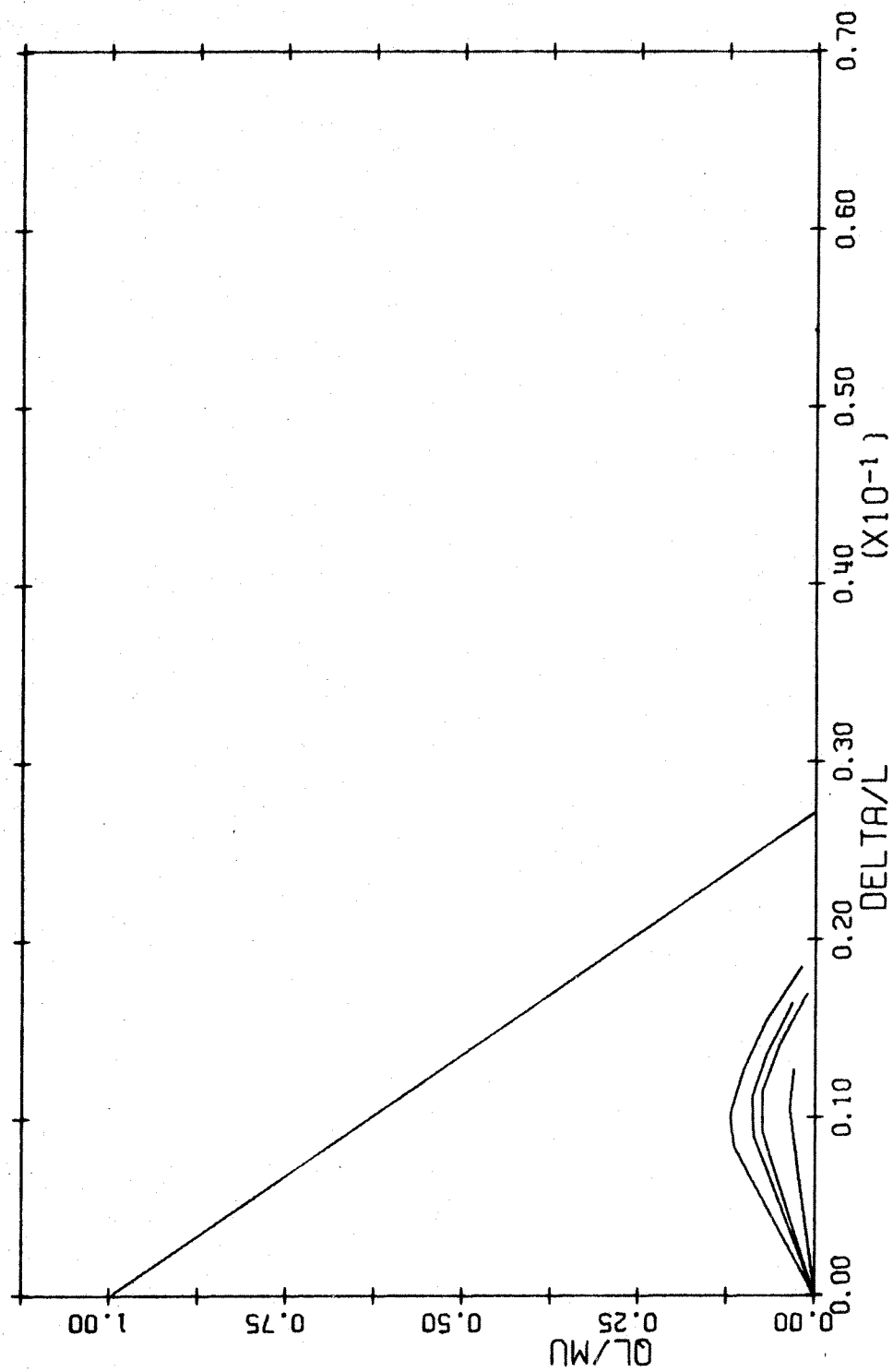

FIG. A-123 LOAD DEFLECTION DIAGRAM. SPIRAL COLUMN.
L/H=35 P/P0=0.3

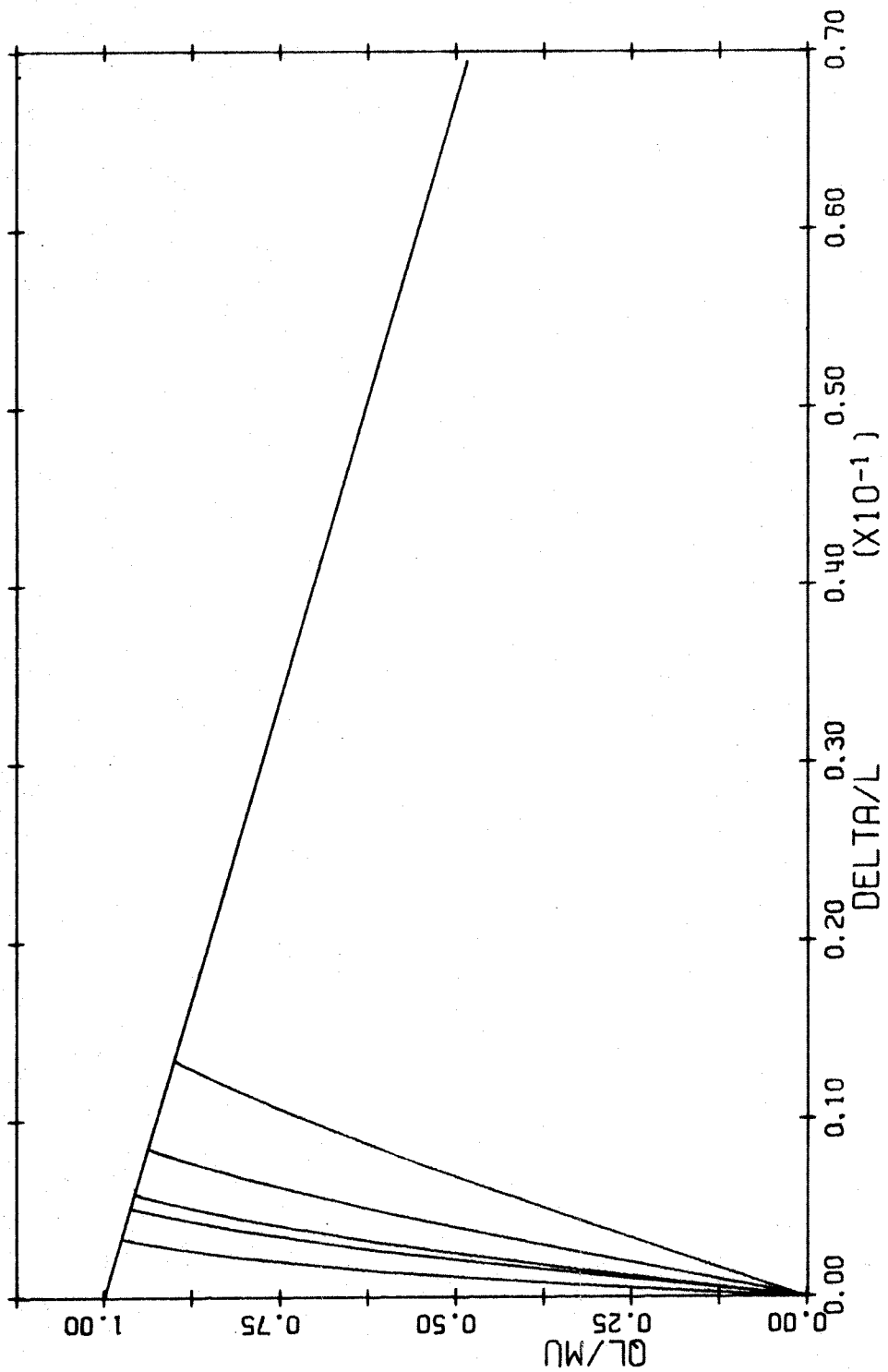

FIG. A-124 LOAD DEFLECTION DIAGRAM. SPIRAL COLUMN.
L/H=5 P/P0=0.4

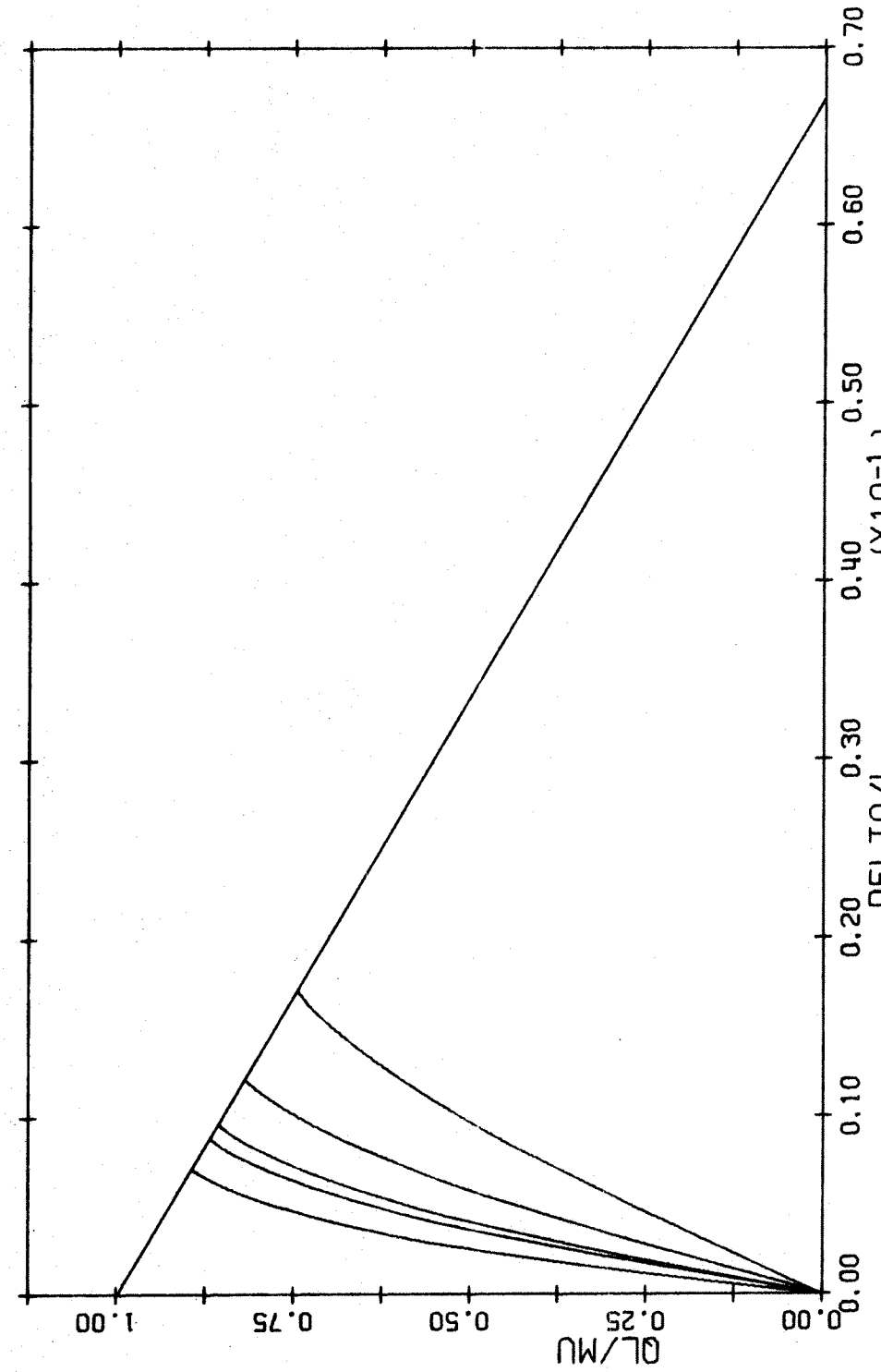

FIG. A-125 LOAD DEFLECTION DIAGRAM. SPIRAL COLUMN.
L/H=10 P/P0=0.4

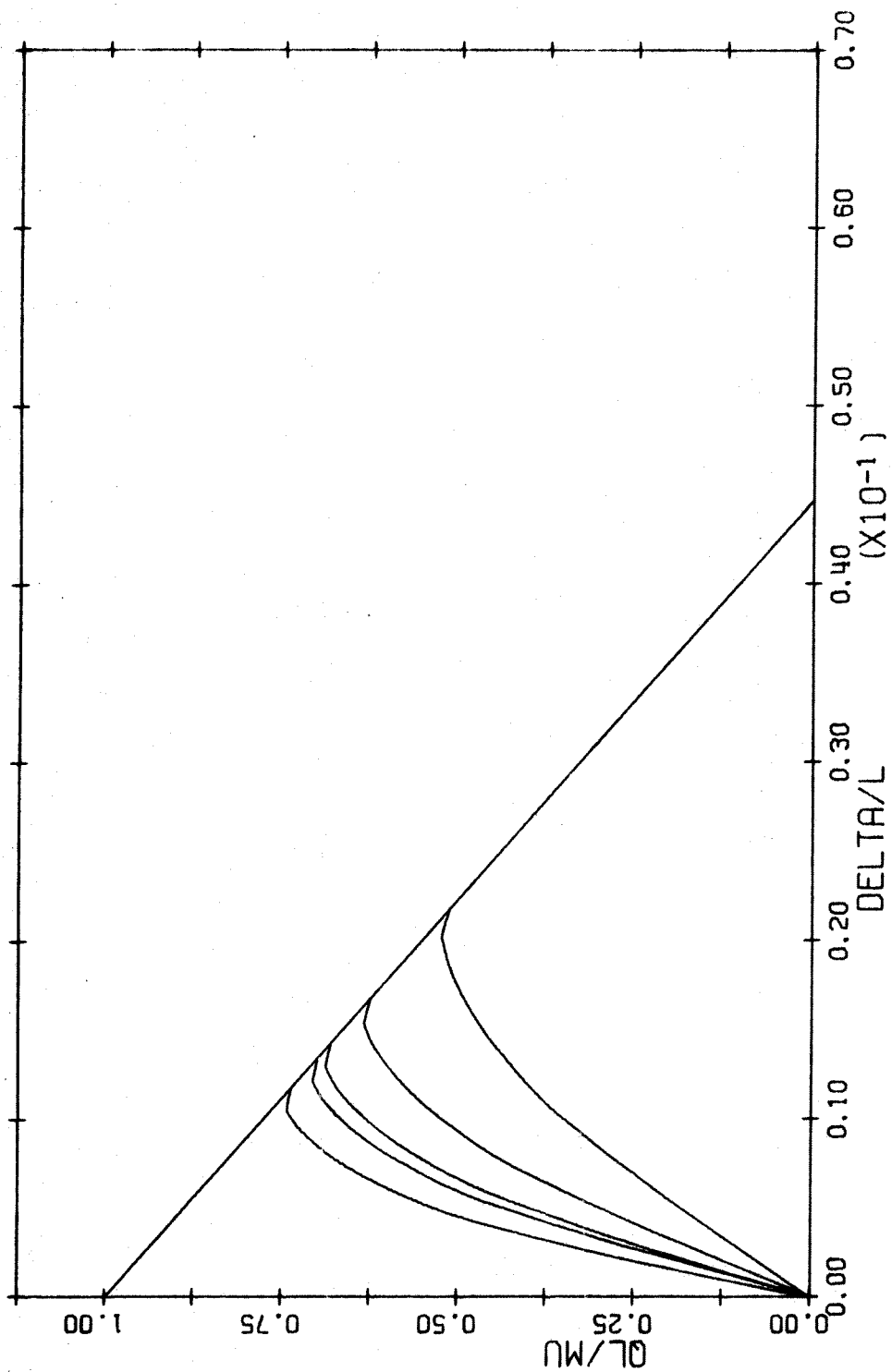

FIG. A-126 LOAD DEFLECTION DIAGRAM. SPIRAL COLUMN.
L/H=15 P/P0=0.4

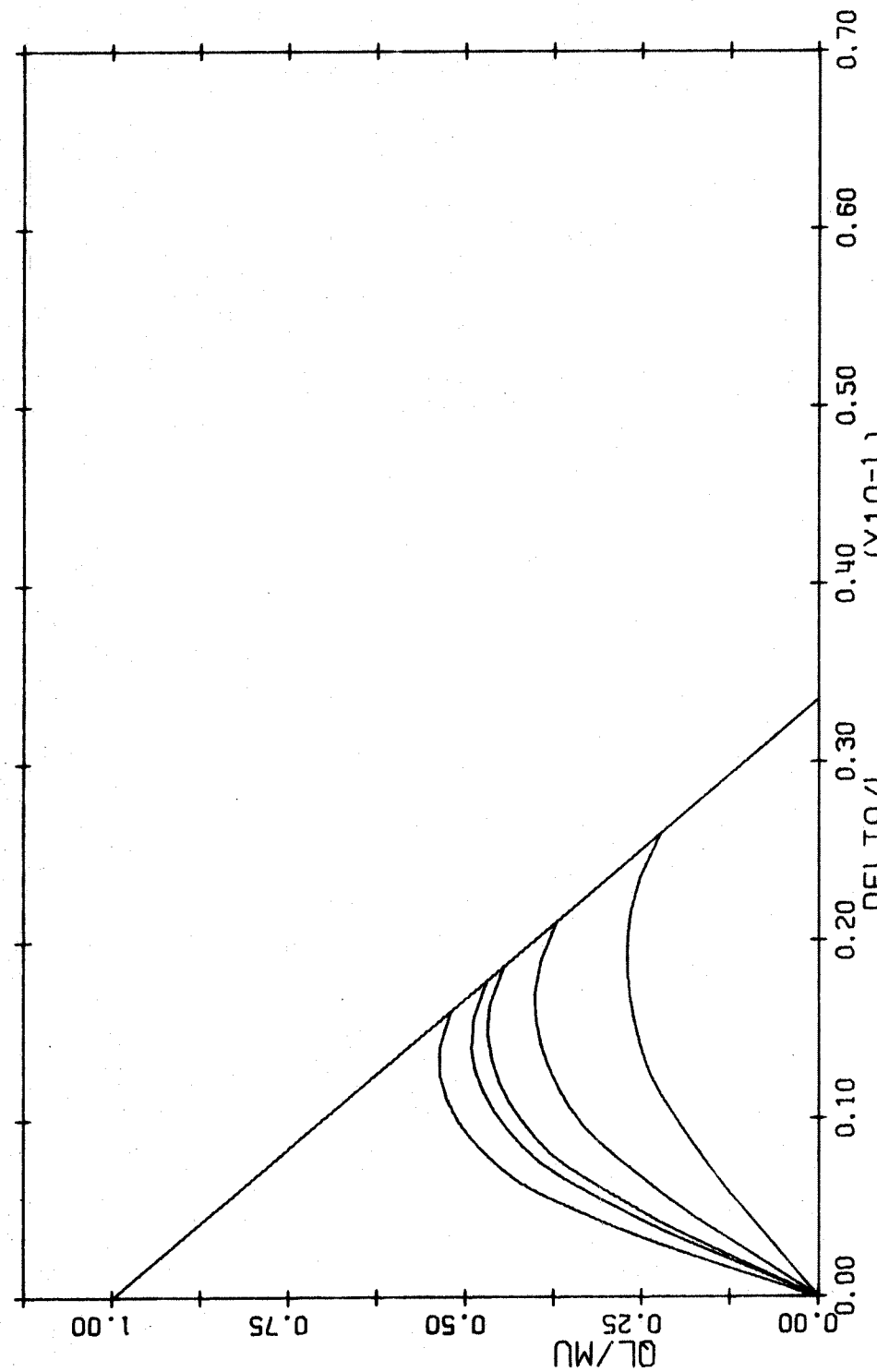

FIG. A-127 LOAD DEFLECTION DIAGRAM. SPIRAL COLUMN.
L/H=20 P/P0=0.4

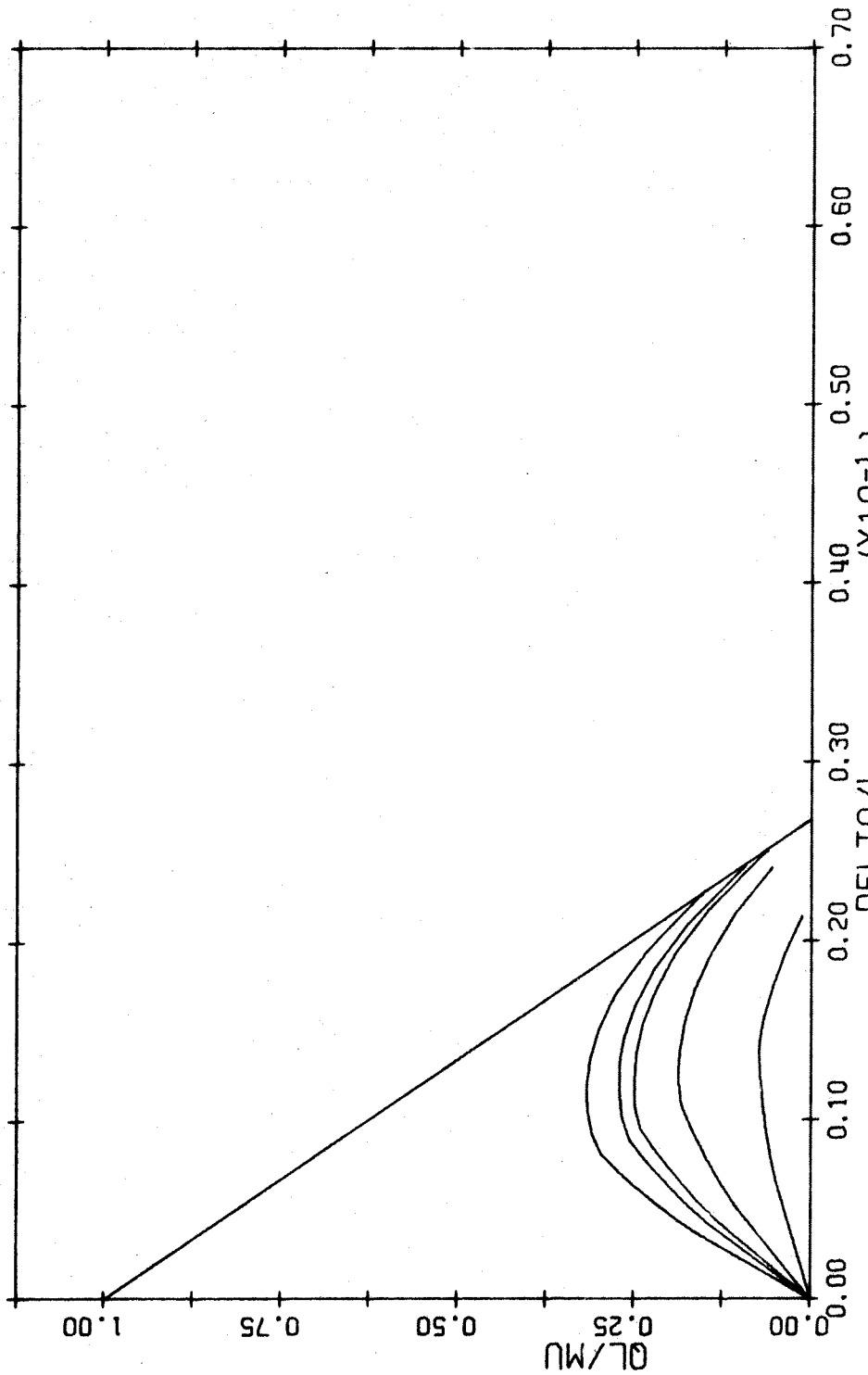

FIG. A-128 LOAD DEFLECTION DIAGRAM. SPIRAL COLUMN.
L/R=25 P/P0=0.4

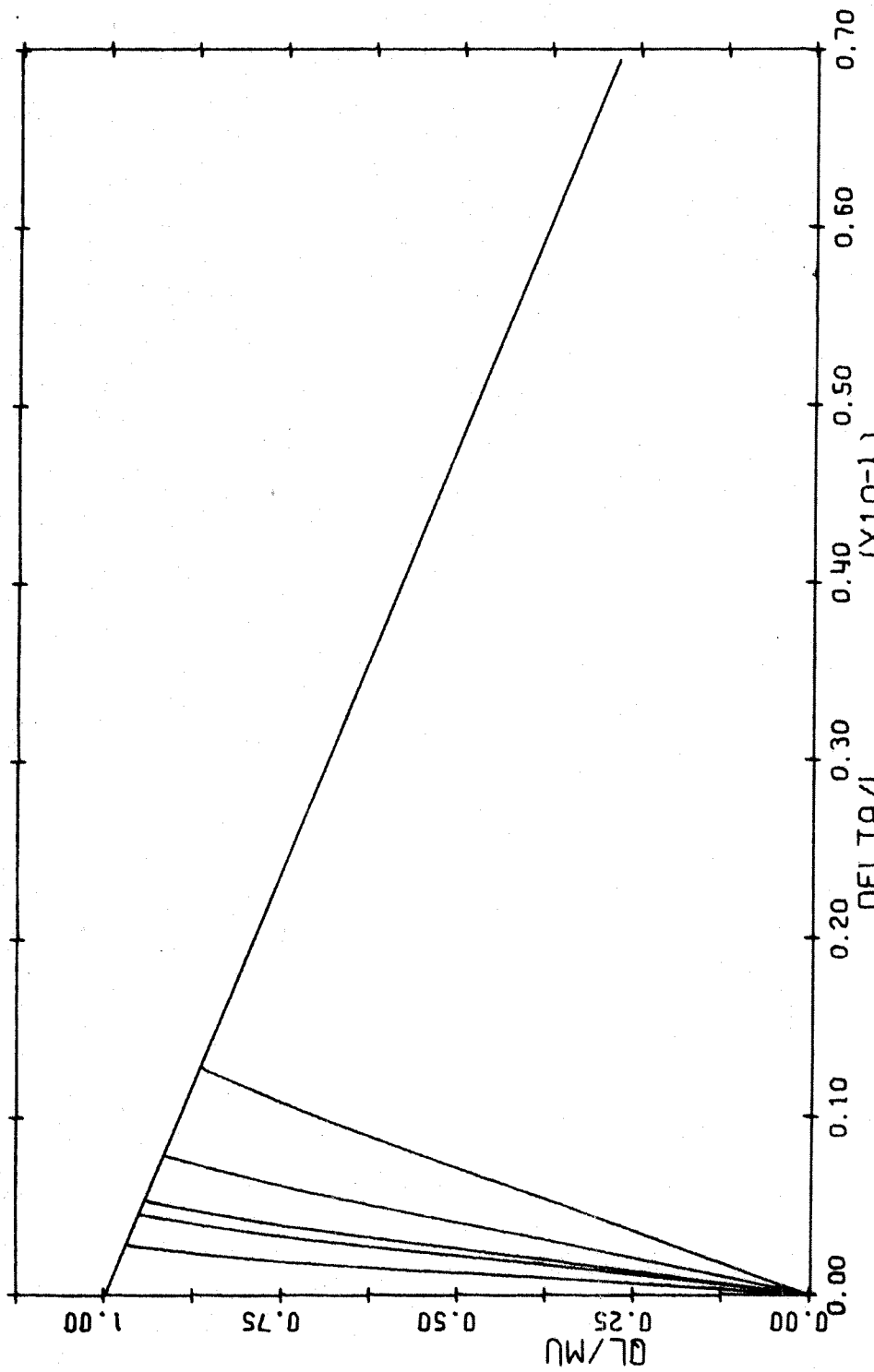

FIG. A-129 LOAD DEFLECTION DIAGRAM. SPIRAL COLUMN.
L/H=5 P/P0=0.5

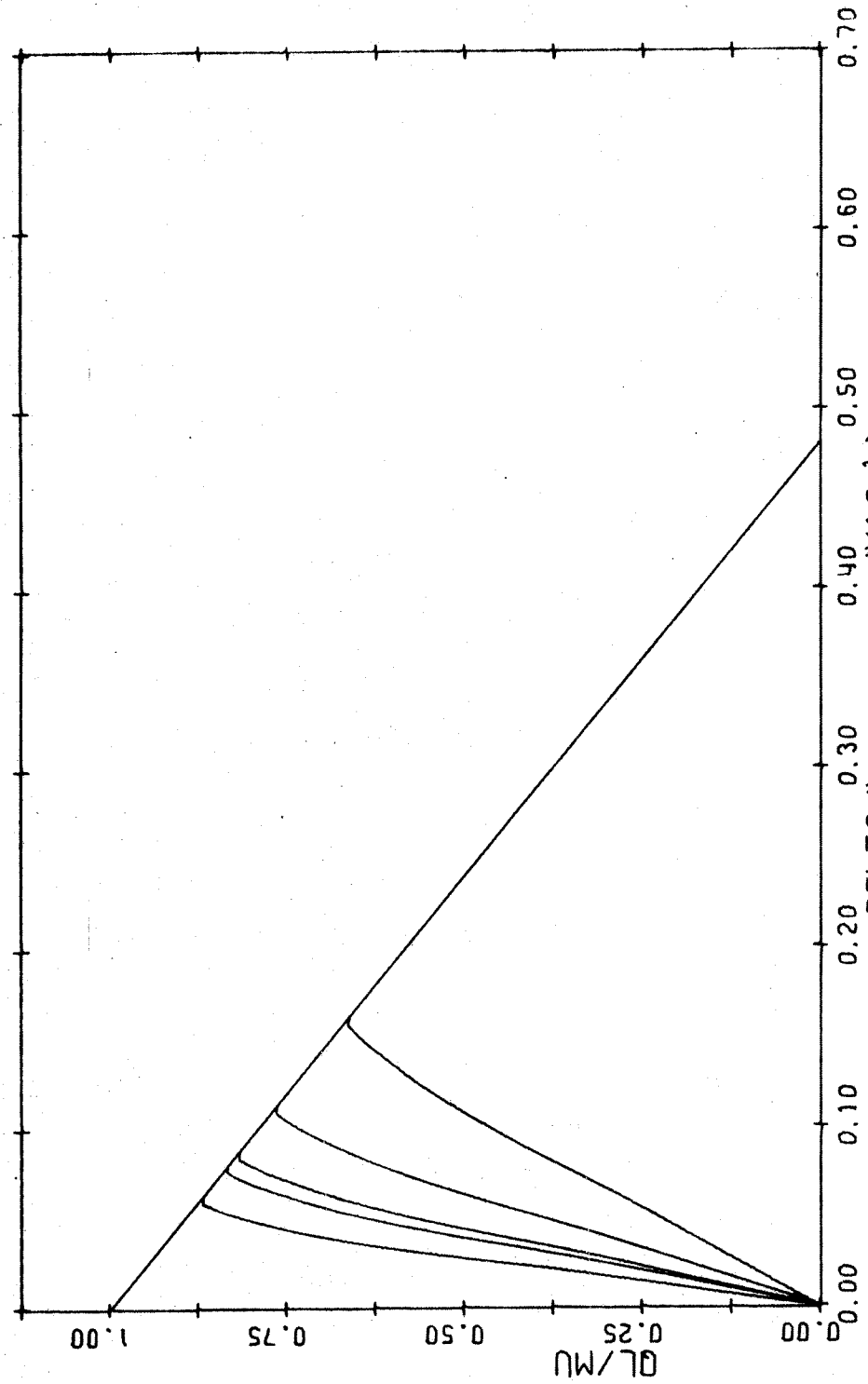

FIG. A-130 LOAD DEFLECTION DIAGRAM. SPIRAL COLUMN.
L/H=10 P/P0=0.5

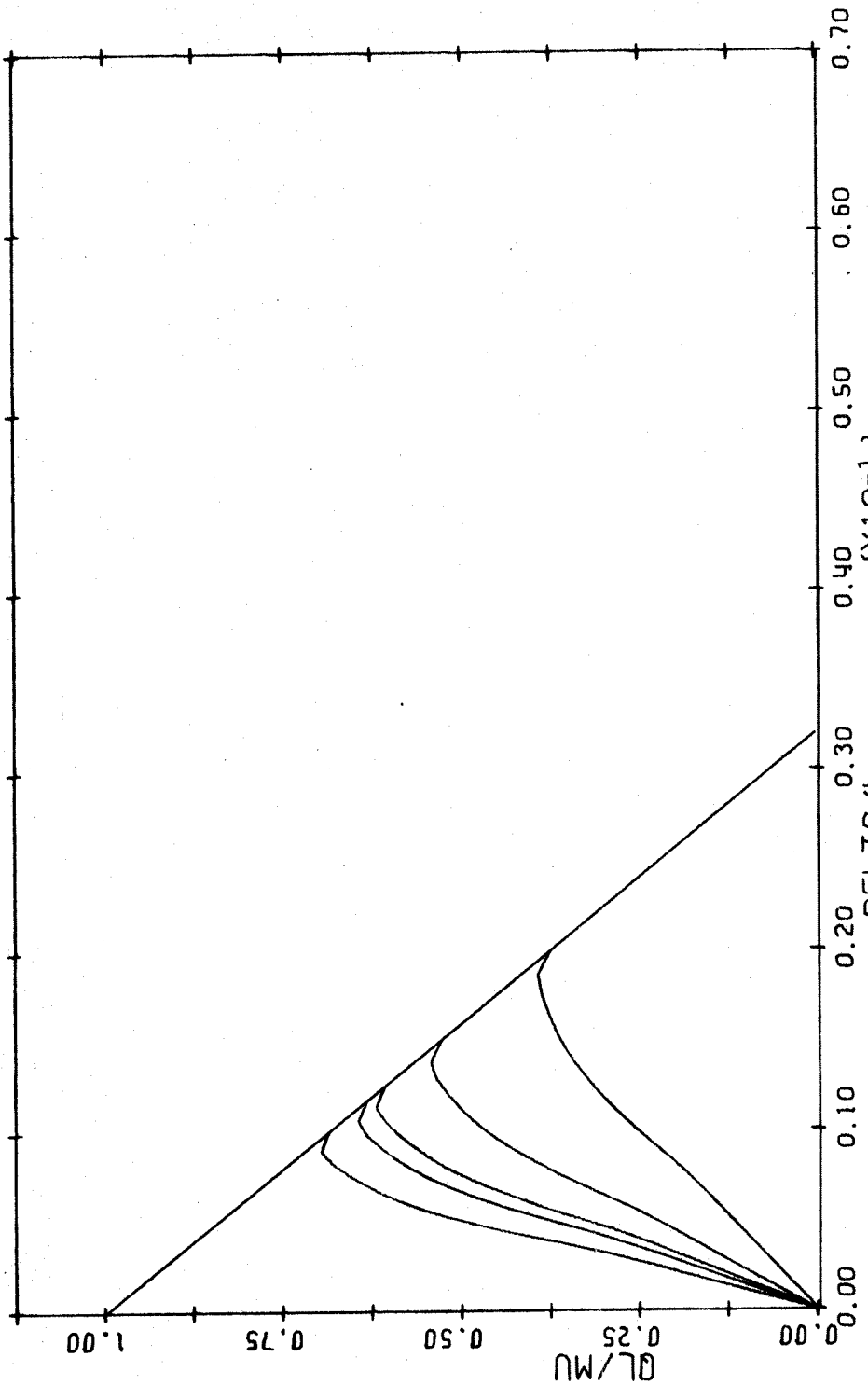

FIG. A-131 LOAD DEFLECTION DIAGRAM. SPIRAL COLUMN.
L/H=15 P/P0=0.5

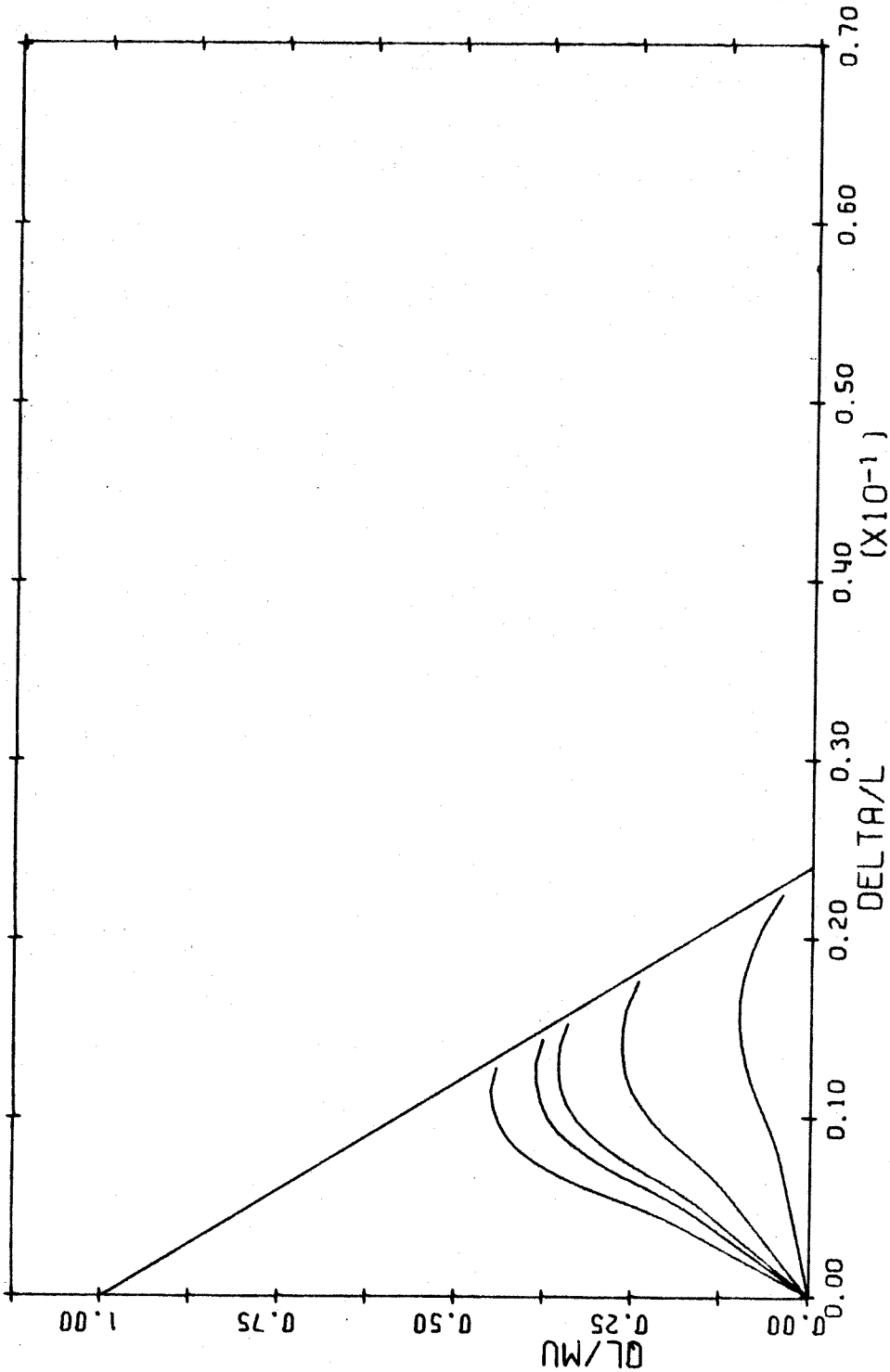

FIG. A-132 LOAD DEFLECTION DIAGRAM. SPIRAL COLUMN.
L/H=20 P/P0=0.5

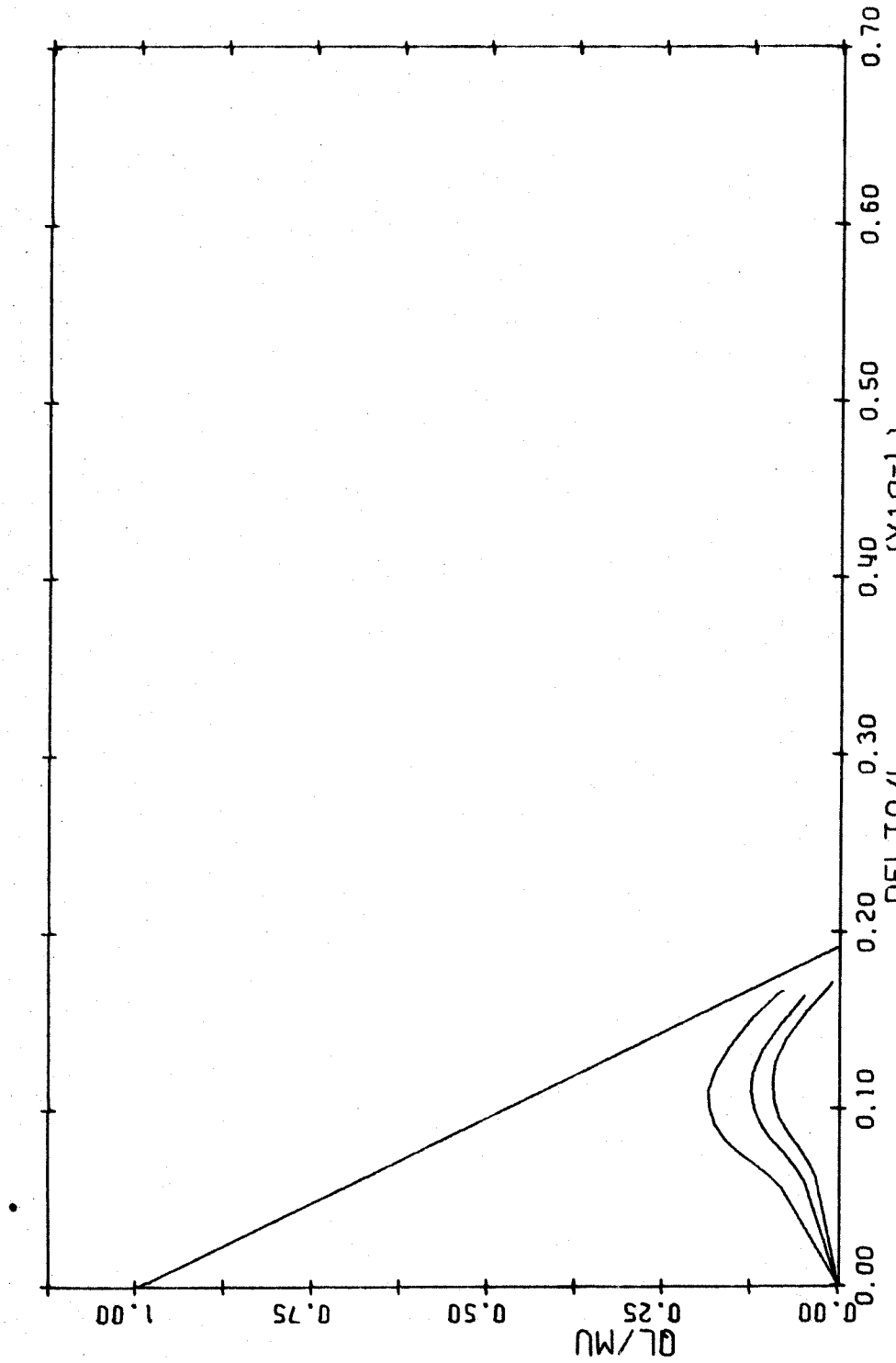

FIG. A-133 LOAD DEFLECTION DIAGRAM. SPIRAL COLUMN.
L/H=25 P/PC=0.5

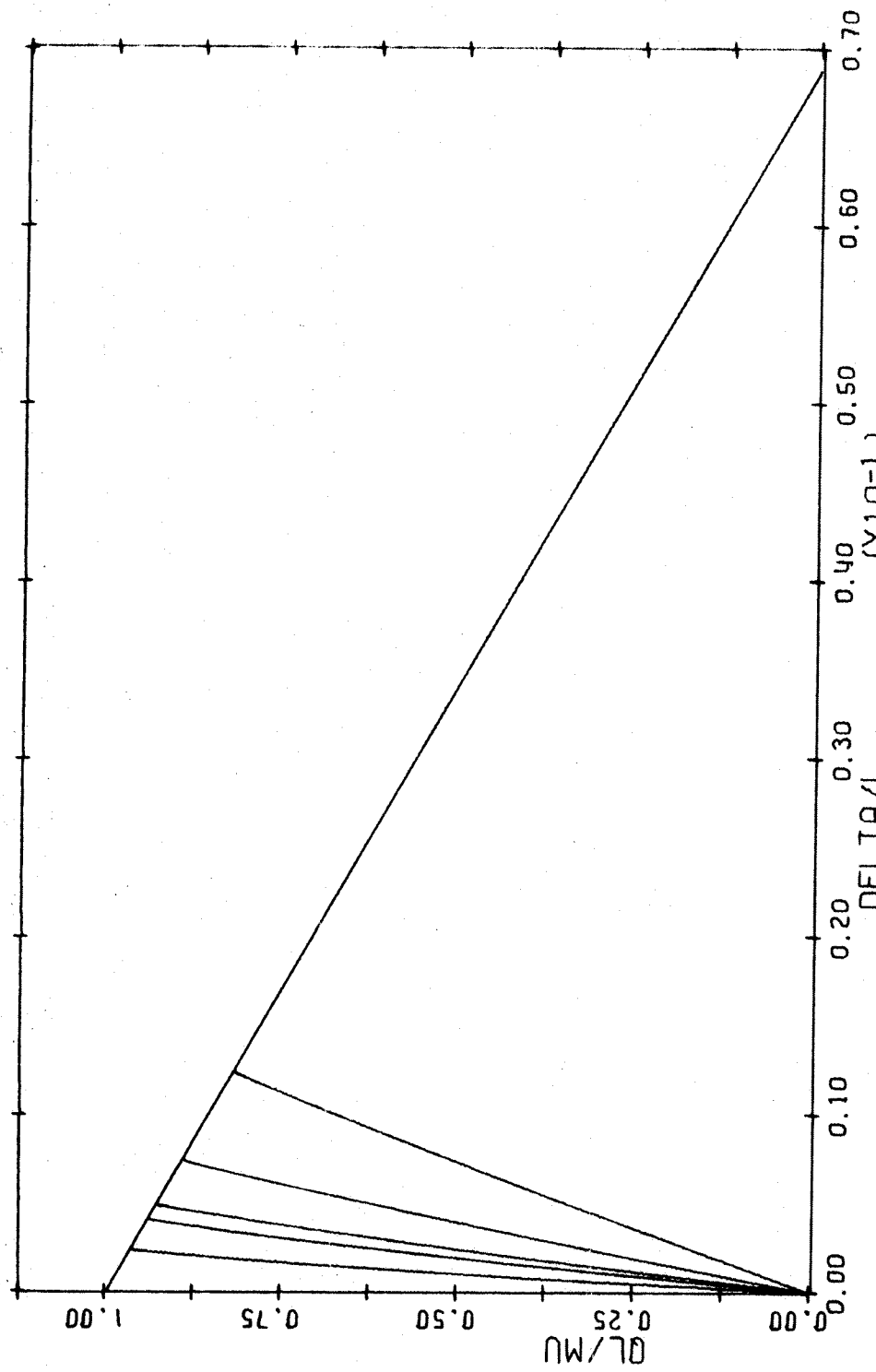

FIG. A-134 LOAD DEFLECTION DIAGRAM. SPIRAL COLUMN.
L/H=5 P/PO=0.6

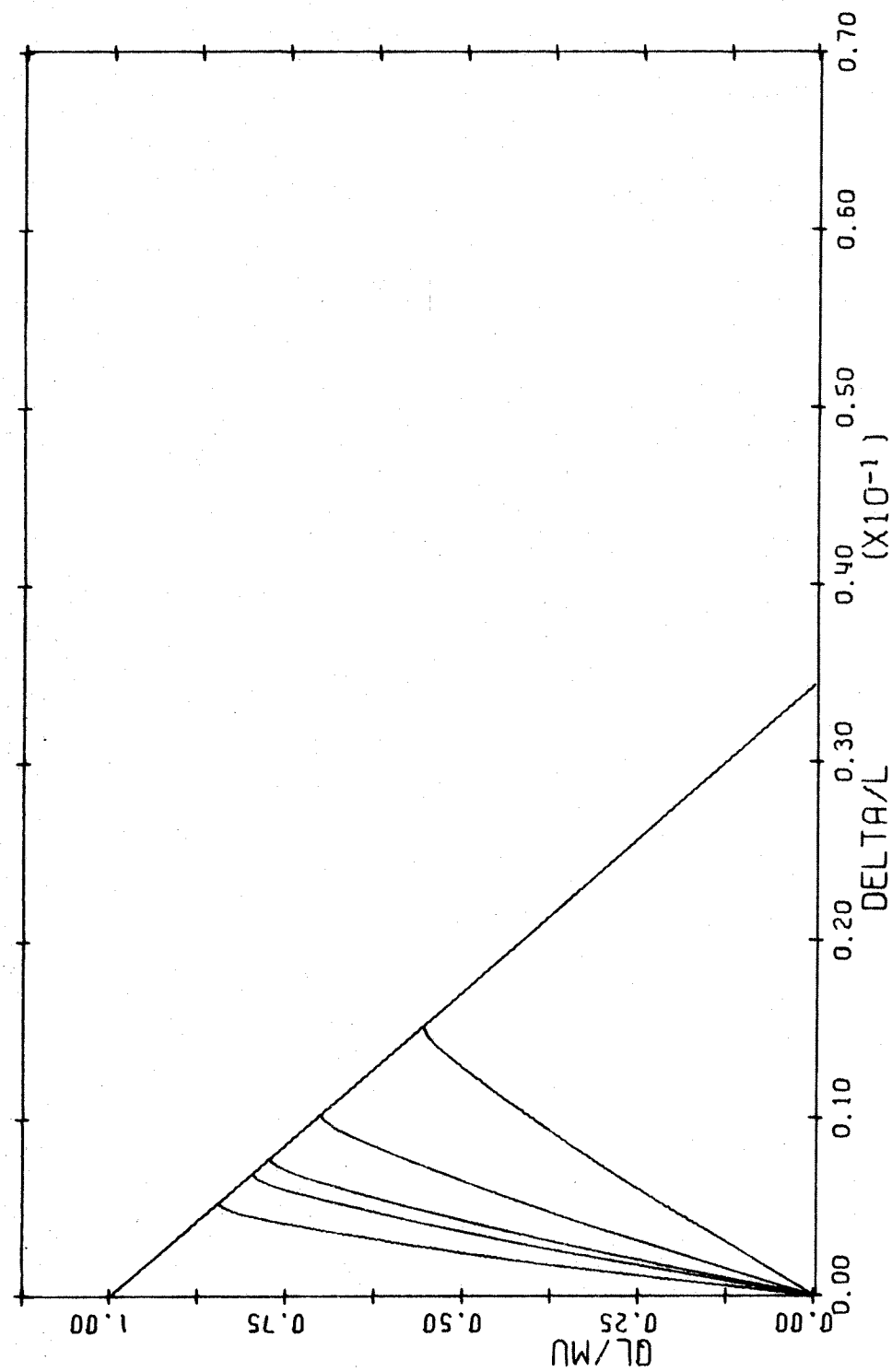

FIG. A-135 LOAD DEFLECTION DIAGRAM. SPIRAL COLUMN.
L/H=10 P/P0=0.5

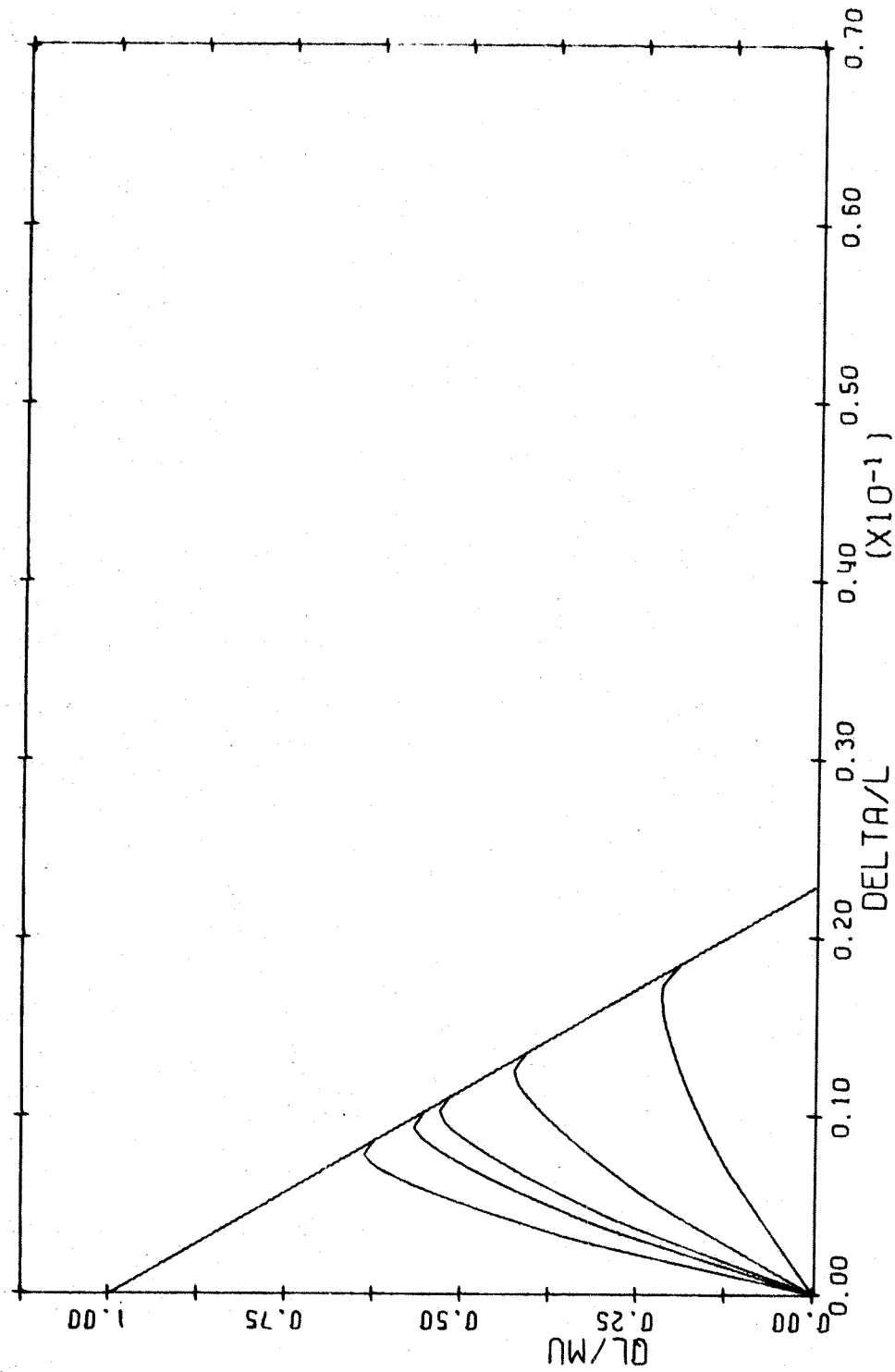

FIG. A-136 LOAD DEFLECTION DIAGRAM. SPIRAL COLUMN.
L/H=15 P/P0=0.6

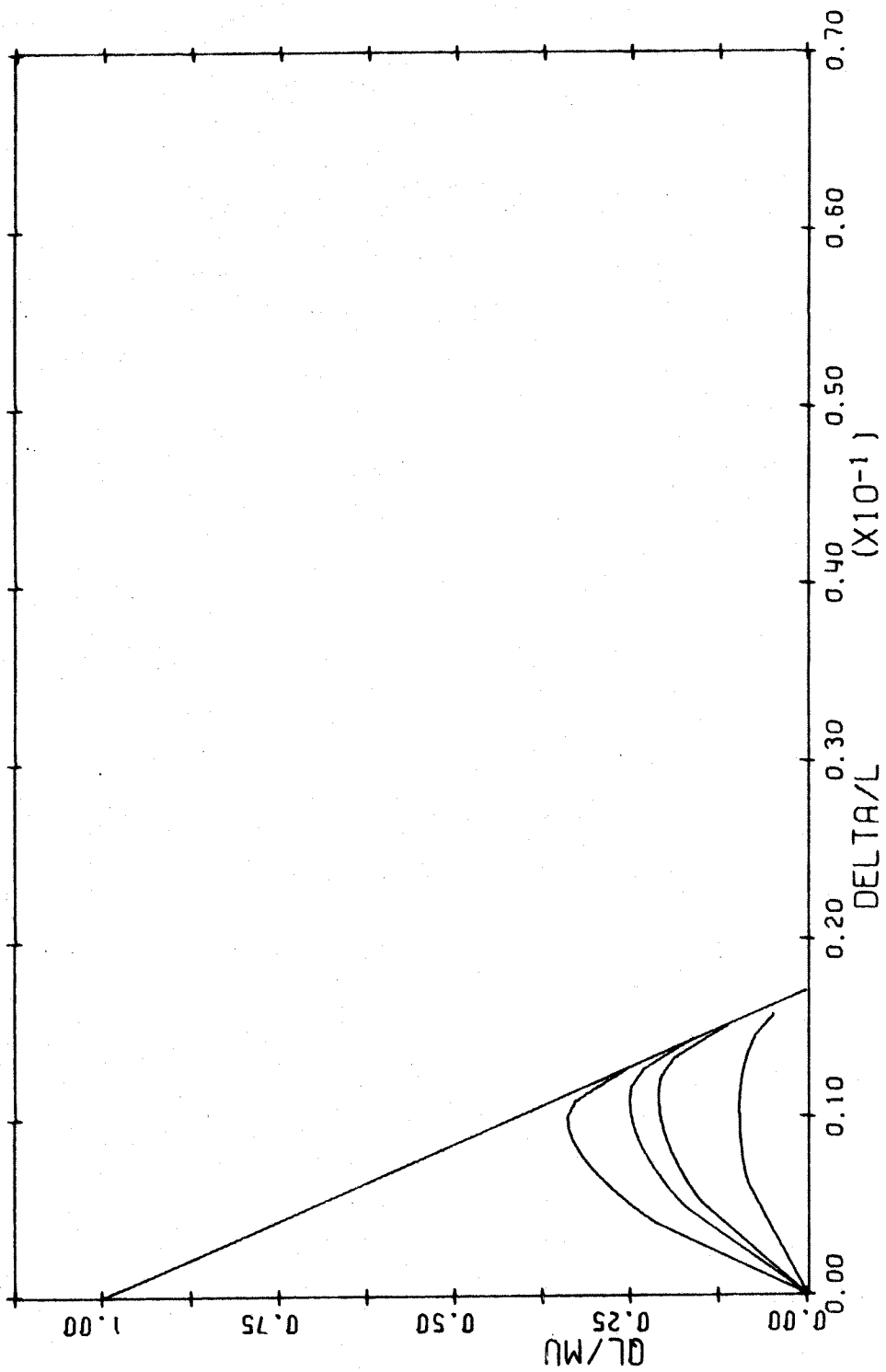

FIG. A-137 LOAD DEFLECTION DIAGRAM. SPIRAL COLUMN.
L/H=20 P/P0=0.5

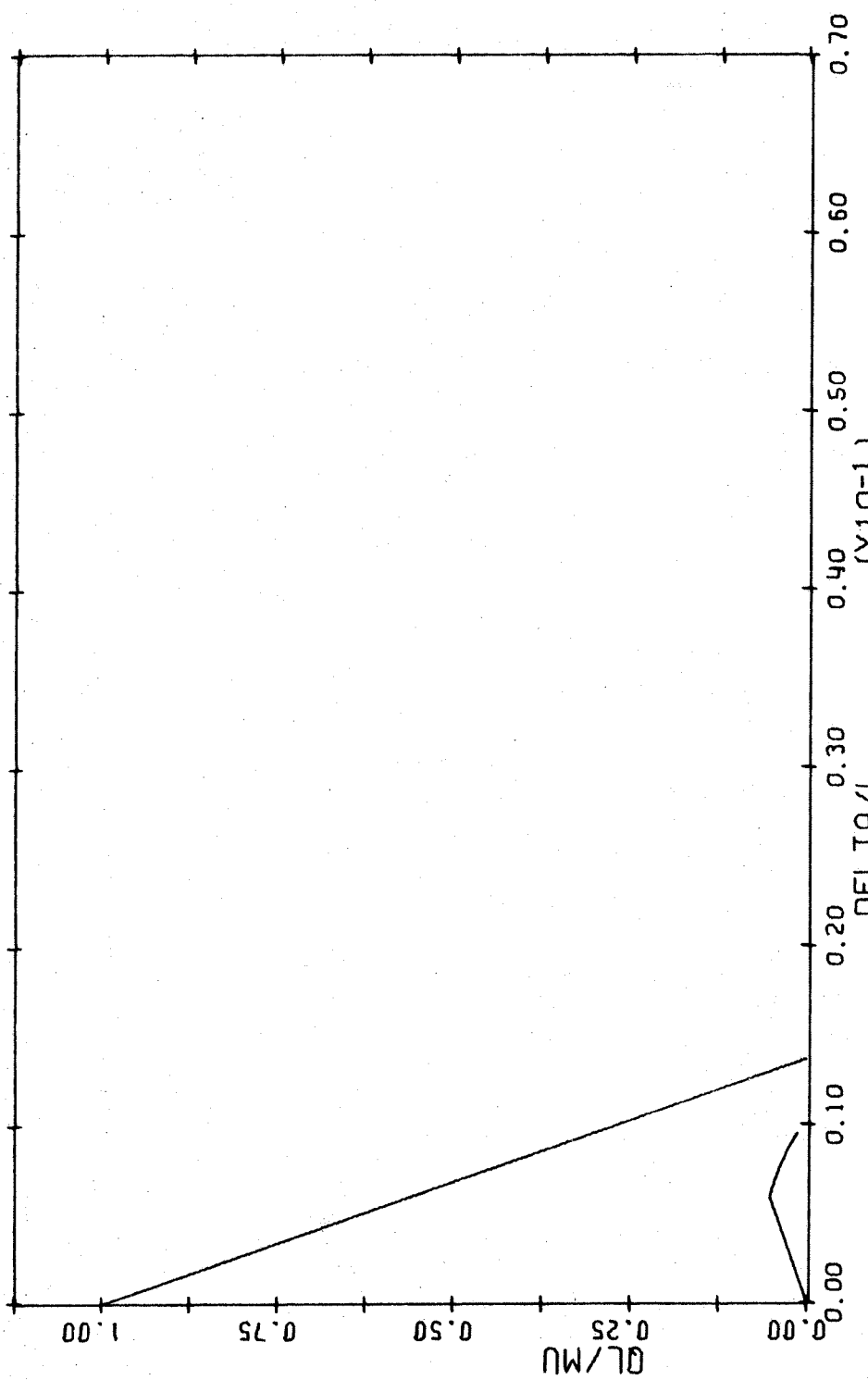

FIG. A-138 LOAD DEFLECTION DIAGRAM. SPIRAL COLUMN.
L/H=25 P/P0=0.6

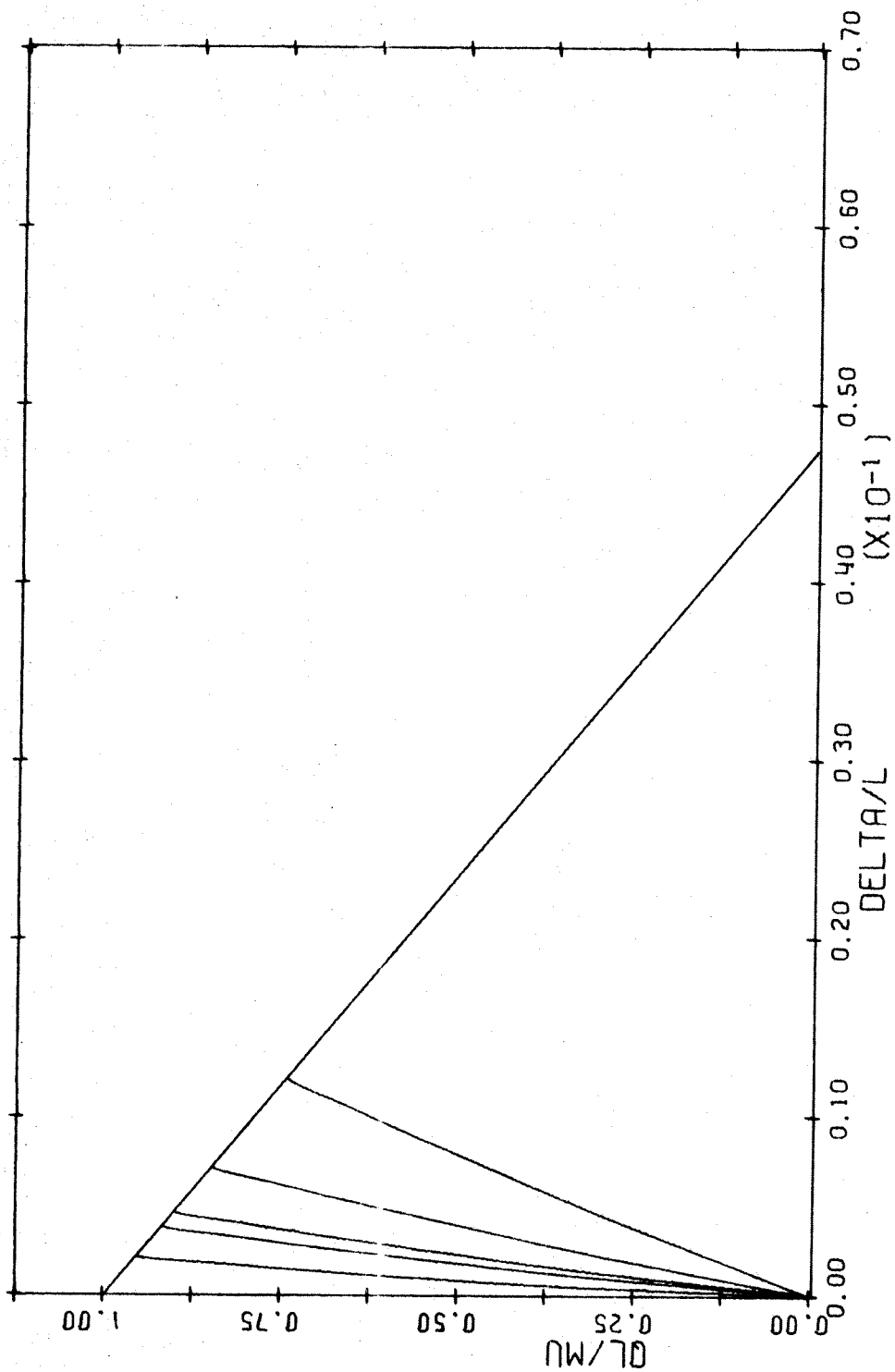

FIG. A-139 LOAD DEFLECTION DIAGRAM. SPIRAL COLUMN.
L/H=5 P/P0=0.7

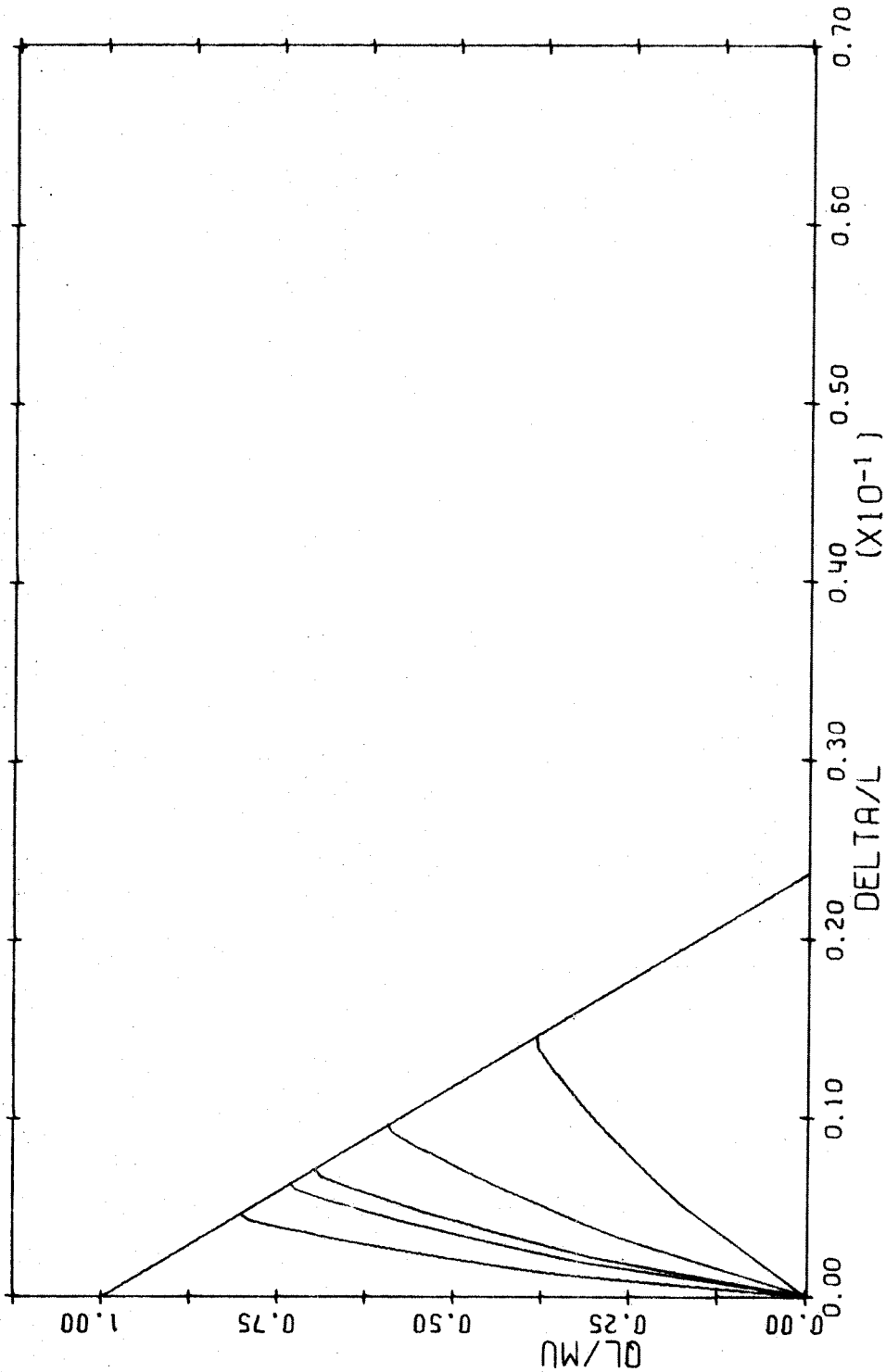

FIG. A-140 LOAD DEFLECTION DIAGRAM. SPIRAL COLUMN.
L/H=10 P/P0=0.7

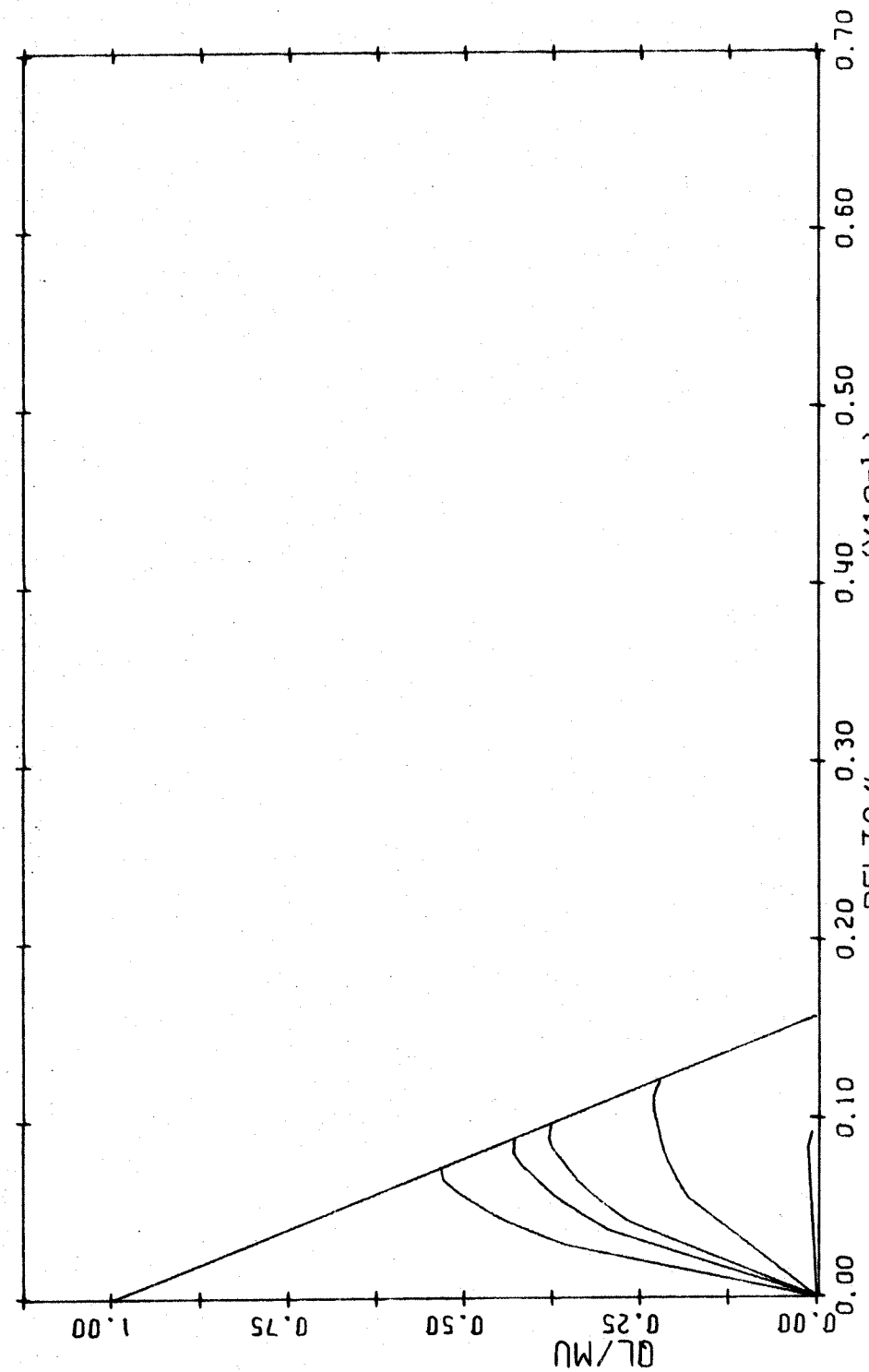

FIG. A-141 LOAD DEFLECTION DIAGRAM. SPIRAL COLUMN.
L/H=15 P/P0=0.7

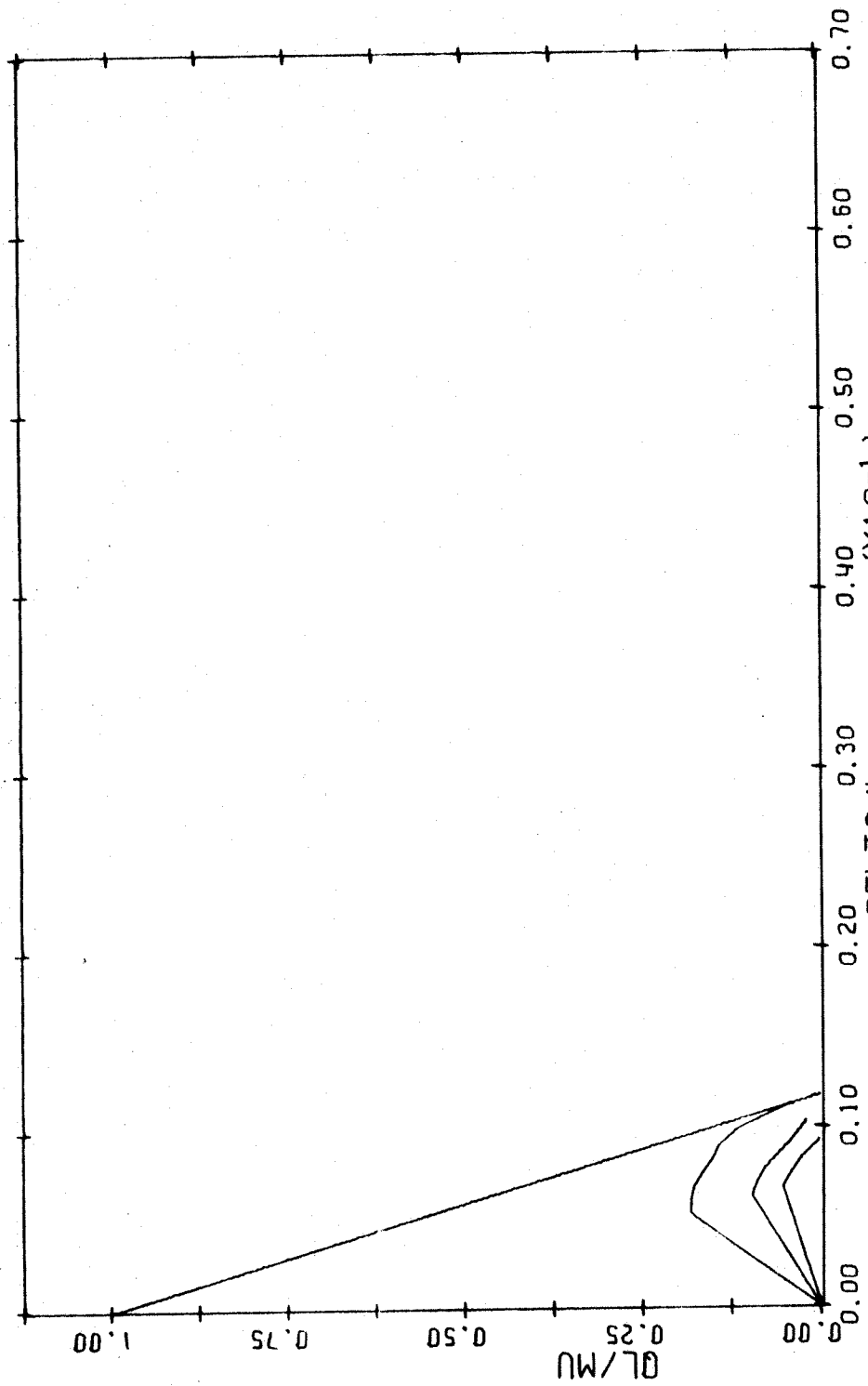

FIG. A-142 LOAD DEFLECTION DIAGRAM. SPIRAL COLUMN.
L/H=20 P/P0=0.7

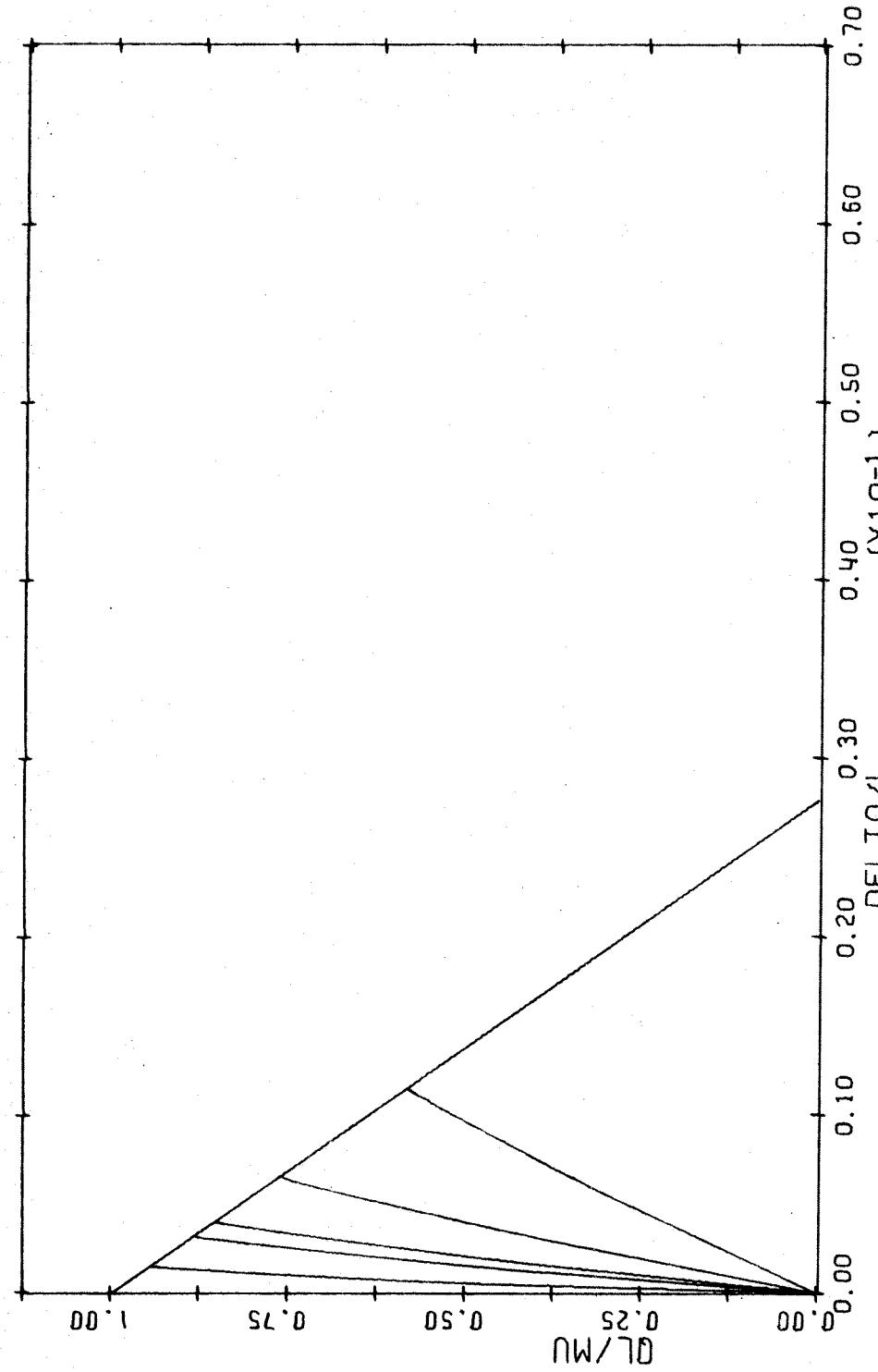

FIG. A-143 LOAD DEFLECTION DIAGRAM. SPIRAL COLUMN.
L/H=5 P/P0=0.8

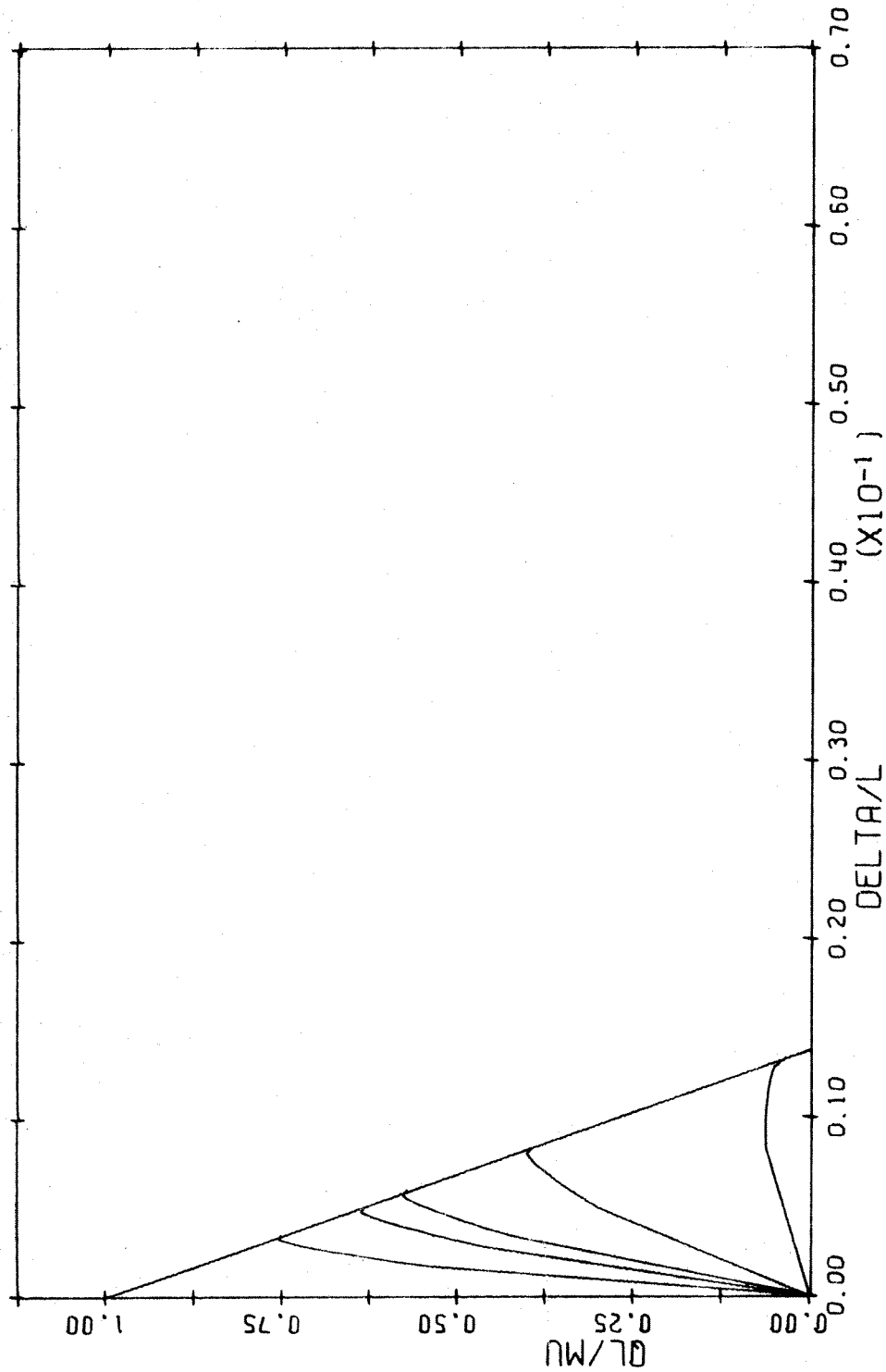

FIG. A-144 LOAD DEFLECTION DIAGRAM. SPIRAL COLUMN.
L/H=10 P/P0=0.8

APPENDIX B

COMPUTER PROGRAMS

B.1 Beam Stiffness Program

B.1.1 General Description

This program is written in FORTRAN and computes the effective elastic stiffness of reinforced concrete beams under gravity load, Lateral load and a combination of the two. The variation in stiffness along the member is taken into account by dividing the beam into a number of short segments which are all of the same length. The moment in each segment is taken as the mean of the moments at the ends of the segment. The EI value of the segment is then determined from the moment-curvature diagram of the cross-section.

When this process has been carried out for all segments the beam is loaded by the M/EI diagram and the conjugate beam theorem is used to compute the flexibility coefficients. The rotational stiffness coefficients are then determined by inverting the flexibility matrix.

The beam is assumed to be divided into three sections, two end sections and a middle section, and the cross-sectional properties are assumed to be the

same within any one section.

When the beam carries gravity load the moments produced by these loads are computed assuming fixed ends.

B.1.2 Input Data

The program can handle any type of moment-curvature diagram with a positive slope. However, non-linear curves must be approximated by a series of straight lines and the coordinates at all points where a change in slope occurs must be read in. The number of points must not exceed 99. The coordinates of the origin are not read in.

The load intensity is specified as a fraction of the moment capacity of the end segment. For gravity loads this fraction is given by the ratio $wl_b^2/12M_u$ where w is the uniformly distributed load, l_b is the length of the beam and M_u is the moment capacity of the end segment. For lateral loads it is given by the ratio of the sway moment to the ultimate moment of the end segment. When the beam is carrying both gravity load and lateral load the sum of the two ratios must not exceed 1.0.

All units are in pounds and inches.

The following input parameters are required:

1. Type of loading.
2. Number of load cases
3. Gravity load.
4. Lateral load
5. Number of segments. All segments are of the same length.
6. Number of segments in left hand end section.
7. Number of segments in middle section.
8. Number of segments in right hand end section.
9. Number of points on M-ϕ curves.
10. EI for gross concrete section.
11. Moment and curvature coordinates of M-ϕ curves.

A detailed description of the input data required starts on the next page.

Card Column	Name used in Program	DATA DESCRIPTION	FORTRAN Format
	CASE	Type of loading. for gravity load only, 2 for lateral load only and 3 for combined loading.	I
2-80	--	Blank	
1-2	NBETA	Number of load cases. NBETA 10.	I2
3-80	--	Blank	
1.80	ALPHA(I)	Ratio of fixed end moment capacity of end segment. Omit if CASE=2. Number of entries equals NBETA. Combine on new card if NBETA >8.	8F 10.0
1-80	BETA(I)	Ratio of sway moment to moment capacity of end segment. Number of entries equals NBETA. Omit if LCASE=1 . Continue on new card if NBETA>8.	8F 10.0
1-5	NSEG	Number of segments which the beam has been divided into.	I5
6-10	NSEG	Number of segments in left hand end section.	I5
11-15	NSEG2	Number of segments in middle section.	I5
16-20	NSEG3	Number of segments in right hand end section.	I5
21-80	--	Blank	

Card Column	Name used in Program	DATA DESCRIPTION	FORTRAN Format
1-5	NP(IJ)	Number of points on M-ϕ curve for positive bending in left hand end section.	I5
6-10	NP(IJ)	Same as above; but for negative bending.	I5
11-80	--	Blank	
1-5	NP(IJ)	Number of points on M-ϕ curve for positive bending in middle section.	I5
6-10	NP(IJ)	Same as above, but for negative bending.	I5
11-80	--	Blank	
1-5	NP(I,J)	Number of points on M-ϕ curve for positive bending in right hand end section.	I5
6-10	NP(I,J)	Same as above, but for negative bending.	I5
11-80	--	Blank	
1-15	ECIG	EI for gross concrete section.	F15.5
16-80	--	Blank	
1-10	EM	Moment coordinate of point on M-ϕ curve for positive bending. Left hand end section.	F10.0
11-20	PHI	Curvature coordinate for same Number of cards= number of points on curve.	F10.0
21-80	--	Blank	

B.1.3 Output

The program prints out the stiffness matrix and the stiffness coefficients. It also prints out the effective elastic EI value for each end of the beam. The units are pounds and inches.

B.1.4 Listing of Program

A listing of the computer program starts on the next page.

```
      DIMENSION NP(99,20),BETA(10),EM(99,2,15),PHI(99,2,15),
     1SM(99,10),THETA(2,2),TM(99,20),EI(99,20),S(2,2),SI(2,2)
      DIMENSION GM(99,10),ALPHA(10)
      DIMENSION ETI(90,10)
C ***
C *** LCASE=1: GRAVITY LOAD ONLY
C *** LCASE=2: LATERAL LOAD ONLY
C *** LCASE=3: GRAVITY LOAD AND LATERAL LOAD COMBINED
C ***
      READ(5,901)LCASE
      READ(5,903)NBETA
      IF(LCASE.EQ.2) GO TO 1
C ***
C *** READ RATIO OF F.E.M. TO ULTIMATE MOMENT OF END SEGMENT
C ***
      READ(5,904)(ALPHA(I),I=1,NBETA)
      IF(LCASE.EQ.1) GO TO 2
C ***
C *** READ RATIO OF SWAY MOMENT TO ULTIMATE MOMENT OF END SEGMENT
C ***
C *** NOTE THAT ALPHA(L)+BETA(L) MUST BE LESS OR EQUAL TO 1.0
C ***
    1 READ(5,904) (BETA(I),I=1,NBETA)
    2 READ(5,900) NSEG,NSEG1,NSEG2,NSEG3
C ***
C *** READ NO. OF POINTS ON M-PHI CURVES, NP(I,J).
C *** I IS THE SEGMENT NUMBER.
C *** J=1 REFERS TO THE M-PHI CURVE FOR POSITIVE BENDING.
C *** J=2 REFERS TO THE M-PHI CURVE FOR NEGATIVE BENDING.
C ***
      KOUNT=0
      READ(5,900) (NP(1,J),J=1,2)
      READ(5,900) (NP(NSEG1+1,J),J=1,2)
      N=NSEG=NSEG3+1
      READ(5,900) (NP(N,J),J=1,2)
      DO 39 I=2,NSEG1
      NP(I,1)=NP(1,1)
   39 NP(I,2)=NP(1,2)
      N=NSEG1+2
      NN=NSEG1+NSEG2
      DO 40 I=N,NN
      NP(I,1)=NP(N-1,1)
   40 NP(I,2)=NP(N-1,2)
      NNN=NN+2
      DO 41 I=NNN,NSEG
      NP(I,1)=NP(NN+1,1)
   41 NP(I,2)=NP(NN+1,2)
      READ(5,913) ECIG
C ***
C *** READ M-PHI COORDINATES (MOMENTS IN LB-IN)
C ***
      DO 3 J=1,2
      NP1=NP(1,J)
      DO 3 K=1,NP1
    3 READ(5,904) EM(1,J,K),PHI(1,J,K)
      DO 42 I=2,NSEG1
      DO 42 J=1,2
```

```
      NP1=NP(I,J)
      DO 42 K=1,NP1
      EM(I,J,K)=EM(1,J,K)
   42 PHI(I,J,K)=PHI(1,J,K)
      DO 43 J=1,2
      NP1=NP(NSEG1+1,J)
      DO 43 K=1,NP1
   43 READ(5,904) EM(NSEG1+1,J,K),PHI(NSEG1+1,J,K)
      DO 44 I=N,NN
      DO 44 J=1,2
      NP1=NP(I,J)
      DO 44 K=1,NP1
      EM(I,J,K)=EM(NSEG1+1,J,K)
   44 PHI(I,J,K)=PHI(NSEG1+1,J,K)
      DO 45 J=1,2
      NP1=NP(NSEG-NSEG3+1,J)
      DO 45 K=1,NP1
   45 READ(5,904) EM(NSEG-NSEG3+1,J,K),PHI(NSEG-NSEG3+1,J,K)
      N2=NSEG1+NSEG2+2
      DO 46 I=N2,NSEG
      DO 46 J=1,2
      NP1=NP(I,J)
      DO 46 K=1,NP1
      EM(I,J,K)=EM(NSEG1+NSEG2+1,J,K)
   46 PHI(I,J,K)=PHI(NSEG1+NSEG2+1,J,K)
C ***
C *** READ LENGTH OF BEAM (BL) IN INCHES
C ***
      READ(5,902) BL
      WRITE(6,921)
      WRITE(6,922)
      WRITE(6,905)LCASE
      IF(LCASE.EQ.2) GO TO 31
      WRITE(6,927)
      WRITE(6,907) (ALPHA(I),I=1,NBETA)
      IF(LCASE.EQ.1) GO TO 38
   31 WRITE(6,910)
      WRITE(6,907) (BETA(I),I=1,NBETA)
   38 WRITE(6,923)BL
      WRITE(6,909) NSEG
      WRITE(6,914)ECIG
      WRITE(6,912)
      WRITE(6,924)
      WRITE(6,925)
      WRITE(6,911)
      SEGL=BL/NSEG
      X=0.
      IF(LCASE.EQ.2) GO TO 4
      DO 5 K=1,NBETA
      X=0.0
      NP1=NP(1,2)
      GL=12.0*ALPHA(K)*EM(1,2,NP1)/(BL**2)
      GM1=-GL*BL**2/12.
      X=X+SEGL
      DO 5 I=1,NSEG
      GM2=GL*(6.0*BL*X-BL**2-6.0*X**2)/12.0
      GM(I,K)=(GM1+GM2)/2.0
      X=X+SEGL
    5 GM1=GM2
      DO 81 L=1,NBETA
```

```
122        81 WRITE(6,931) GM(1,L),GM(NSEG,L)
123         4 IF(LCASE.EQ.1) GO TO 6
124           K=NP(1,2)
125           DO 7 L=1,NBETA
126           X=SEGL
127           SM1=BETA(L)*EM(1,2,K)
128           DO 7 I=1,NSEG
129           SM2=BETA(L)*EM(I,2,K)*((2.0*(BL-X)/BL)-1.0)
130           SM(I,L)=(SM1+SM2)/2.0
131           SM1=SM2
132         7 X=X+SEGL
133           IF(LCASE.GT.1, GO TO 9
134         6 DO 10 L=1,NBETA
135           DO 10 I=1,NSEG
136        10 TM(I,L)=GM(I,L)
137           GO TO 14
138         9 IF (LCASE.EQ.3) GO TO 11
139           DO 12 I=1,NSEG
140           DO 12 J=I,NBETA
141        12 TM(I,J)=SM(I,J)
142           GO TO 14
143        11 DO 13 I=1,NSEG
144           DO 13 J=1,NBETA
145        13 TM(I,J)=GM(I,J)+SM(I,J)
146      C ***
147      C *** COMPUTE EI FOR  EACH ELEMENT
148      C ***
149        61 M=0
150        14 IF (LCASE.GT.1) GO TO 15
151           DO 16 L=1,NBETA
152           DO 16 I=1,NSEG
153           J=2
154           IF(TM(I,L).GT.0.0) J=1
155           IF(ABS(TM(I,L)).GT.EM(I,J,1)) GO TO 17
156           N1=NP(I,J)
157           IF((TM(I,L)-EM(I,J,N1)).GT.10.0) GO TO 200
158           M=L
159           EI(I,L)=EM(I,J,1)/PHI(I,J,1)
160           GO TO 16
161       200 EI(I,L)=0.00000000000001
162           WRITE(6,933)I,BETA(L),ALPHA(L)
163           GO TO 16
164        17 N=2
165        19 IF(ABS(TM(I,L)).GT.EM(I,J,N)) GO TO 18
166           EI(I,L)=(EM(I,J,N)-EM(I,J,N-1))/(PHI(I,J,N)-PHI(I,J,N-1))
167           GO TO 16
168        18 N=N+1
169           IF(N.GT.N1) GO TO 203
170           GO TO 19
171       203 EI(I,L)=0.000000000001
172        16 CONTINUE
173           GO TO 34
174        15 DO 21 L=1,NBETA
175           DO 21 I=1,NSEG
176           J=2
177           IF(TM(I,L).GT.0.) J=1
178           N1=NP(I,J)
179           IF((TM(I,L)-EM(I,J,N1)).GT.10.0) GO TO 201
180           M=L
181           IF(ABS(TM(I,L)).GT.EM(I,J,1)) GO TO 22
```

```
182           EI(I,L)=EM(I,J,1)/PHI(I,J,1)
183           GO TO 21
184       201 EI(I,L)=0.00000000000001
185           WRITE(6,933)I,BETA(L),ALPHA(L)
186           GO TO 21
187        22 N=2
188        23 IF(ABS(TM(I,L)).GT.EM(I,J,N)) GO TO 24
189           EI(I,L)=(EM(I,J,N)-EM(I,J,N-1))/(PHI(I,J,N)-PHI(I, J,N-1))
190           GO TO 21
191        24 N=N+1
192           IF(N.GT.N1) GO TO 202
193           GO TO 23
194       202 EI(I,L)=0.00000000000001
195        21 CONTINUE
196        34 CONTINUE
197           IF(KOUNT.EQ.0) GO TO 72
198           DO 71 L=1,NBETA
199           DO 71 I=1,NSEG
200           IF(EI(I,L).GT.EII(I,L)) EI(I,L)=EII(I,L)
201        71 CONTINUE
202        72 CONTINUE
203           KOUNT=KOUNT+1
204           CALL        ANCOL(SEGL,EI,NBETA,NSEG,TM,LCASE,GL,SM,GM,BL,ALPHA,NP,
205          1 EM)
206           DO 70 L=1,NBETA
207           DO 70 I=1,NSEG
208        70 EII(I,L)=EI(I,L)
209           IF(KOUNT.LT.5) GO TO 61
210     C ***
211     C *** COMPUTE OVERALL BEAM STIFFNESS USING CONJUGATE BEAM METHOD
212     C ***
213     C ***
214     C *** UNIT MOMENT AT LEFT END (1)
215     C ***
216           DO 29 L=1,M
217           THETA(1,1)=0.0
218           THETA(2,1)=0.0
219           THETA(2,2)=0.0
220           THETA(1,2)=0.0
221           X=SEGL/2.0
222           DO 26 I=1,NSEG
223           THETA(1,1)=THETA(1,1)+(((BL-X)/BL)**2)*(SEGL/EI(I,L))
224           THETA(2,1)=THETA(2,1)-(((BL-X)/BL)*(X/BL))*(SEGL/EI(I,L))
225        26 X=X+SEGL
226     C ***
227     C *** UNIT MOMENT AT RIGHT END (2)
228     C ***
229           X=SEGL/2.0
230           DO 27 I=1,NSEG
231           THETA(2,2)=THETA(2,2)+((X/BL)**2)*(SEGL/EI(I,L))
232           THETA(1,2)=THETA(1,2)-((X/BL)*(BL-X)/BL)*(SEGL/EI(I,L))
233        27 X=X+SEGL
234           DET=THETA(1,1)*THETA(2,2)-THETA(2,1)*THETA(1,2)
235           S(1,1)=THETA(2,2)/DET
236           S(1,2)=-THETA(1,2)/DET
237           S(2,1)=-THETA(2,1)/DET
238           S(2,2)=THETA(1,1)/DET
239           DO 28 I=1,2
240           DO 28 J=1,2
241        28 SI(I,J)=S(I,J)*BL/ECIG
```

```
      WRITE(6,925)
      IF(LCASE.EQ.1) GO TO 37
      IF(LCASE.EQ.3) GO TO 36
      WRITE(6,918)BETA(L)
      GO TO 30
   36 PA =ALPHA(L)/BETA(L)
      WRITE(6,919)PA
      GO TO 30
   37 WRITE(6,920)ALPHA(L)
   30 WRITE(6,909) ((S(I,J),J=1,2),I=1,2)
      WRITE(6,915)
      WRITE(6,916) ((S(I,J),J=1,2),I=1,2)
      WRITE(6,929)
      SLOV4=S(1,1)*BL/4.0
      WRITE(6,925)SLOV4
      SLOV4=S(2,2)*BL/4.0
   29 WRITE(6,930)SLOV4
      DO 50 L=1,NBETA
      WRITE(6,912)
      WRITE(6,907) BETA(L)
      WRITE(6,931) (GM(I,L),I=1,NSEG)
      WRITE(6,932)
      WRITE(6,931) (EI(I,L),I=1,NSEG)
   50 CONTINUE
      CALL EXIT
   20 WRITE(6,917)I,BETA(L),J
      IF(M.GT.1) GO TO 34
  900 FORMAT(1615)
  901 FORMAT(I1)
  902 FORMAT(F10.0)
  903 FORMAT(I2)
  904 FORMAT(8F10.0)
  905 FORMAT(1H0,5X,'TYPE OF LOADING =',I2)
  907 FORMAT(1H0,5X,10F8.2)
  908 FORMAT(1H0,5X,'BEAM IS DIVIDED INTO ',I3,' SEGMENTS')
  909 FORMAT(1H0,5X,1P2E15.4)
  910 FORMAT(1H0,5X,'SWAY MOMENT RATIOS:')
  911 FORMAT(1H0,5X,'ROTATIONAL STIFFNESS COEFFICIENTS:')
  912 FORMAT(1H1)
  913 FORMAT(F15.5)
  914 FORMAT(1H0,5X,'ECIG=',F15.1,' LB-IN**2')
  915 FORMAT(1H0,5X,'STIFFNESS COEFFICIENTS EXPRESSED AS K=SL/LI:')
  916 FORMAT(1H0,5X,1P2E15.4)
  917 FORMAT(1H1,5X,'THE MOMENT IN SEGMENT NO.',I3,' IS GREATER THEN THE
     1ULTIMATE MOMENT OF THE SEGMENT. BETA=',F4.2,'BENDING CODE=',I2)
  918 FORMAT(1H0,5X,'BETA =',F5.2)
  919 FORMAT(1H0,5X,'F.E.M./SWAY MOMENT =',F5.2)
  920 FORMAT(1H0,5X,'ALPHA =',F5.2)
  921 FORMAT(1H0,5X,'I N P U T')
  922 FORMAT(6X,'---------')
  923 FORMAT(1H0,5X,'THE LENGTH OF THIS BEAM IS ',F5.1,' IN')
  924 FORMAT(5X,'O U T P U T')
  925 FORMAT(5X,'----------')
  926 FORMAT(1H0)
  927 FORMAT(1H0,5X,'F.E.M. RATIOS:')
  928 FORMAT(1H0,10X,'LEFT END',1PE15.5)
  929 FORMAT(1H0,5X,'EFFECTIVE ELASTIC EI VALUES:')
  930 FORMAT(1H0,10X,'RIGHT END',1PE15.5)
  931 FORMAT(1H0,1P8E10.2)
  932 FORMAT(////)
```

```
      933 FORMAT(1H0,3X,'STIFFNESS OF ELEMENT',I3,' IS ZERO FOR BETA =',
     1F5.2,' AND ALPHA=',F5.2)
          STOP
          END
          SUBROUTINE ANCOL(SEGL,EI,NBETA,NSEG,TM,LCASE,GL,SM,GM,BL,ALPHA,NP
         1,EM)
          DIMENSION ALPHA(10),NP(99,20),EM(99,2,15)
          DIMENSION SM(99,10),TM(99,20),EI(99,20),GM(99,10)
          DIMENSION FEM(5,50)
          DIMENSION A0(50),XBAR(50),P(30),MY(50),IY(50)
          REAL MY,IY
    C *** COMPUTE CENTROID OF ANALOGOUS COLUMN, AREA AND LOAD
          DO 2 L=1,NBETA
          X=SEGL/2.0
          A=0.0
          B=0.0
          C=0.0
          NPI=NP(1,2)
          GL=12.0*ALPHA(L)*EM(1,2,NPI)/(BL**2)
          DO 1 I=1,NSEG
          A=A+SEGL/EI(I,L)
          B=B+X*SEGL/EI(I,L)
          C=C+(GL*X*(BL-X)*SEGL/(2.0*EI(I,L)))
        1 X=X+SEGL
          XBAR(L)=B/A
          A0(L)=A
          P(L)=C
          WRITE(6,102) XBAR(L),A0(L),P(L)
      102 FORMAT(1H0,5X,1P3E10.3)
        2 CONTINUE
    C *** COMPUTE MY AND IY
          DO 3 L=1,NBETA
          AA=0.0
          BB=0.0
          X=SEGL
          NPI=NP(1,2)
          GL=12.0*ALPHA(L)*EM(1,2,NPI)/(BL**2)
          DO 4 I=1,NSEG
          AA=AA+(GL*X*(BL-X)/2.0)*(X-XBAR(L))/EI(I,L)
          BB=BB+SEGL**3.0/(EI(I,L)*12.0) + SEGL*(X-XBAR(L))**2/EI(I,L)
        4 X=X+SEGL
          MY(L)=AA
          IY(L)=BB
        3 CONTINUE
    C *** COMPUTE FIXED END MOMENTS
          DO 5 L=1,NBETA
          FEM(1,L)=P(L)/A0(L)+MY(L)*(-XBAR(L))/IY(L)
        5 FEM(2,L)=P(L)/A0(L)+MY(L)*(BL-XBAR(L))/IY(L)
          DO 6 L=1,NBETA
        6 WRITE(6,101) FEM(1,L),FEM(2,L)
          IF(LCASE.EQ.2) GO TO 12
          DO 7 L=1,NBETA
          GM1=0.
          X=SEGL
          AB1=ABS(FEM(1,L))
          AB2=ABS(FEM(2,L))
          NPI=NP(1,2)
          GL=12.0*ALPHA(L)*EM(1,2,NPI)/(BL**2)
          DO 8 I=1,NSEG
          GM2=GL*X*(BL-X)/2.0
```

```
      GM(I,L)=(GM1+GM2)/2.0-(AB1+(AB2-AB1)*(X-SEGL/2.0)/BL)
      X=X+SEGL
    8 GM1=GM2
    7 CONTINUE
      IF(LCASE.EQ.3) GO TO 10
      DO 9 L=1,NBETA
      DO 9 I=1,NSEG
    9 TM(I,L)=GM(I,L)
      GO TO 12
   10 DO 11 L=1,NBETA
      DO 11 I=1,NSEG
   11 TM(I,L)=SM(I,L)+GM(I,L)
   12 CONTINUE
  101 FORMAT(1H0,5X,1P2E10.3)
      RETURN
      END
```

B.2 Restrained Column Curves and CDC Program

B.2.1 General Description

The program is written in the FORTRAN programming language.

The first part of the program generates a set of Column Deflection Curves for a given axial load and all the geometrical data of the curves are stored.

In the second part of the program the data of the Column Deflection Curves are used to compute restrained column curves for five values of beam restraint.

When the first two parts have been carried out for all values of axial load specified, the program goes on to compute effective elastic EI values, effective length factors and the ratio of the total end moment and the $P\Delta$-moment.

B.2.2 Input Data

The program can handle any type of M-P-ϕ diagram with a positive slope. However, non-linear curves must be approximated by a series of straight lines and the coordinates of all points where a change in slope occurs must be read in. The last point on M-P-ϕ curves terminating with a negative slope is taken as the point of zero slope. The number of such points must not exceed 24 per curve. The coordinates of the origin are not read in.

Two service load conditions may be analysed with each ultimate load case. The load ratios are read in using an implied DO-loop and the sequence must be as follows:

load case 1 { ultimate; maximum service load; minimum service load }

load case 2 { ultimate; maximum service load; minimum service load }

and so on. Thus,fields 1,4,7 etc. are reserved for ultimate loads, 2,5,8 etc. are reserved for maximum service load and minimum service load are entered in fields 3,6,9 etc. The subscripts for ultimate load are then (1+3n), for maximum service loads the subscripts are (2+3n) and for minimum service load (3+3n) where n is an integer ranging from one to the number of load cases entered. If, for a particular load case, values for one or two of the three load ratios are not to be entered the appropriate fields should be left blank and the input parameters START,END,and STEP should be given values such that the program does not use these load ratios during execution. START, END and STEP specify the subscripts of the load ratios to be used during execution of the program. If eight load cases are to be investigated there can be as many as 24 load ratios. To get the results for ultimate load for load cases one through four START must be equal to one, END must be equal to (1+3x4)-3=10, and STEP equals three. The program will then use the load ratios given the subscripts 1,4,7 and 10. If only mimimum service loads were to be investigated the values would be 3,(3+3x4)-3=12 and 3, respectively.

If the load factors are different from 1.70 and 1.275 lines 115 and 113 must be changed accordingly.

Listed below is an outline of the input data required.

1. Parameters to specify for which axial loads the computations are to be carried out.
2. CDC parameters: initial angle, angle increment and segment length.
3. Column properties: type of column, material properties, steel percentage and cover.
4. Number of M-P-ϕ curves.
5. Number of points on M-P-ϕ curves.
6. Axial load ratios.
7. Moment coordinates of all M-P-ϕ curves.
8. Curvature coordinates of all M-P-ϕ curves.
9. Gross area of concrete cross-section.
10. Values of beam restraints.

A detailed description of the input data required begins on the next page.

```
0001              DIMENSION RSTF(5)
0002              DIMENSION DMAX(40,5)
0003              DIMENSION XX(24),YY(24),BIGQ(24,50,5),BIGD(24,50,5),NA(24,50),
                 1 OMEGA(20),X(500),Y(500),X1(2),Y1(2) ,EMP1(200,50),EMM1(200,50),
                 2NP1(24),DELH(200,50,5),OH2MP(200,50,5),PRAT(24),EM(24,15),PHI(50,1
                 35),
                 3  ALPHO(200),EMM(50),V(50),ALPHA(50),H(50),CAY(6),EMF(50),
                 4KOUNT(24,50),LRAT(50,5),SERVO(24,50,5),SERVD(24,50,5)
0004              INTEGER START,END,STEP
0005              REAL LFAC(24)
0006              REAL MOM
0007              REAL MOM1
0008              REAL KB
0009              INTEGER TYPE
0010              READ(5,169) START,END,STEP
0011              READ(5,148) (OMEGA(IK),IK=1,20)
0012              READ(5,125)ALPHAO,NALPH,ALPHIN,RHO
0013              HC=ALPHIN
0014              DO 221 J=1,50
0015              DO 221 K=1,5
0016            221 LRAT(J,K)=0
                C
                C     ALPHO=FIRST VALUE OF ALPHA,NALPH=NO OF CDCS,ALPIN=INCREMENT
                C     RHO=LENGTH OF SEGMENT,TYPE=1-TIED,=2-SPIRAL,=3-OTHER
                C     READ AND PRINT BASIC COLUMN PROPERTIES
                C
0017              READ(5,100)TYPE,FPC,FY,PT,COV
0018              WRITE(6,101)
0019              WRITE(5,142)
0020              WRITE(6,143)
0021              IF(TYPE.EQ.1) GO TO 1
0022              GO TO 2
0023            1 WRITE(6,102)
0024              GO TO 4
0025            2 IF(TYPE.EQ.2) GO TO 3
0026              WRITE(6,104)
0027              GO TO 4
0028            3 WRITE(6,103)
0029            4 CONTINUE
0030              WRITE(6,105)FPC
0031              WRITE(6,140)FY
0032              WRITE(6,106)PT
0033              WRITE(6,141)COV
                C
                C     READ CO-ORDINATES OF P-M-PHI DIAGRAMS, NO IS NUMBER OF DIAGRAMS
                C
0034              READ(5,110)NO
0035              READ (5,126) (NP1(I),I=1,NO)
0036              READ(5,111) (PRAT(I),I=1,NO)
0037              WRITE(6,132)
0038              WRITE(6,133) (NP1(I),I=1,NO)
0039              WRITE(6,134)
0040              WRITE(6,135) (PRAT(I),I=1,NO)
0041              WRITE(6,136)
0042              WRITE(6,146)
```

```
0083                WRITE(6,137)
0084                WRITE(6,144)
0085                DO 204 I=1,NO
0086                NP=NP1(I)
0087                READ (5,111) (EM(I,J),J=1,NP)
0088                WRITE(6,138) I,PRAT(I)
0089                WRITE(6,110)  (EM(I,J),J=1,NP)
0090              204 CONTINUE
0091                WRITE(6,139)
0092                WRITE(6,145)
0093                DO 205 I=1,NO
0094                NP=NP1(I)
0095                READ(5,111)   (PHI(I,J),J=1,NP)
0096                WRITE(6,138)I,PRAT(I)
0097              205 WRITE(6,131)   (PHI(I,J),J=1,NP)
0098                WRITE(6,112)
                  C
                  C     COMPUTE COLUMN DEFLECTION CURVES. CALCULATIONS BASED ON P 9.10 OF
                  C     LEHIGH NOTES. CALCULATIONS ARE FOR B OR T=1 INCH
                  C
0099                IF(TYPE.EQ.1) GO TO 6
0100                IF(TYPE.EQ.2) GO TO 7
0101                READ(5,113)AG
0102                GO TO 8
0103              6 AG=1.0
0104                GO TO 8
0105              7 AG=0.7854
0106              8 CONTINUE
0107                PO=0.85*FPC*AG*(1.0-PT)+FY*PT*AG
0108                READ(5,119) BSTF(1),BSTF(2),BSTF(3),BSTF(4),BSTF(5)
0109                BSTF(1)=BSTF(1)*1.0E8
0110                BSTF(2)=BSTF(2)*1.0E8
0111                BSTF(3)=BSTF(3)*1.0E8
0112                BSTF(4)=BSTF(4)*1.0E8
0113                BSTF(5)=BSTF(5)*1.0E25
0114                WRITE(6,177)BSTF(1),BSTF(2),BSTF(3),BSTF(4),BSTF(5)
0115                DO 70 I=1,40
0116                DO 70 J=1,5
0117              70 LRAT(I,J)=0
0118             211 DO 301 II=1,24
0119                DO 301 JJ=1,50
0120             301 KOUNT(II,JJ)=0
0121                DO 214 KL=1,24
0122                DO 214 KM=1,50
0123                DO 214 KN=1,5
0124                BIGQ(KL,KM,KN)=0.0
0125             214 BIGD(KL,KM,KN)=0.
0126                DO 216 KA=1,24
0127                DO 216 KZ=1,50
0128             216 MA(KA,KZ)=0
0129                DO 228 I=1,24,3
0130             228 LPAC(I)=1.0
0131                DO 229 I=2,24,3
0132             229 LPAC(I)=1.275
0133                DO 230 I=3,24,3
```

```
0094          230 LFAC(I)=1.7
0095              DO 99 I=START,END,STEP
0096              DO 200 L=1,200
0097              DO 200 J=1,50
0098              DO 200 K=1,5
0099              DELH(L,J,K)=0.
0100          200 OH2MP(L,J,K)=0.
0101              IF(I.GT.6) HC=0.0005
0102              ALPHIN=HC
0103              GO TO 208
0104          212 ALPHIN=ALPHIN+HC
0105              DO 224 JB=1,50
0106          224 KOUNT(I,JB)=0
0107          208 P=PRAT(I)*PO
0108              NP=NP1(I)
                  C
                  C     I GIVES AXIAL LOAD,L GIVES ALPHA(0),J GIVES POINT IN COLUMN
                  C     K GIVES RESTRAINING MOMENT
                  C
0109              NSEG=0
0110              WRITE (6,127)
0111              L=1
0112              IF(L.GT.1) GO TO 9
0113              ALPHO(1)=ALPHAO
0114              GO TO 11
0115            9 ALPHO(L)=ALPHO(L-1)+ALPHIN
0116           11 CONTINUE
0117              DO 97 J=1,40
0118              IF(L.GT.1) GO TO 302
0119              NSEG=NSEG+1
0120          302 CONTINUE
0121              KOUNT(I,J)=KOUNT(I,J) + 1
0122              IF(J.EQ.1) GO TO 12
0123              GO TO 20
0124           12 EMM(1)=P*ALPHO(L)*RHO/2.
                  C
                  C     COMPUTE  PHI(J)=AVG.PHI IN JTH INCREMENT
                  C
0125           13 IF(EMM(J).GT.EM(I,1))GO TO 14
0126              PHIJ=(EMM(J)/EM(I,1))*PHI(I,1)
0127              GO TO 18
0128           14 N=2
0129           16 IF(EMM(J).GT.EM(I,N)) GO TO 15
0130              PHIJ=PHI(I,N-1)+((EMM(J)-EM(I,N-1))/(EM(I,N)-EM(I,N-1)))*
                 1 (PHI(I,N)-PHI(I,N-1))
0131              GO TO 18
0132           15 N=N+1
0133              IF(N.GT.NP) GO TO 17
0134              GO TO 16
0135           17 CONTINUE
0136              IF(H(J).LT.25.) GO TO 300
0137              GO TO 98
0138           18 IF(J.GT.1) GO TO 21
0139              V(1)=RHO*ALPHO(L)-RHO**2*PHIJ/2.
0140              ALPHA(1)=ALPHO(L)-RHO*PHIJ
```

```
0141                H(1)=RHO
0142                GO TO 23
0143             20 EMM(J)=P*V(J-1)+P*ALPHA(J-1)*RHO/2.
0144                EMM1(L,J)=EMM(J)
0145                GO TO 13
0146             21 V(J)=(V(J-1)*ALPHA(J-1)*RHO)-(RHO**2*PHIJ/2.)
0147                ALPHA(J)=ALPHA(J-1)-RHO*PHIJ
0148                IF(ALPHA(J).LT.0.) GO TO 98
0149                H(J)=H(J-1)+RHO
0150             23 VOVRH=V(J)/H(J)
0151                GAMMA=VOVRH-ALPHA(J)
0152                EME(J)=V(J)*P
0153                EME1(L,J)=EME(J)
0154                IF(EMM(J).GT.EM(I,NP)) GO TO 17
0155                IF(J.EQ.1) GO TO 500
0156                IF(EMM(J).LT.EMM(J-1)) GO TO 98
0157            500 CONTINUE
                C
                C     COMPUTE QH/2MPC VS DELTA/H AS PER PAGES 18.8 TO 18.10 OF LEHIGH
                C     NOTES WITH MP=2*MN. CAY(I)=K=STIFFNESS OF RESTRAINT
                C
0158                DO 97 K=1,5
0159                CAY(K)=3.0*BSTF(K)/EM(I,NP)
0160                IF(EME(J).GT.EM(I,NP)) EME(J)=EM(I,NP)
0161                THETA=EME(J)/(CAY(K)*EM(I,NP))
0162                DELH(L,J,K)=THETA*GAMMA
0163                QH2MP(L,J,K)=(EME(J)-P*DELH(L,J,K)*H(J))/EM(I,NP)
0164             97 CONTINUE
0165                GO TO 98
0166             98 L=L+1
0167                IF(L..LT.100) GO TO  9
0168                DO 232 L=1,100
0169                DO 232 J=1,50
0170                DO 232 K=1,5
0171                DELH(L,J,K)=0.0
0172            232 QH2MP(L,J,K)=0.0
0173                GO TO 212
                C
                C     PRINT OUT SWAY SUBASSEMBLAGE VALUES FOR A GIVEN VALUE OF P
                C
0174            300 CONTINUE
0175                WRITE(6,115)PRAT(I),P,EM(I,NP)
0176                MN=0
0177                M1=0
0178                DO 152 J=5,NSEG,5
0179                NCUPVP=1
0180                M1=M1+5
0181                MM=1
0182                DO 151 K=1,5
0183                WRITE(6,121)H(J),CAY(K)
0184                WRITE(6,122)
0185                KOUNT1=KOUNT(I,J)
0186                MD=1
0187                KK=1
0188                X(1)=0.
```

```
0189              Y(1)=0.
0190              DO 150 L=1,KOUNT1,KK
0191              IF(NN.GT.1) GO TO 150
0192              IF(ENE1(L,J).GT.EM(I,NP))GO TO 206
0193              IF(QH2MP(L,J,K).LE.0.) GO TO 218
0194              IF(DELH(L,J,K).LT.DELH(L-1,J,K))  GO TO 218
0195              IF(LFAC(I).GT.1.0) GO TO 215
0196              WRITE(6,123) QH2MP(L,J,K),DELH(L,J,K)
0197              IF(QH2MP(L,J,K).LT.BIGQ(I,J,K).OR.DELH(L,J,K).LT.BIGD(I,J,K))
                 1GO TO 215
0198              BIGQ(I,J,K)=QH2MP(L,J,K)
0199              BIGD(I,J,K)=DELH(L,J,K)
0200          215 ND=ND+1
0201              X(ND)=DELH(L,J,K)
0202              Y(ND)=QH2MP(L,J,K)
0203              GO TO 150
0204          206 CONTINUE
0205              IF(DELH(L,J,K).LT.DELH(L-1,J,K)) GO TO 218
0206              IF(LFAC(I).GT.1.0) GO TO 213
0207              WRITE(6,147) QH2MP(L,J,K),DELH(L,J,K),ENE1(L,J)
0208              IF(QH2MP(L,J,K).LT.BIGQ(I,J,K).OR.DELH(L,J,K).LT.BIGD(I,J,K))
                 1GO TO 213
0209              BIGQ(I,J,K)=QH2MP(L,J,K)
0210              BIGD(I,J,K)=DELH(L,J,K)
0211          213 ND=ND+1
0212              X(ND)=DELH(L,J,K)
0213              Y(ND)=QH2MP(L,J,K)
0214              NN=NN+1
0215              GO TO 218
0216          150 CONTINUE
0217          218 NN=1
0218              NF=NCURVE
0219              LRAT(J,K)=LRAT(J,K)+1
0220              IF(LFAC(I).GT.1.0) GO TO 231
0221              SERVQ(I,J,K)=BIGQ(I,J,K)
0222              SERVD(I,J,K)=BIGD(I,J,K)
0223              GO TO 223
0224          231 SERV=DMAX(J,K)/LFAC(I)
0225              IF(SERV.LE.0.0) GO TO 151
0226              L=1
0227          225 IF(QH2MP(L,J,K).GE.SERV)GO TO 226
0228              L=L+1
0229              GO TO 225
0230          226 SERVD(I,J,K)=DELH(L-1,J,K)+((DFLH(L,J,K)-DELH(L-1,J,K))*(SERV-
                 1 QH2MP(L-1,J,K))/(QH2MP(L,J,K)-QH2MP(L-1,J,K)))
0231              SERVQ(I,J,K)=SERV
0232          223 CONTINUE
0233              IF(ND.EQ.1) GO TO 151
0234              IF(SERVQ(I,J,K).EQ.0.0.OR.SERVD(I,J,K).EQ.0.0) GO TO 311
0235              WRITE(2,188)PRAT(I),SERVQ(I,J,K),SERVD(I,J,K),H(J),CAY(K),LFAC(I)
0236          311 CONTINUE
0237              NCURVE=NCURVE+1
0238              NA(I,J)=NA(I,J)+1
0239          151 CONTINUE
0240              A=J*RHO
```

```
0241              X1(1)=0.
0242              Y1(1)=1.
0243              X1(2)=EM(I,NP)/(P*A)
0244              Y1(2)=0.
0245              IF(X1(2).LE.0.0695) GO TO 207
0246              X1(2)=0.0695
0247              Y1(2)=1.0-0.0695*P*A/EM(I,NP)
0248          207 NP=NP+1
0249              IF(ND.EQ.1) GO TO 152
0250          152 CONTINUE
0251           99 CONTINUE
0252              DO 220 J=5,40,5
0253              WRITE(3,162)
0254              DO 220 K=1,5
0255              WRITE(3,163)
0256              WRITE(3,168)H(J),RSTF(K)
0257              WRITE(3,165)
0258              WRITE(3,166)
0259              LOADR=LRAT(J,K)
0260              I=START
0261              DO 220 ISV=1,LOADR
0262              IF(ISV.GT.1) I=I+3
0263              IF(BIGQ(I,J,K).LE.0.0.OR.BIGD(I,J,K).LE.0.0) GO TO 220
0264              NP=NP1(I)
0265              P=PRAT(I)*PO
0266              KR=RSTF(K)
0267              DELTA=BIGD(I,J,K)*H(J)
0268              MOM=BIGQ(I,J,K)*EM(I,NP)+PRAT(I)*PO*DELTA
0269              EI=MOM*H(J)**2/(3.0*DELTA-(MOM*H(J)/KR))
0270              QL=BIGQ(I,J,K)*EM(I,NP)
0271              EFFL=9.8696*EI*(1.0-(QL/MOM))/((H(J)**2)*P)
0272              EMOVPD=MOM/(BIGD(I,J,K)*H(J)*PRAT(I)*PO)
0273              WRITE(3,167) PRAT(I),BIGQ(I,J,K),BIGD(I,J,K),MOM,EMOVPD,EI,EFFL
0274          220 CONTINUE
0275              YY(11)=1.0
0276              XX(11)=0.0
0277              DO 217 KC=1,10
0278          217 YY(KC)=PRAT(KC)
0279          100 FORMAT(1X,I1,2F10.2,2F10.4)
0280          101 FORMAT(1H1,'COLUMN DEFLECTION AND SWAY SUBASSEMBLY CURVES'///)
0281          102 FORMAT(5X,'TYPE - TIED COLUMN')
0282          103 FORMAT(5X,'TYPE - SPIRAL COLUMN')
0283          104 FORMAT(5X,'TYPE - SPECIAL')
0284          105 FORMAT(1H0,5X,'CONCRETE STRENGTH=',F6.0,'PSI')
0285          106 FORMAT(1H0,5X,'(AS+ASP)/AG=',F8.4)
0286          107 FORMAT(1X,'MOMENT CURVATURE DIAGRAMS'///)
0287          109 FORMAT(3X,8X,'M1',9X,'PHI1',11X,'M2',9X,'PHI2',11X,'M3',9X,'PHI3'
                 1,11X,'M4',9X,'PHI4'//)
0288          110 FORMAT(1X,I4)
0289          111 FORMAT (8F10.3)
0290          112 FORMAT(1H0)
0291          113 FORMAT(1X,F8.5)
0292          114 FORMAT(1H0,4X,'PO=',F12.5,'LBS FOR DIAM OR B=T=1 INCH'//)
0293          115 FORMAT(1X,'COLUMN DEFLECTION CURVE FOR P/PO=',F7.4,' AND P=',F8.1,
                 1 10X,'ULTIMATE MOMENT=',1PE10.4)
```

```
0294          116 FORMAT(1H0,'CASE ',I3,'  ALPHA(0)=',F12.5)
0295          117 FORMAT(1H0,'MOMENT FAILURE AT UPPER END OF ',I3,'TH LENGTH INCR')
0296          118 FORMAT(5X,F10.5,5E13.4)
0297          119 FORMAT(1X,5E10.3)
0298          120 FORMAT(1H1,'VALUES FOR SWAY SUBASSEMBLAGE CHARTS'///)
0299          121 FORMAT(1H0,4X,'LENGTH=',F10.5,'  K OF BEAM=',F10.3)
0300          122 FORMAT(12X,'QH/2MPC',8X,'DELTA/H'//)
0301          123 FORMAT(5X,3F15.5)
0302          124 FORMAT(12X,'H',12X,'V',10X,'V/H',9X,'GAMMA'//)
0303          125 FORMAT (F10.7,I4,2F10.7)
0304          126 FORMAT (16I5)
0305          127 FORMAT(1H0)
0306          128 FORMAT (60X,'KOUNT1 =',I5)
0307          129 FORMAT (80X,I5)
0308          130 FORMAT(5F20.0)
0309          131 FORMAT ( 5F20.8)
0310          132 FORMAT(1H0,'NO. OF POINTS ON M-P-PHI CURVES:',/)
0311          133 FORMAT (9(9X,I5))
0312          134 FORMAT (1H0,'AXIAL LOAD RATIOS:',/)
0313          135 FORMAT (10X,9F6.2,///)
0314          136 FORMAT(1H1,30X,'COORDINATES OF M-P-PHI CURVES')
0315          137 FORMAT (5X,'MOMENTS, LB-IN:')
0315          138 FORMAT (1H0,5X,'CURVE NO. ',I2,5X,'P/P0=',F4.2,/)
0317          139 FORMAT (1H1,5X,'CURVATURES:')
0318          140 FORMAT(1H0,5X,'YIELD STRENGTH=',F9.0,'PSI')
0319          141 FORMAT(1H0,5X,'COVER/DEPTH=',F6.2,////)
0320          142 FORMAT(1H0,5X,'MATERIAL AND SECTION PROPERTIES:')
0321          143 FORMAT(5X,'-------------------------------',//)
0322          144 FORMAT(5X,'---------------',//)
0323          145 FORMAT(5X,'-----------',//)
0324          146 FORMAT(31X,'--------------------------',///)
0325          147 FORMAT(5X,2E15.5,5X,'END MOMENT=',1PE10.4)
0326          148 FORMAT(20A4)
0327          160 FORMAT(1H0,'LENGTH OF COLUMN=',F10.3,5X,'BEAM STIFFNESS =',F10.3)
0328          161 FORMAT(11F10.3)
0329          162 FORMAT(1H1)
0330          163 FORMAT(1H0)
0331          164 FORMAT(1H0,5X,'LENGTH OF COLUMN =',F5.1,' IN',10X,'K OF BEAM =',
                 1 E10.2)
0332          165 FORMAT(6X,'-------------------------',10X,'--------------------
                 1',/)
0333          166 FORMAT(8X,'P/P0',3X,'QL/MU',4X,'DELTA/L',4X,'END MOMENT',4X,
                1'E.M/PDELTA',9X,'PI',9X,'EPEL',/)
0334          167 FORMAT(8X,F4.2,2X,F6.4,5X,F6.4,4X,1PE10.3,4X,1PE10.3,4X,1PE10.3,
                14X,F10.3)
0335          168 FORMAT(F5.3,2F15.10,F8.1,F15.1,F10.3)
0336          169 FORMAT(3I5)
0337          171 FORMAT(1H0,'CHECK')
0338          172 FORMAT(8F10.5)
0339          173 FORMAT(2F15.10)
0340          174 FORMAT(1X,'NO. OF CAPDS IN THIS DATA SET =',I4)
0341          175 FORMAT(5X,F15.10)
0342          176 FORMAT(10X,I5)
0343          177 FORMAT(5E10.2)
0344              STOP
```

39. *Fatigue of Reinforcing Bars* by I.C. Jhamb and J.G. MacGregor, February 1972.

40. *Behavior of Welded Connections Under Combined Shear and Moment* by J.L. Dawe and G.L. Kulak, June 1972.

41. *Plastic Design of Steel Frame-Shear Wall Structures* by J. Bryson and P.F. Adams, August 1972.

42. *Solution Techniques for Geometrically Non-Linear Structures* by S. Rajasekaran and D.W. Murray, March 1973.

43. *Web Slenderness Limits for Compact Beams* by N.M. Holtz and G.L. Kulak, March 1973.

44. *Inelastic Analysis of Multistory Multibay Frames Subjected to Dynamic Disturbances* by M. Suko and P.F. Adams, June 1973.

45. *Ultimate Strength of Continuous Composite Beams* by S. Hamada and J. Longworth, August 1973.

46. *Prestressed Concrete I-Beams Subjected to Combined Loadings*, by D.L.N. Rao and J. Warwaruk, November 1973.

47. *Finite Element Analysis for Combined Loadings with Improved Hexahedrons* by D.L.N. Rao and J. Warwaruk, November 1973.

48. *Solid and Hollow Rectangular Prestressed Concrete Beams Under Combined Loading* by J. Misic and J. Warwaruk, September 1974.

49. *The Second-Order Analysis of Reinforced Concrete Frames* by S.E. Hage and J.G. MacGregor, October 1974.